



Thèse présentée pour obtenir le grade de
Docteur de l'Université Louis Pasteur
Strasbourg I

Discipline: Chimie Physique
par Marianne Gaborieau

Solid-state NMR investigation
of spatial and dynamic heterogeneity
in acrylic pressure sensitive adhesives (PSAs)
compared to model poly(n-alkyl acrylates)
and poly(n-alkyl methacrylates)

Soutenue publiquement le 10 mars 2005

Membres du Jury :

Directeur de Thèse: M. Bernard Meurer,
Rapporteur Interne : M. Gilbert Weill,
Rapporteur Externe : Mme Bernadette Charleux,
Rapporteur Externe : M. Piotr Tekely,
Examineur : M. Hans Wolfgang Spiess,
Examineur : M. René-Paul Eustache,

Chargé de Recherche, Strasbourg
Professeur Emérite, Université Strasbourg I
Professeur, Université Paris VI
Directeur de Recherche, Nancy
Professeur, Université de Mayence, Allemagne
Ingénieur de Recherche, Arkema

*Voici le terme d'un long périple
dans l'espace et dans le temps.*

This is the end of a long travel through Space and Time.

Marc Gaborieau, *Le Népal, une introduction à la connaissance du monde népalais*,
Kailash éditions, Paris, 1995, p. 291

*La verdadera ciencia enseña, sobre todo,
a dudar y a ser ignorante.*

True science teaches, above all, to doubt and to be ignorant.

Miguel de Unamuno, *Tragic sense of life*, 1913

à Marc et Catherine[†], Thomas, Julie et Capucine
à Patrice ...

Acknowledgements

Thanks are due to Bernard Meurer for accepting the official supervision of this work.

I would like to gratefully acknowledge Hans W. Spiess for allowing me to conduct my PhD work in his research group at the Max Planck Institute for Polymer Research (Mainz, Germany). This was a fruitful experience on a scientific as well as on a human point of view. I benefited from his never failing and motivating support.

I would like to thank Manfred Wilhelm for his supervision at the beginning of this work, for his readiness to answer my questions on various topics: science, Riesling, Pfalz...

Special thanks to Robert Graf for the never failing assistance concerning all practical spectrometer and NMR problems, for enlightening discussions about polymer physics, for careful reading of the manuscript and help for final corrections, as well as for many nice evenings around a good meal with Katharina ...

I am indebted to Atofina for financial support and for providing the investigated pressure sensitive adhesive samples, to François Beaume for interesting discussions, to René-Paul Eustache, Stéphane Lepizéra, Françoise Cochet and Olivier Colombani for the interest they take in my project.

I am grateful to Bernadette Charleux, Gilbert Weill, and Piotr Tekely for accepting to read this manuscript and report on this work.

Thanks are due to Nawel Khelfallah and Gilbert Weill for helping me organizing the defense.

I am very grateful to Mario Beiner from the University of Halle Wittenberg (Germany) for his invitation and nice welcome in Halle, for numerous and fruitful discussions. My chemist point of view of the nanophase separation was enlightened by his physicist experience.

I would like to thank Prof. Pakula for a friendly and fruitful cooperation on local dynamics in polyacrylates, and Stefan Kahle for numerous dielectric relaxation measurements, analysis and explanations.

In a random order, I would like to express many thanks to the Spiess group and the MPI-P, in particular:

Uta Pawelzik for her kind help during the poly(n-alkyl acrylates) synthesis and an introduction to various characterization techniques

Verona Maus for many urgent DSC measurements and friendly discussions

The "Chemielabor" team for the nice working atmosphere : Ulri Jonas, the Neidhöfers, Kiki, Arancha, Diane, Diana, Michelle, Silvia, Petra, Charles-André, etc.

Michael Neidhöfer, Axel Kretschmer, Robert Graf and Ingrid Fischbach for their patient explanations of the way of operating a spectrometer, and how to properly record NMR data

Katja Klimke and Matt Parkinson for the precious advices and experimental tricks concerning the branching quantification

Manfred Hehn, Hans Peter Reich for the efficient technical assistance with spectrometers, for always finding solutions to the problems arising from annoying samples, mechanics or electronics

Frank Keller for computer assistance on a French-speaking laptop with French keyboard

The unforgettable 3M team of the Massenzimmer: Mark McCormick, Matt Parkinson, Michael Pollard, for my big progress in English language, journeys in time, Jazz-and-beer evenings, discussions about NMR (what about that Mainz 05?) and more, and making me feel at home ... I thank them also, as well as Attila Domján, Sheng-Shu Hou, Christian Krüger, Diana Boos, Timm Doetsch for the nice working atmosphere in room of Massen and Zimmer

Ingrid Fischbach, Katja Klimke, Michael Neidhöfer, for a friendly time together by Bürochef and Alumni

Barbara Doerner-Stute, the good soul of the Spiess group, for her kindness, her patience, her continuous help concerning administrative and morale things.

Corinna Kautz for successfully continuing this difficult task,

Michael Wind for providing the poly(n-alkyl methacrylates) samples together with the characterization of the dynamic heterogeneity, and tricks for low temperature measurements.

The Spiess group and the MPI-P in general for the multicultural experience: among others Gillian from Canada, Erli from Indonesia, Alexandra from Italy, Eva from Spain, Han-Bong from Korea/Saarland, Grazyna from Poland, Julia from Russia/America/Israel, Shi Feng from China, Sanjay from India/Netherlands, Yao from China, Doene, Fatma, Mehmet and Bahar from Turkey, Juana and Carlos from Mexico, Rafa from Catalonia, Laurent and Baptiste from France, Britt from the USA, Karen and Michael from Germany...

Frau Nanz for many urgent printing / cutting / binding

I am grateful to my parents and brother and sisters for encouraging higher studies in a field foreign to them ("and at the end you will tell us why the adhesives stick?"), my grandmother for many phone calls.

A very special thank goes to Patrice for his continuous and attentive help, from countless 6h train trips to careful reading of solid-state NMR or dynamics study, and so much more ...

I would like to apologize to all the ones I did not have enough space or memory to namely thank...

Table of contents

Résumé de la thèse	ix
I. Introduction	ix
A. Contexte	ix
B. Présentation des échantillons	x
C. Démarche	xi
II. Etude du branchement	xi
A. Etat de l'art.....	xi
B. Quantification du branchement par RMN ¹³ C	xi
C. Détection des branches longues par SEC multi-détection	xii
III. Filtre dipolaire et dynamique locale dans des polymères fondus	xiii
A. Présentation des échantillons étudiés	xiii
B. Technique de diffusion de spin ¹ H nucléaire avec filtre dipolaire	xiv
C. Contraste dynamique dans les PnAAs et PnAMAs fondus	xv
D. Sélection réelle et mécanisme de diffusion de l'aimantation.....	xv
E. Quantification de la dynamique locale.....	xvi
F. Interprétation des résultats	xvii
G. Comparaison de tous les échantillons	xviii
IV. Conclusion générale et perspectives	xviii
V. Plan du manuscrit de thèse	xix
Part 0: General introduction	1
Part 1: Literature survey and motivation	5
I. Pressure sensitive adhesive materials ⁷⁻¹⁰	7
A. Definition and applications	7
B. Composition	8
C. Properties and testing	12
D. Influence of chemical and physical factors on the adhesive properties ²	16
E. Mechanism of debonding	20
F. Conclusion	23
II. Basic principles of solid-state nuclear magnetic resonance	24
A. General introduction to NMR	24
B. Introduction to solid-state NMR	28
C. Single pulse excitation	34
D. Cross-polarization (CP) ¹³ C-NMR spectra.....	35
E. Two-dimensional wideline separation (2D-WISE).....	37
F. ¹ H Longitudinal or spin-lattice relaxation T ₁	39
G. Dipolar filter.....	39
H. ¹ H nuclear spin diffusion ^{81,82}	41
I. Nuclear Overhauser effect (NOE) ⁹⁴	48
III. Conclusion and strategy	56
A. Branching	56
B. Chain dynamics.....	57
C. Nanostructuring.....	57

Part 2: Presentation and characterization of PSA and model samples	59
I. Description and characterization of the industrial pressure sensitive adhesive samples.....	61
A. Description	61
B. Solid content, particle size and calorimetric properties	65
C. Adhesive and mechanical properties.....	66
D. Chemical characterization of the samples via solid-state NMR	67
II. Description, synthesis and characterization of model samples.....	71
A. Comparison of poly(n-alkyl acrylates) and poly(n-alkyl methacrylates)	72
B. Presentation of model poly(n-alkyl methacrylate) homopolymers.....	73
C. Synthesis of model poly(n-alkyl acrylate) homopolymers	75
D. Characterization of the poly(n-alkyl acrylate) homopolymers	76
III. Quantification of branching in PSA samples using ¹³C NMR	78
A. Molecular origin of branching and crosslinking in poly(alkyl acrylates)	79
B. Choice of a ¹³ C NMR technique to quantify branching in poly(alkyl acrylates)...	84
C. Branching level quantification and discussion of the branching topology	94
IV. Multiple-detection SEC of the model poly(n-alkyl acrylates)	100
A. Overview of the possible SEC methods ^{199,203}	100
B. Determined molar masses	102
C. Investigation of branching.....	103
D. Conclusion on the multiple detection SEC investigations	107
V. Conclusion on samples presentation and characterization	108
Part 3: Using and misusing the dipolar filter, example of PEMA.....	111
I. Literature survey on nanostructuring in poly(n-alkyl methacrylates) and poly(n-alkyl acrylates).....	113
A. Molecular dynamics and nanophase separation in poly(n-alkyl methacrylates) (Ph.D. work of Wind) ^{5,221}	113
B. Nanophase separation in poly(n-alkyl methacrylates) and poly(n-alkyl acrylates) (habilitation work of Beiner ²²⁰).....	122
C. Conclusion	126
II. Dynamic contrast in poly(ethyl methacrylate), PEMA	127
A. ¹ H static spectra.....	127
B. 2D-WISE.....	128
C. Conclusion on the dynamic contrast	131
III. Monitoring the ¹H magnetization of the more mobile parts after the dipolar filter.....	131
A. New type of sample for the ¹ H nuclear spin diffusion technique with dipolar filter	131
B. Changes done to data analysis	132
C. Results obtained for poly(ethyl methacrylate) at ca T _g +70 K.....	136
IV. Investigation of the actual selection done by the dipolar filter and of the actual subsequent transfer mechanism	138
A. Actual selection done by the dipolar filter	139
B. Coherent or incoherent magnetization transfer ?	141
C. Mathematical equations describing the magnetization decay	143
D. Conclusion on the actual selection and subsequent magnetization transfer	146
V. Conclusion on use and misuse of the dipolar filter	146
A. Summary of the investigation of PEMA at ca T _g +70 K	146
B. Conclusion on the use and misuse of the dipolar filter	147

Part 4: Nuclear Overhauser Effect investigated in model poly(n-alkyl acrylates) using the dipolar filter.....	149
I. Investigation of the dynamic contrast in model poly(n-alkyl acrylates) ...	151
A. ¹ H static spectra.....	151
B. 2D-WISE.....	153
C. Conclusion on the dynamic contrast.....	155
II. Investigation of NOE in the model poly(n-alkyl acrylates) using the dipolar filter.....	156
A. Actual selection done by the dipolar filter.....	156
B. Recording and processing NOE data using the dipolar filter in PEA at T _g +70 K.....	157
C. Temperature dependence of q _{AB} ·τ _C ^{AB} for sample PEA.....	165
D. Temperature dependence of q _{AB} ·τ _C ^{AB} for all PnAA samples.....	166
E. Conclusion on the measurement of NOE in model PnAAs.....	167
III. Interpretation of NOE results in model poly(n-alkyl acrylates).....	168
A. ¹ H longitudinal relaxation in model PnAAs.....	168
B. Relaxation processes in model PnAAs.....	170
IV. Conclusion on NOE in model poly(n-alkyl acrylates).....	175
A. Conclusion.....	175
B. Outlook.....	175
Part 5: Nuclear Overhauser Effect investigated in model poly(n-alkyl methacrylates) using the dipolar filter; comparison with acrylate models and PSAs.....	177
I. Investigation of the dynamic contrast in model poly(n-alkyl methacrylates).....	179
A. ¹ H static spectra.....	179
B. 2D-WISE.....	181
C. Conclusion on the dynamic contrast.....	181
II. Investigation of NOE in the model poly(n-alkyl methacrylates) using the dipolar filter.....	181
A. Actual selection done by the dipolar filter.....	181
B. Recording and processing NOE data using the dipolar filter in PEMA at T _g +67 K.....	184
C. Temperature dependence of q _{AB} ·τ _C ^{AB} for poly(ethyl methacrylate) samples.....	186
D. Temperature dependence of q _{AB} ·τ _C ^{AB} for model PnAMA samples.....	187
E. Discussion of the biexponential behavior observed at low temperatures.....	188
F. Conclusion on the measurement of NOE in model PnAMAs.....	189
III. Interpretation of NOE results in model poly(n-alkyl methacrylates).....	190
A. ¹ H longitudinal relaxation in model PnAMAs.....	190
B. Relaxation processes in model PnAMAs.....	192
IV. Comparison of model and industrial samples.....	195
A. Comparison of all model samples.....	195
B. Comparison of model and industrial samples.....	198
V. Conclusion on NOE in model poly(n-alkyl methacrylates) and on the comparison of all samples.....	201
A. Local nanophase separation.....	201
B. Local relaxation processes detected by the NOE with dipolar filter.....	201
C. Comparison with industrial samples.....	202

Part 6: General conclusion and outlook	203
I. General conclusion	205
A. Branching	205
B. Nanophase separation.....	206
C. NOE with dipolar filter	207
D. Chain dynamics.....	207
II. Outlook.....	208
A. Branching	208
B. Nanophase separation.....	208
C. Chain dynamics.....	209
D. NOE with dipolar filter	209
E. Characterization of PSAs	210
Part 7: Appendices.....	211
I. Properties of the investigated samples	213
A. Synthesis of the industrial pressure sensitive adhesive samples.....	213
B. Synthesis of the model poly(n-alkyl acrylates).....	214
C. Characterization of the first synthesized poly(n-alkyl acrylates).....	217
D. Samples storage.....	218
II. Conditions of the experiments.....	219
A. DSC, TGA, SEC and solution-state NMR.....	219
B. Solid content and mean particle diameter of latices, casting of films.....	220
C. Solid-state NMR	220
III. Viscoelastic properties and stereochemistry of polymers, characterization of homogeneous networks.....	235
A. Basic concepts relative to viscoelastic properties	235
B. Stereochemical definitions and notations ²⁸⁰⁻²⁸² relative to tacticity.....	238
C. Characterization of the crosslinking of homogeneous networks	240
IV. NMR spectra and SEC results	242
A. NMR spectra of model poly(n-alkyl methacrylates).....	242
B. NMR spectra of model poly(n-alkyl acrylates).....	253
C. NMR spectra of PSA samples.....	264
D. SEC results of poly(n-alkyl acrylates)	268
V. Abbreviations and symbols	270
A. Investigated samples	270
B. Monomers, polymers and other chemicals.....	270
C. Nuclear magnetic resonance	271
D. Others	272
VI. Literature references.....	274

Résumé de la thèse

I. Introduction

A. Contexte

Le but des travaux présentés est l'étude des propriétés microscopiques d'adhésifs sensibles à la pression (PSAs) acryliques et de composés modèles. Les PSAs acryliques sont d'importance industrielle : ils sont utilisés principalement dans la confection d'étiquettes et de rubans adhésifs, repositionnables ou non.

Ils sont actuellement caractérisés principalement à travers leurs propriétés macroscopiques, par exemple leurs propriétés adhésives. Ces matériaux nécessitent un compromis entre une faible viscosité (pour le caractère collant) et une forte cohésion (pour le caractère repositionnable), devant être optimisée pour chaque application particulière, ce qui est réalisé à l'heure actuelle à travers le test de nombreuses formulations. La relation entre leurs propriétés microscopiques et macroscopiques est inconnue, bien qu'il soit connu empiriquement que la température de transition vitreuse (T_g), les propriétés viscoélastiques et la réticulation sous toutes ses formes jouent un rôle majeur dans les propriétés adhésives. La distance à la T_g et les propriétés viscoélastiques ont un lien étroit avec la dynamique de chaîne. La réticulation peut être présente sous forme de réticulation covalente (via l'introduction d'agent de réticulation ou bien intrinsèquement du fait de la cinétique de la polymérisation), de liaison hydrogène entre les unités monomères d'acide acrylique ou de réticulation physique (à travers une nanoséparation de phase).

Cette thèse s'inscrit dans une recherche à très long terme visant à comprendre le mécanisme d'adhésion des adhésifs PSA acryliques, en particulier le rôle joué par des propriétés microscopiques comme la nature et le nombre de branches, la dynamique de chaîne, l'hétérogénéité dynamique. Une meilleure compréhension du mécanisme d'adhésion nécessite tout d'abord de développer de nouvelles techniques de caractérisation de la microstructure des échantillons. La résonance magnétique nucléaire (RMN) du solide a été choisie dans ce travail pour caractériser les branches longues, la dynamique de chaîne et l'hétérogénéité dynamique dans des échantillons PSA acryliques et des composés modèles.

B. Présentation des échantillons

Les échantillons fournis par Atofina (pas des grades commerciaux) sont des copolymères statistiques de poly(acrylates d'alkyles), avec différentes chaînes latérales alkyles, contenant aussi d'autres composants. Ils ont été obtenus par copolymérisation en émulsion d'acrylate de 2-éthyl-hexyle, d'acrylate de méthyle, d'acide acrylique et d'un agent de réticulation comonomère (confidentiel). Du fait du procédé de polymérisation semi-continu, des copolymères statistiques sont attendus, avec une plus grande densité d'acide acrylique en surface des particules et en bout de chaînes polymères. De plus, une microstructure branchée est attendue. Ces échantillons, pas complètement solubles dans les solvants classiques, ont été caractérisés tout d'abord par mesure du taux de solide et des tailles de particules des émulsions, détermination de la T_g des films. Les propriétés adhésives et mécaniques des films ont été examinées chez Atofina (confidentielles). La structure chimique des échantillons a été étudiée par RMN du solide ^1H et ^{13}C . En plus de ces échantillons industriels, deux familles d'échantillons modèles ont été étudiées : des homopolymères d'acrylates de n-alkyles et de méthacrylates de n-alkyles.

Les poly(acrylates de n-alkyles) (PnAAs) ont été synthétisés dans ce travail par polymérisation radicalaire conventionnelle en solution d'acrylate de méthyle, d'éthyle, de n-butyle ou de n-hexyle et purifiés par précipitation à froid dans le méthanol. Les homopolymères sont obtenus sans additif, mais avec une microstructure branchée et une distribution des masses molaires large similaires à celles des échantillons industriels. Les masses molaires, déterminées par chromatographie d'exclusion stérique (SEC) multi-détection avec étalonnage universel, sont suffisamment élevées pour avoir une influence négligeable sur les propriétés microscopiques étudiées. Ces échantillons sont atactiques et contiennent des branches.

Les poly(méthacrylates de n-alkyles) (PnAMAs), sont des homopolymères de méthacrylate d'éthyle, de n-butyle ou de n-hexyle synthétisés par polymérisation radicalaire. Ils ont fait l'objet d'études structurales et dynamiques auparavant dans notre groupe. Les PnAMAs diffèrent des PnAAs par un groupe méthyle sur le squelette, résultant en une T_g beaucoup plus élevée ; cependant, un comportement similaire est attendu à la même distance de la T_g du fait de leur formule chimique similaire. En particulier, puisque le but de cette étude à long terme est de caractériser des adhésifs PSA à température ambiante, ce qui correspond à $T_g+70\text{ K}$, l'étude des échantillons modèles devrait être centrée autour de $T_g+70\text{ K}$. Certains échantillons PnAMA présentent un marquage isotopique sélectif ^2H ou ^{13}C . Tous les échantillons PnAMA ont une forte tendance à la syndiotacticité, une absence de

branche et des masses molaires suffisamment élevées pour avoir une influence négligeable sur les propriétés microscopiques étudiées.

C. Démarche

La RMN du solide est une technique appropriée à la caractérisation de divers aspects de la microstructure d'échantillons polymères. Le taux de branchement peut être quantifié par RMN ^{13}C monodimensionnelle, qui peut être appliquée directement aux échantillons industriels. La dynamique de chaîne peut être étudiée avec diverses techniques de RMN du solide ; cependant, cette étude nécessite des échantillons modèles. La taille d'une structure à l'échelle du nanomètre résultant en une hétérogénéité dynamique pourrait être déterminée par la technique de diffusion de spin nucléaire ^1H avec filtre dipolaire ; les analyses devraient être conduites tout d'abord sur des échantillons modèles.

II. Etude du branchement

A. Etat de l'art

Le branchement dans les poly(acrylates d'alkyles) a son origine dans deux réactions : le transfert *intermoléculaire* au polymère crée des branches longues (LCB) qui ont une influence sur les propriétés mécaniques et adhésives, le transfert *intramoléculaire* au polymère crée des branches courtes (SCB) et a une influence sur la vitesse de polymérisation. Le branchement n'est pas complètement compris et ne peut pas être contrôlé, mais il ne peut pas non plus être évité en polymérisation radicalaire ; il est actuellement étudié dans plusieurs groupes de recherche. La meilleure technique de quantification du branchement pour les poly(acrylates d'alkyles) est la RMN ^{13}C monodimensionnelle ; en revanche, branches courtes et branches longues ne sont pas différenciées. Les branches longues peuvent être détectées dans les polymères par rhéologie ou SEC multi-détection.

Avant ce travail, une technique de RMN en solution et une technique de RMN du solide en 28 h avaient été publiées pour la quantification du branchement. Cependant, toutes deux présentent des inconvénients, comme des problèmes de solubilité et de longs temps de mesure. Notre but était de développer une méthode rapide de quantification du branchement, directement sur les échantillons PSA industriels.

B. Quantification du branchement par RMN ^{13}C

La quantification du branchement dans les polyacrylates par RMN ^{13}C souffre principalement d'un faible rapport signal sur bruit (S/N). Pour un échantillon industriel, nous avons comparé plusieurs techniques de RMN du solide ^{13}C pour la quantification du

branchement. La polarisation croisée (CP) sous rotation à l'angle magique (MAS) peut permettre d'augmenter le S/N, mais ce n'est pas une technique quantitative et elle présente une très faible résolution pour l'échantillon étudié. L'irradiation simple sous MAS appliquée à l'échantillon gonflé par du THF présente une résolution suffisante pour la quantification, mais le S/N est faible. Nous avons donc décidé d'adapter aux poly(acrylates d'alkyles) une méthode développée pour le polyéthylène. La mesure est conduite sur l'échantillon pur fondu (150 °C au-dessus de T_g), sous rotation à l'angle magique (MAS), ce qui permet d'analyser l'échantillon entier, y compris sa fraction insoluble. Elle est réalisée par irradiation simple, et permet une estimation fiable du branchement en moins de 3h30 (cf. figure 1). Nous concluons que la meilleure technique pour la quantification du branchement dans les poly(acrylates d'alkyles) est la RMN du solide ^{13}C appliquée à l'échantillon pur fondu sous MAS. Les taux de branchement déterminés sur ces échantillons, de 3 à 5 % des unités monomères, sont en accord avec les valeurs (moins précises) de la bibliographie.

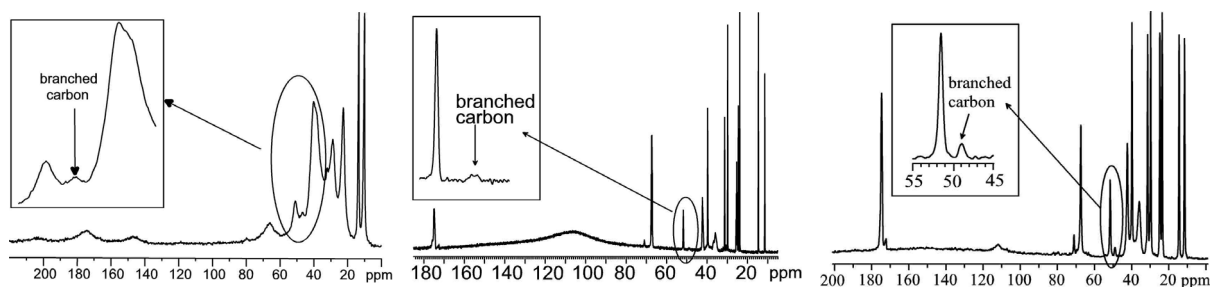


Figure 1 : Spectres RMN ^{13}C de l'échantillon Copo3 ; à gauche, par CP-MAS sur l'échantillon pur ; au centre, par irradiation simple de l'échantillon gonflé par le THF ; à droite, par irradiation simple de l'échantillon pur fondu ; la raie K du point de branchement se trouve à 49 ppm ; cf. partie 2 pour plus de détails.

La RMN ^{13}C ne différencie pas les branches longues des courtes. Cependant, des travaux publiés par d'autres groupes de recherche lors du travail présenté ici montrent que les poly(acrylates d'alkyles) présentent des branches longues et courtes, qu'ils soient polymérisés en solution ou en émulsion. Pour cette raison, il a été décidé d'utiliser la SEC multi-détection pour la caractérisation des branches longues dans les poly(acrylates d'alkyles).

C. Détection des branches longues par SEC multi-détection

L'étude par SEC multi-détection a été limitée aux PnAAs modèles pour des raisons de solubilité. Parmi les différentes méthodes de détermination des masses molaires par SEC, certaines ne sont pas applicables aux poly(acrylates d'alkyles) : l'étalonnage conventionnel (pas d'étalon), l'étalonnage universel utilisant les paramètres de Mark-Houwink-Sakurada (MHS, non reproductible), et la diffusion de lumière multi-angles et aux faibles angles (MALS/LALS, incrément d'indice de réfraction dn/dC trop faible). Nous avons donc utilisé les méthodes de détermination des masses molaires suivantes : étalonnage universel vrai avec viscosimètre en ligne (UC) et triple détection (TD).

La méthode classique de détection de branches longues par SEC pour le polyéthylène est le diagramme de Mark-Houwink : une droite est obtenue pour les échantillons linéaires, une courbe incurvée pour les échantillons ayant de longues branches. Cette technique ne donne aucun résultat concluant pour les PnAAs étudiés, peut-être du fait d'une gamme de masses molaires trop restreinte ou du fait d'une fréquence de branchement non constante. De plus, la présence de branches longues a une influence non seulement sur la viscosité intrinsèque mesurée, mais aussi sur la masse molaire déterminée à un volume d'élution donné. Pour cette raison, nous proposons de détecter les branches longues par le tracé sur une échelle logarithmique des masses molaires déterminées par UC et TD en fonction du volume d'élution. Ce tracé a été réalisé pour tous les PnAAs modèles, et montre une différence systématique entre les courbes obtenues par UC et TD. Cette différence de masses molaires s'explique par la présence de branches longues : à chaque volume d'élution, un mélange de chaînes ayant le même volume hydrodynamique mais des topologies et des masses molaires différentes est présent. La méthode basée sur la diffusion de lumière (TD) détermine la masse molaire moyenne en poids M_w du mélange, celle basée sur la viscosimétrie (UC) détermine la masse molaire moyenne en nombre M_n du mélange.

Des branches longues ont été détectées dans tous les PnAAs modèles. Malheureusement, du fait de diverses difficultés théoriques aussi bien que de problèmes techniques, une quantification de ce LCB n'est pas possible à l'heure actuelle pour les poly(acrylates d'alkyles). Pour permettre cette quantification, il serait nécessaire tout d'abord de coupler la SEC à une technique de séparation des chaînes polymères en fonction de leurs caractéristiques de branchement, puis de développer un modèle théorique fiable reliant des grandeurs mesurées au taux de branchement pour les poly(acrylates d'alkyles).

III. Filtre dipolaire et dynamique locale dans des polymères fondus

A. Présentation des échantillons étudiés

Les PnAAs présentent une structure locale à l'état fondu : une nanoséparation de phase est causée par l'incompatibilité à l'intérieur d'une unité monomère entre le squelette polaire et rigide et la chaîne latérale alkyle apolaire et flexible. Cette structure locale est détectée par diffraction des rayons X aux grand angles (WAXS), mais elle n'est pas bien comprise. Les PnAMAs sont chimiquement similaires aux PnAAs ; ils présentent une structure locale mieux organisée et ont été bien plus étudiés.

La nanoséparation de phase est détectée dans les PnAMAs par WAXS ou diffraction des neutrons, et indirectement par des mesures de dynamique par RMN du solide. Les

diffractogrammes WAXS des polymères fondus montrent trois halos ; dans la bibliographie, deux représentations de cette même structure sont proposées (cf. figure 2). Des mesures de RMN du solide ont permis de détecter un processus de relaxation plus lent que la relaxation $\alpha\beta$ classique dans les polymères fondus ; il est attribué à l'isotropisation des mouvements des chaînes principales.

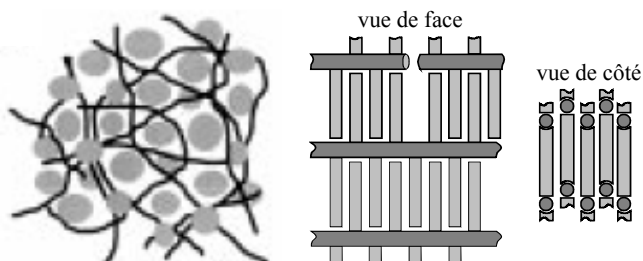


Figure 2 : Modèles pour la représentation de la structure locale de poly(méthacrylates de n-alkyles), les squelettes sont représentés en gris foncé et les chaînes latérales alkyles en gris clair ; à gauche, modèle tridimensionnel de la structure ; à droite, modèle local en couches (cf. partie 3 pour plus de détails).

On peut imaginer que l'existence d'une structure locale dans le polymère fondu pourrait résulter en des domaines organisés moins mobiles séparés par le reste de l'échantillon plus mobile. Si tel était le cas dans les PSA acryliques, cela pourrait avoir une influence sur leur propriétés adhésives à travers une réticulation physique. C'est pourquoi les PnAMAs et les PnAAs représentent des échantillons modèles intéressants pour la caractérisation d'une éventuelle structure locale de phase dans les PSA acryliques.

B. Technique de diffusion de spin ^1H nucléaire avec filtre dipolaire

La technique de diffusion de spin ^1H nucléaire avec filtre dipolaire a été beaucoup utilisée pour quantifier la taille d'hétérogénéités dynamiques sur une gamme de 1 à 50 nm, dans des échantillons où la structure correspondante est associée à un fort contraste dynamique : par exemple des copolymères à blocs à nanoséparation de phase ou des films constitués de particules coeur-couronne avec une grande différence entre les T_g des deux phases.

L'expérience de diffusion de spin ^1H nucléaire se déroule de la façon suivante. Une aimantation macroscopique est tout d'abord créée dans tout l'échantillon. Puis le filtre dipolaire est appliqué, qui résulte en la sélection de l'aimantation seulement dans les parties les plus mobiles. Ensuite l'aimantation diffuse dans l'échantillon au cours d'un temps de mélange pour revenir à l'équilibre ; il ne s'agit pas d'une diffusion physique des molécules mais de la diffusion de l'aimantation d'un site à l'autre. Pour différents temps de mélange, l'aimantation présente dans les parties les plus mobiles est enregistrée. La courbe décroissante obtenue permet d'extraire des informations sur la proportion de parties plus mobiles (via le plateau aux longs temps de mélange) et sur la taille des domaines concernés (via la vitesse de décroissance linéaire aux courts temps de mélange).

C. Contraste dynamique dans les PnAAs et PnAMAs fondus

Des spectres ^1H statiques enregistrés entre $T_g-50\text{ K}$ et $T_g+130\text{ K}$ ont montré pour les PnAAs et PnAMAs que l'échantillon entier devient plus mobile lorsque la température augmente, et ne présente pas de fort contraste dynamique.

Des spectres 2D-WISE (« wideline separation » bidimensionnelle) ont été enregistrés pour caractériser la mobilité des différents sites sélectivement en fonction de leur déplacement chimique ^{13}C . Pour le poly(méthacrylate d'éthyle) entre environ $T_g-10\text{ K}$ et $T_g+80\text{ K}$, les groupes méthyle sont les plus mobiles, celui de la chaîne latérale étant plus mobile que celui de la chaîne principale. Pour les PnAAs à environ $T_g+70\text{ K}$, le groupe méthyle terminal de la chaîne latérale alkyle est plus mobile que la chaîne principale ; de plus, pour le poly(acrylate de n-hexyle), un gradient de mobilité est observé le long de la chaîne latérale alkyle.

D. Sélection réelle et mécanisme de diffusion de l'aimantation

Les échantillons modèles et industriels analysés lors de cette thèse constituent un nouveau type d'échantillon pour la technique de diffusion de spin ^1H nucléaire avec filtre dipolaire, puisqu'ils présentent un contraste dynamique très faible. C'est pourquoi leur étude a nécessité des modifications de l'analyse des données. Les expériences de diffusion de spin ^1H nucléaire réalisées sur le PEMA à $T_g+67\text{ K}$ produisent apparemment des courbes de diffusion de spin typiques, avec un début linéaire suivi d'un plateau (cf. figure 3, gauche).

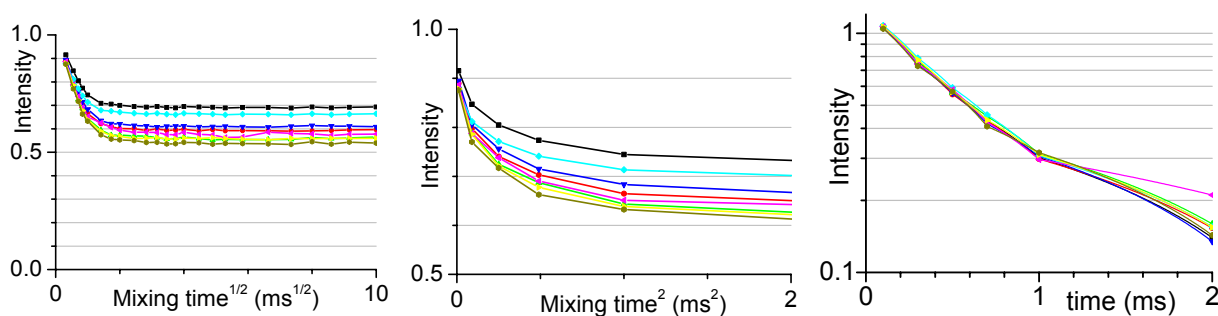


Figure 3 : Evolution de l'aimantation ^1H des parties plus mobiles après le filtre dipolaire pour l'échantillon PEMA à 409 K ($T_g+67\text{ K}$, différents filtres) ; à gauche, en fonction de la racine carrée du temps de mélange ; au centre, en fonction du carré du temps de mélange ; à droite, sur une échelle logarithmique en fonction du temps de mélange, après soustraction de la valeur du plateau.

En supposant que le filtre dipolaire sélectionne la nanostructure, il sélectionnerait la matrice plus mobile et désélectionnerait les nanodomains organisés moins mobiles, ce qui conduirait à une taille de structure de 2 à 7 nm, en accord avec la taille typique de 5 à 10 unités monomères déterminée par RMN ou WAXS.

Cependant, compte-tenu du faible contraste dynamique présent dans l'échantillon, il était nécessaire de vérifier la sélection réellement faite par le filtre dipolaire. Pour cela, l'aimantation des noyaux ^1H après le filtre dipolaire a été transférée sur les noyaux ^{13}C voisins

(par polarisation croisée de Lee-Goldburg pour assurer un transfert local) pour être détectée avec une résolution en déplacements chimiques. Cette expérience a été conduite sur plusieurs échantillons PnAA et PnAMA et montre que le filtre dipolaire sélectionne le groupe méthyle terminal de la chaîne latérale alkyle et parfois partiellement le(s) groupe(s) méthylène suivant(s). Le filtre dipolaire ne sélectionne donc pas de domaine à l'échelle nanométrique, mais des sites isolés. C'est pourquoi, le transfert d'aimantation observé ne se produit pas entre des domaines à l'échelle du nanomètre, mais le long de la chaîne latérale alkyle et en direction de la chaîne principale. Aucune taille de domaine ne peut donc être extraite des données.

Le mécanisme de diffusion de l'aimantation après le filtre dipolaire a aussi été étudié. Un transfert cohérent de l'aimantation par couplage dipolaire résiduel résulterait en une décroissance linéaire de l'aimantation des parties plus mobiles en fonction du carré du temps de mélange. Un transfert non cohérent de l'aimantation par relaxation croisée résulterait en une décroissance linéaire du logarithme de l'aimantation des parties plus mobiles en fonction du temps de mélange. A l'échelle de temps de nos expériences, une dépendance linéaire est observée seulement dans le deuxième cas (cf. Figure 3, centre et droite), indiquant une prédominance du mécanisme de relaxation croisée dans le transfert de l'aimantation après le filtre dipolaire.

E. Quantification de la dynamique locale

Le signal enregistré après le filtre dipolaire dans les PnAAs et PnAMAs est attribué à la décroissance de l'aimantation des groupes terminaux des chaînes latérales alkyles par relaxation croisée. Ceci est équivalent à la décroissance de l'intensité d'une raie située sur la diagonale dans une expérience bidimensionnelle de NOE (effet Overhauser nucléaire). L'expression analytique la plus appropriée existante à notre connaissance pour décrire cette décroissance concerne deux groupes de spins équivalents ; l'équation correspondant à l'entité CH₃-CH₂ a été dérivée de données bibliographiques et utilisée dans ce travail :

$$a(\tau_m) = \frac{3M_0}{10} \cdot \left[\frac{6}{5} + \frac{4}{5} \exp(-5q_{AB}\tau_C^{AB}\tau_m) \right]$$

Cette équation relie l'aimantation $a(\tau_m)$ enregistrée au temps de mélange τ_m avec seulement deux inconnues : un paramètre dipolaire q_{AB} et le temps de corrélation τ_C^{AB} du mouvement moléculaire qui module le couplage dipolaire pour induire la relaxation croisée. Le paramètre dipolaire a été déterminé indépendamment via le calcul de la distance H-H intergroupe moyenne dans une entité CH₃-CH₂ et via la mesure du second moment de spectres ¹H enregistrés pour chaque échantillon très au-dessous de sa T_g dans des conditions statiques. L'ajustage des données expérimentales permet alors l'extraction du temps de

corrélation du mouvement moléculaire qui module le couplage dipolaire pour induire la relaxation croisée.

F. Interprétation des résultats

Pour les PnAMAs au-dessus d'environ T_g+80 K, une décroissance monoexponentielle de l'aimantation est observée, dont a été extrait un temps de corrélation. Pour les PnAMAs entre environ T_g+30 K et T_g+80 K, une décroissance biexponentielle de l'aimantation est observée, qui a été attribuée à deux processus moléculaires distincts. Le processus rapide (correspondant à la décroissance lente) n'est pas quantifiable, il est détecté dans la gamme de températures où une forte anisotropie des mouvements moléculaires due à la nanostructure est reportée. En revanche, le temps de corrélation du processus lent (correspondant à la décroissance rapide) présente la même dépendance linéaire de la température inverse ($1000/T$) de type Arrhenius que le processus unique observé à plus haute température, indiquant un processus local. Ces temps de corrélation ont été comparés avec des diagrammes d'Arrhenius des PnAMAs tirés de la bibliographie. Le processus détecté par relaxation croisée après filtre dipolaire est attribué à la relaxation des nanodomains alkyles, en tant que mouvements couplés de la chaîne principale avec des modes locaux entravés dans les chaînes latérales. Dans le cas des échantillons PEMA, du fait du nombre moins élevé de degrés de liberté internes, le processus de relaxation β est prédominant.

Pour les PnAAs entre environ T_g+20 K et T_g+100 K, une décroissance monoexponentielle de l'aimantation est observée. Pour chaque PnAA, les temps de corrélation extraits présentent une dépendance linéaire de la température inverse ($1000/T$) de type Arrhenius, indiquant un processus local. De plus, une courbe maîtresse est obtenue lorsque ces temps de corrélation sont tracés en fonction de la distance de la T_g ($T - T_g$). Les temps de corrélations extraits ont été comparés avec des données de spectroscopie de relaxation diélectrique ou mécanique, tirés de la bibliographie ou mesurés sur nos échantillons dans le groupe du Prof. Pakula au MPI-P (cf. figure 4). Le processus de relaxation observé par l'expérience de NOE est détecté et quantifié pour la première fois dans cette gamme de températures. S'appuyant sur la nanoséparation de phase dans les PnAAs, les temps de corrélation quantifiés par NOE dans le travail présent ont été attribués à des mouvements locaux entravés des chaînes latérales dans les nanodomains alkyles organisés.

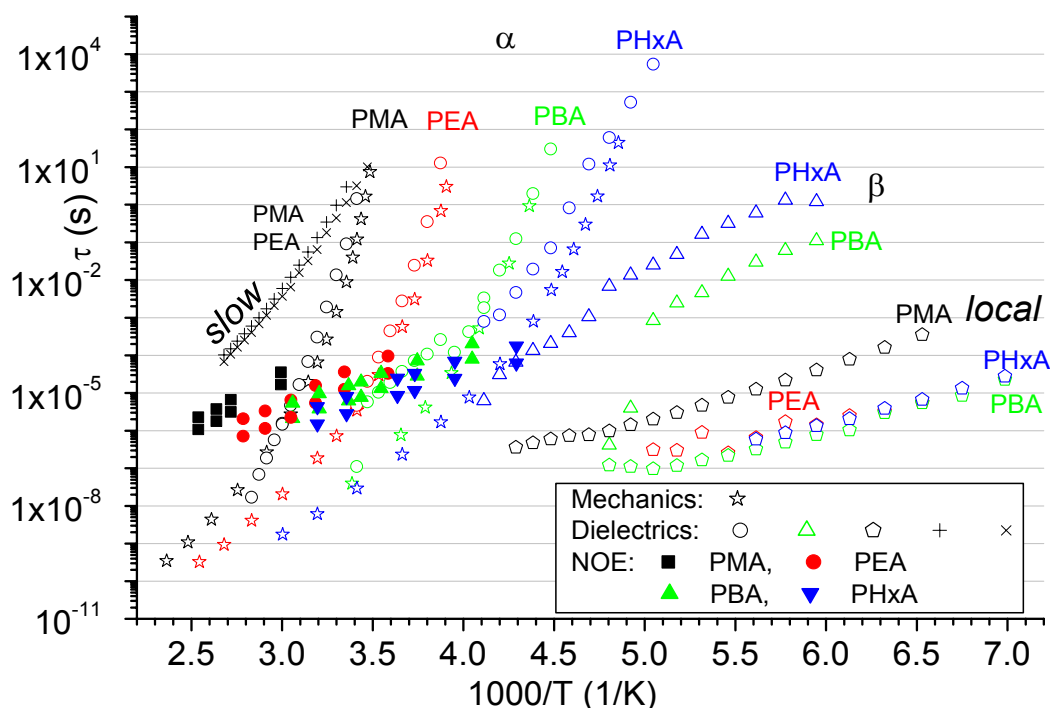


Figure 4: Temps de corrélation extraits des expériences de relaxation croisée (NOE) conduites dans le travail présenté ici sur les PnAAs modèles ; comparaison avec les données mesurées dans le groupe du Prof. Pakula sur les mêmes échantillons par spectroscopie diélectrique ou mécanique ; cf. partie 4 pour plus de détails.

G. Comparaison de tous les échantillons

Les PnAAs modèles sont plus mobiles que les PnAMAs modèles à la même distance de la T_g au-dessus de $T_g + 20$ K. Cela a été démontré par des spectres ^1H et ^{13}C enregistrés dans des conditions statiques. De plus, une structure locale est présente dans les deux familles d'échantillons avec le même ordre de grandeur de taille, mieux organisée dans le cas des PnAMAs. L'expérience de NOE avec filtre dipolaire permet la quantification des processus dynamiques liés à la structure locale dans les deux familles.

Des spectres ^1H statiques et des expériences 2D-WISE montrent pour les échantillons PSA industriels un comportement plus proche de celui des PnAAs que de celui des PnAMAs. Pour les PSAs, l'expérience de NOE avec filtre dipolaire réalisées à température ambiante permet la quantification de temps de corrélation du même ordre de grandeur que ceux des PnAAs. Cependant, ils ne se trouvent pas sur la courbe maîtresse des PnAAs tracées en fonction de la distance de la T_g ; cela pourrait être dû au caractère branché de la chaîne latérale 2EHA.

IV. Conclusion générale et perspectives

Ce travail s'inscrit dans une étude à très long terme visant à améliorer les adhésifs PSA acryliques, nécessitant pour cela une meilleure compréhension de leur procédé de polymérisation ainsi qu'une meilleure compréhension de leur mécanisme d'adhésion. Notre

contribution est l'apport de nouveaux outils analytiques pour cette étude. Il ouvre la voie à de nombreuses études, tant au niveau de la recherche fondamentale qu'à un niveau très appliqué.

Dans le cadre de la compréhension du procédé de polymérisation, nous proposons une technique de RMN ^{13}C du solide par irradiation simple, appliquée au polymère fondu sous MAS, qui fournit la première estimation fiable du taux de branchement dans les poly(acrylates d'alkyles). Elle est applicable directement aux échantillons industriels réticulés et multi-composants. Elle peut encore être optimisée.

Dans le cadre de la compréhension du mécanisme d'adhésion, nous proposons deux nouveaux outils analytiques. Le premier est une méthode de détection des branches longues (LCB) dans les poly(acrylates d'alkyles) par SEC multi-détection. Pour rendre cette méthode quantitative, il faudrait la coupler à une technique de séparation des chaînes polymères en fonction de leur topologie de branchement, et développer des modèles théoriques reliant les signaux des détecteurs aux taux de LCB statistique dans les polyacrylates. Le second outil analytique est la quantification de dynamique moléculaire locale dans les polymères fondus par une expérience de RMN « classique ». L'expérience conventionnelle de diffusion de spin nucléaire ^1H est utilisée ici pour quantifier sélectivement une dynamique locale sur des échantillons sans marquage isotopique et présentant un contraste dynamique. Le filtre dipolaire est alors utilisé pour la détermination de temps de corrélation (et non de taille de domaines comme c'est habituellement le cas). Il serait intéressant de développer des modèles plus élaborés décrivant la relaxation croisée dans des systèmes de spins multiples et d'appliquer la méthode développée dans ce travail à d'autres échantillons à chaîne latérale alkyle, comme des adhésifs PSA ou des poly(itaconates d'alkyles). Il serait par ailleurs passionnant de déterminer les mécanismes moléculaires des différents processus de relaxation dans les PnAAs.

V. Plan du manuscrit de thèse

Après une introduction générale dans la partie 0, une revue bibliographique sur les adhésifs PSA et une introduction à la RMN du solide sont présentées dans la partie 1. La partie 2 est consacrée à la présentation de tous les échantillons, ainsi qu'à l'étude du branchement dans les poly(acrylates d'alkyles). Dans la partie 3, la possibilité d'utilisation du filtre dipolaire pour la quantification de dynamique locale dans les polymères fondus est démontrée sur l'exemple du PEMA. La partie 4 est consacrée à l'étude des PnAAs par cette technique, la partie 5 à celle des PnAMAs. Une conclusion générale et des perspectives sont présentées dans la partie 6.

Part 0: General introduction

Part 0: General introduction

Poly(alkyl acrylates) are of industrial importance, due to their wide use in e.g., pressure-sensitive adhesives (PSAs), paintings, coatings.¹ Adhesion mechanism of acrylic PSAs is influenced by the microscopic and molecular properties of these samples like entanglement length, chemical and physical crosslinking.² Even if the first evidence of a substance being used as adhesive dates back to 4,000 B.C.³, the mechanism of adhesion is still being thoroughly investigated. New characterization techniques are needed. Solid-state nuclear magnetic resonance (NMR)⁴ was chosen to investigate the microstructure as well as the chain dynamics and its heterogeneity in some acrylic PSAs. NMR dates back only to 1946, but it has rapidly become a powerful tool to investigate the structure and dynamics in various media (gases, liquids, solids) for all types of chemical structures, from the diatomic gases to crystalline lattices via proteins and synthetic macromolecules. The long term goal of this study is to progress towards a better understanding of the adhesion mechanism of these samples.

In order to obtain a first glance of the complex behavior of these multi-component industrial samples, we chose to investigate model samples first. Poly(*n*-alkyl acrylate) homopolymers (s. Figure 1) are considered as good model samples, since their chemical composition is simpler than that of the industrial samples. Poly(*n*-alkyl methacrylate) homopolymers (s. Figure 1) have a chemical nature close to that of the poly(*n*-alkyl acrylate) homopolymers, and should exhibit similar properties. Furthermore, they have been studied more extensively in the past few decades,⁵ so that they are also suitable as model samples.

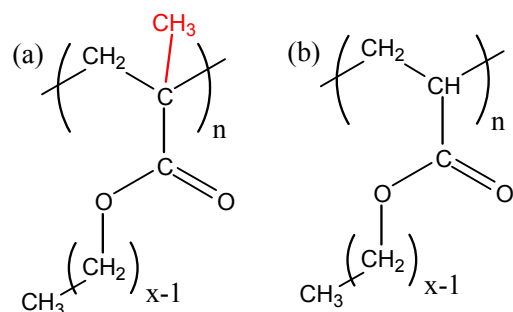


Figure 1: General formula of (a) poly(*n*-alkyl methacrylates) and (b) poly(*n*-alkyl acrylates).

In the first part, a literature survey will be given. The pressure-sensitive adhesives will be presented; in particular, the microscopic characteristics influencing the adhesion properties will be underlined. Then, several solid-state NMR techniques will be introduced, and a methodology will be chosen for the investigation of the industrial PSAs using NMR.

The second part is dedicated to the characterization of the industrial PSA samples. Their synthesis is described first. It should be noted that those samples are not commercial grades, but were synthesized for research purposes. Synthesis and characterization of model samples will be presented next. Then, different NMR methods for the quantification of the branching in the PSA samples will be compared in detail. Multiple detection SEC will be evaluated as a complementary technique for the branching detection in model poly(n-alkyl acrylates).

In the third part, the ^1H nuclear spin diffusion experiment with dipolar filter will be investigated in detail. The dipolar filter⁶, generally used to probe dynamic heterogeneities in polymeric samples, yielding domain sizes on the nanometer length scale, will be applied to poly(ethyl methacrylate). The possible occurrence of nuclear Overhauser effect (NOE) will have to be considered. Molecular dynamics will be investigated via selection by the dipolar filter and NOE for poly(n-alkyl acrylates) in the fourth part, for poly(n-alkyl methacrylates) in the fifth part.

Part 1: Literature survey and motivation

I. Pressure sensitive adhesive materials⁷⁻¹⁰	7
A. Definition and applications	7
B. Composition	8
1. Possible solvent	9
2. Tackifiers	9
3. Used raw materials	9
4. Acrylic pressure sensitive adhesives	10
a) Composition	10
b) Production process	11
c) Adhesive properties	12
C. Properties and testing	12
1. Tack and bonding	13
a) Definition and requirements for tack	13
b) Tests for tack measurement	13
c) Case of acrylic adhesives	14
2. Peel adhesion and debonding ^{21,34}	14
3. Cohesive strength	16
D. Influence of chemical and physical factors on the adhesive properties²	16
1. Glass transition temperature	16
2. Molar mass	16
3. Entanglement network	17
4. Introduction of functional groups	18
5. Crosslinking	18
6. Viscoelastic properties	20
E. Mechanism of debonding	20
1. Early studies	20
2. Energy criterion for adhesive strength in peel test	21
3. Zosel's work on fibrillar debonding in probe tack test	21
4. Creton's work on fibril formation	22
F. Conclusion	23
II. Basic principles of solid-state nuclear magnetic resonance	24
A. General introduction to NMR	24
1. Definition and basic concepts ^{63,64}	24
2. Evolution of magnetization during pulsed NMR experiments for a spin-half nucleus in the rotating frame	26
B. Introduction to solid-state NMR	28
1. Resonance line width, dipolar coupling and motion	28
a) Types of broadening	28
b) Line shape and line width	28
2. Applications of solid-state NMR	30
3. Principle of magic-angle spinning (MAS) ⁶⁹	30
4. Examples of application of MAS	31

C. Single pulse excitation.....	34
1. ^1H -NMR spectra	34
2. ^{13}C -NMR spectra	34
D. Cross-polarization (CP) ^{13}C-NMR spectra.....	35
1. Principle ^{70,71}	35
2. Optimization of the CP contact time ⁷¹	36
3. Lee-Goldburg CP	37
E. Two-dimensional wideline separation (2D-WISE)	37
1. Principle ^{73,76}	37
2. Information obtained from a 2D-WISE spectrum ^{73,76}	38
F. ^1H Longitudinal or spin-lattice relaxation T_1.....	39
G. Dipolar filter	39
1. Concept of mobility	40
2. The dipolar filter ⁶	40
H. ^1H nuclear spin diffusion^{81,82}	41
1. Concept of nuclear spin diffusion	41
2. Goal of the experiment	41
3. Choice of the operating temperature	42
4. Pulse program ⁸⁷ and principle of the experiment.....	43
5. Data analysis ⁸¹	44
a) Recording of the ^1H nuclear spin diffusion curve.....	44
b) Comparison of the longitudinal relaxation with the diffusion times	45
c) Information obtained from the ^1H nuclear spin diffusion curve	45
d) Determination of the plateau value	46
e) Quantification of the domain size	46
f) Measurement of the T_2 relaxation time ⁶⁴	47
I. Nuclear Overhauser effect (NOE)⁹⁴	48
1. The Overhauser effect	48
2. Cross-relaxation mechanism	48
3. Different kinds of NOE experiments.....	50
a) Steady-state NOE.....	50
b) Transient one-dimensional NOE.....	51
c) Two-dimensional NOE spectroscopy (NOESY)	51
4. Equations describing the cross-relaxation between two groups of equivalent spins in NOESY.....	53
a) General case	53
b) Case of an homonuclear spin pair in the slow motion limit ¹¹²	54
c) Case of two groups of equivalent homonuclear spins A_nB_n in the slow motion limit ¹¹²	55
d) Cross-relaxation in other spin systems	55
III. Conclusion and strategy.....	56
A. Branching.....	56
B. Chain dynamics.....	57
C. Nanostructuring	57

Part 1: Literature survey and motivation

The goal of the work presented here is to investigate the microscopic properties of acrylic pressure sensitive adhesives (PSAs). These materials are of industrial importance and are currently characterized mainly according to their macroscopic properties, e.g. adhesive properties. Little is known about the exact relation between their microscopic and macroscopic properties, although it is empirically known that the former play a major role in the latter. Therefore it was decided to characterize the microstructure of the industrial samples using solid-state NMR, in order to progress towards a better understanding of the adhesion mechanism of these samples.

In the paragraph I, the pressure sensitive adhesives (PSAs) will be defined and described. Their possible compositions will be detailed. Their adhesive properties will be exposed, together with the chemical and physical factors influencing them. In the paragraph II, the solid-state nuclear magnetic resonance (NMR) spectroscopy will be introduced. Several techniques will be described. In paragraph III, conclusions will be drawn concerning the relevant solid-state NMR techniques chosen to investigate relevant microscopic properties of the PSA samples.

I. Pressure sensitive adhesive materials⁷⁻¹⁰

The literature review on pressure sensitive adhesives (PSAs) presented here is not exhaustive: it is meant as a comprehensive introduction.

Historically, the first industrially produced PSAs were adhesive tapes and plasters for medical applications, derived from natural rubber and blended with resins.¹¹ One of the first patents on a PSA is credited to Shecut and Day in 1845.⁸ Styrene-butadiene rubber (SBR) were introduced during World War II¹²⁻¹⁵ and poly(styrene-isoprene-styrene) triblock copolymers (SIS) in the 1960s.¹⁶ The suitability of polyacrylates for PSAs was discovered in 1929,¹²⁻¹⁵ but they began to be used as such only shortly after World War II,⁷ attaining their current industrial importance in the 1960s.¹⁷ The PSA sector is among the fastest growing in the adhesive market, making the search for new pressure sensitive products and applications highly competitive.¹⁰ High throughput development of PSAs has recently been reported.¹⁸

A. Definition and applications

An “adhesive” is defined as a “non-metallic material that is capable of joining bodies together by surface adhesion and internal strength (adhesion and cohesion) without the

Part 1, I Pressure sensitive adhesives (PSA's)

structure of the bodies undergoing significant changes".¹⁹ The term "*pressure-sensitive adhesives*" designates "*adhesives which in dry form are aggressively and permanently tacky at room temperature and firmly adhere to a variety of dissimilar surfaces upon mere contact without the need of more than finger or hand pressure.[...] They have sufficiently cohesive holding and elastic nature so that, despite their aggressive tackiness, they can be handled with the fingers and removed from smooth surfaces without leaving a residue*".²⁰ Their primary advantages are convenience and fast application, their main deficiency the weakness of the formed physical bond.⁸

Pressure sensitive products are used mainly for adhesive tapes, labels, and films, but also for medical products, protective masking sheets and specialty products.^{7,10} There are three categories of applications for PSAs.²¹ The removable PSAs must exhibit a high compliance and a totally adhesive rupture, but need only low adhesion. The general-purpose, semi-permanent PSAs need a medium compliance, a relatively good adhesion but no long-term aging resistance. The permanent, semi-structural PSAs require very high adhesion and creep resistance, and a good aging resistance.

PSAs consist of an adhesive which is coated with a flexible *backing*, also named *carrier* (s. Figure 1- I-1), e.g. paper or polypropylene. The backing must often exhibit different adhesion properties to the adhesive on the two sides, so that e.g. a tape roll can be unwound; therefore, one side of the backing is usually coated with either a *release coating* (for an easier debonding of the adhesive) or a *primer* (for a stronger adhesion of the adhesive). The surface on which the pressure sensitive product will be applied is named *adherend* or *substrate*. The function of the adhesive is to keep the backing in contact with the substrate.

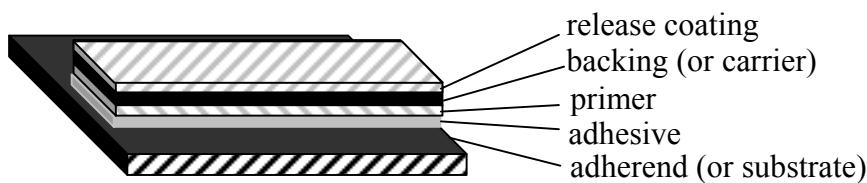


*Figure 1- I-1:
Components of a
pressure sensitive
product and
adherend.*

B. Composition

In addition to the raw material (s. paragraph 3) and the possible solvent (s. paragraph 1), the industrial PSAs may contain a tackifier (s. paragraph 2) and other additives.¹⁰ These additives are peel modifiers, wetting agents, rheology modifiers, crosslinking agents, antioxidants, plasticizers, etc. They are used to induce or enhance a particular property.

1. Possible solvent

The advantages and drawbacks of solvent-based, water-based and hot-melts PSAs are summarized in Table 1- I-1.²² From the 1980's on, the environmental constraints have decreased the consumptions of solvent-based PSAs.¹⁶

	<i>Solvent-based PSAs</i>	<i>Water-based PSAs</i>	<i>Hot-melt PSAs*</i>
<i>Advantages</i>	quick drying form homogeneous films good adhesion to non polar substrate good key on certain plastics	easy cleaning good adhesion to polar substrates good heat and aging resistance environment friendly high solid content	100 % active, environment friendly very fast setting
<i>Drawbacks</i>	flammability toxicity relatively low solid content difficult cleaning	slow drying require heat to dry poor adhesion on non polar substrates presence of surfactants	high equipment costs require heat thermal degradation difficult to clean can melt the substrate

*: used as such, applied at high temperature between two substrates, the stuck device is then cooled down
Table 1- I-1: Advantages and drawbacks of solvent-based, water-based and hot-melt PSAs.²²

2. Tackifiers

Tackifiers are low molar mass materials (usually 500 to 1500 g·mol⁻¹), which induce tack or stickiness. They are mainly based on petroleum streams or on rosin. All rubber based adhesives require tackifiers as a main component, while acrylic PSAs require tackifiers in smaller amounts.

Adding a tackifier decreases the resistance to deformation at low rates, while it increases it at high rates.¹⁹ It also increases the T_g of the mixture (in contrast to a plasticizer), owing to a loosened entanglement network and decreased segmental friction.^{2,10}

3. Used raw materials

A high molar mass, low crystallinity, low T_g polymer is preferred. The compounds of industrial importance are described in Table 1- I-2. The acrylates are additionally described in more detail in paragraph 4. Recently, a polymer which monomer is obtained from a renewable source has been reported as suitable for PSA.²³

<i>Raw material</i>	<i>Main applications</i>	<i>Other characteristics</i>
Natural rubber	general-purpose tapes, diaper tapes, masking tapes	high quality PSA requires tackifier, fillers, antioxidants, plasticizers used in solution (e.g. hexane, toluene)
Polyisobutylene, Butyl rubber*	removable labels (low peel adhesion needed)	used additives: tackifiers, fillers, low molar mass polyisobutylene, amorphous polypropylene
Poly(vinyl alkyl ethers)	tapes, labels	mainly poly(iso-butyl vinyl ether)
Reclaim rubber**	pipe-wrap tape, duct tape, friction tapes	used as a blend of low and high molar mass polymers

Poly(vinyl acetate) copolymers	permanent labels	no tackifier required
Silicone polymers	transdermal tapes for drug delivery, masking tapes for printed circuits	large working temperature range (-100 to 250 °C) linear poly(dimethyl siloxane), or linear copolymers of dimethyl and diphenyl siloxane requires a tackifier
Styrene-isoprene-styrene (SIS) triblock copolymers	hot-melt PSAs, general-purpose tapes, duct tapes, permanent labels	short S blocks and long I block the aggregated polystyrene domains behave like thermolabile crosslinks require tackifiers for both blocks
Styrene-butadiene random copolymers	mainly labels, also medical applications, freezer labels, pipe wrap, electrical tape	exhibit a broader molar mass distribution than the typical styrene-butadiene rubber (SBR), and often a fraction of gel require a tackifier
Acrylic copolymers	tapes: transparent, strapping, transfer, medical, metal-foil	no tackifier required suitable for medical applications s. next paragraph for more details

*: copolymer of isobutylene and a small quantity of isoprene, **: obtained from the digestion of used tires

Table 1- I-2: Raw materials and characteristics of PSAs of industrial importance.

4. Acrylic pressure sensitive adhesives

This paragraph is focused on the acrylic PSAs, the type of PSA samples investigated in this work. Acrylic polymers have been known for a long time, but their utilization as PSAs is relatively recent.²⁴ Acrylic acid was first synthesized in 1843; by 1901 research was carried out on acrylic esters. Poly(methyl methacrylate) was first produced in 1927 by Roehm and Haas, and acrylic dispersions by the BASF AG in 1929. Roehm and Haas patented in 1929 the suitability of polyacrylates for PSAs,¹²⁻¹⁵ but polyacrylates found extensive use in PSAs only in the 1950s. Their applications span over a multitude of tapes, especially transparent, strapping, transfer, medical and metal-foil tapes. Acrylic PSAs are typically water- or solvent-based, but hot-melt acrylic PSAs have also been reported.

a) Composition

Acrylics can be used as single-component adhesive, which means that these acrylate copolymers do not require tackification: this is an advantage, because low molar mass tackifiers can migrate to the surface and thus affect the bond to the substrate.²⁴ Since acrylic PSAs can be prepared free from tackifiers and antioxidants, they are less irritating to skin (provided there is no residual monomer) and therefore preferred for medical applications. Acrylates are superior to the corresponding methacrylates as expected from the large difference in glass transition temperature (s. Figure 2- III-2 in Part 2, III.A).²⁴ For acrylates with alkyl side chains shorter than octyl, the T_g is reduced with increasing length of the alkyl side group (s. Figure 2- III-2 in Part 2, III.A), which leads to an increase in tack strength and

lowering of peel strength and resistance to shear.²⁴ The dominant raw materials are n-butyl acrylate (BA) and 2-ethyl-hexyl acrylate (2EHA) because they lead to a high tackiness;¹⁹ an acrylic PSA is a copolymer of one of them (70-97 %) with a polar monomer (2-10 %, e.g., acrylic acid, AA) and often other monomers (10-25 %, e.g., ethyl acrylate). The formulation depends on the application; the desired T_g for PSA applications at room temperature is between $-50\text{ }^\circ\text{C}$ and $-25\text{ }^\circ\text{C}$, because the working temperature must be in the liquid-rubbery region of the polymer.²⁴ Indeed, the tack of an acrylic polymer shows a maximum with increasing temperature, generally about 50 to 70 $^\circ\text{C}$ above the T_g .^{21,24} n-Butyl, 2-ethyl-hexyl and iso-octyl acrylates give an homopolymer with a T_g of $-50\text{ }^\circ\text{C}$ or less. They are copolymerized with an other monomer (e.g. methyl acrylate) to raise the T_g : the glass transition temperature is a useful indicator for the choice of comonomers, but not a sufficient criterion for fine adjustment of adhesive properties.²⁴ The modifying monomers include methyl and ethyl acrylate, vinyl acetate and methyl methacrylate, among many others. The polar monomer is mainly acrylic acid, but can also be methacrylic acid, acrylamide, acrylonitrile, dimethyl-amino-ethyl methacrylate, hydroxy-ethyl acrylate or methacrylate. The effect of copolymerization is discussed in paragraph D.4.

b) Production process

Acrylic PSAs are produced by solution or more frequently emulsion polymerization.²⁴ Solution polymers give homogeneous films (due to the absence of surfactants, wetting agents and defoamer), they have better resistance to water, solvent and plasticizer, as well as better aging properties and higher shear resistance combined with good tack and peel; on the other hand, they are more expensive than emulsion polymers and exhibit safety problems due to the solvent. As for acrylic dispersions, they are environmentally safe, easy to handle, economical and offer good adhesive properties for most PSA applications. Therefore, emulsion polymers are predominantly used except for the applications where they cannot replace solution polymers. The emulsions are available at 50-55 % solid content. The commercial latices are essentially pigment free.²⁴ Tobing and al.²⁵ compared emulsion and solution copolymer of 2EHA or BA with AA: the solution PSA had a higher shear holding power due to the continuous network (vs. discrete microgels), while the peel and tack are mainly affected by the sol-to-gel ratio regardless of the solution or emulsion character of the PSA. They showed²⁶ that the thermal crosslinking of the emulsion PSA after filmification increased its shear holding power because of the interlinking of the microgels.

c) Adhesive properties

Due to their strong dipolar moment (compared to non-polar polymers), the acrylic PSAs adhere generally more strongly to polar surfaces than rubber-based PSAs, but less well to non-polar surfaces. Owing to their saturated backbone, they are more stable to light and heat than rubber-based adhesives, and retain their properties for years; however, they have lower tack and peel strength. Tackifiers are sometimes added to increase peel adhesion and tack. Acrylic PSAs build up adhesion with time when aging above T_g .

The molar mass of emulsion acrylics has no effect on latex viscosity and may be $10^6 \text{ g}\cdot\text{mol}^{-1}$ and higher. Generally high molar masses result in low tack, molar masses are thus sometimes limited by the introduction of a chain-transfer agent in the polymerization. However, a lower molar mass implies a too low cohesive strength for many applications and, therefore, crosslinking is required. The cohesive strength (s. paragraph C.3) is sometimes improved without crosslinking by grafting pendent high T_g blocks, e.g. polystyrene or poly(methyl methacrylate), to an acrylic polymer;²⁷ then, the same domain structure as with the triblocks SIS described above is obtained, since the polymers are usually not compatible.

C. Properties and testing

The properties required from a pressure sensitive adhesive (PSA) can be divided into three classes along with their specific test methods:²¹

- the adhesive strength (debonding process), tested by peel tests,
- the conformability (bonding process), tested by tack tests,
- the cohesive strength of the adhesive, tested by a shear experiment.

Unlike structural adhesives which change from a liquid to a solid, PSAs do not undergo a phase change from the initial stage of adhesion upon wetting the surface to the final rupture of the adhesive bond.⁷ A balance of cohesive strength and viscoelastic properties is required, allowing the PSA to spread over a surface with application of minimum pressure and be removable from that surface without leaving an adhesive residue.⁷

The most important properties of PSAs and their testing methods will be presented below. Recommended test procedures have been developed and published in the USA by the Pressure Sensitive Tape Council (PSTC)²⁸ and the American Society for Testing and Materials (ASTM)²⁹, in Europe by FINAT³⁰ and the Association des Fabricants Européens de Rubans Auto-Adhésifs (AFERA)³¹. The PSAs are not only characterized by their adhesive properties: resistance to heat, aging and plasticizers are also of importance.¹⁹

The adhesive properties (tack and peel) will be presented first, followed by the cohesive strength.

1. *Tack and bonding*

a) Definition and requirements for tack

Tack is defined as “the property of a material which enables it to form a physical bond of measurable strength immediately upon contact with another surface” (ASTM D 1878-61T).⁷ The wet tack is the ability of an adhesive to form a bond while the adhesive is still wet, the green tack the ability of certain polymers to bond to themselves for several hours after drying, and the pressure sensitive tack, of specific interest within this report, the ability of a dried film to bond tenaciously to most surfaces under light pressure (a few kPa).²² The concept of tack is equivalent to stickiness in every day language, and is often evaluated by pressing a finger into and withdrawing it from the adhesive. Thus, it involves a bonding and a debonding step; poor tack can result from either deficiencies in the initial bonding or low holding power after the bond has been formed. In the absence of the precise definition of applied pressure and separation force (and time), tack remains a qualitative property. Tack can be quantified either as the peak force necessary to remove the probe from the adhesive surface, or as the related tack energy (the area under the tack force/time plot).²

The requirement that the adherend surface is wetted by the adhesive implies that the surface energies (or surface tensions) of adhesive and adherend are favorable for a spreading of the adhesive. Tack values obtained for various adherend materials with the same adhesive increase with the surface energies of the adherends, reaching a maximum when it approaches the surface energy of the PSA.³² The second requirement for good bonding is low viscosity. In general, PSAs have a viscosity in the range of 10^5 - 10^7 Pa·s at ambient temperatures. It is thus desirable that the PSAs are used well above their T_g and have a broad molar mass distribution (or that a portion of the chains be of low molar mass). The third requirement is a short relaxation time of elastic deformation.

b) Tests for tack measurement

Toyama et al.² distinguish three sets of tack values: (a) primary tack determined by rolling ball test and probe-tack at reduced time, (b) secondary tack from probe tack testing at proper contact time, and (c) ultimate tack determined from peel-force measurements after prolonged standing. In addition to these tests, the loop tack test allows the “immediate” tack to be measured.

In the *loop tack test*, a loop of substrate is coated with adhesive on its external side, applied vertically on an adherend without pressure and immediately withdrawn (s. Figure 1-I-2).

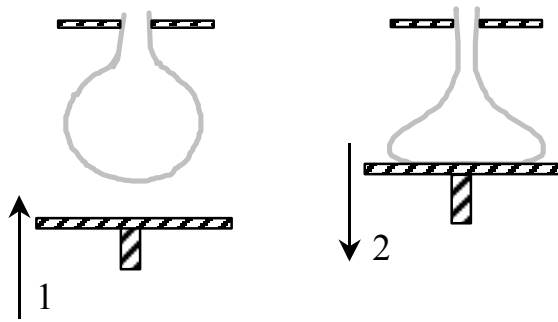


Figure 1- I-2: Geometry and evolution of a loop tack test.

In the *rolling ball tack test*, a ball is rolled down an inclined plane or grooved ramp connected to a tape in a horizontal position (s. Figure 1- I-3). The tack value is the distance that the ball rolls before stopping on the tape; low numbers imply high tack. This test is mainly used in industry. It gives a good indication of tack with elastomer adhesives but is unreliable with water-based systems.²² Furthermore, it differentiates adhesives which give same results with the loop tack test, but do not have the same “stickiness” when tested by imprinting of a finger.

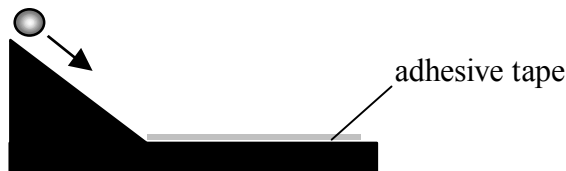


Figure 1- I-3: Geometry of a rolling ball tack test.

In the *probe-tack test*, the bonding strength is measured between the flat end of a cylindrical probe, brought into contact with adhesive on a backing for a measured dwell time and then withdrawn at a specific rate (s. Figure 1- I-4). This test is mainly used in research. A cylindrical probe with an hemispherical head is sometimes used in industry.³³

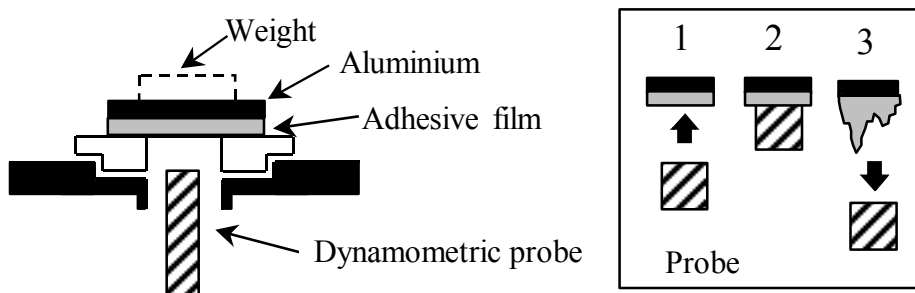


Figure 1- I-4: Geometry and evolution of a probe-tack test.

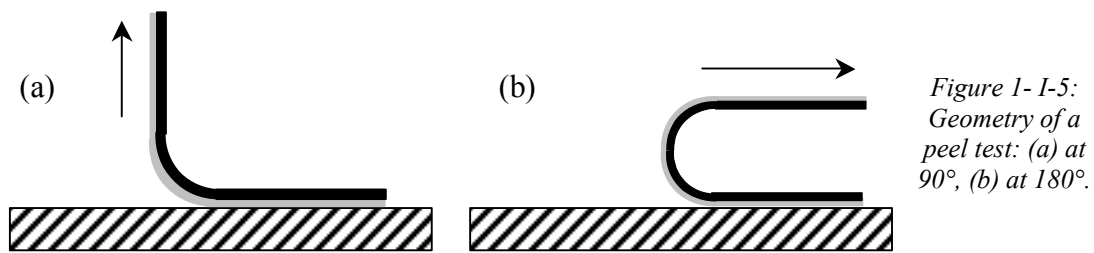
c) Case of acrylic adhesives

Poly(methyl acrylate) ($T_g = 22 \text{ }^\circ\text{C}$) is not tacky, while poly(ethyl acrylate) ($T_g = -8 \text{ }^\circ\text{C}$) is slightly tacky, and poly(n-butyl acrylate) ($T_g = -43 \text{ }^\circ\text{C}$) as well as poly(2-ethylhexyl acrylate) ($T_g = -58 \text{ }^\circ\text{C}$) are extremely tacky at room temperature.¹

2. Peel adhesion and debonding^{21,34}

Adhesion is the ability to remain permanently attached to surfaces in the absence of excessive forces; it depends on both tack and cohesion properties of the PSA. In the *peel-*

adhesion test, a tape is applied to a hard surface under specified conditions and removed at a specified rate to a specified angle with the substrate, usually 90 or 180° (s. Figure 1- I-5).



The adhesion values in a peel test depend on the width and thickness of the adhesive, the thickness and modulus of the backing, as well as the peel angle, peel rate and the application conditions (time, temperature, pressure, roughness of the surface). Assuming constant backing and physical dimensions for the test, however, the forces measured are related to the viscoelastic behavior of the adhesive, as well as the interfacial forces between adhesive and substrate (briefly: to adhesive and cohesive properties of the PSA). Once failure has started, the peel force generally fluctuates about an average value as peeling proceeds. Failure can occur in the adhesive layer or in the substrate (cohesive failure), as well as at either of the two interfaces (adhesive or interfacial failure).² The cohesive failure leaves a residue of adhesive on the substrate (or more rarely of substrate on the adhesive layer), while the adhesive failure leaves no residue. The combination of both is a phenomenon known as slip-stick.² The mode of failure is related to the relaxation properties of the material: the cohesive mode corresponds to the terminal zone of relaxation spectra (lowest frequencies), the adhesive mode to the rubbery zone, and the slip-stick to the glass transition zone.¹⁰

The Figure 1- I-6 describes the peel force as a function of the peel rate (or temperature). At low peel rates (or high temperatures), the peel strength increases with the peel rate, and cohesive failure is observed. Indeed, the effective modulus is low at low deformation rate and an increase in peel rate causes the adhesive to behave as if it were stiffer; it can thus support higher loads before parting from the test surface. At higher peel rates, the peel strength decreases when the peel rate increases, and then becomes constant. In this high peel region, the cohesive strength of the polymer exceeds the adhesive forces and the material separates cleanly from the substrate. At intermediate peel rates, a “slip-stick” failure can be observed.³⁵

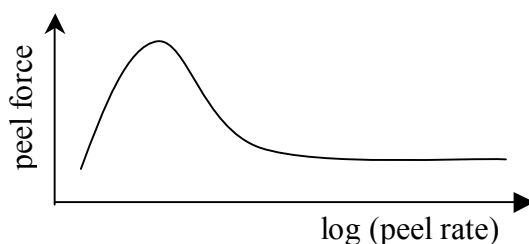


Figure 1- I-6: Peel force as a function of the peel rate.

3. Cohesive strength

Cohesive strength, or resistance to shear, is also called holding power. This is the internal strength of an adhesive material that resists elongational flow or creep under stress in the plane of the surface. To eliminate or minimize creep, the adhesive must be of high molar mass or chemically crosslinked. A further possibility is the use of triblock copolymers to obtain physical crosslinks. In practice the polymer may contain up to 30-50 % gel. It has been experimentally observed that the holding power is inversely related to the adhesive thickness.

The holding power is characterized in the *shear test*, in which a defined area is vertically mounted to a steel bar and a weight is hanged on it (s. Figure 1- I-7). The duration for which the tape can support the load, without failing or slipping a specified distance, is determined. The time to dwell before the load is applied influences the results: acrylics in particular may require longer times to fall or slip if the adhesive is allowed 24 hours to effect a better bond before the weights are attached.

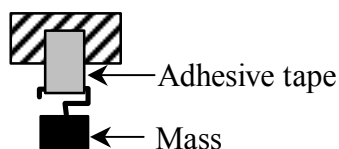


Figure 1- I-7: Geometry of the tests of the resistance to shear and of the determination of the SAFT.

The *Shear Adhesion Failure Temperature* (SAFT) can also be measured: the preceding experimental setup is put into an oven, the temperature is increased and the temperature at which the adhesive in shear exhibit a significant viscous flow and can no longer support an applied stress is recorded.

The shear resistance can be tested alternatively in dynamic shear, where a constant shear rate is imposed and the force is monitored.²¹

D. Influence of chemical and physical factors on the adhesive properties²

1. Glass transition temperature

This was already discussed in paragraph B.4.a.

2. Molar mass

A low molar mass (MM) polymer sample flows rapidly into close contact with adherend surface, but exhibit a low cohesive strength. With increasing MM, peel and tack of PSAs are expected to pass through a maximum (at different MM), while shear resistance is predicted to rise to a very high MM and then drop dramatically (s. Figure 1- I-8). It is generally considered that a polymer must have a degree of polymerization of at last 300 before its mechanical properties are developed on a useful level due to entanglement; but the

MM should be much higher to develop a sufficient resistance to creep, unless the level of non covalent bonding is high.²⁴

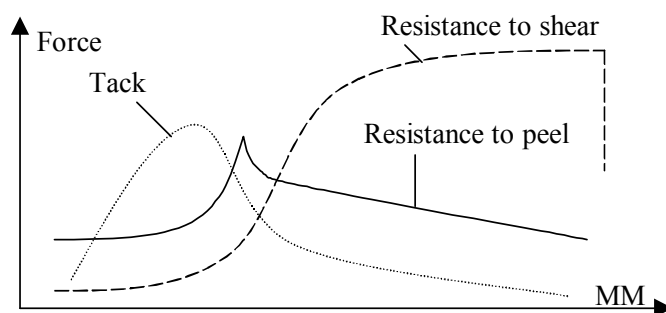


Figure 1- I-8:
Expected influence
of molar mass MM
on adhesive
properties of PSAs.²

In a polymer exhibiting a broad MM distribution, high MM fraction should determine creep resistance, while peel and tack should be dictated by the low MM fraction. However, a polymer exhibiting a broad MM distribution may have a lower cohesive strength than one with a narrow distribution and lower MM. Common acrylic PSAs exhibit a quite broad MM distribution, containing a considerable amount of the low MM fraction; acrylic emulsion polymers contain a considerable gel fraction, so that the MM distribution can only be obtained from the soluble fraction of the films.²⁴

Yang³⁶ developed an emulsion polymerization method with a temperature gradient to obtain highly non-uniform acrylic copolymer PSAs. He found that the polydispersity index should be higher than 10 to ensure a good balance between adhesion and cohesion.

3. Entanglement network

A high average molar mass between entanglements, M_e , increases the performance of the adhesive in two ways through its influence on the plateau modulus.²¹ First, it favors the bond formation at very short contact time. Second, it favors the formation of fibrils during the debonding process (s. paragraph E), thereby increasing the adhesion energy.

Zosel³⁷ studied the debonding of various PSAs (PIB and acrylics) in the probe tack test. He showed that only the PSAs which have a M_e higher than 10^4 to $1.5 \cdot 10^4$ g·mol⁻¹ are able to form fibrils and therefore have a high adhesion energy. This limit corresponds to the well-known Dahlquist's criterion:³⁸ PSAs having an elastic modulus exceeding 10^5 Pa exhibit a poor tack (some exceptions are known³⁹).

Tobing et al.¹⁶ showed that adding a tackifier to an acrylic emulsion PSA can lead to a strong decrease of the shear holding power, while it leads to only a small increase in loop tack and peel strength. Indeed, the entanglement of uncrosslinked chains with the micro-networks present in the particles is impossible due to the increase of M_e , and the tackifier can not tackify the micro-networks.

4. *Introduction of functional groups*

Generally, weak non covalent bonds are formed between a PSA and a substrate, with the following prevailing order: hydrogen bonding, interaction between two permanent dipoles, induction forces between one dipole and a polarisable group, London forces between virtual dipoles. Adhesion and cohesion may be improved by incorporation of judicious functional groups on an adhesive polymer chain with careful consideration of the substrate composition. This can be done by copolymerization.

Acrylic and methacrylic acids are often copolymerized in acrylate adhesive polymers. Dhal et al.⁴⁰ copolymerized n-butyl acrylate with increasing small quantities of acrylic acid. This resulted in an increase in resistance to shear, peel and tack, which is believed to originate in the molecular interactions of –COOH groups with each other. Chan et al.³⁵ copolymerized ethyl acrylate (EA) with acrylic or methacrylic acid. This increased the resistance to shear and the peel strength with respect to pure EA. Furthermore, the tack of samples with increasing acid content presents a maximum for 3 to 4 % monomeric units. At low acid levels, adhesion was improved by better interfacial interactions with the substrate, while at higher acid concentration, the tack is believed to decrease due to hardening of the polymer.

Chan et al.³⁵ copolymerized EA with other polar comonomers: hydroxyethyl acrylate and acrylonitrile. It had similar effects as the introduction of (meth)acrylic acid, but less intense.

They also copolymerized 2EHA with various amounts of non polar comonomers: ethyl acrylate, methyl acrylate, ethyl methacrylate. For increasing 2EHA contents, the shear strength decreases, while the peel strength increases for adhesives fractures and then decreases for cohesive fractures. The tack increases for increasing 2EHA contents even when the fracture becomes cohesive (except for MA, for which a maximum is observed at 60 % 2EHA). These three properties can be reduced to a single master curve using the Williams-Landel-Ferry (WLF) equation for polymers of similar molar mass, showing that the properties are governed by the T_g value. Nevertheless, a change in the molar mass has also strong effects.

5. *Crosslinking*

Generally, covalent crosslinking increases the elastic character of the response to shear and tension at the expense of the viscous one,²⁴ and therefore lowers the ability of the adhesive to establish surface contact.² Hence, only low amounts of crosslinker are required to increase creep and shear resistance, while peel strength and tack are usually adversely affected at all levels of crosslinking (a higher crosslinking degree may yield to a non-tacky

product).²⁴ Crosslinked adhesives may not exhibit a noticeable transition at all, but fail adhesively under all peel rate and temperature conditions.²⁴ The crosslinking should preferably take place through long and flexible chains, in order to retain the flexibility and the high stress relaxation rate, and therefore minimize the effect in adhesion properties without changing the shear and creep improvement.²⁴

Zosel⁴¹ showed that for poly(dimethyl siloxane) (PDMS) samples the tack and peel strength have a pronounced maximum in the range just above the gel point. Plessis et al.^{42,43} studied various poly(n-butyl acrylate), PBA, latices. They showed that crosslinking (less than 50 wt% of gel) increases both the resistance to shear and the peel strength, while an increase in the molar mass increases the resistance to shear and decreases the peel strength. All latices exhibited a very good tack.

For PBA adhesives, an increasing copolymerized styrene amount leads to a decrease in branching level and fraction of gel, while the tack properties are unchanged, the resistance to shear is improved and the peel strength decreased.⁴³

In the case of films cast from dispersions, if the crosslinking is only performed in the particles, there can be little or no increase of shear resistance because failure can happen in the weak phase between the particles. If the phase between the particles is crosslinked too heavily, tack can be reduced greatly because the mechanical properties are dominated by a rigid network structure.²⁴

Secondary bonding (hydrogen bonding, dipole-dipole or dipole-induced dipole interaction) can have the same effect as covalent bonding on the mechanical properties. But such polymers can be soluble, and the strength of such bonds decreases rapidly with increasing temperature because the bond strength decreases with increasing distance between atoms.²⁴ The hydrogen bonding between two carboxyl groups is very important for acrylic adhesives, the length of this rather strong bond represented in Figure 1- I-9 ranges from 2.6 to 3.0 Å for the O-O distance.²⁴

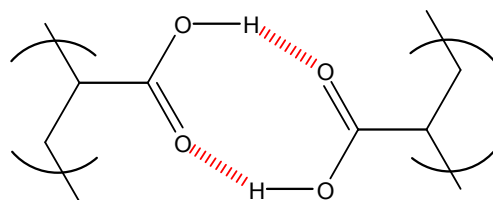


Figure 1- I-9: Hydrogen bond between two carboxyl groups of acrylic acid units in acrylic polymers.

Physical crosslinking in the form of crystallinity (in semi-crystalline polymers) is used in some PSAs instead of chemical crosslinking; but it is not used for acrylics.²

6. Viscoelastic properties

The concepts of viscoelasticity of polymers used in this chapter are presented in appendix (s. Part 7, III.A).

PSAs have the ability to distribute stresses over large volumes of material, thereby avoiding the sharp stress concentrations responsible for the failure of structural glassy adhesives.⁴⁴ This specific ability is directly related to their low storage modulus G' (typically in the 10^4 to 10^6 Pa range) and relatively high viscoelastic character ($\tan\delta$ close to 1).⁴⁴ The wider the temperature range over which G' is in this range, the more effective the PSA.⁷ If G' is too high, the adhesive will lose its tack, and if G' is too low the shear resistance of the material will be reduced.²¹ Similarly, the loss modulus G'' is taken as an indication of the amount of viscoelastic losses during debonding, and therefore needs to be as high as possible for good adhesion.²¹ Nevertheless G' and G'' can generally not be varied independently over a wide range, and a high G'' implies a high G' and a loss of tack. Chang⁴⁵ defined the concept of viscoelastic windows for PSAs: he drew a two-dimensional map with storage and loss moduli G' and G'' as axes, divided in different regions corresponding to different characteristics of the PSA (non-PSA, high shear PSA, cold-temperature PSA, removable PSA, general purpose PSA).

The viscoelastic basis of peel adhesion is demonstrated by the construction of master curves, relating bond strength (i.e. peel energy) to temperature and peel rate for several chemically different PSAs.² Furthermore, different models of the dependence of the peel force on viscoelastic properties have been developed.² It should be noted that the deformation involved in the debonding of an adhesive tape is in the non-linear regime, where the mechanical history of the material should affect its behavior. This could seem to be in contradiction with the obtainment of a WLF master curve.²¹

E. Mechanism of debonding

1. Early studies

The early studies on pressure sensitive properties of polymers focused on the mechanical aspects of peel tests of soft elastomers from rigid substrates or on the effect of surface properties. At that stage, the detachment of the PSA from the surface was implicitly assumed to occur by the propagation of a single interfacial crack.⁴⁴ In 1960, Kaelble⁴⁶ detected the formation of fibrils of adhesive linking the adhesive layer to the substrate during the peel test of a PSA.

2. *Energy criterion for adhesive strength in peel test*

In 1971, Gent, Kinloch et al.⁴⁷⁻⁴⁹ proposed an energy criterion for the adhesive failure of PSAs: a characteristic failure energy per unit area of new surface can be regarded as a characteristic measure of the strength of the adhesive bond, since it is independent of the geometry of the test. They showed that this adhesive failure energy W is the sum of an intrinsic adhesive failure energy W_0 (depending only of the substrate surface and on the adhesive) and of the energy Ψ dissipated viscoelastically within the adhesive (depending on W_0 , on the rate and temperature of debonding) (s. Equation 1- I-1). W can also be expressed as the product of W_0 and a function Φ of rate and temperature of debonding:

$$W = W_0 + \Psi(W_0, T, \nu) = W_0 \cdot (1 + \Phi(T, \nu)) \quad \text{Equation 1- I-1}$$

In the middle of the 1980's, Good⁵⁰ proposed a model for the debonding of adhesives forming fibrils, for both PSAs and "brittle" adhesives. In the case of the PSAs involving fibrillation, he developed mathematical expressions⁵¹ for the energies necessary for elongating the fibrils and for detaching the fibril bases from the substrate. They allow to predict if the rupture will be cohesive or adhesive and if the debonding energy will be high or low (but without quantitative prediction of this energy).

The experimental curves of adhesion energy as a function of temperature and peel-rate obey the WLF time-temperature superposition quite well, indicating that the viscoelastic properties of the PSA govern the debonding process, even in regimes where fracture occurs by extensive fibrillation.²¹

Since the mechanisms of debonding in peel and probe tack tests are similar (fibrillation or propagation of an interfacial crack), the results obtained using one technique is also relevant for the other technique.³⁸

3. *Zosel's work on fibrillar debonding in probe tack test*

In the late 1980's, Zosel^{52,53} developed an instrument measuring the adhesive failure energy in dependence of contact time, contact pressure, rate of separation, temperature, and allowing also to study the stress-strain behavior during bond separation. It is similar to the probe-tack geometry presented in Figure 1- I-4. The adhesive failure energy is measured as the area under the stress-strain curve: at very short contact times, it is the tack of the adhesive, at long contact times its maximum energy of separation. This apparatus allows to study the influence of the molecular structure of a polymer on its adhesive properties. By coupling his instrument with high speed photography perpendicular to the film plane, Zosel^{41,54} showed unambiguously that high strain at break and high adhesive failure energy can be obtained only if the polymer is able to form (and deform) a macroscopic fibrillar structure. This case is

illustrated on Figure 1- I-10: when the probe moves away from the adhesive layer, the adhesive material is split into separate filaments or fibrils which are anchored on both the substrate and the probe surface (a); these fibrils are first increasingly stretched (b), causing the storage and dissipation of energy; the fibrils then begin to separate from the probe surface by purely interfacial failure (c), this failure starts at the rim of the probe where the tensile stress has a maximum; after complete debonding the deformed material recovers (d) and finally restores the original film surface. A photograph representative of step (c) is shown on (e).⁵⁴

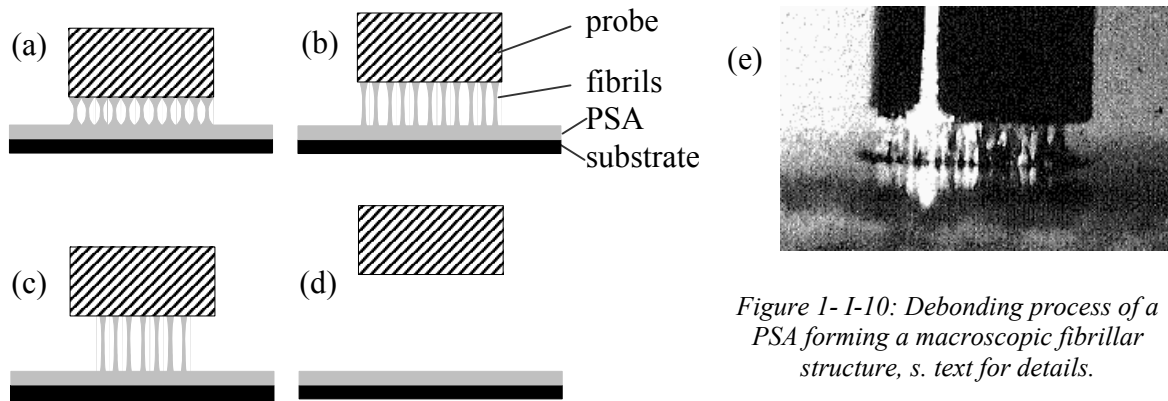


Figure 1- I-10: Debonding process of a PSA forming a macroscopic fibrillar structure, s. text for details.

The stress-strain curves characteristic of PSA debonding^{41,54} are shown on Figure 1- I-11. In the “brittle” case (a), the PSA has a low adhesive failure energy (area below the stress-strain curve). In the “fibrillar” case (b), the PSA forms and deforms fibrils, and the adhesive failure energy is high. The kind of plateau extending to the right corresponds to the fibrils extension.

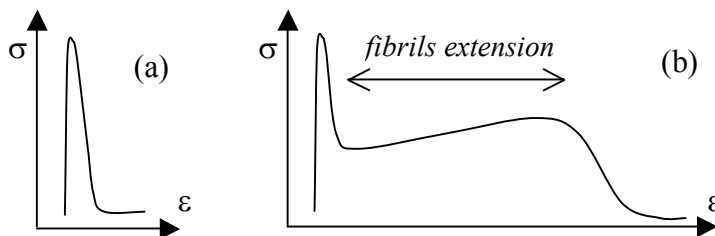


Figure 1- I-11: Elongation stress-strain curves of a PSA during debonding; (a) “brittle” case, (b) “fibrillar” case.

The characteristic size of the PSA fibrils is typically three to four orders of magnitude larger than the size of craze fibrils. Their morphology depends on the adhesive and the experimental geometry, but also on the substrate (in particular its surface roughness).²¹

4. Creton's work on fibril formation

Creton et al.³³ developed an instrument for the probe tack test allowing the simultaneous record of nominal stress and strain curves, as well as pictures of the adhesive film from underneath a transparent substrate. They correlated the debonding sub-processes with the corresponding parts of the stress-strain curve (s. Figure 1- I-11): first formation of cavities randomly at (or near) the probe/film interface during the initial stress increase, then lateral growth of these cavities during the first stress decrease, then elongation of fibrils

during the pseudo-plateau of stress, and finally rupture of the fibrils during the stress decrease.

Lakrouf et al.⁵⁵ defined a Deborah number for this experiment, De , as the product of the strain rate and the relevant relaxation time for the flow of the polymer. This number allows to predict the growth type of the cavities: for $10 < De < 1000$, lateral growth is limited and extensional growth dominates, it is the useful regime for the use as a PSA. Alternatively, Creton et al.³⁸ defined a critical parameter G_0/E , as the ratio of the energies dissipated at the surface and elastically in the bulk: when G_0/E increases, a transition is observed from (a) interfacial crack propagation to (b) cavitation within the adhesive layer followed by rapid detachment of cell walls, then to (c) cavitation followed by extension of the adhesive fibrils to large strains.

In PSAs so far there is little experimental evidence concerning the mechanism of fibril growth. Creton²¹ proposes a picture for macroscopic fibril growth where two processes are competing: fibril drawing from the bulk to a constant extension ratio at the fibril/bulk interface, and fibril creep at a constant stress once the fibril is formed. All experimental observations are consistent with the hypothesis that fibrils grow mainly by chain disentanglement, which can limit the use of very high molar masses or highly branched polymers in an attempt to increase the creep resistance.

Zosel⁵⁶ had studied the increase of the bonding energy for increasing contact force and contact time for smooth and rough probes. His experimental results are in accordance with the theoretical model developed by Creton et al.⁵⁷ for contact formation and true contact area on a rough surface. He proved that the influence of the surface roughness becomes significant at low contact forces and for polymers with comparably high moduli. Chiche et al.⁵⁸ showed that a decreasing probe surface roughness leads to a delay in the formation of the cavities and an acceleration of their lateral expansion.

The cavitation and the fibril extension were also studied theoretically. Gay et al. developed models for predicting the number of cavities which will appear during the probe tack⁵⁹ and the shape of the stress-strain curve⁶⁰. Creton et al. developed a micromechanical model to account for debonding mechanisms of soft adhesives from a hard substrate⁶¹ and a deformation map defining the regions where bulk shape instabilities of crack will propagate⁶².

F. Conclusion

In this comprehensive introduction to pressure sensitive adhesives (PSAs), the main features of these materials have been presented: applications, composition, adhesive properties and testing, influence of chemical and physical factors on adhesive properties,

mechanism of debonding. In particular, the influence on the adhesive properties of the T_g , the viscoelastic properties and all sorts of crosslinking was pointed out. The distance from T_g and the viscoelastic properties are closely related to the chain dynamics. Crosslinking can be present in the form of covalent crosslinking (from the introduction of a crosslinker or extensive long chain branching), of hydrogen bonding between acrylic acid units and of physical crosslinking (e.g. through nanophase separation).

II. Basic principles of solid-state nuclear magnetic resonance

A. General introduction to NMR

1. Definition and basic concepts^{63,64}

Nuclear magnetic resonance (NMR) spectroscopy is a branch of spectroscopy which consists of all studies of the nature of nuclear magnetic energy levels of material systems and of the transitions induced between them through absorption or emission of electromagnetic radiation.⁶⁵ It is possible to record NMR spectra (in gas, solution or solid) of any nuclide having a nuclear spin quantum number I different from 0. For example, ^{12}C is not NMR-active, but ^1H is and ^{13}C as well (^{13}C represents 1 % of the C atoms in natural abundance). Among other NMR-active nuclides, ^2H (deuterium), ^{15}N , ^{29}Si , ^{31}P are widely used for chemical and structural investigations.

Nuclei possess an angular momentum, P , and a charge. The motion of this charge gives rise to an associated magnetic moment, μ , such that $\mu = \gamma \cdot P$, where γ is the magnetogyric ratio, constant for each nuclide (and often designated as gyromagnetic ratio, contrary to IUPAC recommendations). Both angular momentum and magnetic moment are vector quantities. When placed in an external, static magnetic field, B_0 (strictly speaking the magnetic flux density), the microscopic magnetic moments align themselves relative to the field in a discrete number of orientations, because the energy states involved are quantized. For a spin of magnetic quantum number I , there exist $2I+1$ possible spin states, so for ^1H and ^{13}C ($I = 1/2$), there are two possible states, denoted $+1/2$ and $-1/2$, or α and β , or "spin up" and "spin down".

For a spin-half nucleus, the two states can be considered as orientation of the nucleus spin parallel or antiparallel to the static field, the parallel one (or $-1/2$, or α , or "spin up") being of lower energy for positive magnetogyric ratio γ . This situation can be described in terms of classical mechanics, with the field imposing a torque on the moment, which therefore traces a circular path about the applied field, referred to as Larmor precession (s. Figure 1-

II-1). The angular velocity of the precession is $\omega = -\gamma \cdot B_0$. The corresponding frequency $\nu = \omega/2\pi$ is named Larmor frequency of the nucleus.

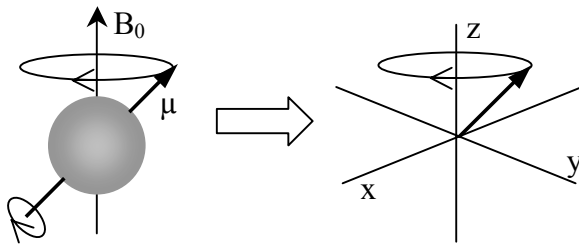


Figure 1- II-1: Precession of a single nucleus caused by a static magnetic field B_0 ; B_0 is conventionally applied along the z-axis and the motion of the nucleus represented as a vector moving on the surface of a cone.

For a spin-half nuclei, the lower energy level has a slight excess of nuclei, as defined by the Boltzmann distribution (s. Equation 1- II-1):

$$N_{up} = N_{down} \cdot \exp\left(\frac{\Delta E}{k \cdot T}\right) \quad \text{Equation 1- II-1}$$

where N_i is the populations of the energy level i , ΔE is the energy difference between the two levels, R the gas constant and T the absolute temperature. The differences between spin energy levels are rather small, so that the corresponding population differences are similarly small, only about 1 spin in 10^4 spins at the highest. This partly explains why NMR is so insensitive compared to other techniques as IR or UV. The tiny population excess of nuclear spins can be represented as a collection of spins distributed randomly about the precessional cone and parallel to the z-axis. This gives rise to a resultant bulk magnetization vector M_0 along the z-axis at equilibrium (s. Figure 1- II-2 (a)). This magnetization M behavior can be described in terms of classical mechanics, it is termed the vector model of NMR.

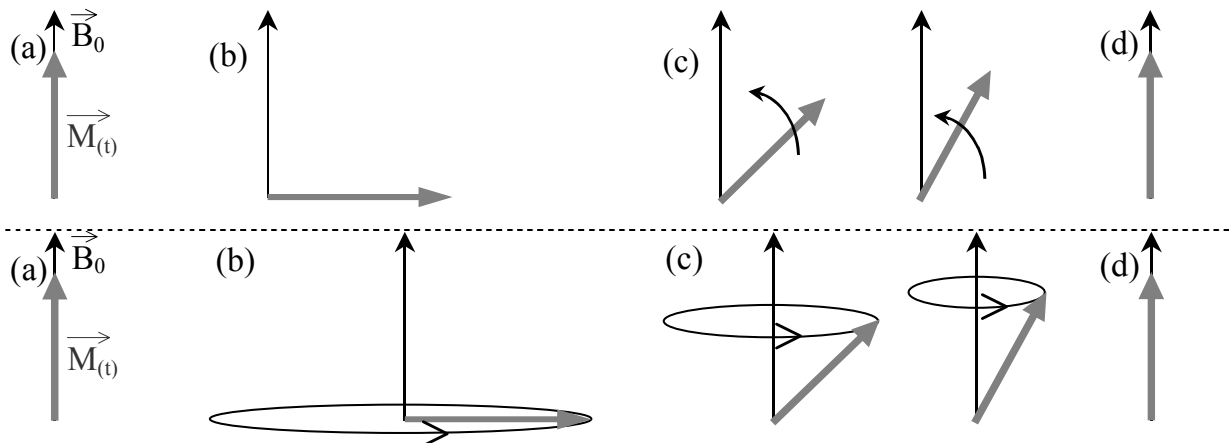


Figure 1- II-2: Evolution of the bulk magnetization in the sample during a pulsed NMR experiment; in the rotating frame (top), and in the laboratory frame (bottom); (a) and (d) at equilibrium, (b) during the acquisition of the data, (c) during the relaxation delay between consecutive transients.

Nuclear magnetic resonance occurs when the nucleus changes its spin state, driven by the absorption of a quantum of energy applied as electromagnetic radiation whose frequency matches the Larmor frequency of the nucleus. During NMR experiments, the sample is irradiated by an oscillating B_1 magnetic field, applied in the xy-plane via the electric current circulating in a coil around the sample. In order to simplify the understanding, the oscillating

B_1 field is decomposed in two counter-rotating magnetic vectors in the xy -plane, and everything is observed from the own frame of one of the B_1 components, where it is static: the rotating frame. In the rotating frame, the second component of B_1 is precessing at twice the Larmor frequency of the nuclei, so that it does not have any effect on the spins and is not considered. It should be stressed that the rotating frame is rotating with respect to the laboratory frame at the Larmor frequency of the studied nucleus, therefore the precession of the spins around the B_0 field appears to be frozen in the rotating frame.

If spins with different chemical surroundings are present in the sample, they will have different Larmor frequencies, so that in the rotating frame of one of them, the other will precess at a frequency which is the slight difference between the two Larmor frequencies. Therefore the different types of spins will appear at different frequencies in the recorded spectrum (corresponding to different chemical shifts). These differences due to the chemical environment are in the ppm range relative to the Larmor frequencies.

2. Evolution of magnetization during pulsed NMR experiments for a spin-half nucleus in the rotating frame

At equilibrium, the bulk magnetization vector is along the z -axis (s. Figure 1- II-2 (a)). During the experiments, radiofrequency (rf) pulses are applied to the sample. Applying a "pulse" to the sample simply consists in turning on the B_1 oscillating field via rf irradiation. The rf electromagnetic field imposes a torque on the bulk magnetization vector, in a direction that is perpendicular to the direction of the B_1 field. For example, applying the rf field along the x -axis will drive the vector from the z -axis toward the y -axis (s. Figure 1- II-3). The phase of the pulse (in the laboratory frame) is defined as the rotation axis (in the rotating frame). The rate at which the magnetization vector moves is proportional to the strength of the applied rf field, so that the total angle from which it turns (tip angle or flip angle) is proportional to the amplitude and duration of the rf pulse. If the rf is turned off just after the vector has reached the y -axis, it is called a 90° pulse; if it is turned off just after it has reached the $-z$ -axis, it is called a 180° pulse, etc.

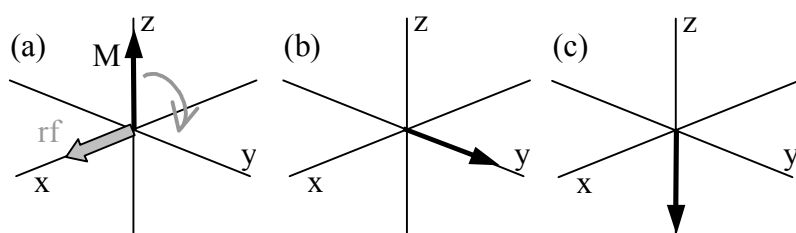


Figure 1- II-3: Effect of a rf pulse on the bulk magnetization in the vector model of the NMR; bulk magnetization (a) at equilibrium when the application of the rf pulse starts, (b) after a 90° pulse, (c) after a 180° pulse.

The idea of applying a sequence of pulses of different phase and flip angle is of central importance to NMR experiments. The concept of repeating a multipulse experiment with

different pulse phases and combining the collected data in an appropriate manner is called phase cycling, and is widely used for selecting the signal of interest in an NMR experiment.

At the end of the pulse program, the response of the sample to the irradiation is recorded via the current induced in the same coil by the change of bulk magnetization in the sample. At that step of the experiment, the magnetization precesses in the laboratory frame at the Larmor frequency around the B_0 axis, and is static in the rotating frame. To be able to record the magnitude of this magnetic field negligible with respect to the static field B_0 , the acquisition of the data is done in the xy -plane (s. Figure 1- II-2 (b)).

Between consecutive transients (single repetitions of the same experiment to accumulate data), time is given to the sample to relax (typically 4 s for ^1H and 10 s for ^{13}C). Relaxation is the process by which the bulk magnetization comes from a non equilibrium state, usually in the xy -plane or along the $-z$ -axis, back to the ground state along the z -axis. This process is schematically shown on Figure 1- II-2 (c) in the case of relaxation from the xy -plane. It can be decomposed into two sub-processes: the transverse or spin-spin relaxation with a time constant T_2 in the xy -plane, and the longitudinal or spin-lattice relaxation with a time constant T_1 along the z -axis. In solution-state NMR, T_1 and T_2 are of the same order of magnitude, while in solid-state NMR T_1 (s timescale) is usually larger than T_2 (ms timescale). T_2 characterizes the decay rate of the recorded signal (and hence the total acquisition time). T_2 relaxation happens through the dephasing of the different individual spin precessing in the perpendicular plane due to their slightly different Larmor frequencies. T_1 characterizes the growth of the overall magnetization back along the z -axis (and hence the relaxation delay that must be waited between consecutive transients). T_1 relaxation happens through the transfer of the excess energy of the spins to the surrounding lattice.

After the relaxation delay, or recycle delay, the system is back to equilibrium (s. Figure 1- II-2 (d)) and the rf irradiation sequence can be repeated.

The recorded signal in the time domain, FID for free induction decay, is finally Fourier-transformed into the frequency domain to obtain the spectrum. It is indeed easier in the frequency domain to read out the resonance frequencies corresponding to the different chemical environments of the nuclei. Furthermore, the simultaneous stimulation of all spins with a single pulse of rf energy (instead of scanning all the frequencies one by one) allows a faster signal-averaging and hence an enormous increasing in signal-to-noise ratio.

B. Introduction to solid-state NMR

1. Resonance line width, dipolar coupling and motion

a) Types of broadening

The resonance lines observed in solid-state NMR are generally much broader than in solution-state NMR. There are three types of resonance line broadening (s. Figure 1- II-4).⁶⁶ An homogeneously broadened line is a sum of lines having the same broadening and no chemical shift difference; it is the case that will be developed in this paragraph. An inhomogeneous line is a sum of non-overlapping individual lines with no coupling between the corresponding spin packets; its line shape is determined by a distribution of shifts. A heterogeneous line is the sum of individual lines with different shifts, and whose corresponding spin packets are coupled to each other.

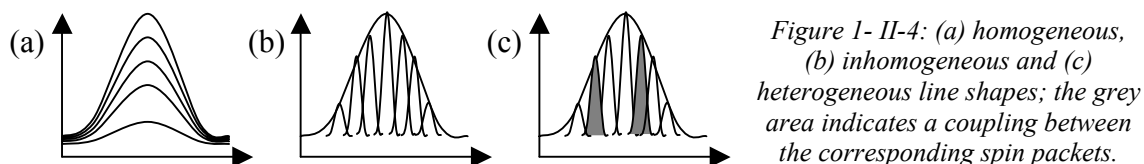


Figure 1- II-4: (a) homogeneous, (b) inhomogeneous and (c) heterogeneous line shapes; the grey area indicates a coupling between the corresponding spin packets.

Homogeneous line broadening is observed due to dipole-dipole couplings. The dipole-dipole coupling is an anisotropic direct spin-spin interaction through space. It is present between all types of spin with $I > 0$. In organic solids, the dominant homonuclear couplings are usually ^1H - ^1H couplings (because ^{13}C - ^{13}C or ^{15}N - ^{15}N can only play a role in isotopically enriched substances) and the most common heteronuclear coupling is the ^1H - ^{13}C coupling. Dipole-dipole couplings effectively depend on both, the distance r_{ij} between the two spins i and j involved as well as the angle θ_{ij} between the internuclear vector and the B_0 field. The dipolar coupling is proportional to D_{ij} :

$$D_{ij} = \frac{\gamma_i \gamma_j}{r_{ij}^3} (1 - 3\cos^2 \theta_{ij}) \quad \text{Equation 1- II-2}$$

where γ_i denotes the magnetogyric ratio of the nucleus i .⁶⁷

b) Line shape and line width

The resonance line width is usually described either as the full width at half maximum (fwhm) or by the second moment. The fwhm is the distance between the points on the curve at which the function reaches half its maximum value. The second moment M_2 of a normalized function $f(\omega)$ with a maximum at ω_0 is defined in Equation 1- II-3.⁶⁷

$$M_2 = \int (\omega - \omega_0)^2 f(\omega) d\omega \quad \text{Equation 1- II-3}$$

For a normalized Gaussian line (s. Table 1- II-1), the second moment is Δ^2 , while the fwhm is $2\Delta\sqrt{2\log 2}$. For a normalized Lorentzian (s. Table 1- II-1), the fwhm is 2δ , while the second moment does not exist because the integral diverges.⁶⁸

Name	Gaussian function	Lorentzian function
Definition	$G(\omega) = \frac{1}{\Delta\sqrt{2\pi}} \exp\left(-\frac{(\omega-\omega_0)^2}{2\Delta^2}\right)$	$L(\omega) = \frac{\delta}{\pi} \frac{1}{\delta^2 + (\omega-\omega_0)^2}$

Table 1- II-1:
Mathematical definitions
of normalized Gaussian
and Lorentzian functions.

In a rigid lattice of strongly coupled spins, the dipole-dipole couplings have two effects.⁶⁷ First, each involved nucleus produces at the location of each neighbor a local magnetic field due to its own Larmor precession. The resulting static component of the local field (along the z-axis) is different at the location of each nucleus, resulting in a slight shift in Larmor frequency, and thus in heterogeneous line broadening. Furthermore, the rotating component of the resulting local field (in the xy-plane) results in an homogeneous line broadening of the order of magnitude of the local field. Second, the coupled spins can undergo flip-flop processes: the "spin up" spin becomes "spin down" and vice versa. The total magnetization is not changed during this process, but step by step, its spatial distribution in the sample evolves in the network of interacting spins. In the case of a rigid lattice of strongly coupled spins, this leads to a ^1H line shape which can usually be approximated to a Gaussian shape, in most cases having a fwhm of the order of magnitude of tens of kHz. It is for example generally the case of ^1H line shapes of polymeric samples well below their T_g , as recorded under static conditions.

It should be noted that for not abundant nuclei like ^{13}C (or ^{15}N), the homonuclear ^{13}C dipole-dipole coupling is negligible with respect to the heteronuclear ^1H - ^{13}C one. The heteronuclear flip-flop contribution is strongly reduced with increasing static magnetic field, therefore with the field used these days the heteronuclear coupling leads to detectable heterogeneous line broadening if the ^1H homonuclear coupling is negligible (e.g. decoupled).

When molecular motion is present, the motion of the spins results in a variation of the induced local field.⁶⁸ If the variation of the spin lattice is fast compared to the instantaneous Larmor precession in the local field due to dipolar couplings, each individual spin "sees" an average local field, which is weaker than the instantaneous local field. Therefore the induced line broadening is smaller. Finally, compared to the rigid lattice case detailed above, it results in line narrowing, usually called motional line narrowing. The faster the molecular motion, the stronger the local field averaging, and hence the narrower the resulting line. The very slow motions have no influence on the line shape. In the case of very fast molecular motions, the assumption of a Lorentzian line shape is satisfying, with a line width of the order of magnitude of the second moment of the static line multiplied by the correlation time of the

motion. In the intermediate regime, no satisfying correlation between the line width and the correlation time of the motion exist, the only developed models requiring strong assumptions.

2. Applications of solid-state NMR

Solid-state NMR methods can be divided into two groups depending if the sample is spun or not. The recorded spectra exhibit usually very broad lines when the sample is kept static. It is possible to spin a rotor containing the sample very fast at a certain angle relative to the static B_0 field during the measurements. If the angle is chosen equal to 54.7° , the technique is called magic angle spinning (MAS, s. paragraph 3), and increases the resolution in the spectrum.

Hence, high resolution spectra are accessible in solids by MAS (the resolution is nevertheless lower than in solution-state NMR). Analyses similar to the ones conducted with solution-state NMR can be carried out: structural studies based on lines assignment according to chemical shifts.

Spectra recorded on static samples usually exhibit a very poor resolution. In that case, the line shape is investigated. The fact that the neat solid sample is analyzed makes it possible to study features of the solid itself (on the contrary to solution-state NMR): its structure (distances, angles), orientation, and reorientations of molecules on a ns to a s timescale.

3. Principle of magic-angle spinning (MAS)⁶⁹

In the case of solid samples, NMR spectra are usually severely broadened by anisotropic nuclear interactions to which the nuclei in the solid are subjected (s. paragraph 1). Although motion is usually present in solid samples, it is generally not sufficient to narrow the NMR lines to the degree found in liquids. In order to reveal fine structures of the type of those found in NMR spectra of liquids, magic-angle spinning (MAS) can be used. The MAS procedure consists in **rotating the solid sample uniformly about an axis inclined at the angle $54^\circ 44'$ to the direction of the static magnetic field of the NMR magnet** (s. Figure 1- II-5). Very *fast rotation* compared to the line width is needed and rotation speeds of more than 25 kHz can now be achieved routinely.

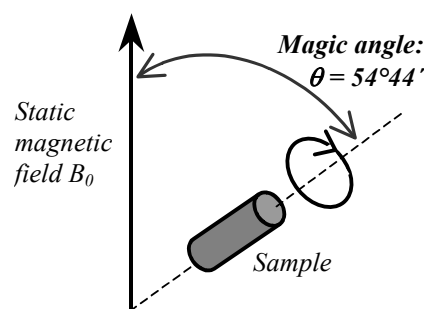


Figure 1- II-5:
Magic angle
spinning (MAS) of a
solid-state NMR
sample.

Rapid isotropic motion eliminates the anisotropic interactions from an NMR spectrum, like in NMR of liquids. For a sample undergoing uniform spinning at any angle θ , calculations of every anisotropic interaction Hamiltonian according to the perturbation theory introduces a factor $(3\cos^2\theta-1)$ in the constant term, and periodic terms depending on the rotation frequency. Such a mathematical expression proves that spinning at the magic angle $\theta_M=54^\circ44'$ for which $(3\cos^2\theta-1) = 0$ should reduce the anisotropic broadening in principle to zero; in addition, rotational sidebands should possibly appear at multiples of the spinning frequency. These predictions are borne out by experiments, at every spinning frequency for the anisotropic shift interactions that results in an heterogeneous broadening, and only if this spinning frequency is higher than the NMR line width in the case of the anisotropic dipole-dipole interactions that causes a homogeneous broadening. Nuclear quadrupole interactions are not completely averaged by simple MAS, but ^1H and ^{13}C nuclei do not possess a magnetic quadrupole moment.

Sufficiently fast MAS leaves only isotropic shift interactions and isotropic J couplings (indirect electron couplings) on NMR spectra, similar to the ones present in NMR spectra of liquids. However, the NMR spectra obtained are still broader than spectra of liquids, because of instrumental factors, residual interactions, as well as T_2 -relaxation and motional effects. The instrumental factors are the inhomogeneity of the laboratory magnetic field, the imperfect adjustment of the magic angle and its instability, the insufficiently fast spinning, and bulk susceptibility effects in inhomogeneous samples. The residual interactions are the residual dipole-dipole interactions (related to insufficiently fast spinning), the chemical shift distributions, the intermolecular J couplings (electron-coupled interactions), the antisymmetric part of the J couplings, some quadrupole and multipole effects (not present in the case of ^1H and ^{13}C nuclei). The spin-spin (or transversal) relaxation contributes to the broadening with a width of order $(\pi T_2)^{-1}$, where T_2 is the spin-spin relaxation time. Under rotational resonance conditions (when the spinning frequency is exactly equal to the frequency difference between two resonance lines), extensive cross relaxation is observed, leading to line broadening. Microscopic molecular motion in solid samples can already narrow the lines but can interfere with MAS. For further narrowing due to MAS, the spinning frequency must be higher than that of the molecular motion.

4. Examples of application of MAS

To illustrate the effect of MAS frequency on NMR spectra of solid samples, we recorded spectra of adamantane, PMMA (s. Figure 1- II-6) and sample Copo1 (s. Part 2, I).

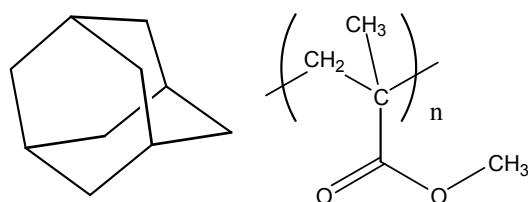


Figure 1- II-6:
Formulas of
adamantane (left)
and PMMA (right).

Adamantane can be used to calibrate ^1H and ^{13}C spectra in solid-state NMR. It is a crystalline powder, but the molecule is ball-shaped, so that it is rotating isotropically in the crystal. This type of microscopic motion leads to significant line-narrowing even in the static ^1H spectrum, and thus adds to the line-narrowing achieved via MAS (s. end of the previous paragraph). ^1H -NMR spectra of adamantane have been recorded static and with different spinning frequencies ω_{MAS} on a Bruker MSL300 spectrometer at a ^1H frequency of 300.13 MHz at room temperature (s. Figure 1- II-7). The ^1H static full width at half maximum is 13.7 kHz, so that the narrowing of the line due to MAS becomes apparent in the spectrum at $\omega_{\text{MAS}} = 3$ kHz but is not complete below $\omega_{\text{MAS}} = 15$ kHz. Furthermore, spinning sidebands are observed, with a frequency separation of ω_{MAS} between two consecutive sidebands.

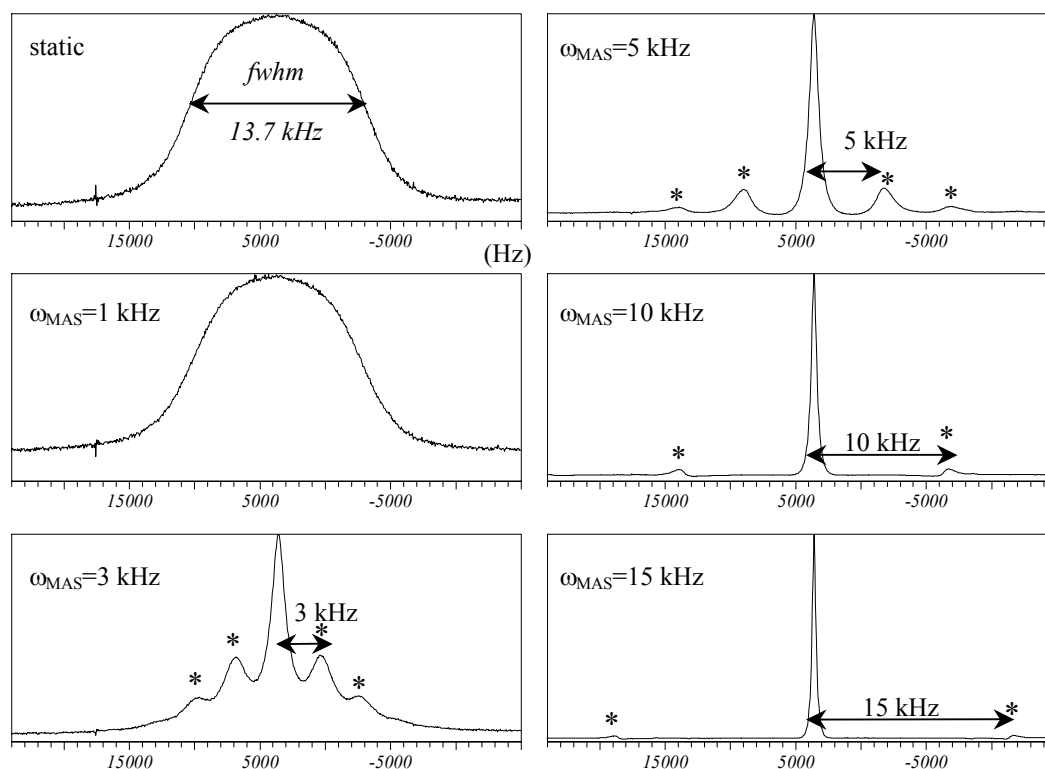


Figure 1- II-7: Influence of the MAS spinning speed on the ^1H -NMR spectrum of adamantane, at room temperature and for a ^1H frequency of 300.13 MHz; spinning sidebands are marked with *.

The effect of MAS on the ^{13}C spectrum is illustrated on Figure 1- II-8. CP-MAS spectra of PMMA have been recorded at different spinning frequencies ω_{MAS} on a Bruker MSL300 spectrometer at a ^{13}C frequency of 75 MHz and at room temperature. Spinning sidebands are observed only for the C=O line, with a frequency separation of ω_{MAS} between two consecutive sidebands. Therefore, the intensity is concentrated in the centerband for

higher spinning frequencies. Furthermore, the resolution is not changed when the spinning frequency is increased from 2 to 5 kHz.

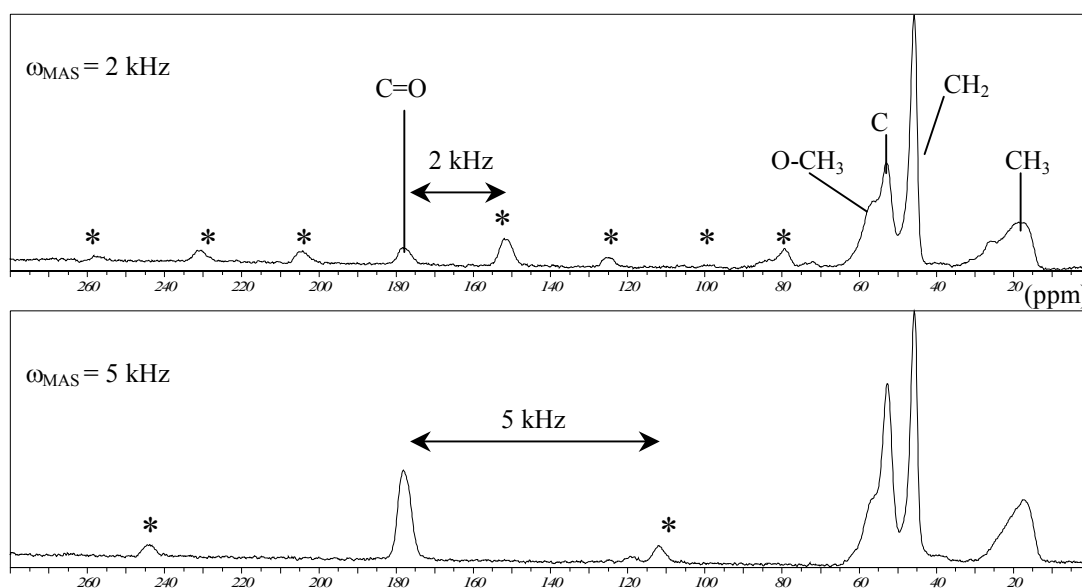


Figure 1-II-8: Influence of MAS spinning speed on ^{13}C CP-MAS spectrum of PMMA, at room temperature and for a ^{13}C frequency of 75 MHz; spinning sidebands are marked with *.

The importance of MAS for our investigations is illustrated by the case of the industrial sample Copo1, statistical copolymer of 2-ethylhexyl acrylate, methyl acrylate and acrylic acid (s. Part 2, I for more details on the composition). ^1H spectra were recorded at $-20\text{ }^\circ\text{C}$, static at a ^1H frequency of 300.13 MHz and under 25 kHz MAS at a ^1H frequency of 500.13 MHz (s. Figure 1-II-9). It should be noted that the line width in kHz of the dipolar broadened lines is independent of the ^1H Larmor frequency, and that for a ^1H Larmor frequency of 500.13 MHz, 1 kHz corresponds to 2 ppm. On this example, it is obvious that MAS dramatically increases the resolution in the spectrum.

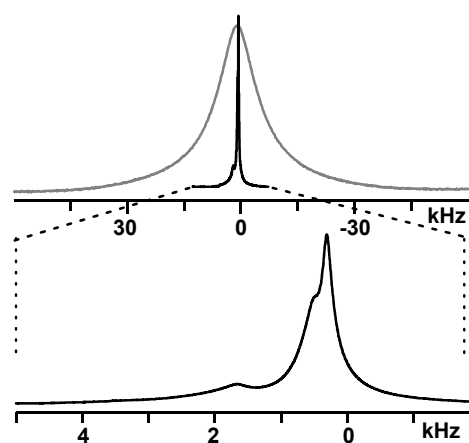


Figure 1-II-9: ^1H solid-state single pulse spectra of sample Copo1 at $-20\text{ }^\circ\text{C}$, static at 300.13 MHz (in grey, above) and under 25 kHz MAS at 500.13 MHz (in black, above and below).

C. Single pulse excitation

1. ^1H -NMR spectra

The ^1H single pulse excitation is the simplest NMR experiment. Its pulse scheme is shown on Figure 1- II-10.

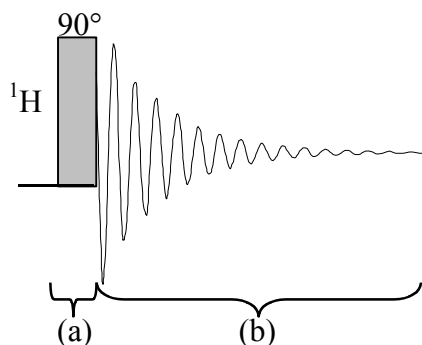


Figure 1- II-10:
Pulse scheme of ^1H
single pulse
excitation.

It should be noted that the timescale can not be represented correctly in the pulse schemes shown here since the pulse durations are of the order of magnitude of a few μs , while the delays between pulses are of the order of magnitude of μs to ms , and the FID is of the order of magnitude of several ms .

At equilibrium, the magnetization is along the main magnetic field B_0 axis. The 90° pulse ((a), applied through an orthogonal magnetic field B_1) rotates it into the orthogonal xy -plane. The detection of the magnetization, (b), is immediately done in the xy -plane, leading to the free induction decay (FID), and to the spectrum after Fourier transformation.

2. ^{13}C -NMR spectra

There are two classical methods to obtain one-dimensional ^{13}C spectra: single pulse excitation and cross-polarization (CP, s. paragraph D.). The ^{13}C single pulse excitation is the simplest ^{13}C NMR experiment. Its pulse scheme is shown on Figure 1- II-11.

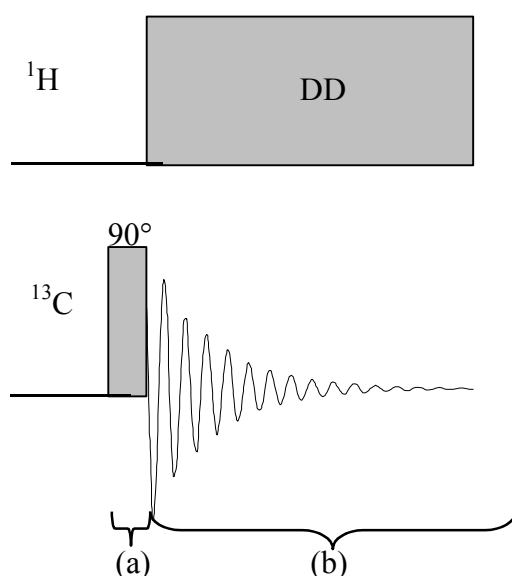


Figure 1- II-11: Pulse
scheme of ^{13}C
single
pulse excitation.

In the single pulse experiment, the pulse program consists of one 90° pulse in the carbon channel, (a), which flips the ^{13}C magnetization of ^{13}C nuclei in the plane perpendicular to B_0 where it is immediately recorded (b). During the data acquisition, the ^{13}C nuclei are decoupled from the surrounding ^1H nuclei by irradiating the ^1H nuclei with a continuous rf

field. This heteronuclear decoupling procedure eliminates the broadening of the ^{13}C lines due to strong heteronuclear dipole-dipole coupling between ^1H and ^{13}C .

D. Cross-polarization (CP) ^{13}C -NMR spectra

1. Principle^{70,71}

In natural abundance, 99 % of carbons are ^{12}C nuclei, while only 1 % are ^{13}C nuclei. Since only the ^{13}C isotope is NMR-sensitive, and its γ is lower than the one of ^1H by a factor of 4, the signal in ^{13}C spectra is very low compared to ^1H spectra. Consequently, methods were developed to increase the sensitivity in spectra of ^{13}C or other rare nuclei.

Cross polarization (CP) is a method used to obtain ^{13}C magnetization not directly from T_1 relaxation (like in the case of single pulse excitation), but indirectly via ^1H magnetization. It usually provides a higher polarization (and therefore more signal), and allows more frequent measurements (because the T_1 relaxation is faster for the hydrogen than for the carbon nuclei). Thus, spectra similar to single pulse ^{13}C spectra can be obtained within a shorter measurement time, provided the sample has only a limited mobility.

The experiment is divided in three parts: the flip of the hydrogen magnetization to the xy-plane (a), the transfer of the magnetization between ^1H and ^{13}C nuclei in the xy-plane (b), and the recording of the FID (c) (s. Figure 1- II-12).

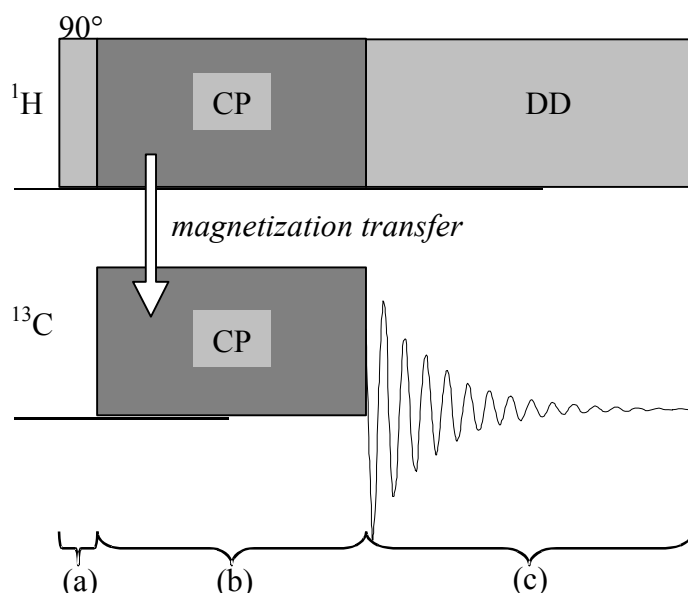


Figure 1- II-12: Pulse scheme for the ^{13}C CP experiment.

In the first part (a) of the experiment, the ^1H magnetization is driven to the xy-plane through a 90° pulse. In the part (b) of the experiment, the cross-polarization (CP) is realized during a defined contact time T_{CP} . During this time, magnetization is exchanged between ^1H and ^{13}C nuclei. This polarization transfer is possible via heteronuclear dipole-dipole interactions since the ^1H nuclei are locked with an rf field $B_1^{1\text{H}}$, while the ^{13}C nuclei are irradiated with a different magnetic field $B_1^{13\text{C}} = 4 \cdot B_1^{1\text{H}}$, so that they finally have the same

precession frequency $\omega^C = \gamma_C \cdot B_1^C = \gamma_H \cdot B_1^H = \omega^H$ in the locking fields. Under these so-called Hartmann-Hahn conditions,⁷² ^1H and ^{13}C nuclear spins can efficiently exchange magnetization. Detection of the FID of the ^{13}C nuclei takes place in the part (c), with dipolar decoupling of the ^1H nuclei.

2. Optimization of the CP contact time⁷¹

The CP magnetization transfer occurs during the part (b) between ^1H and ^{13}C . During this period, both ^1H and ^{13}C loose magnetization (in the orthogonal plane) through $T_{1\rho}$ relaxation phenomena (corresponding to the relaxation under an applied B_1 field). Efficient magnetization transfer is possible only if the relaxation time constants $T_{1\rho}$ are higher than the time constant T_{CH} of the magnetization transfer. As the cross-polarization and the $T_{1\rho}$ relaxation of the ^1H nuclei are the fastest phenomena, the intensity $M_C(t)$ of the ^{13}C nuclei magnetization over the time follows approximately Equation 1- II-4:

$$M_C(t) = M_0 \cdot e^{-t/T_{1\rho}} \cdot (1 - e^{-t/T_{\text{CH}}}) \quad \text{Equation 1- II-4}$$

where M_0 is the initial ^1H magnetization, $T_{1\rho}$ the longitudinal relaxation time of ^1H nuclei under Hartmann-Hahn conditions, and $1/T_{\text{CH}}$ the magnetization transfer rate from ^1H to ^{13}C nuclei under Hartmann-Hahn conditions.

The intensity of the magnetization of a ^{13}C nucleus as a function of the contact time T_{CP} is shown on Figure 1- II-13.

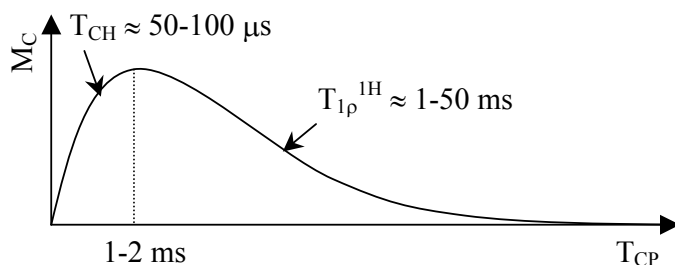


Figure 1- II-13: Intensity of the magnetization of the ^{13}C nuclei M_C as a function of contact time T_{CP} in a CP experiment.

The time constant T_{CH} of the cross-polarization depends on the proximity of ^1H nuclei close to the ^{13}C nucleus, and on their mobility: the closer the ^1H nuclei, the faster the transfer occurs; the more mobile the ^1H nuclei, the weaker the dipole-dipole coupling and the more slowly the transfer occurs. The time constant $T_{1\rho}$ characterizes the relaxation of the ^1H nuclei bound to the ^{13}C nucleus and depends mostly on the mobility of these ^1H nuclei: the more mobile, the slower they relax. Finally, the ^{13}C nuclei bound to ^1H nuclei can be selected by using a short CP contact time, while the ones not bound to a ^1H nucleus can be selected by using a long CP contact time followed by a waiting time without any pulse (to dephase the ^{13}C nuclei signal by attached ^1H nuclei) preceding the detection of the FID (this procedure is known as “gated decoupling”).

The increase of the ^{13}C signal, i.e. the ratio of the intensities obtained using CP and single pulse techniques, has in theory a maximal value of $\gamma_{1\text{H}}/\gamma_{13\text{C}} = 4$. However, this value is seldom achieved. Furthermore, in the case of very mobile samples, less signal is obtained with CP than with single pulse excitation.

3. Lee-Goldburg CP

^1H nuclear spin diffusion is the magnetization transfer taking place in a sample without material transport. It is occurring via flip-flop processes (s. paragraph B.1.b), due to the ^1H - ^1H dipole-dipole couplings which are operative during Hartmann-Hahn cross-polarization with 50 % of their full strength.⁷³ It hinders the recording of a local information, because it spatially averages properties over the groups through which the magnetization has traveled. It is nevertheless possible to prevent ^1H nuclear spin diffusion during CP by the use of Lee-Goldburg cross-polarization (LG-CP) instead of classical CP.

During LG-CP, an off-resonant B_1 field is applied to the ^1H spins, in such way that the effective field in the rotating frame is inclined at the magic angle $\theta_m = 54^\circ 44'$ with respect to the static magnetic field along the z-axis.⁷⁴ The LG irradiation thus significantly suppresses the ^1H - ^1H homonuclear dipole-dipole couplings.⁷⁵ Therefore the ^1H nuclear spin diffusion, mediated by the ^1H - ^1H homonuclear dipole-dipole couplings, is prevented.

E. Two-dimensional wideline separation (2D-WISE)

Information on the mobility in the sample and its correlation with the chemical structure can be obtained from two-dimensional wideline separation (2D-WISE) spectra.

1. Principle^{73,76}

The 2D-WISE experiment is a two-dimensional version of the CP experiment. Its pulse scheme is shown on Figure 1- II-14. The magnetization of the hydrogens of the sample is flipped to the xy-plane through a 90° pulse, then it evolves during a given evolution time t_1 , before magnetization transfer is done between hydrogens and carbons through dipole-dipole couplings under the Hartmann-Hahn conditions⁷²; finally the carbon magnetization is recorded using ^1H dipolar decoupling.

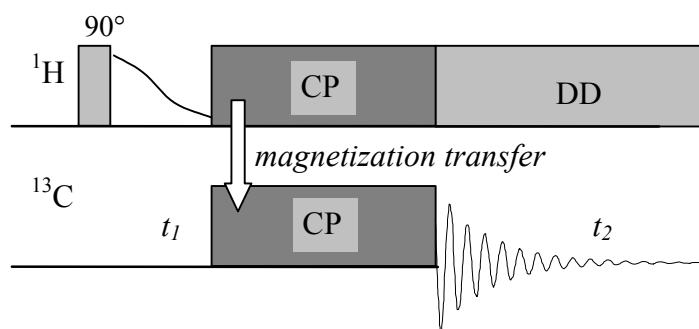


Figure 1-II-14:
Pulse scheme for
2D-WISE
experiment.

Since only 1D data can be directly acquired in conventional NMR (the direct dimension, or t_2 , corresponding to the FID), the second direction must be recorded indirectly. This is done by incrementing the evolution time t_1 (indirect dimension) and recording different FIDs for the various t_1 values. Indeed, the intensity of the virtual ^1H signal after the time t_1 is encoded as the intensity at the beginning of the FID recorded during t_2 . By putting side by side these different FIDs, a 2D time-dataset is obtained. A 2D Fourier transform is applied to this data to obtain a 2D spectrum.

2. Information obtained from a 2D-WISE spectrum^{73,76}

In a 2D-WISE spectrum, the different chemical groups of the molecule are resolved according to their chemical shifts in the ^{13}C (direct) dimension, and the line width in the ^1H (indirect) dimension gives information on the mobility of the corresponding group (the narrower the line, the more mobile the chemical group, s. Figure 1-II-15). It should be noted that rigorously, the ^1H line width does not depend only on the local mobility: CH_3 lines are usually more narrow than the others due to fast rotation, and CH_2 lines are usually broader than the CH lines at equivalent mobility, due to the fact that CH_2 contains a strongly coupled spin pair.

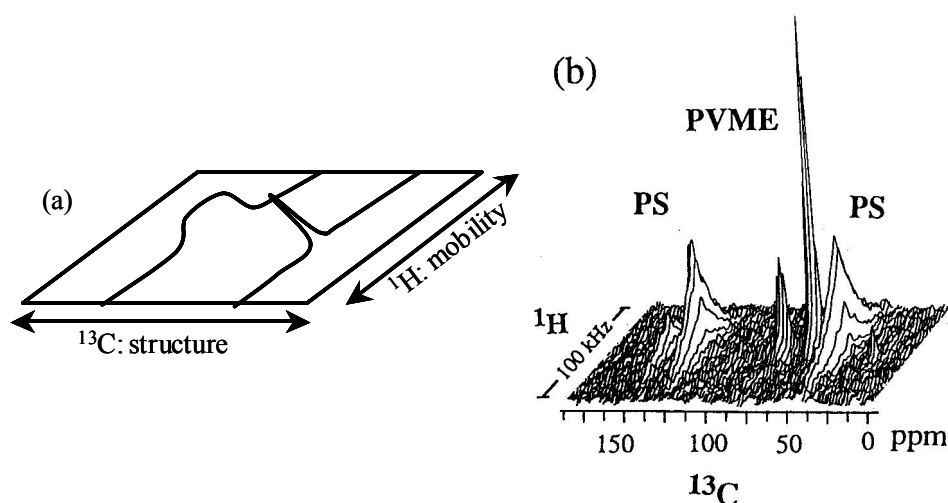


Figure 1-II-15:
Information
contained in a 2D-
WISE spectrum; (a)
scheme, (b) example
of a polymer blend
of more mobile
poly(vinyl methyl
ether) (PVME) and
less mobile
polystyrene (PS)⁷⁶.

^1H nuclear spin diffusion occurring during the CP contact time averages the apparent mobility over the groups through which the magnetization has traveled. In order to record a

local information, it is possible to prevent ^1H nuclear spin diffusion by using the Lee-Goldburg CP instead of classical CP (s. paragraph D.3).

F. ^1H Longitudinal or spin-lattice relaxation T_1

The longitudinal relaxation T_1 (or spin lattice relaxation) was introduced in paragraph A.2. It can be measured by the inversion recovery method introduced by Erwin Hahn.⁷⁷⁻⁷⁹ The pulse scheme for ^1H is shown on Figure 1- II-16. The ^1H magnetization is first flipped to the $-z$ axis via a 180° pulse. Then it relaxes longitudinally along the z -axis during the evolution time τ . Finally it is flipped via a 90° pulse in the xy -plane where it is recorded.

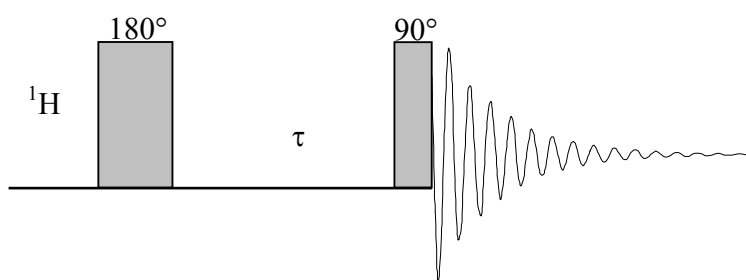


*Figure 1- II-16:
Pulse scheme for the
 ^1H inversion
recovery experiment.*

The final intensity is recorded for a series of τ values. The data are fitted with the Equation 1- II-5 to extract the relaxation time T_1 .

$$M(\tau) = M_0 \cdot [1 - 2 \cdot \exp(-\tau/T_1)] \quad \text{Equation 1- II-5}$$

In the case of an imperfect inversion pulse, the factor 2 is replaced by a variable factor, which is determined via the fit of the experimental data, and should remain close to 2.⁷⁹

The longitudinal relaxation can also be measured using a saturation recovery experiment, which is faster but less accurate.⁸⁰

G. Dipolar filter

The so-called dipolar filter allows to select the magnetization in some parts of a sample according to their mobility. It was introduced by Schmidt-Rohr et al.⁶

1. *Concept of mobility*

Mobility in the NMR sense is closely related to local mobility of the molecule. The terms mobile and non mobile in NMR depend on the experiment carried out.

For most of the NMR techniques, the relevant time scale is the one needed by local molecular reorientations to average out an anisotropic NMR interaction (e.g. dipole-dipole interaction, chemical shift anisotropy). In the case of the dipolar filter technique, the relevant interaction is the dipole-dipole interaction and its averaging time scale corresponds to the transversal T_2 relaxation time. Thus the corresponding local molecular motion takes place in the kHz regime. A molecule with local motion slower than the kHz regime will be considered as non mobile on the NMR time scale, a molecule with local motion faster than the kHz regime will be considered as mobile on the NMR time scale. NMR experiments (e.g. via the dipolar filter) are able to differentiate molecules with motion in the kHz regime as more mobile (resp. less mobile) if the corresponding local molecular motion is faster (resp. slower).

For other NMR experiments, in particular longitudinal T_1 relaxation or NOE (s. paragraph I), the relevant time scale is the Larmor frequency in the tens or hundreds of MHz regime. A molecule exhibiting a local motion with a correlation time shorter than the inverse of the Larmor frequency will be considered in the fast motion limit, in the opposite case it will be considered in the slow motion limit.

Possible causes of reduction of mobility on the NMR time scale in polymeric materials are lowering of the temperature towards T_g , chain branching, entanglement, or slower dynamics of the main chain with respect to the side chain.

2. *The dipolar filter*⁶

The dipolar filter selects the more mobile parts of a sample with regard to the dynamics of the corresponding ^1H nuclei. The selection is thus done based on a contrast between the dipole-dipole interaction strength in the different parts of the sample. Indeed, the ^1H nuclei with a T_2 relaxation constant higher than a critical value have a magnetization at the end of this filter. The dipolar filter consists of a succession of 90° pulses with different phases (s. Figure 1- II-17). It is designed to average all interactions (dipole-dipole couplings as well as the chemical shift) of the ^1H nuclei. However, the windows τ between the pulses are not kept as short as usual, but are set to rather long values of 10-30 μs . This varies the typical limit rate for mobility of less mobile and more mobile parts (its inverse) between 33 and 100 kHz. As a result, the averaging is not effective for large dipole-dipole couplings (in the less mobile parts) and the magnetization of the corresponding ^1H nuclei relaxes (with an exponential decay of short characteristic time T_2). Indeed, spins in the less mobile parts are

strongly coupled, therefore can undergo flip-flops easily and frequently, and dephase very quickly. The remaining magnetization is located at the more mobile ^1H nuclei for which the dipole-dipole coupling is small (and the characteristic time T_2 long), as a result of partial averaging due to high molecular mobility. In this way, only the more mobile regions of the sample are magnetized after application of the dipolar filter. To improve the selectivity, the filter pulse scheme is repeated up to 20 times. We define the filter strength as the ability of the filter to select a lower mobile fraction: it is increased by increasing either the number of cycles or the duration τ .

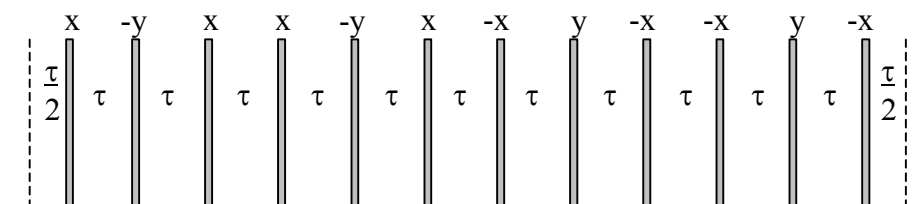


Figure 1- II-17: Pulse scheme for the dipolar filter (the series of 12 pulses is repeated up to 20 times).⁶

H. ^1H nuclear spin diffusion^{81,82}

The term spin diffusion has been introduced by Bloembergen to describe the transport of spin polarization between spatially separated spins; this spatial spin diffusion is the process occurring between equivalent spins.⁸³ The molecular mobility in a sample can be characterized according to its spatial heterogeneity using the ^1H nuclear spin diffusion technique with dipolar filter.⁶

1. Concept of nuclear spin diffusion

Nuclear spin diffusion is the spatial diffusion of the nuclear magnetization, which usually takes place without material transport. It is then mediated by dipole-dipole couplings, and therefore is most efficient among ^1H nuclei. The spins are coupled via dipole-dipole interactions, and each spin is in the energy state "spin up" or "spin down". Only a difference in the amount of "spin up" and "spin down" spins results in a bulk magnetization. A spin pair with one "spin up" and one "spin down" can undergo a coherent flip-flop exchange of magnetization if the two spins are dipolar coupled: the "spin up" spin becomes "spin down" and vice versa. The total magnetization is not changed during this process, but step by step, its spatial distribution in the sample evolves in the network of interacting spins. The magnetization transfer involved in the ^1H nuclear spin diffusion experiment usually consists of a succession of such flip-flop processes.

2. Goal of the experiment

The goal of the ^1H nuclear spin diffusion experiment with dipolar filter⁶ is to determine the percentage of more mobile ^1H nuclei in the sample, as well as the size of the

heterogeneities in dynamic heterogeneous samples. Spatial dynamic heterogeneities are more mobile micro-domains in a less mobile matrix, or vice-versa. From the surface-to-volume ratio of an interface, the domains can be modeled as lamellae, cylinders or spheres.⁸⁴ ^1H nuclear spin diffusion is an appropriate method for characterization of heterogeneity sizes in the range from a half to several tens of nm.^{84,85} Nevertheless, it is not appropriate for a full characterization of the domain shape.⁸⁵ The principle of the experiment is the following: first select the polarization of the more mobile parts only by dephasing the magnetization in the less mobile parts of the sample, then allow the magnetization to diffuse during a certain time t_m and finally record the evolved FID. The original idea of a nuclear spin diffusion experiment is from Goldman and Shen;⁸⁶ the selection is done in the present work through the dipolar filter⁶ (s. paragraph G). It should be noted that the selection in the ^1H nuclear spin diffusion experiment can also be done according to various other criteria, including $T_{1\rho}$ relaxation time or ^1H chemical shift.^{84,87} Nuclear spin diffusion has also been investigated between rare nuclei like ^{13}C .^{88,89} The ^1H nuclear spin diffusion with dipolar filter has been applied already to various polymer samples, including block copolymers,⁸¹ blends,⁸¹ core-shell particles^{82,90} and conetworks (polymer chains covalently bonded by block of another polymer)⁹¹.

3. Choice of the operating temperature

Before conducting a ^1H nuclear spin diffusion experiment, the optimal operating temperature must be chosen. This is done via a study of the ^1H line shape at different temperatures. At low temperatures, the whole sample is little mobile, so that the ^1H spectrum is broad, while at high temperatures, all the fractions of the sample are highly mobile, so that the ^1H resonances are narrow. In the usual case, intermediate temperatures are the interesting ones, because the sample contains both less and more mobile parts: the line exhibits a narrow component and a broad one (s. Figure 1- II-18). The optimal and usual operating temperature is a temperature at which the less and the more mobile parts are present in similar (or stoichiometric) amounts, so that the areas of the more and of the less mobile parts in the spectrum are similar.

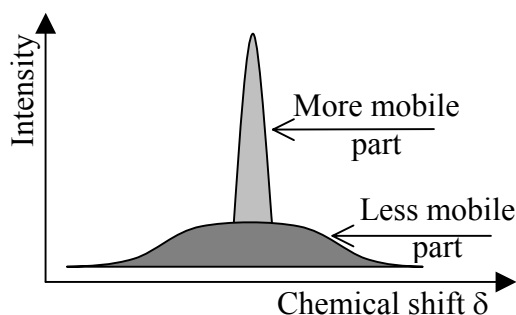


*Figure 1- II-18:
Shape of the ^1H line
of an heterogeneous
sample containing
more and less mobile
parts at intermediate
temperatures.*

4. Pulse program⁸⁷ and principle of the experiment

The ^1H nuclear spin diffusion experiment is a typical exchange experiment, consisting of an evolution or selection period, a mixing time t_m and a detection period. Its pulse scheme is shown on Figure 1- II-19. The spatial evolution of the magnetization in the sample is shown on Figure 1- II-20.

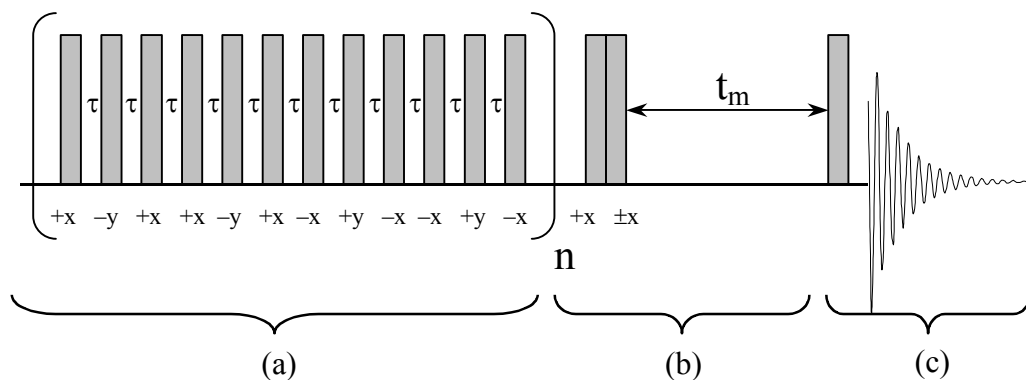


Figure 1- II-19:
Pulse scheme for ^1H nuclear spin diffusion experiment.

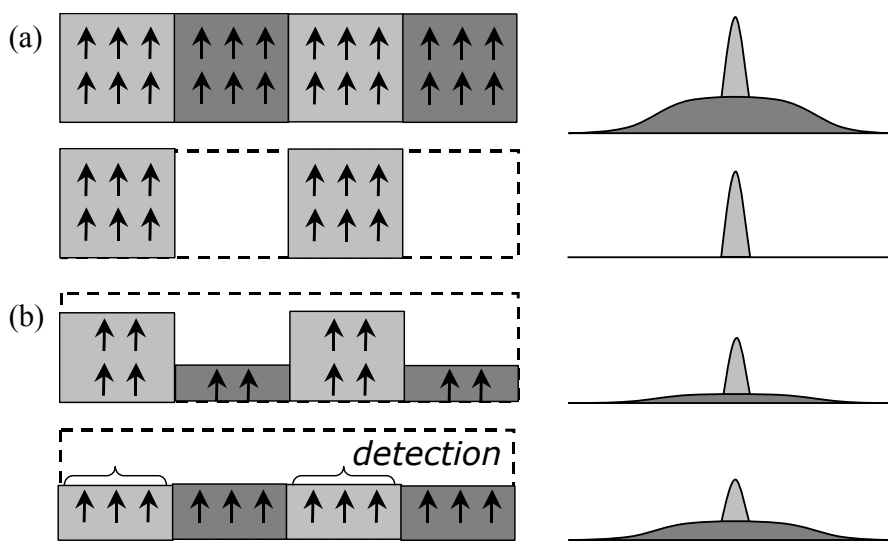


Figure 1- II-20:
Schematic representations of the evolution of the magnetization in the sample during a ^1H nuclear spin diffusion experiment; the more mobile parts are shown in light grey, the less mobile parts in dark grey; left, spatial evolution where the intensity of the magnetization is represented by the number of arrows; right, corresponding schematic ^1H line shape.

The selection of the more mobile parts of the sample is done with a dipolar filter (a) (s. paragraph G). At the end of this filter, only the more mobile ^1H nuclei of the sample possess magnetization. Then the magnetization remaining in the xy -plane is driven to the z -axis. During the mixing time t_m (b), ^1H nuclear spin diffusion (or migration of nuclear polarization) occurs, usually through the effective dipole-dipole coupling among ^1H nuclei. The remaining magnetization diffuses throughout the whole sample, usually mediated via flip-flops, and the heterogeneous distribution of polarization achieved by the dipolar filter equilibrates gradually. Then the magnetization present along the z -axis is driven to the xy -plane where the FID is recorded (c) and analyzed.

The first structural elements reached by the magnetization through diffusion are those in close proximity to the initially polarized ^1H nuclei. The morphological organization within

a sample therefore determines the time dependence of the magnetization equilibration process. Vice-versa, the spin diffusion behavior contains valuable information about typical domain size⁸⁵ and phases geometry.^{84,85}

5. Data analysis⁸¹

a) Recording of the ¹H nuclear spin diffusion curve

Several FIDs are recorded as a function of mixing time t_m and Fourier transformed. The line shape changes in two ways over t_m : the bottom of the line becomes broader and the total intensity (line area) decreases. The broadening of the line indicates that a less mobile part of the sample is observed, so that a part of the magnetization has diffused from a more mobile to a less mobile part of the sample. The decrease of the total intensity is due to T_1 relaxation (or longitudinal relaxation).

The decay of the intensity of the more mobile ¹H magnetization is monitored over the mixing time as the area of the corresponding line. In the usual case of a high mobility contrast, the recorded spectrum indeed exhibits only a narrow line for very small t_m , and for increasing t_m a broad line of increasing area appears below it. The area of the narrow line is then quantified by adjusting a spectral window narrower than the broad line (to eliminate the broad line) and integrating the remaining narrow line.⁸¹

The monitored decay is due to two factors: ¹H nuclear spin diffusion and T_1 relaxation. In order to separate the effects of ¹H nuclear spin diffusion and of T_1 relaxation, the magnetization is alternatively stored along $+z$ and $-z$ during the mixing time t_m , and the corresponding transients are subtracted.⁸⁴ To correct the data for T_1 relaxation, the recorded intensity I of the more mobile parts is divided by the intensity obtained for the same mixing time without application of the dipolar filter.^{81,87}

The so-corrected intensity is then normalized by the initial intensity I_0 . A decreasing curve is therefore obtained for I/I_0 plotted against $\sqrt{t_m}$ (s. Figure 1- II-21). Because of the appearance of multiple-quantum coherences around $t_m=0$, it is impossible to measure reliably the intensity at $t_m=0$.⁸⁴ Fortunately, the dependence upon t_m of the intensity corrected for T_1 relaxation is linear for small t_m , so that the intensity at $t_m=0$ can be extrapolated. The ¹H nuclear spin diffusion curve is then normalized, in such a way that the re-extrapolated intensity at $t_m=0$ is equal to 1, to obtain the final (corrected and normalized) ¹H nuclear spin diffusion curve.⁸⁴

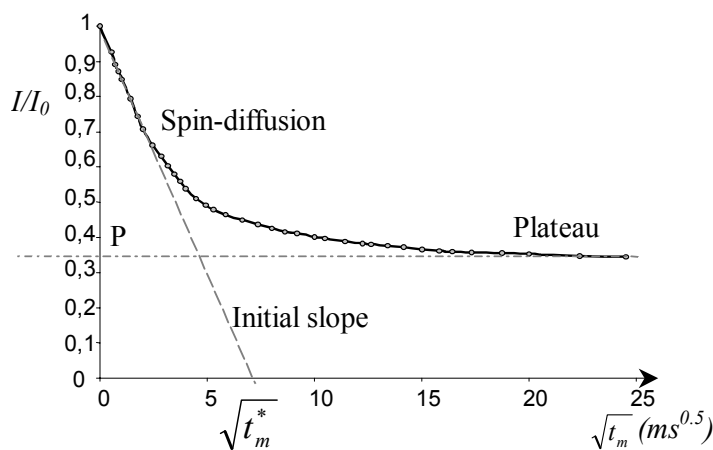


Figure 1- II-21: Typical ^1H nuclear spin diffusion curve, corrected for T_1 relaxation, plotted as the corrected normalized intensity I/I_0 against the square root of the mixing time.

b) Comparison of the longitudinal relaxation with the diffusion times

The use of the z-alternation phase cycling described above could not separate T_1 and spin diffusion effects in the general case.⁹² However, in the case of a spatially homogeneous T_1 , the recorded data can simply be corrected by multiplication of the data by $\exp(+t_m/T_1)$ with a T_1 value easily obtained in a measurement without selection,⁸⁴ or as described above using intensities from a reference experiment. If T_1 exhibits a strong spatial dependence, then this correction for T_1 relaxation is not valid any more, and the only reliable data will be obtained for mixing times much shorter than the shortest T_1 .⁸⁴ In that case of mixing times on the order of magnitude of the T_1 relaxation, the spin diffusion can still be qualitatively distinguished from the T_1 relaxation, if one component was completely suppressed initially and the z-alternation phase cycle is used.⁸⁴

c) Information obtained from the ^1H nuclear spin diffusion curve

The first information obtained from the ^1H nuclear spin diffusion curves is the plateau value P (s. Figure 1- II-21) which corresponds to the percentage of selected magnetization after application of the dipolar filter. It is the percentage of more mobile (in the NMR sense) ^1H nuclei in the sample, according to the chosen filter conditions and temperature.

The second information is the domain size d_{size} (lamella thickness, cylinder or sphere diameter, s. Figure 1- II-22). It should not be confused with the long period d_L determined in X-ray scattering (total thickness of 2 successive lamellae, distance between two consecutive cylinders or spheres).⁸⁴ The domain size d_{size} is related to the intercept of the initial slope with the X-axis (s. next paragraph). It should be noted that, according to the Babinet's principle, the initial decay does not exhibit any difference between the case of less mobile domains in a more mobile matrix and the inverse case.⁸⁴

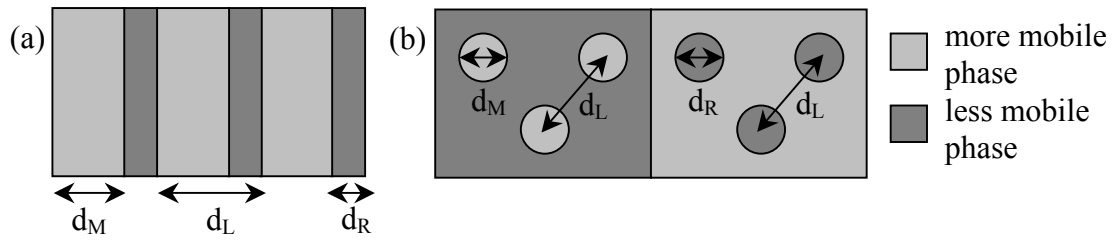


Figure 1-II-22: Domain size d_{size} (d_M or d_R) determined by 1H nuclear spin diffusion, compared to the long period (d_L) determined via X-ray scattering; (a) case of lamellae, (b) case of cylinders or spheres.

d) Determination of the plateau value

Since the transition between the more mobile and the less mobile phases is not an actual interface, but rather an interphase, there is no clear definition of phase around interphase, and therefore a dependence of plateau value on the filter parameters.⁹⁰ With decreasing interphase thickness, the plateau values determined for a given set of dipolar filters become closer to each other. Moreover, a slightly different domain size is determined for each curve. In the usual case of a high mobility contrast, the filter is adjusted to select roughly the stoichiometric proton ratio of more mobile phase.^{81,91}

e) Quantification of the domain size

The domain size d_{size} (d_M or d_R , s. Figure 1-II-22) is calculated using the Equation 1-II-6:

$$d_{size} = \frac{2 \cdot \varepsilon}{\sqrt{\pi}} \cdot \sqrt{D_{eff}} \cdot \sqrt{t_m^*} \quad \text{Equation 1-II-6}$$

where $\sqrt{t_m^*}$ is the intercept of the extension of the initial slope with the X-axis (s. Figure 1-II-21), ε the number of orthogonal dimensions relevant for the effective magnetization diffusion process (1 for lamellae, 2 for cylinders and 3 for spheres), and D_{eff} the effective 1H nuclear spin diffusion coefficient through flip-flops. The inverse of the square root of the effective diffusion coefficient D_{eff} is the arithmetic average of the inverses of the square roots of the 1H nuclear spin diffusion coefficients of the more mobile and less mobile phases D_{mob} and D_{rig} (s. Equation 1-II-7).

$$\frac{1}{\sqrt{D_{eff}}} = \frac{1}{2} \left(\frac{1}{\sqrt{D_{mob}}} + \frac{1}{\sqrt{D_{rig}}} \right) \text{ i.e. } \sqrt{D_{eff}} = \frac{2 \cdot \sqrt{D_{mob}} \cdot \sqrt{D_{rig}}}{\sqrt{D_{mob}} + \sqrt{D_{rig}}} \quad \text{Equation 1-II-7}$$

For polymeric samples with a high dynamic contrast, the value of the less mobile phase 1H nuclear spin diffusion coefficient is usually taken equal to the one measured for PS below its T_g : $0.8 \text{ nm}^2 \cdot \text{ms}^{-1}$,⁸¹ due to the similar hydrogen densities for organic polymers (in the order of magnitude of $0.8 \cdot 10^{23} \text{ cm}^{-3}$). The value of D_{mob} can be determined using its correlation with the relaxation time T_2 . This empirical correlation has been established in the

group of Prof. Spiess (s. Figure 1- II-23),^{81,93} using three different lamellar block copolymers (more mobile polyisoprene and less mobile polystyrene, with different molar masses for the blocks) and a polymer blend (cylinders of more mobile poly(ethylene oxide) in crosslinked poly(hydroxyethyl methacrylate)). The domain sizes of these polymers were known from transmission electron microscopy (TEM) and small-angle X-ray scattering (SAXS). NMR experiments were carried out at different temperatures (from 0 to 50 °C) to obtain several relaxation times in the more mobile phase of each polymer.

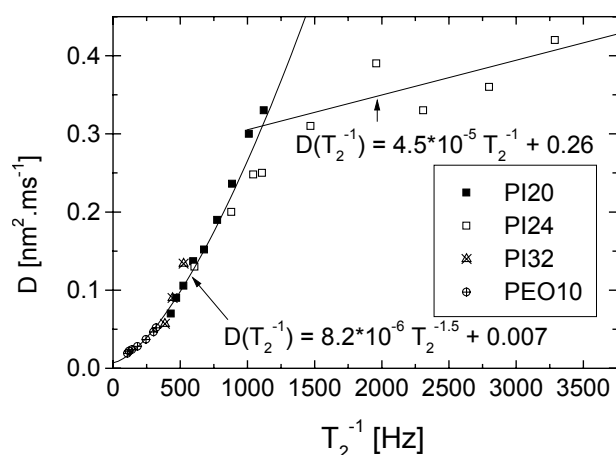


Figure 1- II-23: Correlation between the time constant for transversal relaxation T_2 and the ^1H nuclear spin diffusion coefficient D_{mob} ; PI: polyisoprene, PEO: poly(ethylene oxide).^{81,93}

f) Measurement of the T_2 relaxation time⁶⁴

The T_2 relaxation time has to be measured independently. This measurement can be done either using the Carr-Purcell-Meiboom-Gill (CPMG) experiment, or by measuring the line width of the static ^1H spectrum.

The CPMG experiment consists of a 90° pulse followed by a delay τ' and by a series of 180° pulses, separated by a delay $2 \cdot \tau'$ (s. Figure 1- II-24). The magnetization is refocused by the 180° pulses and the T_2 relaxation constant is the exponential decay constant of the intensity recorded at full echoes (in the middle between consecutive 180° pulses, where the intensity is maximal).

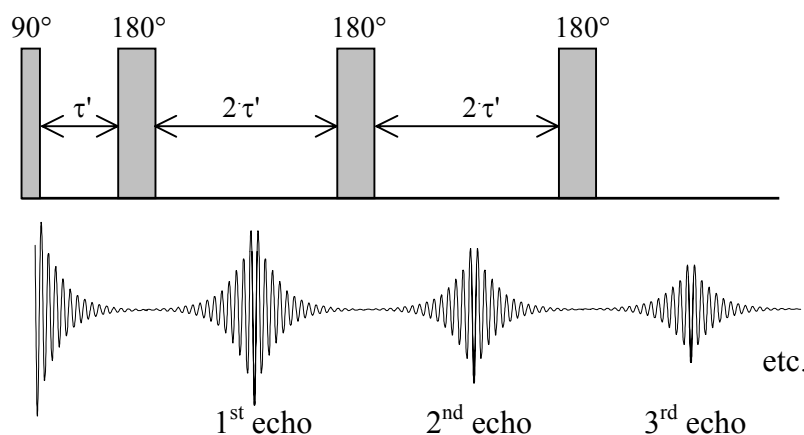


Figure 1- II-24: Pulse scheme of the CPMG experiment to measure T_2 .

It is possible to determine the relaxation time of the more mobile part alone using CPMG experiments, by applying the CPMG pulse scheme immediately after a dipolar filter. The

CPMG experiments allows to quantify T_2 correctly only if the sample is very mobile (liquid-like); otherwise the 180° pulses do not refocus the magnetization fully, and this causes an additional decay of the magnetization.

For samples of intermediate mobility, the T_2 relaxation time can be quantified via the ^1H static line width. Assuming that the line shape is Lorentzian, the full width at half maximum (fwhm) is equal to the ratio $1/(\pi \cdot T_2^*)$. The constant T_2^* is related to the genuine T_2 relaxation time by the equation $1/T_2^* = 1/T_2 + \gamma \cdot \Delta B$, where $\gamma \cdot \Delta B$ characterizes the additional reversible broadening of the line caused by the inhomogeneity of the static field B_0 . Even if the fwhm allows to determine only T_2^* , which is not exactly T_2 , the error done on T_2 that way is smaller than the error done with CPMG for the samples that are not completely mobile.

I. Nuclear Overhauser effect (NOE)⁹⁴

1. *The Overhauser effect*

Albert Overhauser first predicted substantial creation of nuclear polarization via saturation of electron spin resonance, through hyperfine coupling.^{95,96} Felix Bloch then described a similar transfer of magnetization occurring between nuclear spins through dipolar coupling.⁹⁷ This nuclear Overhauser effect (NOE) was first measured in relaxation experiments conducted on anhydrous hydrofluoric acid HF ^{98,99} and various organic compounds: 2,3-dibromothiophene,¹⁰⁰ formic acid and acetaldehyde,¹⁰¹ formyl fluoride CHFO ¹⁰². The use of NOE (change of intensity of one resonance when another is irradiated) in structural problems has been first demonstrated by Anet and Bourn.¹⁰³

NOE has become of central importance in molecular biology where it allows the complete determination of the 3D structures of large biological macromolecules in solution. However, we will not review this by far predominant application of NOE here, but rather concentrate on its less common application to non biological macromolecules. It should be noted that NOE spectroscopy was also used for structural studies in various other compounds like small molecules crystals,¹⁰⁴ coal,¹⁰⁵ hydrogels,¹⁰⁶ dendrimers,¹⁰⁷ transition metal complex ion pairs,¹⁰⁸ coordination and organometallic oligomers¹⁰⁹, surfactants in solution¹¹⁰.

2. *Cross-relaxation mechanism*

Nuclear cross-relaxation is caused by mutual spin flips in pairs of dipolar coupled spins which are induced by motional processes. Cross-relaxation leads to a non coherent transfer of magnetization between the spins and hence to intensity changes, known as NOE. A coherent transfer would imply a periodicity in the time evolution of intensities in a two-spin system, which is not the case in non coherent relaxation processes like NOE. In the case of

cross-relaxation, the fluctuations of the dipolar interaction between two spins indeed induces zero-, single- and double-quantum transitions (and not coherences, s. Figure 1- II-25). Only zero- and double-quantum transitions involve simultaneous flips of both spins and contribute to NOE.¹¹¹ The single-quantum transitions only contribute to independent spin-lattice relaxation of the individual spins.

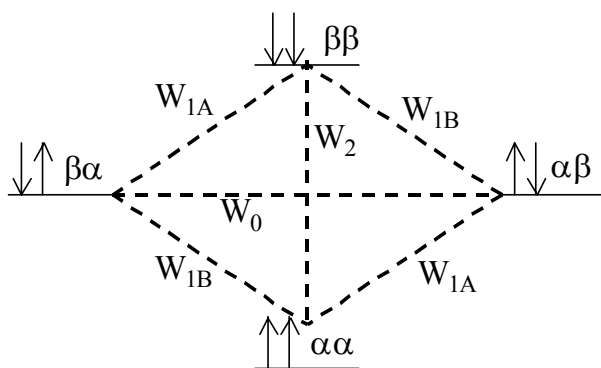


Figure 1- II-25: Energy level diagram for a two spin system, showing definitions for transition probabilities W and spin states; the subscripts 0, 1X, 2 designate respectively zero-quantum transition, single-quantum transition with flip of X spin (left: spin A, right: spin B), double-quantum transition.⁹⁴

The transition probabilities depends on the motional correlation time τ_c . τ_c is the correlation time of the isotropic random process which modulates the dipolar coupling interaction.^{112,113} It is designated by Levitt as the rotational correlation time and roughly defined as the average time taken by a molecule to rotate by one radian in the case of molecular tumbling in liquids.¹¹⁴ The evolution of the transition probabilities with τ_c is shown on Figure 1- II-26. The usefulness of the NOE technique strongly depends on the time scale of the motional processes involved. The fast motion limit, or extreme narrowing limit, corresponds to a motion with a correlation time τ_c much lower than the inverse of the Larmor frequency ω_0 ; it applies to small molecules in non viscous solutions. The slow motion limit, or spin diffusion limit, corresponds to $\tau_c \gg \omega_0^{-1}$; it applies to macromolecules at high magnetic field.

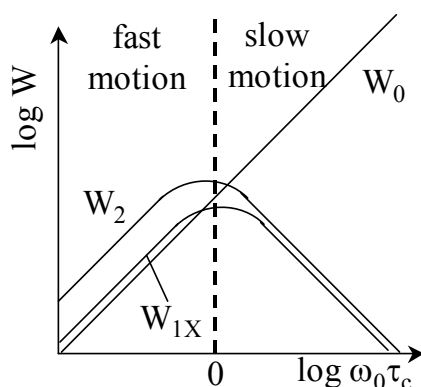


Figure 1- II-26: Evolution of the transition probabilities W with the motional correlation time τ_c (right).⁹⁴

It is clearly seen on Figure 1- II-26 that cross-relaxation occurs predominantly by double-quantum transitions in the fast motion regime, and predominantly by zero-quantum transitions in the slow motion regime.¹¹¹ This results in negative cross-relaxation rates $-R_{AB}$ and $-R_{BA}$ (s. Equation 1- II-8 and Equation 1- II-9 for notations) in the case of fast motion

limit, and in positive cross-relaxation rates in the case of slow motion limit. The physical meaning of positive or negative cross-relaxation rate is represented on Figure 1- II-27. In the slow motion limit, the spin-lattice relaxation is inefficient, and the rate of cross-relaxation is very fast.¹¹⁵ For a critical correlation time of $\frac{\sqrt{5}}{2\omega_0}$, the cross-relaxation rates are equal to zero.

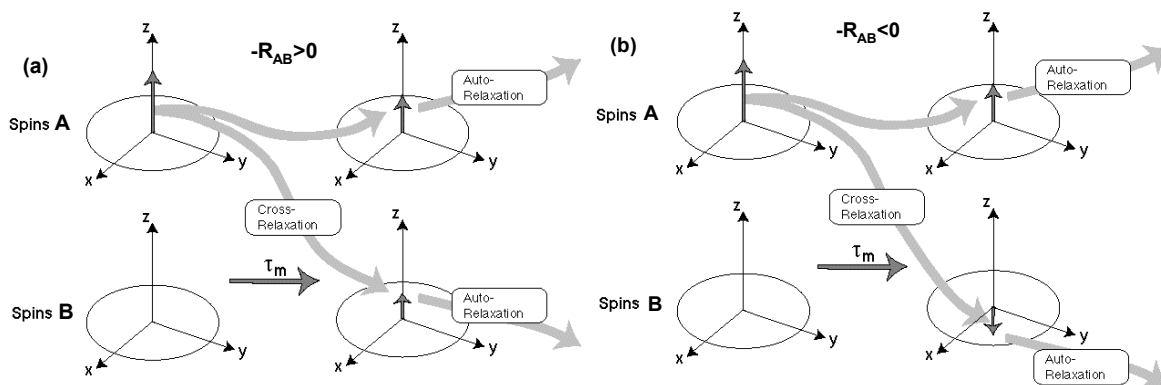


Figure 1- II-27: Visualization of the magnetization transfer process; (a) positive cross-relaxation rate in the slow motion limit, (b) negative cross-relaxation rate in the fast motion limit.¹¹⁴

3. Different kinds of NOE experiments

a) Steady-state NOE

Early 1D NOE measurements were mostly concerned with steady-state Overhauser effects obtained by selectively saturating one spin while observing the intensity changes occurring on other spins. This is expected to induce a positive enhancement in the fast motion limit. In the slow motion limit, it is expected to result in a rapid saturation of all resonances and a lack of sensitivity due to extended spin diffusion¹¹⁶ (i.e. coherent magnetization transfer via dipolar couplings).

Measurements of steady-state NOE were used to investigate structural and dynamical features in bulk polymers. Concerning the structural aspects, the studies followed a method reported at the first occurrence of intermolecular ¹H-¹H NOE experiments¹¹⁷ on a mixture of chloroform, cyclohexane and tetramethylsilane. Intermolecular ¹H-¹H steady state NOE experiments were used to probe miscibility on the molecular level in polymer blends via the proximities between protons in the different polymer chains, for polystyrene/poly(vinyl methyl ether)^{118,119} and polybutadiene/polyisoprene¹²⁰ melts. A similar work was done on a poly(ethylene oxide)/crosslinked polysiloxane semi-interpenetrated network (semi-IPN).¹²¹ Intermolecular ¹H-¹³C NOE experiments were used for the same purpose in various polymer blends.¹²²

Measurements of intramolecular ¹H-¹³C NOE were used to investigate molecular dynamics in polymer melts, either by detecting changes of motional regime by changes of NOE enhancement, or by comparing NOE enhancement variations with e.g., temperature,

with molecular dynamics models. This was done on various polymer melts: polyethylene,¹²³⁻¹²⁵ polypropylene,¹²⁶ polyisoprene,¹²⁷ polybutadiene,¹²⁸ polyoxymethylene¹²⁹.

b) Transient one-dimensional NOE

Compared to steady-state NOE, more specific information can be obtained from transient Overhauser effects where the redistribution of the magnetization is studied as a function of time after a selective inversion of one spin. The first NOE measurements, carried out on HF, were transient ^1H - ^{19}F and ^{19}F - ^1H NOE experiments.⁹⁸ In the fast motion limit, transient 1D NOE is expected to result in weak positive transient enhancement. In the slow motion limit a negative effect is expected to be rapidly washed out by extended spin diffusion.

In the slow motion limit, the initial build up rates of the NOE's depend only on the cross-relaxation coefficient between the irradiated spin and the observed nuclei and thus are directly related to the inverse of the sixth power of the internuclear distances in the three-dimensional structure of the macromolecule.¹³⁰ After reaching a maximum, the lines decay to zero via spin-lattice relaxation, thus allowing to determine spin diffusion pathways in macromolecules.¹³⁰

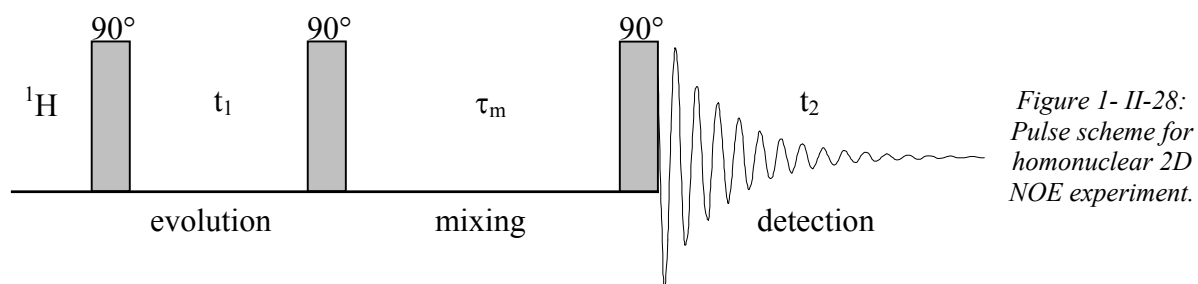
Measurements of 1D ^1H - ^{13}C transient NOE were used to investigate structural features in bulk polymers. In polystyrene and polycarbonate based glassy homopolymers the NOE originates in methyl groups, and the ^1H nuclear spin diffusion leads to decrease in build-up rate and increase in induction delay for increasing distances from the methyl group.¹³¹ In branched polyethylene melts, NOE was used to differentiate branch lengths longer than six carbons according to their respective build-up rate.¹³²

c) Two-dimensional NOE spectroscopy (NOESY)

The original idea of 2D NMR was proposed by Jeener,¹³³ while the theory and experiments were first published by Ernst's group.¹³⁴ It consists in irradiating the sample with a series of two pulses separated by a delay t_1 , before recording the FID during the time t_2 . The t_1 delay is varied and a FID is recorded for each t_1 value. A two-dimensional Fourier transform is applied to the two-dimensional signal intensity (2D since depending on t_1 and t_2), to obtain a two-dimensional spectrum.

The 2D NOE spectroscopy was introduced by Jeener, Ernst et al.¹³⁵ The pulse scheme for the homonuclear experiment is shown in Figure 1- II-28. It consists of a sequence of three non selective 90° pulses. During the variable evolution time t_1 , the components are frequency-labeled. During the fixed mixing time τ_m , cross-relaxation leads to incoherent transfer of magnetization between nearby protons through mutual dipolar interactions. In the obtained 2D spectrum, the intensity on the diagonal depends on the specific relaxation rate of each

nucleus, while the cross peaks relate the components between which magnetization was transferred to each other.



The 2D NOE technique is expected to induce weak negative cross peaks in the fast motion limit, and strong positive cross peaks in the slow motion limit (s. Figure 1- II-29).

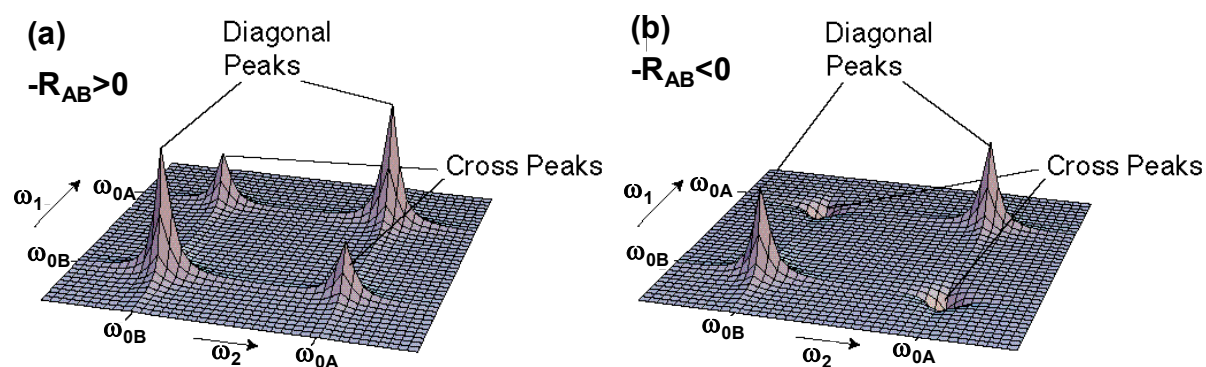


Figure 1- II-29: Schematic form of the NOESY spectrum (a) in the case of slow motion limit, (b) in the case of fast motion limit.¹¹⁴

It should be pointed out that this is opposite to what is expected in a 1D transient experiment. Indeed, the cross-relaxation rates are of same sign in both experiment, but the initial conditions are opposite. Apart from this sign, 2D and transient 1D NOE experiments produce identical enhancements for the whole course of the experiment, except for a factor of 2.¹¹⁵ 2D NOESY has a two advantages over 1D-NOE experiments:¹³⁶ since it consists in a simultaneous investigation of all NOE processes,^{112,113} it saves time and avoids problems arising from a non perfectly selective pre-irradiation. This experiment is extensively used in liquid-state NMR and predominantly applied to the investigation of biological macromolecules in solution, since it allows studies in non deuterated water, thus in native conditions.¹³⁷

2D transient ^1H - ^1H NOE spectroscopy was used under MAS to investigate slow chain motions in SBR elastomers;¹³⁸ a theory relating the cross-relaxation rate with the rotor spinning frequency and the motion correlation time(s) was developed.¹³⁹

The logical extension of 2D NOE experiment is the 3D NOE experiment. Its theoretical aspects were presented together with experimental data,¹⁴⁰ but no application to non biological macromolecules was reported up to now.

4. Equations describing the cross-relaxation between two groups of equivalent spins in NOESY

a) General case

The first relaxation equations including cross-relaxation were presented by Solomon.⁹⁸ The theory underlying two-dimensional studies of cross-relaxation and of transient nuclear Overhauser effect was detailed by Macura and Ernst.^{112,113} A clear and simple explanation of the concepts, the matricial description, and data processing in the slow motion limit is presented by Likic.¹⁴¹ The results detailed by Macura and Ernst^{112,113} will be presented here. As noted above, 2D and transient 1D NOE experiments produce identical enhancements for the whole course of the experiment (except that the 2D NOE rate is the double of the 1D one).¹¹⁵

The cross-relaxation occurring in a system composed of n_A magnetically equivalent A spins and n_B magnetically equivalent B spins with spin quantum number $I=1/2$ is considered here. The respective Larmor frequencies are noted ω_A and ω_B . The vector m , comprising the deviation of the longitudinal magnetization components from equilibrium, obeys Equation 1-II-8, where R_{xx} and R_{xy} respectively correspond to the spin-lattice relaxation rates ρ and the cross-relaxation rates σ in Solomon's notation⁹⁸; \dot{m} designates the time derivative of m .

$$\begin{pmatrix} \dot{m}_A \\ \dot{m}_B \end{pmatrix} = - \begin{pmatrix} R_{AA} & R_{AB} \\ R_{BA} & R_{BB} \end{pmatrix} \begin{pmatrix} m_A \\ m_B \end{pmatrix} \quad \text{Equation 1-II-8}$$

The elements of the cross-relaxation matrix can be expressed by the transition probabilities W , resulting from AA, AB and BB interactions, and by the external relaxation rates R_{1A} and R_{1B} , which take into account possible interactions with further spins (s. Equation 1-II-9). In this equation, the subscripts 0, 1(A) and 2 relate respectively to zero-quantum transition, single-quantum transition (with flip on A nucleus), double-quantum transition; the superscripts ij relate to both nuclei involved in the corresponding transition.

$$\begin{cases} R_{AA} = 2(n_A - 1)(W_1^{AA} + W_2^{AA}) + n_B(W_0^{AB} + 2W_{1A}^{AB} + W_2^{AB}) + R_{1A} \\ R_{AB} = n_A(W_2^{AB} - W_0^{AB}) \end{cases} \quad \text{Equation 1-II-9}$$

The transitions probabilities W obey Equation 1-II-10, with the spectral densities $J_{xy}(\omega)$ and the constants q_{xy} defined in Equation 1-II-11. In the latter, τ_C^{xy} is the correlation time of the isotropic motion which modulates the xy interaction, μ_0 is the permeability of space, γ_x is the magnetogyric ratio of spin x , \hbar is the reduced Planck's constant, and r_{xy} the internuclear xy distance. It should be noted that the equation given for the spectral density is obtained for a rigid molecule undergoing isotropic random motions.¹⁴¹ It should be pointed out

that the investigated phenomenon is local due to its dependence on the inverse sixth power of the internuclear distance.

$$\begin{cases} W_1^{xy} = \frac{3}{2} q_{xy} J_{xy}(\omega_x) & W_{1k}^{xy} = \frac{3}{2} q_{xy} J_{xy}(\omega_k) \\ W_0^{xy} = q_{xy} J_{xy}(\omega_x - \omega_y) & W_2^{xy} = 6 q_{xy} J_{xy}(\omega_x + \omega_y) \end{cases} \quad \text{Equation 1- II-10}$$

$$J_{xy}(\omega) = \frac{\tau_C^{xy}}{1 + (\omega \tau_C^{xy})^2} \text{ and } q_{xy} = \frac{1}{10} \left(\frac{\mu_0}{4\pi} \right)^2 \frac{\gamma_x^2 \gamma_y^2 \hbar^2}{r_{xy}^6} \quad \text{Equation 1- II-11}$$

The evolution of the diagonal and cross-peaks intensities with the mixing time τ_m then obeys Equation 1- II-12, where M_0 is the total equilibrium magnetization of the $n_A + n_B$ nuclei.

$$\begin{cases} a_{AA}(\tau_m) = \frac{n_A M_0}{2(n_A + n_B)} \exp(-R_L \tau_m) \left[\left(1 - \frac{R_{AA} - R_{BB}}{R_C} \right) + \left(1 + \frac{R_{AA} - R_{BB}}{R_C} \right) \exp(-R_C \tau_m) \right] \\ a_{BB}(\tau_m) = \frac{n_B M_0}{2(n_A + n_B)} \exp(-R_L \tau_m) \left[\left(1 - \frac{R_{BB} - R_{AA}}{R_C} \right) + \left(1 + \frac{R_{BB} - R_{AA}}{R_C} \right) \exp(-R_C \tau_m) \right] \\ a_{AB}(\tau_m) = a_{BA}(\tau_m) = -\frac{n_B M_0 R_{AB}}{(n_A + n_B) R_C} \exp(-R_L \tau_m) [1 - \exp(-R_C \tau_m)] \end{cases} \quad \text{Equation 1- II-12}$$

R_L and R_C are defined in Equation 1- II-13.

$$R_C = \sqrt{(R_{AA} - R_{BB})^2 + 4R_{AB}R_{BA}} \text{ and } R_L = \frac{1}{2}(R_{AA} + R_{BB}) - \frac{1}{2}R_C \quad \text{Equation 1- II-13}$$

The complicated general equation Equation 1- II-12 for the time evolution of the diagonal and cross-peaks intensities can be simplified according to several assumptions. *Only the case of slow motion limit in an homonuclear spin system will be considered here.* In the slow motion limit, $\omega_X \tau_C \gg 1$ and in an homonuclear system $(\omega_X - \omega_Y) \tau_C \approx 0$, therefore $W_1^{XY} = W_2^{XY} = 0$, and only the zero-quantum transitions contribute to cross-relaxation. They are responsible for the energy-conserving flip-flop transitions $\alpha\beta \Leftrightarrow \beta\alpha$. These transitions lead to spin diffusion and to an exchange of energy between the two spins. In that case, the cross-relaxation process is a pure spin diffusion process.¹¹² Assuming equal external relaxation rate R_1 for all nuclei, simple equations are derived for the time evolution of the diagonal and cross-peaks intensities.

b) Case of an homonuclear spin pair in the slow motion limit¹¹²

In a two-spin system AB, the zero-quantum transition probability is $W_0^{AB} = q \cdot \tau_C$, and the evolution of the diagonal and cross-peaks intensities with the mixing time τ_m obeys Equation 1- II-14.

$$\begin{cases} a_{AA}(\tau_m) = a_{BB}(\tau_m) = \frac{M_0}{4} \exp(-R_1 \tau_m) [1 + \exp(-2q_{AB} \tau_C^{AB} \tau_m)] \\ a_{AB}(\tau_m) = a_{BA}(\tau_m) = -\frac{M_0}{4} \exp(-R_1 \tau_m) [1 - \exp(-2q_{AB} \tau_C^{AB} \tau_m)] \end{cases} \quad \text{Equation 1- II-14}$$

An example of evolution of the diagonal and cross-peaks intensities with the mixing time τ_m in a two spin system in the slow motion limit is shown on Figure 1- II-30.

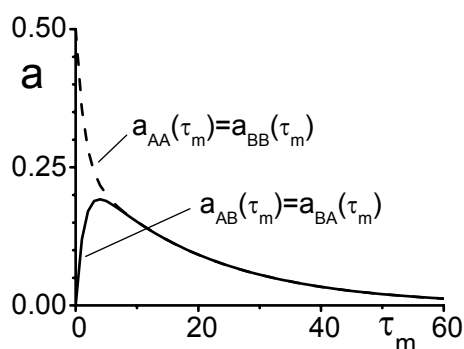


Figure 1- II-30: Example of dependence of the diagonal and cross-peaks intensities with the mixing time τ_m in a 2D NOE experiment conducted on a two spin system AB in the slow motion limit.¹¹²

c) Case of two groups of equivalent homonuclear spins A_nB_n in the slow motion limit¹¹²

In a system composed of two groups of n equivalent nuclei A_nB_n , the zero-quantum transition probability is $W_0^{AB} = n \cdot q_{AB} \cdot \tau_C^{AB}$, and the time evolution of the diagonal and cross-peaks intensities obeys Equation 1- II-15.

$$\begin{cases} a_{AA}(\tau_m) = a_{BB}(\tau_m) = \frac{M_0}{4} \exp(-R_1 \tau_m) [1 + \exp(-2nq_{AB}\tau_C^{AB}\tau_m)] \\ a_{AB}(\tau_m) = a_{BA}(\tau_m) = -\frac{M_0}{4} \exp(-R_1 \tau_m) [1 - \exp(-2nq_{AB}\tau_C^{AB}\tau_m)] \end{cases} \quad \text{Equation 1- II-15}$$

d) Cross-relaxation in other spin systems

Likic¹⁴¹ describes three- and four-spin systems in the slow motion limit, in which the influence of indirect magnetization transfer (from spin A to spin B, then to spin C) competing with cross-relaxation (direct transfer from A to C) in multi-spin systems is illustrated. It leads to multiexponential behavior of the peaks intensities, and thus to erroneous data interpretation when assuming monoexponential behavior.

A theory of transient NOE relaxation for rigid proteins in solution (with only CH_3 rotation as internal motion) was developed by Kalk and Beredsen.¹¹⁶ It shows a cross relaxation rate inversely proportional to the sixth power of the distance between the involved nuclei.

Theories were also developed to describe cross-relaxation rates in linear arrays of spins,¹⁴² and in infinite model systems composed of regular lattices or helices.¹⁴³

An exact solution for NOE enhancement intensities beyond the initial rate region can be obtained for multispin systems using matrix equations; alternatively numerical integration of the Solomon equation can be computed.¹¹⁵

III. Conclusion and strategy

The goal of this Ph.D. work is to characterize industrial pressure sensitive adhesive samples, using solid-state NMR techniques. The samples provided by Atofina are statistical poly(alkyl acrylates) copolymers, with different alkyl side chains, containing also other components (s. Part 2, I). The literature survey on PSAs (s. Part 1, I) showed that these materials are currently characterized mainly according to their macroscopic properties (adhesive, cohesive, mechanical), and that little is known about the exact relation between these macroscopic properties and the molecular chain dynamics or the crosslinking. However, it is empirically known that chain dynamics, as well as crosslinking (e.g. in the form of branching or nanophase separation) play a major role in the adhesive properties of the materials. The solid-state NMR was introduced in paragraph II, and several techniques were detailed. We will now propose several promising ways to characterize nanophase separation, branching and chain dynamics in PSA samples during this Ph.D. work.

A. Branching

Crosslinking in general is of major importance in the adhesive properties of PSAs. Crosslinking can occur in the form of covalent crosslinking (from the introduction of a crosslinker or extensive long chain branching), of hydrogen bonding between acrylic acid units and of physical crosslinking (through nanophase separation). Branching in poly(alkyl acrylates) occurs at a significantly higher level than in e.g., poly(alkyl methacrylates),¹⁴⁴ and is currently under investigation in several research groups (s. Part 2, II.C).

The branching is best quantified in poly(alkyl acrylates) using ^{13}C 1D NMR. Up to now, a solution-state technique using single pulse excitation^{145,146}, as well as a solid-state technique using cross-polarization^{147,148} have been reported. However, both present drawbacks, such as poor solubility or long measuring time. Therefore it would be useful to optimize the chain branching quantification via ^{13}C NMR. Our work on this topic will be presented and discussed in Part 2, II.B, the investigations were conducted directly on the PSA samples.

It should be emphasized here that high resolution ^{13}C NMR allows the quantification of branching, but doesn't differentiate between short chain and long chain branches, because it characterizes the structure of the branch points, which is the same for the two of them in polyacrylates.¹⁴⁹ No experimental method is known to quantify separately these two contributions. However, other methods exist which allow the detection of long chain branches. These are e.g., dynamic mechanical analysis and multiple-detection size-exclusion

chromatography (SEC). However, emulsion poly(alkyl acrylates), as a result of their polymerization process, contain a considerable portion of high molar mass and / or highly branched or crosslinked polymer (gel), which is only swellable but not completely soluble in common solvents.²⁴ Our characterization of some model samples using multiple detection SEC will be detailed in Part 2, III.E.

B. Chain dynamics

The distance from T_g and the viscoelastic properties play a major role in the adhesive properties of PSAs. Both are closely related to chain dynamics. Diverse solid-state NMR techniques allow for the characterization of chain dynamics in polymers.⁴ An elegant way to quantify chain dynamics, combined with the elucidation of molecular mechanism, was presented by Wind^{5,150,151} and Kuebler¹⁵² via 1D and 2D solid-state NMR techniques in poly(*n*-alkyl methacrylate) melts. Due to their similar chemical nature differing only in a methyl group on the backbone (s. Figure 1- III-1), these techniques could be easily applied to poly(alkyl acrylates).

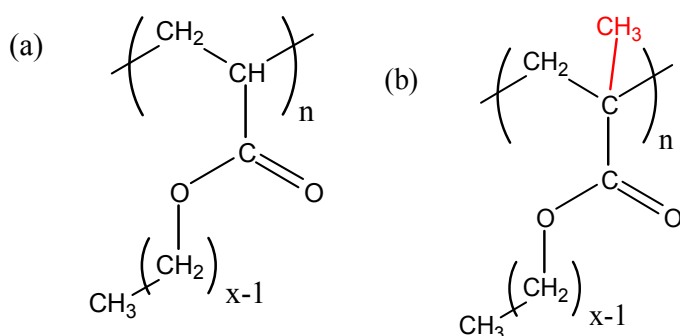


Figure 1- III-1: Chemical structure of (a) poly(*n*-alkyl acrylates) and (b) poly(*n*-alkyl methacrylates).

However, these techniques require ^{13}C and ^2H selectively labeled samples. Thus, they can not be applied directly to the industrial samples, but model samples are needed. The poly(*n*-alkyl acrylates), PnAAs, are appropriate model samples for the investigated industrial PSAs, whose major component is a poly(alkyl acrylates) copolymer. Our work concerning the synthesis of selectively labeled PnAAs is detailed in Part 2, III.C.1.

C. Nanostructuring

As stated above, crosslinking can occur in the form of physical crosslinking through nanophase separation. Physical crosslinking was extensively characterized in styrene-isoprene-styrene triblock copolymer PSAs. A similar kind of nanostructuring, by far much weaker, could occur in acrylic PSAs. Such a nanostructuring has indeed already been revealed in poly(*n*-alkyl methacrylates), PnAMAs^{5,153} (s. Part 3, I). There, the molecular motion is hindered by the presence of organized nanodomains.¹⁵⁰ Due to their similar chemical nature

(s. Figure 1- III-1), the poly(alkyl acrylates) could exhibit a similar local organization, which would influence the adhesive properties of acrylic PSAs.

^1H nuclear spin diffusion is a method of choice to investigate structuring on the nanometer length scale (s. paragraph II, H), provided one of the phases can be selected. In the case of a mobility contrast, as expected here, the dipolar filter is particularly well suited (s. paragraph II, G). In order to detect a possible nanostructuring in poly(alkyl acrylates), the ^1H nuclear spin diffusion technique with dipolar filter has to be tested first on models samples, in which a nanophase separation is present. The PnAMAs are particularly appropriate for this purpose. If this test is conclusive, the same technique could be applied to PnAAs, and then to the multicomponent PSAs. Our work using the ^1H nuclear spin diffusion technique and the dipolar filter is presented in Parts 3 to 5.

Part 2: Presentation and characterization of PSA and model samples

I.	<i>Description and characterization of the industrial pressure sensitive adhesive samples</i>	61
A.	Description	61
1.	Chemical composition.....	61
2.	Synthesis.....	63
3.	Expected copolymer structure.....	64
B.	Solid content, particle size and calorimetric properties	65
1.	Solid content and particle size.....	65
2.	Glass transition temperature.....	65
	a) Differential scanning calorimetry measurements	65
	b) Comparison with literature values	66
3.	Thermogravimetric analysis.....	66
C.	Adhesive and mechanical properties	66
D.	Chemical characterization of the samples via solid-state NMR	67
1.	¹ H spectra	67
2.	¹³ C spectra	68
	a) Single pulse excitation.....	69
	b) ¹³ C CP-MAS	69
3.	Conclusion.....	71
II.	<i>Description, synthesis and characterization of model samples</i>	71
A.	Comparison of poly(n-alkyl acrylates) and poly(n-alkyl methacrylates) ...	72
B.	Presentation of model poly(n-alkyl methacrylate) homopolymers	73
1.	Presentation of the samples	73
2.	Calculation of true molar masses	73
C.	Synthesis of model poly(n-alkyl acrylate) homopolymers	75
1.	Target poly(alkyl acrylates).....	75
2.	Free-radical polymerization of the acrylates.....	75
D.	Characterization of the poly(n-alkyl acrylate) homopolymers	76
1.	Differential scanning calorimetry and thermogravimetric analysis	76
2.	Size exclusion chromatography (SEC).....	76
3.	Branching level and tacticity	76
	a) Branching level (BL)	76
	b) Tacticity	77
III.	<i>Quantification of branching in PSA samples using ¹³C NMR</i>	78
A.	Molecular origin of branching and crosslinking in poly(alkyl acrylates) ..	79
1.	Possible branch topologies	79
2.	The origin of branching and crosslinking in poly(alkyl acrylates)	80

a)	Kinetic scheme of alkyl acrylate polymerization ^{144,185,186}	80
b)	Discussion of the branching/crosslinking origin and topology.....	82
3.	Effects of branching and crosslinking on the material properties	83
4.	Characterization of the crosslinking of homogeneous networks.....	84
B.	Choice of a ¹³C NMR technique to quantify branching in poly(alkyl acrylates).....	84
1.	Determination of chemical shifts	85
a)	Determination of chemical shifts of other components	85
b)	Line assignment for 2EHA, MA and AA monomeric units	85
2.	Solution-state NMR.....	86
a)	Published works	86
b)	Our work	87
3.	Solid-state NMR with cross-polarization	87
4.	Solid-state NMR with single pulse excitation on swollen sample	89
a)	Published works	89
b)	Our work	90
5.	Solid-state NMR with single pulse excitation in the melt.....	91
a)	Published work.....	91
b)	Our work	91
6.	Conclusion on the choice of the ¹³ C NMR technique	93
C.	Branching level quantification and discussion of the branching topology. 94	
1.	Branching quantification from ¹³ C NMR spectrum	94
a)	Published works	94
b)	Our work	95
2.	Branching topology	96
a)	Zosel's work on poly(n-butyl acrylate) latices	96
b)	McCord's work on copolymerization of poly(alkyl acrylates).....	96
c)	Chiefari's work on poly(alkyl acrylates) in solution	96
d)	Lovell's work on n-butyl acrylate and 2-ethylhexyl acrylate in emulsion and solution polymerization	97
e)	Plessis' work on the branching of n-butyl acrylate and 2-ethylhexyl acrylate during emulsion polymerization	97
f)	Farcet's work on branching of PBA in bulk and emulsion.....	98
g)	Gilbert's work on branching of PBA in emulsion	98
h)	Castignolles' work on branching of PBA and P2EHA in solution.....	99
i)	IUPAC working party on "Modeling of polymerization kinetics and processes"	99
3.	Conclusion on the branching levels and branching topology.....	99
IV.	Multiple-detection SEC of the model poly(n-alkyl acrylates)	100
A.	Overview of the possible SEC methods^{199,203}	100
B.	Determined molar masses	102
C.	Investigation of branching	103
1.	Detection of long chain branching	103
2.	Quantification of long chain branching.....	105
a)	Models.....	105
b)	Case of poly(alkyl acrylates)	106
D.	Conclusion on the multiple detection SEC investigations.....	107
V.	Conclusion on samples presentation and characterization.....	108

Part 2: Presentation and characterization of PSA and model samples

All the samples investigated during the present Ph.D. work are presented in this Part 2. Apart from the industrial PSA samples provided by Atofina, the complex solid-state NMR investigations required model samples. All the characterizations using rather fast methods will be detailed in this part. The investigations using more complex solid-state NMR methods will be presented in the following parts 3 to 5.

The industrial pressure-sensitive adhesive samples will be described in paragraph I, together with their simplest characterization. Then the available model poly(n-alkyl methacrylates) and the synthesized model poly(n-alkyl acrylates) will be presented in paragraph II, together with their simplest characterization. In paragraph III, the branching quantification in PSA samples using solid-state NMR will be detailed. In paragraph IV, the multiple detection SEC investigation of the model poly(n-alkyl acrylates) will be shown.

I. Description and characterization of the industrial pressure sensitive adhesive samples

A. Description

1. Chemical composition

The samples provided by ATOFINA (Cerdato, Serquigny, France) were obtained via emulsion copolymerization of 2-ethyl-hexyl acrylate, methyl acrylate, acrylic acid and a crosslinking comonomer (s. Figure 2- I-1). They are not commercial grades, but similar to commercial samples and synthesized for research purposes. Since the nature of the crosslinker is confidential, it will only be designated by CL below. The crosslinking is assumed not to be covalent but rather to occur via hydrogen bonds between CL monomeric units and acrylic acid monomeric units.

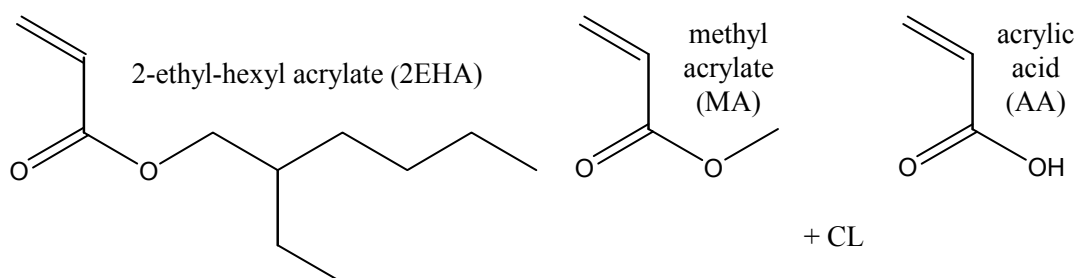


Figure 2- I-1: Comonomers used to synthesize the studied samples.

The quantitative composition of the samples is given in Table 2- I-1. The samples Copo2 and Copo3 differs only by the synthesis temperature (85 °C for Copo3, 60 °C for all other PSA samples).

Sample	Composition (wt%)
Homo2EHA	2EHA + AA (1 %)
Copo1	2EHA (80 %) + MA (19 %) + AA (1 %)
Copo2	2EHA (79.5 %) + MA (18.75 %) + AA (1 %) + CL (0.38 %) + MMA (0.38 %)
Copo3	2EHA (79.5 %) + MA (18.75 %) + AA (1 %) + CL (0.38 %) + MMA (0.38 %)

Table 2- I-1: Quantitative composition of the PSA samples.

The samples were provided in the form of a latex. The sample Copo1 contains a biocide, which prevents bacteria from growing in the sample, and should not be detected in the NMR experiments since only 0.1 % of a 0.1 % solution has been added to the sample. The crosslinker CL is added in form of a comonomer mixture containing exactly 50 % of CL and 50 % of methyl methacrylate, and the percentage given below is the percentage of CL alone and not the one of the added mixture. All the percentages given for chemicals in this work are weight percentages. It should be noted that a 80 / 20 2-ethyl-hexyl acrylate / methyl acrylate weight ratio corresponds to a 66 / 33 molar ratio. The molar masses of the polymers in the samples is expected to be higher than 500,000 g.mol⁻¹, based on confidential DMA results. Indeed, as a result of their polymerization process, emulsion poly(alkyl acrylates) contain a considerable portion of high molar mass and / or highly branched or crosslinked polymer (gel), which is only swellable but not completely soluble in common solvents, so that the molar mass distribution could only be obtained from the soluble fraction of these films).²⁴

The only additives expected to be seen during NMR measurements are the surfactants. The latex samples contain one anionic and one non-ionic surfactant, whose characteristics are given in Table 2- I-2. The role of the anionic surfactant is to provide electrostatic stability, the role of the non ionic one to provide steric stability (this one is rather soluble in the polymerizing particle as long as it is swollen with monomer). The surfactants are available in the form of an aqueous solution, with 70 % content for the non-ionic one, 30.7 % for the anionic one.

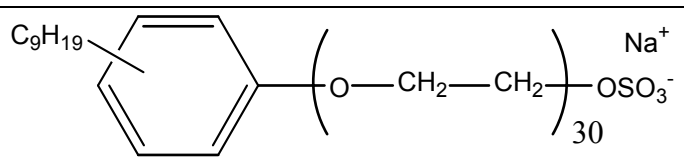
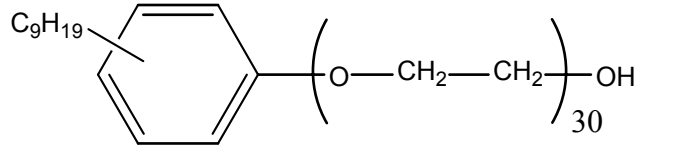
Name, type	Formula	wt% in samples
Disponil AES63IS, anionic		1 %
Disponil NP307, non ionic		1 %

Table 2- I-2: Description of the surfactants.

2. Synthesis

The samples were synthesized at Cerdato using a semi-batch (or semi-continuous) process. It is schematically described on Figure 2- I-2, a more detailed description can be found in appendix in Part 7, I.A.

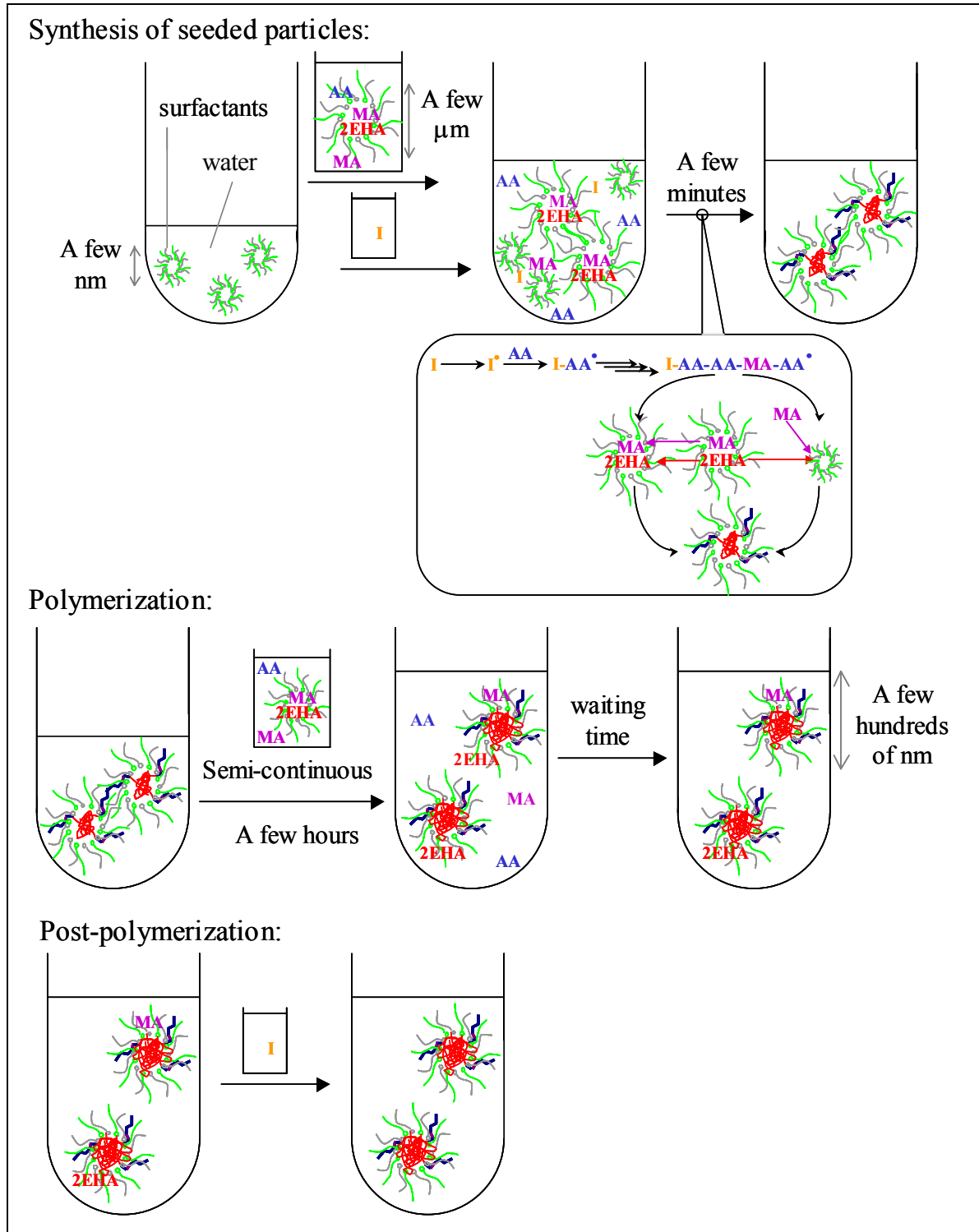


Figure 2- I-2: Schematic description of the three steps of the semi-continuous seeded emulsion polymerization of the industrial PSA samples.

3. Expected copolymer structure

In free-radical emulsion copolymerization, the homogeneity of the monomer sequences along the polymer chains depends on the reactivity ratios and the relative water solubilities of the monomers, as well as on the type of polymerization process employed.¹⁵⁴ In the case of the copolymerization of two monomers A and B, the terminal model¹⁵⁵ associated with the Q-e scheme developed by Alfrey and Price¹⁵⁶ is often used to predict the statistics of the monomeric unit sequences for some monomers. For the free radical copolymerization of 2EHA and MA, the following values can be calculated: $r_{2EHA}=0.91$ and $r_{MA}=0.94$.¹⁵⁷ These two ratios are very close to 1, meaning that a statistical copolymer should be obtained. Concerning the behavior of AA, its copolymerizations with 2EHA and MA are governed by r_{AA} values higher than 1, what would imply that AA tends to homopolymerize. Finally, the composition implied by the reactivity ratios alone would be a statistical copolymer, in which AA tends to form blocks.

However, many studies proved that the terminal model is not valid, because it doesn't take into account the influence of the penultimate unit.¹⁵⁸⁻¹⁶¹ Therefore, the Q-e scheme based on it is also not valid. Finally, the reactivity ratios for the copolymerization (r_1 and r_2 based on the terminal model) are only experimental fitting parameters, which can be used only for the pair of monomers on which they were determined. Since they have not been determined for 2EHA/MA, MA/AA or 2EHA/AA pairs, we can not apply them to our samples.

Since the microstructure of the polymer can not be determined using reactivity ratios, it can be estimated with regard to the water solubility and the type of polymerization process. The water solubilities of the three comonomers are very different (s. Table 2- I-3), therefore the polymerization tends to be heterogeneous: AA is partitioned between the aqueous and the polymer phase, while 2EHA and MA are located almost only in the latter one. Furthermore, since the initiator is water soluble, the initiation and the first steps of propagation occur in the aqueous phase, so that the monomeric units located at the end of the polymer chains are preferentially AA, and then MA.

<i>Monomer</i>	<i>Water solubility (g of monomer per 100 g of water)</i>	<i>Ref.</i>
2EHA	0.01	162
MA	5.2	163
AA	Infinite	164

*Table 2- I-3:
Solubility of
the involved
monomers in
water.*

The polymerization process implies the most homogeneous possible copolymerization: it is a semi-continuous process, under monomer-starved conditions. Consequently, a statistical copolymer is expected. Furthermore, with this process, the monomer concentration is low in

the particles during the polymerization, while the polymer concentration is high. Thus it promotes a high degree of inter- or intramolecular transfer to the already formed polymer, resulting in a branched polymer structure:¹⁴⁶ We expect a branching level of few percents of the monomeric units.

Finally, **branched statistical copolymers** are expected, with possibly a higher density of AA monomeric units at the surface of the particles and at the end of the polymer chains.

B. Solid content, particle size and calorimetric properties

A classical characterization of the samples has first been realized through measurement of the solid content and the particle size of the latices, as well as measurement of the T_g of the films. This first step had two goals: first, to be sure that the received sample didn't degrade during the transportation, and second to create a databank on the analysis of our samples with the apparatus in Mainz, in order to check the non-degradation of the samples over time. The values specified by Atofina won't be reported here for confidentiality reasons.

1. Solid content and particle size

The solid content was measured by gravimetry and the particle size by light scattering. The results for the PSA latices are indicated in Table 2- I-4.

Sample	Homo2EHA	Copo1	Copo2
Solid content	56 %	55 %	55 %
Mean particle diameter	260 ± 6 nm	214 ± 6 nm	210 ± 6 nm

Table 2- I-4: Solid content and particle size of the PSA samples.

2. Glass transition temperature

a) Differential scanning calorimetry measurements

The results of the DSC measurements are shown in Table 2- I-5. Only one T_g is detected for each sample, which is in accordance with the expected statistical character of the copolymers.

Sample	Homo2EHA	Copo1	Copo2
T_g (°C)	213 (-60 °C)	225 (-48 °C)	226 (-47 °C)
ΔC_p ($J.g^{-1}.K^{-1}$)	0.35	0.35	0.35

Table 2- I-5: T_g of the PSA samples, measured with DSC at 10 $K.min^{-1}$.

A first order endothermic peak is observed around 40 °C for the sample Homo2EHA. It is in fact the superposition of the melting peaks of the anionic and non-ionic surfactants, respectively located at 39 and 45 °C. They probably correspond to the crystallization of the oligo(ethylene oxide) units (as a comparison, pure high molar mass poly(ethylene oxide), PEO, exhibits a melting point of 65 °C). These values were measured on pure surfactants samples (available as aqueous solutions, which were freeze-dried), using the same temperature cycle as for the polymer samples. It should be noted that this peak is seen only for the homopolymer of 2EHA, which has the lowest T_g . Furthermore, this peak is clearly

seen even if the total amount of surfactants is 1 wt%, since the first order transitions (e.g. melting) are more energetic than the second order ones (e.g. glass transition).

b) Comparison with literature values

Several values can be found for the T_g of 2EHA, varying from 188 K (dilatometry¹⁵⁴) to 223 K^{162,165}, depending on the method used for the measurement. A value of 215 K measured by DSC at 20 K.min⁻¹ has been reported,¹ which is in accordance with the value reported here.

The T_g of a copolymer of two monomers A and B can be approximately calculated from several equations,¹⁶⁶ of which the probably most well known is the Fox-equation¹⁶⁷:

$$\frac{1}{T_g} = \frac{w_A}{T_{gA}} + \frac{w_B}{T_{gB}} \quad \text{Equation 2- I-1}$$

where w_A and w_B are the mass fractions of the monomeric units A and B, T_{gA} and T_{gB} are the respective glass transition temperatures of the corresponding homopolymers in Kelvin. The glass transition temperatures of the involved comonomers are given in Table 2- I-6.

Homopolymer	T_g (K)
poly(2EHA)	215 (-58 °C)
poly(MA)	295 (22 °C)
poly(AA)	403 (130 °C)

Table 2- I-6: Glass transition temperatures of the involved comonomers, measured with DSC at 20 K.min⁻¹.

A statistical copolymer of 80 % of 2EHA with 20 % MA would have a T_g of:

$$\frac{1}{T_g} = \frac{w_{2EHA}}{T_{g2EHA}} + \frac{w_{MA}}{T_{gMA}} = \frac{0.8}{215} + \frac{0.2}{295} = 0.004399, \text{ thus } T_g = 227K \text{ } (-46^\circ\text{C})$$

which is in agreement with the measured values.

As a conclusion, *all the measured T_g values are in good agreement with the values found in the literature.*

3. Thermogravimetric analysis

The results of the TGA measurements are shown Table 2- I-7.

Sample	Homo2EHA	Copo1	Copo2
Decomposition temperature (K)	399 (T_g+186 K)	375 (T_g+151 K)	381 (T_g+155 K)

Table 2- I-7: Characterization of the PSA samples with TGA.

At temperatures higher than the measured decomposition temperature, transesterification could occur in the samples.¹⁶⁸ Therefore it was chosen not to exceed T_g+110 K in the investigations done in the present Ph.D. work.

C. Adhesive and mechanical properties

The mechanical and adhesive properties of films cast from the PSA samples were investigated at Cerdato. For testing the adhesive properties, the latex samples were coated to a poly(ethylene terephthalate) backing. With this setup, rolling ball tack, loop tack, 180° peel

adhesion, static shear and SAFT tests were done (s. Part 1, I.C. for a description of the tests). The results of these tests are confidential.

The following mechanical properties of the PSA samples were investigated at Cerdatto: master curves representing the storage and loss moduli (G' and G'') as a function of the frequency, the dependence of storage and loss moduli on the temperature, the dependence of the $\tan \delta$ value (ratio of the G' to the G'' moduli) on the temperature (s. Part 7, III.A for a short reminder of viscoelastic properties). These mechanical properties are confidential.

It sometimes happens that a sample exhibits a higher G' value in the rubber plateau than other samples (indicating that it is more crosslinked), but also a worse cohesion. A possible explanation would be an heterogeneous distribution of the crosslinking points in the sample, preventing the crosslinking points to percolate in the material (s. Figure 2- I-3).

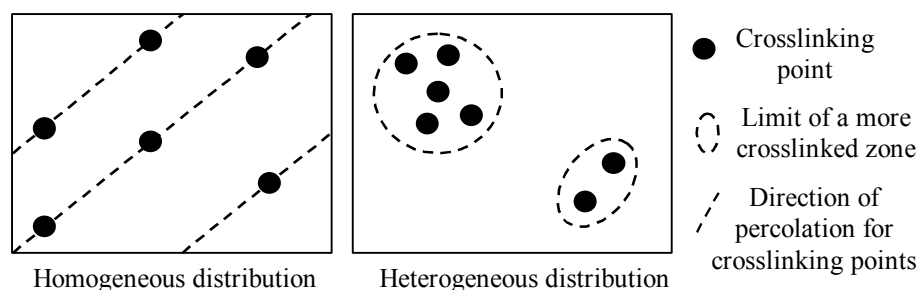


*Figure 2- I-3:
Possible distributions
of the branching
points in PSA
samples.*

D. Chemical characterization of the samples via solid-state NMR

1. 1H spectra

The chemical structure of the samples was studied using 1H solid-state NMR. A good resolution was achieved by recording the spectra with single pulse excitation, at a 1H Larmor frequency of 500.13 MHz, using fast MAS. The lines of the spectra were assigned to the corresponding 1H nuclei of the polymer (s. Figure 2- I-4 for the assignment and Figure 2- I-5 for the proton identification by number of the next carbon atom), according to incremental calculations of the chemical shift for each proton.

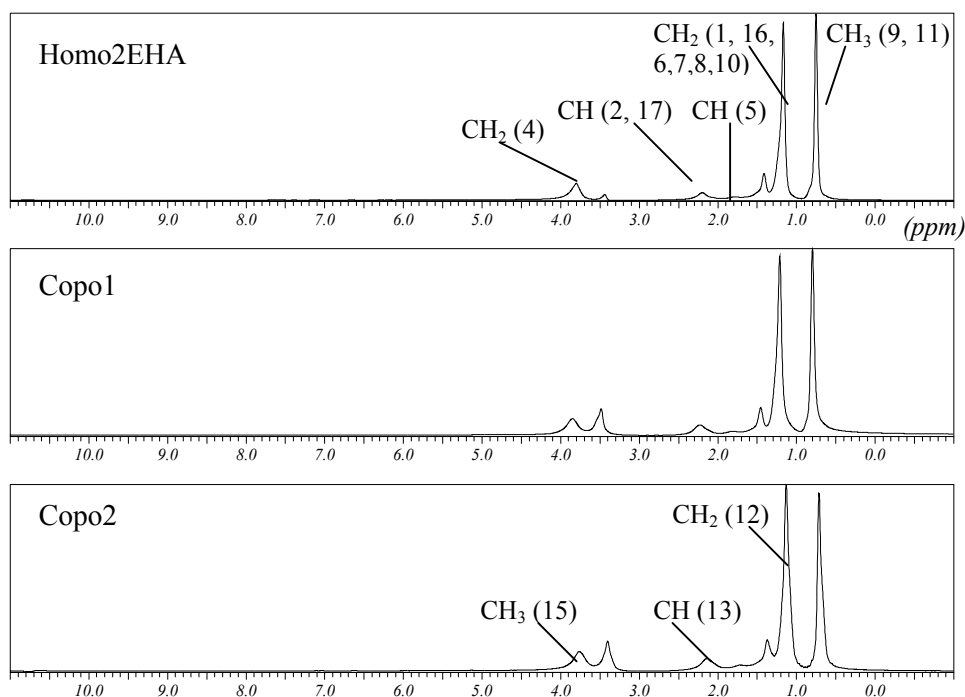


Figure 2- I-4: ^1H solid-state NMR spectra of the PSA samples, ^1H frequency: 500.13 MHz, 60 °C, 25 kHz MAS (80 °C and 12 kHz MAS for sample Copo1); the line assignment is the same for Copo1 and Copo2, it contains also the lines assigned for Homo2EHA.

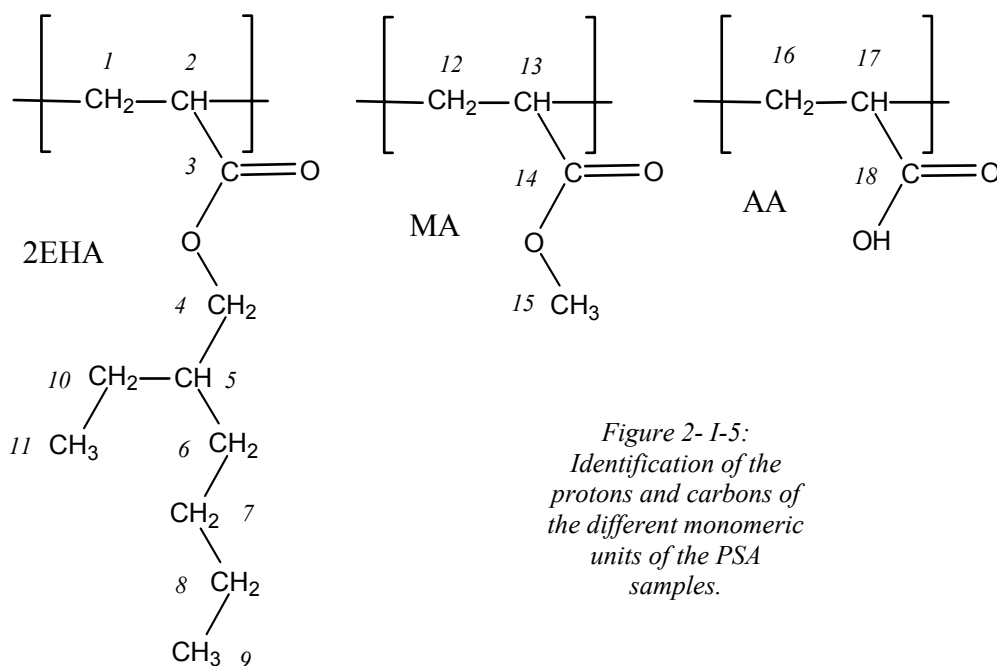


Figure 2- I-5: Identification of the protons and carbons of the different monomeric units of the PSA samples.

2. ^{13}C spectra

The chemical structure of the samples was also studied using ^{13}C solid-state NMR. There are two classical methods to obtain one-dimensional ^{13}C spectra, combined with MAS: single pulse excitation and cross-polarization (CP-MAS) (s. Part 1, II.C and D. for more details).

a) Single pulse excitation

The lines were assigned to the corresponding ^{13}C atoms of the different monomeric units (s. Figure 2- I-6), according to incremental calculations of the chemical shift for each ^{13}C nucleus (s. paragraph E.1.).

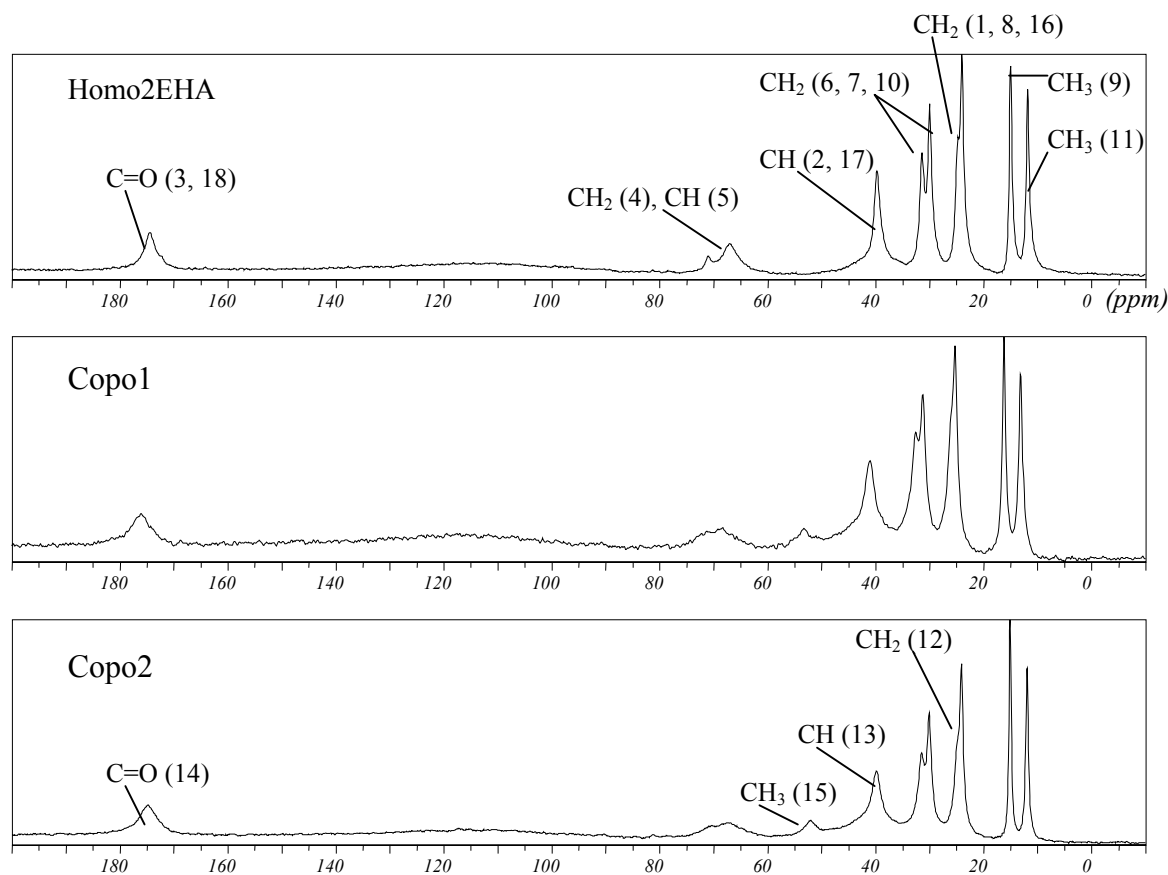


Figure 2- I-6: ^{13}C single pulse excitation NMR spectra of the PSA samples, ^1H frequency: 300.13 MHz, 5 kHz MAS, room temperature; the line assignment is the same for Copo1 and Copo2, it contains also the lines assigned for Homo2EHA.

b) ^{13}C CP-MAS

For each sample, the CP contact time was varied, in order to study its influence on the intensities of the lines (s. Figure 2- I-7 to Figure 2- I-9). The lines of the spectra are located at the same chemical shifts as the lines obtained by single pulse experiments.

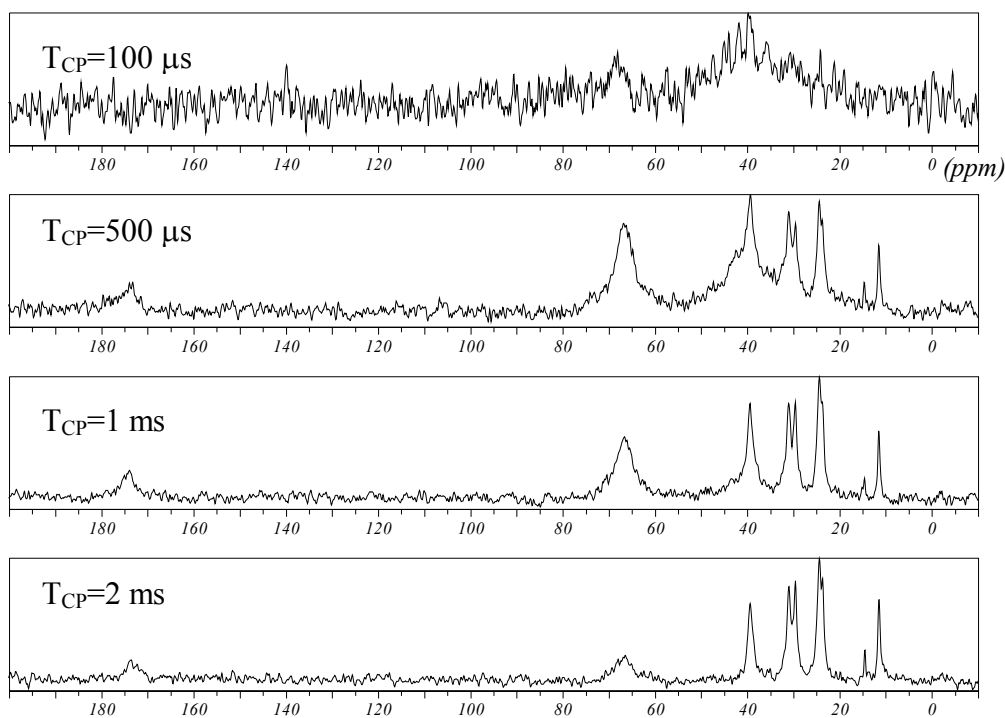


Figure 2- I-7: ^{13}C CP-MAS spectra of the sample Homo2EHA recorded for different CP contact times, ^1H frequency: 300.13 MHz, 5 kHz MAS, room temperature.

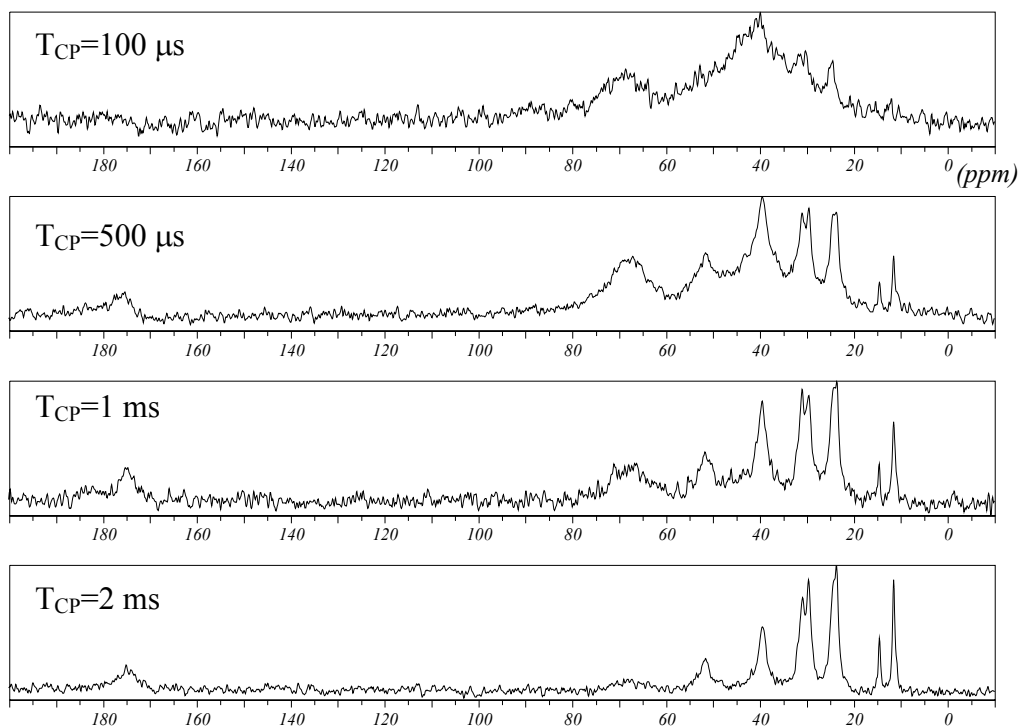


Figure 2- I-8: ^{13}C CP-MAS spectra of the sample Copo1 recorded for different CP contact times, ^1H frequency: 300.13 MHz, 5 kHz MAS, room temperature.

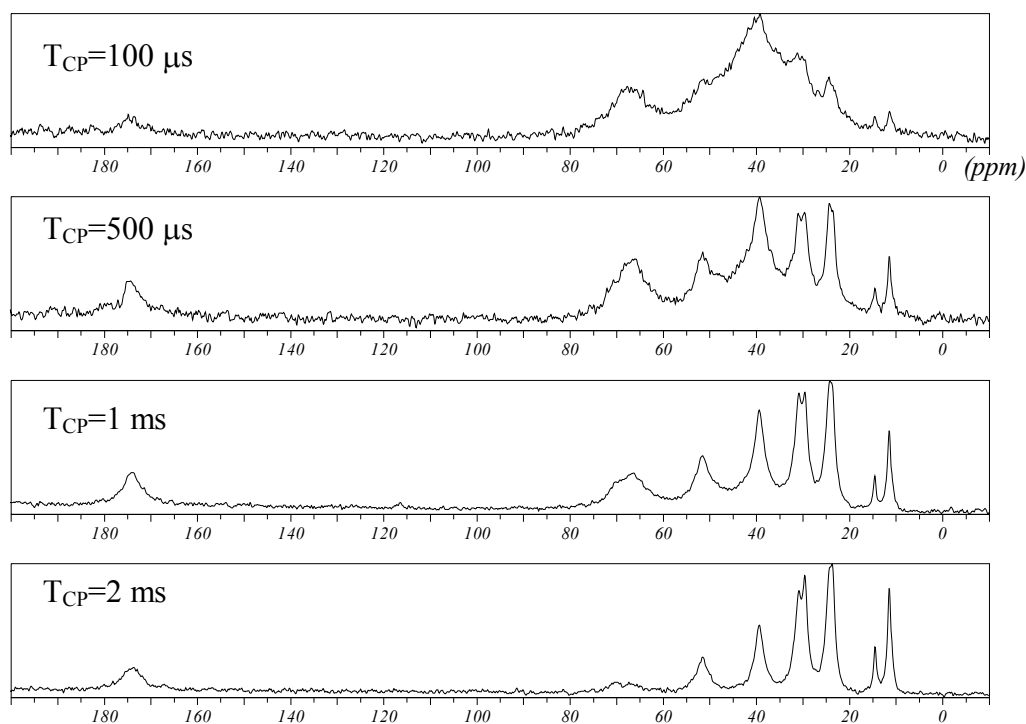


Figure 2- 1-9: ^{13}C CP-MAS spectra of the sample Copo2 recorded for different CP contact times, ^1H frequency: 300.13 MHz, 5 kHz MAS, room temperature.

At least one broad line can be distinguished from the noise for the samples Copo1 and Copo2, what is not the case for the sample Homo2EHA. This can be explained by the higher rigidity of the first two samples, which have a higher T_g due to the presence of the MA comonomer.

3. Conclusion

It has been checked by ^1H and ^{13}C solid-state NMR spectroscopy that the chemical structure of the industrial sample corresponds to the one expected from monomers used in the synthesis.

Furthermore, it is observed that at room temperature single pulse excitation gives significantly higher signal-to-noise ratio and resolution than CP for the investigated PSA samples.

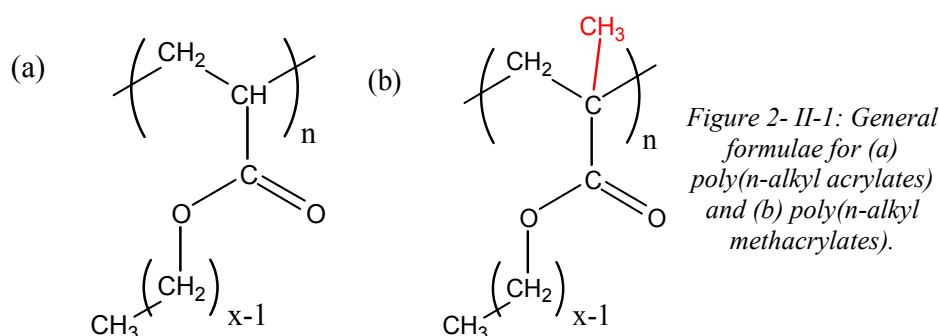
II. Description, synthesis and characterization of model samples

The model samples are poly(n-alkyl methacrylates), PnAMAs and poly(n-alkyl acrylates), PnAAs. All were used as model samples for the investigations using the dipolar filter. Furthermore, ^{13}C and ^1H selectively labeled PnAAs were meant to be used as model samples for the investigations of chain dynamics. PnAAs and PnAMAs in general will be compared first in paragraph A. Then, the PnAMAs available in our group will be described in

paragraph B. Finally, the synthesis and characterization of PnAAs will be detailed in paragraphs C and D.

A. Comparison of poly(n-alkyl acrylates) and poly(n-alkyl methacrylates)

The poly(n-alkyl acrylates), PnAAs, and poly(n-alkyl methacrylates), PnAMAs, have a very similar chemical structure, since they only differ in a methyl group on the backbone (s. Figure 2- II-1).



Nevertheless, the presence or absence of the methyl group gives rise to very different physical properties for the two families of polymers. In particular, the PnAMAs have a much stiffer backbone, so that the dynamics of the polymer chains is much slower than in PnAAs; this results in a much higher T_g for the PnAMAs with small alkyl side chains (shorter than 8 carbons, s. Figure 2- II-2). It should be noted that the tacticity has an influence on the T_g of the polymer only for PnAMAs.¹⁶⁹ PnAAs produced by free-radical polymerization are atactic, while PnAMAs produced by free-radical polymerization have a high syndiotactic content.

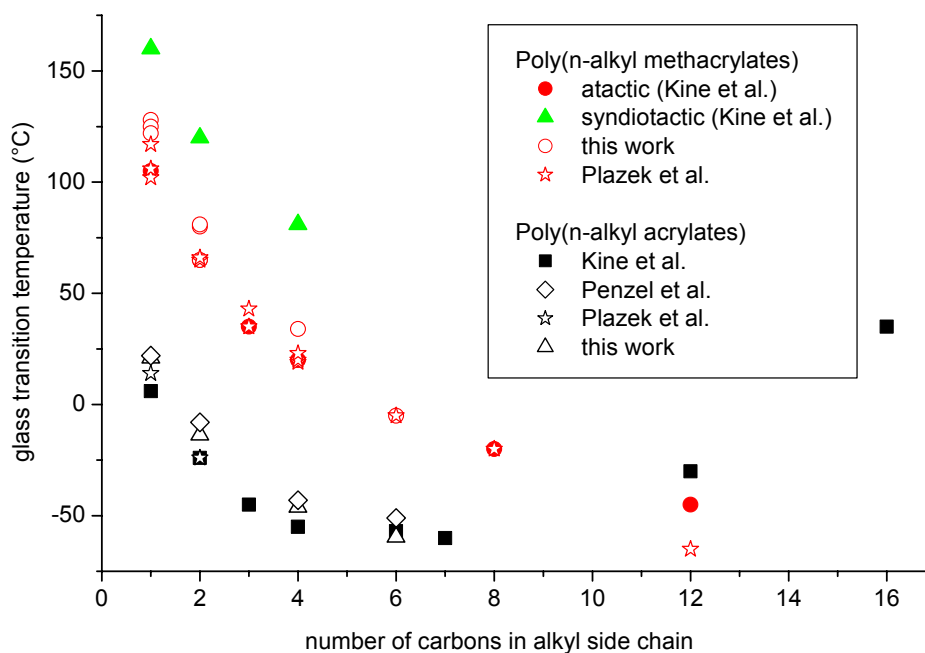


Figure 2- II-2: Glass transition temperature of PnAAs and PnAMAs as a function of the length of the alkyl side chain, from Kine et al.¹⁶², Plazek et al.¹⁶⁹, Penzel et al.¹ and this work.

Besides these very different physical properties, the two families of polymers have a polar backbone (including the carbonyl group) and flexible non polar alkyl side chains in common. Therefore similar dynamic and structural features as the ones observed in PnAMAs could be present also in PnAA's. It has to be noted that *comparison studies carried out on PnAMAs and PnAAs have to be conducted not at the same temperature, but at the same temperature difference relative to T_g* . In particular, since the long term goal of our study is to investigate PSA samples at room temperature, corresponding to T_g+70 K, the investigation of the model samples should be centered at T_g+70 K.

B. Presentation of model poly(n-alkyl methacrylate) homopolymers

1. Presentation of the samples

The model poly(n-alkyl methacrylate), PnAMA, samples were provided by Wind. They were obtained by free-radical polymerization. The glass transition temperature (T_g) was measured with differential scanning calorimetry (DSC) at $10 \text{ K}\cdot\text{min}^{-1}$. Furthermore, all samples have a high tendency to syndiotacticity (60 to 70 % of rr triads were measured with high resolution NMR in solution in CDCl_3 , s. Part 7, III.B. for definitions and notations). More details can be found in the Ph.D. thesis of Wind⁵ and Kuebler¹⁵².

Sample	Polymer, label	T_g (K)
PMMADMC	poly(ethyl methacrylate), ^2H on main chain (100 %)	398 (125 °C)
PEMA	poly(ethyl methacrylate), no label	342 (69 °C)
PEMA13C	poly(ethyl methacrylate), ^{13}C at C=O (20 %)	338 (65 °C)
PEMADSC	poly(ethyl methacrylate), ^2H on side chain (100 %)	353 (80 °C)
PEMADMC	poly(ethyl methacrylate), ^2H on main chain (100 %)	345 (72 °C)
PBMA	poly(n-butyl methacrylate), no label	302 (29 °C)
PBMA13C	poly(n-butyl methacrylate), ^{13}C at C=O (20 %)	307 (34 °C)
PHMA13C	poly(n-hexyl methacrylate), ^{13}C at C=O (20 %)	277 (4 °C)

Table 2- II-1: Presentation and glass transition temperature of the model PnAMAs.

2. Calculation of true molar masses

The average molar masses M_n and M_w were determined using size exclusion chromatography (SEC) calibrated with PMMA standards, in THF at room temperature.^{5,152} As will be detailed in paragraph IV.A, the conventional calibration done with PMMA standards yields true molar masses only if the investigated polymers are of same chemical nature, i.e. PMMA. In the case of PEMA, PBMA, PHMA, the true molar masses can be calculated from those determined with PMMA calibration by using universal calibration. The universal calibration equation of Benoît,^{170,171} $[\eta]_A \cdot M_A = [\eta]_B \cdot M_B$, is combined with the Mark-Houwink-Sakurada (MHS) equation, $[\eta] = K \cdot M^\alpha$, where $[\eta]$ is the intrinsic viscosity, M the molar mass, K and α the MHS parameters which can be found in the literature. Equation 2- II-1 is

obtained, which allows to convert the molar mass M_{PMMA} determined for polymer X using PMMA calibration into the true molar mass M_X of polymer X.¹⁷²

$$M_X = \left(\frac{K_{\text{PMMA}}}{K_X} M_{\text{PMMA}}^{\alpha_{\text{PMMA}}+1} \right)^{\frac{1}{\alpha_X+1}} \quad \text{Equation 2- II-1}$$

The MHS parameters K and α are given in Table 2- II-2 for the investigated PnAMAs. It should be noted that the parameter given for PMMA, PEMA and PBMA are recommended by the IUPAC working party on “modeling of polymerization kinetics and processes”, and thus selected among different literature values. On the contrary, the parameters given for PHMA are extracted from a single literature source.

Sample	$K \cdot 10^5$ (dL.g ⁻¹)	α	ref.
PMMA	9.44	0.719	¹⁷³
PEMA	9.70	0.714	¹⁷³
PBMA	14.8	0.664	¹⁷³
PHMA	1.94	0.76	¹⁷⁴

Table 2- II-2: Mark-Houwink-Sakurada (MHS) parameters for investigated PnAMAs in THF at 30 °C.

Using Equation 2- II-1, the true molar masses were calculated from the molar masses previously determined using conventional calibration with PMMA standards.

Sample	PMMA calibration ^{5,152}			True molar masses			Difference (%)	
	M_n	M_w	M_w/M_n	M_n	M_w	M_w/M_n	M_n	M_w
PMMADMC	68 300	124 500	1.83	-	-	-	-	-
PEMA	112 900	153 300	1.36	115 000	156 200	1.36	1.8	1.9
PEMA13C	54 500	120 000	2.20	55 400	122 200	2.21	1.6	1.8
PEMADSC	117 100	170 000	1.46	119 300	173 300	1.45	1.8	1.9
PEMADMC	76 400	105 700	1.38	77 700	107 600	1.38	1.7	1.8
PBMA	44 600	80 400	1.80	48 500	89 100	1.84	8.7	9.8
PBMA13C	125 700	203 300	1.83	141 400	232 400	1.64	11.8	13.4
PHMA13C	129 800	278 800	2.15	65 500	138 300	2.11	-65.8	-76.4

Table 2- II-3: Molar masses of the model PnAMAs; M_n and M_w are given in g.mol⁻¹; the error is calculated with respect to the average of the two values.

It is observed that the difference between the molar masses obtained using PMMA calibration and the true molar masses is very low for PEMA samples (lower than 2 percents); it is lower than the experimental error coming from the SEC analysis itself, evaluated at roughly 5 to 10 % for M_w and 15 to 20 % for M_n .¹⁷⁵ It should be noted that a difference in tacticity could lead to an additional 20 % error in the case of PEMA,¹⁷⁶ but that the PMMA standards and the investigated PEMA samples had a similar syndiotactic content. In this case, the use of the molar masses determined using PMMA calibration introduces a negligible error. It is not the case of the PBMA samples, for which the introduced error is approximately as high as the experimental error, and can not be neglected any more. However, the order of magnitude of the measured value is still valid. In the case of PHMA sample on the contrary, the molar masses determined using a PMMA calibration are totally erroneous. An error larger

than 60 % is observed with respect to average of the two molar masses, which corresponds to an error of 100 % with respect to the true molar masses. Therefore it is necessary in the case of PHMA samples to consider the universal calibration and recalculate the true molar masses. The difference in behavior of model PnAMAs might be attributed a different solubility in THF at 30 °C.

It should be noted that the molar masses are high enough to have no influence on the local chain dynamics investigated in Parts 3 to 5.

C. Synthesis of model poly(n-alkyl acrylate) homopolymers

1. Target poly(alkyl acrylates)

Model poly(alkyl acrylates) were needed for studying the chain dynamics and for the investigations using the dipolar filter (s. Part 1, III.C). Our aim was to synthesize alkyl acrylates homopolymers with different linear alkyl side chains (s. Figure 2- II-1(a)) to study the influence of alkyl side chain length. Since these polymers tend to crystallize for alkyl side chains longer than octyl,¹⁷⁷ we decided to synthesize the homopolymers with the following alkyl side chains: methyl (PMA, x=1), ethyl (PEA, x=2), butyl (PBA, x=4), hexyl (PHxA, x=6).

Apart from the non labeled polymers, it would have been interesting to synthesize also labeled ones for the investigation of the chain dynamics (s. Part 1, III.B). However, the synthesis of labeled alkyl acrylates turned out to be much more time consuming than the one of labeled methacrylate monomers (s. Part 7, I.B.2), and thus too time consuming for a Ph.D. work where the main focus is on characterization. Therefore we decided to synthesize only non labeled samples and to study them using appropriate NMR methods to spare synthetic efforts.

The model samples have to be as similar as possible to the industrial ones (e.g., concerning the branching level and the broad molar mass distribution). Therefore we chose to homopolymerize the n-alkyl acrylates using conventional free-radical polymerization and not controlled free-radical polymerization or anionic polymerization. To avoid the presence of surfactants in the model samples, we chose to carry out the polymerizations in toluene solution and not in emulsion.

2. Free-radical polymerization of the acrylates

Each n-alkyl acrylate has been polymerized as a 4.7 mol.L⁻¹ solution in toluene initiated by 0.5 mol% of AIBN with respect to the acrylic monomer. The polymerization has been carried out at 60 °C under nitrogen for 20 hours. The obtained polymers were purified by precipitation at low temperature. More details can be found in appendix in Part 7, I.B.1.

D. Characterization of the poly(n-alkyl acrylate) homopolymers*1. Differential scanning calorimetry and thermogravimetric analysis*

Differential scanning calorimetry (DSC) and thermogravimetric analysis (TGA) were carried out at 10 °C.min⁻¹. The results of DSC and TGA are given in Table 2- II-4. The detected T_g is in accordance with the values found in the literature for each sample (taking into account the influence of the heating rate on the detected T_g).

<i>Sample</i>	PMA	PEA	PBA	PH _x A
<i>T_g (K) DSC, 10 K.min⁻¹</i>	294 (21 °C)	259 (-14 °C)	227 (-46 °C)	213 (-60 °C)
<i>T_g (K) 20 K.min⁻¹</i>	295	265	230	222
<i>Decomposition temperature (TGA, K)</i>	500 (T _g +206 K)	507 (T _g +248 K)	514 (T _g +288 K)	520 (T _g +307 K)

*Table 2- II-4:
Characterization
of the model
PnAAs using DSC
and TGA.*

It should be noted that decomposition of the PBA and PH_xA samples was observed during NMR measurements after several hours at ca T_g+150 K.

2. Size exclusion chromatography (SEC)

Poly(alkyl acrylates) can not be properly characterized using SEC with conventional calibration (s. paragraph IV). Multiple detection SEC has to be used for the determination of the molar masses. The investigations done using multiple detection SEC require a short presentation of the possible multiple detection techniques, and allow to draw conclusions also concerning branching in the samples. Therefore, they will be detailed in the separate paragraph IV.

3. Branching level and tacticity

The tacticity and the branching level of the model PnAAs were measured on ¹³C *solution-state* NMR spectra of the samples dissolved in CDCl₃ at a ¹³C frequency of 125.76 MHz.

a) Branching level (BL)

According to the literature, the chain branching is much higher in poly(alkyl acrylates) than in e.g. poly(alkyl methacrylates) or polystyrene: it can reach a few percents of the monomeric units (s. paragraph III, C.2). The branching level (BL, in percents of the monomeric units) is measured by dividing the hundredfold of the area of the branched quaternary carbon line in a ¹³C spectra with the sum of the areas of this carbon and the corresponding non-branched tertiary carbons on the same spectrum (s. Figure 2- II-3).

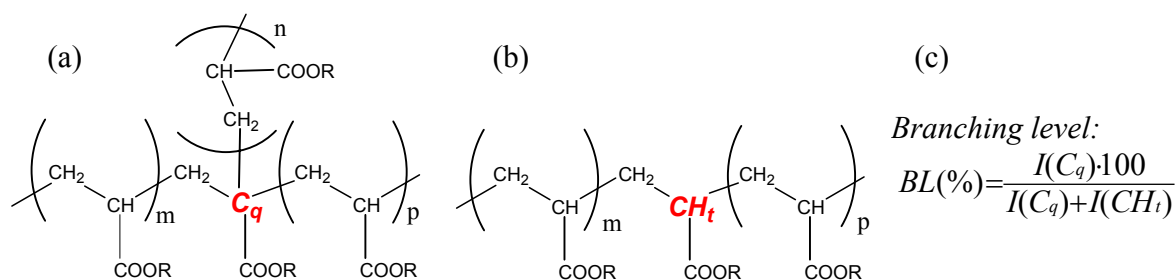


Figure 2- II-3: Branching in poly(alkyl acrylates), R=alkyl; (a) branched chain with a quaternary carbon C_q , (b) linear chain with the corresponding tertiary carbon CH_t , (c) formula used to calculate the branching level.

The ^{13}C chemical shifts assignment (including the branched C_q carbon) can be found in the literature at 47.2-48.4¹⁴⁹ and 46.5-48.0¹⁷⁸ ppm for PBA and at 47.2-48.4¹⁴⁵ and 48.0¹⁴⁸ ppm for P2EHA, for solution-state and solid-state NMR. Since the chemical structure of the PnAAs are similar, the ^{13}C chemical shifts of the C_q carbon in the four model polymers are similar. The integration of C_q and CH_t signals was done for the model PMA, PEA, PBA and PHxA. The representative example of PEA is given in Figure 2- II-4 and all the results are given in Table 2- II-5.

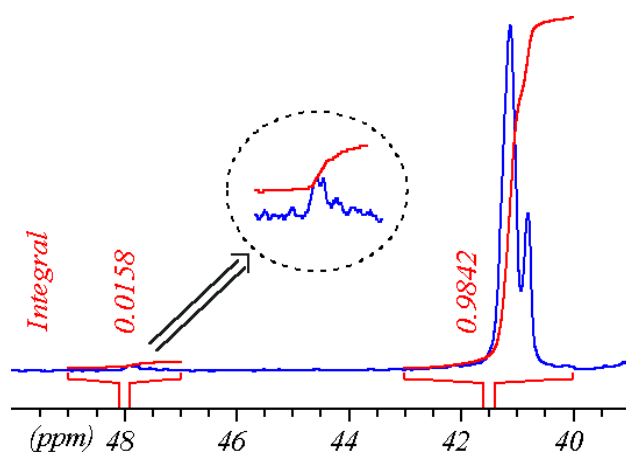


Figure 2- II-4: Integration of branched C_q and non branched CH_t for the model PEA (^{13}C solution-state NMR at 125.76 Hz in CDCl_3 , at room temperature).

Sample	BL (%)	δ of C_q (ppm)
PMA	2.1 ± 0.5	47.1 to 47.9
PEA	1.6 ± 0.5	47.4 to 48.1
PBA	2.3 ± 0.5	47.1 to 48.4
PHxA	1.8 ± 0.5	47.2 to 48.4

Table 2- II-5: Branching levels for the model PnAAs.

b) Tacticity

Definitions and notations are detailed in appendix (s. Part 7, III.B). For PMA, the different triads can be detected on the CH line at 41.3-41.6 ppm. Incomplete¹⁷⁹ and complete¹⁸⁰ assignments of the different triads can be found in the literature. For PEA, PBA and PHxA the different triads can be detected on the O- CH_2 line at 60.4-60.6 ppm for PEA, at 64.4-64.6 ppm for PBA and PHxA. The assignment can be found in the literature for PEA¹⁷⁹, PBA¹⁸⁰ and poly(pentyl acrylate)¹⁸¹. Since it is the same for PBA and poly(pentyl acrylate), it

is assumed to be the same also for PBA and PHxA. The integration of the triad signals was done for the model PMA, PEA, PBA and PHxA. The representative examples of PMA and PHxA are given in Figure 2- II-5 and all the results are given in Table 2- II-6.

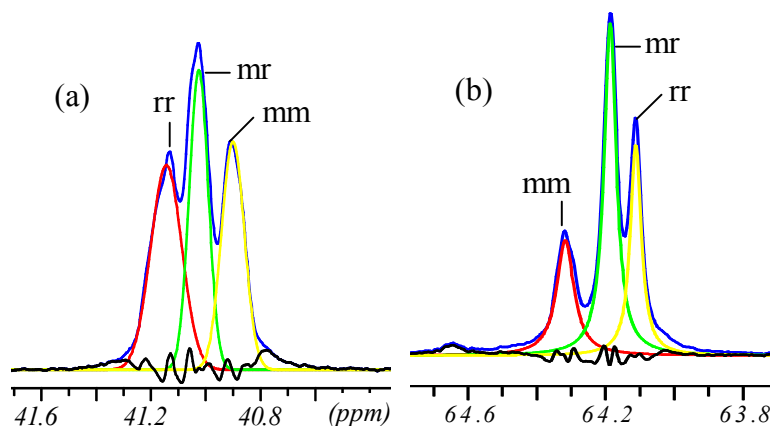


Figure 2- II-5: Integration of triads signals for (a) PMA and (b) PHxA (^{13}C solution-state NMR spectra at 125.76 MHz in CDCl_3 , at 29 and 33 $^{\circ}\text{C}$); the curves in black are the recorded spectrum and the difference of it and of the fitted lines; the curves in red, green and yellow are the fitted lines.

Sample	δ (ppm)	Assignment	Content (%)	Tacticity
PMA	41.14	rr	36.8	atactic (tendency to syndio- and isotacticity)
	41.02	mr	33.1	
	40.90	mm	30.1	
PEA	60.37	rr	23.2	atactic
	60.23	mr	51.3	
	60.15	mm	25.5	
PBA	64.31	mm	20.8	atactic (slightly isotactic)
	64.18	mr	52.0	
	64.10	rr	27.2	
PHxA	64.32	mm	23.9	atactic
	64.19	mr	48.5	
	64.11	rr	27.6	

Table 2- II-6: Tacticity of the model PnAAs.

n.b.: The spectra were first recorded at a frequency of 75.47 MHz, but the signal-to-noise ratio (S/N) obtained in one week-end at 50 $^{\circ}\text{C}$ was sufficient to quantify only the tacticity, and not the branching level.

III. Quantification of branching in PSA samples using ^{13}C NMR

Branching in poly(n-alkyl acrylates) is not fully understood and cannot be controlled, nor avoided in free-radical polymerization. Branching characterization is a relevant issue in polymeric materials in general, as it has a significant influence on the material properties.¹⁸²

^{13}C NMR spectroscopy (solid-state or solution-state) allows to quantify branching in polymeric samples. However, ^{13}C NMR spectroscopy is highly sensitive to short- and mid-chain branching but typically cannot distinguish branches of 6 carbon atoms or more.¹⁸² High resolution NMR indeed characterizes the structure of the branch points, which is the same for all of them.¹⁴⁹ SEC and rheological measurements are both sensitive to long chain branching

in the molecule at branch lengths of about 20 carbon atoms or more.¹⁸² It thus becomes evident that no single analytical technique can uniquely describe the complete branching state of a macromolecule.¹⁸² Spectroscopic (¹³C NMR) and chromatographic (multiple detection SEC) techniques can supplement each other, as neither is capable of fully describing the molecular architecture imparted by the various types of branching.¹⁸²

Our investigation of branching in poly(alkyl acrylates) samples is composed of two parts. The ¹³C NMR investigations aim to quantify the total branching level (s. this paragraph), and the multiple detection SEC investigations aim to gain information on the branching topology (s. paragraph IV).

Concerning the ¹³C NMR investigations, our aim was to propose a fast method for branching quantification, directly applicable to the industrial PSA samples. The branching is best quantified in poly(alkyl acrylates) using ¹³C 1D NMR. Up to now, a solution-state technique,^{146,183} as well as a solid-state technique^{147,148} in 28 h have been reported to quantify the branching. However, both exhibit drawbacks, respectively solubility problems and long measuring time. Therefore it would be useful to optimize the chain branching quantification via ¹³C NMR. The molecular origin of branching in polyacrylates will be presented in paragraph A. Then literature survey and our work will be presented and compared, first concerning the possible NMR techniques to measure branching (s. paragraph B), then concerning the branching levels and branching topology (s. paragraph C).

A. Molecular origin of branching and crosslinking in poly(alkyl acrylates)

1. Possible branch topologies

In order to understand the different possible branch topologies, a few definitions from the “glossary of basic terms in polymer science” published by IUPAC¹⁸⁴ are cited below. A *branch* is defined as an oligomeric or polymeric offshoot from a macromolecular chain. A *branch point* is a point on a chain at which a branch is attached (in a network, it may be termed *junction point*). A *short-chain branch* is an oligomeric branch, i.e. a branch having an intermediate molecular weight and essentially comprising a small plurality of units derived, actually or conceptually, from molecules of low relative molecular mass. A *long-chain branch* is a polymeric branch, i.e. a branch having a high relative molecular mass and essentially comprising the multiple repetition of units derived, actually or conceptually, from molecules of low relative molecular mass. A *star macromolecule* is a macromolecule containing a single branch point from which linear chains (i.e. arms) emanate. A *comb macromolecule* is a macromolecule comprising a main chain with multiple trifunctional branch points, from each of which a linear side chain emanates; if at least some of the branch

points are of functionality greater than three, the macromolecule is a *brush macromolecule*. A branched macromolecule should not be mistaken for a *graft macromolecule*, i.e. a macromolecule with one or more species of block connected to the main chain as side-chains, these side-chains having constitutional or configurational features that differ from those in the main chain.

The possible branch topologies are illustrated on Figure 2- III-1. A particular branch topology is also included, in which multiple branching leads to a “tree-geometry”, with branches on branches; this topology is typical of low density polyethylene (LDPE).

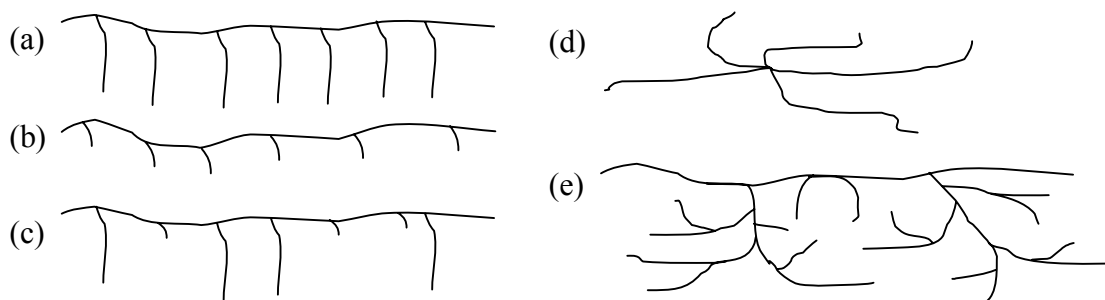


Figure 2- III-1: Possible branch topologies; (a) comb macromolecule with long-chain branches, (b) comb macromolecule with short-chain branches, (c) comb macromolecule with long- and short-chain branches, (d) star macromolecule, (e) “tree-geometry” originating in multiple branching and resulting in branches on branches.

2. The origin of branching and crosslinking in poly(alkyl acrylates)

The kinetic scheme of alkyl acrylate polymerization is presented first, before a discussion on the origin of branching and crosslinking topology.

a) Kinetic scheme of alkyl acrylate polymerization^{144,185,186}

The kinetic scheme of alkyl acrylate polymerization is shown in the next figures: initiation (s. Figure 2- III-2), propagation (s. Figure 2- III-3), termination (s. Figure 2- III-4), transfer reactions (s. Figure 2- III-5) and other side reactions (s. Figure 2- III-6).

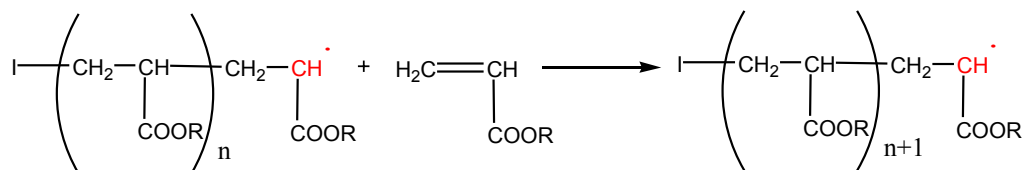
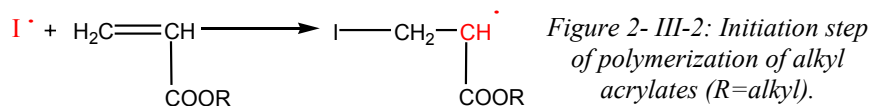


Figure 2- III-3: Propagation step of polymerization of alkyl acrylates (head-to-tail addition, R=alkyl).

Part 2, III Branching quantification in PSA samples

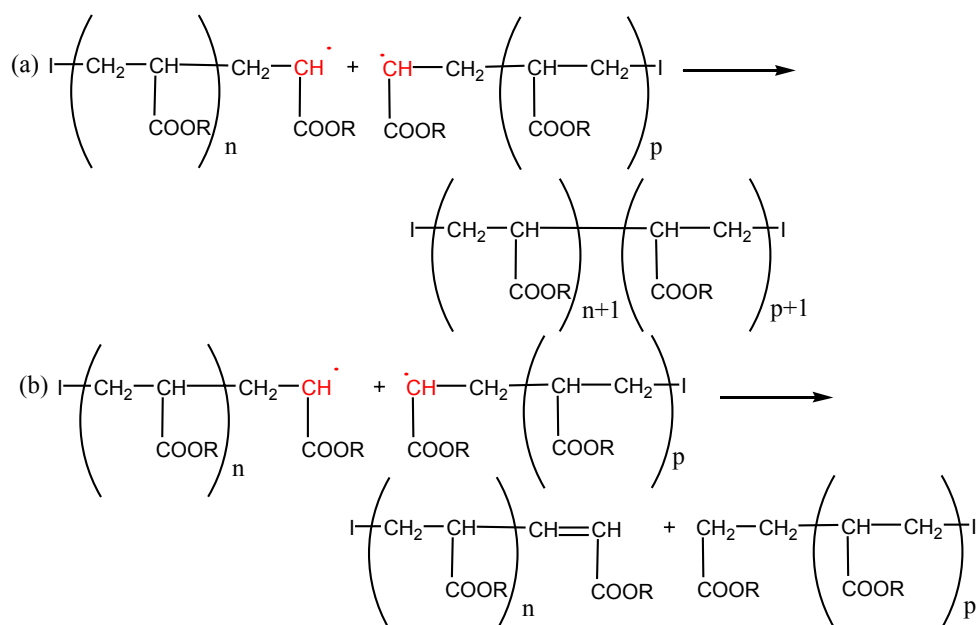


Figure 2- III-4: Termination step of polymerization of alkyl acrylates; (a) by combination, (b) by disproportionation (R=alkyl).

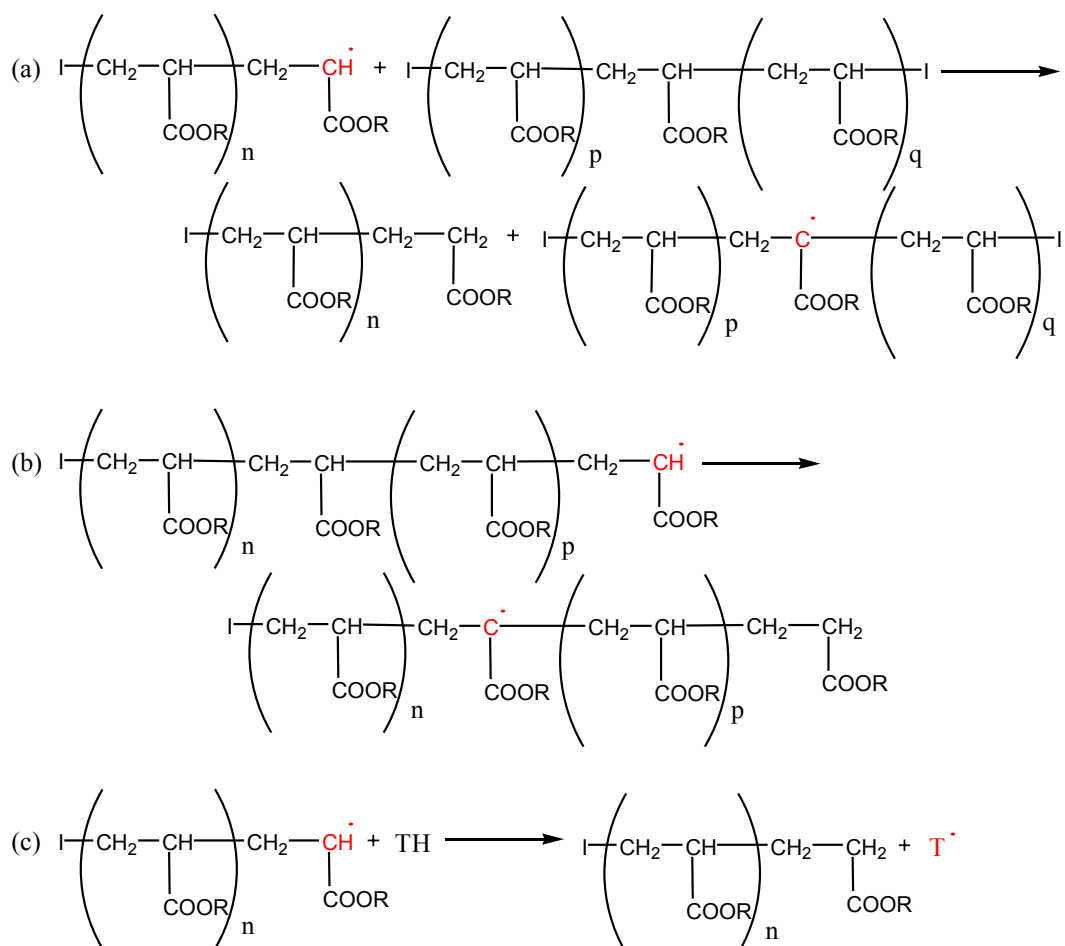


Figure 2- III-5: Transfer reactions of the polymerization of alkyl acrylates; (a) intermolecular chain transfer to polymer, (b) intramolecular transfer to polymer (back-biting if p is small); (c) transfer to any species, after which the produced T[·] radical can act as an initiator (R=alkyl).

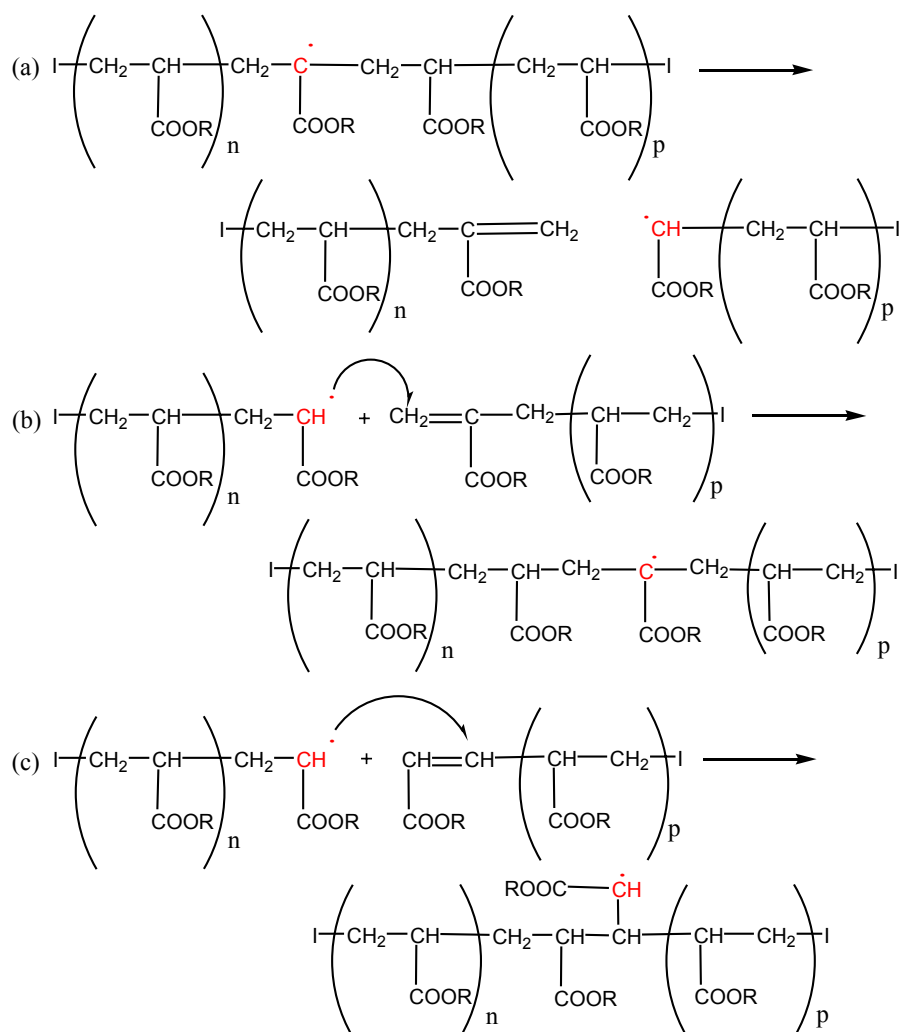


Figure 2- III-6: Other side reactions of the polymerization of alkyl acrylates; (a) β -scission, (b) propagation to a terminal bond produced by β -scission, (c) propagation to a terminal bond produced by termination by disproportionation (R =alkyl).

The transfer to polymer produces a tertiary radical which can reinitiate (leading to branches) or undergo β -scission. The β -scission occurs in a polymer chain containing a tertiary radical and produces a macromonomer (polymer chain with a terminal double bond). Macromonomers are produced in β -scission or in termination by disproportionation, and could further copolymerize (leading also to branches).

b) Discussion of the branching/crosslinking origin and topology

Acrylic monomers tend to exhibit a significantly more frequent transfer to polymer (s. Figure 2- III-5) than styrene or methacrylic monomers.¹⁴⁴ This results in branching of poly(alkyl acrylates), especially during emulsion polymerization (because the local concentration of polymer is higher than during solution polymerization).¹⁴⁶ Via termination by combination of branched polymers (s. Figure 2- III-4), it can lead to crosslinking, although it is possible to prepare highly branched and not crosslinked polyacrylates.

The amount of intermolecular chain transfer to polymer is characteristic of the monomer, and is difficult to control directly even by varying the polymerization temperature

(because its temperature dependence is unknown). On the contrary, introducing a crosslinker makes it possible to control more precisely the amount of crosslinking (by varying the crosslinker concentration, but this only increases the amount of crosslinking). Secondary bonding is also often used for crosslinking, e.g. by introduction of acrylic acid units in a poly(alkyl acrylates) to form hydrogen bonds.

In the case of branching, the nature of the resulting branches depends on the type of transfer to polymer occurring during the synthesis. Short-chain branches (SCB) result from intramolecular transfer to polymer (s. Figure 2- III-5) with a low p value (usually 1, 2 or 3). Long-chain branches (LCB) result from intermolecular chain transfer to polymer, or from intramolecular transfer to polymer with high p value. These two transfer modes are sometimes both designated as intermolecular chain transfer to polymer, because they both lead to a LCB.

3. Effects of branching and crosslinking on the material properties

The presence of short chain branching (SCB) affects the crystallinity (in semi-crystalline polymers), chemical reactivity, hardness, glass-transition temperature, and so forth, whereas long chain branching (LCB) has a more pronounced effect on viscoelastic properties such as the intrinsic viscosity, sedimentation behavior, and angular distribution of scattered radiation of dilute solutions, as well as the viscosity and elasticity of melts.¹⁸² Branching also plays a role in the adhesive properties of PSAs; the effect of branching and crosslinking on mechanical and adhesive properties was already detailed in Part 1, I.D.5.

In dispersion films, the crosslinking can take place either internally (i.e., inside the particles) or in the phase between the particles, as shown in Figure 2- III-7.²⁴ During the latex film formation, the coupling between the particles is due to interdiffusion of polymer chains and chain ends across the interface, leading to formation of physical entanglements between former separated particles.¹⁸⁷ This interdiffusion occurs only above T_g .¹⁸⁸ In a study of the mechanical behavior of crosslinked poly(*n*-butyl methacrylate) (PBMA), Zosel et al.¹⁸⁹ explained the brittleness of the film, after annealing of the sample, by the absence of physical interdiffusion of polymer chains between the particles, because of the intra-particle crosslinking. As a conclusion, intra-particle crosslinking in a latex can hinder the formation of an homogeneous film, while intra-particle branching can result in a dramatic increase in reptation time.

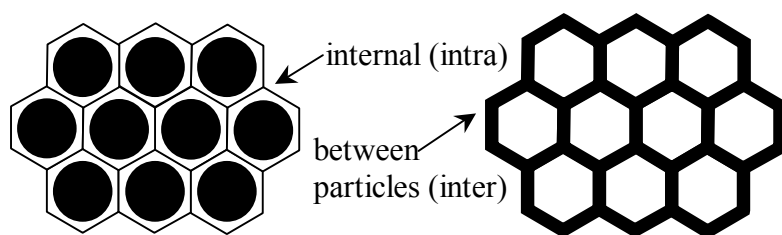


Figure 2- III-7: Types of crosslinking patterns in acrylic emulsions.²⁴

4. Characterization of the crosslinking of homogeneous networks

Several methods are known to characterize crosslinking in networks, but always assuming an homogeneous network. Since the investigated industrial PSAs are partly soluble, they can not be considered as homogeneous networks. Therefore the techniques have not been used in the present work. However, considering the importance of crosslinking in the adhesive properties of PSAs, a brief overview of these methods is given in appendix in Part 7, III.C.

B. Choice of a ^{13}C NMR technique to quantify branching in poly(alkyl acrylates)

The method of choice for the characterization of the branching appears to be ^{13}C NMR. Indeed, branched and not branched backbone carbons exhibit different chemical shifts. Our aim was to develop a fast method for branching quantification, directly on the industrial PSA samples. This requires both spectral resolution and sensitivity. To increase the sensitivity in solid-state NMR, it is possible to use CP-MAS at low temperature. To increase the spectral resolution, it is necessary to increase the effective mobility, either by using solution-state NMR, or by swelling the samples and use fast MAS, or by melting the sample and use slow MAS.

The most studied poly(alkyl acrylates) are poly(*n*-butyl acrylate), PBA, and poly(2-ethylhexyl acrylate), P2EHA. In the case of P2EHA, Heatley et al.¹⁴⁵ determined that transfer to polymer occurs predominantly by abstraction of the hydrogen atom on the tertiary CH from the backbone and not from the side group (s. Figure 2- III-8).

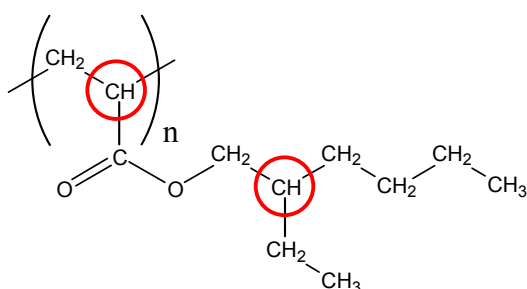


Figure 2- III-8: Poly(2-ethylhexyl acrylate); in circles the hydrogen atoms bond to tertiary carbons.

A list of the chemical shifts of all detected lines in the industrial PSA samples will be given first, before an overview of the possible ^{13}C NMR techniques. For each technique, the present work will be compared to published works.

1. Determination of chemical shifts

It is important to determine first the chemical shifts of all involved species. The only components that could be detected by ^1H or ^{13}C NMR in the investigated industrial PSAs (except the acrylic monomers) are surfactants, crosslinker, water (and possible solvent when there is one). In order to perform a complete assignment of the spectra, the chemical shift of their characteristic lines must be determined first.

a) Determination of chemical shifts of other components

Solution-state NMR was used to determine the chemical shifts of the surfactants present in the studied samples. The assignment of all the observed lines is given in the Table 2- III-1.

Sample	Nucleus	δ (ppm)	Intensity (%)	Assignment
Disponil NP307	^1H	0.6 to 1.8	13	alkyl group C_9H_{19}
		3.7	84	ethoxy chain $-(\text{CH}_2-\text{CH}_2-\text{O})-$
		6.8 and 7.2	3	aromatic ring
Disponil AES63IS	^1H	0.7, 0.9, 1.3 and 1.7	13	alkyl group C_9H_{19}
		3.7	84	ethoxy chain $-(\text{CH}_2-\text{CH}_2-\text{O})-$
		6.8 and 7.2	3	aromatic ring
Disponil NP307 and AES63IS	^{13}C	10 to 40	12	alkyl group C_9H_{19}
		72	80	ethoxy chain $-(\text{CH}_2-\text{CH}_2-\text{O})-$
		116, 129, 143 and 158	8	aromatic ring

Table 2- III-1: Assignment of the NMR signals of the surfactants (s. Table 2- I-2 for chemical structures).

The chemical shifts of the crosslinker are known but are confidential.

The different chemical shifts of the solvents used in the experiments can be found in the literature and are summarized in the Table 2- III-2.

Solvent	Nucleus	δ (ppm)	Assignment
D_2O	^1H	4.8	H_2O , HOD
CDCl_3	^1H	7.27	CHCl_3
	^{13}C	77.2	CDCl_3
DMF-d_7	^1H	2.75 and 2.90	methyl groups
		8.03	aldehyde group
	^{13}C	29.8 and 34.9	methyl groups
		163.2	aldehyde group
THF-d_8	^1H	1.75	CH_2 group in β from O
		3.60	CH_2 group in α from O
	^{13}C	25.4	CH_2 group in β from O
		67.6	CH_2 group in α from O

Table 2- III-2: Chemical shifts of the solvents used in the NMR experiments (the ^1H chemical shifts reported are the ones of residual protonated species).

b) Line assignment for 2EHA, MA and AA monomeric units

The ^{13}C chemical shifts of the different nuclei of 2EHA, MA and AA monomeric units have been assigned by comparison of the measured values with calculated values (from

incremental calculations¹⁹⁰) and with values from the literature^{145,148,180} (s. Table 2- III-4 and Table 2- III-3, as well as Figure 2- I-5 for the identification of the carbon atoms).

Monomeric unit	δ (ppm) in copolymers (measured)	Assignment		δ (ppm) in homopolymers (calculated)	δ (ppm) in homopolymers (literature) ¹⁸⁰
MA	35.7 to 36.9	12	CH ₂	24 to 25	34.5 to 35.9
	42.2	13	CH	40	41.3 to 41.6
	51.7	15	O-CH ₃	48	51.5
	175.0	14	C=O		174.9
AA	35.9 to 36.7	16	CH ₂	25	38.7 to 41.5
	42.2	17	CH	42	47.7-49.8
	175.0	18	C=O		187.3

Table 2- III-3: Assignment of the ¹³C chemical shifts of MA and AA monomeric units.

δ (ppm) in copolymers (measured)	Assignment		δ (ppm) in homopolymer (calculated) ¹⁹ ₀	δ (ppm) in homopolymer (literature) ¹⁴⁸	δ (ppm) in homopolymer (literature) ¹⁴⁵
11.4	9	CH ₃ , side-group	11	10.3	14
14.5	11	CH ₃ , side-group	14	13.4	10.7
23.8	8	CH ₂ , side-group	23	22.6	23.0
24.5	10	CH ₂ , side-group	26	23.5	23.5
29.8	7	CH ₂ , side-group	30	28.6	28.9
31.2	6	CH ₂ , side-group	33	30.1	30.1
35.9 to 36.7	1	CH ₂ , backbone	24 to 25	34.8 to 35.6	33.5 to 37.3
39.6	5	CH, side-group	45	38.5	38.5
42.2	2	CH, backbone	40	41.2	41.5
48.5	2'	branched C _q , backbone	51	48.0	47.2 to 48.4
67 to 68	4	O-CH ₂ , side-group	71	66.0	66.9
172.6	3'	branched or terminal C=O		171.2	
175.0	3	C=O		173.5	174.3

Table 2- III-4: Assignment of the ¹³C chemical shifts of 2EHA monomeric units.

2. Solution-state NMR

Solution-state NMR exhibits the advantages of wider accessibility, as well as higher spectral resolution.

a) Published works

Lovell et al.¹⁴⁶ investigated branching in PBA latices using ¹³C solution-state NMR at 75.5 MHz of solutions or gels in C₆D₆, after dialysis. They quantified the branching levels with the relative intensities of the branched and non-branched carbon lines without NOE enhancement. In the same group, Ahmad et al.¹⁴⁹ recorded ¹³C NMR spectra of the PBA in solution in CDCl₃, at room temperature and 125.8 MHz.

Heatley et al.¹⁴⁵ investigated P2EHA. The samples were dried under vacuum, then dissolved in CDCl₃ and single pulse ¹³C spectra were recorded at 125 MHz using continuous proton decoupling and either a flip angle of 45 ° with a delay of 0.5 s between transients, or inverse gated decoupling with a delay of 10.5 s between transients.

Two more works were published during the present Ph.D. work. Farcet et al.¹⁹¹ investigated PBA homopolymers. The branching level was quantified using ¹³C solution-state NMR in CDCl₃ at 125.76 MHz using a flip angle of 20 °, a recycle delay of 20 s, and inverse gated decoupling to suppress NOE. Gilbert et al.¹⁹² investigated PBA latices, dialyzed prior to analysis. Branching levels were quantified using solution ¹³C NMR at 100 MHz.

These successful investigations of PBA and P2EHA model samples show the feasibility of branching quantification using ¹³C solution-state NMR in CDCl₃ for some poly(alkyl acrylates) samples.

b) Our work

The branching level was successfully investigated in the model PnAA samples using ¹³C solution-state NMR; it was presented in paragraph II.D.3.a.

In the case of the industrial PSA samples however, the solubility in CDCl₃ is low, so that 3 days measurements at 33 °C do not give sufficient signal-to-noise ratio (S/N) for the branching quantification. To overcome the latter problem, a spectrum of Homo2EHA (the most soluble of the three samples) was recorded in solution in C₂D₂Cl₄ at 100 °C for 3 days. The S/N was still not sufficient to detect any branching line (s. Figure 2- III-9). Therefore it was decided to investigate the branching in industrial PSAs using solid-state NMR.

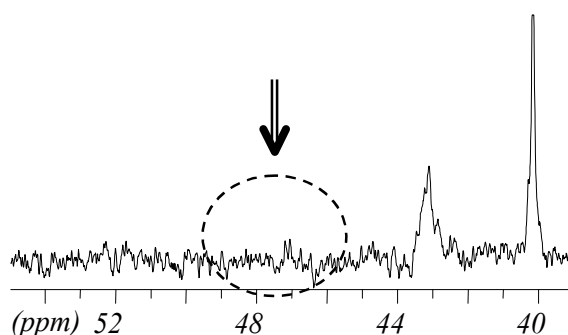


Figure 2- III-9: Part of the ¹³C solution-state NMR spectrum of Homo2EHA (125.76 MHz, in C₂D₂Cl₄, 100°C, 56h): no branching line can be detected around 48 ppm.

3. Solid-state NMR with cross-polarization

Solid-state NMR in general exhibits the advantage over solution-state NMR of investigating the whole sample, regardless of solubility problems. There is no published work concerning the quantification of branching in poly(alkyl acrylates) using cross-polarization. However, the branching quantification requires an optimization of the S/N, and the S/N might be increased by the use of cross-polarization (s. Part 1, II.D). In contrast to ¹³C single pulse excitation, the CP-MAS experiment is not quantitative, because it is more sensitive to less

mobile carbons. A calibration using single pulse excitation experiments is thus necessary. It will then be interesting only if it is much quicker than quantification using single pulse excitation.

The preliminary solid-state NMR study of the branching was done on the sample Copo3, which differs from Copo1 only by a higher synthesis temperature. Therefore it could present a higher amount of branches than the other studied samples. ^{13}C solid-state CP-MAS spectra of sample Copo3 were recorded at low temperature ($-20\text{ }^\circ\text{C}$), at 125.76 MHz, under 3.6 kHz MAS with a repetition time of 3 s between consecutive transients, and a total number of 5120 transients. The MAS speed was chosen so that no spinning sideband of another line could interfere with the line of the branched carbon that has to be quantified and the lines of the backbone carbons, and not too high so that it should not fully average the dipolar coupling needed for the polarization transfer. A $4\text{ }\mu\text{s}$ 90° proton pulse was used, as well as a ramp for the ^1H pulse during the contact time¹⁹³ and a TPPM composite pulse decoupling of 63 kHz for the protons during the acquisition. The ramp is used to compensate for the imperfection of the experimental setup and the possible spectrometer drift effects. 4 mm outer diameter rotors were used. CP-MAS spectra were recorded at low temperature. The contact time was optimized at $500\text{ }\mu\text{s}$ with regard to the line of the quaternary branched carbon at 48 ppm (s. Figure 2- III-10).

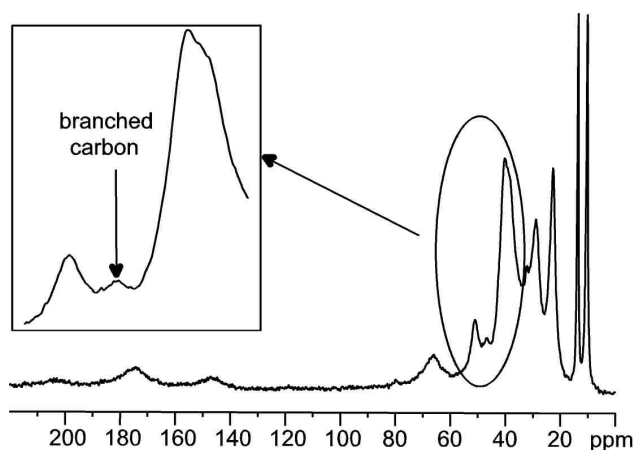


Figure 2- III-10: ^{13}C CP-MAS spectrum of sample Copo3 at 75.47 MHz, 3.6 kHz MAS, $-20\text{ }^\circ\text{C}$, 4h30.

The S/N scales with the square root of the measuring time. Therefore the S/N achieved in this work in 4h30 must be multiplied by 6 to be compared to the S/N achieved by Plessis et al.¹⁴⁸ in 28 h using single pulse excitation (s. paragraph 4.a). Then both are of the same order of magnitude. Therefore, it doesn't compensate for the additional work of deconvolution of the spectrum and calibration with ^{13}C single pulse excitation experiments. For that reason, ^{13}C CP-MAS has not been used to quantify the branching level.

4. Solid-state NMR with single pulse excitation on swollen sample

a) Published works

The abbreviation HR-MAS (high-resolution MAS) is often used to designate the technique consisting in recording routinely ^{13}C single pulse spectra of swollen samples under MAS. Plessis quantified branching levels in PBA and P2EHA using HR-MAS.^{17,148} The films were first dried under vacuum, then slightly swollen with THF and packed in a 7 mm rotor. The single pulse ^{13}C spectra were recorded at 45 °C on a Bruker Avance DSX300 at 1.3 kHz MAS, using inverse gated decoupling and composite phase decoupling, with a recycle delay of 4 s. At least 25 000 transients were acquired for each spectrum, which corresponds to a minimum measuring time of 28 h, and is the shortest measuring time found in literature for quantitative measurements. A typical spectrum is shown for PBA on Figure 2- III-11.

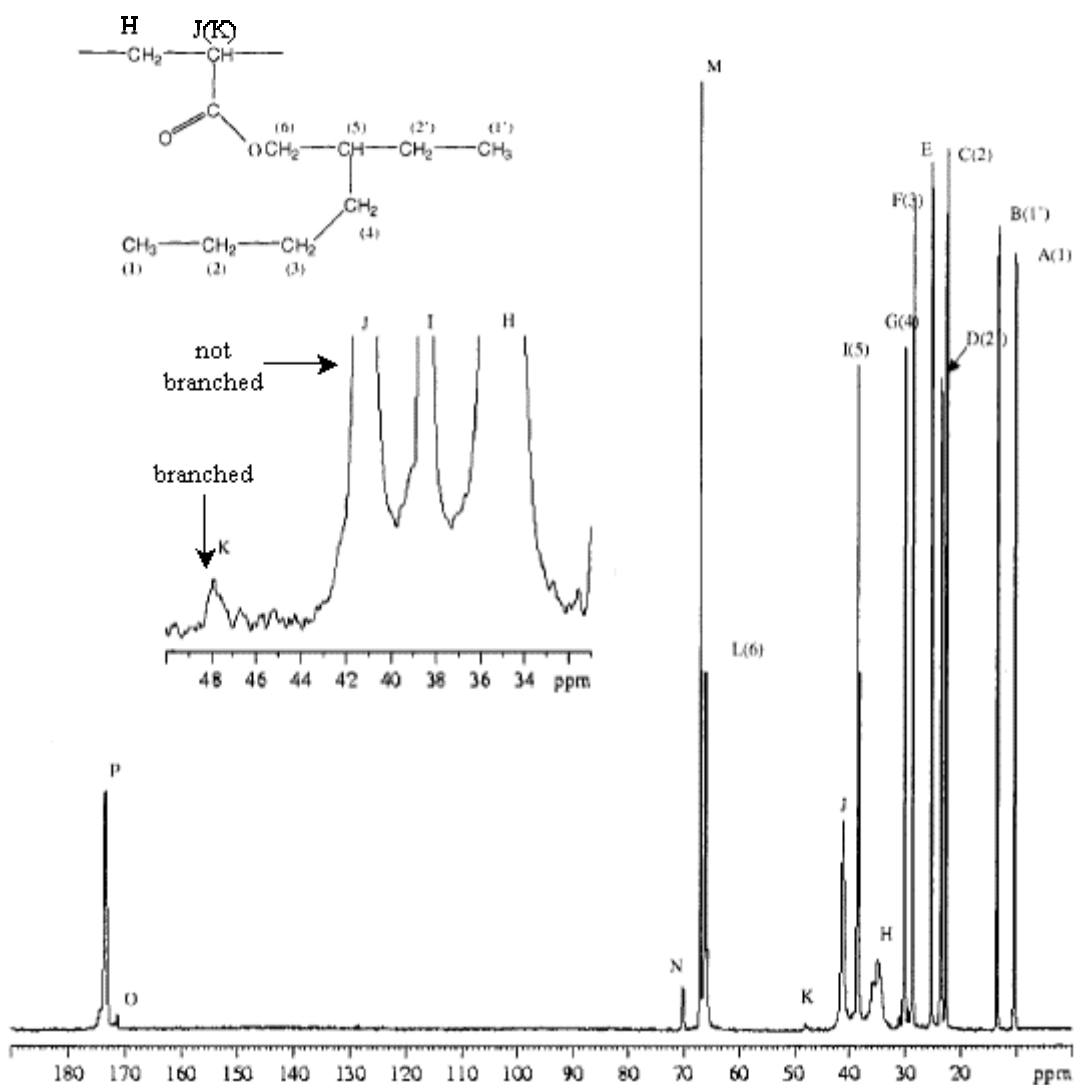


Figure 2- III-11: Single pulse ^{13}C spectrum of swollen 2EHA homopolymer and lines assignment including the quaternary line due to branching.¹⁴⁸

b) Our work

The swelling agent was chosen according to the following criteria: it has to be a good solvent of 2EHA and MA monomeric units to be able to swell them, and it must have a high boiling point to allow the swollen sample to be heated to increase the resolution. Due to their relative polarity, poly(alkyl acrylates) with short side-groups are soluble in polar solvents, aromatic hydrocarbons and chlorinated hydrocarbons; common solvents include THF, DMF, acetone, butanone, ethyl acetate, CHCl_3 ;¹ the swelling ability of the solvents increases in the following order: alcohols, aliphatic hydrocarbons, aromatic hydrocarbons, ketones and esters.²⁴ DMF and THF are thus good swelling agents for the poly(alkyl acrylates). DMF has a high boiling point (153 °C), what allows to heat the sample at 80°C, but it has a line overlapping one of the backbone carbons (s. paragraph 1), what prevents us from using it for the quantification. Therefore THF was chosen (as by Plessis): it has a lower boiling point (66 °C) but it can be heated to 50 °C for several hours as swelling agent.¹⁴⁸ The spectra were recorded on samples containing roughly 50 % of swelling agent.

The single pulse ^{13}C experiments were carried out at a frequency of 125.76 MHz, under 5 kHz MAS, with 4 μs 90° pulse, continuous wave decoupling at 50 kHz, and a delay of 5 s between consecutive transients. 2096 transients were acquired at room temperature, and 4 mm outer diameter rotors were used. The acquisition time of the FID was optimized to 102 ms: a too short duration leads to a decrease in resolution (via convolution), while a long duration requires a lower decoupling power, which also leads to broadening of the lines; moreover, the irradiation duration has to be lower than 2 % of the delay between consecutive transients to avoid damages in the electronic parts. The ^{13}C T_1 relaxation time of the sample was measured using the saturation recovery method to optimize the delay between consecutive transients: for all the lines except the carbonyl group, the T_1 value is in the range 200 ms to 1 s, so that the delay between consecutive transients is kept at 5 s.

A typical spectrum is shown on Figure 2- III-12. The very broad line centered around 105 ppm arises from the material forming the cap of the rotor (Kelf). The S/N obtained in 3 h is not high enough to quantify the branching, but is promising: the S/N obtained in 28 h *should allow for a quantification, like Plessis et al.¹⁴⁸ did. Nevertheless, a faster quantification seems unrealistic.*

It can be argued that some progresses could still be done using single pulse excitation. However, they would require a degradation of the sample (by mixing a relaxation agent, which can not be extracted afterwards) or the use of especially modified probeheads or advanced pulse sequences, which would severely reduce the applicability of the method by non-NMR specialists.

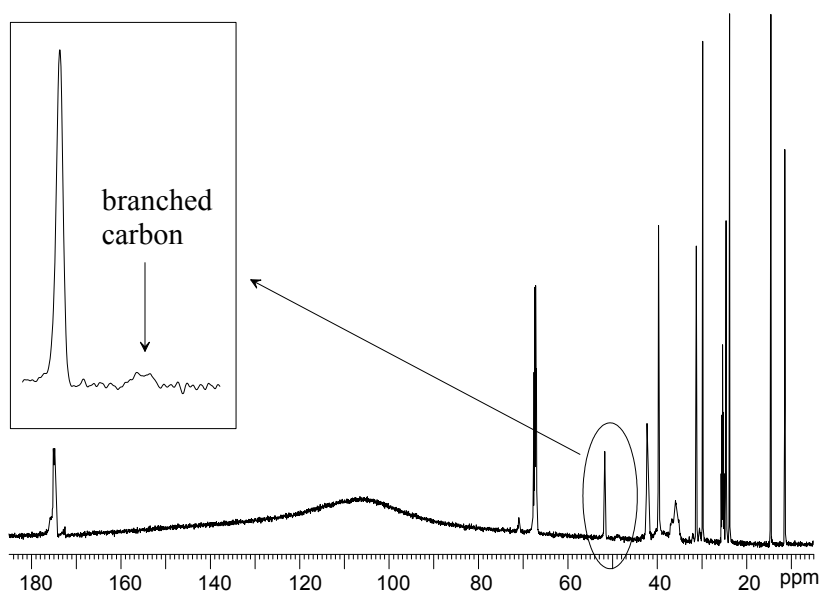


Figure 2-III-12: Single pulse ^{13}C spectrum of sample Copo3 swollen in THF, at 125.76 MHz, under 5 kHz MAS, at room temperature, 3h.

Therefore, it was chosen not to continue investigating swollen samples, but rather to study the PSA samples in the melt.

5. Solid-state NMR with single pulse excitation in the melt

Similarly to swollen samples, the molten samples exhibit a high mobility and thus a high resolution (considering solid-state NMR).

a) Published work

The branching quantification in polymeric samples *in the melt*, using solid-state NMR under slow MAS, was developed in our group by Pollard et al. with polyethylene.¹³² They could detect branching levels down to 0.02 % of the monomeric units in one day in this chemically simple polymer. The measurements are done on the *pure sample*, which allows to measure a bigger sample amount (and therefore get more signal), as well as to measure the *whole sample* including its insoluble fraction (crosslinked or high molar mass). This method had never been applied to any other polymer than polyethylene.

b) Our work

The chain branching level was quantified in the PSA samples using the solid-state NMR method developed by Pollard et al.¹³² for PE. The measurements were carried out in the melt (at 90 °C or 100 °C) to increase the mobility of the sample, and hence the resolution of the spectrum. 7 mm outer diameter rotors were used.

The first ^{13}C NMR spectrum was recorded for sample Copo3 at 100 °C on a Bruker DSX300 spectrometer, at a ^{13}C Larmor frequency of 75.47 MHz, under 3 kHz MAS, using single pulse excitation with a 5 μs 90° pulse, inverse gated decoupling, TPPM composite pulse decoupling at 50 kHz and a relaxation delay of 10 s (to obtain a quantitative spectrum). The spectrum is shown on Figure 2-III-13. The signal-to-noise ratio obtained in 3h30 is more

than sufficient to quantify the chain branching level in the sample using the area of the quaternary branched carbon at 49 ppm (J).

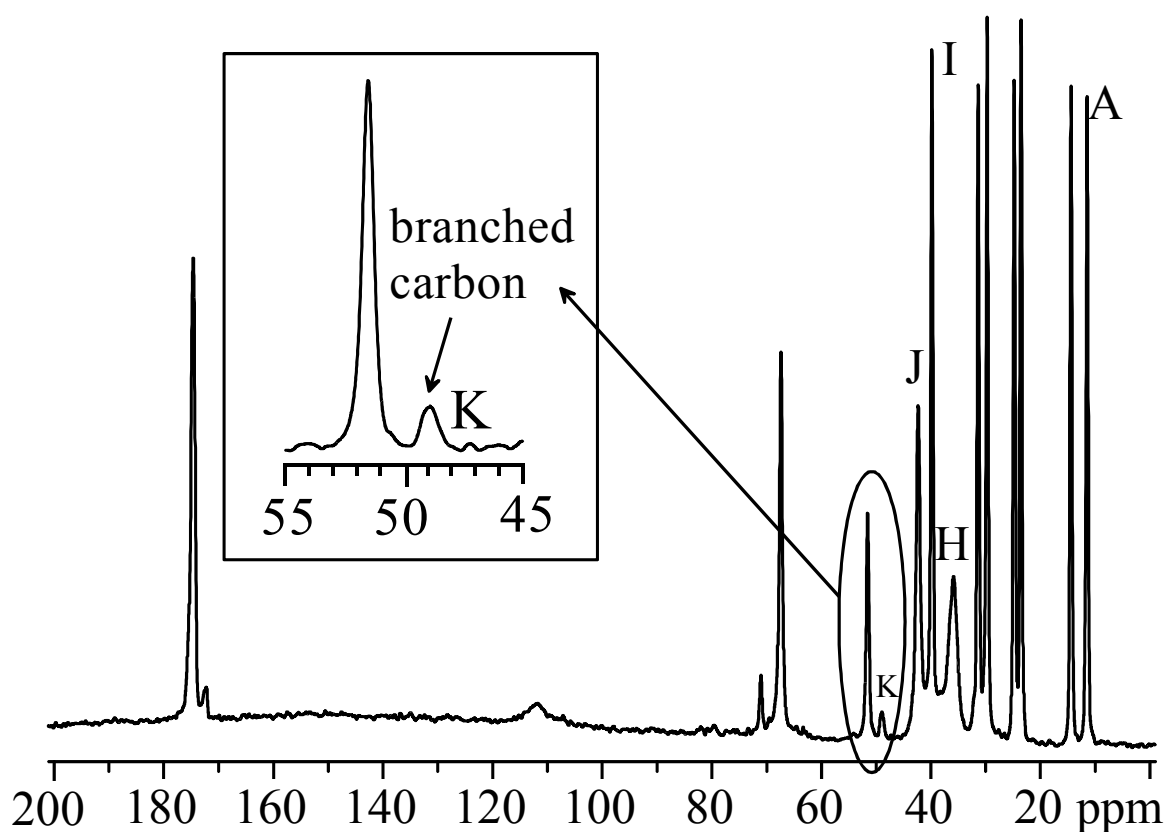


Figure 2- III-13: ^{13}C single pulse NMR spectrum of molten Copo3 (75.47 MHz for ^{13}C , pure sample, 3 kHz MAS, 100°C, 3h30): the chain branching line K at 49 ppm can be quantified precisely.

In order to carry out an even faster quantification, the static magnetic field was increased. The ^{13}C NMR spectrum of samples Homo2EHA and Copo2 were recorded at 90 °C on a Bruker DSX500 spectrometer, at a ^{13}C Larmor frequency of 125.76 MHz, under 2.8 kHz MAS, using single pulse excitation with a 5 μs 90° pulse, inverse gated decoupling, continuous wave decoupling at 42 kHz and a relaxation delay of 10 s to record quantitative spectra. A spectrum is shown for sample Copo2 on Figure 2- III-14. The signal-to-noise ratio obtained in 18 h is higher than for a Larmor frequency of 75.47 MHz (not shown), and sufficient to quantify precisely the chain branching level in the sample. However, on the contrary to a Larmor frequency of 75.47 MHz, at a Larmor frequency of 125.76 MHz spinning side bands are present between 10 and 60 ppm, so that the MAS frequency has to be chosen more carefully in order to avoid overlapping between these side bands and the integrated lines.

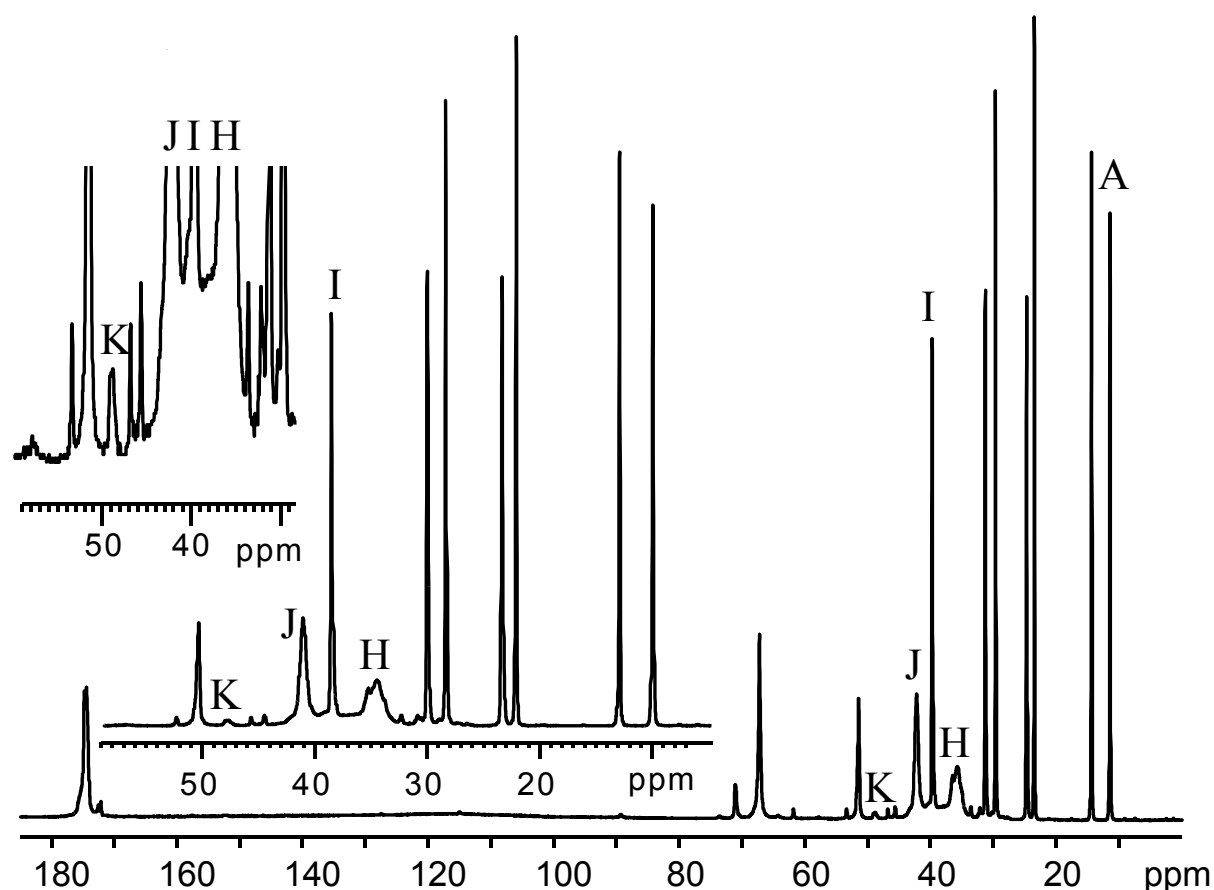


Figure 2-III-14: ^{13}C single pulse NMR spectrum of molten Copo2 (125.76 MHz for ^{13}C , pure sample, 2.8 kHz MAS, 90°C, 18 h): the chain branching line K at 49 ppm can be quantified precisely.

6. Conclusion on the choice of the ^{13}C NMR technique

Several ^{13}C NMR techniques have been used to investigate branching in poly(alkyl acrylates), and our work has been compared with the published works on this topic. It has been shown that solution-state NMR is suitable for model PnAAs, for which it was preferred due to easier accessibility. However, on the contrary to solid-state NMR, it provides a lower signal-to-noise ratio for identical measuring time, and the risk of not taking into account possible microgels. Therefore this technique should not be recommended in cases where a very precise branching quantification is required.

The industrial PSA samples exhibit a too low solubility in common NMR solvents to be investigated by solution-state NMR, and were thus investigated using solid-state NMR. CP-MAS spectra do not exhibit a significantly higher signal-to-noise ratio than single pulse excitation spectra, and on the other hand exhibit a low resolution due to low temperature and are not quantitative. Therefore CP-MAS was not used for quantification. *Single pulse excitation spectra of swollen samples are suitable for branching quantification*, as shown by Plessis et al.,^{148,178} but the experimental optimizations done in the present work did not achieve a faster quantification. A new method was proposed for quantification of branching in poly(alkyl acrylates). It is adapted from a branching quantification method for PE¹³², using

single pulse excitation under slow MAS in the melt. It is faster and more precise than the methods published up to now for poly(alkyl acrylates), and can be applied directly to industrial PSA samples. Therefore this method should be recommended in cases where a very precise branching quantification is required, e.g. for the determination of a kinetic constant.

C. Branching level quantification and discussion of the branching topology

The way of extracting the branching level from the recorded ^{13}C NMR spectrum will be presented in paragraph 1, while the branching levels and branching topology will be detailed and discussed in paragraph 2.

1. Branching quantification from ^{13}C NMR spectrum

a) Published works

Ahmad et al.¹⁴⁹ define the mole percent of branched repeat units in PBA samples by referencing the integrals of the quaternary carbon and of the adjacent CH and CH₂ groups to the total integral for backbone carbons. The corresponding Equation 2- III-1 is explicitly written and used by Farcet et al. for PBA homopolymers.¹⁹¹ In this equation, A(x) is the area of the line x and the carbons H, J, K, X, Y are defined on Figure 2- III-15.

$$BL = \frac{(A(K) + A(X+Y)/6)/2}{A(K) + A(X+Y)/2 + A(J+H)/2} \cdot 100 \quad \text{Equation 2- III-1}$$

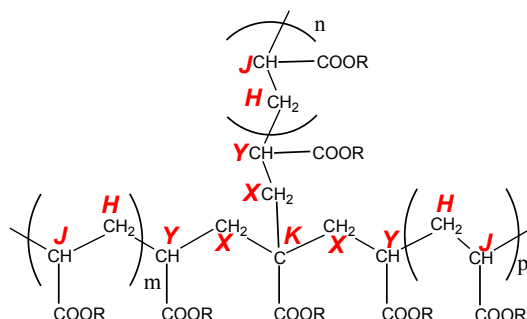


Figure 2- III-15: Structure of the branched carbons in polyacrylates, with definition of the different moieties used for branching quantification by Farcet et al.¹⁹¹ (R alkyl).

Plessis et al. used Equation 2- III-2 to quantify the branching level BL in PBA in % of monomeric units.¹⁷⁸ The carbons H, J, K, X are defined on Figure 2- III-16.

$$BL = \frac{A(K)}{A(K) + A(X+J+H)/2} \cdot 100 \quad \text{for PBA} \quad \text{Equation 2- III-2}$$

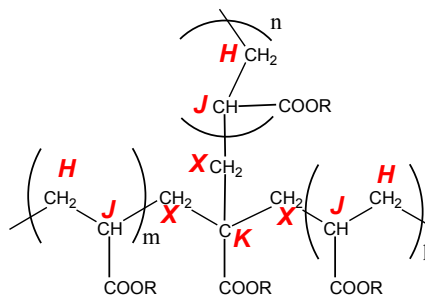


Figure 2- III-16: Structure of the branched carbons in polyacrylates, with definition of the different moieties seen in NMR (R alkyl).

Heatley et al.¹⁴⁵ investigated P2EHA and showed that the adjacent CH₂ (X) is overlapping with the side chain CH signal. Therefore, Plessis et al. used Equation 2- III-3, from which A(X) is absent, to quantify the branching level BL in P2EHA in % of monomeric units.¹⁴⁸

$$BL = \frac{A(K)}{A(K) + A(J+H)/2} \cdot 100 \text{ for P2EHA} \quad \text{Equation 2- III-3}$$

b) Our work

The most precise way of calculating the branching level in poly(alkyl acrylates) is Equation 2- III-1, used by Ahmad et al.¹⁴⁹ and Farcet et al.¹⁹¹. However, our PSA samples contain 2EHA monomeric units and in that case the branch CH₂ signal is not resolved.¹⁴⁵ Therefore Equation 2- III-3¹⁴⁸ has to be used.

The determination is complicated here by the fact that a copolymer and not an homopolymer is investigated. Luckily, each backbone carbon exhibits the same chemical shift in the three monomeric units (s. paragraph B.1 for the chemical shift assignment and Figure 2- III-17 for the molecular assignment). Therefore, the hundredfold of the ratio of area of K with the sum of area of K and half the areas of H and J has to be done to calculate the branching level.

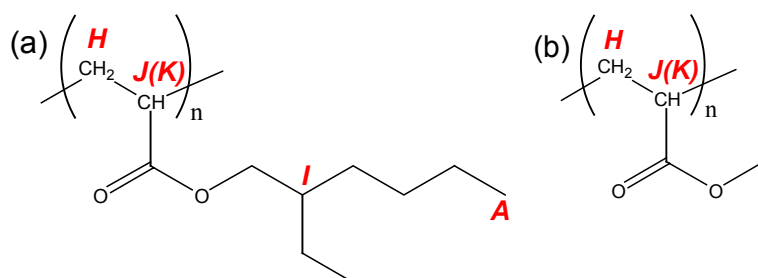


Figure 2- III-17:
Definition of the NMR
lines of interest for the
quantification of
branching for 2EHA and
MA monomeric units; K
designates the branched
carbon, J the non
branched one.

However, the lines corresponding to H and J are not sufficiently resolved (s. Figure 2- III-13 and Figure 2- III-14) and have to be integrated together with the line corresponding to I. In order to calculate the areas of H and J alone, an area equal to the one of I has to be subtracted from the area of H and I and J together. The line A is perfectly resolved and also corresponds to one carbon (CH₃) in the side chain of 2-ethyl hexyl acrylate comonomer. Therefore, the branching level BL, in percents of the monomeric units, can be expressed as:

$$BL = \frac{A(K) \cdot 100}{A(K) + \frac{A(H+J)}{2}} = \frac{A(K) \cdot 100}{A(K) + \frac{A(H+I+J) - A(A)}{2}} \quad \text{Equation 2- III-4}$$

The determined branching levels, expressed in percents of the monomeric units, are reported in Table 2- III-5.

Sample	Homo2EHA	Copo1	Copo2	Copo3
BL	4.7	5.2	3.4	6.0

Table 2- III-5: Branching level quantified in the PSAs, in percents of the monomeric units.

It should be noted that the branching level is higher in the PSA samples than in the PnAAs (1.5 to 2.5 % of the monomeric units, s. paragraph II.D.3.a). This general trend was expected from the synthesis procedures (free radical polymerization, respectively in emulsion under monomer starved conditions and in solution).

2. Branching topology

^{13}C NMR allows to determine the total branching level, but does not differentiate between SCB and LCB. The branching topology was investigated using multiple detection SEC only for model PnAAs (s. paragraph IV), due to incomplete solubility of the industrial PSAs. Considering the importance of the branching topology in the industrial PSA samples, a survey of the published works concerning branching topology in poly(alkyl acrylates) in general will be presented here. When measured, the branching levels will be indicated.

a) Zosel's work on poly(n-butyl acrylate) latices

Zosel et al.¹⁸⁹ have synthesized various PBA latices with different amounts of either crosslinking monomer (difunctional methallyl methacrylate, MAMA), or chain transfer agent (tert-dodecyl mercaptan, DMCT). Studying the viscoelastic behavior of these samples at small strains and 23 °C, they proved that PBA made without any additive is slightly crosslinked, since the storage modulus G' is higher than the loss modulus G'' for the low frequencies (or high temperatures). Furthermore, at least 0.3 % DMCT must be introduced during the polymerization to obtain a non-crosslinked behavior with viscous flow. It should be noted that the samples recognized as crosslinked by this method were not only branched, but really crosslinked, because they presented a gel fraction.

b) McCord's work on copolymerization of poly(alkyl acrylates)

McCord et al.¹⁹⁴ have studied the microstructure of short-chain branches in PE copolymers with (meth)acrylates synthesized at high pressure, using ^1H , ^{13}C , 1D and 2D liquid-state NMR. They have shown that (a) the short-chain branching mechanism also involves comonomeric units in the chain, (b) most of the intramolecular back-biting originates from ethylene, and not from the comonomer radicals, and (c) hydrogens opposing acrylate side groups are prone to abstraction by backbiting.

c) Chiefari's work on poly(alkyl acrylates) in solution

Chiefari et al.¹⁹⁵ report the synthesis in solution (in toluene, n-butyl acetate, n-butanol and n-amyl acetate) of several polyacrylate macromonomers through propagation, transfer to polymer and β -scission. They suggest that the predominant mechanism for the transfer to polymer is intramolecular (back-biting) at lower monomer concentrations, and intermolecular

at higher ones. This would lead to mostly SCB in the former case, and to LCB in the latter one.

d) Lovell's work on n-butyl acrylate and 2-ethylhexyl acrylate in emulsion and solution polymerization

Lovell et al.¹⁴⁶ synthesized PBA latices at 75 °C. They estimated branching levels of 2 to 4 % of the monomeric units. In the same group, Ahmad et al.¹⁴⁹ performed polymerization of BA in cyclohexane at 70 °C and measured branching levels ranging from 1 to 6 % of the monomeric units.

Also in the same group, Heatley et al.¹⁴⁵ carried out polymerization of 2-ethylhexyl acrylate (2EHA) in solution in cyclohexane at 70 °C. Branching levels ranging from 2 to 8 % of the monomeric units were quantified. It was proved that the extent of transfer to polymer increases for 2EHA with increasing conversion and decreasing initial monomer concentration; furthermore the extent of transfer is higher for 2EHA than for BA polymerized under the same conditions.

e) Plessis' work on the branching of n-butyl acrylate and 2-ethylhexyl acrylate during emulsion polymerization

Plessis studied the seeded semi-continuous emulsion polymerization of BA and 2EHA at 75 °C under starved conditions.¹⁷ Plessis et al.¹⁴⁷ showed that highly branched PBA was formed (0.9 to 3.4 % of branched monomeric units). The PBA contains up to 50 to 60 % gel (weight fraction of the polymer insoluble in THF under reflux), and interestingly, no correlation between branching level and gel content was found. This indicates that the branching level measured by NMR is predominantly caused by intramolecular transfer to polymer leading to short-chain branches.

A kinetic model was developed to simulate this polymerization.¹⁹⁶ The experimental dependence of branching level on initiator concentration, the experimental dependence of gel fraction and mass-average molar mass of the soluble part on conversion were fitted for many experiments with a solid content ranging from 55 to 60 % and percentages of gel ranging from 1.7 to 2.8 %. To obtain correct fits, intra- and intermolecular transfer to polymer needed to be introduced, as well as the lower reactivity of the tertiary radical and propagation to the terminal bonds, but β -scission was not taken into account. The fit of the experimental values by the model indicated that most of the branches were SCB produced by back-biting and not LCB. This is in accordance with the fact that an increase in the initiator concentration leads to an increase in branching level (which involves both SCB and LCB), but does not much affect the gel content (which involves only LCB).

Plessis et al. also studied briefly the emulsion polymerization of 2EHA,¹⁴⁸ for which they fitted two experiments with the model developed for BA. They showed that this monomer exhibits the same features as BA and concluded that the two monomers follow a similar polymerization scheme. According to this mechanism, the main branching mechanism for 2EHA would be back-biting, so that most of the branches would be SCB. Nevertheless, some LCB are also formed since there is gel formation. Branching levels of 1.4 and 2.3 % were measured.

The emulsion polymerization of BA was then studied in more detail by Plessis et al.¹⁷⁸ They proved that the introduction of a chain transfer agent decreases the gel fraction, while it does not affect the branching level.⁴² Therefore, the dominant transfer to polymer is intramolecular, leading to SCB. Moreover they demonstrated that the introduction of styrene as a comonomer dramatically decreases the gel fraction, and only slightly decreases the branching level.⁴³

Plessis et al. quantified branching levels ranging from 0.2 to 0.7 % of the monomeric units in PBA synthesized in solution and in bulk (obtained by pulsed laser photopolymerization, PLP).¹⁹⁷

f) Farcet's work on branching of PBA in bulk and emulsion

Farcet et al.¹⁹¹ investigated PBA homopolymers prepared via nitroxide-mediated controlled radical polymerization in bulk and miniemulsion at 112 °C. Branching levels ranging from 1 to 1.8 % were measured, increasing with the monomer conversion.

Some of the polymer were investigated using MALDI-TOF-MS, and the spectra did not exhibit the 1:2:1 proportion of chains with respectively 0, 1, and 2 nitroxide chain ends, that would be expected if intermolecular chain transfer to polymer was the dominant process throughout the polymerization. They concluded that the branches seem to be produced predominantly by intramolecular transfer to polymer (presumably back-biting). However, a small portion of chains seem to undergo intermolecular chain transfer to polymer.

g) Gilbert's work on branching of PBA in emulsion

Gilbert et al. investigated PBA synthesized via free radical emulsion polymerization, between 60 and 80 °C, either using the batch procedure, or the seeded procedure under starved conditions.¹⁹² Branching levels ranging from 0 to 6.7 % were quantified.

During dynamic mechanical measurements on the samples, they detected no reduction in the plateau modulus observed at high frequencies; this indicates that no large amount of LCB (long branches) is present. Furthermore, the results are compatible with an enlargement of the reptation tube due to a large amount of SCB (short branches). These conclusions should

be drawn carefully since the influence of molar mass on rheological properties is masking the influence of chain branching, as was already observed by Ahmad et al.¹⁹⁸

h) Castignolles' work on branching of PBA and P2EHA in solution

Castignolles^{199,200} synthesized PBA and P2EHA by pulsed laser polymerization (PLP) in solution in toluene at temperatures ranging from $-34\text{ }^{\circ}\text{C}$ to $22\text{ }^{\circ}\text{C}$. The obtained polymers were investigated by SEC. The chromatograms and the comparison of the molar masses calculated by triple detection and universal calibration (s. paragraph IV.C) indicate the presence of long branches in the samples. However, no conclusion can be drawn on the quantity of LCB as the current correlation between hydrodynamic volume and LCB fails.

i) IUPAC working party on "Modeling of polymerization kinetics and processes"

Asua et al. reviewing the work published on the polymerization kinetics of alkyl acrylates, and in particular simulation works^{201,202}.¹⁸⁶ They conclude that intramolecular transfer to polymer occurs in solution polymerization of BA via PLP, leading to SCB.

3. *Conclusion on the branching levels and branching topology*

The spectra recorded on the industrial PSAs with the ^{13}C solid-state NMR method developed in the present work have been used to extract branching levels. Equations from published work have been discussed and adapted to the case of copolymers. The measured branching levels are in the same range as those given in published works.

The nature of the chain branches (SCB or LCB) was not known at the beginning of this Ph.D. work. It was only sure that branching occurs by abstraction of the backbone proton opposite the acrylate side group and not by abstraction of a side group proton. The different works published during this Ph.D. indicate that branching would occur in poly(alkyl acrylates) mainly by back-biting during *emulsion* polymerization, leading to a predominance of SCB over LCB. In the case of *solution* polymerization, the LCB amount would be sufficient to be detected by multiple detection SEC, and the occurrence of SCB was demonstrated by simulation. In both cases (emulsion and solution), a "tree-geometry" (s. Figure 2- I-1 in paragraph A.1) is then expected for the PnAAs synthesized by free-radical polymerization.

The branching levels determined for the model PnAAs synthesized via solution polymerization (1.5 to 2.5 %) are comparable to those determined by Ahmad et al. for BA obtained with a similar synthesis (1 to 6 %)¹⁴⁹, and rather lower than those determined by Heatley et al. for P2EHA obtained with a similar synthesis (2 to 8 %)¹⁴⁵. The branching levels determined for the industrial samples (3.5 to 5.5 %) are significantly higher than those

determined by Plessis for P2EHA using also emulsion polymerization (1.4 and 2.3 %) ¹⁴⁸; considering the much lower S/N obtained by Plessis (ca 2) than the one obtained in this work (at least 7), it is concluded that the values measured by Plessis are less precise and underestimated.

IV. Multiple-detection SEC of the model poly(n-alkyl acrylates)

Poly(alkyl acrylates) can not be properly characterized using SEC with conventional calibration (s. below). Therefore we will detail the different methods of SEC in paragraph A, before giving the obtained molar masses with the chosen methods in paragraph B. Then the investigation of long chain branching will be detailed in paragraph C, and conclusions will be drawn in paragraph D.

A. Overview of the possible SEC methods ^{199,203}

SEC is a separation method of polymer chains, in a series of columns (by a size exclusion mechanism), according to their hydrodynamic volume (and not to their molar mass). Different methods to determine the molar mass are then possible, depending on the used detector(s).

The most simple SEC setup uses *only a refractometer* (or another “concentration” detector), which is sensitive to the quantity of polymer. In that case, a calibration curve $\log M = f(V_e)$ (correlating the molar mass M of the polymer chains with the corresponding elution volume V_e) is first done with polymer standards, and then used to determine the molar mass of polymer samples of the same chemical nature as the standards: it is the *conventional calibration (CC)*. If no standard is available for the studied polymer, it is also possible to apply the *universal calibration (UC)* to convert the calibration curve $\log MM = f(V_e)$ for polymers of another chemical nature. This conversion is done considering the UC relation of Benoît at a given V_e for polymers A and B: $[\eta]_A \cdot M_A = [\eta]_B \cdot M_B$, ^{170,171} and the Mark-Houwink-Sakurada (MHS) equation: $[\eta] = K \cdot M^\alpha$, ¹⁷² where $[\eta]$ is the intrinsic viscosity, M the molar mass, K and α the MHS parameters which can be found in the literature, but are not universal.

It is possible to use *a refractometer and a viscosimeter*, doing a proper *universal calibration (UC)*. Here, the calibration curve $\log(M[\eta]) = f(V_e)$ is determined with polymer standards, using the viscosimeter instead of the MHS parameters to determine $[\eta]$. This calibration curve is then used for the determination of the molar mass distribution of polymer samples of any chemical nature.

Finally a *refractometer combined with light scattering* (LS) can be used. This setup requires no calibration curve. It utilizes the Rayleigh equation for the determination of the molar mass: $\frac{k \cdot C}{R_\theta} = \frac{1}{M \cdot P(\theta)} + 2 \cdot A_2 \cdot C$, where k is a constant for a given polymer, C is the concentration, R_θ the ratio of the light intensity scattered at the angle θ to the initial intensity, M the molar mass, $P(\theta)$ the form factor and A_2 the second virial coefficient. The term $2 \cdot A_2 \cdot C$ is neglected (since C is very low in SEC), C is determined by the refractometer, R_θ by the LS. The form factor $P(\theta)$ can be determined:

- when θ is very low, $P(\theta)=1$. This is the *low angle laser light scattering (LALLS)*.
- when R_θ is measured at several angles, the value of M is extrapolated at $\theta=0$ where $P(\theta)=1$. This method is named the *multi-angle laser light scattering (MALLS)*.
- when R_θ is measured at 90° using LS and $[\eta]$ is measured additionally via a *viscosimeter*, $P(\theta)$ is calculated using a Flory formula correlating $P(\theta)$ with M and $[\eta]$. This method is called *triple detection (TD)*.

It should be noted that other detectors can be in principle coupled to the SEC. This has been reported with osmometry,²⁰⁴ and receives more attention with MALDI-TOF-MS.²⁰⁵

It is interesting to compare the advantages and drawbacks of the different methods. The CC is the easiest, fastest and least expensive method, as well as the most accurate and robust, but is applicable only to polymers for which standards exist, namely PS and PMMA. The UC using the MHS parameters is also simple, but not really universal since it is limited to the polymers for which reliable MHS parameters can be found in the literature; it is in particular not valid for branched polymers like polyacrylates.²⁰⁰ The UC using a viscosimeter is truly universal. However, CC and UC methods have the big drawback of needing a calibration curve, which depends on the separation mechanism in the columns (purely steric exclusion or also contribution of some adsorption phenomena).

The LS methods have in common the advantage of not needing a calibration curve, and the drawback of necessitating to know the refractive index increment dn/dc of the polymer in the eluent. While the LALLS technique suffers from the lowest signal-to-noise ratio, the MALLS technique necessitates a perfect optics to know the scattering angles precisely. The TD is the least noisy LS method, but is based on the assumption that a Flory equation is valid, which was not proved.

B. Determined molar masses

The determination of reliable molar masses of PnAAs is not possible using SEC, unless a multi-detection SEC is used (UC, LALLS, MALLS or TD). These methods were not available at the Polymer Analysis service of the MPI-P in Mainz (Germany), where only a conventional calibration was possible. Therefore, another SEC analysis was performed in Paris (France) in the Laboratoire de Chimie des Polymères using a triple detector device.²⁰⁶

An example of molar mass distributions is shown on Figure 2- IV-1 for sample PMA. It can be noted that TD and LS yield higher molar masses than UC, this will be commented below.

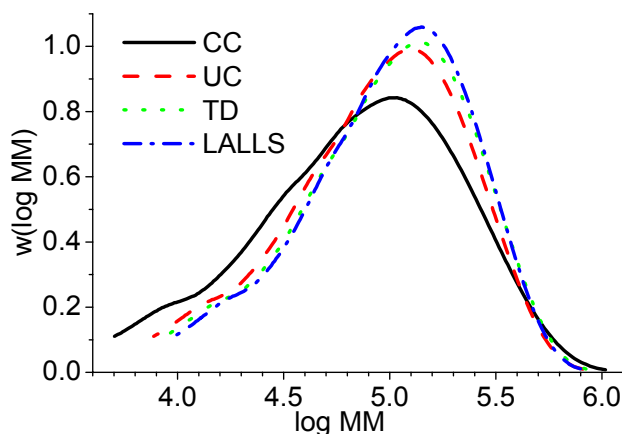


Figure 2- IV-1:
Molar mass
distribution of
sample PMA
determined by
different techniques
on a single run with
the TDA in Paris
(CC done with PS
standards).

The average molar masses determined for the model PnAA samples using SEC are given in Table 2- IV-1. The results obtained for all the synthesized PnAA samples (including the samples synthesized in small quantities to test the synthesis procedure) are presented in appendix (s. Part 7, I.C).

Samples		CC in Mainz			TDA in Paris				
		PMMA	PtBMA	PS	CC PS	Diff.	UC	TD	LALLS
PMA	M_n	44 600	51 600	36 900	39 900	+8	55 000	61 000	65 700
	M_w	133 000	139 000	110 000	119 000	+8	128 000	138 000	139 000
	M_w/M_n	3.0	2.7	3.0	3.0	0	2.3	2.3	2.1
PEA	M_n	84 700	96 100	70 000	80 700	+14	69 300	62 900	112 000
	M_w	216 000	222 000	184 000	221 000	+18	169 000	200 000	215 000
	M_w/M_n	2.6	2.3	2.6	2.7	+4	2.4	3.2	1.9
PBA	M_n	67 200	76 500	55 600	51 800	-7	100 000	89 900	119 000
	M_w	230 000	236 000	197 000	228 000	+15	318 000	248 000	273 000
	M_w/M_n	3.4	3.1	3.6	4.4	+20	3.2	2.8	2.3
PHxA	M_n	87 200	97 800	75 200	58 800	-24	88 500	144 000	165 000
	M_w	300 000	306 000	288 000	269 000	-7	395 000	335 000	347 000
	M_w/M_n	3.4	3.1	3.8	4.6	+19	4.5	2.3	2.1

Table 2- IV-1: Characterization of the model PnAAs using SEC; in the column Diff. the relative difference of CC with PS standards in Mainz and in Paris is given; M_n and M_w are indicated in $g \cdot mol^{-1}$.

A few general remarks should be made about these results. First, CC-SEC results from Mainz and Paris are reproducible. Furthermore, the M_n value can not be determined very

precisely (e.g., TD and LALLS values of PEA). This is caused by the presence of oligomers in the samples (according to IUPAC round robin tests, this can lead to an uncertainty of up to 800 % on the M_n value for PS,²⁰⁷ due to a different definition of the baseline and of the peak integration limits). It can be noted that the non-uniformity with respect to molar mass is higher measured by CC than by UC, TD and LALLS. Moreover, the LALLS results is more noisy than the TD or UC results, as can be seen on Figure 2- IV-4.

Two conclusions may be drawn. First, the most reliable molar masses for our branched PnAAs are obtained with UC and TD. Moreover, LS is more sensitive to high molar masses than viscosimetry, so that TD (and LALLS) give higher M_n and M_w than UC. Second, the sample PMA contains shorter polymer chains than PEA, PBA and PHxA.

C. Investigation of branching

As stated in paragraph III, spectroscopic (^{13}C NMR) and chromatographic (multiple detection SEC) techniques can supplement each other, as neither is capable individually of completely describing the molecular architecture imparted by the various types of branching.¹⁸²

The investigation of branching in the model PnAAs using multiple detection SEC has been done in two steps. First by proving the actual detection of long chain branches, second by attempting to quantify the amount of LCB. It should be noted that it was not applied to industrial samples because of their lack of solubility.

1. Detection of long chain branching

The presence of LCB results in a shrinkage of the hydrodynamic volume, and therefore in a decrease of the intrinsic viscosity at constant molar mass.²⁰⁸ In the case of a constant branching frequency for all molar masses, this effect is more pronounced for high molar masses, so that LCB results in a downward curvature in the plots of the intrinsic viscosity $[\eta]$ versus the molar mass on a log-log scale (s. Figure 2- IV-2).¹⁸²

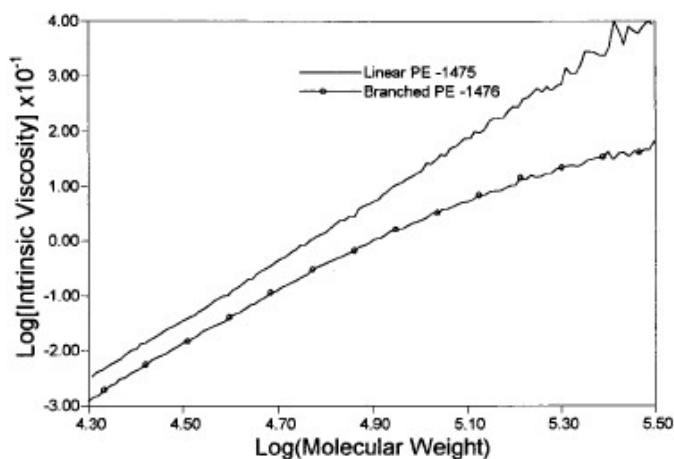


Figure 2- IV-2: Plot of the intrinsic viscosity as a function of the molar mass on a log-log scale for polyethylene; the linear chains exhibit a linear dependence, while the branched chains with a constant branching frequency exhibit a downwards curvature.¹⁸²

Similar curves have been plotted for all PnAAs. The example of PMA is shown on Figure 2- IV-3, some others are given in appendix with all the MHS parameters values used from literature (s. Part 7, IV.D.1). It should be noted that the MHS parameters quoted from literature were all determined for PMA samples synthesized using free-radical polymerization, thus very likely branched. It is clearly seen that no curvature is observed for our samples, probably due to an insufficient molar mass range or a non constant branching frequency. However, we lack a linear equivalent to be able to compare the respective intrinsic viscosities at a given molar mass. Furthermore, it should be underlined here that LCB has an influence on the intrinsic viscosity, but also on the determined molar mass, so that the plot of the intrinsic viscosity versus molar mass is rather difficult to interpret.

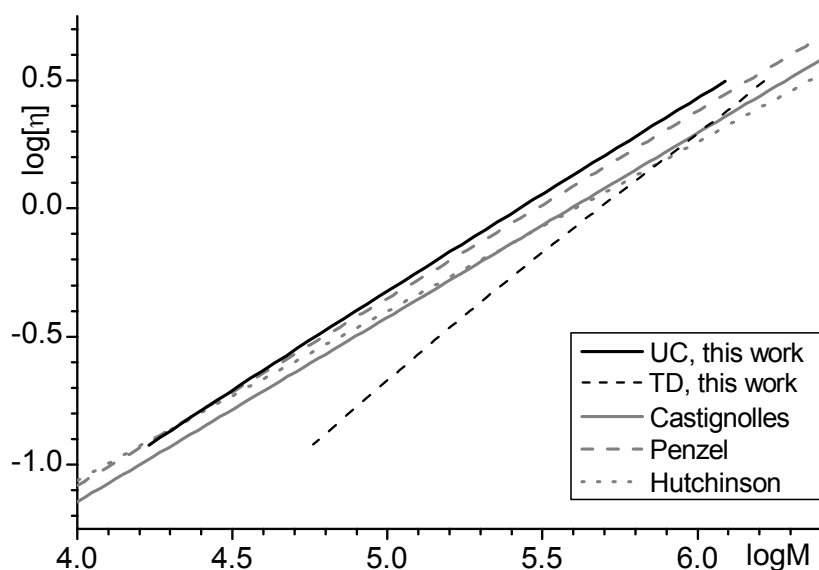


Figure 2- IV-3: Intrinsic viscosity as a function of the molar mass on a log-log scale for the investigated PMA sample, as well as other PMA samples (MHS parameters from literature: Castignolles,²⁰⁰ Penzel,²⁰⁹ Hutchinson^{210,211}).

Another plot is proposed as more appropriate to prove the detection of the LCB. It is the comparison of the plots of the molar mass versus the elution volume obtained by UC and LS. The case of sample PEA is shown on Figure 2- IV-4. The molar mass determined at a given elution volume on the same run depends on the SEC method used: UC, or LS-based (TD, LALLS). Due to the logarithmic scale used on the molar masses axis, this difference is definitely significant. The chromatogram is indicated to show that this difference is present in the elution volume range where the sample is detected. This difference is not observed when linear samples are injected, but is observed for a variety of branched poly(alkyl acrylates).²⁰⁰ Therefore, it must be caused by the presence of LCB.

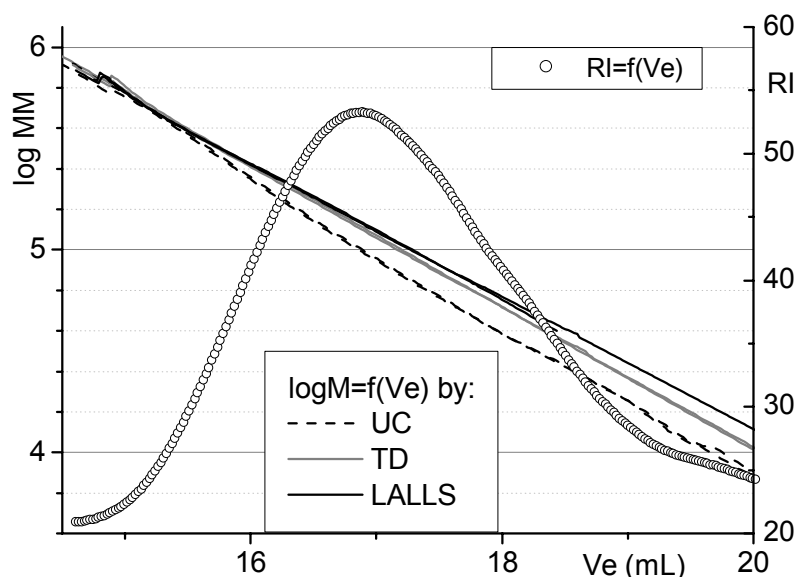


Figure 2-IV-4: Molar mass as a function of the elution volume for sample PMA, on a logarithmic scale; the different molar masses have been determined respectively by UC, TD and LALLS; the chromatogram is indicated on the same elution volume scale.

The explanation of the higher molar masses determined light scattering (TD or LALLS) as compared to UC was detailed by Castignolles.²⁰⁰ In the case of statistically branched samples, the SEC separation is not complete. The separation is done according to hydrodynamic volume, so that at each elution volume, there is a mixture of chains with different branching levels, exhibiting different molar masses but identical hydrodynamic volume. The techniques based on light scattering determine the mass average molar mass of this mixture.^{212,213} The UC determines the number average molar mass of this mixture, which is lower than its mass average molar mass.²⁰⁰ Since an average molar mass is determined at each elution volume, and since this average depends on the used method, only apparent molar masses and no true molar mass are determined.

2. Quantification of long chain branching

a) Models

Several models exist which should allow the quantification of LCB using multiple detection SEC with online viscosimeter.^{182,214,215} They are based on comparison of the branched molecule with its linear equivalent, following a theory developed by Zimm and Stockmayer.²¹⁶ Considering the contraction caused by LCB, the branching ratio g is defined as the ratio of the radii of gyration of the branched and linear molecules of same molar mass (s. Equation 2-IV-1).²¹⁶ Alternatively, the experimental ratio g' is defined as the ratio of the intrinsic viscosities of the branched and linear molecules of same molar mass (s. Equation 2-IV-1).²¹⁶ Both are linked by the Debye/Bueche viscosity shielding ratio ϵ through $g' = g^\epsilon$.¹⁸²

$$g = \left(R_{g, \text{branched}} / R_{g, \text{linear}} \right)_M \quad \text{and} \quad g' = \left([\eta]_{\text{branched}} / [\eta]_{\text{linear}} \right)_M \quad \text{Equation 2-IV-1}$$

In real polymeric systems, distributions of molar masses and of branching numbers are present. In that case, and for trifunctional branching points, the following relationship between the branching ratio g and the weight average branching number B_n is calculated.²¹⁶

$$g = \frac{6}{B_n} \left\{ \frac{1}{2} \sqrt{\frac{2+B_n}{B_n}} \ln \left(\frac{\sqrt{2+B_n} + \sqrt{B_n}}{\sqrt{2+B_n} - \sqrt{B_n}} \right) - 1 \right\} \quad \text{Equation 2-IV-2}$$

This function is a monotonic decreasing function of B_n (s. Figure 2-IV-5), so that the determination of g leads to a unique value of B_n . However, to our knowledge this equation was not experimentally validated.

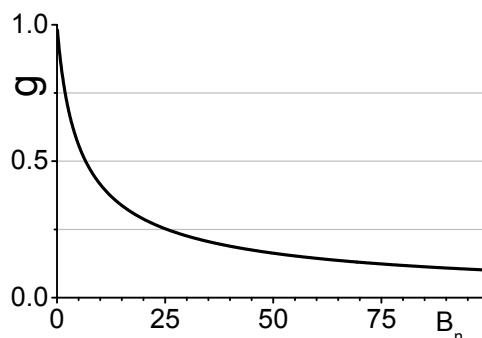


Figure 2-IV-5:
Branching ratio g
versus weight average
branching number B_n .

The intrinsic viscosities are experimentally accessible through the viscosimetric detected SEC for the investigated branched samples and through MHS equation¹⁷² of the linear reference. The radii of gyration are experimentally accessible only through SEC-MALLS for the investigated branched samples,¹⁸² or through an equation relating it to the intrinsic viscosity, the molar mass and the α MHS parameter.²¹⁷

The main weakness of the method using g' consists in the dependence of the ε exponent upon polymer chemical nature, solvent and temperature, and possibly also upon molar mass.¹⁸² ε is related to the draining characteristics of the polymer in solution. Experimental values of ε range from 0.5 (for high molar mass regular stars) to 1.5 (for comb polymers in good solvents), most of them being in the range from 0.7 to 0.8.¹⁸²

b) Case of poly(alkyl acrylates)

The TDA device used in this work was not equipped with MALLS detection, so that LCB would have to be calculated using the g' ratio. To our knowledge, the ε value for branched poly(alkyl acrylates) synthesized using conventional free-radical polymerization is not known. Furthermore, the MHS parameters for linear reference are known only for PBA.^{200,214} Data processing for the quantification of LCB would thus require to first determine MHS parameters on linear polyacrylates synthesized by anionic polymerization.

Moreover, a technical problem is observed on the TDA equipment used. Indeed, the intrinsic viscosity calculated by the software at a given elution volume depends on the

technique used for molar mass calculation from the same set of raw data: UC, TD or LALLS (s. Figure 2- IV-6). This should not be the case. A possible explanation of this observation is a change of the integration limits depending on the molar mass determination method, which is illustrated on Figure 2- IV-1. The concentration used to calculate the intrinsic viscosity from the viscosimeter signal is indeed calculated through integration of the refractometer signal over the whole chromatogram.²¹⁷ The significant difference observed depending on the molar mass determination method is technically not satisfying.

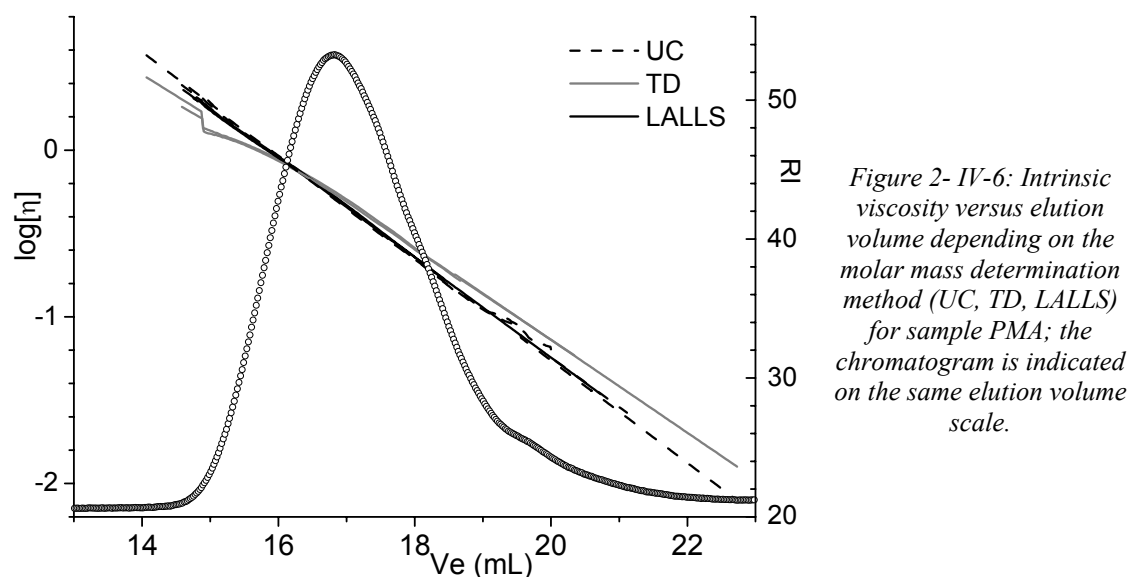


Figure 2- IV-6: Intrinsic viscosity versus elution volume depending on the molar mass determination method (UC, TD, LALLS) for sample PMA; the chromatogram is indicated on the same elution volume scale.

Furthermore, due to the incomplete separation of branched macromolecules in SEC (s. paragraph 1), the measured intrinsic viscosity is an average intrinsic viscosity for the mixture detected at a given elution volume. In order to determine an intrinsic viscosity corresponding to a single type of macromolecule, the chains must thus be separated according to their branching level (and branching topology) prior to viscosimetric measurement. This could be achieved by coupling the SEC with another separation technique, e.g. critical chromatography or HPLC. The incomplete separation of the polymer chains is also technically not satisfying.

As a conclusion, *no quantification of LCB in model PnAAs using multiple detection SEC is currently possible.*

D. Conclusion on the multiple detection SEC investigations

Poly(alkyl acrylates) can not be properly characterized with SEC using conventional calibration, due to long chain branching (LCB). However, it has been shown that a reliable estimation of the molar masses can be obtained using multiple detection techniques, namely universal calibration, triple detection and LALLS. Furthermore, multiple detection SEC is a very sensitive tool to detect LCB in polymeric samples.

LCB was detected in all investigated model PnAAs, but its quantification necessitates complementary extensive investigations, both on theoretical and experimental levels. Nevertheless, it would be interesting to continue these investigations. It would indeed yield a quantification of LCB, which could then be compared to the overall branching quantification done on the model PnAAs using ^{13}C NMR, and lead to a better understanding of the branching topology in those samples.

The quantification of LCB will necessitate for comparison of a linear sample of similar molar mass, the synthesis of which has to be realized via anionic polymerization (and subsequent characterization is needed). Then the quantification of LCB could be done via the branching ratio g or the g' ratio. On one hand, SEC-MALLS analysis is necessary to determine the branching ratio g . We are not equipped with SEC-MALLS, and first trials of SEC-MALLS of poly(alkyl acrylates) did not give convincing results.²⁰⁰ On the other hand, the use of the g' ratio necessitates to do assumptions concerning the exponent ε in the relationship $g' = g^\varepsilon$ or extensive literature research, as well as probable modelization work, in order to determine a more reliable relationship between g' and the weight average branching number B_n .

V. Conclusion on samples presentation and characterization

All the samples investigated during the present Ph.D. work have been presented. The industrial PSA samples were provided by Atofina and are copolymers of alkyl acrylates. Model poly(n-alkyl methacrylates), isotopically labeled or not, were available in our group. Model poly(n-alkyl acrylates) have been synthesized. Poly(alkyl acrylates) exhibit a high branching levels, which influence their physical properties, in particular their adhesive properties, and prevent from using SEC with conventional calibration to determine reliable molar masses. Therefore, more complex ^{13}C solid-state NMR investigations have been carried out to quantify the branching. Furthermore, multiple detection SEC investigations have been conducted to determine reliable molar masses and detect LCB.

A new solid-state NMR method for quantifying the branching level in poly(alkyl acrylates) is proposed. The measurement is done on the *pure sample in the melt*, under slow MAS, which allows to measure the *whole sample* including its insoluble fraction (on the contrary to solution-state NMR). It is conducted using single pulse excitation, and allows for a precise branching quantification in less than 3h30, which is significantly faster than the method used by Plessis et al. in 28 h, due to a significant signal-to-noise ratio improvement. It is concluded that our quantification of the branching level is *faster and more precise than the*

one developed by Plessis et al. Furthermore, it has been *applied successfully to industrial PSA samples*, which are copolymers of poly(alkyl acrylates), and contains as well other components.

Poly(alkyl acrylates) can not be properly characterized with SEC using conventional calibration. However, it has been shown that a reliable estimation of the molar masses can be obtained using multiple detection techniques, namely universal calibration, triple detection and LALLS. Furthermore, LCB was detected in all investigated model PnAAs using those techniques. Its quantification would necessitate complementary extensive investigations, both on theoretical and experimental levels.

Part 3: Using and misusing the dipolar filter, example of PEMA

I.	<i>Literature survey on nanostructuring in poly(n-alkyl methacrylates) and poly(n-alkyl acrylates)</i>	113
A.	Molecular dynamics and nanophase separation in poly(n-alkyl methacrylates) (Ph.D. work of Wind)^{5,221}	113
1.	Isotropization of atactic poly(ethyl methacrylate)	114
a)	Geometry of the isotropization ¹⁵¹	114
b)	Time scale of the isotropization ¹⁵¹	115
c)	Length scale of the isotropization ¹⁵⁰	117
2.	Influence of the tacticity on the isotropization process of poly(ethyl methacrylate) ¹⁵⁰	118
3.	Influence of the side chain length on the isotropization process ¹⁵⁰	119
4.	Local structure of poly(n-alkyl methacrylates) ¹⁵³	120
B.	Nanophase separation in poly(n-alkyl methacrylates) and poly(n-alkyl acrylates) (habilitation work of Beiner²²⁰)	122
C.	Conclusion	126
II.	<i>Dynamic contrast in poly(ethyl methacrylate), PEMA</i>	127
A.	¹H static spectra	127
B.	2D-WISE	128
1.	Sample PEMA13C	128
2.	Sample PEMADSC	130
C.	Conclusion on the dynamic contrast	131
III.	<i>Monitoring the ¹H magnetization of the more mobile parts after the dipolar filter</i>	131
A.	New type of sample for the ¹H nuclear spin diffusion technique with dipolar filter	131
B.	Changes done to data analysis	132
1.	Recording of the ¹ H nuclear spin diffusion curve.....	133
a)	Choice of the height instead of the area of the recorded ¹ H line	133
b)	Correction for longitudinal relaxation	133
2.	Determination of the plateau value	134
3.	Determination of the average diffusion coefficient	135
4.	Choice of the dimensionality	136
C.	Results obtained for poly(ethyl methacrylate) at ca T_g+70 K	136
1.	Modeling of the structured nanodomains.....	136
2.	Monitoring ¹ H magnetization after the dipolar filter	137
3.	Conclusion	138

IV. Investigation of the actual selection done by the dipolar filter and of the actual subsequent transfer mechanism.....	138
A. Actual selection done by the dipolar filter	139
1. Discussion of the experimental conditions	139
2. Obtained results for PEMA at ca T_g+45 K	140
3. Conclusion	141
B. Coherent or incoherent magnetization transfer ?	141
1. Importance of this question.....	141
2. Discussion of the type of magnetization mechanism.....	142
C. Mathematical equations describing the magnetization decay.....	143
1. Equivalence to 2D-NOE experiment	143
2. Case of two groups of equivalent homonuclear spins $A_{nA}B_{nB}$ in the slow motion limit	145
3. Magnetization decay for the more mobile parts.....	145
D. Conclusion on the actual selection and subsequent magnetization transfer	146
V. Conclusion on use and misuse of the dipolar filter.....	146
A. Summary of the investigation of PEMA at ca T_g+70 K	146
B. Conclusion on the use and misuse of the dipolar filter	147

Part 3: Using and misusing the dipolar filter, example of PEMA

It was stated in Part 1, III.C that a possible nanostructuring in a pressure-sensitive adhesive (PSA) could play a role in its adhesive properties, and that the ^1H nuclear spin diffusion technique with dipolar filter might allow to characterize such a nanostructuring. It was also mentioned that poly(n-alkyl methacrylates), PnAMAs, are appropriate model samples for such study. The goal of this chapter is thus to investigate the possibility of characterizing local nanostructuring by using the ^1H nuclear spin diffusion technique with dipolar filter.

The model PnAMAs have already been described in Part 2, II.B. A literature survey on their tendency to local nanophase separation will be presented in paragraph I, showing their suitability as model samples in the present investigation of local nanostructuring. Poly(ethyl methacrylate), PEMA, is retained as example; its dynamic contrast is investigated in paragraph II. The results obtained at T_g+70 K with the ^1H nuclear spin diffusion technique with dipolar filter will be detailed in paragraph III, together with the modifications implemented in the data analysis. The actual magnetization selection and equilibration mechanism will be demonstrated in paragraph IV, followed by a conclusion on the use and misuse of the dipolar filter in paragraph V.

I. Literature survey on nanostructuring in poly(n-alkyl methacrylates) and poly(n-alkyl acrylates)

The study of nanophase separation in homopolymers with alkyl side chain²¹⁸ is closely related to the study of the relaxation behavior of these polymers, which began in the 1950s for the poly(n-alkyl methacrylates).²¹⁹ We chose to present here only the results that are of direct relevance for the discussion of our own results, namely parts of the Ph.D. work of Wind⁵ on molecular dynamics and nanophase separation in poly(n-alkyl methacrylates), and parts of the habilitation work of Beiner²²⁰ on relaxation and nanophase separation in poly(n-alkyl methacrylates), PnAMAs, and poly(n-alkyl acrylates), PnAAs.

A. Molecular dynamics and nanophase separation in poly(n-alkyl methacrylates) (Ph.D. work of Wind)^{5,221}

Heating an amorphous polymer above its glass transition generally yields an isotropic melt. In this respect, poly(n-alkyl methacrylates), PnAMAs, are of special interest, since these macromolecules exhibit highly anisotropic motional processes in the molten state, as

shown by Kulik et al.²²² For poly(ethyl methacrylate), PEMA, and its higher homologues, the time scales of the usual segmental α -relaxation and the isotropization process are clearly separated.

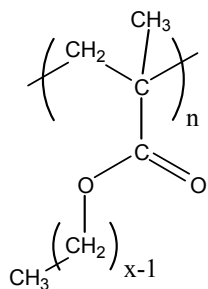


Figure 3- I-1: Poly(*n*-alkyl methacrylates), PEMA for $x=2$.

1. Isotropization of atactic poly(ethyl methacrylate)

The isotropization process is a relaxation process which leads the macromolecule from a state where some motions are anisotropic within a given time window, to a state where the motions are isotropic. The isotropization in atactic poly(ethyl methacrylate), a-PEMA, was characterized using solid-state NMR on a sample of PEMA statistically labeled with ^{13}C on 20 % of the C=O groups. It has a T_g of 338 K, a high molar mass, and in fact a high syndiotactic content (63 % of rr triads), s. Part 2, III.B for more details.

a) Geometry of the isotropization¹⁵¹

2D ^{13}C exchange spectra⁷⁶ were recorded under static conditions, with a mixing time of 2 ms, at various temperatures above T_g (s. Figure 3- I-2). In this experiment, the intensity at a spectral point (ω_1, ω_2) is the joint probability that a species having a frequency ω_1 at the beginning of the experiment has a frequency ω_2 after the mixing time t_m . Neither elliptic patterns, characteristic of discrete reorientations at defined angles, nor patterns characteristic of isotropic rotational diffusion, simulated for various correlation times, were observed.

At a lower temperature, $394\text{ K} = T_g + 56\text{ K}$, the intensity near the diagonal represents the diffusive motions of the main chain at small angles, while the non structured distribution of intensity over the whole 2D exchange plane represents the reorientation processes with wide angles and variable amplitude. A spectrum simulated assuming an isotropic random jump model and a single correlation time ($t_1 = 3.3 \cdot 10^{-3}\text{ s}$ at 394 K) reflected all characteristic properties of the experimental spectrum (s. Figure 3- I-2). The fact that a single correlation time is involved, and not a distribution of correlation times, was proved by measurement of Hahn-echo decay curves.

At higher temperatures, $405\text{ K} = T_g + 67\text{ K}$ and $416\text{ K} = T_g + 78\text{ K}$, the recorded spectra were also successfully simulated using a random jump model (s. Figure 3- I-2).

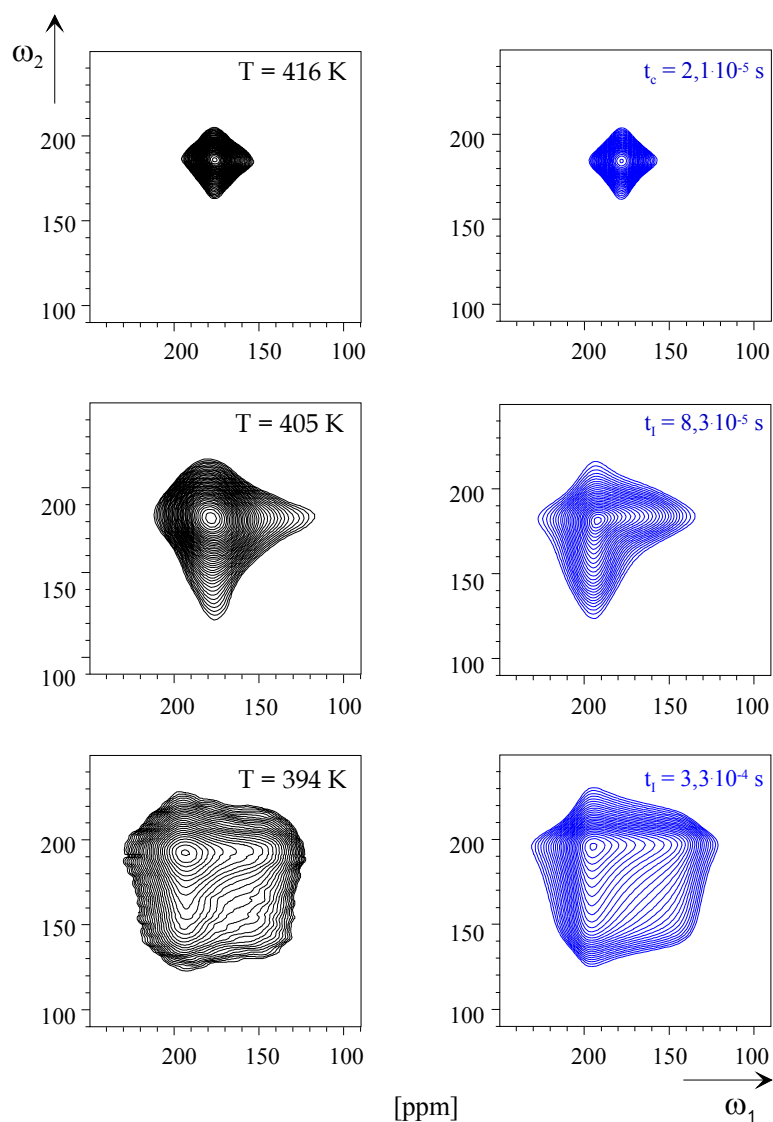
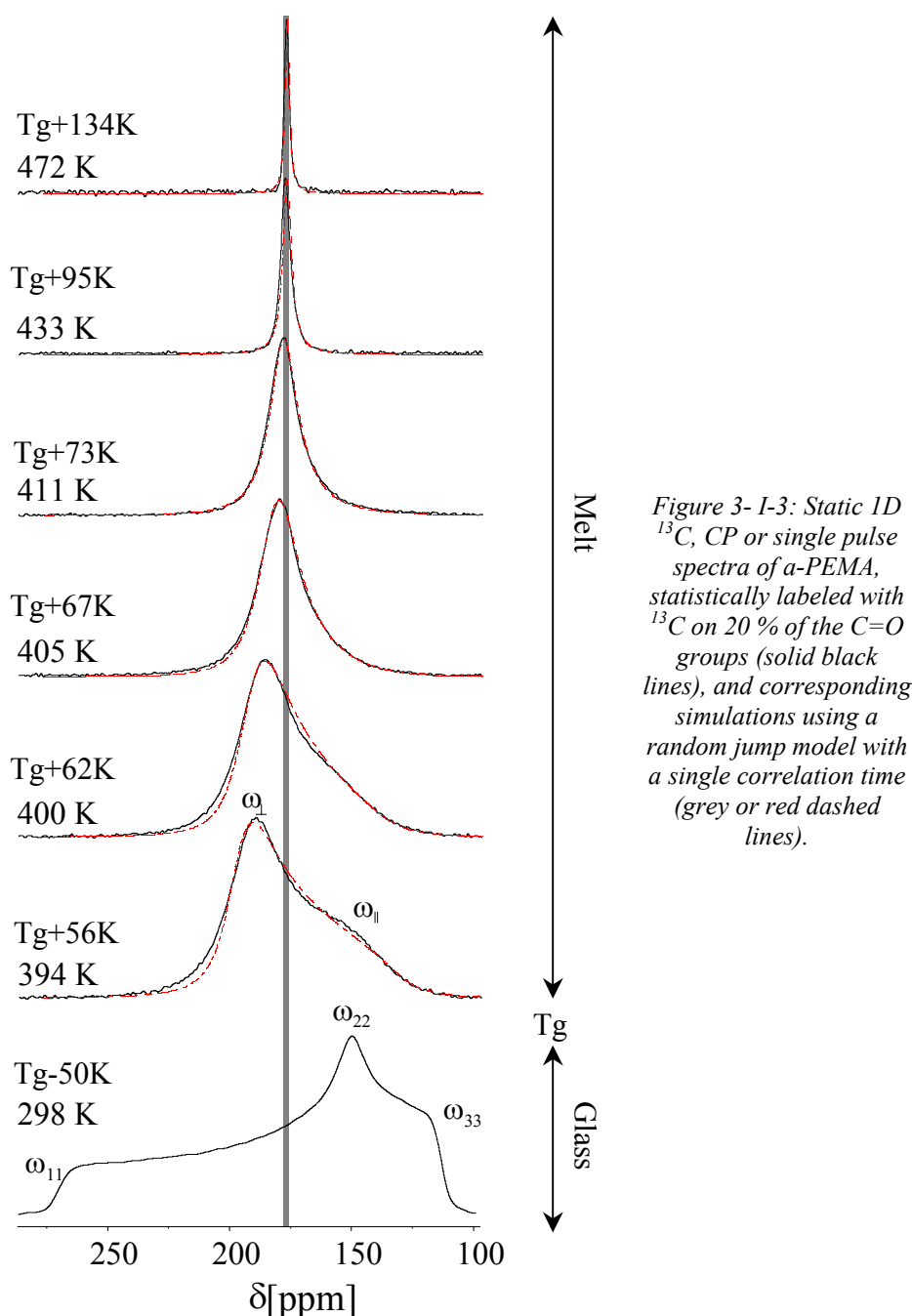


Figure 3- I-2: Static 2D ^{13}C exchange spectra of a-PEMA, statistically labeled with ^{13}C on 20 % of the C=O groups (on the left side), and corresponding simulations using a random jump model with a single correlation time (on the right side); the mixing time was 2 ms; T_g is 338 K.

b) Time scale of the isotropization¹⁵¹

The geometry of the isotropization motion had been established using the 2D exchange experiments presented above. Therefore 1D line shape analysis could be used for a faster determination of correlation times. 1D ^{13}C static, cross-polarization (CP) or single pulse excitation, spectra were recorded for the labeled a-PEMA, at various temperatures. Each spectrum was simulated using a random jump model to obtain the single correlation time of the isotropization motion (s. Figure 3- I-3).



All measured correlation times related to the isotropization motion of a-PEMA were plotted against the inverse temperature on an Arrhenius diagram for this polymer (s. Figure 3- I-4) to compare them with known correlation times of α - and β -relaxation processes taken from literature.²²¹ These α - and β -relaxation processes are historically named so from dielectric spectroscopy measurements, where the slowest observed process was named α -relaxation, the next faster one was named β -relaxation. The α -process corresponds to cooperative motions of polymer chains, usually the cooperative reorientation of several monomeric units in the main chain also called glass transition. The β -process corresponds to local motions, in the case of side chain polymers like PnAMAs it is usually the reorientation of individual ester side chains. Above the crossover temperature, both α - and β -relaxation

merge into the $\alpha\beta$ -relaxation. The Arrhenius diagram of a-PEMA shows that the isotropization is clearly slower than the α - and $\alpha\beta$ -relaxations.

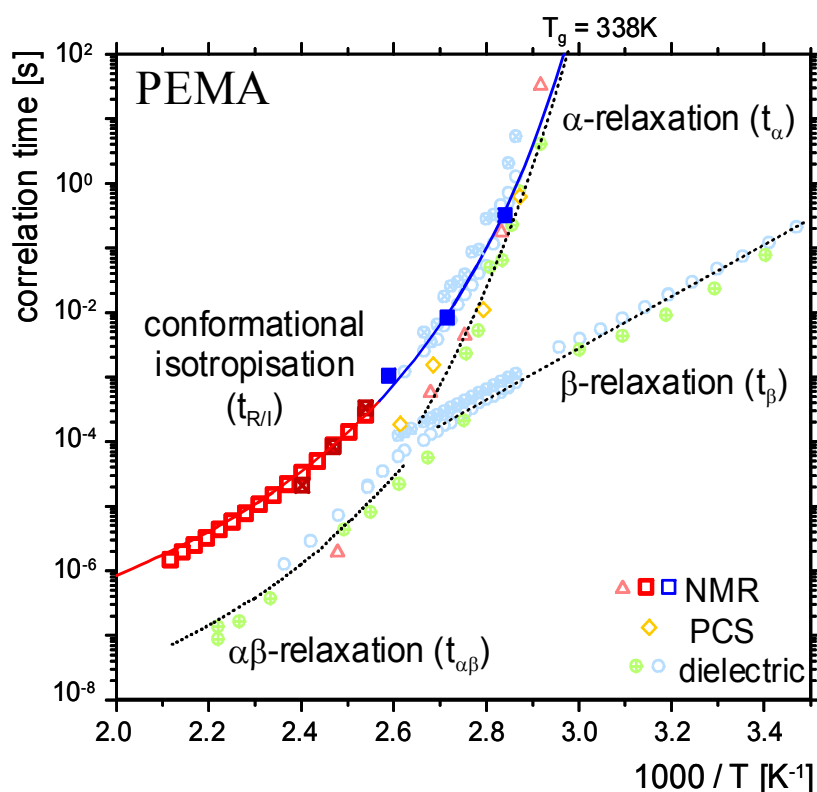


Figure 3- I-4: Arrhenius diagram of the separation of the dynamic time scales in a-PEMA melts. All the data were scaled with a T_g of 338K. The measured correlation times $t_{R/I}$ of the main chain measured using 1D ^{13}C and 2D ^{13}C exchange NMR¹⁴⁷ were compared with the correlation times of α -, β - and $\alpha\beta$ -relaxations taken from literature (PCS is photon correlation spectroscopy).²²¹

The β -relaxation time scale exhibit an Arrhenius behavior, while the α -relaxation and the isotropization time scales are described by a Williams-Landel-Ferry (WLF) equation²²³ (s. Appendix in Part 7, III.A.3):

$$\log\left(\frac{t(T)}{t(T_0)}\right) = -\frac{C_1(T-T_0)}{C_2+(T-T_0)}$$

where $t(T)$ is the correlation time at the temperature T (K), and C_1 and C_2 are constants characteristic of the material. The reference temperature T_0 is often chosen equal to T_g , which generally results in values of ca $C_1^g = 17.4$ and $C_2^g = 51.6$ K for the α -relaxation process. In the case of a-PEMA shown here, the reference temperature was chosen equal to $T_g = 338$ K, which leads to $C_1^g = 10.6$ and $C_2^g = 52.6$ K for the isotropization process. (This is clearly different from the parameters obtained for $\alpha\beta$ -relaxation of a-PEMA from dielectric spectroscopy: $C_1^g = 15$ to 21, $C_2^g = 65$ K, $T_g = 335$ K).

c) Length scale of the isotropization¹⁵⁰

The length scale of the isotropization in a-PEMA was probed by recording static 1D ^{13}C CP spectra of a-PEMA samples of different mass-average molar masses M_w with ^{13}C in natural abundance, at T_g+56 K (s. Figure 3- I-5). These samples were synthesized by anionic polymerization in order to obtain narrow molar mass distributions. The spectra of the

polymers containing 56 and 12 monomeric units can be described by a random jump model with a single correlation time corresponding to the one of the α -PEMA of higher M_w which proves that the isotropization process occurs in these polymers. On the contrary, the oligomer containing on average four monomeric units exhibits a spectrum which is fully averaged by isotropic motions, without an axial-symmetric tensor, and the measured correlation time is the one of the $\alpha\beta$ -relaxation; this proves that the isotropization motion does not occur in it. Finally, it can be deduced that ***the isotropization motion involves a segment of polymer chain containing 5 to 12 monomeric units.***

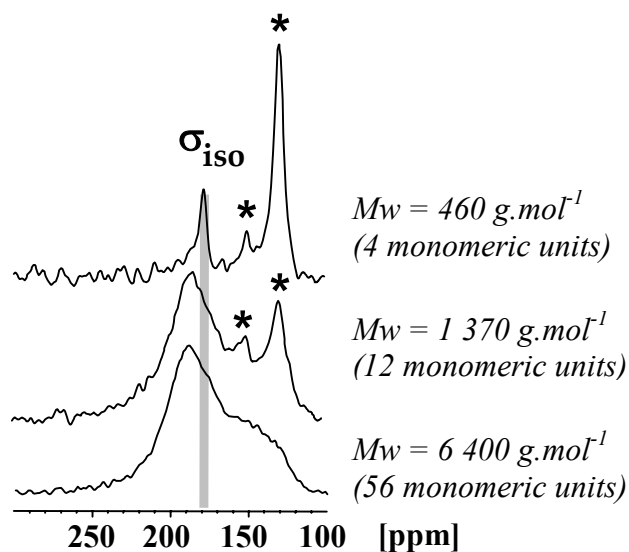


Figure 3- I-5: Static 1D ^{13}C CP spectra of a-PEMA, with ^{13}C in natural abundance at $T_g+56\text{K}$ (the lines marked with an asterisk * arise from the polymerization initiator, diphenyl hexyl lithium).

2. Influence of the tacticity on the isotropization process of poly(ethyl methacrylate)¹⁵⁰

The length scale of the isotropization process in a-PEMA (5 to 12 monomeric units) is the same as the statistical length of syndiotactic sequences in a-PEMA, so that the isotropization process could be related to the tacticity of PEMA. High molar mass isotactic PEMA (i-PEMA) was synthesized using anionic polymerization in toluene. Since the relaxation behavior of i-PEMA had never been characterized before, non labeled i-PEMA was used to determine the time scales of α - and $\alpha\beta$ -relaxations (using mechanical and dielectric spectroscopy) and the time scale of β -relaxation (via solid-state NMR). The time scale of the isotropization process in i-PEMA was determined by recording 2D ^{13}C exchange and 1D ^{13}C , CP or single pulse spectra of a sample statistically labeled with ^{13}C at 20 % of C=O groups. The results are shown on Figure 3- I-6. The parameters of the WLF equation describing the isotropization process of i-PEMA are $T_g=290\text{ K}$, $C_1^g=11.5$, $C_2^g=58\text{ K}$. Since the WLF parameters of i-PEMA and a-PEMA are the same for the isotropization process, as well as for α -relaxation, ***the isotropization process of PEMA is observed for both syndio- and isotactic sequences.***

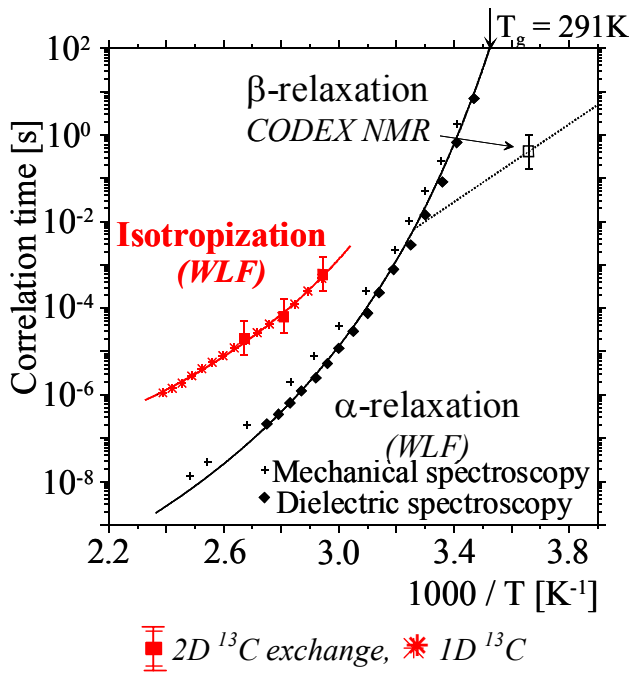


Figure 3- I-6: Arrhenius diagram of the separation of the dynamic time scales in i-PEMA melts. All the data were scaled with a T_g of 290 K.

3. Influence of the side chain length on the isotropization process¹⁵⁰

Several poly(n-alkyl methacrylates) were synthesized, statistically labeled with 20 % ¹³C on C=O. The side chain length was varied: methyl (PMMA), ethyl (PEMA), n-butyl (PBMA), n-hexyl (PHxMA). They all exhibit a high molar mass, their T_g determined by differential scanning calorimetry (DSC) are shown in Table 3- I-1 (s. Part 2, III.B for details).

Sample	PMMA	PEMA	PBMA	PHxMA
T_g (DSC at 10K/min)	401	338	307	277

Table 3- I-1: T_g of atactic poly(n-alkyl methacrylates), 20 % statistically ¹³C labeled on C=O.

The time scale of the isotropization motion was investigated for each of these polymers by recording static 1D ¹³C, CP or single pulse excitation, spectra at different temperatures and fitting them using a random jump model to determine the correlation time of the isotropization motion (s. Figure 3- I-7). It appears that the isotropization process can be described by similar and consistent sets of WLF parameters for all poly(n-alkyl methacrylates) except PMMA.

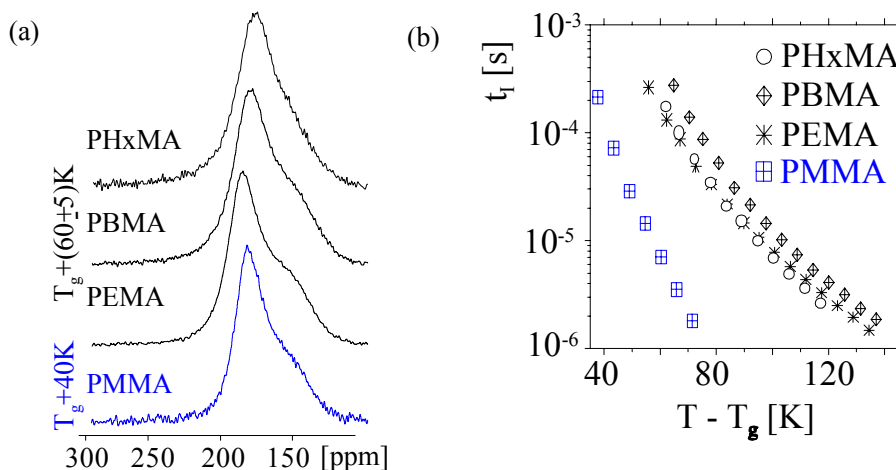


Figure 3- I-7: (a) Static 1D ¹³C CP spectra of various poly(n-alkyl methacrylates) statistically labeled with ¹³C on 20 % of the C=O groups; (b) Arrhenius diagram of the correlation times, extracted by fitting these spectra using a random jump model with a single correlation time.

The time scale of the isotropization process measured by Wind¹⁵⁰ has been compared to the time scale of the $\alpha\beta$ -relaxation for each polymer except PMMA by plotting them on an Arrhenius diagram (s. Figure 3- I-8). The correlation times for α -, β , and $\alpha\beta$ -relaxations quoted by Wind were measured by NMR, photon correlation spectroscopy, dielectric spectroscopy, mechanical spectroscopy and calorimetric measurements. These diagrams show that the $\alpha\beta$ -relaxation time scale comes closer to the isotropization time scale when the side chain length is increased.

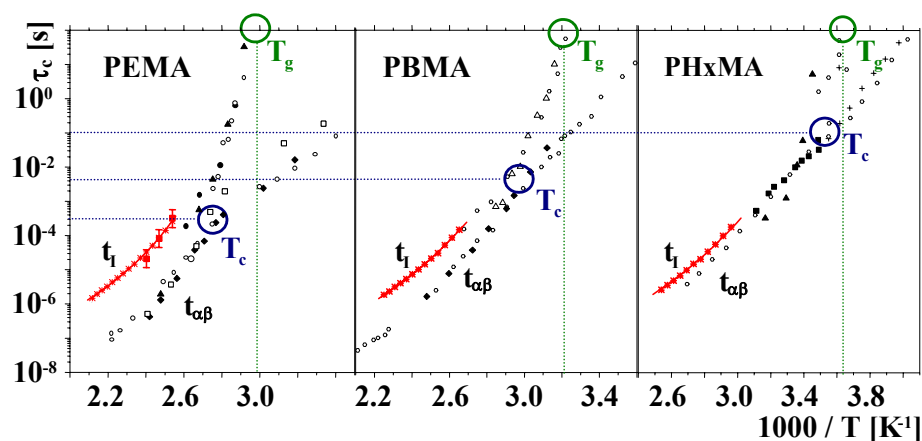


Figure 3- I-8: Arrhenius diagrams of the separation of the dynamic time scales in poly(*n*-alkyl methacrylate) melts.

4. Local structure of poly(*n*-alkyl methacrylates)¹⁵³

The local structure of the PnAMAs was studied using wide-angle X-ray scattering (WAXS). The WAXS studies of these polymers show the presence of two or three clearly different peaks, except for PMMA (since the systems are amorphous, the term halo would be correct, but the term peak is more usual and will be used here). Apart from the peak (I) around 13 nm^{-1} , a peak (II) appears around 8 nm^{-1} for lower homologues and a peak (III) in the range 3.5 to 6 nm^{-1} (s. Figure 3- I-9).

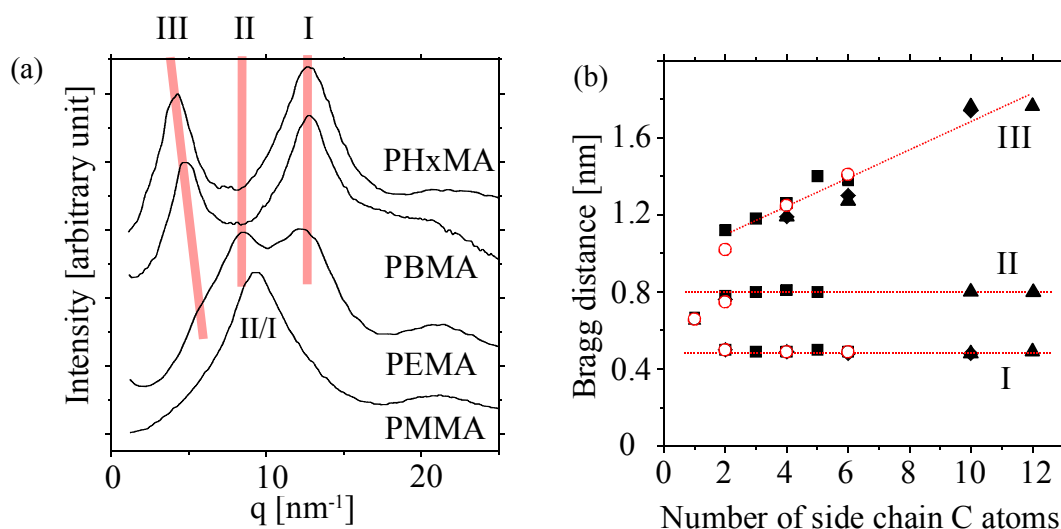
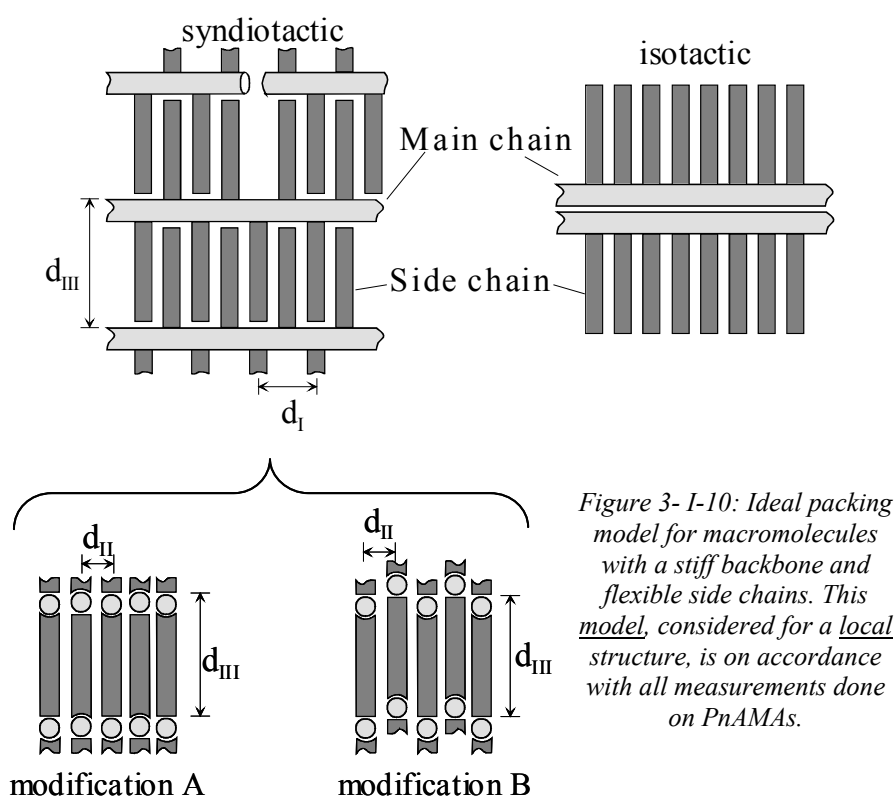


Figure 3- I-9: (a) WAXS curves of poly(*n*-alkyl methacrylates) at 300 K. (b) Corresponding Bragg distances as a function of the number of carbons in the ester side group; the data recorded by Michael Wind (hollow circles) are plotted together with other values from the literature (full squares, triangles, and diamonds).⁵

Several arguments of different origins were used to assign the observed peaks to structural features of the poly(n-alkyl methacrylates). The peak (I) is assigned to side chain groups according to a wide-angle neutron scattering (WANS) study of selectively deuterated polymers. This peak corresponds to an intrasegmental phenomenon since its intensity is independent of the temperature. Furthermore, a change in temperature around the glass transition has no influence on it, so that it can be assigned to non-bonded neighbors atoms. The peak (II) is assigned to main chain groups according to a WANS study of selectively deuterated polymers; this peak corresponds to an intersegmental phenomenon since its intensity increases with increasing temperature; furthermore the increase of the corresponding distance with temperature is related to the decrease of the density in the polymer. The peak (III) is assigned to side chain groups and intersegmental phenomena according to a WANS study.

A structure had already been proposed by Adam²²⁴ to describe the structure of macromolecules with incompatible stiff main chains and flexible side chains (polyesters, polyamides and polyimides). This structure was proposed again here to describe *locally* the PnAMAs (s. Figure 3- I-10), since it is in accordance with all the observations detailed before.



The driving force of the nanophase separation in PnAMAs is the incompatibility of stiff polar main chains with the flexible non polar alkyl side chains. It should be noted that the term polar will be used in this work for the main chain including the COO group, even if

this group would be considered as little polar by most chemists. In the case of syndiotactic PnAMAs, two arrangements of the main chains are possible (modifications A and B), and modification B is the most probable due to steric hindrance. ***This model must be considered as an abstract limiting structure to illustrate the local order in the real systems, on a length scale of 5 to 10 monomeric units.*** This structure and the stability that it implies would explain the anisotropic motion observed in the polymethacrylate melts.

B. Nanophase separation in poly(n-alkyl methacrylates) and poly(n-alkyl acrylates) (habilitation work of Beiner²²⁰)

Beiner et al.²¹⁹ recorded the evolution of shear loss modulus with temperature for different PnAMAs at 10 rad.s^{-1} . Besides α -, β - and $\alpha\beta$ -relaxations, an additional relaxation process at low temperatures was observed for all members above propyl ($x=3$, s. Figure 3-I-1 for notation). It is shown on Figure 3-I-11. This process is very little or not active in dielectric relaxation, but active in temperature modulated DSC, indicating a cooperative relaxation process of the alkyl side chains. It was called polyethylene-like glass transition, α_{PE} . Since the α -process is associated with the glass transition measured using conventional DSC, the samples exhibit two glass transition-type processes. The α_{PE} -relaxation process, active in the glassy homopolymers, can originate from a phase separation between polar main chains and non polar side chains on a nanometer length scale. It can also originate from a dynamic pattern, fluctuating in time and space, with two inherent time and length scales. The static picture of the nanophase separation is preferred by Beiner et al., and is in accordance with the existence of two pronounced peaks in WAXS (peaks I and III of Figure 3-I-9).

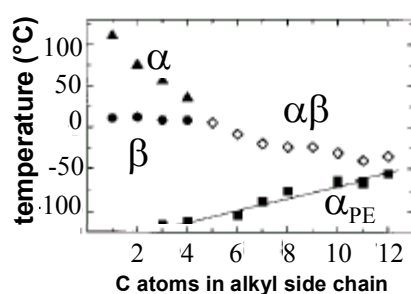
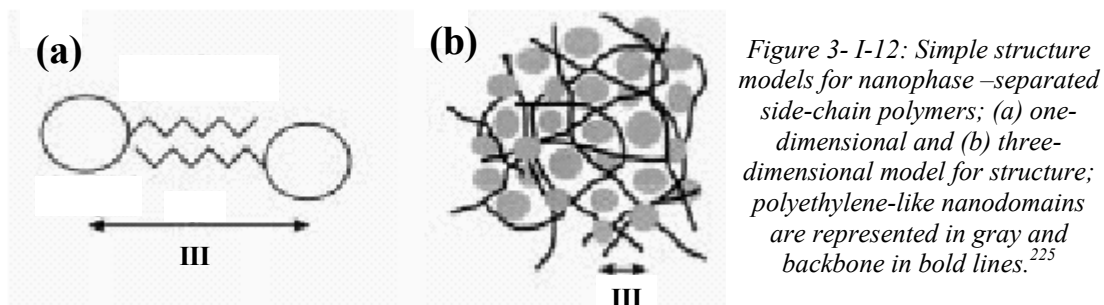


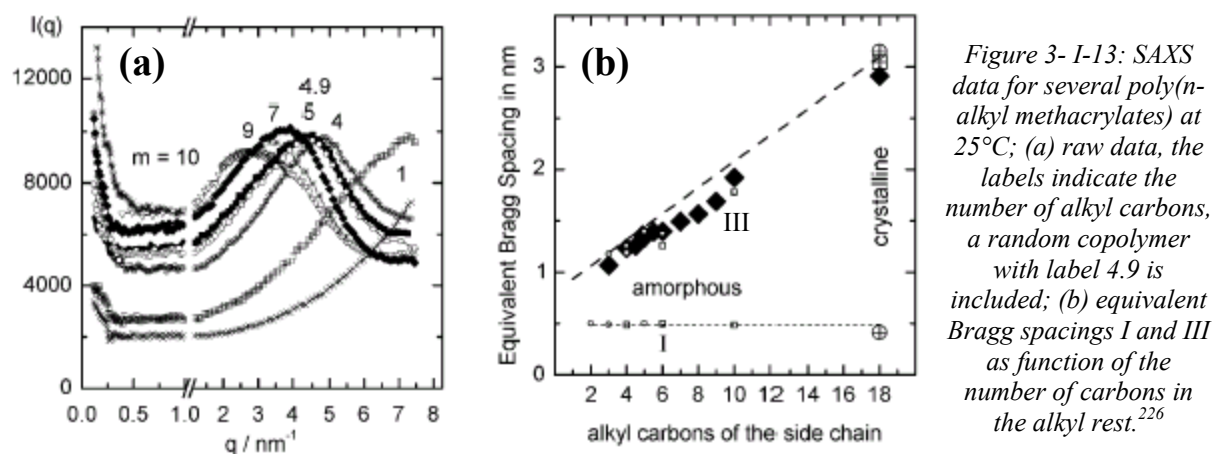
Figure 3-I-11: Relaxation temperatures for different relaxation processes α , β , $\alpha\beta$ and α_{PE} as a function of side chain length; the symbols correspond to the maxima positions in the shear loss moduli at 10 rad.s^{-1} .²¹⁹

Beiner²²⁵ reviewed the results concerning the relaxation behavior in the crossover region between α and $\alpha\beta$ relaxation, as well as the nanophase separation for PnAMAs. The coexistence of two glass transitions is rather unusual for homopolymers, but typical of microphase separated block copolymers and other systems showing a static structure on a larger scale. Therefore, a kind of local phase separation is also expected for the amorphous poly(n-alkyl methacrylates) with a long enough alkyl side chain (more than three carbon atoms), due to the incompatibility of the polar backbones and the non polar side chains. Two

of the three peaks observed in WAXS are discussed. The main peak at 0.5 nm (I in Figure 3-I-9) was attributed to chain-to-chain distance since it is a typical Van der Waals separation of non-bonded neighbors. The peak at 1 to 1.8 nm (III in Figure 3-I-9) was attributed to either the backbone to backbone distance or to the typical repeating distance of the polyethylene-like nanodomains in the melt (s. Figure 3-I-12).



Beiner et al.²²⁶ summarized the structural and dynamic heterogeneities in higher homologues of PnAMAs in which no side-chain crystallization occurs. They show small-angle X-ray scattering (SAXS) data for side chains ranging from n-butyl ($x=4$) to n-decyl ($x=10$), as well as n-octadecyl ($x=18$) and a random copolymer of n-hexyl and n-butyl ($x=4.9$) (s. Figure 3-I-13). They observe that the higher Bragg spacing increases monotonically with the alkyl side-chain length, but not linearly. The dependence has an exponent close to 0.5 for propyl to nonyl, indicating a Gaussian coil-like conformation of the side chain. Interestingly, random copolymers behave similar to homopolymers with the same average side chain length. The morphology of the PnAMAs is a situation with alkyl nanodomains containing the aggregated alkyl groups of different monomeric units surrounded by carboxylic groups (belonging to main chains). However, the shape of the 1 to 2 nm large alkyl nanodomains is not clear so far.



Hempel et al.²²⁷ characterized PnAMAs with longer alkyl side chains (10 to 18 carbons), using SAXS, calorimetric and dielectric methods. They showed that PnAMAs

undergo partial crystallization of the nanodomains composed of alkyl side chains for side chains longer than 12 carbons.

Pascui et al.²²⁸ studied the molecular dynamics of poly(n-hexyl methacrylate) (x=6) in the range T_g to T_g+40 K using solid-state NMR, in order to assign the molecular dynamics of the different subunits of the monomeric units to the different relaxation processes that were detected by dielectric and mechanical relaxations. They used ^{13}C 1D-exchange techniques under MAS and developed a method to correct the data for ^1H nuclear spin diffusion which occurs in the samples under MAS at the same time scale as the investigated molecular reorientations (even in the samples naturally abundant in ^{13}C). They probed the dynamics of the side-chain using the O-CH₂ group, and showed that it is involved only in the localized β -process. They probed the dynamics of the main chain using the quaternary carbon and showed that it is involved in the localized β -process as well as in the cooperative α -process. They showed that the COO group dynamics is dominated by the β -process around T_g , while at higher temperatures both α and β contribute to it.

Beiner and Huth²²⁹ showed that *nanophase separation of incompatible main and side-chain parts is a general phenomenon in amorphous polymers with long alkyl side chains*. This conclusion was achieved by comparing relaxation dynamics and scattering data for PnAAs, PnAMAs, poly(di-n-alkyl itaconates) and hairy rod polyimides. SAXS data exhibit two main peaks (s. Figure 3- I-14 and Figure 3- I-15 for the peak III). As detailed above, this indicates *an aggregation of the alkyl groups from different monomeric units, belonging to one or different polymer chains, in the amorphous material. This side chain aggregation occurs on a length scale of 1 to 2 nm*.

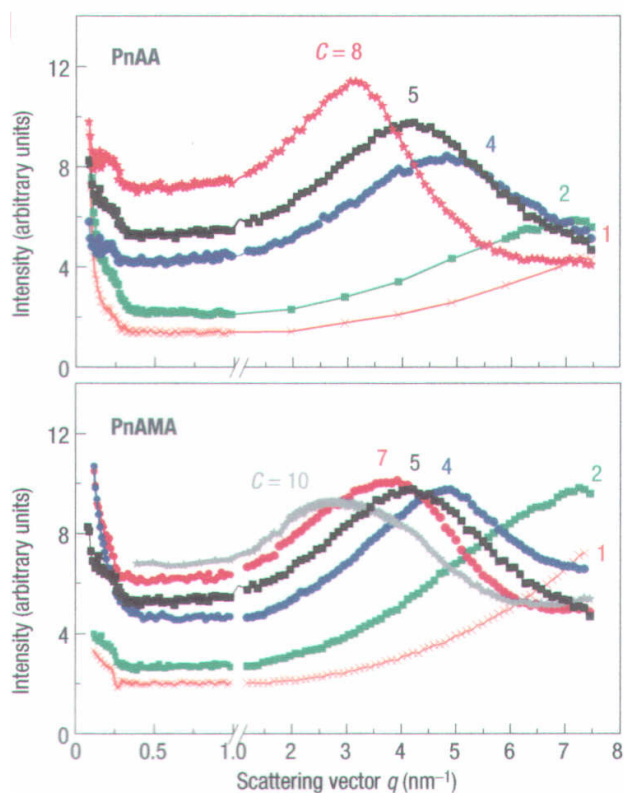


Figure 3- I-14: Peak III in SAXS data at 25°C for PnAAs (top) and PnAMAs (bottom),¹⁵³ C is the number of carbons in the alkyl side chain.

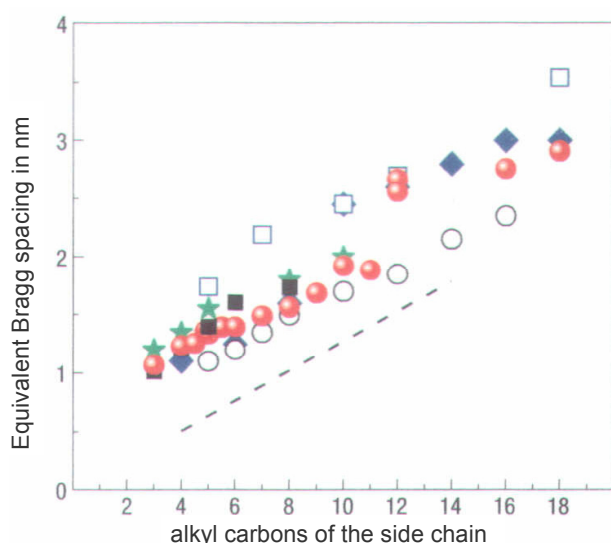


Figure 3- I-15: Equivalent Bragg spacing III from SAXS data vs number of carbons in alkyl side chain, for PnAAs (filled squares), PnAMAs (filled circles), polyitaconates (stars), polyimides (diamonds), poly(alkylbenzimidazol-alt-thiophenes) (open squares), poly-1-olefins (open circles). The dashed line indicates the length of extended alkyl groups (all trans).²²⁹

A similar polyethylene-like glass transition is observed in all families cited above,²²⁹ which depends only on the alkyl side chain length, but not on nature of the main chain (s. Figure 3- I-16). In PnAAs and PnAMAs the size of cooperatively rearranging regions (CRRs²³⁰) involved in the α_{PE} process is a few nanometers (as extracted from calorimetric data or measured by solid-state NMR). This is comparable to the size of the alkyl nanodomains. Therefore Beiner and Huth interpret the α_{PE} process as an hindered glass transition in self-assembled alkyl nanodomains.

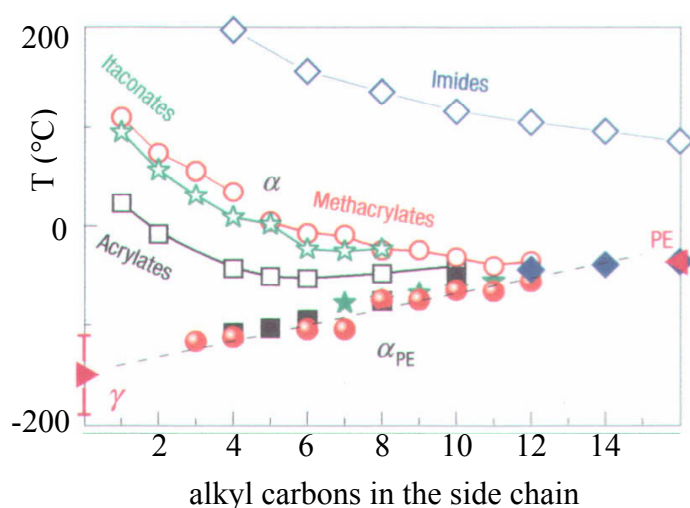


Figure 3- I-16: Relaxation temperature of the α process and of the polyethylene-like α_{PE} process vs alkyl side chain length for different polymer series; the data are taken from dielectric and shear data at 10 rad.s^{-1} for PnAAs (squares) and PnAMAs (circles), and from shear data at 6.28 rad.s^{-1} for polyitaconates (stars) and polyimides (diamonds); the T_g for amorphous polyethylene and the relaxation temperature of the γ -process in semi-crystalline polyethylene are given for comparison (triangles).²²⁹

Hiller et al. investigated a series of n-butyl methacrylate samples with different degrees of polymerization (1, 2, 6, 10, 25, 52, 405) using SAXS.²³¹ They observed that the main features of the nanophase structure are nearly identical for all polymers and oligomers containing more than 25 monomeric units. Furthermore, this structure is significantly different only for the shortest oligomers (less than 10 monomeric units), especially for the monomer and the dimer. This confirms the conclusion of Wind¹⁵⁰ from NMR results (s. paragraph A) that the isotropization motion, and hence the nanophase separation, involves a segment of polymer chain containing 5 to 12 monomeric units.

C. Conclusion

X-ray scattering (SAXS) data show a similar behavior for PnAAs and PnAMAs²²⁹ (s. Figure 3- I-15). In addition to the van der Waals peak below 1 nm, both exhibit a peak at a Bragg distance linearly increasing with the alkyl side chain length. However, a major difference between PnAMAs and PnAAs should be emphasized here: an intermediate peak is clearly seen for lower PnAMAs and not for the PnAAs. This intermediate peak was assigned⁵ to the distance between two consecutive side chains attached to the same backbone. Therefore the PnAAs *probably* adopt a local nanostructure, similar to PnAMAs, but are less ordered within the respective domains. This type of structure, more or less ordered, has already been observed for stiff macromolecules with incompatible flexible side chains, for which a layered geometry was observed (s. Figure 3- I-17).²²⁴

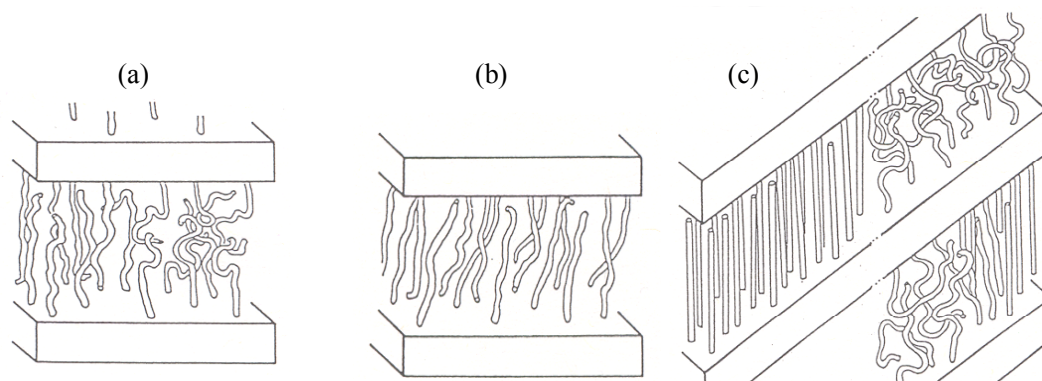


Figure 3- I-17: Layered structures observed for "hairy rods"⁴: (a) almost no order within the layer, (b) order within the layer, (c) order within the layer only present in some parts of the sample.

As a conclusion, both PnAMAs and PnAAs exhibit a local ordering on the nanometer length scale, as it is the case for numerous side chain polymers.²³² This ordering most probably results in a dynamic contrast: the structured nanodomains should be less mobile than the rest of the sample. Therefore both sample families are appropriate model samples for a ^1H nuclear spin diffusion investigation with dipolar filter. However, since the nanostructure is more pronounced in the PnAMAs, those are assumed to be better model samples for this investigation. The most studied PnAMA is PEMA. Furthermore, the investigations should be conducted at the same distance from T_g for all samples, and the temperature of interest for the industrial samples is room temperature, i.e. ca T_g+70 K. Finally, we chose to investigate first PEMA at T_g+70 K.

II. Dynamic contrast in poly(ethyl methacrylate), PEMA

The dynamic contrast is the difference in mobility between the more mobile and the less mobile parts of a sample. It was characterized in PEMA by solid-state NMR, in particular ^1H static spectra and 2D-WISE experiments.

A. ^1H static spectra

All recorded spectra are shown in the appendix (Part 7, IV.A.1), a few representative spectra are shown in Figure 3- II-1 (remarks on the small very narrow line are made in appendix in Part7, I.C). At none of these temperatures, the simple superposition of a broad and a narrow line is observed: the line gets narrower in a visually homogeneous way with increasing temperature. *This means that the whole sample is becoming more mobile with increasing temperature, and exhibits no strong dynamic contrast.* However, less pronounced dynamic contrast within the sample might still be present and probed using the dipolar filter.

In this case, the static spectra would be a superposition of two lines with similar line widths, so that it would be difficult to visually differentiate them.

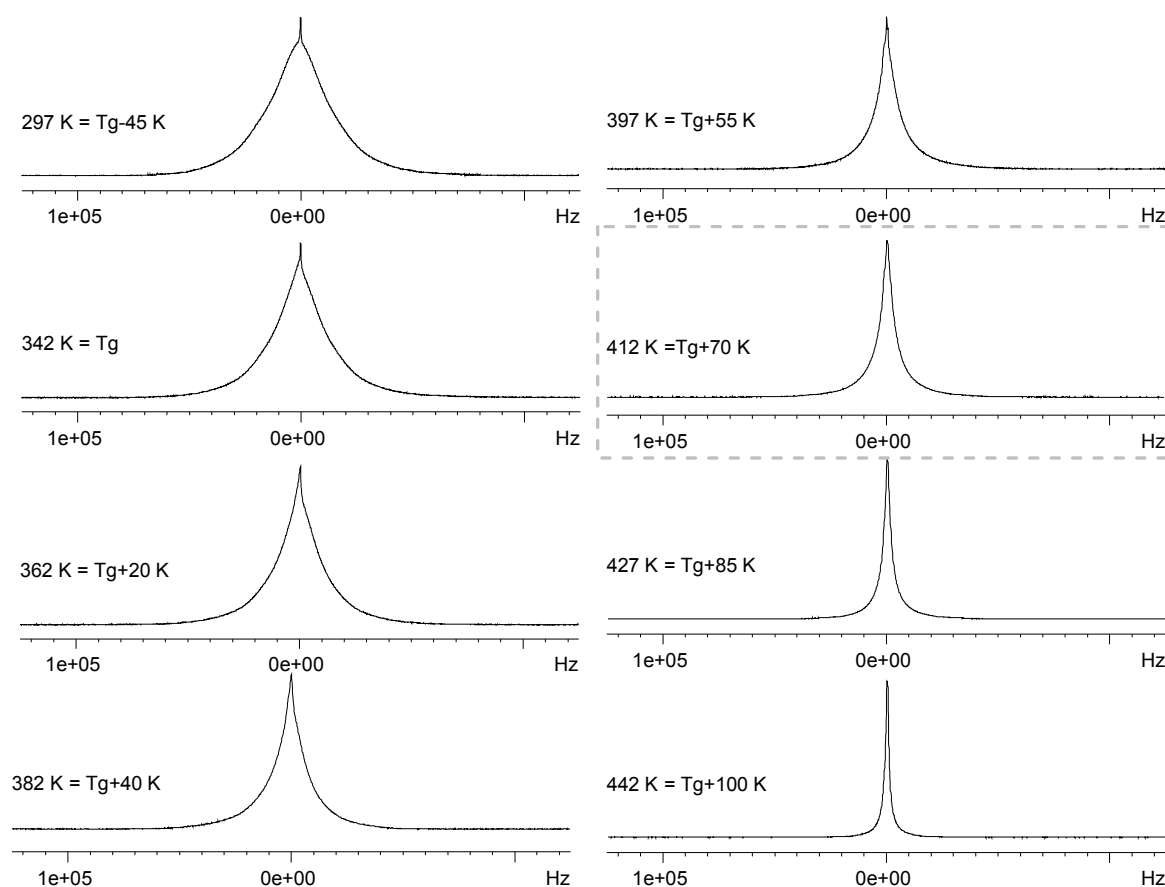


Figure 3- II-1: Influence of the temperature on the shape of the ^1H spectrum of sample PEMA (spectra recorded at a ^1H Larmor frequency of 300.13 MHz, under static conditions); the dotted frame indicates the temperature at which the investigation using the dipolar filter was carried out first.

B. 2D-WISE

In order to characterize more precisely the dynamic contrast in PEMA with a higher structural resolution, the 2D-WISE technique was used. This technique is described in Part 1, II.E. In a 2D-WISE spectrum the different chemical groups of the molecule are resolved according to their chemical shifts in the ^{13}C (direct) dimension and are correlated with the line width in the ^1H (indirect) dimension. This experimental procedure provides information on the mobility of the corresponding group: the narrower the line, the more mobile the chemical group.

1. Sample PEMA13C

In the case of sample PEMA13C, all parts of the monomeric units are detected. The contour spectra and the extracted 1D ^{13}C spectra are shown in the appendix (Part 7, IV.A.2). The 1D ^1H spectra extracted from the 2D-WISE spectra are presented in Figure 3- II-2. The ^{13}C chemical shifts assignment is detailed in Table 3- II-1. It should be noted that the line

width of the quaternary C and C=O signals can not be interpreted in terms of mobility only, due to the absence of directly bond ^1H nuclei.

At $T_g-11\text{ K}$, no significant line width difference is observed for the side chain and main chain CH_3 and CH_2 groups. At $T_g+35\text{ K}$, the lines exhibit the following order for decreasing mobility: CH_3 groups, then CH_2 groups. At $T_g+81\text{ K}$, the lines exhibit the following order for decreasing mobility: side-chain CH_3 , then main chain CH_3 , then CH_2 groups.

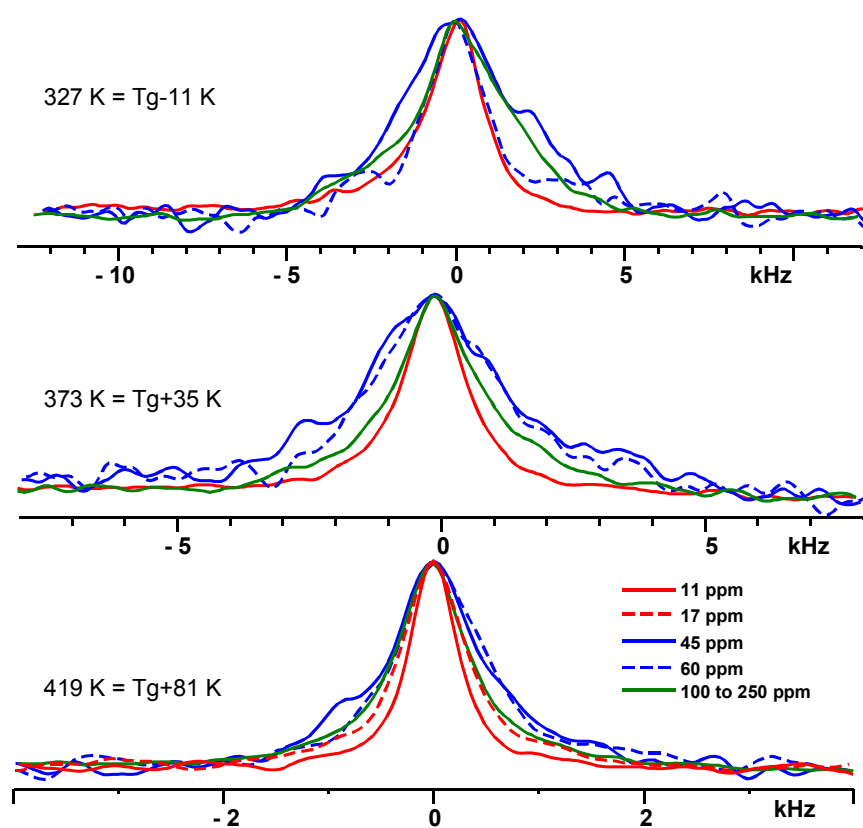


Figure 3- II-2: 1D ^1H spectra extracted from the 2D-WISE spectrum of sample PEMA13C (^1H Larmor frequency of 300.13 MHz, static, LG-CP and π -pulse during t_1).

δ (ppm)	Assignment ¹⁰⁶
11	side chain CH_3
17	main chain CH_3
45	main chain C
60	side chain CH_2 and main chain CH_2
100 to 250	C=O

Table 3- II-1: Assignment of the ^{13}C chemical shifts of poly(ethyl methacrylate).

It should be pointed out here that the apparent difference in mobility is decreased by possible ^1H nuclear spin diffusion during the CP contact time (s. Part 1, II.E). Therefore Lee-Goldburg CP was used here. However, an accurate adjustment of the Lee-Goldburg conditions is only possible under MAS, due to the presence of heteronuclear dipolar couplings under static conditions. The ^1H nuclear spin diffusion was thus not properly suppressed but only weakened in the 2D-WISE recorded here under static conditions.

Finally, the apparent difference in mobility is lower than the actual one, but still high enough to be detected.

As a conclusion, *the CH₃ groups are the most mobile ones, and the side chain CH₃ is more mobile than the main chain one*, as observed at T_g+81 K where they can be differentiated. *The CH₂ groups are less mobile groups than the CH₃ groups*. It should be noted that main chain and side chain CH₂ groups cannot be differentiated in this experiment because of the poor spectral resolution in the ¹³C dimension.

2. Sample PEMADSC

The sample PEMADSC is deuterated on the side chain, so that only the main chain is ¹H-NMR-active. Therefore only the CH₃ and CH₂ groups of the main chain contribute to the spectral intensity (respectively at 17 to 20 and 50 to 55 ppm)¹⁸⁰.

The contour spectra and the extracted 1D ¹³C spectra are shown in the appendix (Part 7, IV.A.2). The 1D ¹H spectra extracted from the 2D-WISE spectra are shown in Figure 3-II-3. For all the temperatures, it can be clearly seen that *the CH₃ group is more mobile than the CH₂ group*. This is due to the fast rotation of the CH₃ group.

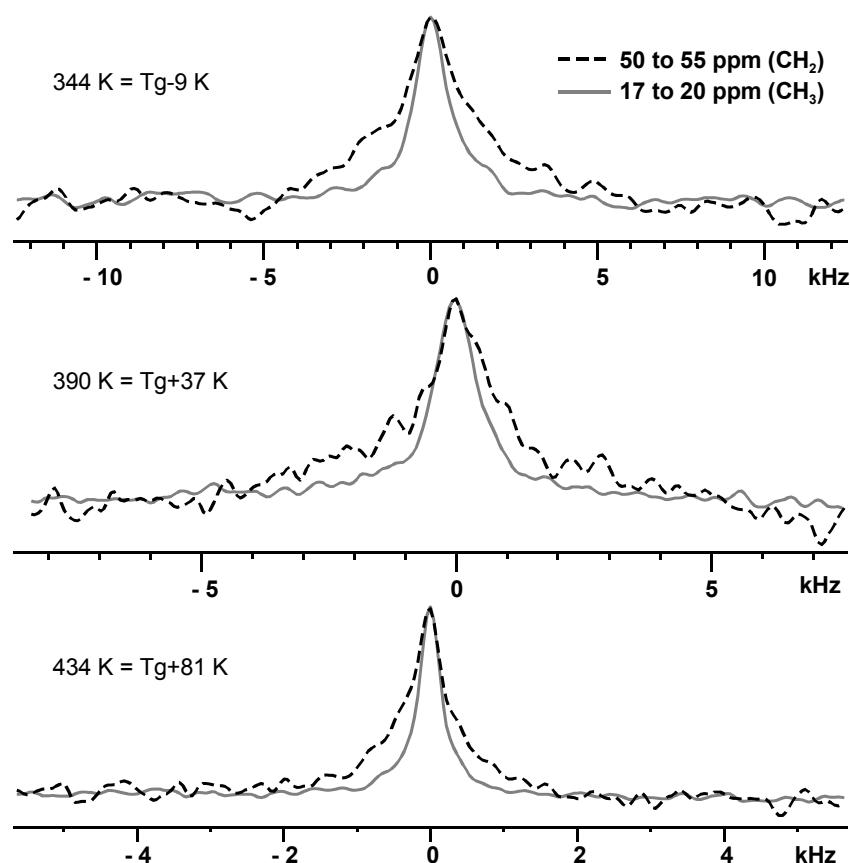


Figure 3- II-3: 1D ¹H spectra extracted from the 2D-WISE spectrum of sample PEMADSC (¹H Larmor frequency of 300.13 MHz, static, LG-CP and π -pulse during t_1).

C. Conclusion on the dynamic contrast

^1H static spectra were recorded on PEMA at temperatures ranging from $T_g-45\text{ K}$ to $T_g+115\text{ K}$. They showed that the whole sample is becoming continuously more mobile with increasing temperature, and does not exhibit a strong dynamic contrast.

2D-WISE spectra were recorded at temperatures ranging from ca $T_g-10\text{ K}$ to $T_g+80\text{ K}$ for samples PEMADSC and PEMA13C. It was shown that the CH_3 groups are more mobile than the CH_2 groups, the CH_3 of the side chain being more mobile than the CH_3 of the main chain. Furthermore, the main chain and the side chain CH_2 are not differentiated.

Finally, the dynamic contrast is very low in PEMA sample, but might still be present and detected by other solid-state NMR experiments like ^1H nuclear spin diffusion technique using the dipolar filter (s. next paragraph).

III. Monitoring the ^1H magnetization of the more mobile parts after the dipolar filter

The sample PEMA, as well as all model and industrial sample investigated in this work, represent a new kind of sample for the ^1H nuclear spin diffusion technique with dipolar filter, since they exhibit a very low dynamic contrast, as explained in paragraph A. Therefore, its investigation required several changes in the data analysis, which are presented in paragraph B. The obtained results are detailed in paragraph C.

A. New type of sample for the ^1H nuclear spin diffusion technique with dipolar filter

The ^1H nuclear spin diffusion technique using the dipolar filter⁶ had been previously applied to various polymers, including block copolymers,⁸¹ blends,⁸¹ core-shell particles^{82,90} and conetworks (polymer chains covalently bonded by blocks of another polymer)⁹¹. These different samples had in common a phase separation on the nanometer length scale in the material, leading to the formation of *two phases composed of one homopolymer each*. Various geometries have been observed for the phase separations. Furthermore, all samples exhibited *two glass transition temperatures* (T_g), each corresponding to one phase, and the difference between the T_g values was substantial in each sample: from 80 K to 160 K in the block copolymers,⁸¹ 170 K in the blend sample,⁸¹ 160 K in the core-shell particles,^{82,90} and from 150 K to 175 K in the conetworks⁹¹. In all cases, the ^1H nuclear spin diffusion experiments were conducted at an intermediate temperature between the two T_g s. This

implies a high difference of mobility between the phases at the measurement temperature, i.e. a *high mobility contrast*. The case of the conetworks is illustrated on Figure 3- III-1 by the ^1H static line shape. The more mobile phase (PIB) exhibits a narrow line, while the less mobile one (PHEMA) exhibits a broad line. The difference in the line width of the two phases (in Hz) is higher than one order of magnitude.⁹¹

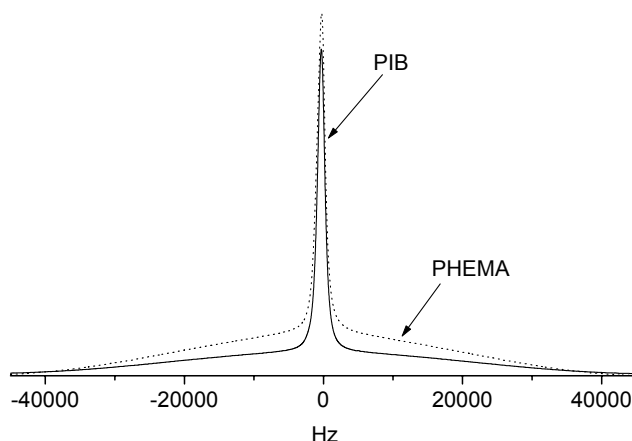


Figure 3- III-1: ^1H static NMR spectra of two amphiphilic conetwork samples with different compositions; they are composed of poly(2-hydroxyethyl methacrylate) (PHEMA) chains covalently bonded by polyisobutylene (PIB) blocks; the solid line marks the spectrum of the 63 % w/w and the dotted line the 24 % w/w PIB containing sample.⁹¹

In order to characterize pressure-sensitive adhesives, we have applied the ^1H nuclear spin diffusion technique to *statistical copolymers and homopolymers* (s. sample descriptions in Part 2, I to III). The statistical copolymers are industrial latices composed of statistical copolymers of 2-ethyl hexyl acrylate, acrylic acid (and methyl acrylate for some of them). The homopolymers are poly(n-alkyl acrylates) (methyl, ethyl, butyl and hexyl members) and poly(n-alkyl methacrylates) (ethyl, butyl and hexyl members). All samples exhibit a *single* T_g , as measured by differential scanning calorimetry (s. Part 2, I to III). It implies that all samples will exhibit a rather homogeneous mobility, i.e. a *low mobility contrast*, for all accessible temperatures. This is indeed the case, as will be detailed in Parts 4, I and Part 5, I. The representative example of PEMA was detailed in paragraph II: the whole sample is becoming more mobile with increasing temperature, and exhibits no significant difference in the mobility of all parts of the sample. However, less pronounced dynamic contrast within the sample is present, and the ^1H spectra is in fact a superposition of lines with a similar line width, that can not be distinguished visually. This type of samples exhibit a low mobility contrast and is therefore more complicated to investigate with the ^1H nuclear spin diffusion technique with dipolar filter, what has not been done before.

B. Changes done to data analysis

The classical data analysis was detailed in Part 1, II.H.5.

1. Recording of the ^1H nuclear spin diffusion curvea) Choice of the height instead of the area of the recorded ^1H line

In a ^1H nuclear spin diffusion experiment, the magnetization of the more mobile ^1H nuclei is usually monitored as the area of the narrower line. This technique is difficult to apply here, because the contrast in mobility (and thus the line width difference) is too low. Typical spectra recorded for sample Copo2 are shown on Figure 3- III-2. It is obvious that a broader component appears over t_m . Nevertheless, the line width difference between the initial line and the appearing broader line is too low to eliminate only one of them by reducing the spectral window. Furthermore, it is difficult to integrate only one line in the total ^1H spectrum without including the other one. This could possibly be achieved after an elaborate deconvolution, which is very time-consuming and difficult at low signal-to-noise ratio. Therefore it was decided to simply *monitor the height of the maximum of the total ^1H spectrum as a function of the mixing time*, which is more sensitive to the narrower component. This estimate allows to monitor the time dependence of the magnetization exchange. The absolute values of the degree of exchange, e.g. the plateau value, should, however, be interpreted with care.

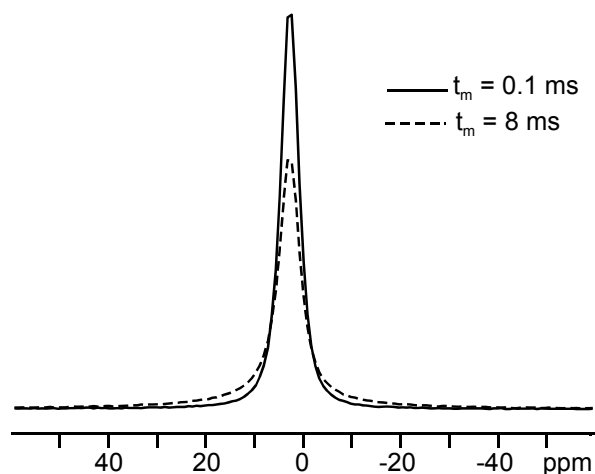


Figure 3- III-2:
Gradual broadening
of the basis of the line
during the ^1H nuclear
spin diffusion
experiment, for
sample Copo2
(dipolar filter with
15 μs delay and 8
cycles, t_m : mixing
time).

b) Correction for longitudinal relaxation

In the case of samples with a very low mobility contrast, the T_1 relaxation was characterized in the samples using the inversion recovery experiment. It exhibited a monoexponential decay, characteristic of a spatially homogeneous T_1 relaxation, or for samples with a relaxation sink and extensive ^1H nuclear spin diffusion. Furthermore, all T_1 times are longer than 450 ms (s. Part 4, III.A and Part 5, III.A). The part of the diffusion curves that were processed for all the samples (initial linear slope and beginning of the plateau) correspond to $\sqrt{t_m}$ values smaller than 10 $\sqrt{\text{ms}}$ (s. curves in appendix in Part 7, IV), and thus to t_m values smaller than 100 ms. This is much smaller than the T_1 relaxation values.

Therefore the corresponding parts of the ^1H nuclear spin diffusion curves could be easily corrected for T_1 relaxation using the procedure described in Part 1, II.H.5.a and b.

The relevance of the T_1 correction and its accuracy are illustrated in Figure 3- III-3. For a few representative samples and temperatures, the normalized intensity is plotted as a function of $\sqrt{t_m}$ before and after T_1 correction. The judicious $\sqrt{t_m}$ values were chosen as follows: initial point, end of the linear decay, (end of the second linear decay, when it exists, s. Part 5), random point on the plateau. It can be clearly seen that the T_1 correction introduces a non negligible difference in normalized values, and that a plateau can be obtained only after T_1 correction.

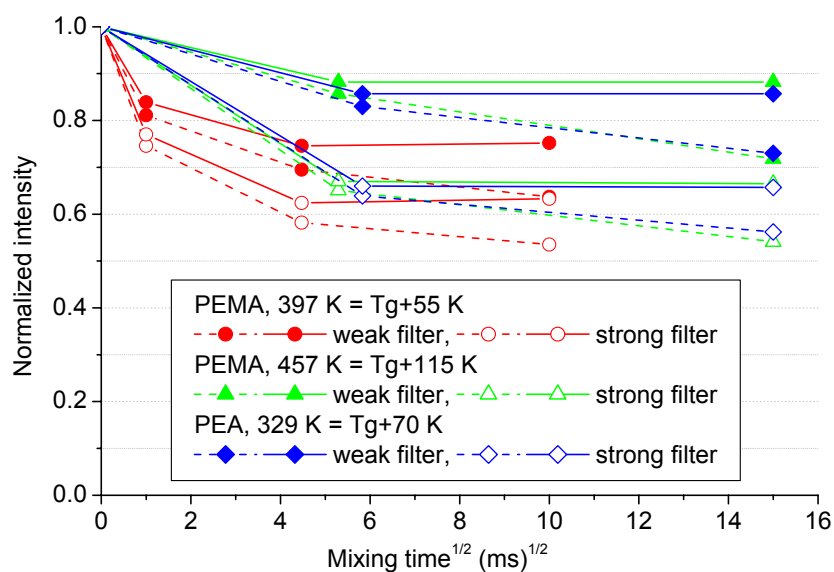


Figure 3- III-3: Illustration of the relevance and accuracy of the T_1 correction in the experiments using the dipolar filter for representative samples and temperatures; for each sample and temperature, the two extreme filters are shown; the dotted and solid lines represent the intensities resp. before and after T_1 correction.

2. Determination of the plateau value

For some experiments, the curve was slowly decaying for long mixing times (s. Figure 3- III-4). In that case, the beginning of plateau can be seen before the slow decay. The height of this short plateau was chosen as plateau value to determine the selected mobile content (s. dashed line). The quality of the T_1 correction indeed decreases with increasing mixing times, since the approximation that t_m is much smaller than T_1 becomes less and less valid, as explained in Part 1, II.H.5.b).

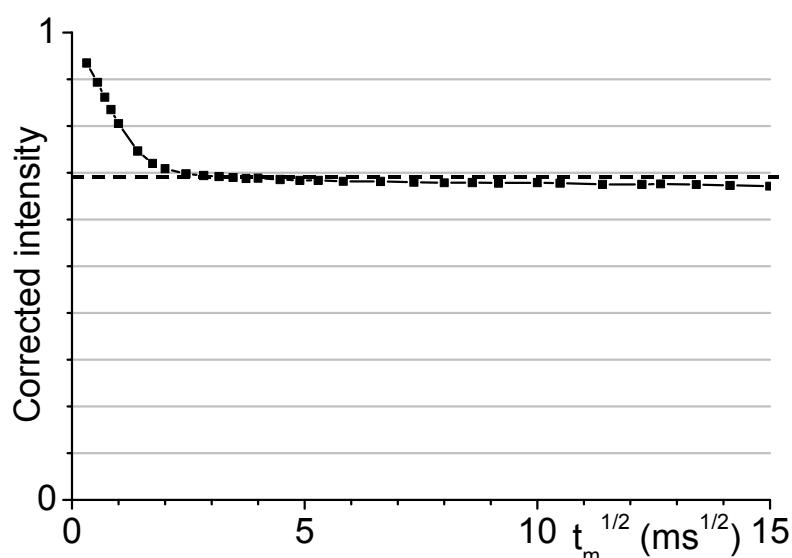


Figure 3- III-4:
Corrected magnetization decay of the mobile parts for sample PBMA at 372 K (T_g+70 K), using a dipolar filter with 10 μs delay and 1 cycle; the dashed line shows the value considered for the plateau value.

3. Determination of the average diffusion coefficient

The average diffusion coefficient D_{eff} is calculated from the diffusion coefficients of the more and the less mobile phase, resp. D_{mob} and D_{rig} , as indicated in Equation 3- III-1.

$$\frac{1}{\sqrt{D_{\text{eff}}}} = \frac{1}{2} \left(\frac{1}{\sqrt{D_{\text{mob}}}} + \frac{1}{\sqrt{D_{\text{rig}}}} \right) \quad \text{Equation 3- III-1}$$

In our case of low mobility contrast, the whole sample is much more mobile than polystyrene below its T_g , so that the less mobile phase can not be assumed to have a diffusion coefficient of $0.8 \text{ nm}^2 \cdot \text{s}^{-1}$. Furthermore, it is practically possible to determine only one value of diffusion coefficient. Since both phases have a similar mobility and ^1H spin density, they have similar diffusion coefficients. Therefore the average of the diffusion coefficients is close to the diffusion coefficient of the more mobile phase. It should also be noted that due to the way of averaging, the diffusion coefficient of the more mobile phase has more influence on the average than the other one, since it is lower. Finally, it was decided to *determine the diffusion coefficient of the more mobile phase only, and assume that it is similar to the one of the less mobile phase, thus to the average diffusion coefficient.*

The diffusion coefficient of the more mobile phase has been determined via the T_2 relaxation time.⁸¹ Both methods (CPMG experiment, line width) have been used for all samples. It was decided to *consider only the value coming from the line width measurement* for two reasons. First, the line is broader at the temperature of the ^1H nuclear spin diffusion measurements than at higher temperatures (indicating an intermediate mobility). Second, the diffusion coefficients determined through CPMG are higher than the ones determined from the line width of the ^1H static spectrum (after a dipolar filter), and both methods overestimate the diffusion coefficient; therefore the lower value is assumed to be more accurate.

4. Choice of the dimensionality

The last unknown left in the Equation 3- III-2 at that stage is the dimensionality ε of the detected structure (s. Part 1, II.H.5.e for notations).

$$d_{\text{size}} = \frac{2 \cdot \varepsilon}{\sqrt{\pi}} \cdot \sqrt{D_{\text{eff}}} \cdot \sqrt{t_m^*} \quad \text{Equation 3- III-2}$$

We have no indication concerning the geometry of the structure. Furthermore, we could not get information on it through, e.g., X-ray diffraction which detects a smaller structure (s. paragraph I), or electron microscopy for which the contrast is too low in homopolymers (or statistical copolymers). However, there is no reason why the structure should be composed of regular cylinders or lamellae or spheres.

Therefore we decided to choose a dimensionality value as general as possible for an irregular structure. This kind of structure is illustrated on Figure 3- III-5 by the case of a hard sphere model of the dynamic heterogeneities in glass formers close to T_g .^{233,234} It should be underlined that these dynamic heterogeneities probably have no link with the dynamic heterogeneities investigated here. These aggregates of spheres have a dimensionality between 2 and 3: it is the number of orthogonal directions along which the magnetization can go out of the domain in a short way. Finally, for simplicity reasons, it was decided to *assume a dimensionality of 2 in the investigated samples.*

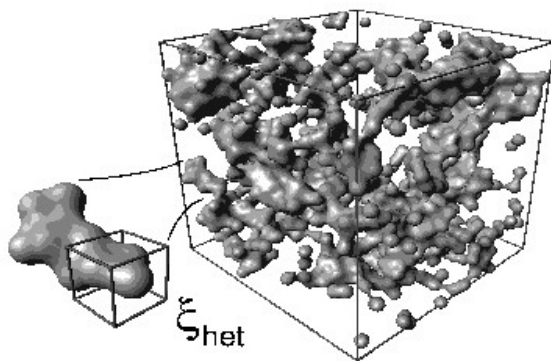
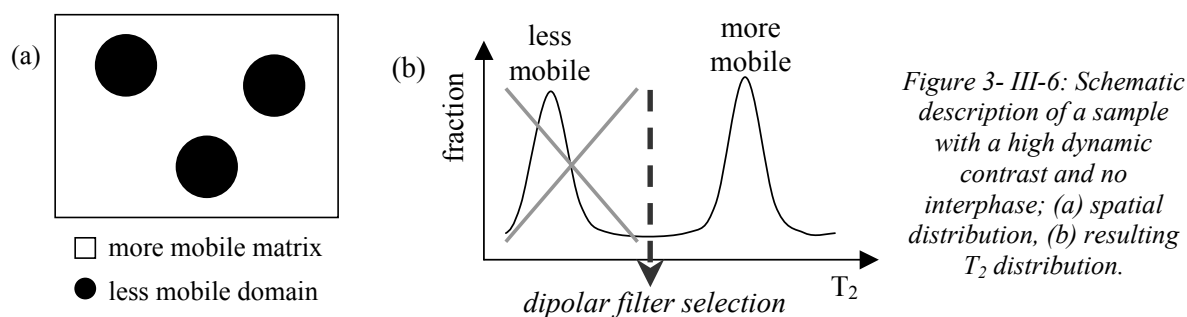


Figure 3- III-5: Computer simulation of dynamic heterogeneities in hard-sphere model for the glass formers close to T_g .²³³

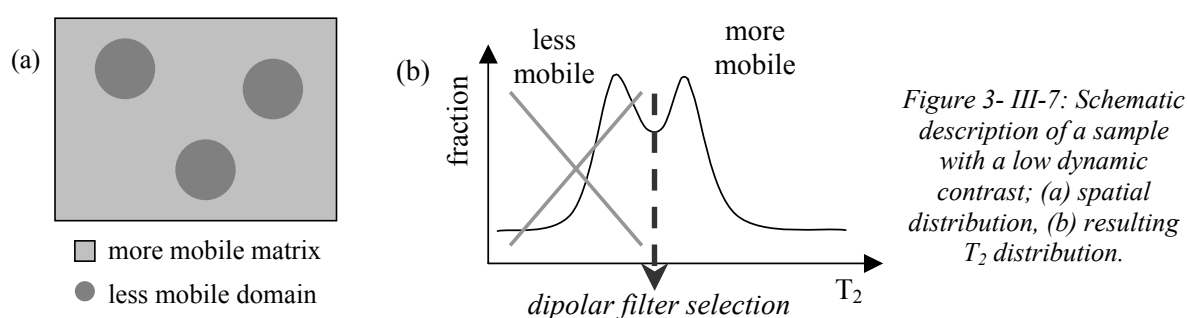
C. Results obtained for poly(ethyl methacrylate) at ca T_g+70 K

1. Modeling of the structured nanodomains

In a sample exhibiting a high dynamic contrast and no interphase, the distribution of the transverse relaxation times T_2 values would be bimodal, and the application of slightly different dipolar filters between these two populations would always select the same mobile fraction (s. Figure 3- III-6).



In the investigated model PEMA the dynamic contrast is very low. Therefore the bimodal distribution of the transverse relaxation times T_2 is narrower, and the application of different dipolar filters at different places of this distribution is able to select slightly different mobile fractions (s. Figure 3-III-7).



2. Monitoring ^1H magnetization after the dipolar filter

In PEMA at $T_g+67\text{ K}$, ^1H polarization transfer occurs after the dipolar filter. It is proved by the gradual broadening of the basis of the line with increasing mixing time. The broadening of the basis of the line is due to parts of the samples with stronger dipole-dipole couplings (and lower mobility). These parts are deselected by the dipolar filter, and receive magnetization during the mixing time.

The evolution of the ^1H magnetization of mobile species with the mixing time after the dipolar filter is plotted on Figure 3-III-8 for sample PEMA at $T_g+67\text{ K}$.

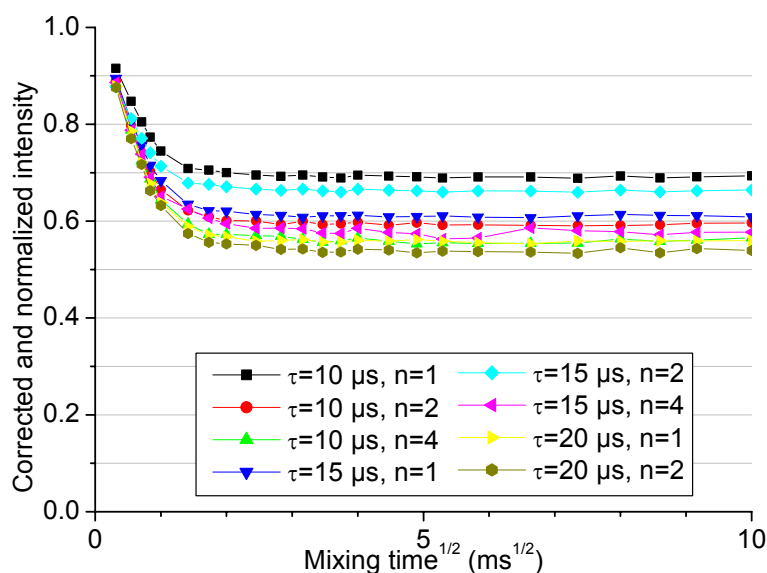


Figure 3-III-8: Evolution of the ^1H magnetization of mobile species with the square root of the mixing time for the sample PEMA at 409 K (T_g+67 K, n cycles of 12 τ -spaced pulses in the dipolar filter).

This evolution is the typical evolution of the normalized and corrected intensity as a function of $\sqrt{t_m}$ in a ^1H nuclear spin diffusion experiment using the dipolar filter: a magnetization decay apparently linear in the square root of the mixing time for small mixing times and a plateau for long mixing times. Assuming that the dimensionality of the selected parts is 2 (s. paragraph B.4), and estimating the effective diffusion coefficient from the ^1H static line width after the dipolar filter (s. paragraph B.3), apparent domain sizes of 2.8 to 5.7 nm are determined. Furthermore, the plateau values range from 53 to 70 %.

3. Conclusion

As a conclusion, if it is assumed that the dipolar filter detects the nanostructuring in PEMA at T_g+67 K, then the dipolar filter would deselect the organized nanodomains, which are less mobile than the rest. These nanodomains have no reason to exhibit a particular shape, therefore a dimensionality of 2 is a fair assumption. The ^1H magnetization of the selected more mobile parts with time apparently shows a typical diffusive behavior. The detected structure would have a size of a 3 to 6 nm, which is in accordance with the typical length of 5 to 10 monomeric units determined in NMR¹⁵⁰ and X-ray scattering²³¹ studies.

IV. Investigation of the actual selection done by the dipolar filter and of the actual subsequent transfer mechanism

The data were processed in the preceding paragraph assuming that the dipolar filter would select domains on the nanometer length scale, and that the following magnetization transfer would occur by ^1H nuclear spin diffusion, i.e. coherent flip-flop processes. However, these assumptions are questionable, in particular considering the weak dynamic contrast

involved. An alternative is that the different mobilities within a monomeric unit would provide the basis for the selection by the dipolar filter.

The actual selection done by the dipolar filter will be determined in paragraph A, then the actual magnetization transfer mechanism will be discussed in paragraph B. Finally, the mathematical equations describing the magnetization decay of the mobile parts will be given in paragraph C, and conclusions will be drawn in paragraph D on the kind of information on the sample which can be extracted.

A. Actual selection done by the dipolar filter

1. Discussion of the experimental conditions

In order to check which selection the dipolar filter actually does, the selected signal was transferred to ^{13}C nuclei and acquired in the ^{13}C channel, to gain chemical shift resolution. The magnetization transfer from ^1H to ^{13}C nuclei is done via cross-polarization, CP (s. Part 1, II.D). To probe a very local information, it is necessary to avoid ^1H nuclear spin diffusion during the CP contact time, and thus to use Lee-Goldburg CP, LG-CP (s Part 1, II.D.3).

It would be best to carry out the LG-CP experiments under the exact same conditions as the experiments using the dipolar filter described in the preceding paragraph, namely under static conditions and at T_g+70 K. It should be noted indeed that both, the dipolar filter selection and the following magnetization transfer could change when going from static to MAS conditions. However, the static conditions exhibit the double drawback of the lower chemical shift resolution and of the impossibility to properly adjust the Lee-Goldburg irradiation on ^1H nuclei (s. paragraph II.B.1). At T_g+70 K under static conditions, the chemical shift resolution is high enough to differentiate all chemical groups of the monomeric unit of PEMA. Nevertheless, the improper adjustment of the Lee-Goldburg conditions leads to extensive ^1H nuclear spin diffusion during the CP contact time and thus prevents from determining the actual selection done by the dipolar filter.

Therefore, it was decided to carry out the LG-CP investigations under MAS. It should be noted that the 4 mm MAS probeheads available at the DSX300 do not have a temperature range as extended as the static probehead: they are limited to 393 K, which corresponds to T_g+45 K for sample PEMA. Finally, it was decided to carry out the LG-CP investigations on sample PEMA under MAS, at 390 K, i.e. ca T_g+45 K. (The temperature should not have a major influence on the selection and magnetization transfer mechanism well above T_g , s. Parts 4 and 5).

2. Obtained results for PEMA at $ca T_g+45 K$

The pulse schemes used to investigate the selection done by the dipolar filter using Lee-Goldburg CP are presented in Figure 3- IV-1. In the experiment (a), a simple LG-CP spectrum is recorded to obtain a reference spectrum. In the experiment (b), a dipolar filter is applied directly followed by LG-CP spectrum, in order to determine the parts of the sample actually selected by the dipolar filter. Experiment (c) corresponds to (b), where a mixing time τ_m is introduced between the dipolar filter and LG-CP, in order to observe the sample back at equilibrium. The corresponding spectra for sample PEMA at $T_g+45 K$ are shown on Figure 3- IV-2. The carbonyl signal was too weak to be detected and is not shown here.

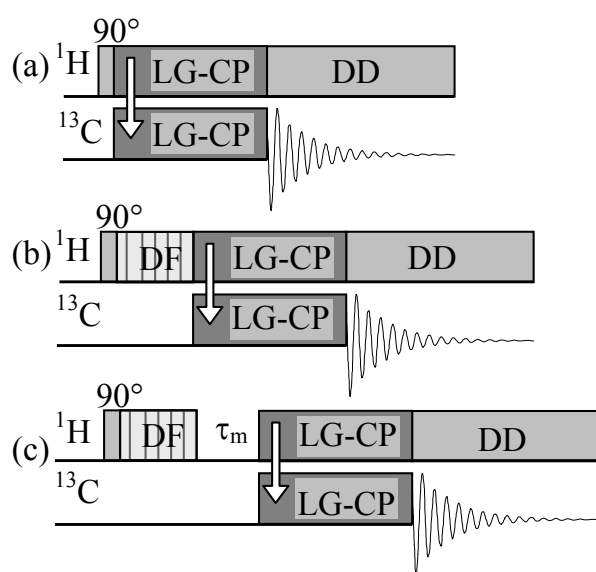


Figure 3- IV-1: Pulse schemes used to investigate the selection done by the dipolar filter in model samples using Lee-Goldburg CP; the abbreviations LG-CP, DD, DF and τ_m designate respectively Lee-Goldburg cross-polarization, dipolar decoupling, dipolar filter and mixing time.

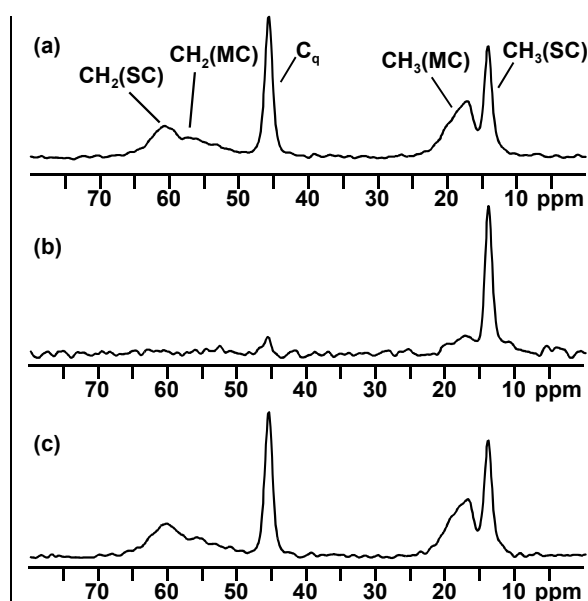


Figure 3- IV-2: ^{13}C LG-CP spectra of sample PEMA at 390 K ($ca T_g+45 K$ at 75.47 MHz under 3 kHz MAS; the corresponding pulse schemes are shown on the figure on the left; the CP contact time was 500 μs , the dipolar filter had a 20 μs delay and 1 cycle; the abbreviations MC, SC and q designate main chain, side chain and quaternary respectively.

The ^{13}C LG-CP spectrum shown on Figure 3- IV-2(a) exhibits a chemical shift resolution high enough to resolve all the chemical sites of the monomeric unit of PEMA. Furthermore, it gives their reference intensities in a LG-CP spectrum.

It can be clearly seen on the ^{13}C LG-CP spectrum on Figure 3- IV-2(b) that *the dipolar filter actually selects essentially the CH_3 group of the side chain of PEMA*. A small amount of CH_3 groups of the main chain is also selected. It should be noted that the plateau values observed on Figure 3- III-8, which correspond to the selected mobile fraction under static conditions, are in the range from 0.5 to 0.7. This is in agreement with a selection of all the side chain CH_3 groups and partly the main chain CH_3 groups, which represent a fraction between 0.3 and 0.6 of the $10^1 H$ nuclei of the monomeric unit of PEMA.

The ^{13}C LG-CP spectrum shown on Figure 3- IV-2(c) is identical to the one shown on Figure 3- IV-2(a), proving that the magnetization is back at equilibrium 50 ms after the application of the dipolar filter.

3. Conclusion

It was assumed for the data processing in paragraph III that the dipolar filter deselects the structured nanodomains present in PEMA, which would be less mobile than the rest. This would lead to the selection of some whole monomeric units, and the deselection of whole other ones. Therefore it would result in the presence of all the chemical parts of the monomeric units in the ^{13}C LG-CP spectrum recorded after the dipolar filter and no mixing time.

However, the LG-CP investigations conducted on PEMA at T_g+45 K clearly showed that the dipolar filter actually selects essentially the CH_3 group of the side chain. This proves that the assumption of the detection of structured domains on the nanometer length scale using the dipolar filter is wrong in PEMA at ca T_g+45 K. Indeed, the dipolar filter selects the end group of the alkyl side chain only.

B. Coherent or incoherent magnetization transfer ?

1. Importance of this question

It was assumed in paragraph III that the magnetization transfer would occur via coherent energy conserving flip-flops, as it is the case in a typical ^1H nuclear spin diffusion experiment. It was proved in paragraph A, however, that the dipolar filter selects essentially the end group of the alkyl side chain and not domains on the nanometer length scale. Therefore, we do not observe magnetization transfer from a domain to an other domain, as it is the usual case in a ^1H nuclear spin diffusion experiment, but rather magnetization transfer from the end group of the alkyl side chain along the alkyl side chain and further to the main chain.

Such a magnetization transfer along an alkyl side chain can occur via either coherent or incoherent transfer. In the case of coherent transfer, the residual dipolar couplings would cause zero-quantum transitions, i.e. coherent flip-flops, what is called, in the limit of many flip-flop transitions, ^1H nuclear spin diffusion. In the case of incoherent transfer, the fluctuation of the dipolar coupling due to the chain motion would cause cross-relaxation occurring via incoherent zero-quantum or double-quantum transitions, what is called NOE. In the case of coherent transfer, and in the limit of many steps, the data should be processed using the diffusion equations detailed in Part 1, II.H.5 and paragraph III.B. (It should be

noted that in the case of a single coherent step, an oscillatory transfer would be observed). In the case of incoherent transfer, the data should be processed using cross-correlation equations presented in Part 1, II.I. Therefore it is necessary to determine the type of magnetization transfer before processing the data.

2. Discussion of the type of magnetization mechanism

Fritzhanms et al.¹³⁹ investigate the magnetization transfer mechanism in multidimensional NOE experiments carried out on elastomers under MAS; they indicate coherent transfer in the case of static measurements, and incoherent transfer in the case of MAS measurements. Demco et al.²³⁵ conducted a detailed study of SBR elastomers at T_g+70 K using NOE experiments under static conditions, and claim a coherent transfer mechanism for the short mixing times. This results in a quadratic decay of the magnetization M_z with the mixing time τ_m , described by Equation 3- IV-1, where M_0 is the initial magnetization and $\langle DC \rangle$ the average residual dipolar coupling. The quadratic behavior is experimentally observed for mixing times up to 400 μ s.

$$M_z = M_0 \cdot (1 - 0.5 \cdot \langle DC \rangle \cdot \tau_m^2) \quad \text{Equation 3- IV-1}$$

In our investigation of PEMA around T_g+70 K under static conditions, a coherent transfer of magnetization is also expected for very short mixing times, on the same time range of 400 μ s or shorter, due to the lower mobility of PEMA. However, the time of 400 μ s would be between our second and third experimental points. Furthermore, the magnetization decay of interest in our study is on the order of several ms (s. Figure 3- III-8 and Parts 4, 5 and 7), thus of a factor 10 to 100 longer than the time range of coherent transfer. Indeed, plotting our experimental magnetization decays as a function of the square of the mixing time did not result in a linear behavior for very short mixing times (s. Figure 3- IV-3).

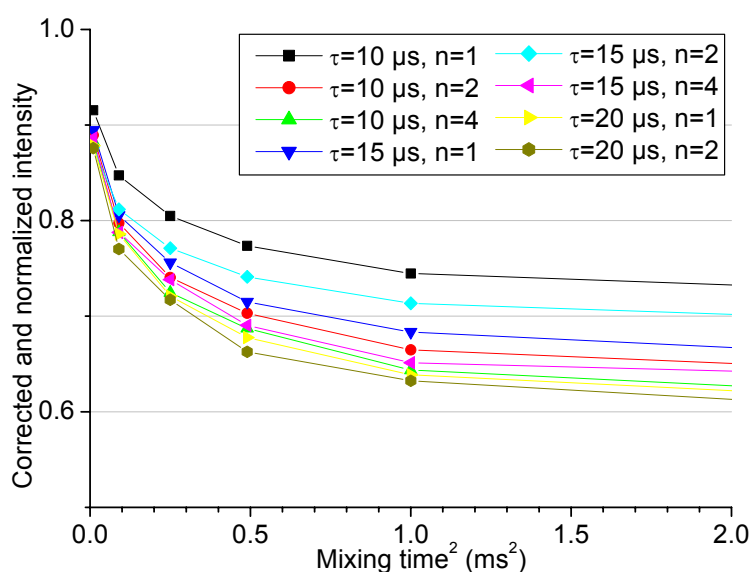
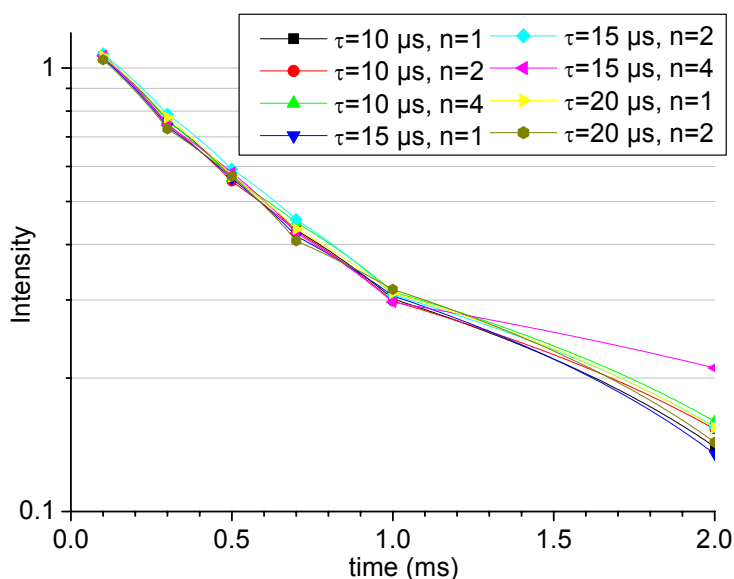


Figure 3- IV-3:
Evolution of the ^1H magnetization of mobile species with the mixing time, after subtraction of plateau value and normalization, on a logarithmic scale, for the sample PEMA at 409 K (T_g+67 K, n cycles of 12 τ -spaced pulses in the dipolar filter).

Therefore, it is concluded that *in PEMA at ca T_g+70 K the magnetization transfer occurs after the dipolar filter predominantly via incoherent zero- and double-quantum transitions.*

A further argument can be quoted in favor of an incoherent magnetization transfer. Filip et al.²³⁶ developed a theory describing MAS spectra using a combination of formalized Floquet theory and perturbation theory. They show that for high spinning frequencies, the weaker dipolar couplings are refocused by MAS, and for sufficiently high spinning frequency the system can be described as an isolated spin pair. Since only the stronger residual dipolar couplings are left under MAS, the transfer should look coherent. Under static conditions on the contrary, a superposition of strong and weak dipolar coupling is observed (with a broad range), which looks like incoherent.

Therefore our magnetization transfer data should be processed considering incoherent zero-quantum and double-quantum transitions, i.e. a NOE mechanism (s. Part 1, II.I). This transfer mechanism indeed results in an exponential decay of the magnetization, as detailed in the following paragraph C. This exponential decay is in complete agreement with the linear behavior observed for the recorded magnetization decay after subtraction of the plateau value, normalization and plot on a logarithmic scale (s. Figure 3- IV-4).



*Figure 3- IV-4:
Evolution of the 1H
magnetization of mobile
species with the mixing
time, after subtraction of
plateau value and
normalization, on a
logarithmic scale, for the
sample PEMA at 409 K
(T_g+67 K, n cycles of 12
 τ -spaced pulses in the
dipolar filter).*

C. Mathematical equations describing the magnetization decay

1. Equivalence to 2D-NOE experiment

It was concluded in paragraph B that the magnetization transfer after application of the dipolar filter in PEMA at T_g+70 K occurs predominantly via incoherent zero-quantum and double-quantum transitions, i.e. a NOE mechanism. The NOE experiments and data processing were detailed in Part 1, II.I, where it was seen that different initial conditions and different transfer conditions are possible.

In our experiments, the line height is monitored (and not its area), which is equivalent to integrate over a thin slice of the spectrum, or to integrate only the mobile component of a superposition of a more mobile component and a less mobile component. Furthermore, in our experiments, magnetization is present initially only at the more mobile sites, and is transferred in the course of our experiment to all more and less mobile sites. Thus our monitoring way is formally equivalent to an experiment where two components A and B would be resolved on the chemical shift scale, where all the magnetization would be present at A sites initially, where the magnetization would be transferred between all A and B sites in the course of the experiment via cross-relaxation, and where only the A component would be integrated (s. Figure 3- IV-5). This latter case is also equivalent to a 2D NOE experiment, where the AA line would be initially selected, and where cross-relaxation would occur over time during A and B, and where the AA line would be monitored over time as its integral in two dimensions (s. Figure 3- IV-5).

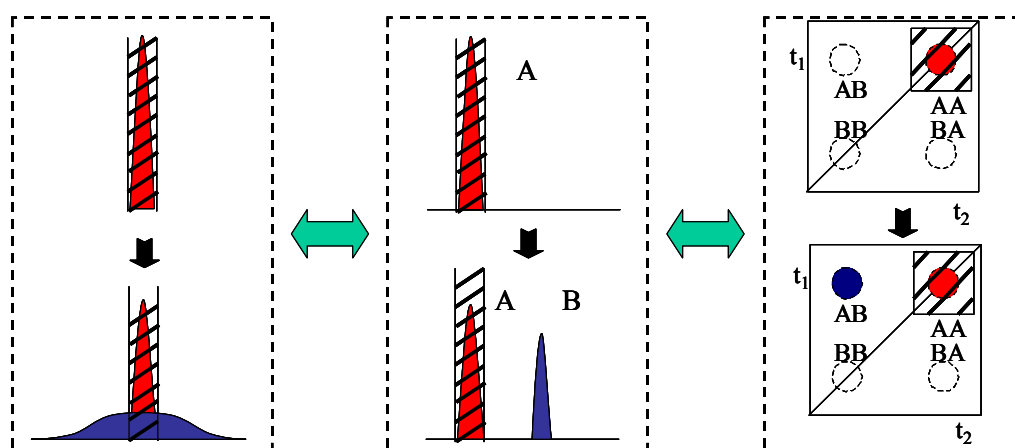


Figure 3- IV-5: Formal equivalence between our NOE experiment (left) and two other experiments (middle and right); the dashed surface represent the integrated component; in the middle experiment, from two components resolved on the chemical shift scale, the component A would be initially selected and then monitored over time during cross-relaxation between A and B; in the right experiment, the AA component would be initially selected, and then monitored over time during cross-relaxation between A and B.

Finally, our way of monitoring the magnetization decay is equivalent to the integration over time of a diagonal line in a 2D NOE experiment. It should be noted that our initial conditions (only the monitored line has magnetization) differ from the classical 2D NOE initial conditions, where all diagonal lines have magnetization. However, “having magnetization” only means that for this particular species, there is of the order of magnitude of ppm (parts per millions!) excess of spin orientation in one direction. Therefore, it doesn’t make a difference for the cross-relaxation at the level of the single spins if only one species A has initially magnetization or if all species A and B have.

Finally, the mathematical equations detailed in Part 1, II.I for the time evolution of the diagonal lines intensity in a 2D NOE study directly apply here to our one-dimensional monitoring of the more mobile sites magnetization.

2. Case of two groups of equivalent homonuclear spins $A_{n_A}B_{n_B}$ in the slow motion limit

The investigated samples are macromolecules in bulk, therefore they are in the slow motion limit. In an homonuclear system composed of a group of n_A equivalent A nuclei and a group of n_B equivalent B nuclei in the slow motion limit, the time evolution of the diagonal and cross-peaks intensities is not explicitly given by Macura and Ernst.^{112,113} However, it can be easily calculated from Equation 1- II-12 (s. Part 1, II.I.4.a for equations and notations).

In the slow motion limit, $\omega_X\tau_C \gg 1$ and in an homonuclear system $(\omega_X-\omega_Y)\tau_C \approx 0$, therefore $W_1^{XY}=W_2^{XY}=0$, and only the zero-quantum transitions contribute to cross-relaxation, with a transition probability of $W_0^{AB}=q_{AB}\tau_C^{AB}$.

The elements of the cross-relaxation matrix are thus reduced to $R_{AA}=n_B W_0^{AB}+R_1$, $R_{BB}=n_A W_0^{AB}+R_1$, $R_{AB}=-n_A W_0^{AB}$ and $R_{BA}=-n_B W_0^{AB}$. Assuming equal external relaxation R_1 for A and B nuclei, the quantities R_C and R_L can then be calculated as follows:

$$R_C = \sqrt{(n_B W_0^{AB} + R_1 - n_A W_0^{AB} - R_1)^2 + 4n_A n_B W_0^{AB}} = \sqrt{(n_B - n_A)^2 W_0^{AB^2} + 4n_A n_B W_0^{AB^2}} = \sqrt{(n_B + n_A)^2 W_0^{AB^2}}$$

$$\text{and } R_L = \frac{1}{2}(n_B W_0^{AB} + R_1 + n_A W_0^{AB} + R_1) - \frac{1}{2}(n_B + n_A) W_0^{AB} = R_1 + W_0^{AB} \left(\frac{n_B + n_A - n_B - n_A}{2} \right)$$

$$\text{yielding } R_C = (n_B + n_A) W_0^{AB} \text{ and } R_L = R_1.$$

It can then be calculated that $\frac{R_{AA}-R_{BB}}{R_C} = \frac{n_B W_0^{AB} + R_1 - n_A W_0^{AB} - R_1}{(n_A + n_B) W_0^{AB}} = \frac{n_B - n_A}{n_A + n_B}$.

Finally, the equations describing the intensities of the diagonal lines and of the cross lines are shown in Equation 3- IV-2.

$$\left\{ \begin{array}{l} a_{AA}(\tau_m) = \frac{n_A M_0}{2(n_A + n_B)} \exp(-R_1 \tau_m) \left[\left(1 + \frac{n_A - n_B}{n_A + n_B} \right) + \left(1 - \frac{n_A - n_B}{n_A + n_B} \right) \exp(-(n_A + n_B) q_{AB} \tau_C^{AB} \tau_m) \right] \\ a_{BB}(\tau_m) = \frac{n_B M_0}{2(n_A + n_B)} \exp(-R_1 \tau_m) \left[\left(1 - \frac{n_A - n_B}{n_A + n_B} \right) + \left(1 + \frac{n_A - n_B}{n_A + n_B} \right) \exp(-(n_A + n_B) q_{AB} \tau_C^{AB} \tau_m) \right] \\ a_{AB}(\tau_m) = a_{BA}(\tau_m) = -\frac{n_A n_B M_0}{(n_A + n_B)^2} \exp(-R_1 \tau_m) [1 - \exp(-(n_A + n_B) q_{AB} \tau_C^{AB} \tau_m)] \end{array} \right. \quad \text{Equation 3- IV-2}$$

3. Magnetization decay for the more mobile parts

In the present work, the magnetization decay of the more mobile parts is described by Equation 3- IV-3 where n_A , n_B , M_0 are constants, q_{AB} is a parameter, R_1 is rate of leakage of magnetization towards the lattice, τ_m is the mixing time and τ_C^{AB} is the correlation time of the molecular motion involved.

$$a_{AA}(\tau_m) = \frac{n_A M_0}{2(n_A + n_B)} \exp(-R_1 \tau_m) \left[\left(1 + \frac{n_A - n_B}{n_A + n_B} \right) + \left(1 - \frac{n_A - n_B}{n_A + n_B} \right) \exp(-(n_A + n_B) q_{AB} \tau_C^{AB} \tau_m) \right] \quad \text{Equation 3- IV-3}$$

Thus, the processing of the data recorded after application of the dipolar filter allows us to extract information on the molecular dynamics, via the determined the correlation time of the involved molecular motion τ_C^{AB} .

D. Conclusion on the actual selection and subsequent magnetization transfer

Using LG-CP and ^{13}C detection, it was shown in paragraph A that the dipolar filter in PEMA at ca $T_g + 70$ K does not select domains of the sample on the nanometer length scale, but it selects only the CH_3 end group of the alkyl side chain. Therefore the observed magnetization transfer is not occurring between domains on the nanometer length scale, but along the alkyl side chain and further to the main chain. It was then proved in paragraph B that the actual magnetization transfer mechanism is not coherent zero-quantum transitions (i.e. coherent flip-flops) like in the usual ^1H nuclear spin diffusion experiment, but that this transfer occurs predominantly via incoherent zero- and double-quantum transitions (i.e. cross-relaxation) like in the usual NOE experiments. Furthermore, it was shown in paragraph C that the usual equations developed for NOE experiments describe the magnetization decay observed here. In those equations, the extracted information is proportional to the correlation time of the molecular motion which modulates the dipolar coupling to give rise to the cross-relaxation. Therefore, *processing the recorded magnetization decay of the more mobile parts after the dipolar filter in PEMA at ca $T_g + 70$ K allows us to extract information on the chain dynamics, and not on the nanostructure like in the usual ^1H nuclear spin diffusion experiment.*

V. Conclusion on use and misuse of the dipolar filter

A. Summary of the investigation of PEMA at ca $T_g + 70$ K

The poly(n-alkyl methacrylate), PnAMA, samples exhibit a nanostructure based on the tendency to phase separation between their polar stiff backbone and their non polar flexible side chains. This results in the presence of less mobile structured domains of a few nanometers, as reviewed in paragraph I. Therefore, they could be investigated by the ^1H nuclear spin diffusion technique with dipolar filter, in order to quantify the size of the less mobile domains. It was chosen to investigate first poly(ethyl methacrylate), PEMA, at ca $T_g + 70$ K.

Based on ^1H and 2D-WISE spectra recorded at different temperatures under static conditions, it was shown in paragraph II that the whole sample is becoming more mobile with increasing temperature above T_g , and does not exhibit a strong dynamic contrast. Furthermore, the CH_3 groups are the most mobile ones, and that the side chain one is more mobile than the main chain one.

The application of the ^1H nuclear spin diffusion technique with dipolar filter to PEMA at T_g+67 K was presented in paragraph III. Some adaptations had to be done to the usual data processing due to the weak dynamic contrast. After correction for T_1 relaxation, the recorded magnetization decay for the more mobile parts exhibits a typical diffusional behavior, namely a linear decay with the square root of the mixing time at short mixing times and a plateau at long mixing time. The data were processed assuming that the less mobile nanodomains are deselected by the dipolar filter and that the subsequent magnetization transfer occurs via coherent flip-flops. The detected structure would then have a size of a 3 to 6 nm, which is in accordance with the typical length determined in NMR¹⁵⁰ and X-ray scattering²³¹ studies.

Using LG-CP and ^{13}C detection however, it was shown in paragraph IV that the dipolar filter in PEMA at ca T_g+70 K selects only the CH_3 end group of the alkyl side chain, and does not select domains on the nanometer length scale. The subsequent magnetization transfer thus occurs along the alkyl side chain and further to the main chain, and not between domains on the nanometer length scale. It was also shown that the actual magnetization transfer mechanism is not coherent zero-quantum transitions (i.e. coherent flip-flops) like in the usual ^1H nuclear spin diffusion experiment, but that this transfer occurs predominantly via incoherent zero- and double-quantum transitions (i.e. cross-relaxation) like in the usual NOE experiments. Furthermore, the usual equations developed for NOE experiments describe the magnetization decay observed here, so that *processing the recorded magnetization decay of the more mobile parts after the dipolar filter allows us to extract information on the chain dynamics, and not on the nanostructure like in an usual ^1H nuclear spin diffusion experiment.*

B. Conclusion on the use and misuse of the dipolar filter

As a conclusion, it should be emphasized that *the results obtained with the ^1H nuclear spin diffusion technique with dipolar filter should in general be considered carefully.* The existence of a nanostructure associated with a dynamic contrast, as well as the typical diffusional behavior of the magnetization decay are not sufficient proofs of the actual characterization of the nanostructure. This is particularly the case for weak dynamic

contrasts. Therefore the *actual selection done by the dipolar filter has to be checked* by a complementary technique.

A second finding within this thesis should be pointed out. *New possibilities have been opened for the dipolar filter.* It has been proved in this chapter that *it can be applied to samples exhibiting a very weak dynamic contrast*, and still provide a proper selection based on mobility. Furthermore, the application of the usual ^1H nuclear spin diffusion technique with dipolar filter to PEMA at ca T_g+70 K turned out to be a NOE experiment. Therefore it is *a new way of investigating and quantifying molecular dynamics*, as opposed to extract structural information like in all previous applications of the dipolar filter.

Part 4: Nuclear Overhauser Effect investigated in model poly(*n*-alkyl acrylates) using the dipolar filter

I.	<i>Investigation of the dynamic contrast in model poly(<i>n</i>-alkyl acrylates)</i>	151
A.	¹ H static spectra.....	151
B.	2D-WISE.....	153
C.	Conclusion on the dynamic contrast.....	155
II.	<i>Investigation of NOE in the model poly(<i>n</i>-alkyl acrylates) using the dipolar filter</i>	156
A.	Actual selection done by the dipolar filter.....	156
B.	Recording and processing NOE data using the dipolar filter in PEA at T _g +70 K.....	157
1.	Conducted experiments and recorded magnetization.....	158
2.	Mathematical equation governing the recorded magnetization decay.....	159
3.	Determination of the q _{AB} parameter.....	160
a)	Case of the distance calculation for a CH ₃ -CH ₂ moiety.....	160
b)	Case of the second moment.....	162
4.	Methodology for extraction of the q _{AB} ·τ _C ^{AB} product.....	164
5.	Measured data and extracted results.....	165
C.	Temperature dependence of q _{AB} ·τ _C ^{AB} for sample PEA.....	165
D.	Temperature dependence of q _{AB} ·τ _C ^{AB} for all PnAA samples.....	166
E.	Conclusion on the measurement of NOE in model PnAAs.....	167
III.	<i>Interpretation of NOE results in model poly(<i>n</i>-alkyl acrylates)</i>	168
A.	¹ H longitudinal relaxation in model PnAAs.....	168
B.	Relaxation processes in model PnAAs.....	170
IV.	<i>Conclusion on NOE in model poly(<i>n</i>-alkyl acrylates)</i>	175
A.	Conclusion.....	175
B.	Outlook.....	175

Part 4: Nuclear Overhauser Effect investigated in model poly(n-alkyl acrylates) using the dipolar filter

It has been demonstrated in Part 3 that the application of the ^1H nuclear spin diffusion technique with dipolar filter to homopolymers exhibiting a weak dynamic contrast can lead to erroneous results when considered not carefully enough. It has been shown that first the dipolar filter selects the end group of the alkyl side chain, and second the following magnetization transfer is incoherent.

These results indeed open new possibilities for the dipolar filter: by selecting end groups of alkyl chains, and following the subsequent magnetization transfer occurring by cross-relaxation inside a monomeric unit, it allows to investigate the involved molecular dynamics selectively. This experiment has been applied to poly(n-alkyl methacrylates), PnAMAs and poly(n-alkyl acrylates), PnAAs, which are models for industrial PSA samples. The work done on PnAA's will be described in detail in Part 4, the work done on PnAMAs in Part 5. First measurements done on industrial PSA samples will be shown in Part 5.

Concerning the model PnAAs, the investigation of the dynamic contrast will be presented in paragraph I, the results of the NOE experiments using the dipolar filter in paragraph II. These results will be interpreted in terms of molecular dynamics in paragraph III.

I. Investigation of the dynamic contrast in model poly(n-alkyl acrylates)

The dynamic contrast (difference in mobility between the more mobile and the less mobile parts of a sample) was characterized in the model PnAAs by solid-state NMR, in particular ^1H static spectra and 2D-WISE experiments.

A. ^1H static spectra

All spectra are shown in the appendix (Part 7, IV.B). For the model PnAA samples the line shapes were similar to those of the sample PEMA at the same distance from T_g (s. Figure 3- II-1 in Part 3, II.A), apart from two exceptions. Therefore it can be concluded that these samples exhibit no strong dynamic contrast.

The first exception concerns the sample PMA. This sample is not completely dry, since a very narrow line characteristic of small, highly mobile molecules is present (s. Figure 4- I-1) in the spectra. These small molecules may be solvents or oligomers, and could not be

eliminated after storage in a dessicator at room temperature under vacuum for a few months. The relatively high fraction of small molecules most probably acts as a plasticizer, increasing the chain mobility and thus decreasing the line width. For this sample, the full width at half maximum (fwhm) of the line was measured without taking into account the presence of the narrow line.

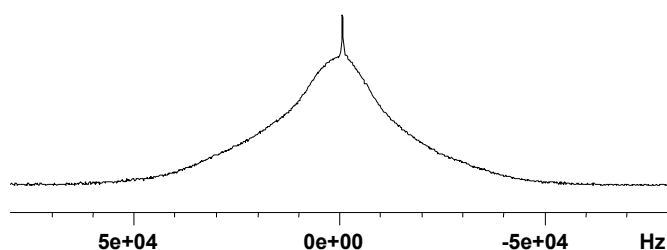


Figure 4- I-1: Line shape of ^1H spectrum for sample PMA at $T_g - 30^\circ\text{C}$ (spectrum recorded at a ^1H Larmor frequency of 300.13 MHz, under static conditions).

The second exception concerns all PnAA samples at high temperatures: contrary to the PnAMAs, the resolution is here sufficient to observe several lines (s. Figure 4- I-2). The spectra were therefore fitted with the individual lines for all the temperatures where it was possible, in order to evaluate the fwhm of the individual lines and not of the recorded superposition of lines. The fraction of the individual fitted lines was always in accordance with the theoretical fractions expected from the chemical structure. The weighted average of the individual line widths was taken into account.

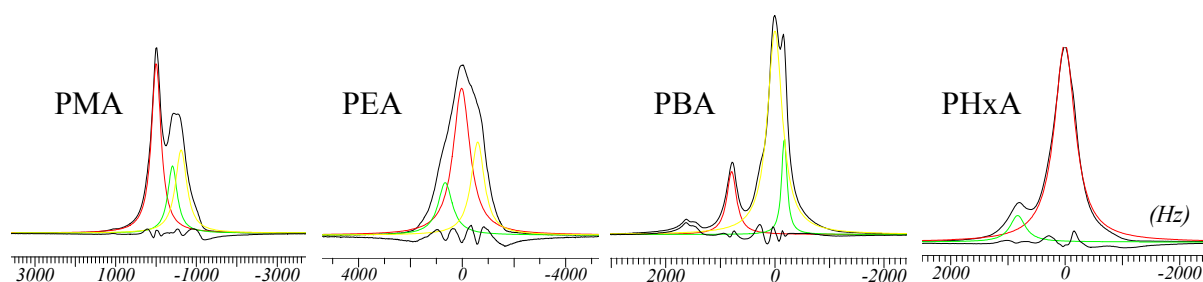


Figure 4- I-2: Line shape of ^1H spectra for samples PMA, PEA, PBA and PHxA at $T_g + 121^\circ\text{C}$, $T_g + 115^\circ\text{C}$, $T_g + 110^\circ\text{C}$, $T_g + 108^\circ\text{C}$ respectively (spectra recorded at a ^1H Larmor frequency of 300.13 MHz, under static conditions); the recorded spectrum is shown in black, the fitted individual lines are shown in red, yellow and green, the difference between the sum of the fitted lines and the experimental spectrum is shown in black.

A summary of the fwhm as a function of temperature for all the model PnAA samples is shown in Figure 4- I-3. For all samples, at none of the temperatures where experimental data have been acquired, a simple superposition of one broad and one narrow line is observed. The observed line(s) become narrower in a visually homogeneous way with increasing temperature. *This means that the whole sample is becoming more mobile with increasing temperature, and does not exhibit a strong dynamic contrast.* However, less pronounced dynamic contrast within the sample might be possible and experimentally accessible. In this case, the static spectra would be a superposition of lines with similar widths, so that it would be difficult to differentiate them via visual inspection.

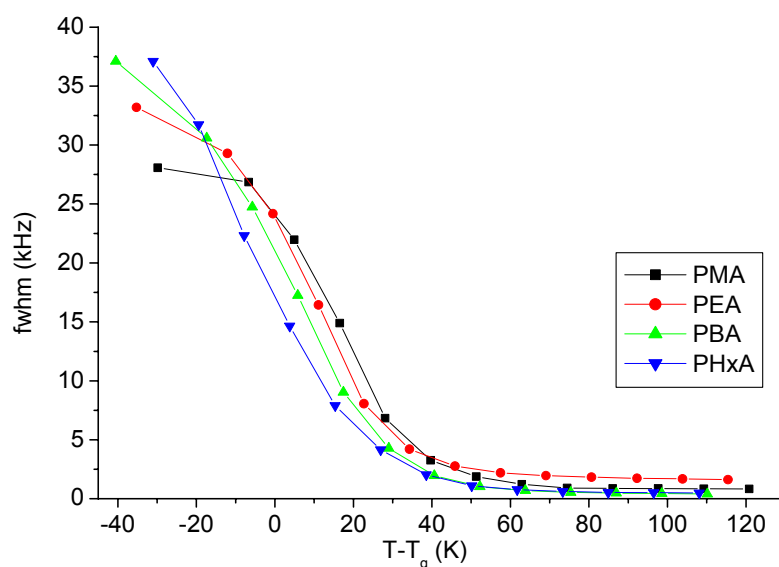


Figure 4- I-3:
Influence of the temperature on the fwhm of the ^1H spectrum of the model PnAAs (spectra recorded at a ^1H Larmor frequency of 300.13 MHz, under static conditions).

It can be noted that the line width of all PnAAs exhibits a similar temperature dependence relative to T_g . However, they exhibit significant line width differences at a given temperature, reflecting a significant difference in mobility. Below T_g , the following order is observed for decreasing mobility: PMA, then PEA, then PBA, then PHxA. Above T_g , the inverse order is observed, except above T_g+40 K, where PMA has a mobility intermediate between PEA and the others.

Furthermore, the steep decay observed for the fwhm as a function of temperature corresponds to a sharp glass transition, similar for all samples. This glass transition starts at a temperature much lower than the glass transition temperature T_g measured by DSC. This is due to the fact that DSC mainly detects the glass transition of the backbone, while the alkyl side chain is already mobile at lower temperatures.

B. 2D-WISE

In order to characterize more precisely the dynamic contrast in the model PnAAs, the 2D-WISE technique (fully described in Part 1, II.E) was used. In a 2D-WISE spectrum, the different chemical groups of the molecule are resolved according to their chemical shifts in the ^{13}C (direct) dimension; furthermore, the line width in the ^1H (indirect) dimension gives a rough information on the mobility of the corresponding group: the narrower the line, the more mobile the chemical group. Measurements were done at T_g+70 K for all PnAAs. The contour spectra and the extracted 1D ^{13}C spectra are shown in the appendix (Part 7, IV.B). The 1D ^1H spectra extracted from the 2D-WISE spectra are presented in Figure 4- I-4. The ^{13}C chemical shifts assignment is detailed in Table 4- I-1.

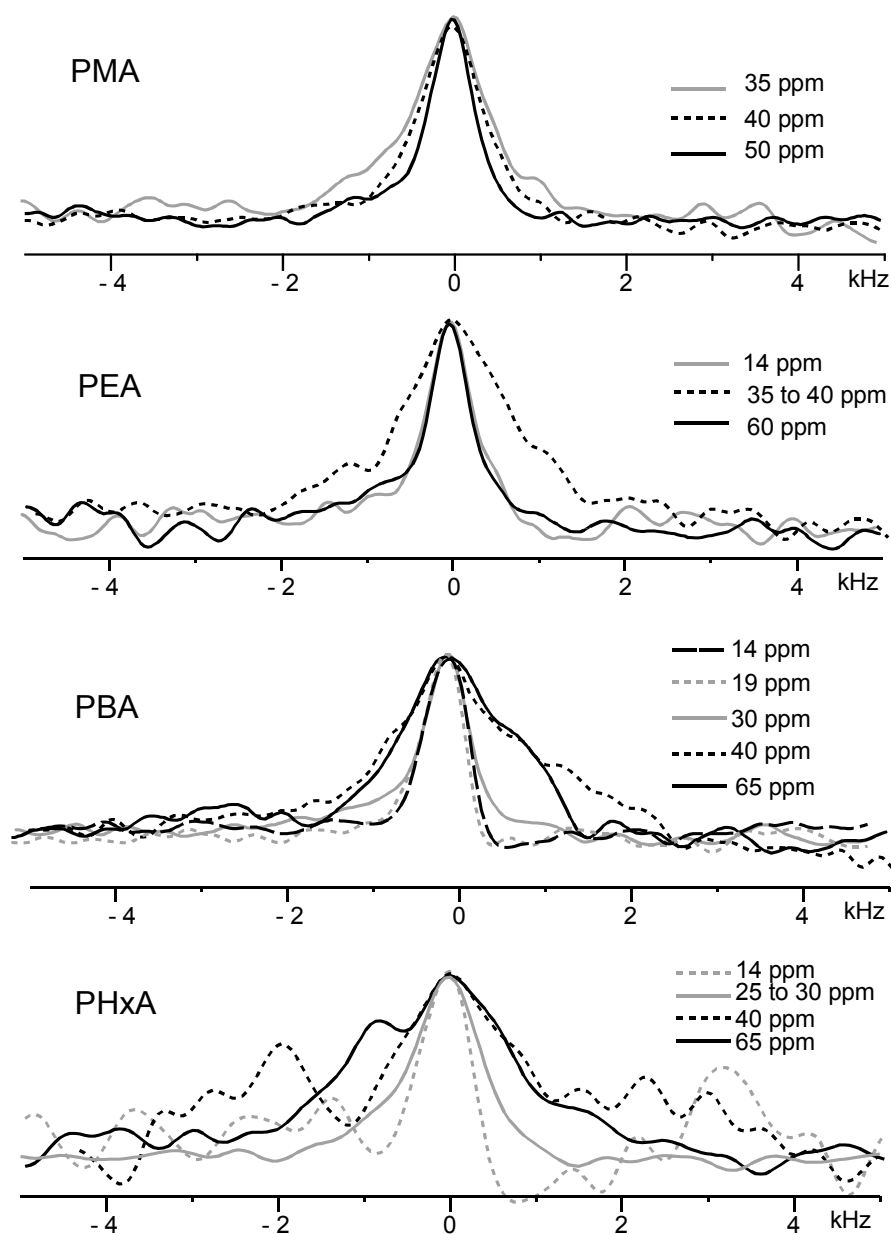


Figure 4- I-4: 1D ^1H spectra extracted from the 2D-WISE spectra of model PnAAs at $T_g+70\text{ K}$ (^1H Larmor frequency of 300.13 MHz, static, LG-CP and π -pulse during t_1).

δ (ppm)	Assignment (PMA) ¹⁸⁰	δ (ppm)	Assignment (PEA) ¹⁸⁰
35	CH ₂ (SC)	14	CH ₃ (SC)
42	CH (MC)	35	CH ₂ (MC)
52	O-CH ₃ (SC)	42	CH (MC)
175	C=O	60	O-CH ₂ (SC)
δ (ppm)	Assignment (PBA) ¹⁸⁰	δ (ppm)	Assignment (PHxA)
14	CH ₃ (SC)	14	CH ₃ (SC)
19	CH ₂ -CH ₃ (SC)	22, 26, 29, 32	CH ₂ (SC, except OCH ₂)
30	CH ₂ -CH ₂ -CH ₃ (SC)	35	CH ₂ (MC)
35	CH ₂ (MC)	42	CH (MC)
40	CH (MC)	65	O-CH ₂ (SC)
64	O-CH ₂ (SC)	175	C=O
175	C=O		

Table 4- I-1: Assignment of the ^{13}C chemical shifts of PnAAs (MC: main chain, SC: side chain).

It should be noticed that in the WISE spectra of none of the samples the C=O group is detected. There are two reasons. First, it is not covalently bonded to a ^1H nucleus, which results in a very low cross polarization efficiency. Second, the ^{13}C chemical shift tensor is much broader for C=O than for the other groups.

For PMA, the lines exhibit the following order for decreasing mobility: side chain CH_3 , then main chain CH, then main chain CH_2 . For PEA, the lines exhibit the following order for decreasing mobility: side chain CH_3 and O- CH_2 groups, then main chain CH and CH_2 groups. For PBA, the lines exhibit the following order for decreasing mobility: side chain CH_3 and CH_2 groups (except O- CH_2), then main chain CH and side chain O- CH_2 . Furthermore, the main chain CH_2 line (35 ppm) overlaps with the main chain CH (40 ppm) line, as can be deduced from the relative intensities in the extracted ^{13}C spectrum. *Thus, in PMA, PEA and PBA at T_g+70 K, the side chain end is clearly more mobile than the main chain.* This explains the decrease in overall line width observed for increasing side chain length above T_g (with the exception of PMA above T_g+40 K). It should be noted that the mobility of the CH group is overestimated by the ^1H line width (compared to CH_2 groups), due to the presence of a strongly coupled spin pair in the CH_2 groups. However, since it is always detected among the less mobile groups, it does not change the mobility order.

For sample PHxA, the lines exhibit the following order for decreasing mobility: side chain CH_3 , then side chain CH_2 groups (except O- CH_2), then side chain O- CH_2 . The signal of the main chain is too low to allow for any conclusion. *Thus, in PHxA at T_g+70 K, an obvious mobility gradient is observed along the alkyl side chain, starting from the more mobile CH_3 end group.*

C. Conclusion on the dynamic contrast

From the line shape of ^1H spectra recorded under static conditions, it can be concluded that the investigated PnAAs exhibit no strong dynamic contrast. However, the investigations conducted via 2D-WISE to gain chemical shift resolution showed mobility differences at T_g+70 K. Indeed, the side chain end is clearly more mobile than the main chain in PMA, PEA and PBA, while in PHxA, an obvious mobility gradient along the alkyl side chain starting at the more mobile CH_3 end group is observed.

II. Investigation of NOE in the model poly(n-alkyl acrylates) using the dipolar filter

The principle of the Nuclear Overhauser Effect measurement using the dipolar filter has been described in Part 3. The actual selection done by the dipolar filter will be investigated in paragraph A, while the exact data processing will be explained in paragraph B on the example of PEA at T_g+70 K. The temperature dependence of the extracted correlation time will be determined in paragraph C for sample PEA, in paragraph D for all PnAAs.

A. Actual selection done by the dipolar filter

For reasons outlined in Part 3, IV.A.1, the LG-CP experiments using the dipolar filter were carried out under 3 kHz MAS on samples PEA and PBA at ca T_g+70 K. In the first experiment, a simple LG-CP spectrum was recorded to obtain a reference spectrum. In the second experiment, a dipolar filter was applied and immediately afterwards a LG-CP spectrum was recorded, in order to determine the parts of the sample actually selected by the dipolar filter. In the third experiment, the same dipolar filter was applied, followed by a rather long mixing time and subsequent recording of a LG-CP spectrum, in order to observe the sample relaxing back at equilibrium. The corresponding spectra are shown on Figure 4- II-1 and Figure 4- II-2. The weak carbonyl signal is not shown here.

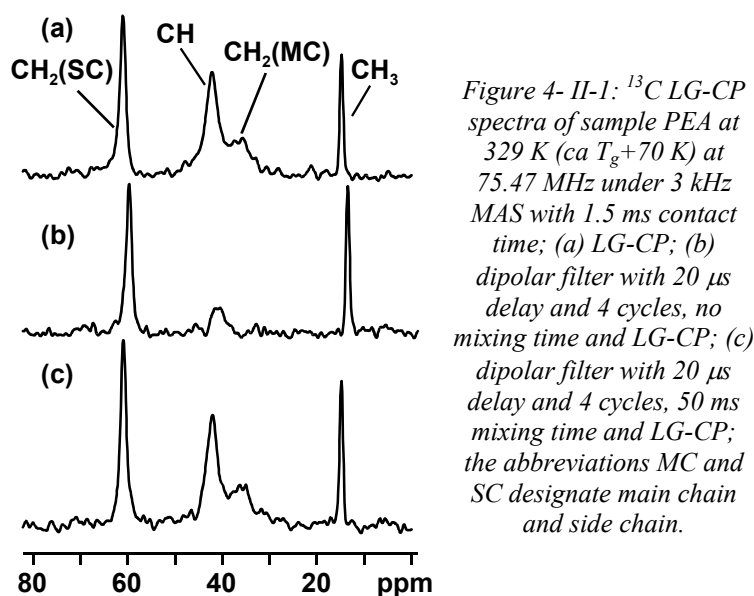


Figure 4- II-1: ^{13}C LG-CP spectra of sample PEA at 329 K (ca T_g+70 K) at 75.47 MHz under 3 kHz MAS with 1.5 ms contact time; (a) LG-CP; (b) dipolar filter with 20 μs delay and 4 cycles, no mixing time and LG-CP; (c) dipolar filter with 20 μs delay and 4 cycles, 50 ms mixing time and LG-CP; the abbreviations MC and SC designate main chain and side chain.

The ^{13}C LG-CP spectrum shown on Figure 4- II-1(a) exhibits a chemical shift resolution sufficient to resolve all chemical parts of the monomeric unit of PEA. Furthermore, it gives their reference intensities in a LG-CP spectrum. It can be clearly seen on the ^{13}C LG-CP spectrum on Figure 4- II-1(b) that the dipolar filter actually selects the CH_3 end group of the side chain and partly the next CH_2 group, i.e. it selects the end of the side chain of PEA. It

should be noted that a negligible amount of CH groups of the main chain is also selected. The ^{13}C LG-CP spectrum shown on Figure 4- II-1(c) is similar to the one shown on Figure 4- II-1(a), proving that the magnetization is back at equilibrium 50 ms after the application of the dipolar filter.

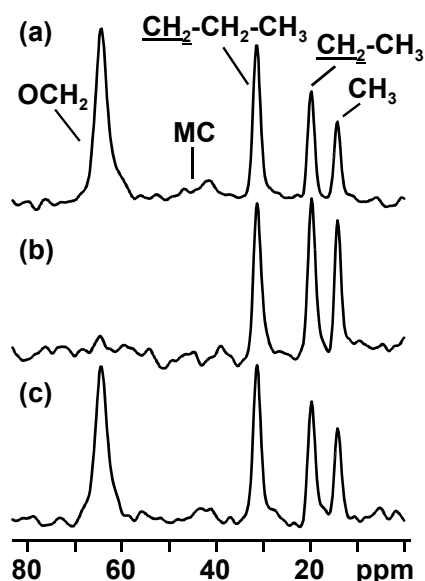


Figure 4- II-2: ^{13}C LG-CP spectra of sample PBA at room temperature (ca T_g+70 K) at 75.47 MHz under 3 kHz MAS with 3 ms contact time; (a) LG-CP; (b) dipolar filter with 20 μs delay and 8 cycles, no mixing time and LG-CP; (c) dipolar filter with 20 μs delay and 8 cycles, 50 ms mixing time and LG-CP; the abbreviation MC designates main chain.

It can be seen on Figure 4- II-2(a) that all the chemical parts of the monomeric unit of PBA are resolved in the ^{13}C LG-CP spectrum. However, the intensity of the main chain lines is not high enough to be properly detected; it may relax efficiently via $T_{1\rho}$ during the CP contact time. On the spectrum shown on Figure 4- II-2(b), it is observed that the dipolar filter actually selects the CH_3 end group of the side chain and partly the next two CH_2 groups, i.e. it selects the end of the alkyl side chain in PBA. The spectra displayed on Figure 4- II-2(c) and Figure 4- II-2(a) are identical. This shows a return to equilibrium 50 ms after the application of the dipolar filter.

As a conclusion, the LG-CP investigations carried out on PEA and PBA at ca T_g+70 K proved that *the dipolar filter actually selects only the CH_3 end group of the side chain and partly the next CH_2 group(s)*. As observed for PEMA in Part 3, IV.A.3, the dipolar filter does not select domains on a nanometer length scale in PnAAs, but it actually selects the end of the alkyl side chain.

B. Recording and processing NOE data using the dipolar filter in PEA at T_g+70 K

The example of PEA at T_g+70 K will be presented here. The results obtained as a function of temperature for this sample will be shown in paragraph C, the results obtained for the other PnAAs in paragraph D.

1. Conducted experiments and recorded magnetization

NOE investigations using the dipolar filter were conducted on sample PEA at 329 K, i.e. T_g+70 K. In those experiments, a dipolar filter is applied to the sample, after which the remaining magnetization is stored along the Z-axis, and then a variable mixing time is waited before recording the ^1H signal. The height of the recorded line is monitored as a function of the mixing time. It is first divided by the height of the recorded line after the same mixing time in the absence of dipolar filter in order to compensate for longitudinal relaxation. The obtained quantity corresponds to the intensity of the selected more mobile parts. Several dipolar filters were used, with delays ranging from 10 to 20 μs , and cycles numbers ranging from 4 to 12. The evolution of the recorded magnetization with mixing time is shown on Figure 4- II-3.

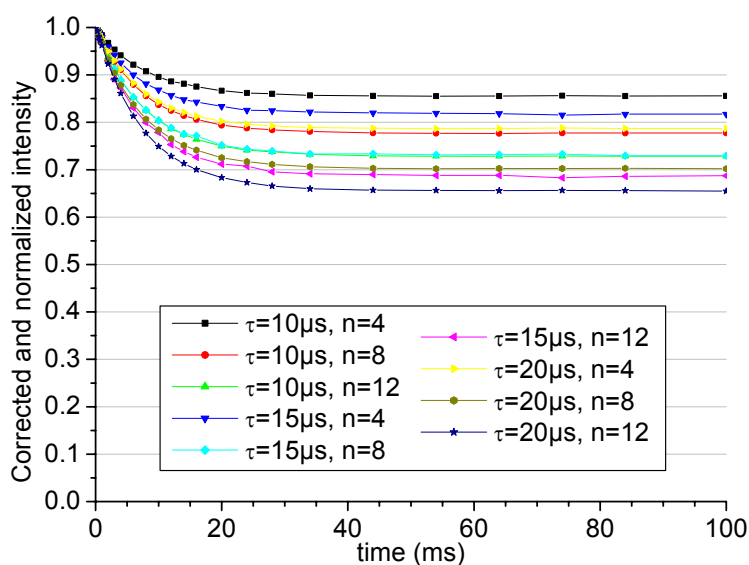


Figure 4- II-3: Evolution of the ^1H magnetization of mobile species with the mixing time for the sample PEA at 329 K (T_g+70 K, n cycles of 12 τ -spaced pulses in the dipolar filter).

It was shown in paragraph A that the dipolar filter actually selects the CH_3 end group of the alkyl side chain, and partly the adjacent CH_2 group. The discussion developed in Part 3, IV.B on the actual mechanism for transfer magnetization after the dipolar filter in PEMA at T_g+70 K is also valid for PEA at T_g+70 K: the magnetization transfer occurs after the dipolar filter via incoherent zero- and double-quantum transitions, also called cross-relaxation or NOE. This is also in accordance with the linear dependence upon mixing time of the recorded magnetization plotted on a logarithmic scale (s. Figure 4- II-4). Since the PEA at T_g+70 K is in the slow motion limit, zero-quantum transitions (i.e. flip-flops) are predominant.

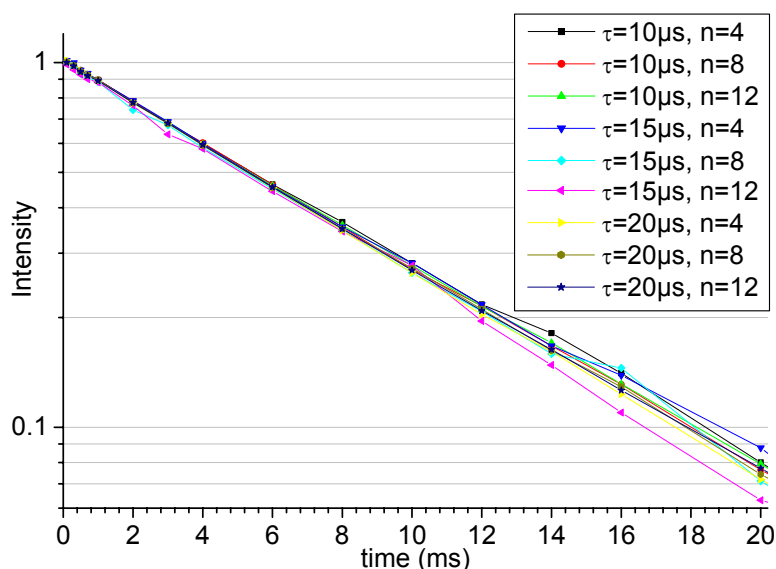


Figure 4- II-4: Evolution of the ¹H magnetization of mobile species on a logarithmic scale with the mixing time for the sample PEA at 329 K (T_g+70 K, n cycles of 12 τ -spaced pulses in the dipolar filter).

2. Mathematical equation governing the recorded magnetization decay

The mathematical equation governing the monitored decay is the one describing the decay of the intensity of a diagonal line in a 2D-NOE experiment in the slow motion limit, as justified in Part 3, IV.C. Furthermore, the initial magnetization is mainly located at the CH₃ end group of the alkyl side chain. Therefore we chose to use the decay equation calculated for two groups of equivalent nuclei in Part 3, IV.C.2, and to consider a CH₃-CH₂ moiety. It should be emphasized here that it does not correspond to the whole PEA monomeric unit, but that no analytical equation is available for moieties larger than two groups of equivalent nuclei. Moreover, since the initial magnetization is mainly located at the CH₃ end group, the CH₃-CH₂ contribution should be dominant in the initial magnetization decay. The same equation will be used for all the other PnAAs in paragraph D; the case of PMA will then be problematic, since its CH₃ group does not have an adjacent CH₂. However, no available model appears more satisfying, so that the same equation is used as for the other PnAAs. In the case of samples PBA and PH_xA, it could be argued that a CH₂-CH₂ behavior is superimposed to the CH₃-CH₂ one, due to the partial selection of CH₂ group(s) by the dipolar filter. However, the only difference between the results extracted using the CH₃-CH₂ and the CH₂-CH₂ models is the extraction of the product $4q_{AB} \cdot \tau_C^{AB}$ instead of $5q_{AB} \cdot \tau_C^{AB}$ (s. Equation 4- II-1), thus a factor 4/5 on the determined correlation times. Considering the inaccuracy of the determined correlation times, originating in particular in the determination of the q_{AB} factor, this can be neglected. Finally, it was decided to process the recorded data using the CH₃-CH₂ model for all PnAAs.

The evolution with mixing time τ_m of the intensity of a diagonal line in a 2D-NOE experiment concerning a CH₃-CH₂ moiety follows Equation 4- II-1 (s. Equation 3- IV-12 in Part 3, IV.C.2).

$$a_{AA}(\tau_m) = \frac{n_A M_0}{2(n_A + n_B)} \exp(-R_L \tau_m) \left[\left(1 + \frac{n_A - n_B}{n_A + n_B} \right) + \left(1 - \frac{n_A - n_B}{n_A + n_B} \right) \exp(-(n_A + n_B) q_{AB} \tau_C^{AB} \tau_m) \right] \quad \text{Equation 4- II-1}$$

In this equation, $n_A=3$, $n_B=2$, M_0 is a constant, R_L is the rate of leakage of magnetization towards the lattice, q_{AB} is a parameter defined in Equation 4- II-2 and τ_C^{AB} is the correlation time of the involved molecular motion.

$$q_{AB} = \frac{1}{10} \left(\frac{\mu_0}{4\pi} \right)^2 \frac{\gamma_A^2 \gamma_B^2 \hbar^2}{r_{AB}^6} \quad \text{Equation 4- II-2}$$

After correction of the longitudinal relaxation as explained in Part 3, III.B.1.b and paragraph 1, the exponential factor $\exp(-R_L \tau_m)$ is compensated and the corrected intensity follows Equation 4- II-3:

$$a_{AA}(\tau_m) = \frac{3M_0}{10} \left[\frac{6}{5} + \frac{4}{5} \exp(-5q_{AB} \tau_C^{AB} \tau_m) \right] \quad \text{Equation 4- II-3}$$

In this equation, everything is known except q_{AB} and τ_C^{AB} . Fitting the experimental data allows to determine the product $q_{AB} \cdot \tau_C^{AB}$. Thus, a parallel determination of q_{AB} leads to extraction of the correlation time of the involved motion τ_C^{AB} .

3. Determination of the q_{AB} parameter

The q_{AB} constant can be determined by two different ways. First, it can be calculated according to Equation 4- II-2, where all the terms are known factors, except the internuclear distance r_{AB} , which has to be calculated (s. paragraph a). Second, it can be calculated as a value proportional to the second moment of the ^1H line recorded below T_g under static conditions (s. paragraph b).

a) Case of the distance calculation for a $\text{CH}_3\text{-CH}_2$ moiety

In the homonuclear $^1\text{H}\text{-}^1\text{H}$ case, the q_{AB} factor can be calculated for an internuclear distance of $1 \text{ \AA} = 10^{-10} \text{ m}$ from the magnetogyric ratio of ^1H ($26.7522128 \cdot 10^{-7} \text{ rad.s}^{-1} \cdot \text{T}^{-1}$)²³⁷ and the physical constants $\mu_0/4\pi$ and \hbar (10^{-7} N.A^{-1} and $6.6260755 \cdot 10^{-34} / 2\pi \text{ J.s}^{-1} \cdot \text{rad}^{-1}$ respectively)²³⁸. This yields a value of $56.9627 \cdot 10^9 \text{ rad}^2 \cdot \text{s}^{-2}$ for q_{AB} . In order to extract the correlation time τ_C^{AB} in s from the product $q_{AB} \tau_C^{AB}$ determined using a mixing time in s, the q_{AB} parameter must be calculated in s^{-2} and not $\text{rad}^2 \cdot \text{s}^{-2}$. Thus the value in $\text{rad}^2 \cdot \text{s}^{-2}$ has to be divided by $(2\pi)^2$, yielding $q_{AB} = 1.44288 \text{ s}^{-2}$ for $^1\text{H}\text{-}^1\text{H}$ and $r_{AB} = 1 \text{ \AA}$.

Then, the calculation of the actual internuclear distance allows for determining the actual q_{AB} value. The distance between a ^1H nucleus of the CH_3 and the ^1H nucleus of the CH_2 group is a function of the dihedral angle involved. Thus an average of this distance over all dihedral angles has to be done.

The H-C-C-H bonds are first assumed to be planar. This system is shown on Figure 4-II-5. In this system, the H-H internuclear distance is equal to

$$c=1.523+a+b=1.523+1.113[\sin(20^\circ)+\sin(19.4^\circ)]=2.273 \text{ \AA}$$

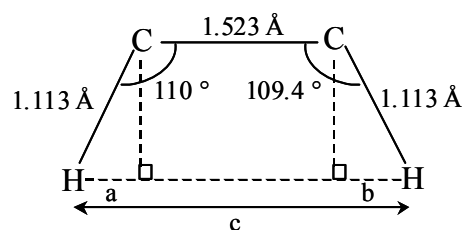


Figure 4-II-5: Planar configuration of the H-C-C-H bonds in a $\text{CH}_3\text{-CH}_2$ moiety, with corresponding angles and distances (CH_2 left, CH_3 right).

After introduction of the dihedral angle φ , the system is represented on Figure 4-II-6.

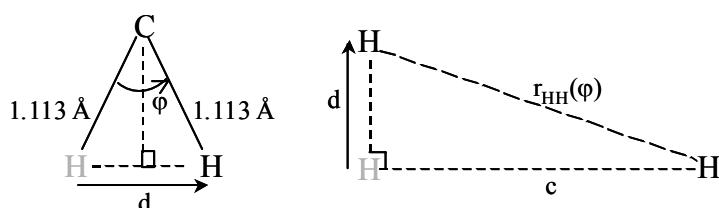


Figure 4-II-6: Representation of the H-C-C-H bonds in a $\text{CH}_3\text{-CH}_2$ moiety, taking into account the dihedral angle φ , (left perpendicular to the C-C direction, right parallel to the C-C direction).

In this system the internuclear distance d is calculated first, to allow the calculation of the dependence of the internuclear distance of interest, $r_{\text{HH}}(\varphi)$, upon dihedral angle φ (s. Equation 4-II-4):

$$d=2 \times 1.113 \times \sin\left(\frac{\varphi}{2}\right)=2.226 \times \sin\left(\frac{\varphi}{2}\right) \text{ and}$$

$$r_{\text{HH}}(\varphi)=\sqrt{c^2+d^2}=\sqrt{2.273^2+\left[2.226 \times \sin\left(\frac{\varphi}{2}\right)\right]^2}=\sqrt{5.167+4.955 \times \sin^2\left(\frac{\varphi}{2}\right)} \quad \text{Equation 4-II-4}$$

In order to calculate q_{AB} from $r_{\text{HH}}(\varphi)$, an average of $r_{\text{HH}}(\varphi)$ has to be calculated over all dihedral angles φ . It had first to be decided which kind of average should be calculated. The average could be done indeed according to $r_{\text{HH}}(\varphi)$ or various powers of $r_{\text{HH}}(\varphi)$. It was decided to average r_{HH} according to the dipolar coupling, which is proportional to r_{HH}^{-3} (s. Equation 1-II-2 in Part 1, II.B.1.a), and thus to calculate the average of $r_{\text{HH}}(\varphi)^{-3}$ values. This was done the following way: first calculating 100 values of angles equally distributed between 0 and 180°, then calculating the value of $r_{\text{HH}}(\varphi)^{-3}$ for each angle, and finally calculating the average distance r_{HH}^{-3} to extract from it the average distance r_{HH} . It was checked that 100 angle values are enough to determine $r_{\text{HH}}(\varphi)$ with a precision of 0.001 Å. The determined average distance is $r_{\text{HH}}=2.670 \text{ \AA}$.

$$\text{The } q_{\text{AB}} \text{ constant is thus } q_{\text{AB}}=\frac{1.44288 \cdot 10^9}{2.670^6}=3.983 \text{ kHz}^2 \text{ for a } \text{CH}_3\text{-CH}_2 \text{ moiety.}$$

n.b.: it should be noted that it is very important to consider an average distance to calculate q_{AB} . Indeed, the dihedral angle has a significant influence on the q_{AB} value: it ranges from 413 kHz^2 for the minimal distance of $r_{HH}(0^\circ)=2.273 \text{ \AA}$ to 55 kHz^2 for the maximal distance of $r_{HH}(180^\circ)=3.182 \text{ \AA}$ via 258 kHz^2 for the optimal dihedral angle of 49.9° ($r_{HH}(49.9^\circ)=2.459 \text{ \AA}$). On the contrary, the type of average considered has much less influence on the q_{AB} value: the latter is 133 kHz^2 for an average according to r_{HH} , 144 kHz^2 for an average according to $1/r_{HH}$, and 177 kHz^2 for an average according to $1/r_{HH}^6$.

b) Case of the second moment

The equation describing the q_{AB} factor (s. Equation 4- II-2, in MKSA unit system) is very similar to the one describing the second moment M_2 of the rigid lattice. In the case of a powder of crystalline sample exhibiting a cubic lattice, M_2 is expressed as Equation 4- II-5,^{239,67} in CGS unit system, where I is the spin quantum number, and d the lattice constant.

$$M_2 = \frac{51}{10} \gamma^4 \hbar^2 I(I+1) \frac{1}{d^6} \quad \text{Equation 4- II-5}$$

The knowledge of the relationship between the q_{AB} factor and the second moment M_2 is useful for two reasons. First, the second moment can be calculated by numerical integration from an experimental ^1H spectrum (recorded well below T_g and under static conditions), which avoids the assumption of the $\text{CH}_3\text{-CH}_2$ moiety and the calculation of the average internuclear distance presented in the paragraph a. Second, it is an independent way of determining the same parameter q_{AB} , therefore useful for comparison with the result of the calculation presented in paragraph a. For a better understanding, the second moment will be defined first. Then its general mathematical formula will be given, and simplified according to various assumptions, in order to compare it to the q_{AB} factor.

The moments of an NMR line are defined using integrals of the mathematical function $f(\omega)$ describing the line shape. The first moment M_1 is defined as Equation 4- II-6, it corresponds to the average frequency of the spectrum.²⁴⁰

$$M_1 = \frac{\int_0^\infty \omega \cdot f(\omega) d\omega}{\int_0^\infty f(\omega) d\omega} \quad \text{Equation 4- II-6}$$

The second moment M_2 is defined as Equation 4- II-7, it is of the order of the square of the line width.²⁴⁰ Its unit is Hz^2 in the MKSA unit system. Rigorously, the full width at half maximum, $fwhm$, obeys to the equation $fwhm^2 = 2 \cdot \ln 2 \cdot M_2$ in the case of a gaussian line shape, and the second moment is not defined in the case of a lorentzian line shape due to the divergence of the integral (s. Part 1, II.B.1.b).⁶⁷ The second moment of a rigid lattice designates the second moment calculated on a spectrum recorded under static conditions, on a

sample where rigorously no molecular motion occurs (in practice, this could be a crystalline sample, or a polymeric sample well below its T_g).

$$M_2 = \frac{\int_0^\infty (\omega - M_1)^2 \cdot f(\omega) d\omega}{\int_0^\infty f(\omega) d\omega} \quad \text{Equation 4- II-7}$$

In the MKSA unit system, the homonuclear second moment for a rigid lattice is expressed as Equation 4- II-8²⁴¹ or Equation 4- II-9^{242,243} where μ_0 is the permeability of space, γ is the magnetogyric ratio of the spins, \hbar is the reduced Planck's constant, I the spin quantum number, N is the number of spins, r_{ij} is the internuclear ij distance, and θ_{ij} is the angle of the \vec{r}_{ij} vector with the applied magnetic field.

$$M_2 = \frac{3}{5} \left(\frac{\mu_0}{4\pi} \right)^2 \gamma^4 \hbar^2 I(I+1) \frac{1}{N} \sum_i \sum_j \frac{1}{r_{ij}^6} \quad \text{Equation 4- II-8}$$

$$M_2 = \left(\frac{\mu_0}{4\pi} \right)^2 \gamma^4 \hbar^2 \frac{I(I+1)}{3} \sum_j \left[\frac{3}{2} \frac{(1-3\cos^2\theta_{ij})^2}{r_{ij}^6} \right] \quad \text{Equation 4- II-9}$$

Both equations are equivalent. Indeed, assuming that all nuclei are equivalent, all the sums $\sum_j \frac{1}{r_{ij}^6}$ are equal, so that $\frac{1}{N} \sum_i \sum_j \frac{1}{r_{ij}^6} = \sum_j \frac{1}{r_{ij}^6}$.⁶⁷ Furthermore, the average of $(1-3\cos^2\theta_{ij})^2$ over all the orientations in a powder sample is equal to 4/5.⁶⁷ Introducing the equivalence of all nuclei in the first equation and the averaging over all orientations in the second one, then taking into account the value $I=1/2$ for ^1H nuclei, the following expression is obtained for M_2 (s. Equation 4- II-10).

$$M_2 = \frac{9}{20} \left(\frac{\mu_0}{4\pi} \right)^2 \gamma^4 \hbar^2 \sum_j \frac{1}{r_{ij}^6} \quad \text{Equation 4- II-10}$$

Then a further assumption has to be done in order to simplify the residual sum. Two simple cases will be considered here: an isolated spin pair and a simple cubic lattice. In the case of the isolated spin pair, only one internuclear distance r has to be taken into account, therefore $\sum_j \frac{1}{r_{ij}^6} = \frac{1}{r^6}$. The resulting second moment is shown in Equation 4- II-11.^{244,245}

$$M_2(\text{spin pair}) = \frac{9}{20} \left(\frac{\mu_0}{4\pi} \right)^2 \gamma^4 \hbar^2 \frac{1}{r^6} \quad \text{Equation 4- II-11}$$

In the case of a cubic lattice, the sum can be expressed as a function of the distance to the next neighbor r (equal to the lattice constant) as $\sum_j \frac{1}{r_{ij}^6} = \frac{17}{2r^6}$.⁶⁷ The resulting second moment is shown in Equation 4- II-12.

$$M_2(\text{cubic lattice}) = \frac{153}{40} \left(\frac{\mu_0}{4\pi} \right)^2 \gamma^4 \hbar^2 \frac{1}{r^6} \quad \text{Equation 4- II-12}$$

It should be underlined here that our case is rigorously neither a spin pair nor a cubic lattice, but that it can be considered as situated in-between.

As a conclusion, by simple comparison of Equation 4- II-2 with Equation 4- II-11 and Equation 4- II-12, it is deduced that $M_2(\text{spin pair}) = \frac{9}{2} q_{AB} = 4.5 q_{AB}$ and $M_2(\text{cubic lattice}) = \frac{153}{4} q_{AB} = 38.25 q_{AB}$. It should be underlined here that our case is rigorously neither a spin pair nor a cubic lattice. The factor of 8.5 found between the results of the two approaches originates mainly in the presence of 6 next neighbors (and some more remote ones) in the case of the cubic lattice versus a single one in the case of the spin pair. The geometry of our system is not sufficiently known to draw conclusions on the number and positions of the neighbors. However, even considering only intramolecular interactions, several neighbors are present, so that the simple cubic lattice approximation is much more realistic than the spin pair approach. Therefore it was decided to use exclusively the former one. Finally, the numerical value of q_{AB} can be obtained in dividing the experimental value of M_2 by a factor of 38.25.

4. Methodology for extraction of the $q_{AB} \cdot \tau_C^{AB}$ product

The decay of the monitored magnetization follows Equation 4- II-3. In order to fit experimental data, programs were written using the Matlab[®] (The MathWorks) software. These programs handle simultaneously a series of measurements done at one temperature using different parameters for the dipolar filter. The general shape of a curve described by Equation 4- II-3 is an exponential decay followed by a plateau, from which the exponential decay rate $5q_{AB}\tau_C^{AB}$ is extracted.

The plateau value was first determined as the average of all experimental values measured for mixing times longer than a chosen one. This determined plateau value was subtracted from all experimental values in order to obtain an exponential decay only (s. Equation 4- II-13).

$$f(\tau_m) = \frac{3M_0}{10} \frac{4}{5} \exp(-5q_{AB}\tau_C^{AB}\tau_m) \quad \text{Equation 4- II-13}$$

Then, the experimental data were normalized so that the exponential decay begins at 1 for $\tau_m=0$. The resulting data are described by Equation 4- II-14.

$$g(\tau_m) = \exp(-5q_{AB}\tau_C^{AB}\tau_m) \quad \text{Equation 4- II-14}$$

Finally, the resulting data were fitted with a monoexponentially decaying function to extract the $5q_{AB}\tau_C^{AB}$ values.

5. Measured data and extracted results

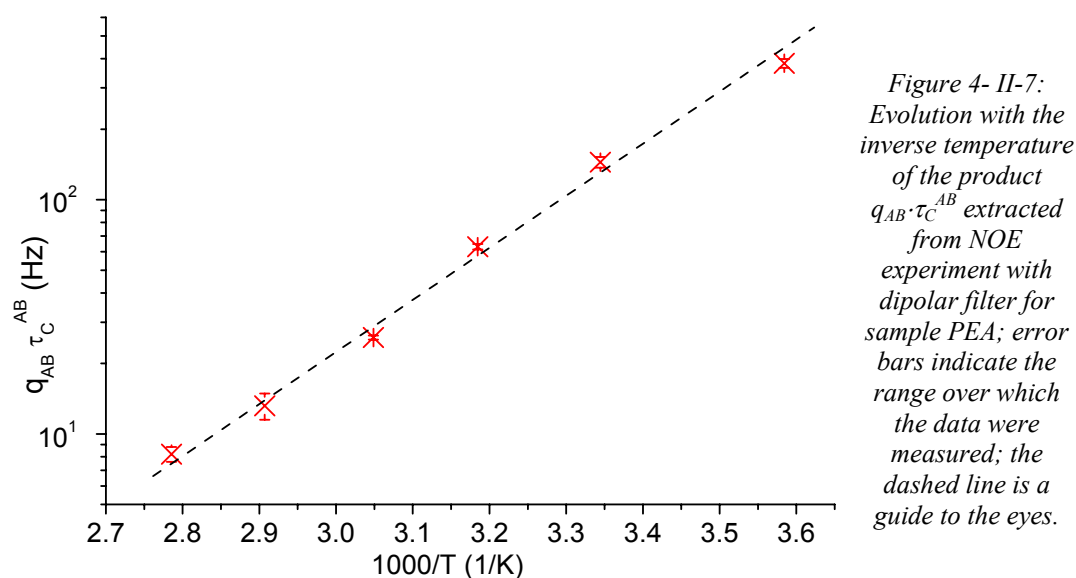
In the case of PEA at T_g+70 K, the fits yielded as series of $5q_{AB}\tau_C^{AB}$ values characterized by an average of 129.18 Hz, a range of 5.17 Hz and a standard deviation of 1.90 Hz. A simple division by a factor of 5 yielded a series of $q_{AB}\tau_C^{AB}$ values characterized by an average of 25.84 Hz, a range of 1.03 Hz and a standard deviation of 0.38 Hz.

The q_{AB} value was determined by two independent ways. First, the assumption of a $\text{CH}_3\text{-CH}_2$ moiety and the calculation of the average internuclear distance yielded a value of $q_{AB}=3.983 \text{ kHz}^2$ (s. paragraph 3.a). Second, the numerical integration of a ^1H spectrum recorded under static conditions at T_g-35 K (s. Part 7, IV.B.1) yielded a second moment value of $M_2=441.60 \text{ kHz}^2$; after division by a factor of $153/4=38.25$, this yielded values of $q_{AB}=8.89 \text{ kHz}^2$ (s. paragraph 3.b).

Finally, the first method yielded a correlation time of $\tau_C^{AB}=6.48\cdot 10^{-6}$ s (with a range of $1.3\cdot 10^{-7}$ s and a standard deviation of $9.5\cdot 10^{-8}$ s). The second method yielded an value of $2.23\cdot 10^{-6}$ s for the correlation time τ_C^{AB} (with a range of $4\cdot 10^{-8}$ s and a standard deviation of $2\cdot 10^{-8}$ s). These correlation times are different but of the same order of magnitude. For an easier comprehension, only values of $q_{AB}\tau_C^{AB}$ products will be given in this paragraph II for all PnAA samples.

C. Temperature dependence of $q_{AB}\tau_C^{AB}$ for sample PEA

The NOE experiment with dipolar filter was carried out on PEA at temperatures ranging from T_g+20 K to T_g+100 K. For each temperature, various parameters were used for the dipolar filter, and the data were processed as presented in paragraph B. The shape of the curves were identical to those obtained at T_g+70 K, only the numerical values varied. The obtained $q_{AB}\tau_C^{AB}$ products are shown on Figure 4- II-7. All numerical values are given in appendix in Part 7, IV.B.3. It is observed that the dependence on inverse temperature is nearly linear. A linear regression of the extracted $q_{AB}\tau_C^{AB}$ products yields an activation energy of 18 kJ.mol^{-1} .



D. Temperature dependence of $q_{AB} \cdot \tau_C^{AB}$ for all PnAA samples

The NOE experiment with dipolar filter was carried out on all PnAAs at temperatures ranging from T_g+40 K to T_g+100 K for sample PMA, and from T_g+20 K to T_g+100 K for samples PEA, PBA and PHxA. For each temperature, various parameters were used for the dipolar filter, and the data were processed as presented in paragraph B. The shape of the curves were similar to those obtained for sample PEA, with different numerical values. It should be noted that at high temperatures (T_g+85 K and T_g+100 K), several lines are resolved in the ^1H spectrum, except for sample PEA (s. paragraph I.A and Part 7, IV.B.1). However, the processing of all lines intensity as a function of mixing times yielded independently the same exponential decay rate. Therefore only one $q_{AB} \cdot \tau_C^{AB}$ product is extracted from measurements done at the same temperature. The obtained $q_{AB} \cdot \tau_C^{AB}$ products are shown on Figure 4- II-8. All numerical values are given in appendix in Part 7, IV.A.3. It is observed that the dependence on inverse temperature is nearly linear. Linear regressions of the extracted $q_{AB} \cdot \tau_C^{AB}$ products yield activation energies of 22, 18, 13 and 12 $\text{kJ} \cdot \text{mol}^{-1}$ for the samples PMA, PEA, PBA and PHxA respectively.

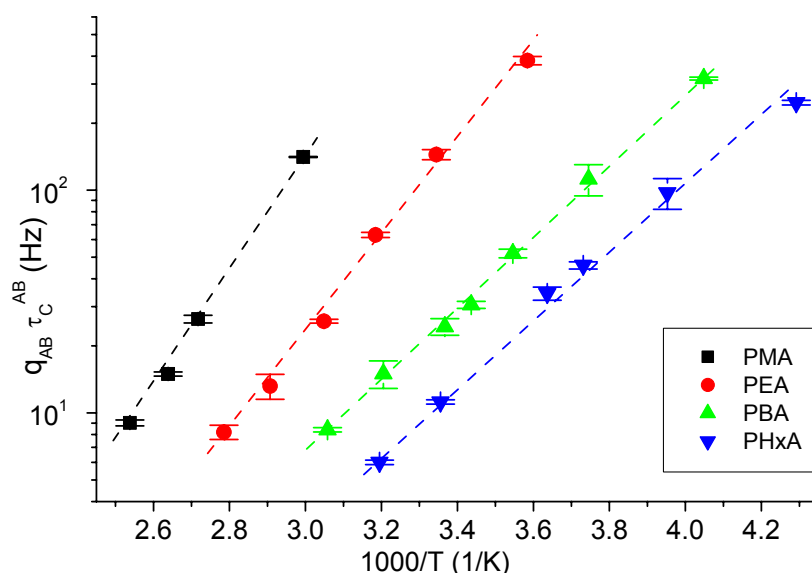


Figure 4- II-8:
Evolution with the inverse temperature of the product $q_{AB} \cdot \tau_C^{AB}$ extracted from NOE experiment with dipolar filter for all model PnAAs; error bars indicate the range over which the data were measured; the dashed lines are guides to the eyes.

Furthermore, the products $q_{AB} \cdot \tau_C^{AB}$ fall on a master curve when plotted as a function of the distance from T_g (s. Figure 4- II-9).

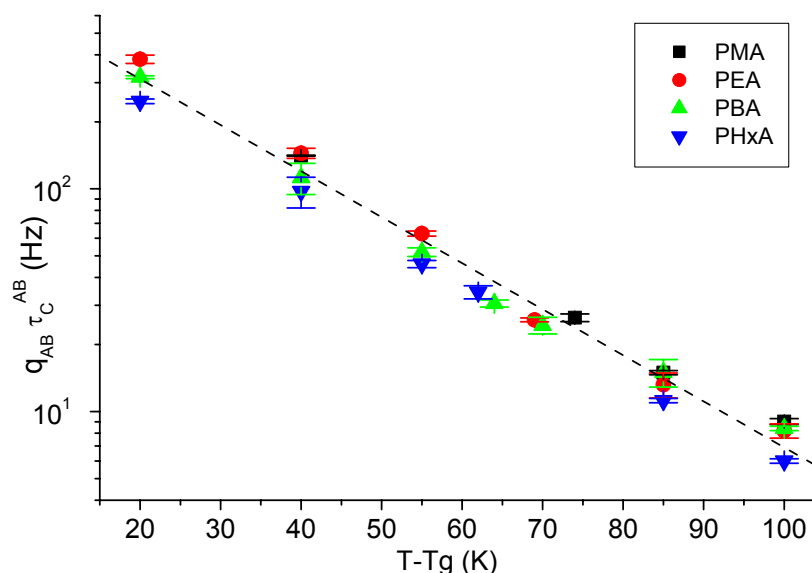


Figure 4- II-9:
Evolution with the distance from T_g of the product $q_{AB} \cdot \tau_C^{AB}$ extracted from NOE experiment with dipolar filter for all model PnAAs; error bars indicate the range over which the data were measured; the dashed line is a guide to the eyes.

E. Conclusion on the measurement of NOE in model PnAAs

The investigated PnAAs exhibit no strong dynamic contrast, as shown in paragraph I. However, the side chain was found to be clearly more mobile than the main chain in PMA, PEA and PBA, while in PHxA, there is an obvious mobility gradient along the alkyl side chain starting at the more mobile CH_3 end group. Applying the dipolar filter to these samples results in a selection according to mobility. It has been demonstrated using Lee-Goldburg CP and ^{13}C detection that the dipolar filter indeed selects the end of the alkyl side chain in PEA and PBA at T_g+70 K, i.e. the CH_3 end group and partly the next CH_2 group(s) (s. paragraph A). For sample PEA at T_g+70 K (s. paragraph B), it has been shown that applying the ^1H nuclear spin diffusion experiment with dipolar filter does not result in a coherent magnetization transfer and in the determination of domain size as it is usually the case. On the

contrary, it results in a non coherent magnetization transfer and yields information on the chain dynamics via the extraction of a correlation time τ_C^{AB} (as it was shown for sample PEMA in Part 3). The mathematical equation describing this cross-relaxation process was detailed; it allows for the determination of the product $q_{AB} \cdot \tau_C^{AB}$. Then, two independent methods were presented for the determination of the q_{AB} parameter, in order to deduce the correlation time τ_C^{AB} . The methodology used to process the experimental data was detailed. Finally, the evolution of the $q_{AB} \cdot \tau_C^{AB}$ product with temperature over the range from ca T_g+20 K to T_g+100 K was determined for all PnAAs. The interpretation of those numerical results will be done below.

III. Interpretation of NOE results in model poly(n-alkyl acrylates)

The various NMR data obtained during this work (NOE with dipolar filter, T_1 relaxation, line width) may give valuable information on the chain dynamics in model PnAAs. ^1H T_1 relaxation data will be presented in paragraph A. The correlations times determined in the present work will be compared to other relaxation data found in the literature or measured by other techniques in paragraph B.

A. ^1H longitudinal relaxation in model PnAAs

^1H longitudinal (or spin-lattice, or T_1) relaxation times have been measured on model PnAAs using the inversion recovery technique (s. Part1, II.F). The measurements were done under the same conditions as the NOE experiments with dipolar filter: at a Larmor frequency of 300.13 MHz, under static conditions, and approximately over the range from T_g to T_g+100 K. It should be emphasized here that the T_1 relaxation times shown in the present paragraph characterize the magnetization relaxation, and are by nature fully different of the correlation times τ_m extracted from NOE measurements, which are related to local motions of the polymer chain leading to magnetization decay on another timescale.

For each measurement, a single exponential behavior was observed. This can result either from an identical relaxation time of all protons in the monomeric unit, or from the faster relaxation of some ^1H nuclei, combined with extensive ^1H nuclear spin diffusion or extensive cross-relaxation. Kalk and Berendsen indeed developed a model describing a rigid protein in solution with only CH_3 rotation as intramolecular motion (and thus relaxation sink); they observed that in the case of efficient cross-relaxation, CH_3 rotation leads to a short and unique T_1 relaxation time for all protons of the molecule.¹¹⁶ They concluded that, due to NOE, there can be no straightforward conclusion on local motion from T_1 relaxation data for fields

above 100 MHz and molecular weights above 20 000 g.mol⁻¹.¹¹⁶ In the PnAAs, the single exponential behavior was thus attributed to the faster relaxation of some ¹H nuclei, combined with extensive ¹H nuclear spin diffusion or extensive cross-relaxation. The extracted relaxation times are shown on Figure 4- III-1. It should be noted that for PMA, PBA and PHxA at high temperatures, several lines are resolved, but they all exhibit nearly identical relaxation times.

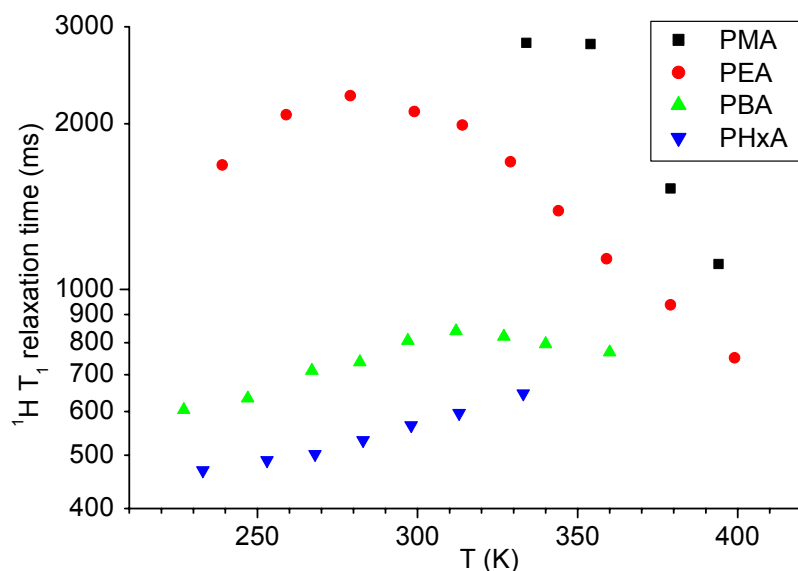


Figure 4- III-1:
Evolution with temperature of the single ¹H longitudinal (or spin-lattice) relaxation time measured using the inversion recovery technique on model PnAAs (300.13 MHz Larmor frequency, under static conditions).

It is clearly seen that the T_1 relaxation time decreases with alkyl side chain length. Furthermore, PMA and PEA exhibit significantly higher T_1 relaxation times than PBA and PHxA. These observations were interpreted as follows. In PMA and PEA samples, which have a short alkyl side chain, there is no motional mode close enough from the Larmor frequency to induce fast relaxation. On the contrary, in PBA and PHxA, which have longer alkyl side chains, and thus more motional modes, there is a motional mode which exhibits a frequency in good range to relax efficiently (the CH₃ rotation is probably too fast, but one of the CH₂ side groups would have an appropriate motional mode). The ¹H-¹H cross-relaxation, or the ¹H nuclear spin diffusion, then induces a fast relaxation of all parts of the molecule.

It is also observed that the temperature dependence of the T_1 relaxation time is weaker in PBA and PHxA. The T_1 relaxation time does not exhibit a common dependence for all PnAAs upon temperature (s. Figure 4- III-1) or distance from T_g (s. Figure 4- III-2). Furthermore, it does not exhibit an evolution comparable to the one of the $q_{AB\tau_C}^{AB}$ factor extracted from the NOE measurements with dipolar filter (s. Figure 4- II-9). Considering the resulting difficulty of using ¹H T_1 relaxation data in the interpretation of NOE data, as well as the complexity of the various underlying motional modes, it was decided not to interpret the ¹H T_1 relaxation data any further.

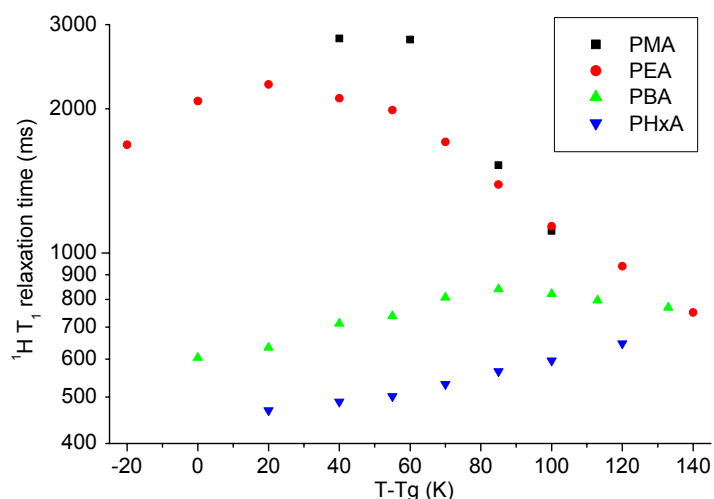


Figure 4- III-2:
Evolution with distance from T_g of the single ^1H longitudinal (or spin-lattice) relaxation time measured using the inversion recovery technique on model PnAAs (300.13 MHz Larmor frequency, under static conditions).

It should be emphasized here that the ^1H T_1 relaxation times are long enough to observe NOE effect on the time scale of a few tens of ms.

B. Relaxation processes in model PnAAs

It was shown in paragraph II.A that the dipolar filter selects the end of the alkyl side chains in PnAAs, but rigorously not only the end CH_3 group. It has then been discussed in paragraph II.B.2 that the $\text{CH}_3\text{-CH}_2$ model does not fully describe the NOE measurements in the investigated PnAAs, even if it is the most appropriate analytical one. For these reasons, the extracted correlations times should be considered carefully.

A correlation time can be deduced from an extracted $q_{\text{AB}} \cdot \tau_{\text{C}}^{\text{AB}}$ product either via the calculation of the q_{AB} parameter for a $\text{CH}_3\text{-CH}_2$ moiety, or via the measurement of the second moment from an experimental ^1H spectrum (s. paragraph II.B.3). Both methods have been used in the present work. The extracted correlation times are plotted together with mechanical and dielectric relaxation data from literature (s. Figure 4- III-3 to Figure 4- III-6). Due to the lack of reliable literature data for the local relaxation processes in most of the PnAAs, dielectric and mechanical spectroscopy measurements were conducted on the investigated PnAAs in the group of Prof. Pakula at the MPI-P.²⁴⁶ The moduli were calculated from the measured permittivity, and the maxima of the moduli as a function of frequency were fitted using Havriliak-Negami functions;²⁴⁷ the results are also indicated on Figure 4- III-3 to Figure 4- III-6.

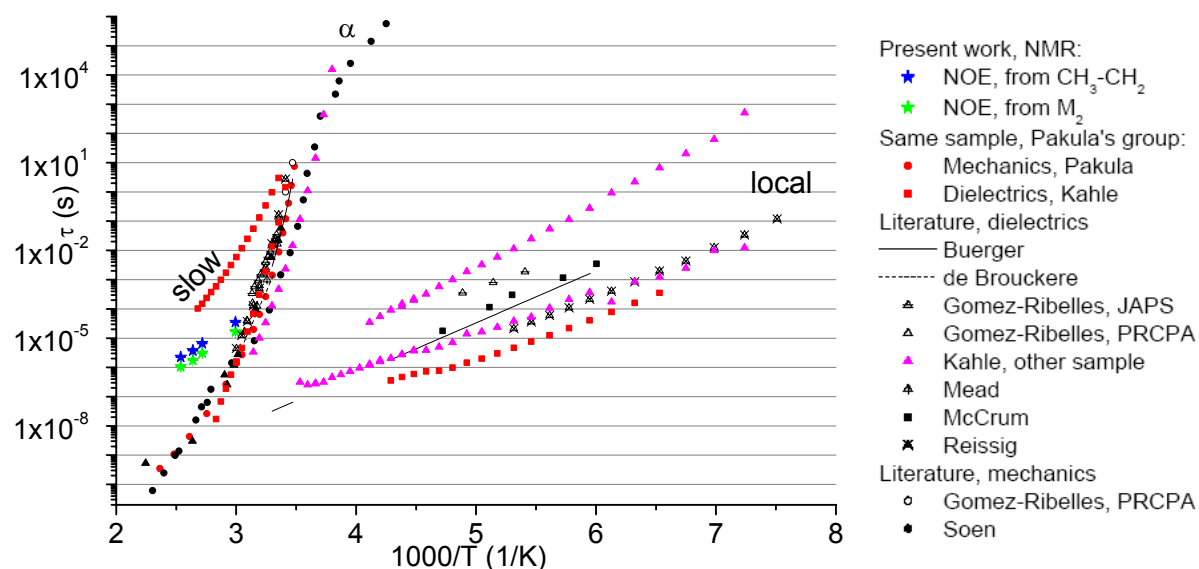


Figure 4- III-3: Correlation times extracted from the NOE measurements performed in the present work for sample PMA, comparison with data measured in the group of Prof. Pakula on the same sample via dielectric and mechanical spectroscopy²⁴⁶, comparison with literature data (Buerger²⁴⁸, de Brouckere²⁴⁹, Gomez Ribelles JAPS²⁵⁰, Gomez Ribelles PRCPA²⁵¹, Kahle²⁵², McCrum²⁵³, Mead²⁵⁴, Reissig²⁵⁵, Soen²⁵⁶).

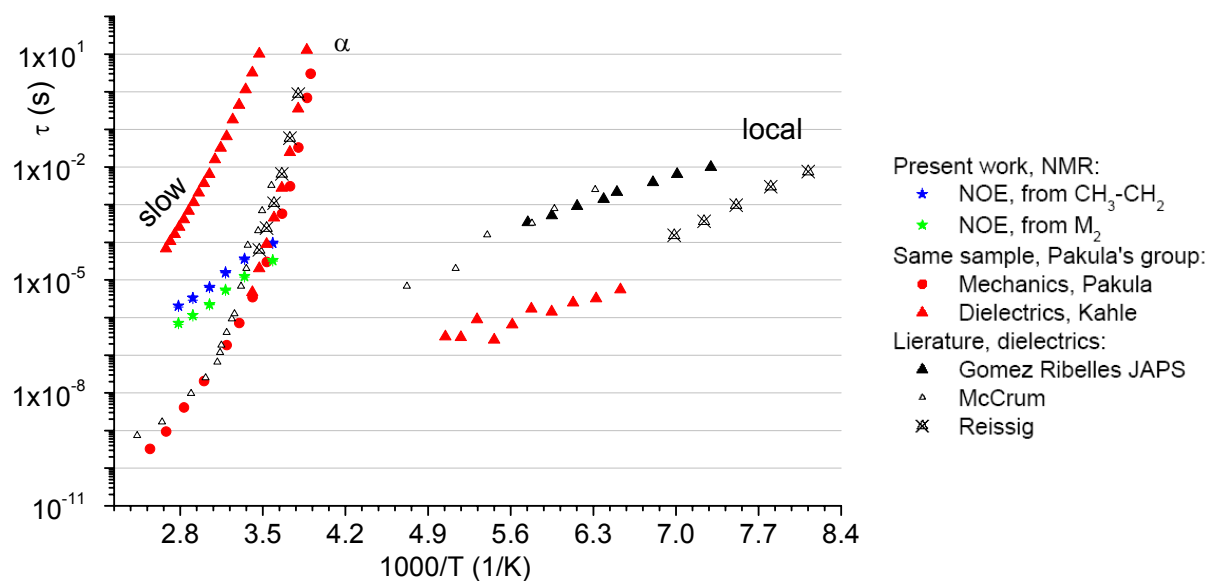


Figure 4- III-4 : Correlation times extracted from the NOE measurements performed in the present work for sample PEA, comparison with data measured in the group of Prof. Pakula on the same sample via dielectric and mechanical spectroscopy²⁴⁶, comparison with literature data (Gomez Ribelles JAPS²⁵⁰, McCrum²⁵³, Reissig²⁵⁵).

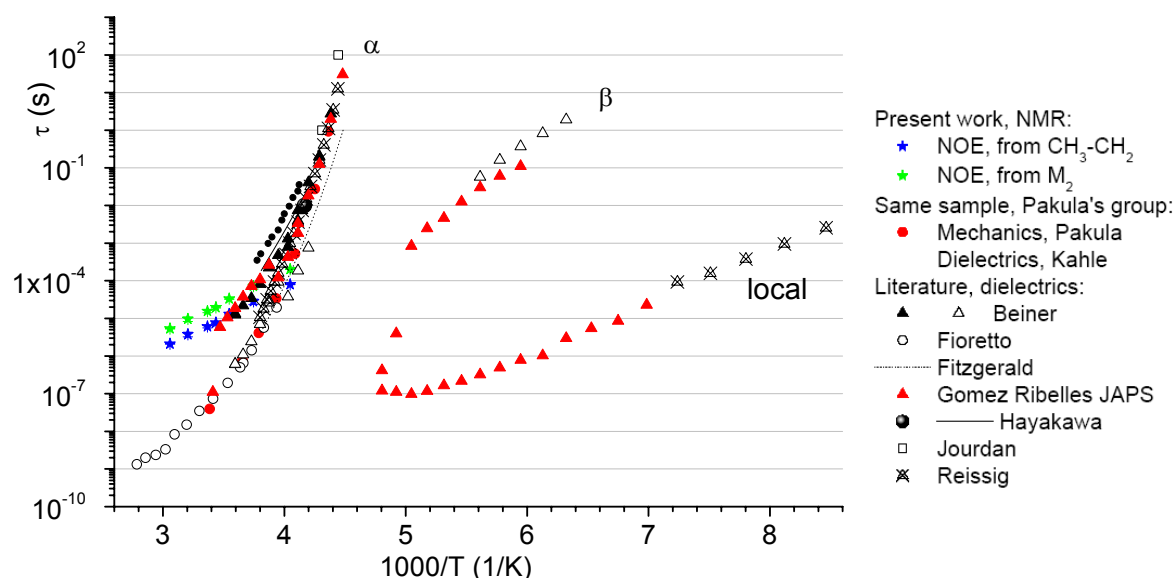


Figure 4- III-5: Correlation times extracted from the NOE measurements performed in the present work for sample PBA, comparison with data measured in the group of Prof. Pakula on the same sample via dielectric and mechanical spectroscopy²⁴⁶, comparison with literature data (Beiner²²⁹, Fioretto²⁵⁷, Fitzgerald²⁵⁸, Gomez Ribelles JAPS²⁵⁰, Hayakawa²⁵⁹, Jourdan²⁶⁰, Reissig²⁵⁵).

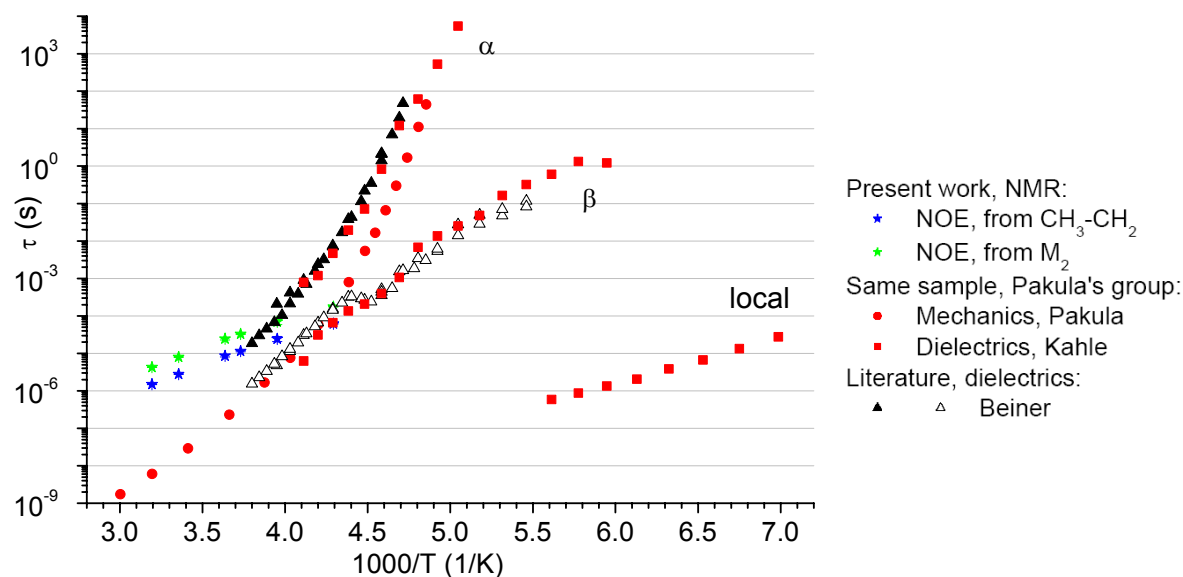


Figure 4- III-6: Correlation times extracted from the NOE measurements performed in the present work for sample PHxA, comparison with data measured in the group of Prof. Pakula on the same sample via dielectric and mechanical spectroscopy²⁴⁶, comparison with literature data (Beiner²²⁹).

The correlation times determined independently via the calculation of q_{AB} and via the second moment are different but of the same order of magnitude for each measurement, thus in fair agreement considering the approximations involved in both cases. Furthermore, no relaxation process is detected by the other methods on the same time and temperature ranges with the same temperature dependence. ***Thus the relaxation process observed by the NOE experiment is detected and quantified for the first time on this temperature range.*** All samples exhibit a linear dependence of the determined correlation time upon inverse

temperature. The investigated temperature range is broad enough to detect a possible curvature, e.g. if a WLF relaxation process would take place. The observed linearity thus indicates rather a local relaxation process than a collective process related to main chain motions. Therefore it will be compared below to the other local relaxation processes, namely the β -relaxation process and the relaxation process labeled as “local”. Linear regressions of all concerned correlation and relaxation times as a function of temperature were done, and the results are detailed in appendix (s. Part 7, IV.B.3).

For sample PHxA, the activation energy of the process detected by NOE, $12 \text{ kJ}\cdot\text{mol}^{-1}$, is intermediate between those of the local relaxation and of the β -relaxation ($10 \text{ kJ}\cdot\text{mol}^{-1}$ and from 15 to $25 \text{ kJ}\cdot\text{mol}^{-1}$ respectively). The same is observed for PBA sample, with respective activation energies of $13 \text{ kJ}\cdot\text{mol}^{-1}$, $10 \text{ kJ}\cdot\text{mol}^{-1}$ and $18 \text{ kJ}\cdot\text{mol}^{-1}$ for the process detected by NOE, the local and the β -relaxations. In the cases of PEA and PMA, it is also seen that the activation energies of the process detected by NOE (respectively $18 \text{ kJ}\cdot\text{mol}^{-1}$ and $22 \text{ kJ}\cdot\text{mol}^{-1}$) are higher than those of the local relaxation (ranging respectively from 8 to $14 \text{ kJ}\cdot\text{mol}^{-1}$ and from 11 to $19 \text{ kJ}\cdot\text{mol}^{-1}$). For samples PEA and PMA, no β -relaxation process was detected by dielectric spectroscopy in the curves of moduli as a function of frequency. However, it could be present but insufficiently resolved from the α -relaxation process, due to proximity in frequency and a lower intensity of the β -relaxation. It might be detected while processing the recorded data as a function of temperature, or using mechanical measurements with another geometry.

The α -relaxation is usually attributed to motions of the main chains, $\alpha\beta$ -relaxation to motions of the main chains coupled to reorientations of the side chains, β -relaxation to reorientations of the whole COO-alkyl side chains, and local relaxation to reorientations of parts of these side chains in PnAAs.²⁵³ Thus ***the process detected by NOE is naturally attributed to reorientations of parts of the side chains***, i.e. to a superposition of β -relaxation and more local relaxation. It is very surprising that the corresponding motions of the side chain are slower than those of the main chain (α - and $\alpha\beta$ -relaxations) on the temperature range where the measurements were carried out. However, it should be noted that the motions detected by the NOE experiment with dipolar filter are not the slowest ones, as indicated by the process labeled as slow, and detected by dielectrics for samples PMA and PEA (for which only the order of magnitude can be trusted in the present state of data processing). Furthermore, it should be underlined here that different relaxation processes may be detected by NOE with dipolar filter and by dielectric spectroscopy, due to the detection method. The dielectrics indeed primarily detects motions via the permanent dipole located at the carbonyl

group in the laboratory frame, while the NOE probes motions more locally via relative motions of neighboring ^1H nuclei causing a modulation of the dipolar coupling in their local molecular frame.

However, *in the context of locally organized samples, it is conceivable that the side chain motions would be slower than those of the main chain* (s. work Beiner et al.²²⁹ for PnAMAs and PnAAs in Part 3, I.B). In those samples, organized nanodomains of alkyl side chains are separated by main chains. Then the positions of the main chains might fluctuate in the regions between organized nanodomains, while the alkyl side chains motions might be hindered inside the organized alkyl nanodomains and thus slower. *The NOE experiment would then detect hindered motions of the side chains inside the nanodomains, resulting from β -relaxation and more local relaxations.*

The correlation times extracted from NOE measurements are plotted together with mechanical and dielectric relaxation data measured on the same sample on Figure 4- III-7. The process detected by NOE seems to be approaching the *slow process* similarly to the way the β -relaxation approaches the α -relaxation. It would be fascinating to investigate if these two processes actually merge at a higher temperature into a process similar to the $\alpha\beta$ -relaxation.

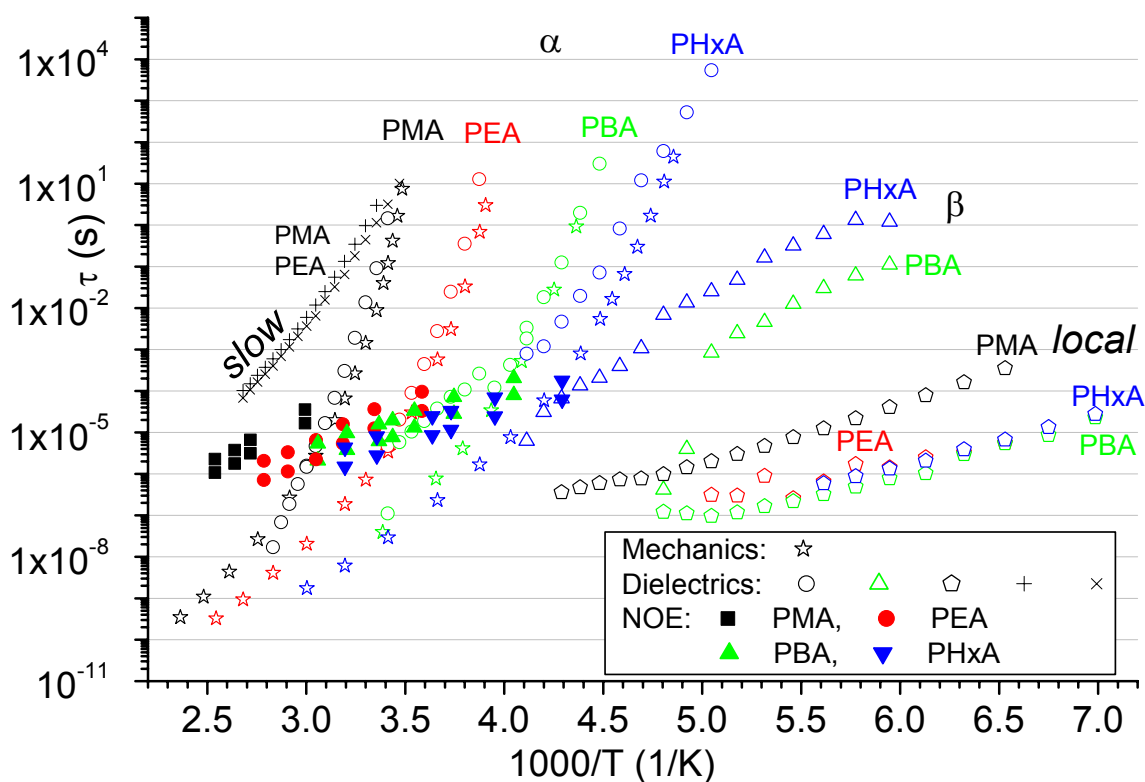


Figure 4- III-7: Correlation times extracted from the NOE measurements performed in the present work for model PnAAs using the NOE experiment with dipolar filter, comparison with data measured in the group of Prof. Pakula on the same samples via dielectric and mechanical spectroscopy²⁴⁶.

IV. Conclusion on NOE in model poly(n-alkyl acrylates)

A. Conclusion

Applying the ^1H nuclear spin diffusion technique with dipolar filter to homopolymers exhibiting a weak dynamic contrast can allow to carry out NOE measurements (s. Part 3). This NOE technique with dipolar filter has been applied successfully to model PnAAs, which are model samples for industrial acrylic PSAs.

The investigated PnAAs do not exhibit a strong dynamic contrast (from the line shape of ^1H spectra recorded under static conditions). However, the side chain end is clearly more mobile than the main chain in PMA, PEA and PBA, while in PHxA, there is an obvious mobility gradient along the alkyl side chain starting at the more mobile CH_3 end group (from 2D-WISE). Applying the dipolar filter to these samples results in a selection according to mobility: the end of the alkyl side chain is selected, i.e. the CH_3 end group and partly the next CH_2 group(s). The following magnetization transfer occurs in a non-coherent way via cross-relaxation, and thus yields information on the involved local dynamics via the extraction of a correlation time τ_C^{AB} . *A methodology was developed for extracting the product $q_{\text{AB}} \cdot \tau_C^{\text{AB}}$ from the recorded data, as well as for calculating the q_{AB} parameter (in two independent ways) to deduce the correlation time τ_C^{AB} .*

The extracted correlation times τ_C^{AB} were compared with mechanical and dielectric relaxation data, from literature or measured on the same samples in the group of Prof. Pakula at the MPI-P. *The relaxation process detected by the NOE experiment is detected and quantified for the first time on this temperature range.* Based on the picture of Beiner at al.²²⁹ of local nanophase separation in PnAAs, *the correlation times quantified by the NOE measurements in the present work have been attributed to hindered local motions of the side chains in organized alkyl nanodomains.* It might be related to the slow relaxation, exhibiting a WLF behavior on a time scale slower than the α -relaxation.

B. Outlook

In order to process the NOE data, the PnAAs were modeled as $\text{CH}_3\text{-CH}_2$ moieties, due to the initial selection of mainly the end CH_3 group of the alkyl side chain, and due to the absence of more elaborate analytical equations to describe NOE (to our knowledge). However, a $\text{CH}_3\text{-CH}_2$ moiety does not model the whole monomeric unit of PEA, PBA and PHxA, and definitely fails to model the one of PMA. Thus the determined correlation times

τ_C^{AB} suffer from this inaccuracy of the available model, and should be considered carefully. *It would be useful to look for and develop more elaborate analytical models or simulation programs to process the recorded NOE decay, in order to extract more accurate correlation times τ_C^{AB} for the model PnAAs.*

Concerning the complementary dielectric and mechanical measurements, it would be helpful to obtain data on the β -relaxation process in the samples PMA and PEA. A new processing of the already recorded dielectric data plotted as moduli vs temperature for a given frequency could allow the detection of this process, due to a better separation from the α -relaxation on a temperature scale than on a frequency scale. Alternative mechanical measurements with a different sample geometry could also allow to detect the β -relaxation process.

It would be very interesting to investigate a possible link between the process detected by NOE and the slow relaxation process detected by dielectric spectroscopy in samples PMA and PEA. First, a more accurate quantification of the slow process should be done by processing the dielectric data, then its presence in samples PBA and PHxA should be investigated. The slow process as well as the process detected by NOE should be investigated at higher temperatures, in particular in order to look for a possible merging.

**Part 5: Nuclear Overhauser Effect investigated
in model poly(n-alkyl methacrylates) using the
dipolar filter; comparison with acrylate models
and PSAs**

I.	<i>Investigation of the dynamic contrast in model poly(n-alkyl methacrylates)</i>	179
A.	¹H static spectra	179
B.	2D-WISE	181
C.	Conclusion on the dynamic contrast	181
II.	<i>Investigation of NOE in the model poly(n-alkyl methacrylates) using the dipolar filter</i>	181
A.	Actual selection done by the dipolar filter	181
B.	Recording and processing NOE data using the dipolar filter in PEMA at T_g+67 K	184
1.	Conducted experiments and recorded magnetization.....	184
2.	Mathematical equation governing the recorded magnetization decay	185
3.	Determination of the q _{AB} parameter	185
4.	Methodology for extraction of the q _{AB} ·τ _C ^{AB} product	185
5.	Measured data and extracted results.....	186
C.	Temperature dependence of q_{AB}·τ_C^{AB} for poly(ethyl methacrylate) samples	186
D.	Temperature dependence of q_{AB}·τ_C^{AB} for model PnAMA samples	187
E.	Discussion of the biexponential behavior observed at low temperatures.	188
F.	Conclusion on the measurement of NOE in model PnAMAs	189
III.	<i>Interpretation of NOE results in model poly(n-alkyl methacrylates)</i> ..	190
A.	¹H longitudinal relaxation in model PnAMAs	190
B.	Relaxation processes in model PnAMAs	192

IV.	<i>Comparison of model and industrial samples</i>	195
A.	Comparison of all model samples	195
1.	Mobility from NMR.....	195
2.	Local structure from NMR and X-ray scattering.....	197
3.	Local relaxation NOE experiment with dipolar filter.....	197
B.	Comparison of model and industrial samples	198
1.	Dynamic contrast.....	198
2.	NOE experiment with dipolar filter.....	199
V.	<i>Conclusion on NOE in model poly(n-alkyl methacrylates) and on the comparison of all samples</i>	201
A.	Local nanophase separation	201
B.	Local relaxation processes detected by the NOE with dipolar filter	201
C.	Comparison with industrial samples	202

Part 5: Nuclear Overhauser Effect investigated in model poly(n-alkyl methacrylates) using the dipolar filter; comparison with acrylate models and PSAs

The application of the ^1H nuclear spin diffusion technique with dipolar filter can lead to erroneous results for homopolymers exhibiting a weak dynamic contrast. It allows in fact to investigate the local molecular dynamics. This experiment has been applied to poly(n-alkyl acrylates), PnAAs (s. Part 4). The same investigation is presented in this part for poly(n-alkyl methacrylates), PnAMAs. First measurements done on industrial PSA samples will also be shown.

Concerning the model PnAMAs, the dynamic contrast has been investigated (s. paragraph I) and NOE experiments using the dipolar filter have been performed (s. paragraph II). The results will be interpreted in terms of chain dynamics (s. paragraph III). Results obtained for the model PnAMAs will be compared to those obtained for model PnAAs (already detailed in Part 4) and industrial PSA samples (s. paragraph IV).

I. Investigation of the dynamic contrast in model poly(n-alkyl methacrylates)

The dynamic contrast (difference in mobility between the more mobile and the less mobile parts of a sample) was characterized in the model PnAMAs by solid-state NMR, in particular ^1H static spectra and 2D-WISE experiments.

A. ^1H static spectra

All the recorded spectra are shown in the appendix (Part 7, IV.A). A few representative spectra are shown in Part 3, II.A (Figure 3- II-1) for sample PEMA. For all investigated model PnAMAs the line shape was similar at the same distance to T_g (except for sample PHMA13C at low temperatures). The line gets narrower in a visually homogeneous way with increasing temperature. As detailed in Part 3, II.A, *this means that the whole sample is becoming more mobile with increasing temperature, and exhibits no strong dynamic contrast*. Nevertheless, less pronounced dynamic contrast within the sample might still be present and probed using the dipolar filter.

A characteristic spectrum of PHMA13C is shown in Figure 5- I-1: this sample is not completely dry, the remarks concerning sample PMA in Part 4, I.A apply here as well.

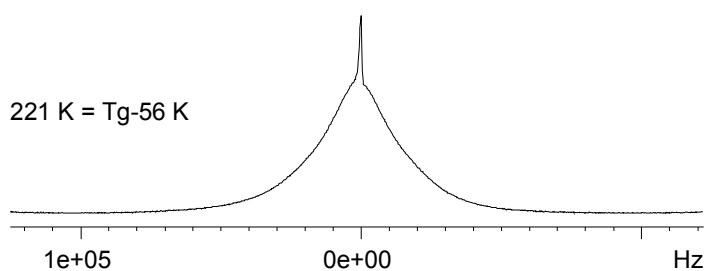


Figure 5- I-1: Line shape of ^1H spectrum of sample PHMA13C at T_g-56 °C (spectrum recorded at a ^1H Larmor frequency of 300.13 MHz, under static conditions).

A summary of the fwhm as a function of temperature for all the PnAMA samples is shown in Figure 5- I-2. It can be noted that all investigated PnAMAs have a similar line width evolution at the same distance from T_g . However, they exhibit significant line width differences at a given temperature. The fwhm of PEMADMC (poly(ethyl methacrylate) deuterated on the main chain) is smaller than the ones of the non deuterated poly(ethyl methacrylate) samples, since only the more mobile side chain is recorded. Furthermore, the fwhm of PHMA13C is smaller than the ones of all the other non deuterated model PnAMAs, since the small molecules present inside sample PHMA13C play the role of a plasticizer. Furthermore, for the non deuterated samples above T_g-20 K, the line width is decreasing with increasing alkyl side chain length. Significant differences between non labeled and ^{13}C labeled samples for a few temperatures have not been attributed.

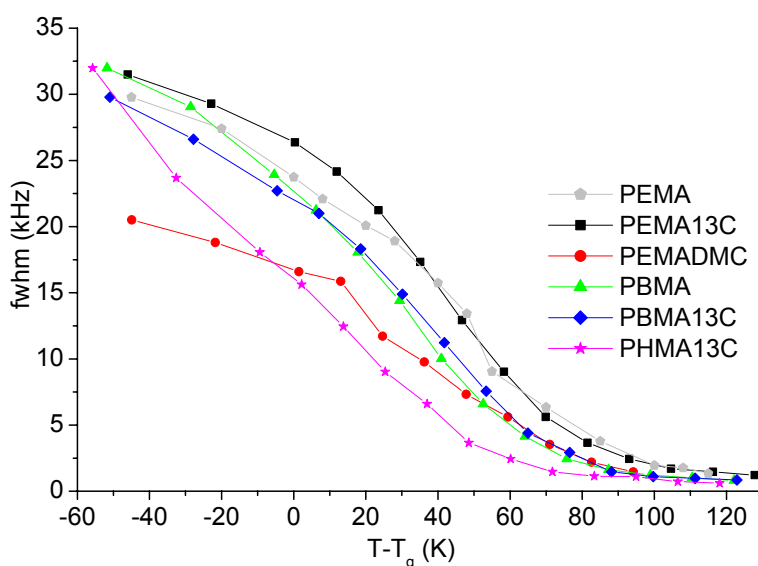


Figure 5- I-2: Influence of the temperature on the fwhm of the ^1H spectrum of the model PnAMAs (spectra recorded at a ^1H Larmor frequency of 300.13 MHz, under static conditions).

For all samples, a slow decay of the fwhm as a function of temperature is observed, which corresponds to a broad glass transition. The slowness of this decay is attributed to the local structure of the samples, present between ca $T_g+30\text{K}$ and ca $T_g+80\text{K}$ on the NMR time scale, which induces strongly anisotropic motions and thus stronger dipolar couplings (s. Part 3, I.). This glass transition starts at a temperature much lower than the glass transition temperature T_g measured by DSC. This is due to the fact that DSC mainly detects the glass transition of the backbone, while the alkyl side chain is already mobile at lower temperatures.

Furthermore, for increasing alkyl side chain length, the fwhm at T_g decreases, indicating that the glass transition process starts at a lower temperature.

B. 2D-WISE

The 2D-WISE technique was used to characterize more precisely the dynamic contrast in the model PnAMAs. It was detailed in Part 3, II.B.

C. Conclusion on the dynamic contrast

The investigated PnAMAs exhibit no strong dynamic contrast from the line shape of ^1H spectra recorded under static conditions. However, 2D-WISE investigations on poly(ethyl methacrylate) samples revealed mobility differences. Indeed, the CH_3 groups are the most mobile ones, and the side chain one is more mobile than the main chain one.

Finally, the dynamic contrast is very low in PnAMA sample, but might still be present and detected by other solid-state NMR techniques like the dipolar filter (s. next paragraph).

II. Investigation of NOE in the model poly(n-alkyl methacrylates) using the dipolar filter

The principle of the Nuclear Overhauser Effect measurement using the dipolar filter dipolar filter is described in Part 3. The actual selection done by the dipolar filter will be investigated in paragraph A, while the exact data processing will be explained in paragraph B on the example of PEMA at T_g+70 K. The temperature dependence of the extracted correlation time will be determined in paragraph C for sample PEMA, in paragraph D for all investigated PnAMAs. The biexponential behavior observed at low temperatures will be discussed in paragraph E.

A. Actual selection done by the dipolar filter

For reasons detailed in Part 3, IV.A.1, the LG-CP experiments using the dipolar filter were carried out under 3 kHz MAS on samples PEMA, PEMADMC and PBMA, at ca T_g+70 K for PBMA and at ca T_g+45 K for the others. In the first experiment, a simple LG-CP spectrum was recorded to obtain a reference spectrum. In the second experiment, a dipolar filter was applied and immediately afterwards a LG-CP spectrum was recorded, in order to determine the parts of the sample actually selected by the dipolar filter. In the third experiment, the same dipolar filter was applied, followed by a rather long mixing time and the recording of a LG-CP spectrum, in order to observe the sample relaxing back at equilibrium.

For samples PEMA and PBMA, a LG-CP spectrum was also recorded for an intermediate mixing time. The corresponding spectra are shown on Figure 5- II-1, Figure 5- II-2 and Figure 5- II-3. The carbonyl signal is not observed.

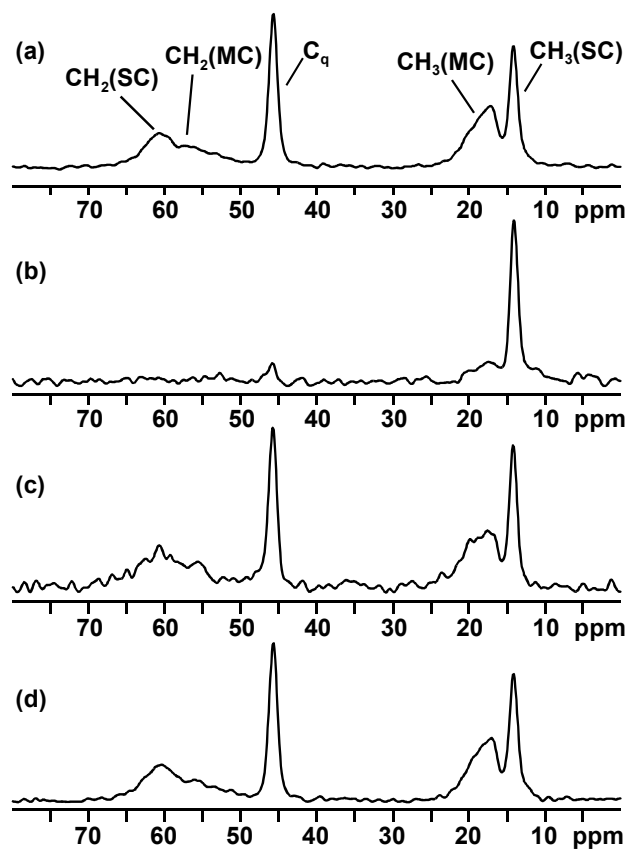


Figure 5- II-1: ^{13}C LG-CP spectra of sample PEMA at ca 390 K (ca T_g+45 K) at 75.47 MHz under 3 kHz MAS with 500 μs contact time; (a) LG-CP; (b) dipolar filter with 20 μs delay and 1 cycle, no mixing time and LG-CP; (c) dipolar filter with 20 μs delay and 1 cycle, 1 ms mixing time and LG-CP; (d) dipolar filter with 20 μs delay and 1 cycle, 50 ms mixing time and LG-CP; the abbreviations MC and SC designate main chain and side chain.

The spectra shown on Figure 5- II-1 (a), (b), and (d) have been commented in Part 3, IV.A.2. The dipolar filter actually selects only the CH_3 group of the alkyl side chain in sample PEMA. It can be noticed that this selection of the CH_3 end group occurs more accurately than in the PnAAs. Furthermore, it is seen on Figure 5- II-1 (c) that there is no significant difference in the spectra recorded after 1 ms or 50 ms mixing time. This will be discussed in Part II.E.

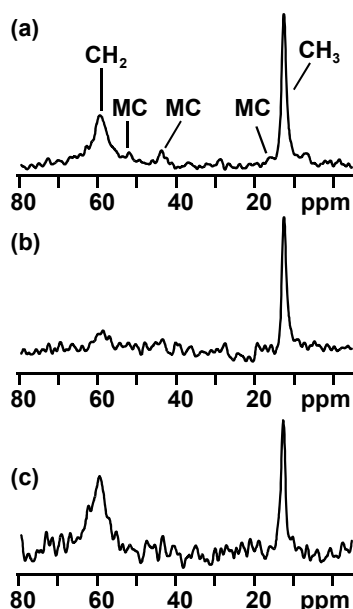


Figure 5- II-2: ^{13}C LG-CP spectra of sample PEMADMC at ca 390 K (ca T_g+45 K) at 75.47 MHz under 3 kHz MAS with 500 μs contact time; (a) LG-CP; (b) dipolar filter with 10 μs delay and 1 cycle, no mixing time and LG-CP; (c) dipolar filter with 10 μs delay and 1 cycle, 8 ms mixing time and LG-CP; the abbreviation MC designate the main chain.

No signal is recorded for the carbons of the main chain in sample PEMADMC (Figure 5- II-2 (a)), as expected for this sample deuterated on the main chain. Furthermore, this ^{13}C LG-CP spectrum gives the reference intensities in a LG-CP spectrum. It can be clearly seen on the ^{13}C LG-CP spectrum on Figure 5- II-2 (b) that the dipolar filter actually selects the CH_3 end group of the side chain, i.e. it selects the end of the side chain of PEMADMC. It should be noted that a negligible amount of CH_2 groups of the main chain is also selected. The ^{13}C LG-CP spectrum shown on Figure 5- II-2 (c) is identical to the one shown on Figure 5- II-2 (a), proving that the magnetization is back at equilibrium 8 ms after the application of the dipolar filter.

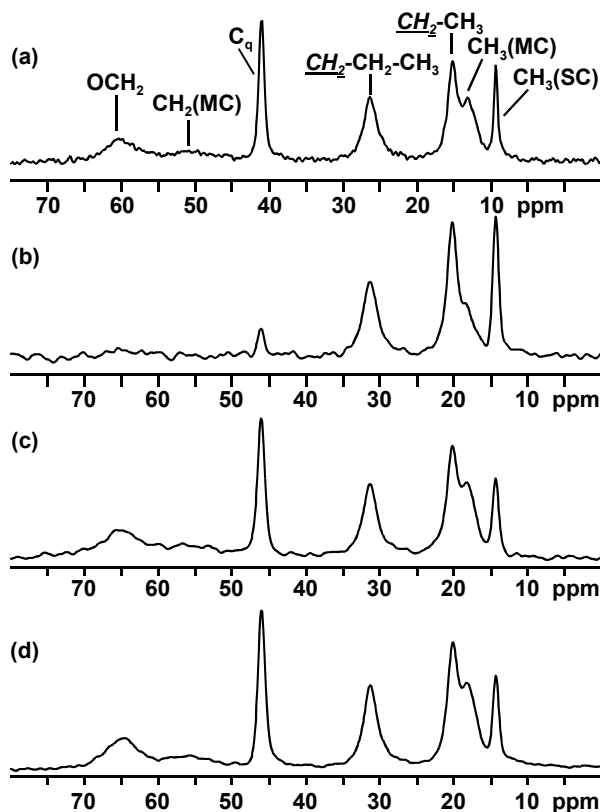


Figure 5- II-3: ^{13}C LG-CP spectra of sample PBMA at ca 370 K (ca T_g+70 K) at 75.47 MHz under 3 kHz MAS with 500 μs contact time; (a) LG-CP; (b) dipolar filter with 15 μs delay and 1 cycle, no mixing time and LG-CP; (c) dipolar filter with 15 μs delay and 1 cycle, 5 ms mixing time and LG-CP; (d) dipolar filter with 15 μs delay and 1 cycle, 50 ms mixing time and LG-CP; the abbreviation MC designates main chain.

All the chemical sites of the monomeric unit of PBMA are resolved in the ^{13}C LG-CP spectrum (Figure 5- II-3 (a)). The dipolar filter actually selects the CH_3 end group of the side chain and partly the next two CH_2 groups and the main chain CH_3 group (Figure 5- II-3 (b)), i.e. it selects the end of the alkyl side chain and partly the α -methyl group in PBMA. The spectra recorded without mixing time and with 50 ms mixing time are identical (Figure 5- II-3 (a) and (d)), indicating a return to equilibrium 50 ms after the application of the dipolar filter. Furthermore, no difference in the spectra recorded after 5 ms or 50 ms mixing time (Figure 5- II-1 (c)). This will be discussed in Part II.E.

As a conclusion, the LG-CP investigations carried out on PEMA and PEMADMC at ca T_g+45 K proved that *the dipolar filter actually selects only the CH_3 end group of the alkyl side chain in poly(ethyl methacrylate)*. It was proved that *the dipolar filter actually selects only the CH_3 end group of the alkyl side chain and partly the next CH_2 groups in PBMA* at ca T_g+70 K, as well as partly the α -methyl group.

B. Recording and processing NOE data using the dipolar filter in PEMA at T_g+67 K

1. Conducted experiments and recorded magnetization

NOE investigations using the dipolar filter were conducted on sample PEMA at 409 K, i.e. T_g+67 K (s. Part 4, II.B.1 for details). The evolution of the recorded magnetization with mixing time is shown on Figure 5- II-4. It was proved (s. Part 3, IV.B) that the magnetization transfer occurs after the dipolar filter via incoherent zero- and double-quantum transitions, also called cross-relaxation or NOE. Since the PEMA at T_g+67 K is in the slow motion limit, zero-quantum transitions (i.e. flip-flops) are predominant.

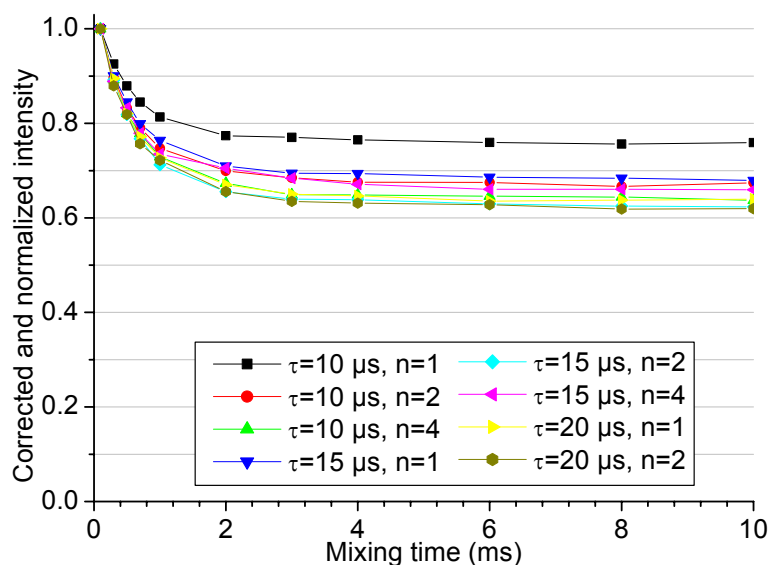


Figure 5- II-4:
Evolution of the ^1H magnetization of mobile species with the mixing time for the sample PEMA at 409 K (T_g+67 K, n cycles of 12τ -spaced pulses in the dipolar filter).

2. Mathematical equation governing the recorded magnetization decay

The mathematical equation governing the monitored decay is the one describing the decay of the intensity of a diagonal line in a 2D-NOE experiment in the slow motion limit, as justified in Part 3, IV.C. Furthermore, the initial magnetization is located at the CH₃ end group of the alkyl side chain. Therefore we chose to use the decay equation calculated for two groups of equivalent nuclei in Part 3, IV.C.2, and to consider a CH₃-CH₂ moiety, as was already done and discussed for model PnAAs in Part 4, II.B.2. The validity of the CH₃-CH₂ approximation should be discussed again here. Indeed, it is rigorously valid for sample PEMADMC, where only a CH₃ and a CH₂ group are present, and in which the dipolar filter properly selects the CH₃ group.

The evolution with mixing time τ_m of the intensity a_{AA} of a diagonal line in a 2D-NOE experiment concerning a CH₃-CH₂ moiety follows Equation 5- II-1, where τ_C^{AB} is the correlation time of the involved molecular motion (s. Equation 4- II-3 in Part 4, II.B.2). Fitting the experimental data allows to determine the product $q_{AB} \cdot \tau_C^{AB}$. Thus, a parallel determination of q_{AB} leads to extraction of the correlation time of the involved motion τ_C^{AB} .

$$a_{AA}(\tau_m) = \frac{3M_0}{10} \left[\frac{6}{5} + \frac{4}{5} \exp(-5q_{AB} \tau_C^{AB} \tau_m) \right] \quad \text{Equation 5- II-1}$$

3. Determination of the q_{AB} parameter

Two possible ways of determining the q_{AB} parameter have been discussed in Part 4, II.B.2. This discussion is also valid for the model PnAMAs.

4. Methodology for extraction of the $q_{AB} \cdot \tau_C^{AB}$ product

The methodology for the extraction of the $q_{AB} \cdot \tau_C^{AB}$ product from the experimental magnetization decay was already detailed in Part 3, IV.B. It was done exactly the same way for the model PnAMAs at high temperatures (roughly higher than $T_g + 80$ K for samples PEMA, PEMADMC, and PBMA).

For the lower temperatures, a biexponential behavior was observed for the recorded magnetization decay from 1 to 0. In that case, the data were fitted using the Microcal™ Origin® software. The slow decay was fitted first as a linear decay of the logarithm of the magnetization versus mixing time. Then the fast decay was fitted as one component of a biexponential decay where the other component was set as the slow decay determined previously. Both extracted values of the $q_{AB} \cdot \tau_C^{AB}$ products will be indicated. It should be emphasized that the slower recorded magnetization decay corresponds to the faster involved molecular motion, and thus will be designated as “fast” in the following.

5. Measured data and extracted results

In the case of PEMA at T_g+67 K, the fits yielded as series of $5q_{AB}\tau_C^{AB}$ values characterized by an average of 1376 Hz, a range of 77 Hz and a standard deviation of 28 Hz for the monoexponential decay. $q_{AB}\tau_C^{AB}$ values are then characterized by an average of 275.2 Hz, a range of 15.4 Hz and a standard deviation of 5.6 Hz.

The numerical integration of a ^1H spectrum recorded under static conditions at T_g-45 K (s. Part 7, IV.B.1) yielded a second moment value of $M_2=342.25$ kHz²; thus a value of $q_{AB}=8.95$ kHz² for a cubic lattice.

Finally, the $\text{CH}_3\text{-CH}_2$ moiety method yielded a correlation time of $\tau_C^{AB}=6.91\cdot 10^{-5}$ s (with a range of $1.9\cdot 10^{-6}$ s and a standard deviation of $1.4\cdot 10^{-6}$ s). The second method yielded a value of $3.08\cdot 10^{-5}$ s for the correlation time τ_C^{AB} (with a range of $9\cdot 10^{-7}$ s and a standard deviation of $3\cdot 10^{-7}$ s). Considering the significant difference between this values of τ_C^{AB} , only values of $q_{AB}\cdot\tau_C^{AB}$ products will be given in this paragraph II for all investigated PnAMA samples.

C. Temperature dependence of $q_{AB}\cdot\tau_C^{AB}$ for poly(ethyl methacrylate) samples

The NOE experiment with dipolar filter was carried out at temperatures ranging from T_g+55 K to T_g+115 K for PEMA, and from T_g+60 K to T_g+100 K for PEMADMC. For each temperature, various parameters were used for the dipolar filter, and the data were processed as detailed in paragraph B. The obtained $q_{AB}\cdot\tau_C^{AB}$ products are shown on Figure 5- II-5 for samples PEMA and PEMADMC. All numerical values are given in appendix in Part 7, IV.A.3. It is observed that the dependence of $q_{AB}\cdot\tau_C^{AB}$ on inverse temperature is nearly linear. Furthermore, the values determined for sample PEMADMC are in agreement with those determined for sample PEMA, validating the assumption of the predominance in the initial magnetization decay of the cross-relaxation from the CH_3 to the CH_2 group inside the alkyl side chain. A linear regression of the extracted $q_{AB}\cdot\tau_C^{AB}$ products yields an activation energy of 27 kJ.mol⁻¹.

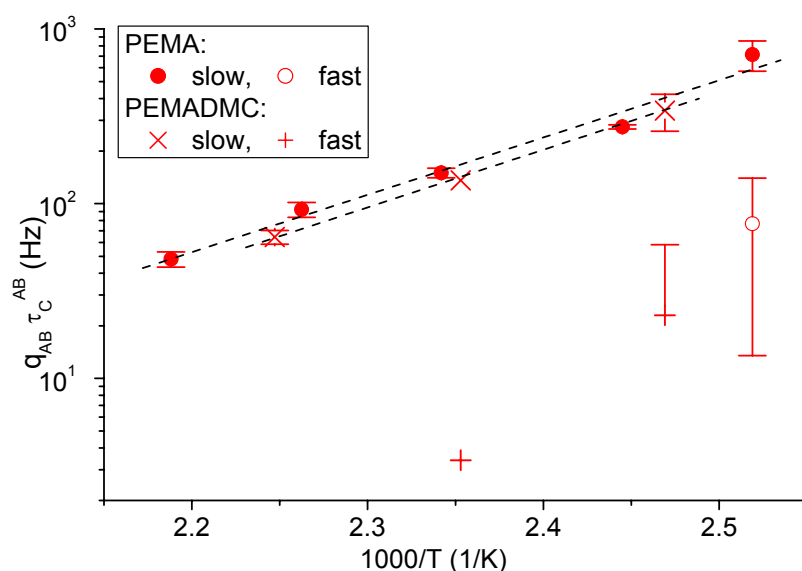
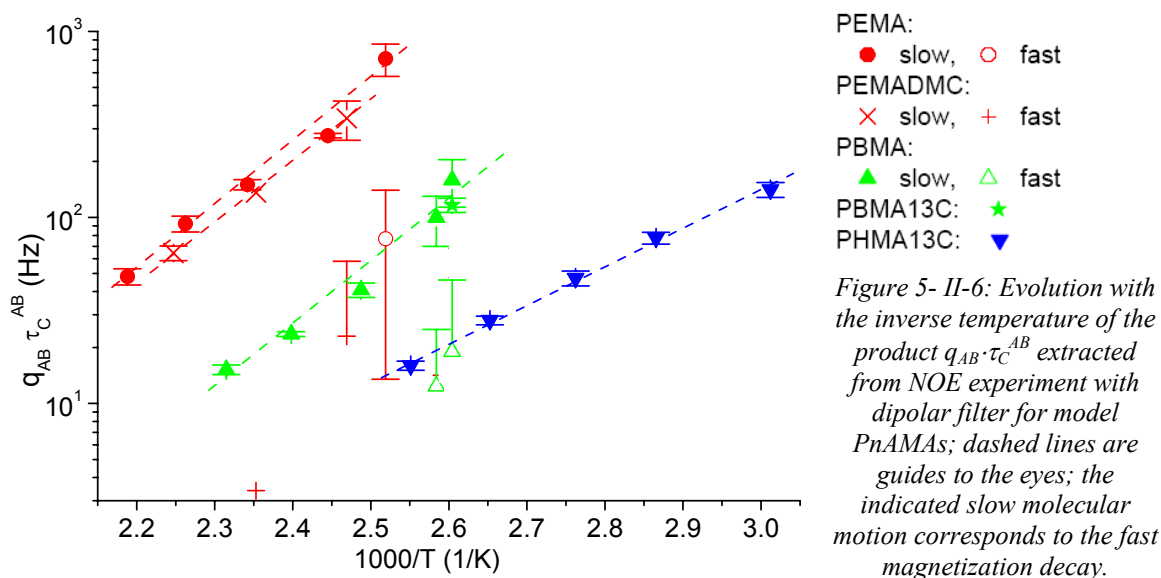


Figure 5- II-5:
Evolution with the inverse temperature of the product $q_{AB} \cdot \tau_C^{AB}$ extracted from NOE experiment with dipolar filter for samples PEMA and PEMADMC (the products are indicated for the slow and fast involved molecular motion, corresponding respectively to the fast and slow recorded magnetization decay).

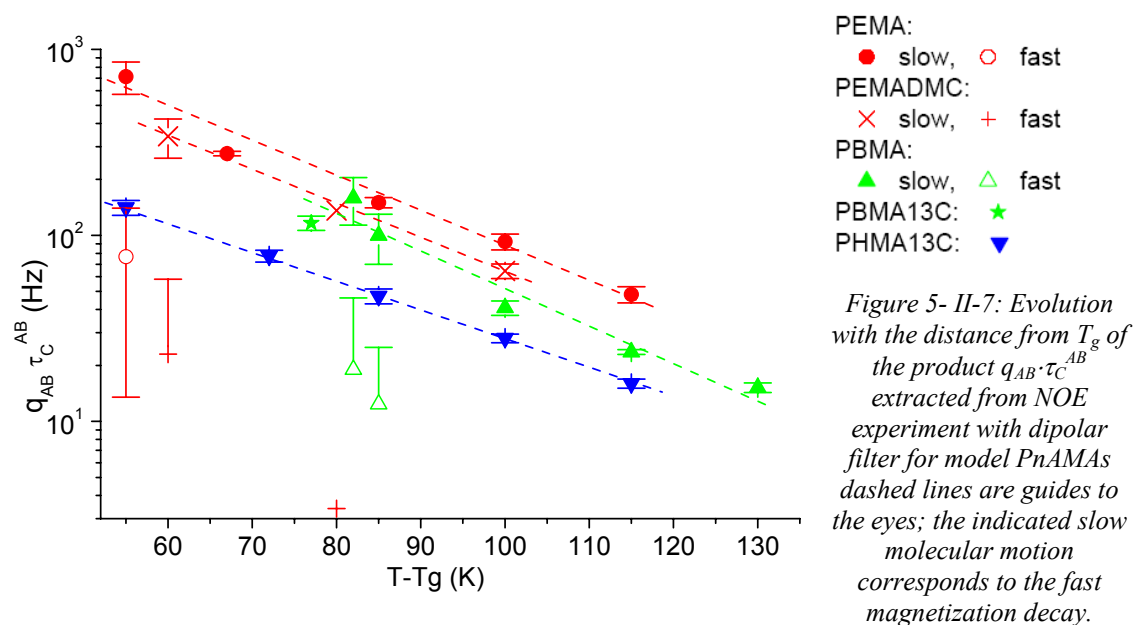
It should be noted that the shape of the curves for high temperatures (above T_g+60 K for PEMA and above T_g+90 K for PEMADMC) were identical to those obtained at T_g+67 K for PEMA, only the numerical values varied. At lower temperatures, the recorded magnetization exhibited a biexponential decay, which will be discussed in paragraph E.

D. Temperature dependence of $q_{AB} \cdot \tau_C^{AB}$ for model PnAMA samples

The NOE experiment with dipolar filter was carried out on other model PnAMAs, at temperatures ranging from T_g+82 K to T_g+130 K for sample PBMA, from T_g+55 K to T_g+115 K for sample PHMA13C, and at T_g+77 K for sample PBMA13C. For each temperature, various parameters were used for the dipolar filter, and the data were processed as detailed in paragraph B. The shape of the curves were similar to those obtained for sample PEMA, with different numerical values. The obtained $q_{AB} \cdot \tau_C^{AB}$ products are shown on Figure 5- II-6 (all numerical values are given in appendix in Part 7, IV.A.3). It is observed in all cases that the dependence on inverse temperature is nearly linear. Linear regressions of the extracted $q_{AB} \cdot \tau_C^{AB}$ products yield activation energies of 27, 28 to 30, and 17 $\text{kJ} \cdot \text{mol}^{-1}$ for the samples PEMA (together with PEMADMC), PBMA (together with PBMA13C), and PHMA13C respectively.



Contrary to model PnAAs (s. Part 4, II.D), the products $q_{AB} \cdot \tau_C^{AB}$ do not fall on a master curve when plotted as a function of the distance from T_g (s. Figure 5- II-7).



E. Discussion of the biexponential behavior observed at low temperatures

In the NOE experiment with dipolar filter, a biexponential decay is observed for the recorded magnetization for samples PEMADMC and PBMA below T_g+90 K, and for sample PEMA below T_g+60 K. Thus, the superposition of two cross-relaxation phenomena with different rates is seen. These two processes could be either processes occurring in different parts of the monomeric units, or processes occurring in the same part of the monomeric unit but at different rates. It should be noted that this phenomenon could hardly be due to an improper correction for T_1 relaxation, since a well defined plateau is observed after the end of the second decay.

The end of the faster recorded magnetization decay (corresponding to the slower involved molecular motion) is observed around 1 ms for sample PEMA at T_g+40 K, and around 5 ms for sample PBMA at T_g+77 K. Therefore, in the investigations of the selection done by the dipolar filter presented in paragraph A, a LG-CP spectrum was recorded after 1 ms or 5 ms mixing time respectively for sample PEMA at ca T_g+45 K and sample PBMA at ca T_g+70 K. No significant difference was observed between this spectrum and the spectrum observed after 50 ms mixing time and return to equilibrium. Therefore the two different rate do not have a molecular origin, but rather a dynamical origin. It is concluded that the cross-relaxation processes occurring with different rates are not occurring in different parts of the monomeric units.

Thus, the biexponential decay is attributed to cross-relaxation processes occurring in the same part of the monomeric unit but at different rates. This behavior is observed for poly(ethyl methacrylate) and poly(n-butyl methacrylate) over the range from ca T_g+40 K to ca T_g+60 K or T_g+90 K. This corresponds to the temperature range where the strong anisotropy of the molecular motion due to the local structure has been reported (from ca T_g+30 K to ca T_g+80 K on the NMR time scale, s. Part 3, I). Therefore it is concluded that the NOE measurement detects the local structure. The NOE experiment with dipolar filter is thus able to detect the faster involved molecular motion (without allowing a precise quantification, s. error bars on Figure 5- II-6). This detection is done in a non isotopically labeled sample, using rather simple NMR techniques: a classical exchange experiment combined with the dipolar filter.

F. Conclusion on the measurement of NOE in model PnAMAs

Applying the dipolar filter to PnAMAs results in a selection according to mobility. It indeed selects only the CH_3 end group of the alkyl side chain in PEMA and PEMADMC at ca T_g+45 K; in PBMA at ca T_g+70 K, it actually selects the CH_3 end group of the alkyl side chain and partly the next CH_2 groups, as well as partly the α -methyl group (s. paragraph A). Correlation times τ_C^{AB} were extracted from the recorded NOE magnetization decay. A biexponential behavior of this decay is observed at low temperatures in PEMA, PEMADMC and PBMA samples; it is attributed to the structure present in the sample over the same temperature range (s. Part 3, I), resulting in a strong anisotropy of the motion.

Finally, the $q_{\text{AB}} \cdot \tau_C^{\text{AB}}$ product has a linear evolution with inverse temperature for PnAMAs over the range from ca T_g+50 K to ca T_g+130 K, which will be interpreted below.

III. Interpretation of NOE results in model poly(n-alkyl methacrylates)

Valuable information on the chain dynamics in model PnAMAs may be obtained through the comparison of various NMR data obtained during the present Ph.D. work (NOE with dipolar filter, T_1 relaxation, line width). ^1H T_1 relaxation data will be presented in paragraph A. The correlations times determined in the present work will be compared to other relaxation data found in the literature or measured by other techniques in paragraph B.

A. ^1H longitudinal relaxation in model PnAMAs

^1H longitudinal (or spin-lattice, or T_1) relaxation times have been measured on model PnAMAs using the inversion recovery technique (s. Part1, II.F). The experiments were carried out under the same conditions as the NOE experiments with dipolar filter: at a Larmor frequency of 300.13 MHz, under static conditions, and approximately over the range from T_g to T_g+100 K. A single exponential behavior was observed for each measurement. This can result either from an identical relaxation time of all protons in the monomeric unit, or from the faster relaxation of some ^1H nuclei, combined with extensive ^1H nuclear spin diffusion or extensive cross-relaxation (already discussed in Part 4, III.A). The single exponential behavior was attributed to the latter for the model PnAMAs. The extracted relaxation times are shown on Figure 5- III-1.

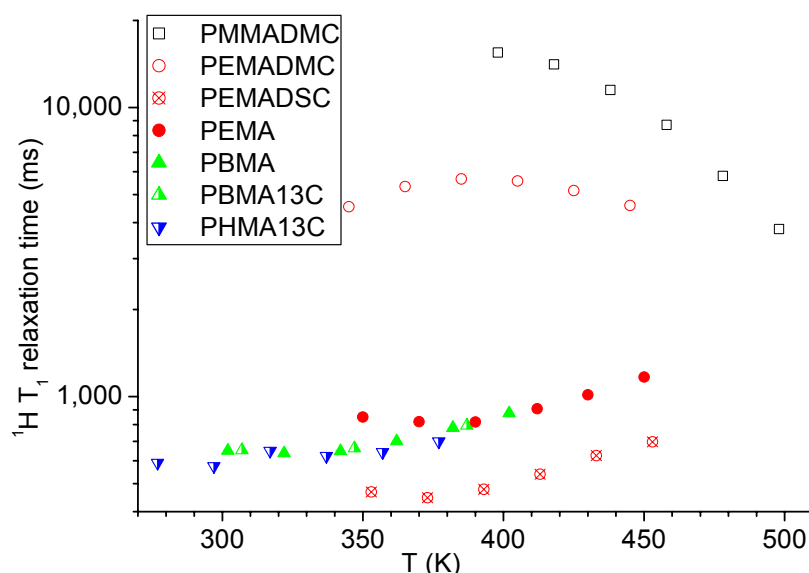


Figure 5- III-1:
Evolution with temperature of the single ^1H longitudinal relaxation time measured using the inversion recovery technique on model PnAMAs (300.13 MHz Larmor frequency, under static conditions).

^{13}C labeling has no influence on the measured ^1H T_1 , as identical values are measured for PBMA and PBMA13C samples. This allows to compare sample PHMA13C with the non labeled PEMA and PBMA: the T_1 relaxation time decreases with alkyl side chain length for the non deuterated samples. Furthermore, the ^1H longitudinal relaxation for PEMA is significantly slower than for PEMADSC (deuterated on the side chain), and one order of

magnitude faster than for PEMADMC (deuterated on the main chain). This is attributed to the hindered rotation of the α -CH₃ group (main chain methyl group), which would be in the frequency range of the Larmor frequency (300 MHz), and thus relaxes efficiently (s. calculation below). Therefore PEMADSC, in which only the main chain is protonated, relaxes very fast through ¹H nuclear spin diffusion or cross-relaxation towards the relaxation sink. In PEMA, where protons are present further from the relaxation sink, the relaxation is significantly slower. In PEMADMC, the relaxation sink is absent and thus the relaxation is one order of magnitude slower. The CH₃ group in the side chain is probably rotating too fast to relax efficiently. Therefore, with increasing alkyl side chains length (and increasing number of motional modes), there should be a mode closer to the Larmor frequency, thus allowing more efficient relaxation, i.e. shorter ¹H T₁ relaxation time. Indeed the relaxation time is longer for PMMADMC than PEMADMC: in PMMADMC only the side chain CH₃ has protons, while in PEMADMC, the side group CH₂ is also present. This is also observed through the decreasing relaxation time with increasing side chain length in samples PEMA, PBMA and PHMA13C.

The frequency of the hindered rotation of the α -CH₃ group in PnAMAs exhibits an Arrhenius behavior at high temperatures (higher than 150 K for PMMA).²⁶¹ The activation energy was determined by various research groups in the range from 27 to 29 kJ.mol⁻¹ (varying slightly with tacticity).²⁶² Tanabe et al. report a rotation frequency of 20 MHz at 260 K for poly(methyl methacrylate), poly(ethyl methacrylate) and poly(n-butyl methacrylate), measured as the minimum of the T₁ relaxation time.²⁶³ They report measurements on other polymeric samples and deduce a rotation frequency of 50 MHz at 270 K and an activation energy of 27 kJ.mol⁻¹ for any CH₃ group bonded to a quaternary carbon;²⁶³ however, this value is not in agreement with the frequency of 20 MHz at 260 K, so that it was not considered here. For all PnAMAs a frequency of 20 MHz at 260 K, and an activation energy of 28 kJ.mol⁻¹ were considered in a first approximation. The frequency f is assumed to follow an Arrhenius behavior (s. Equation 5- III-1, where A is the prefactor, E_a the activation energy, R the gas constant and T the absolute temperature).

$$f = A \cdot \exp\left(-\frac{E_a}{RT}\right) \quad \text{Equation 5- III-1}$$

Knowing the frequency f_1 (20 MHz) at the temperature T_1 (260 K), the frequency f_2 at the temperature T_2 can be calculated using Equation 5- III-2.

$$f_2 = f_1 \cdot \exp\left[\frac{E_a}{R} \left(\frac{1}{T_1} - \frac{1}{T_2}\right)\right] \quad \text{Equation 5- III-2}$$

The obtained frequencies are shown in Table 5- III-1. The rotation frequency is equal to the Larmor frequency between 300 and 350 K, and is of the order of magnitude of the Larmor frequency (300 MHz) over the temperature range over which the ^1H T_1 relaxation measurements were conducted on PEMA, PBMA and PHMA13C in the present work (from 277 K to 460 K, s. Figure 5- III-1). It should be noted that these values are in agreement with rotation frequencies of the order of 314 MHz determined roughly between 200 and 400 K in syndiotactic PMMA samples via ^{13}C T_1 relaxation minima.²⁶⁴

Temperature (K)	260	300	350	400	450	500
Frequency (MHz)	20	110	560	1 900	4 700	10 000

Table 5- III-1: Rotation frequencies of the $\alpha\text{-CH}_3$ group in PnAMAs, determined considering an Arrhenius behavior, a frequency of 20 MHz at 260 K and an activation energy of 28 $\text{kJ}\cdot\text{mol}^{-1}$.

The ^1H T_1 relaxation times measured in the present work do not exhibit a common dependence for all investigated PnAMAs upon temperature (s. Figure 5- III-1) or distance from T_g (s. Figure 5- III-2). Furthermore, it does not exhibit an evolution comparable to the one of the $q_{\text{AB}}\tau_{\text{C}}^{\text{AB}}$ factor extracted from the NOE measurements with dipolar filter (s. Figure 5- II-7). Considering the resulting difficulty of using ^1H T_1 relaxation data in the interpretation of NOE data, as well as the complexity of the various underlying motional modes, the ^1H T_1 relaxation data were not interpreted any further.

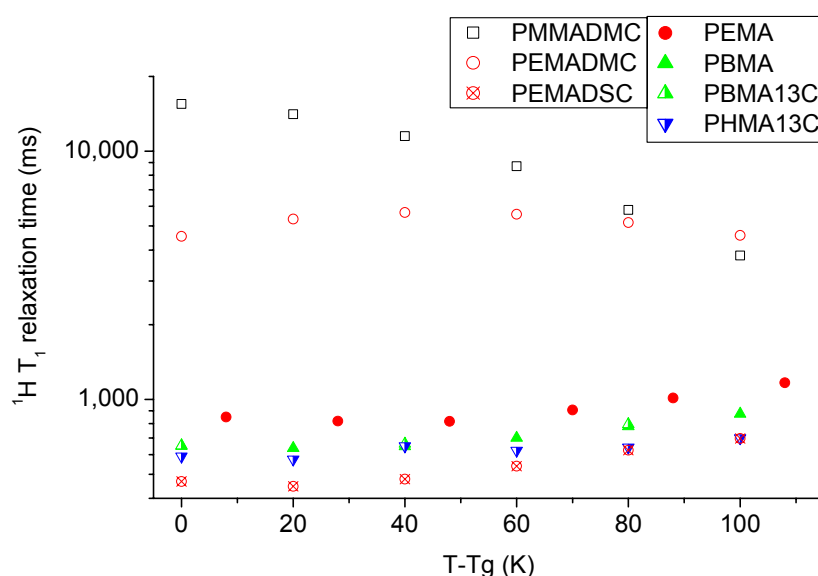


Figure 5- III-2: Evolution with distance from T_g of the single ^1H longitudinal (or spin-lattice) relaxation time measured using the inversion recovery technique on model PnAMAs (300.13 MHz Larmor frequency, under static conditions).

It should be emphasized here that the ^1H T_1 relaxation times are long enough to observe NOE effect on the time scale of a few tens of ms.

B. Relaxation processes in model PnAMAs

It has then been discussed in paragraph II.B.2 that the $\text{CH}_3\text{-CH}_2$ model used to fit the NOE data is rigorously valid only for the sample PEMADMC. For the other PnAMAs, the extracted correlations times should be considered carefully. The extracted correlation times are plotted together with various relaxation data from the literature^{5,150,221} (NMR, photon 192

correlation spectroscopy, calorimetry, dielectric spectroscopy, mechanical spectroscopy, s.

Figure 5- III-3 to Figure 5- III-5).

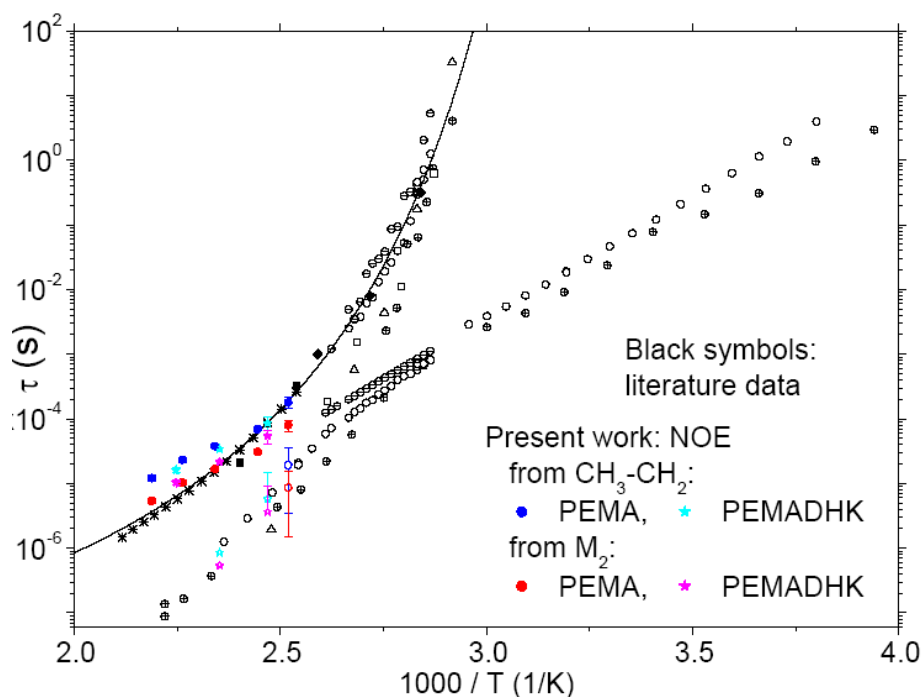


Figure 5- III-3 : Correlation times extracted from the NOE measurements performed in the present work for samples PEMA and PEMADMC, comparison with literature data^{5,150,221}; for NOE in case of a biexponential decay: full symbols for fast decay and open symbols for slow decay in the case of a biexponential decay of the recorded magnetization.

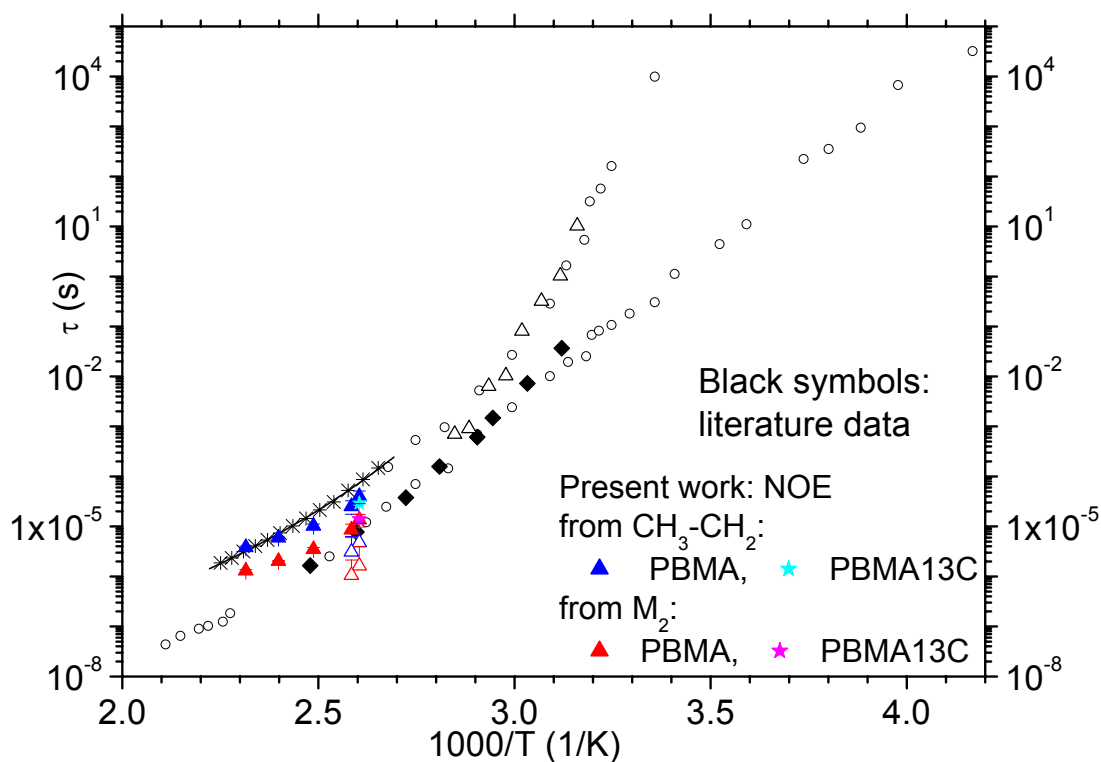


Figure 5- III-4: Correlation times extracted from the NOE measurements performed in the present work for samples PBMA and PBMA13C, comparison with literature data^{5,150}; for NOE in case of a biexponential decay: full symbols for fast decay and open symbols for slow decay in the case of a biexponential decay of the recorded magnetization.

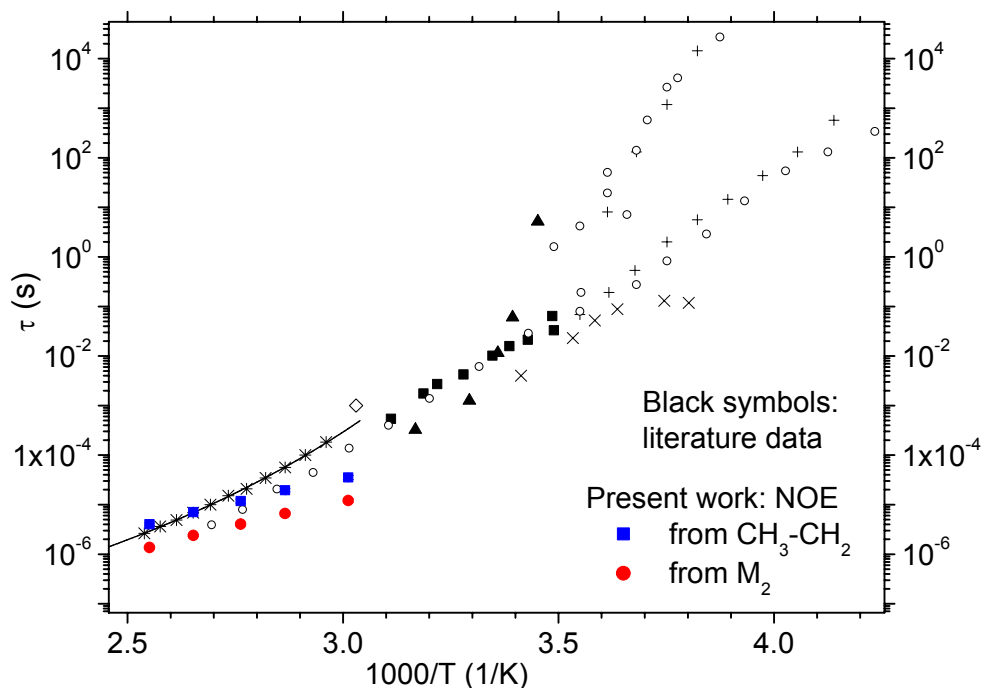


Figure 5-III-5: Correlation times extracted from the NOE measurements performed in the present work for samples PHMA13C, comparison with literature data^{5,150}.

The correlation times determined independently via the calculation of q_{AB} and via the second moment are different but of the same order of magnitude for each measurement, thus in fair agreement considering the approximations involved in both cases. Furthermore, the ^{13}C labeling on 25 % of the carbonyl groups do not have a significant influence on the NOE experiment, as shown for samples PBMA and PBMA13C. Similarly, deuterating the main chain has little influence on the NOE experiment, as observed for samples PEMADMC and PEMA.

A linear dependence of the determined correlation time upon inverse temperature is observed for all samples on a broad temperature range, indicating a local Arrhenius-type relaxation process. Therefore it will be compared preferentially to the β -relaxation process, which is also a local relaxation process. Linear regressions of all concerned correlation and relaxation times as a function of temperature were done, and the results are detailed in appendix (s. Part 7, IV.A.3).

For samples PEMA and PEMADMC, the activation energy of the slow process detected by NOE, $27 \text{ kJ}\cdot\text{mol}^{-1}$, is the same as the one of the β -relaxation ($27 \text{ kJ}\cdot\text{mol}^{-1}$ to $31 \text{ kJ}\cdot\text{mol}^{-1}$). Both processes also have the same prefactor (10^{-14} s). The β -relaxation corresponds to the reorientation of the COO-alkyl side group in PnAMAs.²⁶⁵ ***Therefore the slow process detected by NOE corresponds most probably also to the reorientation of the COO-alkyl side group in PEMA samples.*** Moreover, the correlation times of the slow process detected by NOE correspond to those of the isotropization process on the same

temperature range, within the experimental error. Thus *it is possible that the slow process detected by NOE also corresponds to the relaxation of the organized alkyl nanodomains* (s. work of Wind et al.²²¹ presented in Part 3, I.A). Furthermore, *the correlation times of the fast process detected by NOE correspond to those of the $\alpha\beta$ -relaxation process in the same temperature range* (this should be considered carefully due to the significant experimental error). All those observations are in agreement with the picture of the local phase separation in PnAMAs (s. Part 3, I). One possible explanation would be that *the slow process detected by the NOE experiment would be the hindered motion of the side chain to disengage from the organized nanodomains*, at high temperatures were it would be coupled to the corresponding motions of the main chains, which would thus be the relaxation of the organized nanodomains. In that context the fast process detected by NOE could be the $\alpha\beta$ -relaxation, corresponding to the anisotropic cooperative relaxation of the main chain, coupled to side chain motions.

For the PBMA and PHMA samples, a similar argumentation can be conducted. The main difference is that the slow process detected by NOE moves away from the β -relaxation process with increasing side chain length (the respective activation energies are ca 29 kJ.mol⁻¹ and 49 kJ.mol⁻¹ for PBMA samples, 17 and ca 50 kJ.mol⁻¹ for PHMA samples). This is in agreement with the arguments developed above, considering that *the NOE would detect motions inside the side chain as slow process, which is a superposition of the β -relaxation process and more local relaxation modes for PBMA and PHMA samples*. Indeed, with increasing side chain length, the number of more local modes exhibiting a lower activation energy than the β -relaxation increases, thus decreasing the activation energy of the detected slow process. It would be interesting to dispose of complementary data on these local modes. Furthermore, for PHMA samples only one process is detected, which is in accordance with the very similar correlation times of the $\alpha\beta$ -relaxation and of the isotropization processes.

IV. Comparison of model and industrial samples

A. Comparison of all model samples

1. Mobility from NMR

Above T_g+20 K, the PnAAs are more mobile than the PnAMAs. This is indicated first by a lower fwhm of ¹H static spectra as a function of temperature (s. Figure 5- IV-1), due to the broader glass transition in PnAMAs. It is also indicated by ¹³C static spectra. Spectra recorded on a Tecmag spectrometer for sample PEA at 75.47 MHz with single pulse

excitation and Hahn echo acquisition are shown in Figure 5- IV-2 next to the PEMA13C spectra recorded by Wind^{5,150,151}. A large axial-symmetric C=O tensor in the case of PEMA13C below T_g+100 K indicates a highly anisotropic motion of the main chain. A narrower, nearly isotropic symmetric tensor line shape in the case of PEA above T_g+30 K indicates a nearly isotropic motion of the main chain. It can be concluded that *at the same distance to T_g , the main chain has a more anisotropic motion in PEMA than PEA*. This indicates stronger constraints in the PEMA structure. It is in accordance with the higher mobility detected in PEA compared to PEMA, at the same distance to T_g , above T_g+20 K.

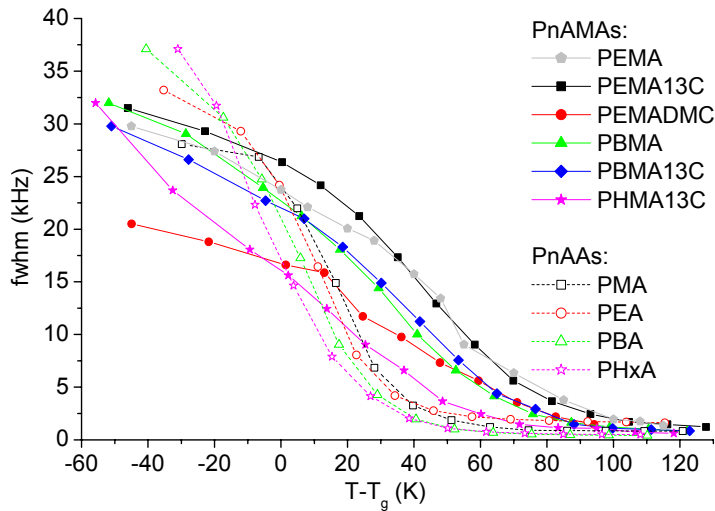


Figure 5- IV-1: Influence of the temperature on the fwhm of the ^1H spectrum of all investigated model samples (spectra recorded at a ^1H Larmor frequency of 300.13 MHz, under static conditions).

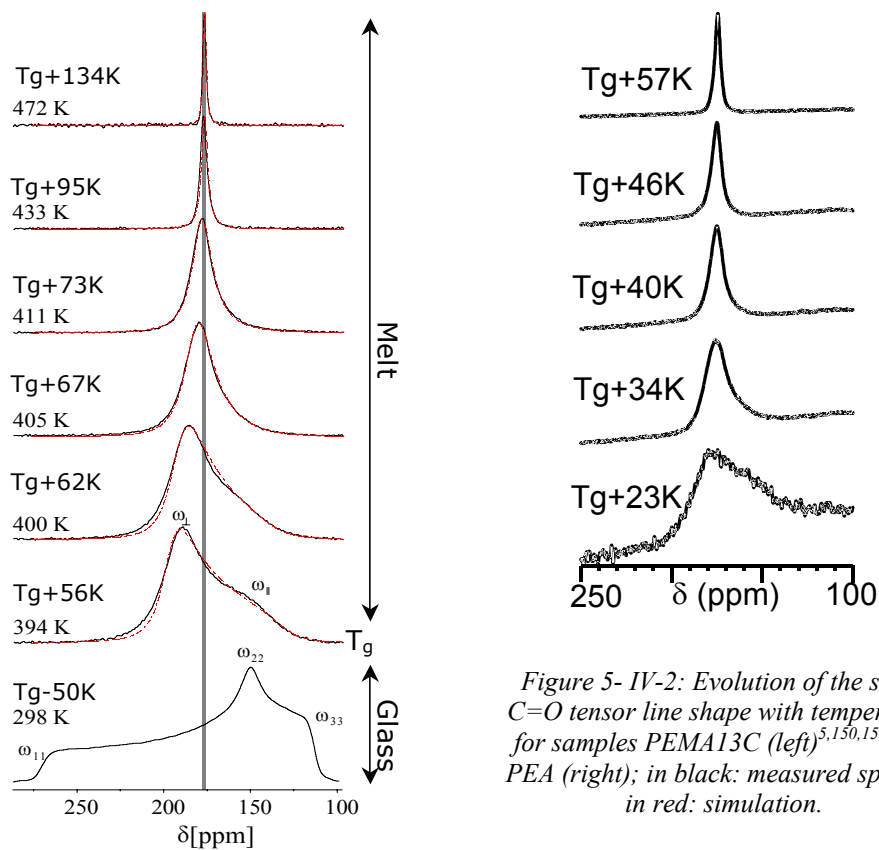


Figure 5- IV-2: Evolution of the static C=O tensor line shape with temperature for samples PEMA13C (left)^{5,150,151} and PEA (right); in black: measured spectra, in red: simulation.

2. Local structure from NMR and X-ray scattering

The features detected by X-ray scattering and solid-state NMR for PnAAs and PnAMAs are summarized in Table 5- IV-1. It can be concluded that *similar local structures are present in PnAAs and PnAMAs, with a better organization in PnAMAs* (more regular and less flexible structure).

		PnAMAs	PnAAs
X-rays	nanostructure	yes	yes
	correlation between side chains in their domains	yes	no
^{13}C NMR	anisotropic main chain motion	high	low
^1H NMR	mobility above $T_g + 20\text{ K}$	lower	higher

Table 5- IV-1:
Comparison of the features detected with X-ray scattering and static solid-state NMR for PnAMAs and PnAAs.

It is expected that PnAMAs are better organized than PnAAs for three reasons. First, their tacticity is different: PnAAs are atactic while PnAMAs are highly syndiotactic when produced by free-radical polymerization (s. Part 2). The higher tacticity of PnAMAs should lead to a higher tendency to order. Second, the PnAAs exhibit chain branching (2 % of the monomeric units, s. Part 2, II), while chain branching has never been detected in PnAMAs. Order should be disturbed around the branching points. Third, the PnAMA backbone contains a CH_3 group where the PnAA backbone contains a less bulky hydrogen. Therefore, the PnAA backbone is much more flexible than the PnAMA one.

An *idealized structure* can be proposed for the PnAAs and PnAMAs, which is shown in Figure 5- IV-3. The shown slices must be repeated to obtain a *local structure, with alternating layers of side chains and main chains*^{5,153} *or with nanodomains of side chains separated by main chains*²²⁵. It must be emphasized here that these structures are idealized ones, meaning that it is not as well organized in reality. Moreover, this structure is valid only for a few monomeric units long along the backbone.

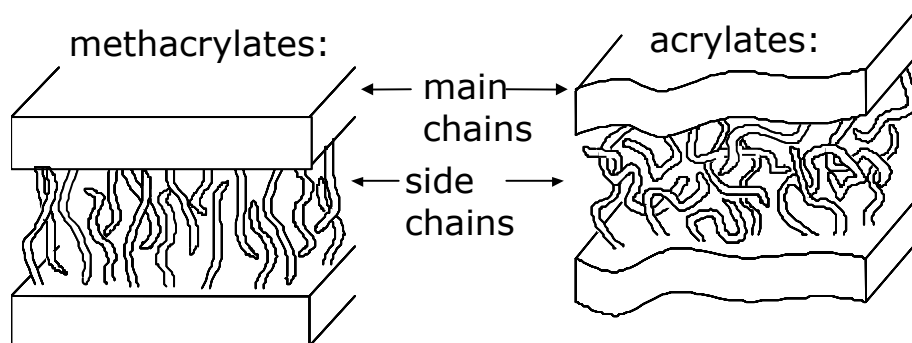


Figure 5- IV-3: Idealized local structures proposed for poly(*n*-alkyl methacrylates) and poly(*n*-alkyl acrylates); s. text for details.

3. Local relaxation NOE experiment with dipolar filter

A concise comparison of the information obtained for model PnAAs and PnAMAs using the NOE experiment with dipolar filter will be presented in paragraph V.B.

B. Comparison of model and industrial samples

1. Dynamic contrast

The dynamic contrast was characterized in the PSAs by solid-state NMR, in particular ^1H static spectra and 2D-WISE experiments. All the recorded ^1H static spectra are shown in the appendix (Part 7, IV.C.1). As for model samples, the whole samples become more mobile with increasing temperature, and exhibit no strong dynamic contrast. The fwhm as a function of temperature is compared for all samples in Figure 5- IV-4. The PSA samples exhibit the same behavior as the model PnAA samples for the fwhm as a function of temperature (at the same distance from T_g).

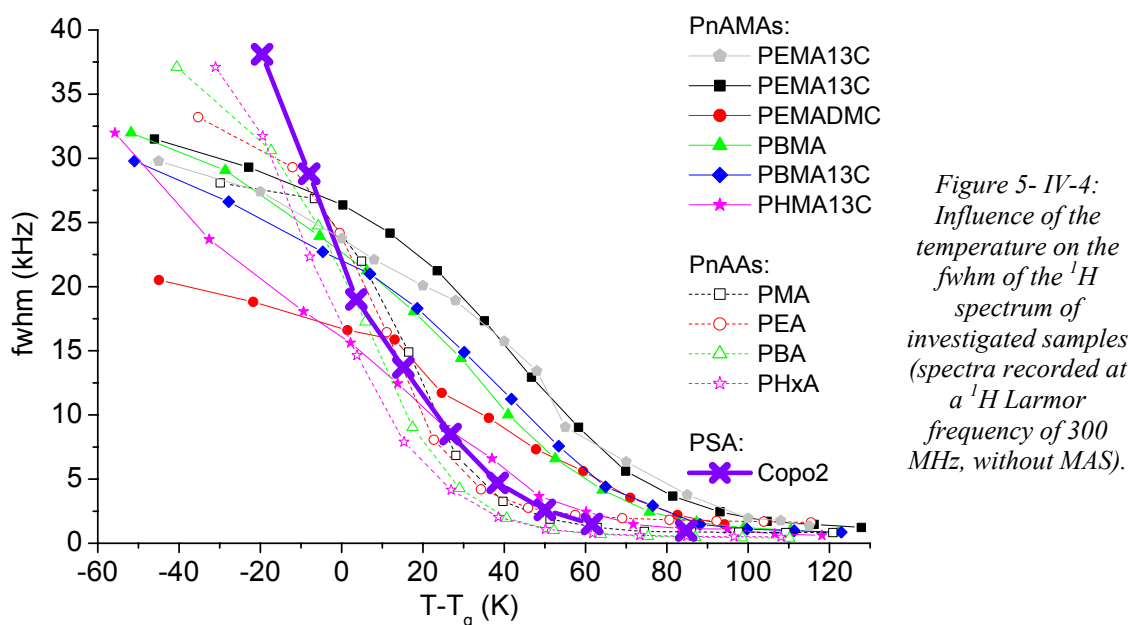


Figure 5- IV-4:
Influence of the
temperature on the
fwhm of the ^1H
spectrum of
investigated samples
(spectra recorded at
a ^1H Larmor
frequency of 300
MHz, without MAS).

The 1D ^1H spectra extracted from the 2D-WISE spectra are shown in Figure 5- IV-5. The contour plots and the extracted 1D ^{13}C spectra are shown in the appendix (Part 7, IV.C.2). The ^{13}C chemical shifts assignment is detailed in Part 2, III.B.1.b. A comparison of the CH_2 line widths demonstrate that the side chain (except O-CH_2) is more mobile than the main chain, as it is also the case in the model samples.

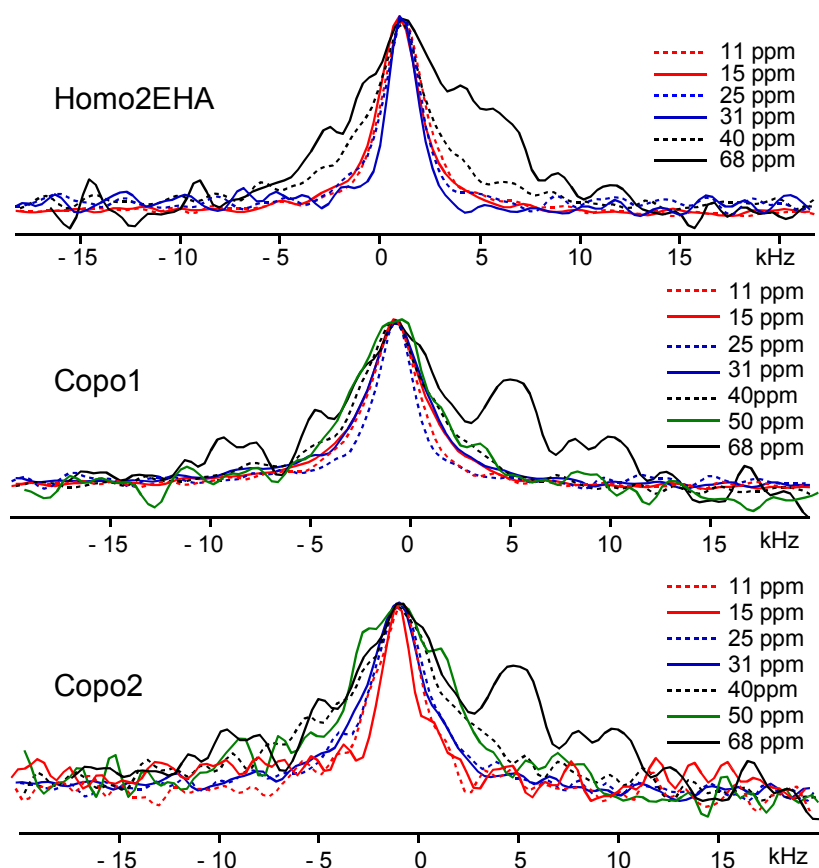


Figure 5- IV-5: 1D ¹H spectra extracted from the 2D-WISE spectra of PSA samples at room temperature (¹H Larmor frequency of 300.13 MHz, static, LG-CP and π -pulse during t_1).

2. NOE experiment with dipolar filter

The NOE experiment with dipolar filter was applied to the industrial PSA samples at room temperature. For all samples, a monoexponential decay of the recorded magnetization was observed. Data were processed using the same methodology as for the model samples, in order to extract the $q_{AB} \cdot \tau_C^{AB}$ product. Then the correlation time τ_C^{AB} was deduced using the q_{AB} value calculated for a CH₃-CH₂ moiety. It should be noted that no ¹H spectrum was recorded well below T_g for the industrial samples, due to their low T_g and the technical difficulty to cool down below it. However, the determination of τ_C^{AB} via the q_{AB} value or the second moment should yield similar results, as demonstrated for all model samples.

The extracted correlation times are plotted together with those of the model PnAAs, on Figure 5- IV-6 versus inverse temperature, on Figure 5- IV-7 versus distance from T_g . It is clearly seen that an identical correlation time is detected for both copolymers (Copo1 and Copo2), which is slightly different of the one of the homopolymer. None of them falls on the master curve observed for model PnAAs as a function of the distance from T_g . This could be due to the branched character of the 2EHA alkyl side chain, while the model PnAAs all have linear alkyl side chains. It would explain why the copolymers Copo1 and Copo2, which contain 33 % of linear methyl side chains exhibit a behavior closer from the model PnAAs than the homopolymer Homo2EHA, containing only branched 2EHA side chains (s. Figure 5-

IV-7). When observed as a function of temperature, the correlation times determined for the PSAs are in the same range as those determined for the model PSAs (s. Figure 5- IV-6).

The molecular nature of the motion detected by NOE can not be known as the temperature dependence of the correlation times from NOE, and the relaxation from other methods, have not been determined.

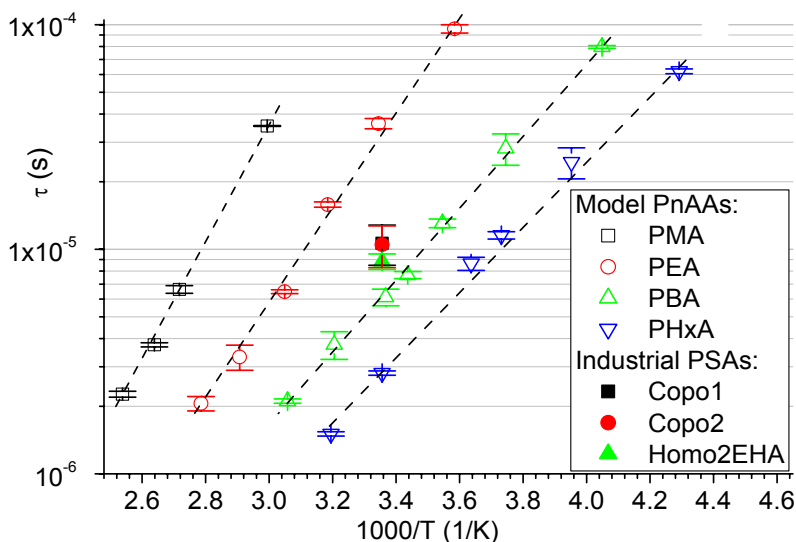


Figure 5- IV-6: Evolution with the inverse temperature of the correlation time τ_c^{AB} extracted from NOE experiment with dipolar filter for industrial PSAs; comparison with the correlation times extracted for the model PnAAs; for all samples, the q_{AB} value was calculated for a CH_3-CH_2 moiety; the dashed lines are guides for the eyes.

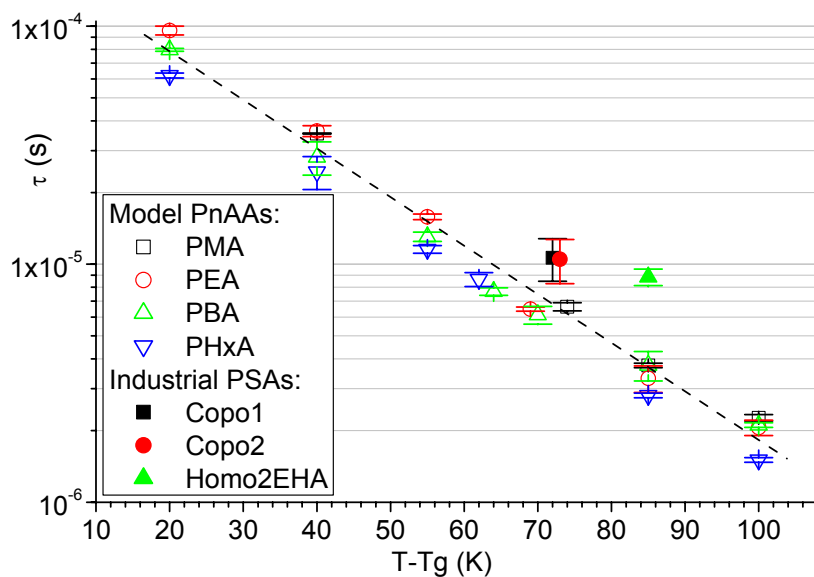


Figure 5- IV-7: Evolution with the distance from T_g of the correlation time τ_c^{AB} extracted from NOE experiment with dipolar filter for industrial PSAs; comparison with the correlation times extracted for the model PnAAs; for all samples, the q_{AB} value was calculated for a CH_3-CH_2 moiety; the dashed lines are guides for the eyes.

V. Conclusion on NOE in model poly(n-alkyl methacrylates) and on the comparison of all samples

A. Local nanophase separation

PnAMAs and PnAAs exhibit similar features of weak mobility contrast and higher mobility in the alkyl side chain than in the main chain. Moreover, both exhibit a local nanophase separation, which is better organized in PnAMAs than in PnAAs. This results in strongly anisotropic chain motions on the range from ca T_g+30 K to ca T_g+80 K. On that temperature range, the NOE experiment with dipolar filter detects this anisotropy via a biexponential behavior of the recorded magnetization decay. Therefore *the NOE experiment with dipolar filter could be used to detect a local nanophase separation resulting in strongly anisotropic chain motions in other side chain polymers, on non isotopically labeled samples and using relatively simple NMR techniques* (the classical exchange experiment combined with the dipolar filter).

B. Local relaxation processes detected by the NOE with dipolar filter

For PnAMAs, ^1H T_1 relaxation data revealed mostly the strong influence of the $\alpha\text{-CH}_3$ rotation and did not help for the molecular interpretation of the NOE data. The results obtained using the NOE experiment with dipolar filter have been interpreted in the context of local nanophase separation present in PnAMAs. *The correlation times of the slow process quantified by the NOE measurements in the present work has been attributed to the relaxation of the alkyl nanodomains, as a coupled motions of the main chain and of hindered local modes in the side chain. In the case of PEMA samples, due to less numerous internal degrees of freedom, the β -relaxation process is predominant.* For the PnAAs, only one process was detected by the NOE experiment. However, all processes detected for PnAAs and PnAMAs can be interpreted in the frame of a locally phase separated structure.

The model of the $\text{CH}_3\text{-CH}_2$ moiety for processing the NOE data is not rigorously valid for PnAMAs, except for PEMADMC. *More elaborate analytical models or simulation programs would be useful to extract more accurate correlation times τ_C^{AB} for the model PnAMAs (except PEMADMC) from the recorded NOE decay.* Furthermore, *in order to assign the relaxation processes detected by the NOE experiment with dipolar filter, some relaxation times of the local relaxation processes faster than the β -relaxation in the PBMA and PHMA would be helpful* (these data could be obtained via literature search, and possibly by conducting complementary experiments).

C. Comparison with industrial samples

Concerning the dynamic contrast as detected via the ^1H static line width and 2D-WISE, the industrial PSA samples investigated in the present work exhibit features closer to those of the model PnAAs than to those of the model PnAMAs. The correlation times extracted from NOE measurements conducted at room temperature are in the same range as those of model PnAAs, but they do not fall on the master curve observed for PnAAs as a function of the distance from T_g . This could be explained by the branched character of the 2EHA side chain.

Part 6: General conclusion and outlook

<i>I.</i>	<i>General conclusion</i>	205
A.	Branching	205
B.	Nanophase separation	206
C.	NOE with dipolar filter	207
D.	Chain dynamics	207
<i>II.</i>	<i>Outlook</i>	208
A.	Branching	208
B.	Nanophase separation	208
C.	Chain dynamics	209
D.	NOE with dipolar filter	209
E.	Characterization of PSAs	210

Part 6: General conclusion and outlook

I. General conclusion

The adhesion mechanism of acrylic PSAs is empirically known to be influenced by microscopic and molecular properties of the samples, e.g. chain dynamics and crosslinking (which can be related to branching, nanophase separation, etc.). However, little is known about their exact relation because little was done to characterize the microscopic and molecular properties. The goal of the present Ph.D. work has been to characterize the microstructure and chain dynamics in industrial acrylic pressure sensitive adhesive samples by solid-state NMR. On a long term, it is aimed to progress towards a better understanding of the adhesion mechanism of acrylic PSAs.

The PSA samples provided by Atofina are statistical poly(alkyl acrylates) copolymers, with different alkyl side chains, containing also other components. It should be noted that those samples are not commercial grades, but were synthesized for research purposes. Model poly(n-alkyl acrylates), PnAAs, were synthesized using conventional free-radical polymerization in solution. Model poly(n-alkyl methacrylates), PnAMAs, which have a similar chemical nature and are extensively characterized, have also been investigated.

A. Branching

Branching in poly(alkyl acrylates) occurs at a significantly higher level than in e.g. poly(alkyl methacrylates), and is currently under investigation in several research groups. LCB plays a role in the adhesive properties, therefore it is important for poly(alkyl acrylates) not only to quantify the branching level, but also to determine its nature (relative amounts of LCB and SCB).

The different method of branching level quantification via ^{13}C NMR (in solution, in the swollen polymer, using CP and in the molten state) have been compared. The best method consists in recording a solid-state ^{13}C NMR spectrum of the molten polymer using single pulse excitation (s. Figure). It is applicable directly on the pure PSA samples. This technique, only applied to polyethylene up to now, proved to be significantly the most accurate one to quantify the branching level in poly(alkyl acrylates).

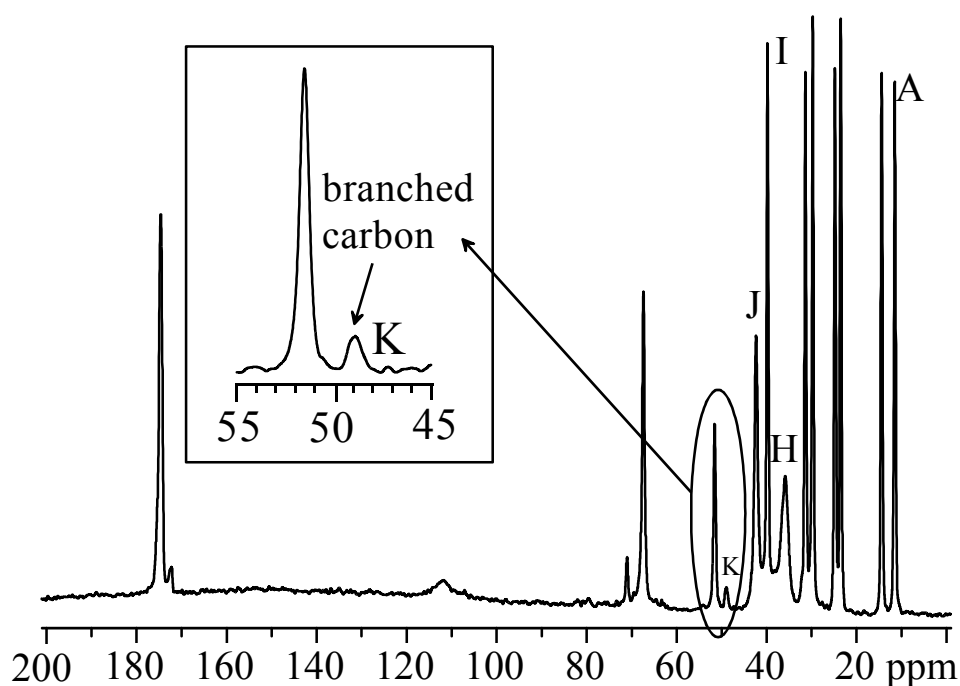


Figure 6-1-1: ^{13}C single pulse NMR spectrum of molten Copo1 (75.47 MHz for ^{13}C , pure sample, 3 kHz MAS, 100°C, 3h30): the chain branching line K at 49 ppm can be quantified precisely; s. Part 2 for more details.

Multiple detection SEC investigations were carried out on model PnAAs to obtain information on the branching nature (SEC is not applicable to industrial PSA samples due to their imperfect solubility). The difference of the molar masses determined at a given elution volume by universal calibration and light scattering-based techniques indicates the presence of LCB. However, no satisfying model was found to quantify it.

B. Nanophase separation

A local nanophase separation occurs in PnAAs and PnAMAs between the side chains and the backbones, with higher organization in PnAMAs. This nanophase separation could result in physical crosslinking, playing a role in the adhesive properties. Among NMR methods, the ^1H nuclear spin diffusion technique with dipolar filter seemed *a priori* to be a good candidate to determine the size of the nanodomains. This experiment had been previously exclusively used to quantify domain sizes in samples exhibiting structures on the nanometer length scale associated to a strong dynamic contrast. In fact, in the case of PnAAs and PnAMAs, the ^1H nuclear spin diffusion technique with dipolar filter quantifies a time scale of local motions via a NOE mechanism. Thus no size information was obtained.

However, the above described NOE experiment may indirectly detect the nanophase separation in PnAMAs via a biexponential behavior of the recorded magnetization decay, on the temperature range where the nanophase separation results in strong anisotropic chain motions.

C. NOE with dipolar filter

The classical ^1H nuclear spin diffusion technique with dipolar filter can be used as NOE experiment to investigate the local chain motion in samples exhibiting a weak dynamic contrast. In the PnAAs and PnAMAs, the selection done by the dipolar filter is based on mobility, and the following magnetization transfer occurs via non coherent cross-relaxation or NOE. A methodology was developed to extract the correlation time of the involved dynamic processes for PnAAs and PnAMAs, by two independent ways which proved to yield results in good agreement.

D. Chain dynamics

The correlation times determined for model PnAAs and PnAMAs using the NOE experiment were compared with complementary relaxation data obtained mainly by dielectric and mechanical spectroscopy, as well as other NMR techniques. For the model PnAAs, literature data are rare, therefore their relaxation behavior was determined for the same samples in the group of Prof. Pakula at the MPI-P by mechanical and dielectric spectroscopy (s. Figure). For PnAMAs, numerous reliable data were available.

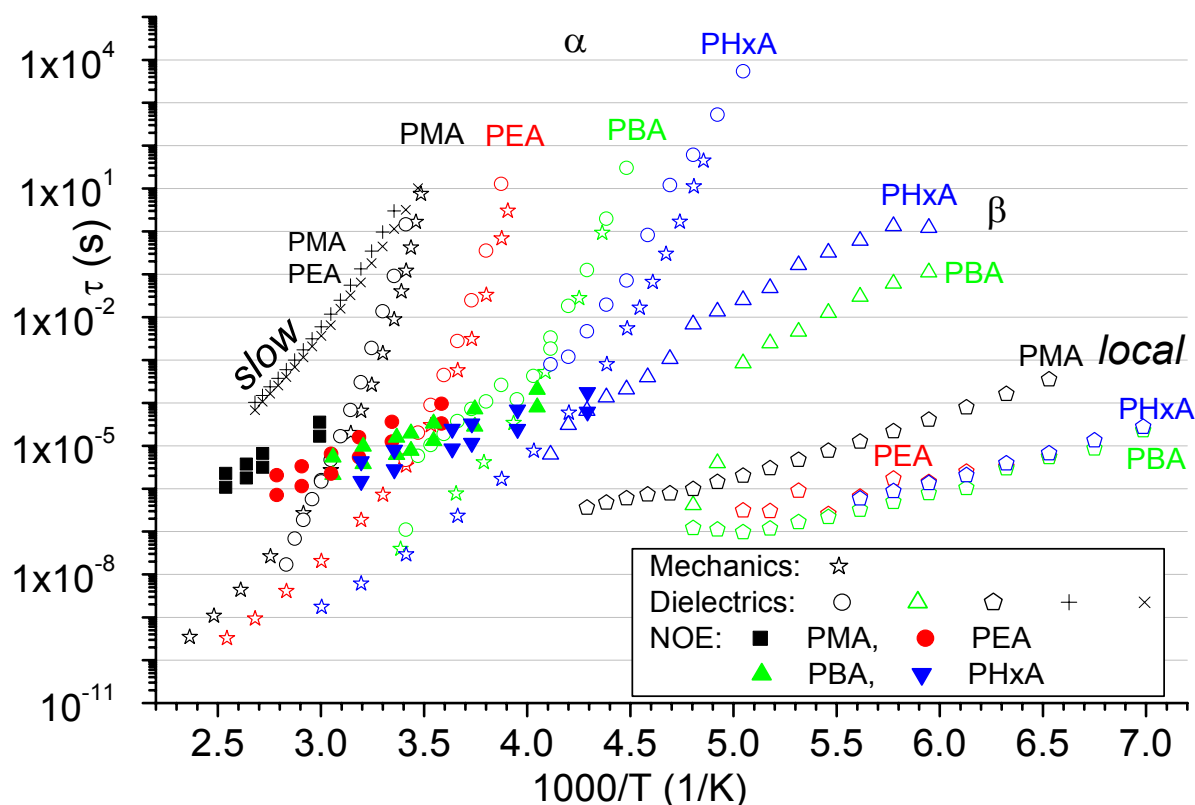


Figure 6- I-2: Correlation times extracted from the NOE measurements performed in the present work for model PnAAs, comparison with data measured in the group of Prof. Pakula on the same samples via dielectric and mechanical spectroscopy; s. Part 4 for more details.

The correlation times of the processes detected by the NOE experiment were interpreted in the context of local nanophase separation in PnAAs and PnAMAs. *For the*

PnAAs the correlation times quantified by the NOE measurements in the present work are attributed to hindered local motions of the side chains in organized alkyl nanodomains. For the PnAMAs, the correlation times of the slow process quantified by the NOE measurements in the present work has been attributed to the relaxation of the alkyl nanodomains, as a coupled motions of the main chain and of hindered local modes in the side chain. In the case of PEMA samples, due to a lower number of internal degrees of freedom, the β -relaxation process is predominant.

II. Outlook

The present work has opened numerous relevant topics to be investigated, on a fundamental research level as well as on a very applied level.

A. Branching

The solid-state ^{13}C NMR of the molten polymer makes it possible to quantify branching levels in any poly(alkyl acrylate) sample, even multi-component and crosslinked ones. The significant gain in accuracy opens new possibilities, for example the determination of accurate kinetic constants for the transfer to polymer. This would allow a better control of the industrial production processes, as well as of the obtained material properties. In the specific case of acrylic PSAs, controlling the LCB level would help to adjust the crosslinking density and thus the adhesive properties.

The quantification of LCB alone in poly(alkyl acrylates) might be possible by multiple-detection SEC. However, work should be invested to obtain reliable hardware and software, as well as satisfying models for the effects of LCB on SEC separation and detection.

B. Nanophase separation

The NOE experiment with dipolar filter would be interestingly applied to other side chain polymers as a tool to detect local nanophase separation. It does not allow simple time scale quantification, but it has the advantage of being easily accessible: the samples do not need to be labeled and the NMR techniques (dipolar filter, typical exchange experiment) are available on classical spectrometers. Possible interesting polymer samples would be side chain polymers in general (acrylates, methacrylates, itaconates, etc.). In particular, the investigation of PnAA samples exhibiting different branching characteristics (no branching from anionic polymerization, controlled branching from copolymerization with

macromonomers, statistical branching from free-radical polymerization) would allow to investigate the effects of branching on the nanophase separation.

C. Chain dynamics

Complementary relaxation data are necessary to properly assign the local molecular motion associated to the correlation time detected by the NOE experiment with dipolar filter.

On a short term, reference correlation times are needed for the β -relaxation in PMA and PEA. These might be determined by reprocessing the existing dielectric relaxation data as a function of temperature instead of processing them as a function of frequency. An alternative measurement method is mechanical spectroscopy with a different geometry. For the PnAMAs, reference correlation times are needed for the local relaxations faster than the β -relaxation in the glassy state. They might be obtained by extensive literature search or complementary measurements, e.g. via dielectric spectroscopy. This is currently being investigated.

It would be very interesting to *investigate a possible link between the process detected by NOE and the slow relaxation process detected by dielectric spectroscopy* in samples PMA and PEA. First, a more accurate quantification of the slow process should be done by processing the existing data, then its presence in samples PBA and PHxA should be investigated. The slow process as well as the process detected by NOE should be investigated at higher temperatures, in particular in order to look for a possible merging.

The chain dynamics is by far not as well understood for the PnAAs as for the PnAMAs. On a long term, it would be fascinating to investigate the actual molecular mechanism associated with the different relaxation processes already quantified for the PnAAs. This has already been achieved for PnAMAs, by applying various solid-state NMR techniques to selectively ^2H or ^{13}C labeled samples. The synthesis of selectively labeled monomers is tedious, but it would allow to progress in the understanding of the material properties in general. The comparison of samples exhibiting different branching characteristics (no branching from anionic polymerization, controlled branching from copolymerization with macromonomers, statistical branching from free-radical polymerization) would allow to investigate the effects of branching on chain dynamics.

D. NOE with dipolar filter

The accuracy of the correlation times measured using the NOE experiment with dipolar filter may be improved by a better mathematical model for the description of the recorded magnetization decay. To our knowledge, the most elaborate analytical model is a $\text{CH}_3\text{-CH}_2$

moiety, which is rigorously valid only for sample PEMADMC. More elaborate analytical equations or simulation programs are needed to describe a full monomeric unit, or at least side chain parts longer than a $\text{CH}_3\text{-CH}_2$ moiety.

Furthermore, the NOE experiment with dipolar filter can be applied to a variety of other polymer samples to investigate local dynamics, provided that there is a dynamical contrast. This contrast can be weak. Due to a detection in the local molecular frame, it might allow to quantify the time scale of slow local relaxation processes at temperatures where other method like dielectric spectroscopy can not detect them in the laboratory frame. In particular, it would be interesting to check its applicability to multi-component samples like the industrial PSAs, for which only preliminary measurements were carried out.

E. Characterization of PSAs

Crosslinking in industrial PSAs might be adjusted using a comonomer forming hydrogen bonds. The exact mechanism of this crosslinking could be investigated using advanced solid-state NMR methods (e.g. multiple quantum techniques). Model PnAA homopolymers containing a few percents of this comonomer should be investigated first.

Finally, the characterization of PSAs by solid-state NMR opens the way to new models for the adhesion mechanism of acrylic PSAs. These models, considering accurate LCB and SCB levels as well as a possible local nanophase separation, may allow a better understanding of the adhesion mechanism, and hence an easier tailoring of the future industrial acrylic PSAs with respect to their respective applications.

Part 7: Appendices

I.	<i>Properties of the investigated samples</i>	213
A.	Synthesis of the industrial pressure sensitive adhesive samples	213
B.	Synthesis of the model poly(n-alkyl acrylates)	214
1.	Synthesis and purification of the non-labeled poly(n-alkyl acrylates).....	214
a)	Synthesis	214
b)	Purification.....	214
2.	Approach for the synthesis of labeled samples	215
a)	Target samples	215
b)	Synthetic pathways	216
c)	Conclusion	217
C.	Characterization of the first synthesized poly(n-alkyl acrylates)	217
D.	Samples storage	218
II.	<i>Conditions of the experiments</i>	219
A.	DSC, TGA, SEC and solution-state NMR	219
B.	Solid content and mean particle diameter of latices, casting of films	220
C.	Solid-state NMR	220
1.	Experimental conditions.....	220
a)	Chemical characterization of the PSA samples	220
b)	¹ H static spectra.....	221
c)	LG-CP investigations.....	222
d)	2D-WISE.....	223
e)	NOE experiments using the dipolar filter	223
f)	¹ H longitudinal relaxation	223
2.	Remark on the adjustment of the receiver gain in the NOE experiments using the dipolar filter	224
3.	Temperature calibration of the static NMR experiments	225
a)	Motivation.....	225
b)	Literature data	225
c)	Experimental conditions	226
d)	Intermediate calibration using published data	227
e)	Check of the intermediate calibration with melting points	228
f)	Final calibration	228
g)	Remarks	229
h)	Molecules on which melting points have been measured.....	229
i)	Typical ²⁰⁷ Pb and ¹ H static spectra	231

III. Viscoelastic properties and stereochemistry of polymers, characterization of homogeneous networks.....	235
A. Basic concepts relative to viscoelastic properties.....	235
1. Viscoelasticity in simple shear or uniaxial deformation ^{277,278}	235
2. Forced oscillations ^{277,278}	236
3. Master curves ¹⁴²	237
4. Viscoelastic window for PSAs	237
B. Stereochemical definitions and notations²⁸⁰⁻²⁸² relative to tacticity	238
C. Characterization of the crosslinking of homogeneous networks.....	240
IV. NMR spectra and SEC results	242
A. NMR spectra of model poly(n-alkyl methacrylates).....	242
1. ¹ H static spectra	242
2. 2D-WISE spectra.....	249
3. NOE data	252
B. NMR spectra of model poly(n-alkyl acrylates)	253
1. ¹ H static spectra	253
2. 2D-WISE spectra.....	261
3. NOE data	263
C. NMR spectra of PSA samples	264
1. ¹ H static spectra	264
2. 2D-WISE spectra.....	266
3. NOE data	267
D. SEC results of poly(n-alkyl acrylates).....	268
1. Plots of the intrinsic viscosity as a function of the molar mass	268
2. Plots of the molar mass as a function of the elution volume.....	269
V. Abbreviations and symbols	270
A. Investigated samples	270
B. Monomers, polymers and other chemicals.....	270
C. Nuclear magnetic resonance	271
D. Others.....	272
VI. Literature references.....	274

Part 7: Appendices

I. Properties of the investigated samples

A. Synthesis of the industrial pressure sensitive adhesive samples

The samples were synthesized at Cerdato using a semi-batch (or semi-continuous) process. This process allows to adjust product properties by changes in the type of monomer or the experimental parameters (e.g. temperature, pH).²⁴

The polymerization is done using four different mixtures. The first one is an emulsion of surfactants and water, and is present from the beginning in the reactor (micelle diameter of several nm). The second one is a pre-emulsion composed of the monomers, surfactants and water (micelle diameter of a few nm). The two last ones are “initiator” solutions in water.

The radical polymerization itself consists of three steps. The synthesis of seeded particles (or nucleation) is first done in situ. Therefore, the two “initiator” solutions and a small part of the monomer pre-emulsion are added to the emulsion in the batch, and the polymerization is carried out. The reaction mixture at the beginning of this step consists of a continuous water phase and an emulsion of monomer droplets (of a few μm). Most of the monomer is localized in the large droplets, but some monomer is also dissolved in water.²⁴ The mechanism is the following: AA and MA are soluble in water (respectively totally and partially), so that various quantities of these monomers are present in the water phase. The radical initiator initiates their polymerization in the water phase to give first oligomers. When an oligomer continues to polymerize, its water solubility gradually decreases, and for a critical size it either enters a monomer micelle, or precipitates and is then stabilized by surfactants which form a new micelle. The particles are created within a few minutes.²⁴ The carboxylic acid comonomer forms a major component of the water-soluble chains on the surface of the particle, providing both steric and electrostatic stabilization of the colloid.²⁶⁶

The second step is the polymerization itself. It is carried out semi-continuously, by continuously adding the rest of the monomer pre-emulsion to the seeded particles emulsion, within a few hours. The reaction mixture at the beginning of this step consists of monomer swollen polymer particles and monomer droplets; ca. 90 % of the monomer is present in the droplets.²⁴ The monomer molecules continue to diffuse through the aqueous phase into the seeded particles where the polymerization takes place. The surfactant

molecules stabilize the growing particles. At the end of the polymerization, the particle diameter is of a few hundreds of nm. This second step can also be considered as two different steps: at the end of the polymerization, the polymer concentration is higher in the particles than at the beginning. It is also higher than in solution polymerization, so that the obtained polymer is expected to be more branched.²⁴ (s. Part 2, III for a discussion of branching).

The third step is the polymerization of all the monomer residues. It takes place after all the pre-emulsion has been fed, and a waiting time is over. A post-polymerization initiator is added, which initiates the residual monomer in the polymer droplets and in the aqueous phase. This decreases the residual monomer amount to a value of a few ppm. This post-polymerization step is important for adhesive purpose (the monomer is a plasticizer that decreases the cohesive strength of the PSA), as well as safety purpose (the acrylic monomers are highly toxic).

B. Synthesis of the model poly(n-alkyl acrylates)

1. Synthesis and purification of the non-labeled poly(n-alkyl acrylates)

a) Synthesis

Prior to polymerization, the n-alkyl acrylate monomers (Aldrich) were distilled under vacuum in a Kugelrohr distillation apparatus to remove the inhibitor, and then stored in the freezer. The recrystallized AIBN was also stored in the freezer.

Each n-alkyl acrylate has been polymerized as a 4.7 mol.L⁻¹ solution in toluene initiated by 0.5 mol% of AIBN with respect to the acrylic monomer. The polymerization has been carried out at 60 °C under nitrogen for 20 hours. The conversion is quasi-complete (99 % measured after evaporation of residual monomer and solvent in a fume hood). After successful tests with 1 g of monomer (s. paragraph C for the characteristics of the polymers), the polymerizations have been done again starting with 3 to 5 g of each monomer. Only the polymers synthesized with several g of monomers were investigated using solid-state NMR and will be presented in this thesis.

b) Purification

After the polymerization, the polymers had to be purified to eliminate the solvent, the possible residual monomer and the AIBN-products. After dissolving the reaction mixture in an equal volume of dichloromethane, the polymer has been precipitated in methanol, filtered and finally dried in an oven (60 °C) under vacuum for one night.

Since the polymers have a very low T_g ($-14\text{ }^\circ\text{C}$ to $-60\text{ }^\circ\text{C}$ for PEA, PBA and PHxA), they are viscous and sticky at room temperature, so that it is difficult to separate them from the filter and to recover them from the tools they stick on. Therefore the purification has to be done below the T_g of the polymers. During the purification, the methanol beaker was regularly cooled by holding it in a Dewar vessel containing liquid nitrogen, to reach approximately the melting point of methanol ($-98\text{ }^\circ\text{C}$). The polymer precipitated at the bottom of the beaker, and the methanol solution was then filtered on a cellulose filter with $1\text{ }\mu\text{m}$ pores; this was done in such a way that the polymer and the stirrer were left in the beaker. The vessel used for the filtration was previously cooled in the freezer for a few hours. The beaker containing the polymer and the stirrer was cooled again using liquid nitrogen, to reach a temperature below the glass transition temperature of the polymer. Then the polymer was broken to separate it from the stirrer.

This protocol has been applied with satisfactory yields: 98 % for PMA, 78 % for PEA, 94 % for PBA and 92 % for PHxA. In the case of purification at room temperature, the yield was significantly lower (only 53 % for PBA).

2. Approach for the synthesis of labeled samples

a) Target samples

Apart from the non isotopically labeled poly(*n*-alkyl acrylates), it would have been interesting to synthesize also selectively labeled ones for the investigations of the chain dynamics. Indeed, we could then have carried out on those samples a dynamical study similar to the one Wind⁵ and Kuebler¹⁵² have done on the poly(*n*-alkyl methacrylates). These polymers would be typically statistically 20 % ^{13}C labeled on C=O (to study the main chain relaxation dynamics), or be fully deuterated on the main chain or on the side chain (to compare main and side chain dynamics and to study selective ^1H nuclear spin diffusion) (s. Figure 7- I-1).

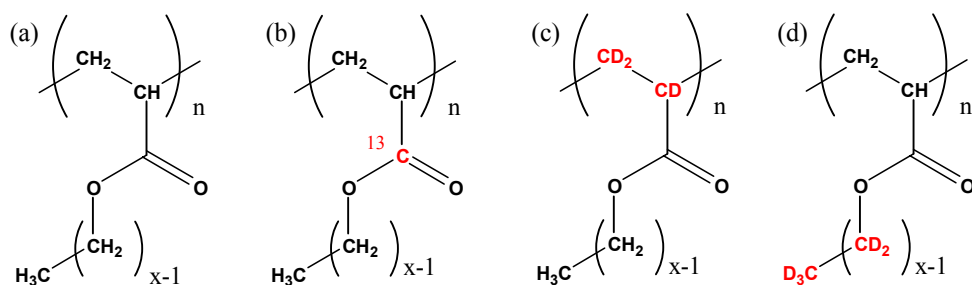


Figure 7- I-1: Poly(*n*-alkyl acrylates); (a) general formula, (b) ^{13}C labeled on C=O, (c) deuterated on the main chain, (d) deuterated on the side chain.

b) Synthetic pathways

Since the labeled monomers are not commercially available, they have to be specifically synthesized. The retained strategy was the esterification of acrylic acid with a linear alcohol; alternative starting products to acrylic acid are acryloyl chloride or methyl acrylate (s. Figure 7- I-2).

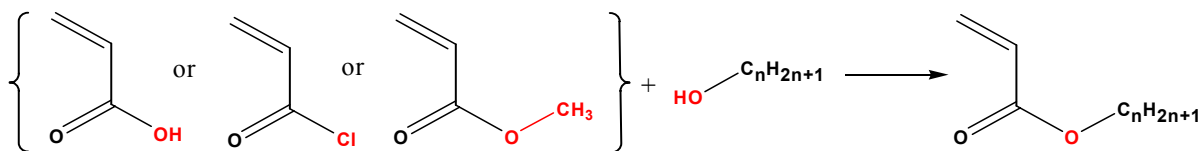


Figure 7- I-2: Synthesis of *n*-alkyl acrylate monomers by esterification of acrylic acid (or acryloyl chloride or methyl acrylate).

Labeled acrylic acid and/or labeled linear alcohol had to be used. The fully deuterated linear alcohols are commercially available, but not the labeled acrylic acid (deuterated or ^{13}C labeled). This implies that the synthesis of the acrylic acid itself would have to be done, starting from labeled materials, but it is too tedious to be done during a Ph.D. thesis where the main focus is on characterization. It was then decided to synthesize only the homopolymers deuterated on the side chain as labeled model samples.

The search of a synthetic pathway to the homopolymers deuterated on the side chain was aggravated by the necessity to handle only small quantities (as the materials are expensive). The esterification was tried using phosphorous pentoxide to eliminate the water formed during the reaction, which is the reaction used in our group to esterify the methacrylic acid (s. Figure 7- I-3a). Nevertheless, the yield was poor and it was impossible to separate the obtained methyl acrylate from the starting materials. The esterification was then tried by the Mitsunobu reaction²⁶⁷ (s. Figure 7- I-3b), and the yield was satisfactory, but once again the purification of the obtained methyl acrylate was not successful.

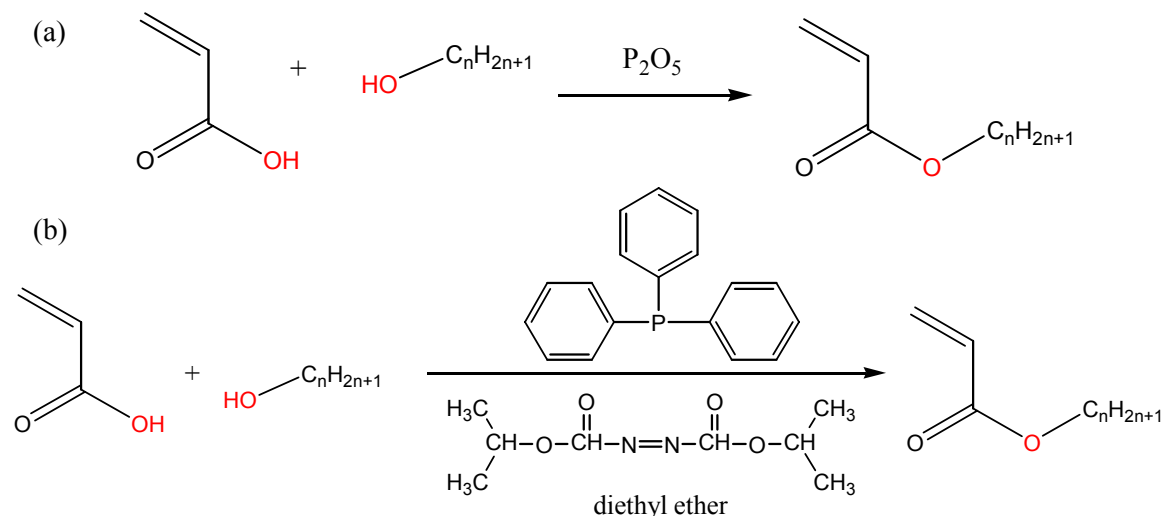


Figure 7- I-3: Esterification of acrylic acid by a linear alcohol (a) using phosphorous pentoxide, (b) using the Mitsunobu reaction.

Therefore, it was decided to conduct a literature search for other possible pathways, but no route could be found which would be applicable to small quantities, starting from acrylic acid, acryloyl chloride or methyl acrylate. The synthetic route of transesterification of ethyl acrylate used by Atofina at the CRDE is also not applicable to small quantities.

c) Conclusion

The synthesis of labeled n-alkyl acrylates has proved to be tedious. Therefore we chose to investigate non labeled model homopolymers with appropriate NMR methods to spare the synthetic effort.

C. Characterization of the first synthesized poly(n-alkyl acrylates)

The T_g measured using DSC at $10 \text{ K}\cdot\text{min}^{-1}$ are given in Table 7- I-1. The conditions are detailed in paragraph II.

Sample	PMA1	PEA1	PEA2	PBA1	PBA2	PBA3	PHxA1
T_g (K)	294	261	260	227	225	226	217

Table 7- I-1: T_g of the first synthesized model PnAAs.

The average molar masses determined in Mainz and Paris are given in Table 7- I-2 (s. paragraph II.A and Part 2, III.E for more experimental details).

Samples		CC in Mainz			TDA in Paris				
		PMMA	PtBMA	PS	CC PS	Diff	UC	TD	LALLS
PMA1	M_n	35 900	39 700	30 600	31 200	+2	31 700	44 600	65 100
	M_w	142 000	150 000	126 000	121 300	-4	114 700	139 000	144 000
	M_w/M_n	4.0	3.8	4.1	3.9	-5	3.6	3.1	2.2
PEA1	M_n	218 000	231 000	190 000	161 000	-20	127 000	172 000	247 000
	M_w	327 000	332 000	306 000	335 000	+9	252 000	303 000	320 000
	M_w/M_n	1.5	1.4	1.6	2.1	+27	2.0	1.8	1.3
PEA2	M_n	104 000	117 000	88 600	83 400	-6	72 600	94 400	101 000
	M_w	200 000	208 000	182 000	173 000	-5	132 000	162 000	164 000
	M_w/M_n	1.9	1.8	2.1	2.1	0	1.8	1.7	1.6
PBA1	M_n	-	126 000	96 200	96 300	+0	179 000	147 000	181 000
	M_w	-	255 000	232 000	257 000	+10	356 000	278 000	319 000
	M_w/M_n	-	2.0	2.4	2.7	+12	2.0	1.9	1.8
PBA2	M_n	-	50 700	42 900	60 300	+34	113 000	105 000	124 000
	M_w	-	249 000	227 000	242 000	+6	335 000	264 000	288 000
	M_w/M_n	-	4.9	5.3	4.0	-28	3.0	2.5	2.3
PBA3	M_n	-	38 100	33 100	42 700	+25	76 100	79 400	98 400
	M_w	-	266 000	246 000	244 000	-1	334 000	265 000	295 000
	M_w/M_n	-	7.0	7.4	5.7	-26	4.4	3.3	3.0
PHxA1	M_n	72 300	80 100	62 100	56 000	-10	76 400	148 000	161 000
	M_w	308 000	313 000	296 200	288 000	-3	423 000	352 000	359 000
	M_w/M_n	4.3	4.0	4.8	5.1	+6	5.5	2.4	2.2

Table 7- I-2: Characterization of the first synthesized PnAAs using SEC; M_n and M_w are given in $\text{g}\cdot\text{mol}^{-1}$, the difference Diff. between CC PS in Mainz and in Paris is given in %.

D. Samples storage

All the model PnAMAs were analyzed using ^1H solid-state static spectra at a Larmor frequency of 300.13 MHz. For some of the samples, the recorded ^1H spectra exhibited a very narrow line below T_g in addition to the expected very broad line. This narrow line arises from a very mobile component and has been assigned to small molecules present in the sample (solvent, monomer from the synthesis, or water from the air), and not to the sample itself. Storing the samples in a dessicator under vacuum for a few days has proved to make the very narrow line disappear (e.g. for sample PEMADMC, s. Figure 7-I-4) or at least decrease drastically in intensity. A stronger drying of the samples (e.g., at a higher temperature) can not be done without a risk of degradation. The deconvolution of the recorded spectra made it possible to quantify the small molecule content in the different samples, before and after storage in the dessicator: from 0 to 4 %. All model PnAMA and PnAA samples have therefore been stored in a dessicator under vacuum to remove the small molecules.

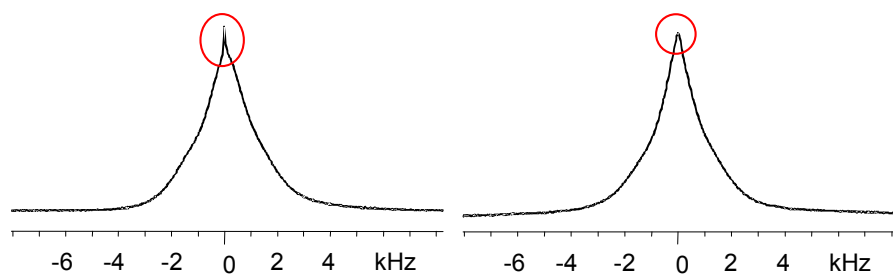


Figure 7- I-4: Presence of small molecules in sample PEMADMC, detected on ^1H static spectra at $T_g-40\text{K}$ (305 K, 300.13 MHz); left: after normal storage in the room, right: after 8 days storage in a dessicator under vacuum.

It should be noted that the PSA samples were not stored under vacuum, because they are not used as adhesives under vacuum. These samples do not contain antifreeze stabilizers, so that a storage at a temperature below $5\text{ }^\circ\text{C}$ could affect the stability of the emulsion. On the contrary, a storage at a temperature above $20\text{ }^\circ\text{C}$ could cause the rapid growth of the bacteria coming from the air and that could contaminate the emulsion. Therefore, a storage temperature between $10\text{ }^\circ\text{C}$ and $15\text{ }^\circ\text{C}$ seems best suited. The samples were stored at $11\text{ }^\circ\text{C}$. Average shelf lives of at least six months to one year without sedimentation are expected nowadays, and most acrylic dispersions meet these expectations.²⁴

II. Conditions of the experiments

A. DSC, TGA, SEC and solution-state NMR

The glass transition temperature (T_g) of the polymers have been obtained using differential scanning calorimetry (DSC) on a Mettler Toledo Star System. The measurements were done at a nitrogen flow of 30 mL.min⁻¹, with the following temperature cycle: heating from -100 °C to 150 °C at 10 °C.min⁻¹, then cooling from 150 °C to -100 °C at 10 °C.min⁻¹, and finally heating from -100 °C to 150 °C at 10 °C.min⁻¹. The first heating and cooling steps are used to erase the thermal history of the sample and detect evaporation of little molecules possibly trapped in the samples. The measurements were done on the second heating step.

The thermogravimetric analysis (TGA) was carried out on a TG 50 Mettler device under nitrogen atmosphere; the temperature was increased from room temperature to 900 °C at 10 °C.min⁻¹. The sample mass was recorded during this increase, and the left limit of its decrease was measured: it is the temperature at which molecules begin to evaporate from the samples (detected as the loss of one percent of the mass), indicating sample decomposition.

The size exclusion chromatography (SEC) was done in Mainz with a conventional SEC equipment comprising a Waters 515 pump, 3 columns from PSS (with pores of 10⁶, 10⁴ and 500 nm respectively), a RI 101 ERC refractometer, the software WinGPC6. Eluent was THF at 30 °C and 1 mL.min⁻¹. The SEC was done in Paris with a Triple Detector Array (TDA, from Viscotek) equipment composed of an online degasser, pump, manual injector, a precolumn and three columns (two mixed-C and one 10² Å) from Polymer Lab., the TDA (including in serie RALLS, LALLS at 7°, refractometer and finally viscosimeter), the software Trisec 2000. Eluent was THF at 40 °C and 1 mL.min⁻¹.

¹³C solution-state NMR spectra of the model PnAAs dissolved in CDCl₃ were recorded on a Bruker DRX500 at a ¹³C frequency of 125.76 MHz. The spectra were recorded at 29 to 33 °C, except for PEA (room temperature). Single pulse excitation with a 6.70 μs 90° pulse and inverse gated decoupling was used with a relaxation delay of 10 s to record quantitative spectra 19 500 to 21 000 transients were recorded. The ppm-scale was calibrated with the middle line of CDCl₃ at 77.00 ppm.

Solution-state NMR was also used to determine the chemical shifts of the surfactants present in the PSAs. The surfactants, available in aqueous solution, were lyophilized (i.e. freeze-dried), then dissolved in D₂O, and TMS was added as an internal standard. The spectra were recorded on a Bruker AMX300 spectrometer at a ¹H frequency

of 300.13 MHz, with ^1H and ^{13}C single pulse excitation, and the ppm scale was calibrated with the TMS resonance at 0 ppm.

B. Solid content and mean particle diameter of latices, casting of films

The solid content of the latices is measured as follows: around 2 g of the latex sample are put in a 1g aluminum shell. Then the samples are dried at 100 °C under vacuum for 1 night. All masses are precisely weighted (precision: ± 0.01 g). Three measurements are done simultaneously, and the average value is calculated.

The mean diameter of the particles in the latices were measured by light scattering on a Zetasizer 5000 (Malvern Instruments Ltd., Malvern, UK) with a cell ZET 5110. The dispersions were diluted in water, until a slightly turbid dispersion was obtained. The photomultiplier should indeed record between 50 and 140 kcounts.s⁻¹ to reduce dead time problems, avoid multiple scattering and increase sensitivity. The measurements were done at room temperature, with an incident wavelength of 633 nm. The angle between the incident beam and the recorded scattered beam was 90°. For each measurement, 30 records were done and their average was calculated.

Films were cast from the latex samples on microscope object slides. Only new object slides were used, and washed twice with ethanol and twice with acetone beforehand, in order to eliminate grease. Some latex sample was then put on the surface and spread with a spatula. During the first trial, the samples were left 50 minutes in the room, until the film became transparent, then dried 1 night at 80 °C under vacuum, and then left in the room again. This films were slightly yellow and considered as having been somehow degraded in the oven. Therefore we chose to let the samples dry at room temperature for at least seven days; weighting and DSC proved that they were dry.

C. Solid-state NMR

1. Experimental conditions

a) Chemical characterization of the PSA samples

^1H MAS spectra with a good resolution were recorded with single pulse excitation, on a Bruker DSX500 spectrometer at a ^1H Larmor frequency of 500.13 MHz, using fast MAS. The operating temperature has been chosen according to the following arguments: it should not be too high, in order not to destroy the hydrogen bonds assumed to crosslink the sample; but the higher the temperature is, the higher the resolution of the spectrum, allowing for a better chemical characterization of the sample. Therefore spectra were recorded at different temperatures for the crosslinked sample (s. Figure 7- II-1).

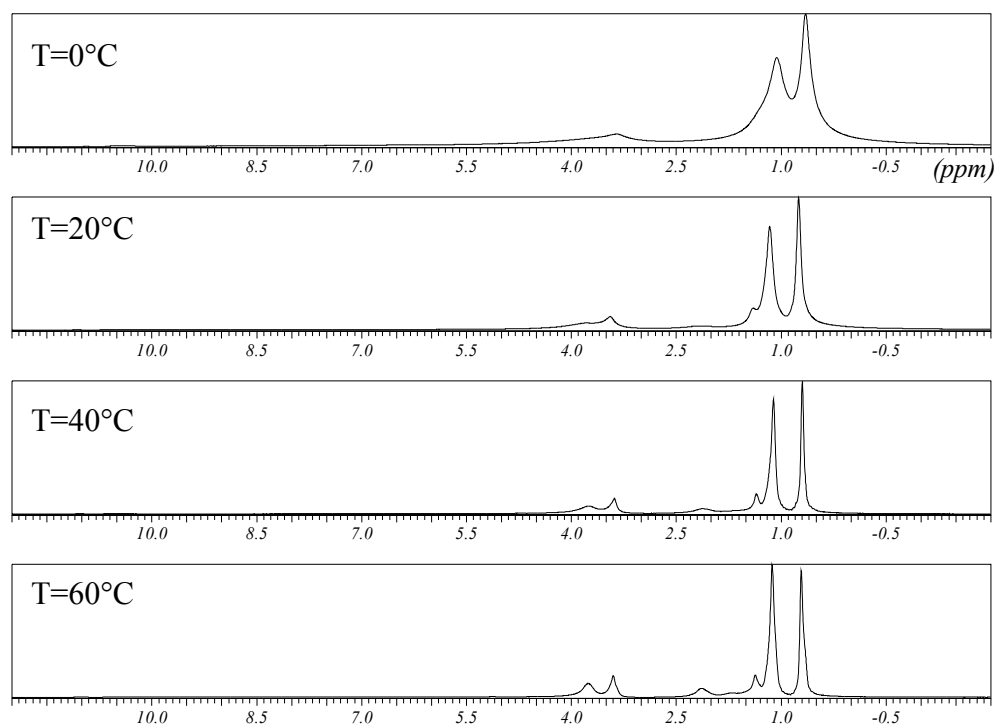


Figure 7-II-1:
 ^1H -NMR
 spectra of
 sample Copo2,
 ^1H frequency:
 500.13 MHz,
 25 kHz MAS.

No line is observed in the 10 to 12 ppm range, where the hydrogen-bonded ^1H nuclei are expected. Furthermore, the higher the temperature, the better the resolution, but no line disappears (it would have proved the existence of crosslinking through hydrogen bonds). Finally, it was decided to record the spectra at 60 °C and 25 kHz MAS, except for Copo1, for which only 12 kHz MAS was possible (due to a technical problem), and which was recorded at 80 °C to enhance the resolution.

The ^{13}C single pulse excitation and CP spectra were recorded on a Bruker MSL300 spectrometer, at a ^{13}C Larmor frequency of 75.47 MHz, with 5 kHz MAS, at room temperature.

b) ^1H static spectra

Static ^1H spectra were recorded for all model samples on a Bruker DSX300 spectrometer, at a ^1H frequency of 300.13 MHz, using single pulse excitation under static conditions. A 4 μs 90 ° pulse was used. MAS was avoided in order to prevent interference between different homodipolar averaging mechanisms. Temperatures ranged between circa T_g-40 K (where the full width at half maximum of the lines, fwhm, levels off) and ca T_g+120 K (where a low fwhm is obtained, due to motional averaging). For sample PEMADSC, the spectra were recorded using single pulse excitation followed by a solid echo²⁶⁸ in order to avoid artifacts coming from the absence of the first points of the FID; no line width was extracted for this sample

^1H spectra were recorded for sample Copo2 on a Bruker DSX300 spectrometer at a ^1H Larmor frequency of 300.13 MHz, under static conditions, at temperatures ranging from T_g to T_g+70 °C. A 4 μs 90° pulse was used. ^1H spectra were also recorded for samples Homo2EHA, Copo1 and Copo2 on a Bruker MSL300 spectrometer at a ^1H Larmor frequency of 300.13 MHz, under static conditions, at temperatures ranging from – 20 K to 60 K. A 6 μs 90° pulse was used.

c) LG-CP investigations

The Lee-Goldburg CP spectra were recorded on a Bruker DSX300 spectrometer, at a ^{13}C Larmor frequency of 75.47 MHz using 4 mm MAS rotors. They were recorded under 3 kHz MAS. 3 μs 90° pulses were used on the ^1H channel, and relaxation delays of 3 s. The LG-CP irradiation was adjusted on the ^1H nuclei the following way. First, the corresponding offset irradiation frequency was calculated. Second, the irradiation power was finely tuned by optimizing the best resolved ^{13}C multiplets while the under ^1H decoupling was done under LG-CP irradiation. It should be noted that no temperature calibration was available for this probehead, so that the display temperature is indicated and not the actual sample temperature; however, the error done under slow MAS should be small and anyway not significant for the qualitative measurements carried out.

The following series of experiments was conducted: first a simple LG-CP spectrum, second, a LG-CP spectrum recorded immediately after a dipolar filter, third a LG-CP spectrum recorded after the same dipolar filter experiment and a mixing time (possibly several mixing times). The experiments were conducted on PEMA at ca 390 K (ca T_g+45 K) with a CP contact time of 500 μs , a filter with 20 μs delay and 1 cycle, mixing times of 1 ms and 50 ms, and respectively 1 536, 25 600, 32 768, 46 080 transients for the four spectra. The experiments were conducted on PEMADMC at ca 390 K (ca T_g+45 K) with a CP contact time of 500 μs , a filter with 10 μs delay and 1 cycle, a mixing time of 8 ms, and respectively 4 096, 8 192, 15 360 transients for the three spectra. The experiments were conducted on PBMA at ca 370 K (ca T_g+70 K) with a CP contact time of 500 μs , a filter with 15 μs delay and 1 cycle, mixing times of 5 ms and 50 ms, and respectively 1 024, 5 120, 10 240, 15 360 transients for the four spectra. The experiments were conducted on PEA at ca 329 K (ca T_g+70 K) with a CP contact time of 1.5 ms, a filter with 20 μs delay and 4 cycles, a mixing time of 20 ms, and respectively 2 560, 5 120, 8 192 transients for the three spectra. The experiments were conducted on PBA at room temperature (ca T_g+70 K) with a CP contact time of 3 ms, a filter with 20 μs delay and 8

cycles, a mixing time of 50 ms, and respectively 3 072, 8 192, 8 192 transients for the three spectra.

d) 2D-WISE

The spectra were recorded on a Bruker DSX300 spectrometer, at a ^1H Larmor frequency of 300.13 MHz and a ^{13}C frequency of 75.47 MHz. They were recorded for all samples (model and industrial) under static conditions, because of the impossibility to pack the industrial samples in a rotor which would spin for more than one day.

A $5\ \mu\text{s}$ 90° ^1H pulse was used, followed by a 180° pulse in the middle of t_1 to refocus the chemical shifts, $500\ \mu\text{s}$ contact time for the Lee-Goldburg cross-polarization (except for samples Homo2EHA and Copo1: 1 ms), and 2 s delay between consecutive transients. For the PnAMAs, 128 to 164 transients were acquired in the indirect ^1H dimension, and 256 to 288 transients in the direct ^{13}C dimension. 2D-WISE spectra were recorded for sample PEMADSC at $T_g-9\ \text{K}$, $T_g+37\ \text{K}$ and $T_g+84\ \text{K}$, for sample PEMA13C at $T_g-11\ \text{K}$, $T_g+35\ \text{K}$ and $T_g+81\ \text{K}$. For the PnAAs, 144 to 176 transients were acquired in the indirect ^1H dimension, and 240 to 304 transients in the direct ^{13}C dimension, and the 2D-WISE spectra were recorded at $T_g+70\ \text{K}$. For the PSAs, 128 transients were acquired in the indirect ^1H dimension, and 320 transients in the direct ^{13}C dimension, and the 2D-WISE spectra were recorded at room temperature.

e) NOE experiments using the dipolar filter

NOE experiments using the dipolar filter were carried out on a Bruker DSX300 spectrometer at a ^1H frequency of 300.13 MHz, under static conditions. 90° pulses of $4\ \mu\text{s}$ were used. The delay τ between pulses in the dipolar filter was varied from 10 to $20\ \mu\text{s}$, and the number n of cycles in the dipolar filter from 1 to 12, depending on the sample and the temperature. The measurements were carried out at temperatures ranging from $T_g+75\ \text{K}$ to $T_g+100\ \text{K}$ on sample PMA, from $T_g+20\ \text{K}$ to $T_g+100\ \text{K}$ on samples PEA, PBA and PHxA, from $T_g+55\ \text{K}$ to $T_g+115\ \text{K}$ on sample PEMA, from $T_g+60\ \text{K}$ to $T_g+100\ \text{K}$ on sample PEMADMC, from $T_g+45\ \text{K}$ to $T_g+130\ \text{K}$ on sample PBMA, at $T_g+77\ \text{K}$ on sample PBMA13C, from $T_g+55\ \text{K}$ to $T_g+115\ \text{K}$ on sample PHMA13C, and at room temperature for all PSA samples.

f) ^1H longitudinal relaxation

^1H longitudinal relaxation measurements were carried out on all model samples using the inversion recovery technique (s. Part 1, II.F), at a ^1H Larmor frequency of 300.13 MHz, under static conditions. 90° pulses of $4\ \mu\text{s}$ were used and 27 data points recorded (only 15 data points for sample PMMADHK). The covered temperature range

was from T_g+8 K to T_g+108 K for sample PEMA, from T_g to T_g+80 K for sample PBMA13C, from T_g+40 K to T_g+10 K for sample PMA, from T_g-20 K to T_g+140 K for sample PEA, from T_g to T_g+133 K for sample PBA, from T_g+20 K to T_g+120 K for sample PHxA, and from T_g to T_g+100 K for all other samples.

2. Remark on the adjustment of the receiver gain in the NOE experiments using the dipolar filter

The receiver gain has to be adjusted in order to record the highest signal-to-noise ratio, without saturating the receiver (and thus introducing artifacts in the recorded spectra). In the recorded NOE data after a dipolar filter, the FID intensity decreases for increasing mixing times. Therefore, the receiver gain was initially adjusted for the smallest mixing time, where the FID intensity is maximal.

However, the receiver gain must be adjusted for the mixing time for which the intensity of a single transient is maximal. It does not necessarily coincide with the mixing time for which the intensity of the total FID (sum of the single transients) is maximal. They coincide in the absence of a dipolar filter, but not when a dipolar filter is used.

The evolution of the magnetization during a NOE experiment using the dipolar filter is the following. The equilibrium magnetization, situated along the Z-axis, is first flipped in the XY-plane. Then the dipolar filter is applied, after which only the magnetization of the selected mobile fraction is still in phase, while the rest is dephased. The magnetization which is still in phase is next flipped on, and stored along the Z-axis. During the mixing time, NOE occurs, as well as a longitudinal relaxation of the dephased components of the magnetization from the XY-plane to the Z-axis. At the end of the mixing time, the magnetization along the Z-axis is flipped back to the XY-plane where it is recorded.

In order to be able to correct for T_1 relaxation by dividing the recorded data by equivalent data recorded without dipolar filter (s. Part 3), the following phase cycle must be applied.⁸⁴ First, the magnetization M is stored for the mixing time along the +Z-axis, and recorded as M_1 in the direction corresponding to the +Z-axis. Second, the same magnetization M is stored for the mixing time along the -Z-axis, and recorded as M_2 in the direction corresponding to the -Z-axis. When these two single transients are added, the following operation is in fact conducted: $M_1 - (-M_2) = M_1 + M_2$. In the absence of dipolar filter, $M = M_1 = M_2$, and $M_1 + M_2 = 2M$. When the dipolar filter is used, the dephased components relax to the +Z-axis, thus increasing M_1 and decreasing M_2 (along the -Z-axis, and consequently increasing it along the +Z-axis). For long mixing times, if the receiver

gain is too high, both M_1 and M_2 saturate the receiver in the direction corresponding to the +Z-axis, and the maximal value Max is recorded. In that case, $M_1 + M_2 = \text{Max} - \text{Max} = 0$, the first points of the total FID are zero, leading to a strong oscillation of the baseline of the spectrum after Fourier transformation and thus to a fast decrease of the line intensity. This problem starts at a given mixing time and then becomes worse with increasing mixing time. This starting mixing time decreases for increasing dipolar filter strength. Nevertheless, it doesn't affect the measurement for mixing times shorter than this starting mixing time.

However, this problem can be easily avoided, by adjusting the receiver gain for the longest mixing time when the dipolar filter is used, and for the shortest mixing time, when no dipolar filter is used.

3. *Temperature calibration of the static NMR experiments*

a) Motivation

The temperature indicated on the spectrometer display is not exactly the temperature within the sample. One reason for this is the geometry of the probehead: the thermocouple measuring the temperature is not located in the sample, but in the heating gas flow before the sample, introducing a geometrical error. Furthermore, there might be an internal correction in the temperature regulation program to compensate for this geometrical error.

The T_g values cover a wide temperature range for all model samples (213 K to 398 K, s. Part 2, I and III). For the model samples, the ^1H static spectra and the NOE experiments using the dipolar filter have been conducted at temperatures ranging from ca $T_g - 40$ K to $T_g + 130$ K, (s. Part 4 and 5). Therefore we needed to calibrate the actual sample temperature (as a function of the display temperature) for the probeheads used for those measurements over their whole temperature range.

b) Literature data

Lead nitrate, $\text{Pb}(\text{NO}_3)_2$, is a thermometer appropriate for NMR experiments for two reasons.²⁶⁹ First, it is highly NMR sensitive (through the ^{207}Pb nucleus) and possesses sharp NMR lines. Second, its chemical shifts are strongly varying with temperature. It is thermally stable at temperatures below 400 °C.²⁷⁰ Nevertheless, it lacks a proper standard for the calibration of the ppm scale.²⁷¹

The temperature dependence of the isotropical chemical shift of lead nitrate was determined by several groups for MAS measurements. Bielecki and Burum determined it from 143 K to 423 K using three melting points (also determined by calorimetry), under

2 kHz MAS, and found a linear relationship.²⁶⁹ Takahashi et al. determined it from 303 K to 673 K using four melting points and two phase transitions (also determined by calorimetry), under 2.5 kHz MAS, and found a quadratic relationship.²⁷⁰

The ^{207}Pb spectrum of lead nitrate recorded under static conditions is very broad due to its large chemical-shift anisotropy. In order to be able to use the relationships established under MAS, the isotropic chemical shift must be extracted from the powder spectrum. Beckmann and Dybowski did so for the temperature range from room temperature to 370 K, and determined a linear relationship between the temperature T (in K) and the chemical shift of the maximum of the powder spectrum δ_{max} (which corresponds to one principal value, in ppm).²⁷²

$$\delta_{\text{max}}(T) = -\{3670.6 \pm 0.1 \text{ ppm}\} + \{0.666 \pm 0.0003 \text{ ppm/K}\}T \quad \text{Equation 7- II-1}$$

However, they did not check this relationship by measuring any melting point.

Since there is no appropriate standard to calibrate the ^{207}Pb scale,²⁷¹ the scale has to be indirectly calibrated. Otherwise, only the slope of the relationships between ^{207}Pb chemical shifts and temperature cited above can be used. The indirect ppm scale calibration can be done by calculating the ^{207}Pb frequency at 0 ppm from the ^1H frequency measured at 0 ppm for tetramethylsilane.⁵ Nevertheless, due to the uncertainty on the magnetogyric coefficients γ used in this calculation, this method is not precise. The indirect calibration can also be done by measuring a given temperature (e.g., melting point) known from calorimetric measurements with NMR experiments. Together with the slope taken from the literature, this allows to establish the calibration of the temperature in the sample.

It should be noted that the calibration problem of the ppm scale could be avoided by measuring ^{119}Sn spectra of $\text{Sm}_2\text{Sn}_2\text{O}_7$ in which tin oxide is an internal standard.²⁷³ However, this NMR thermometer is not appropriate for static measurements, because the lines are too broad,²⁷⁴ and the ^{119}Sn frequency can not be reached by all probeheads. Vanadocene has also been reported as an appropriate thermometer for MAS measurements.²⁷⁵

c) Experimental conditions

The temperature calibration was carried out on the 7.5 mm static probeheads of a Bruker DSX300 and of a Bruker DSX500 spectrometers. The temperature range was 200 to 540 K on the DSX300 and 200 to 473 K on the DSX500, the nitrogen flow was $1200 \text{ L}\cdot\text{h}^{-1}$ on the DSX300 and $1000 \text{ L}\cdot\text{h}^{-1}$ on the DSX500. The temperature range over which the calibration has been done was chosen as follows. The probehead should not be used below 203 K, so that we set the minimal display temperature at 200 K. Both

probeheads were built up to be used up to 573 K, but it is impossible to reach display temperatures higher than 540 K on the DSX300, and this can be achieved only using 1200 L.h⁻¹ nitrogen. On the DSX500, the program regulating the temperature had a higher allowed value set at 473 K.

On the DSX300, the measurements were done with the top of the magnet hole partially open to evacuate the heat. ²⁰⁷Pb single pulse excitation was used at a frequency of 67.8 MHz, with 3 μs 90 ° pulses, and 64 transients were acquired without decoupling with a relaxation delay of 5 s. On the DSX500, the measurements were done with a Dewar glass tube set above the probehead to evacuate the heat. ²⁰⁷Pb single pulse excitation was used at a frequency of 104.6 MHz, with 4 μs 90 ° pulses, and 64 transients were acquired without decoupling with a relaxation delay of 5 s. The spectra were acquired after at least 15 min equilibration at each temperature; it was checked for the lowest and the highest temperature that there was no detectable change in the spectrum, and therefore in temperature, after 15 min.

The chemical structures of all investigated compounds and typical spectra are displayed respectively in paragraphs h and i.

d) Intermediate calibration using published data

In a first step, we assumed that there was no error done at 300 K, i.e., that the sample temperature was also 300 K for this display temperature. Using the published slope²⁷² (s. Equation 2- IV-1), this led to the following intermediate calibrations (in K): $T_{\text{sample}}=1.089 \cdot T_{\text{display}}-26$ for the DSX300 over the range from 200 to 540 K and $T_{\text{sample}}=1.050 \cdot T_{\text{display}}-13$ for the DSX500 over the range from 200 to 473 K.

In the next step, a phase transition was determined for a liquid crystal, 4-hexyloxybenzoic acid-(4'-ethoxy)-phenyl ester,²⁷⁶ using ¹H static spectra under the same heating conditions as the ²⁰⁷Pb spectra. The phase transition from mesophase to liquid of this molecule by heating was chosen because it is fast and reversible. It was determined at 367.2 K with a Buechi melting point device at 0.1 K.min⁻¹. It corresponds to the second narrowing of the peaks on the ¹H spectrum (the first narrowing being the transition from solid to mesophase). ¹H spectra were recorded with 0.1 K steps and 15 min equilibration time on the DSX300, and with 0.25 K steps and 20 min equilibration time on the DSX500. The melting point was detected at 369.4 K on the DSX 300 and at 360.2 K at the DSX500. The intermediate calibration curves determined above were then shifted in the T_{sample} direction to take into account the melting point of the liquid crystal. The following second intermediate calibration curves were then obtained: $T_{\text{sample}}=1.089 \cdot T_{\text{display}}-30$ for the

DSX300 over the range from 200 to 540 K and $T_{\text{sample}}=1.050 \cdot T_{\text{display}}-9$ for the DSX500 over the range from 200 to 473 K.

e) Check of the intermediate calibration with melting points

We decided to check the validity of this second intermediate calibration by measuring two other melting points, one at a very low and one at a very high temperature. The end of the melting by heating had been previously determined as the right limit of the melting peak (and not the minimum!) in differential scanning calorimetry (DSC) at $1 \text{ K} \cdot \text{min}^{-1}$; it was 207 K for dimethyl formamide, 429 K for citric acid. It corresponds on ^1H static spectra to the disappearance of the broad component. It has been measured respectively at 223.0 K and 414.5 K display temperatures on the DSX300 (steps of 0.5 K with 20 min equilibration), at 211.0 K and 411.0 K display temperatures on the DSX500 (steps of 0.5 K with 15 min equilibration).

The measured points (sample temperature as a function of display temperature) are not located on the second intermediate calibration curve determined above, but they are aligned with the melting point of the liquid crystal. Therefore we had to choose for the final calibration between the set of three melting points on one hand, and the ^{207}Pb spectra together with the published slope and one melting point on the other hand.

We decided to take the set of three aligned melting points, determined independently with ^1H spectra and with two calorimetric methods, to determine the final calibration curve. In this way, we do not rely on the published data. Nevertheless, the data measured on the ^{207}Pb spectra are needed to check if this calibration is linear, and to estimate its precision. Therefore we corrected the data measured on the ^{207}Pb spectra, so that their linear fit $T_{\text{sample}}=f(T_{\text{display}})$ is identical to the linear fit $T_{\text{sample}}=f(T_{\text{display}})$ of the set of three melting points. These corrected ^{207}Pb data were then fitted again, to obtain the final calibrations with their errors.

f) Final calibration

A temperature calibration is presented for the 7.5 mm static probeheads of the Bruker DSX300 and DSX500 spectrometers. It should be noted that we have determined the $T_{\text{sample}}=A \cdot T_{\text{display}}+B$ calibration, while the temperature correction is done in the NMR program using the equation $T_{\text{display}}=\text{Slope} \cdot T_{\text{sample}}+\text{Offset}$, where $\text{Slope}=1/B$ and $\text{Offset}=-B/A$. The final calibration, as well as the Slope and Offset coefficients and the experimental conditions are reported in Table 7- II-1.

<i>Spectrometer</i>	<i>DSX300</i>	<i>DSX500</i>
<i>Range</i>	200 to 540 K (display) 179 to 573 K (sample)	200 to 473 K (display) 182 to 500 K (sample)

<i>Calibration (in K)</i>	$T_{sample} = \{1.159 \pm 0.006\} T_{display} - \{53 \pm 2.3\}$	$T_{sample} = \{1.162 \pm 0.006\} T_{display} - \{50 \pm 2.2\}$
<i>Slope</i>	0.8626	0.8604
<i>Offset (in K)</i>	46	43
<i>Conditions</i>	1200 L.h ⁻¹ nitrogen Top of magnet hole partially open	Nitrogen flow equivalent to 1000 L.h ⁻¹ air at 20 °C Dewar glass tube above probehead

Table 7- II-1: Final temperature calibration of the 7.5 mm static probeheads of the Bruker DSX300 and DSX500 spectrometers; the equation correlating the actual temperature in the sample with the temperature indicated on the display (without correction) is given, as well as the coefficients to be entered in the program to do the automatic temperature correction and the conditions for which these are valid.

g) Remarks

On both probeheads, the temperature in the sample is higher than the display temperature for high temperatures, and lower than it for low temperatures. This seems to be in contradiction with the location of the thermocouple in the hot (or cold) gas flow before it reaches the sample. Two reasons could explain this apparent contradiction. First, the thermocouple might not be situated exactly in the gas flow, but next to it; this is impossible to check without breaking a seal in the probehead. Second, there might be an internal correction of the display temperature in the program regulating it to compensate for the difference between the temperatures at the thermocouple and in the sample.

The same work has also been done for the temperatures above room temperature with air as gas. The calibration determined was the same as with nitrogen on the DSX500, and different from it on the DSX300. This does not make sense and could be due to the fact that the gas flow is directly measured using a metal ball located in the flow on the DSX500, while it is probably indirectly measured through its pressure on the DSX300. Moreover, the entering air pressure is very different from the entering nitrogen pressure, and changing with time (because of regular compression). Therefore the calibration with air as gas can not be trusted (which is not a problem in our case, since all measurements were done under nitrogen).

h) Molecules on which melting points have been measured

The molecules on which melting points have been measured are shown on Figure 7- II-2. The melting (to the isotropic melt) of the liquid crystal (a) is fast and reversible, and has a narrow temperature range (melting point determined at 367.2 K, i.e. 94.1 °C, with a Buechi melting point device at 0.1 K.min⁻¹). The melting of dimethylformamide (b) and citric acid (c) are slower and have a wider temperature range (right limit of melting peaks determined respectively at 207 K, i.e. -66 °C, and 429 K, i.e. 156 °C, with DSC at 1 K.min⁻¹). The melting of dimethylformamide (b) is reversible, while the melting of citric acid (c) is not. Indeed, citric acid decomposes and evaporates just above its melting point.

Some experimental tricks should be mentioned here for packing these substances. The liquid crystal and the dimethylformamide can be packed in zirconium rotors with a KelF cap without hole. The citric acid can be packed in a zirconium rotor, but neither with a normal KelF cap (it would shrink at high temperatures), nor with a BN cap (it would break if citric acid evaporates). It should be packed with an old KelF cap, already shrunk, wrapped with Teflon tape to fit exactly in the rotor. Moreover, since the melting of citric acid is not reversible, new citric acid should be packed in the rotor every time it has molten.

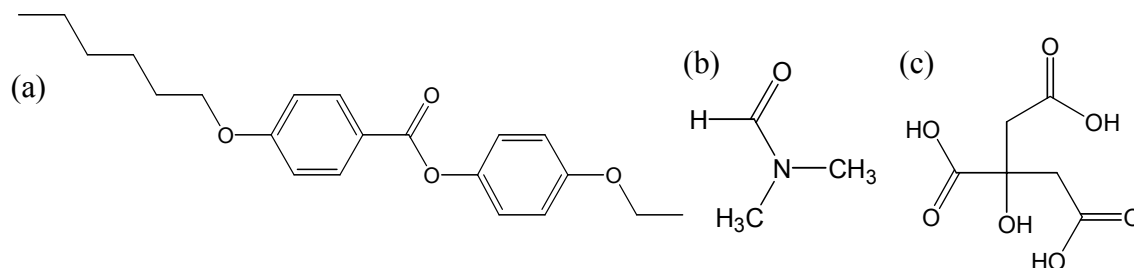


Figure 7- II-2: Molecules on which melting points have been measured; (a) 4-hexyloxy-benzoic acid-(4'-ethoxy)-phenyl ester (liquid crystal), (b) dimethylformamide, (c) citric acid.

Other substances should be mentioned here, and are presented in Figure 7- II-3. Dimethyl terephthalate (a) has a fast and reversible melting over a narrow temperature range at 414 K, i.e. 141 °C, but it is not appropriate for ^1H static NMR measurements of the melting point, since the solid can not be distinguished from the liquid which exhibits a broad line (the liquid probably orientates in the magnetic field). Hydroquinone (b) has a reversible melting point at 445 K, i.e. 172 °C, and is appropriate for ^1H static NMR measurements of the melting point.

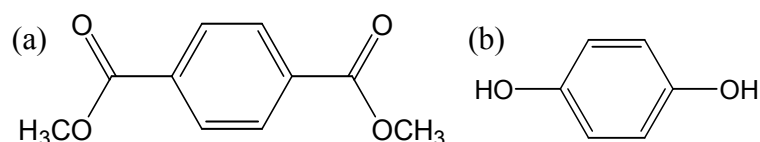


Figure 7- II-3: (a) dimethyl terephthalate, (b) hydroquinone.

i) Typical ^{207}Pb and ^1H static spectra

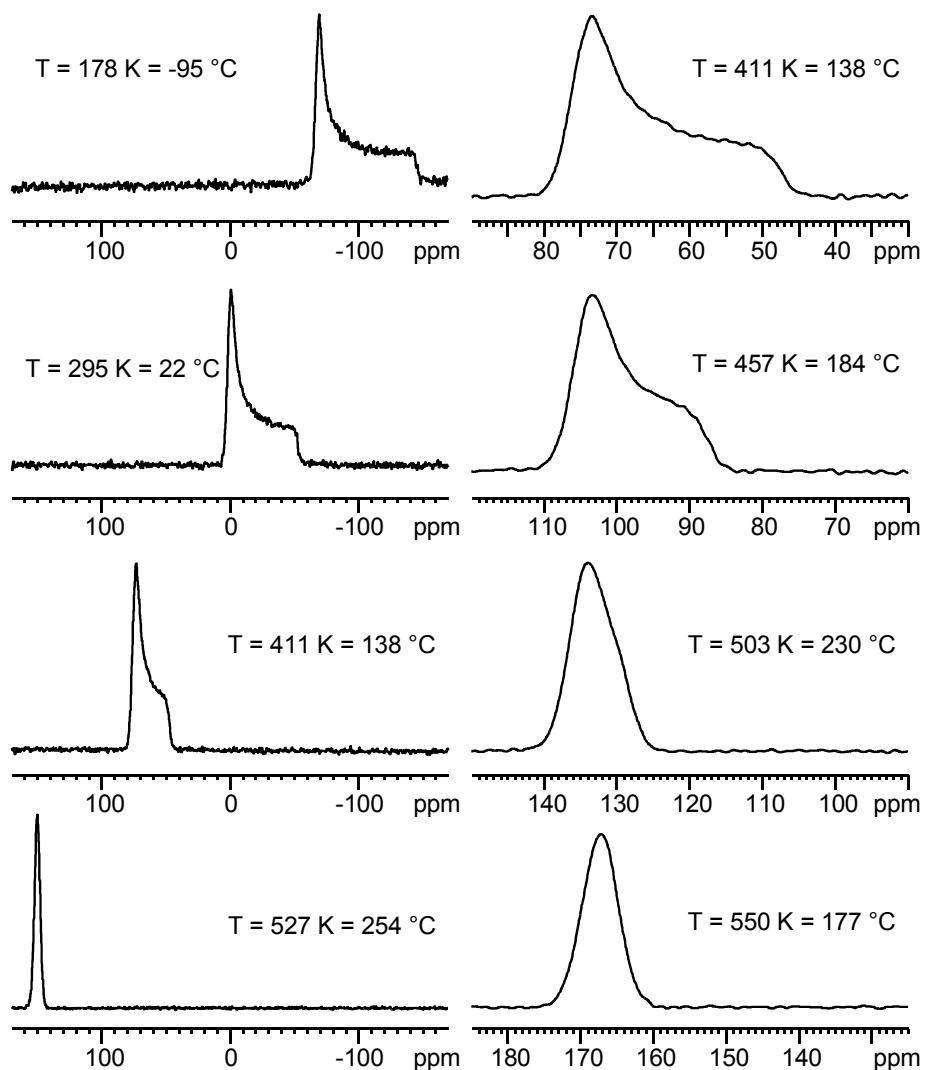


Figure 7- II-4: Typical static ^{207}Pb spectra recorded on the Bruker DSX300, with single pulse excitation, without decoupling, with 64 scans; the shift of the chemical shift with temperature is illustrated on the left, the narrowing of the tensor at high temperatures on the right; actual sample temperature is indicated in the figure; the zero of the ppm scale was set at the tensor maximum at 295 K.

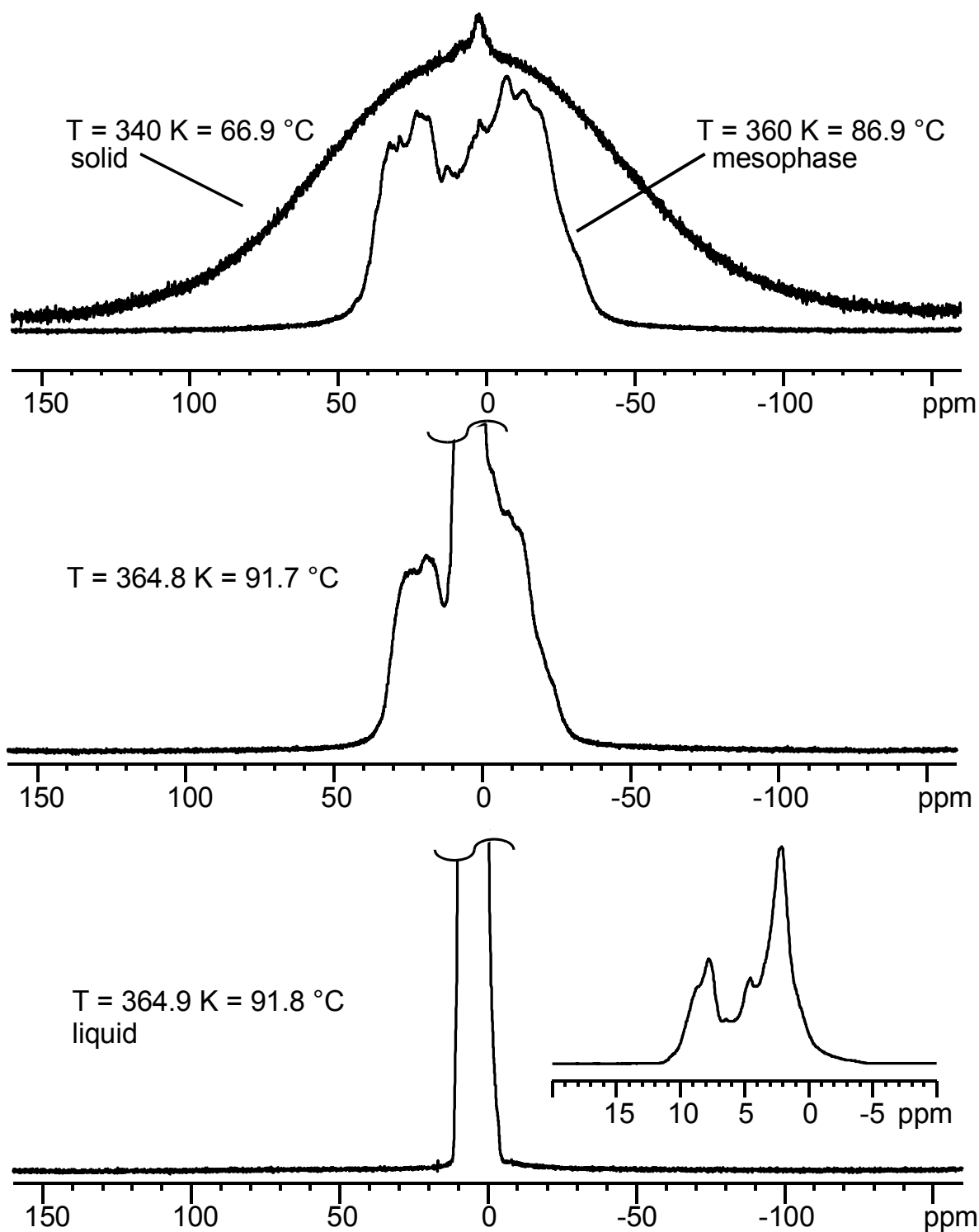


Figure 7- II-5: Typical static ^1H spectra recorded for 4-hexyloxy-benzoic acid-(4'-ethoxy)-phenyl ester (liquid crystal) at a Larmor frequency of 500 MHz; above: spectra of the solid and the mesophase, middle: spectrum of a mixture of mesophase and liquid, below: spectrum of liquid; display temperatures without correction are indicated.

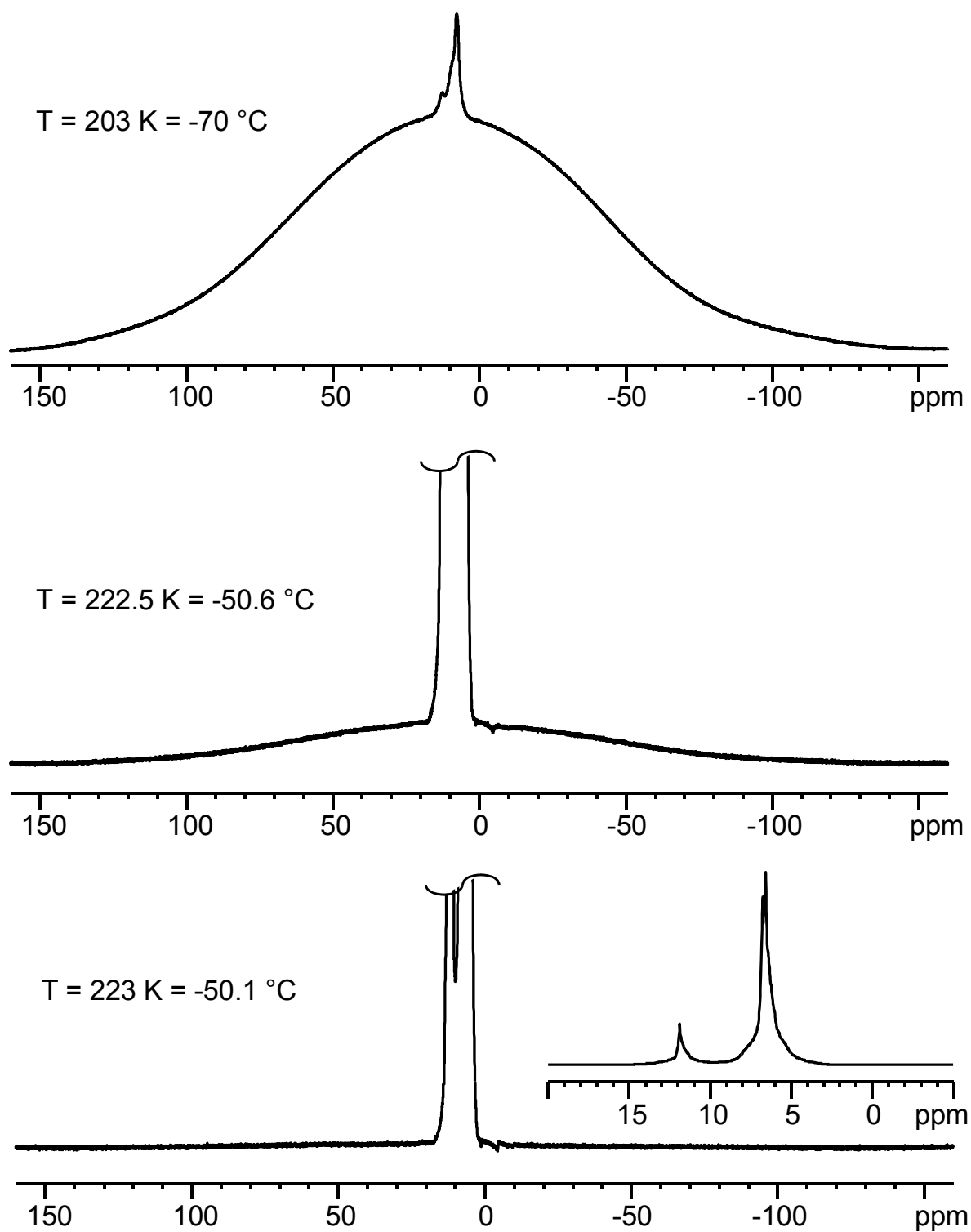


Figure 7- II-6: Typical static ^1H spectra recorded for dimethylformamide at a Larmor frequency of 300.13 MHz; above: spectra of the solid, middle: spectrum of a mixture of solid and liquid, below: spectrum of liquid; display temperatures without correction are indicated.

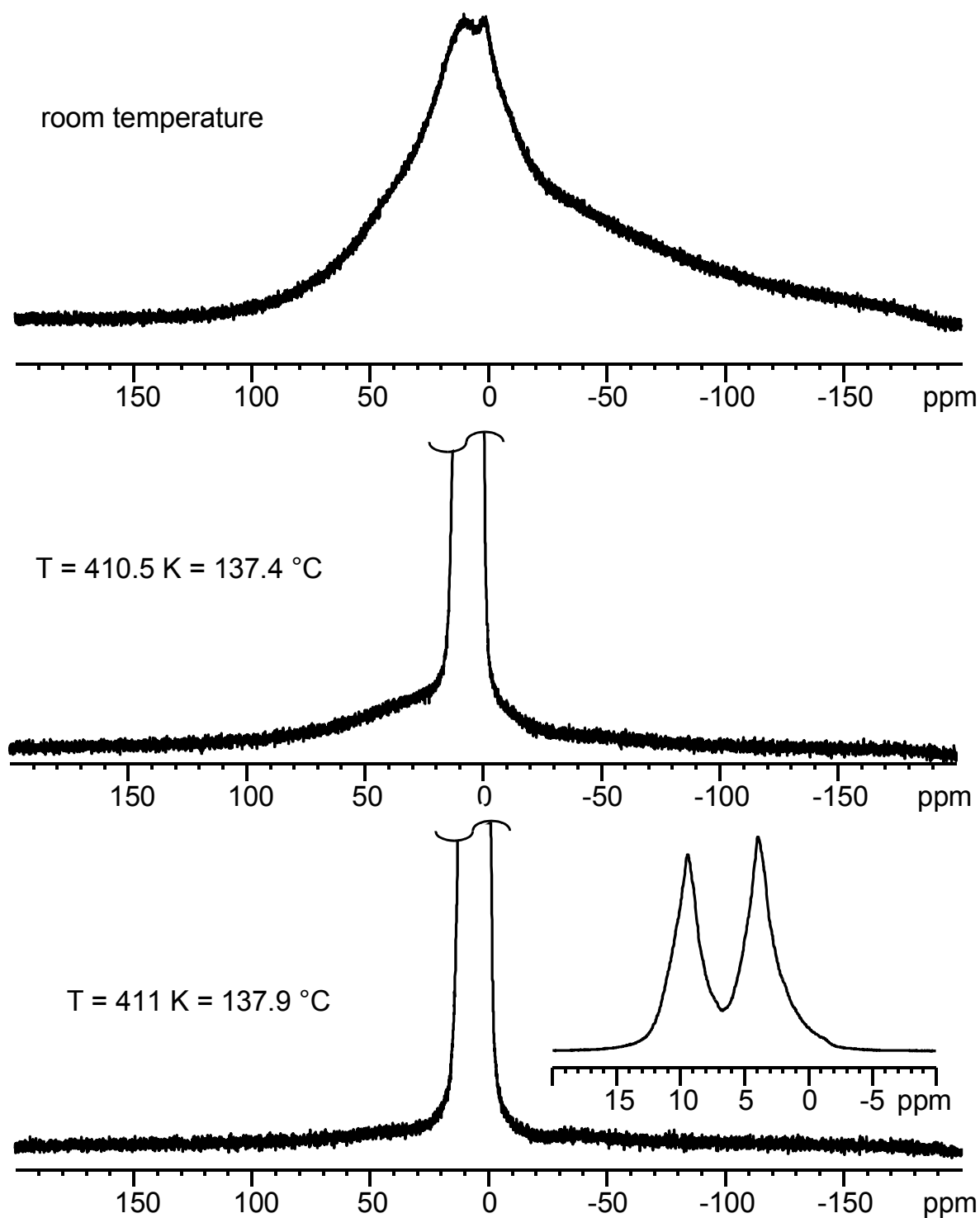


Figure 7- II-7: Typical static ^1H spectra recorded for citric acid at a Larmor frequency of 300.13 MHz; above: spectra of the solid, middle: spectrum of a mixture of solid and liquid, below: spectrum of liquid; display temperatures without correction are indicated

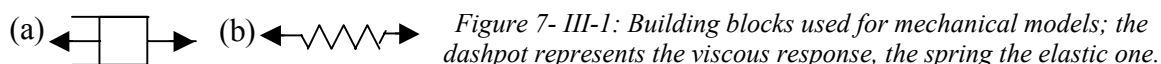
III. Viscoelastic properties and stereochemistry of polymers, characterization of homogeneous networks

A. Basic concepts relative to viscoelastic properties

1. Viscoelasticity in simple shear or uniaxial deformation^{277,278}

Viscoelasticity is the time-dependent response of a liquid or a solid subjected to stress or strain. Both viscous and elastic responses are needed for the description of viscoelastic behavior. Indeed, deformation (the relative displacement of points of a body) can be divided into two types: flow and elasticity. *Flow* is irreversible deformation: when the stress is removed, the material does not revert to its original configuration. This implies that work is converted to heat. *Elasticity* is reversible deformation: the deformed body recovers its original shape, and the applied work is largely recoverable. *Viscoelastic materials* show both flow and elasticity. Polymers are viscoelastic materials.

In mechanical models, the viscous component of the response to applied stress is represented by a dashpot, the elastic one by a spring (s. Figure 7- III-1).



Elastic deformation is a function of the applied *stress* (force normalized to area) and is expressed in terms of relative displacement or *strain*. Strain may be expressed in terms of relative change in volume, length or other measurement depending on the nature of the stress.

A *modulus* is the quotient of stress and strain, where the type of stress and strain is defined by the type of deformation employed. The *bulk modulus* K is the quotient of hydrostatic pressure and bulk compression, the *Young's modulus* E is the quotient of uniaxial stress, and stress at the limit of zero strain (and may be named tensile modulus if determined using tensile deformation), the *shear modulus* G is the quotient of shear stress and shear strain.

An *elastic modulus* or *modulus of elasticity* is a modulus of a body for which the applied stress is proportional to the resulting strain (s. Figure 7- III-2). The material is then said to have a linear viscoelastic behavior, and the measurement is done in the *linear regime*.

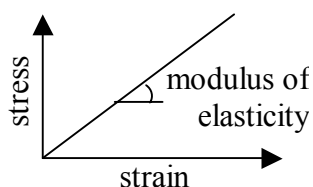


Figure 7- III-2: Definition of the elastic modulus as the slope of the stress as a function of strain, in case this modulus is constant.

The dimensionless *Deborah number*, De , is defined as the fluid's characteristic relaxation time divided by a time constant characterizing the flow.²⁷⁹ For a high Deborah number, the material responds elastically, whereas for a low Deborah number it exhibits a viscous behavior.

2. Forced oscillations^{277,278}

Forced oscillations are the deformations of a material by the application of a small sinusoidal strain γ such that $\gamma = \gamma_0 \cdot \sin(\omega t)$, where γ_0 is the strain amplitude, ω the angular velocity, and both are positive constants. For a linear viscoelastic behavior, a sinusoidal stress σ results from the sinusoidal strain with $\sigma = \sigma_0 \cdot \sin(\omega t + \delta)$, where σ_0 is the stress amplitude and δ the *phase angle* or *loss angle* between stress and strain.

The *storage modulus* (G' in simple shear, E' in uniaxial deformation) is the ratio of the amplitude of the stress in phase with the strain, to the amplitude of the strain: $G' = \sigma_0 \cdot \cos\delta / \gamma_0$. The *loss modulus* (G'' in simple shear, E'' in uniaxial deformation) is the ratio of the amplitude of the stress 90° out of phase with the strain, to the amplitude of the strain: $G'' = \sigma_0 \cdot \sin\delta / \gamma_0$. The *complex modulus* (G^* in simple shear, E^* in uniaxial deformation) is the ratio of the complex stress σ^* ($\sigma^* = \sigma_0 \cdot \exp(i(\omega t + \delta))$) to the complex strain γ^* ($\gamma^* = \gamma_0 \cdot \exp(i\omega t)$). It is related to the storage and loss moduli via $G^* = G' + iG''$. It should be noted that the real part of the complex strain is the strain which is actually applied to the material. Furthermore, the material actually experiences the real part of the complex stress.

The storage modulus G' is a measure of elasticity: it is associated with the energy stored in elastic deformation. It is high when a polymer is in its glassy state, and drops dramatically with increasing temperature as the polymer goes through its glass transition and becomes soft and rubbery (s. Figure 7- III-3). If the polymer is crosslinked, the storage modulus does not drop so far after the glass transition (the exact level depends on the degree of crosslinking). The loss modulus G'' is associated with viscous energy dissipation, i.e. damping. The *loss factor* (or *loss tangent*), $\tan\delta$, is the tangent of the phase angle difference δ between stress and strain during forced oscillations. It is also equal to the ratio of loss to storage moduli: $\tan\delta = G''/G'$.

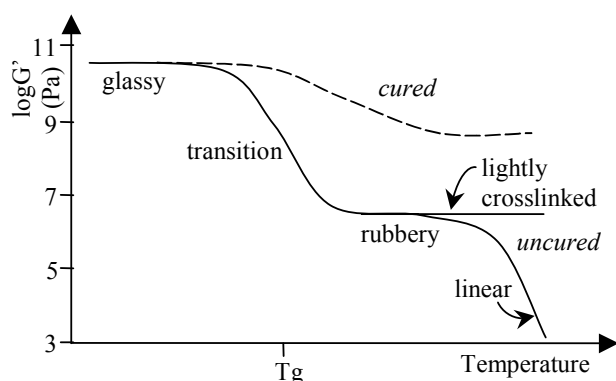


Figure 7-III-3: Generalized modulus-temperature curves for polymeric materials showing the high modulus glassy state, glass transition regions for cured and uncured polymers, plateau regions for crosslinked polymers, and the drop-off modulus for a linear polymer.

3. Master curves¹⁴²

It is currently impossible to investigate the full range of the relaxation spectrum at a single temperature with a single experimental technique. However, a change in temperature may bring relaxation features of interest within an accessible time scale. *Time-temperature equivalence* in its simplest form implies that the viscoelastic behavior at two temperatures can be related by a change in time scale only (shift of the modulus value by an amount $\log(a_T)$). For time-temperature superposition to be exact, the spectrum of relaxation times must continuously shift to shorter times when the temperature is increased. Materials with this characteristic are said to be thermorheologically simple (e.g., no phase transition is encountered). For such polymers, it is possible to predict the behavior for viscoelastic deformation under variable temperature conditions.

Williams, Landel and Ferry showed that the shift factor-temperature relation close to T_g was approximately identical for all amorphous polymers, having the form of the Williams-Landel-Ferry equation²²³ (*WLF equation*):

$$\log(a_T) = \frac{C_1 \cdot (T - T_r)}{C_2 + (T - T_r)} \quad \text{Equation 7-III-1}$$

where C_1 and C_2 are constants and T_r is a reference temperature appropriate for a particular polymer, usually taken equal to T_g . The WLF equation is typically valid over the range T_g to $T_g + 100$ °C.

4. Viscoelastic window for PSAs

Chang⁴⁵ defined the concept of viscoelastic windows for PSAs (s. Figure 7-III-4).

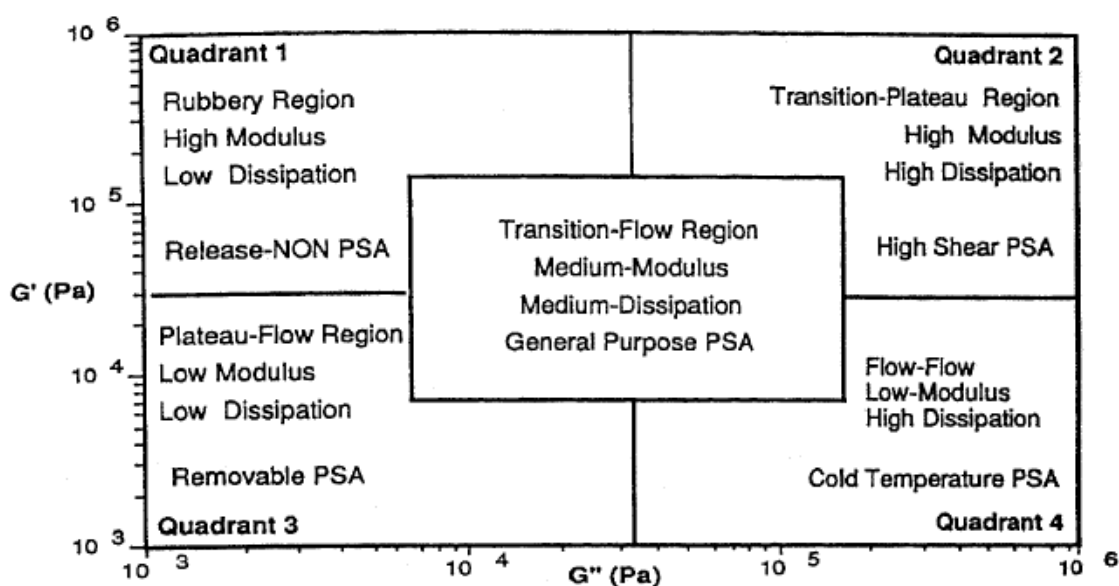


Figure 7-III-4: Representation of the concept of viscoelastic windows for PSAs as a two-dimensional map with storage and loss moduli G' and G'' as axes, divided in different regions corresponding to different characteristics of the PSA (non-PSA, high shear PSA, cold-temperature PSA, removable PSA, general purpose PSA).⁴⁵

B. Stereochemical definitions and notations²⁸⁰⁻²⁸² relative to tacticity

Tacticity means the orderliness of the succession of configurational repeating units in the main chain of a polymer molecule (a configurational repeating unit is a constitutional repeating unit, the configuration of which is defined at one or more sites of stereoisomerism, the pseudochiral carbon(s)). The configuration (which refers to the different arrangements of the atoms and substituents in a molecule which can be interconverted only by the breakage of chemical bonds) should not be mistaken with the conformation (which refers to the different arrangements of the atoms and substituents in a molecule which come about from rotations around single bounds). A *tactic polymer* is a regular polymer, the molecules of which can be described in terms of only one species of configurational repeating unit in a single sequential arrangement: an *isotactic polymer* is a succession of identical configurational base units, a *syndiotactic polymer* an alternation of enantiomeric configurational base units. An *atactic polymer* a succession of an equal number of all possible configurational base units in a random sequence distribution.

When two consecutive pseudochiral carbons bearing different substituents are contiguous, their relative configurations are called erythro (when they are identical) or threo (when they are enantiomeric). When two consecutive pseudochiral carbons bearing the same substituents are linked by a symmetric connecting group (CH_2 in the case of polyacrylates and polymethacrylates), their relative configurations are called *meso*,

abbreviation *m* (when they are identical) or *racemo*, abbreviation *r* (when they are enantiomeric) (s. Figure 7- III-5).

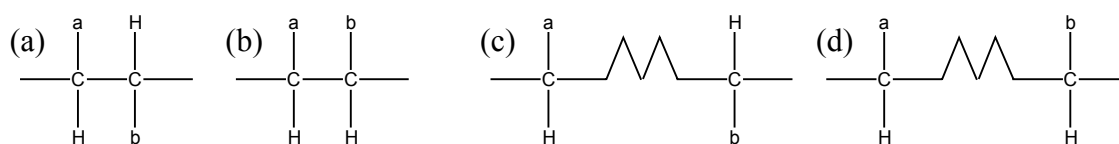


Figure 7- III-5: Relative configurations of consecutive prochiral carbons in a polymer chain ; (a) erythro, (b) threo, (c) meso or *m*, (d) racemo or *r*, /\!/ represents a symmetric connecting unit.

A series of two, three, four, five, etc. consecutive configurational base units, containing therefore two, three, four, five, etc. consecutive pseudochiral carbons, may be called respectively diad, triad, tetrad, pentad, etc. In vinyl polymers (and in particular in polyacrylates and polymethacrylates), there are meso (or *m*) and racemo (or *r*) diads. A triad is the combination of two diads among *m* and *r*, which can be *mm*, *mr* or *rr*; they may be called *isotactic*, *heterotactic* and *syndiotactic triads*, respectively.

The fractions of diads and triads are designated by (*m*), (*r*), and (*mm*), (*mr*), (*rr*) respectively. They satisfy by definition a sum equal to unity: (*m*)+(*r*)=1 on one hand, (*mm*)+(*mr*)+(*rr*)=1 on the other hand. Furthermore, the triads being a combination of two diads, the following equations are also true: (*m*)=(*mm*)+(*mr*)/2 and (*r*)=(*rr*)+(*mr*)/2. A perfect atactic polymer is one with a random distribution of diads and triads, in which therefore (*r*)=(*m*)=0.50, (*mm*)=(*rr*)=0.25 and (*mr*)=0.50. The completely isotactic polymer has (*m*)=(*mm*)=1. The completely syndiotactic polymer is defined by (*r*)=(*rr*)=1. For random distributions with (*m*) \neq (*r*) \neq 0.50 or (*rr*) \neq (*mm*) \neq 0.25, one has different degrees of syndiotacticity or isotacticity. Isotacticity predominates when (*m*)>0.5 or (*mm*)>0.25 and syndiotacticity predominates when (*r*)>0.5 or (*rr*)>0.25.

High resolution, ^1H and ^{13}C , NMR is the technique of choice for the determination of the polymer sequence distributions (diads, triads, tetrads, etc.). The obtained results can be analyzed by statistical propagation models to gain insight into the stereochemistry of polymerization, where P_m is the probability of an active center to give a diad *m*. The most frequently used are the Bernoulli statistical model (which assumes that only the chain end unit in the propagating chain is important in determining the polymer stereochemistry, resulting in (*mm*)= P_m^2 , (*mr*)= $2P_m(1-P_m)$, (*rr*)= $(1-P_m)^2$), and the first-order Markov model (which describes a polymerization where the penultimate unit is important in determining the subsequent stereochemistry, resulting in (*mm*)= $(1-P_{mr})P_{rm}/(P_{mr}+P_{rm})$, (*mr*)= $2P_{mr}P_{rm}/(P_{mr}+P_{rm})$, (*rr*)= $(1-P_{rm})P_{mr}/(P_{mr}+P_{rm})$).

C. Characterization of the crosslinking of homogeneous networks

Several methods are known to characterize crosslinking in networks, assuming an homogeneous network. They allow the determination of a molar mass between entanglements or a crosslinking density. Since the investigated industrial PSAs are partly soluble, they can not be considered as homogeneous networks. Therefore the techniques detailed here have not been used in the present work. However, considering the importance of crosslinking in the adhesive properties of PSAs, a brief overview of these methods is given here.

Highly crosslinked homogeneous polymer networks can be characterized by measurement of their linear viscoelastic behavior. In the rubber-like state, the storage modulus G' is independent of the analysis frequency and is related to crosslink density via the equation $G' = \frac{\rho}{Mc} RT$, where ρ is the density, R the gas constant, T the temperature (in Kelvin) and Mc the mean molar mass between two crosslink points.¹⁸⁹ In the case of a copolymer of a monofunctional acrylate and a bifunctional one, well above T_g , the equation $Mc+e = \frac{3\rho RT(1-x)}{G'}$ relates the dependence of the storage modulus G' on the temperature T to the molar mass $Mc+e$ of network chains between chemical crosslinks (c) and chain entanglements (e) and the volume fraction x of monofunctional acrylate.²⁸³

Homogeneous polymer networks can also be characterized by swelling measurements in a solvent for the corresponding non-crosslinked polymer. The swelling is governed by the Flory-Huggins equation: $\ln(1 - v_p) + v_p + \chi \cdot v_p^2 + v \cdot V_1 \cdot (v_p^{1/3} - \frac{v_p}{2}) = 0$, where v is the crosslink density, v_p the volume fraction of the polymer in the swollen gel, V_1 the molar volume of the solvent and χ the Flory-Huggins parameter describing the interaction between the polymer and the swelling agent.¹⁸⁹ The crosslink density can be determined by measuring the solvent uptake of the poly(alkyl acrylate) films (suitable solvents are THF or DMF, in which the non-crosslinked poly(alkyl acrylates) are completely soluble). The relationship between swelling and crosslink density can be derived from a model used to describe rubber elasticity.¹

Vega et al.²⁸⁴ have studied poly(dimethyl siloxane) model networks using transverse ^1H relaxation T_2 in solid-state NMR. The networks contained elastic chains (attached to the network at both ends) and pendant chains (attached to the network at one end) but no soluble molecules. Pendant chains have an isotropic motion while elastic chains have an anisotropic one, and ^1H -NMR is sensitive to the different behaviors. A fit of

Part 7, III (Appendix) Viscoelasticity and stereochemistry, homogeneous networks
the transverse magnetization decays measured by a Hahn spin echo pulse sequence yielded the proportion of pedant chains.

Barth et al.²⁸⁵ have studied the crosslink density in homogeneously crosslinked natural rubber samples using NMR imaging. They recorded the spatial dependence of the longitudinal relaxation in the rotating frame $T_{1\rho}$, and fitted them with the defect diffusion model to obtain the crosslink density.

IV. NMR spectra and SEC results

A. NMR spectra of model poly(n-alkyl methacrylates)

1. ^1H static spectra

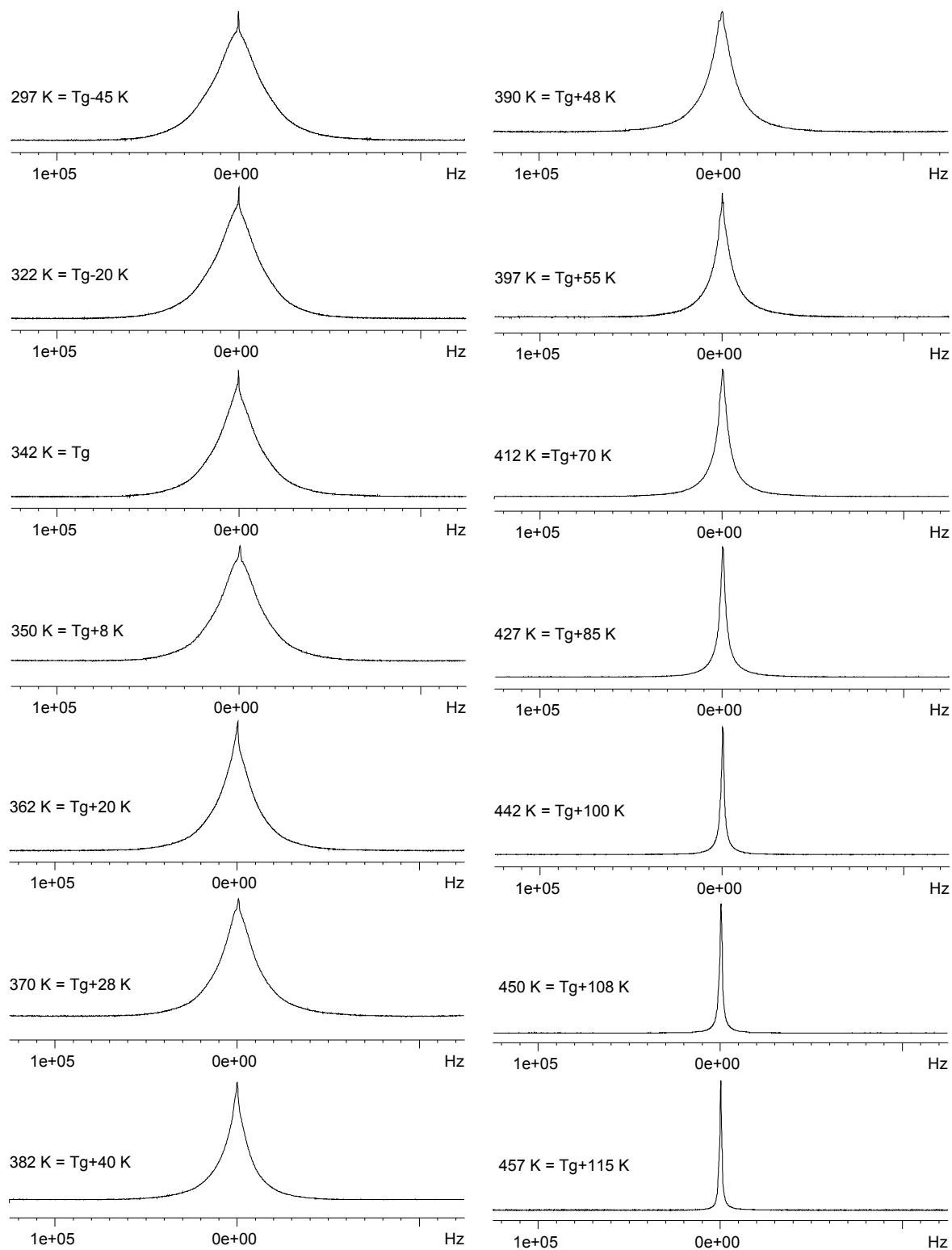


Figure 7- IV-1: Influence of the temperature on the shape of the ^1H spectrum of sample PEMA (spectra recorded at a ^1H Larmor frequency of 300.13 MHz, under static conditions).

Part 7, IV (Appendix) NMR spectra and SEC results

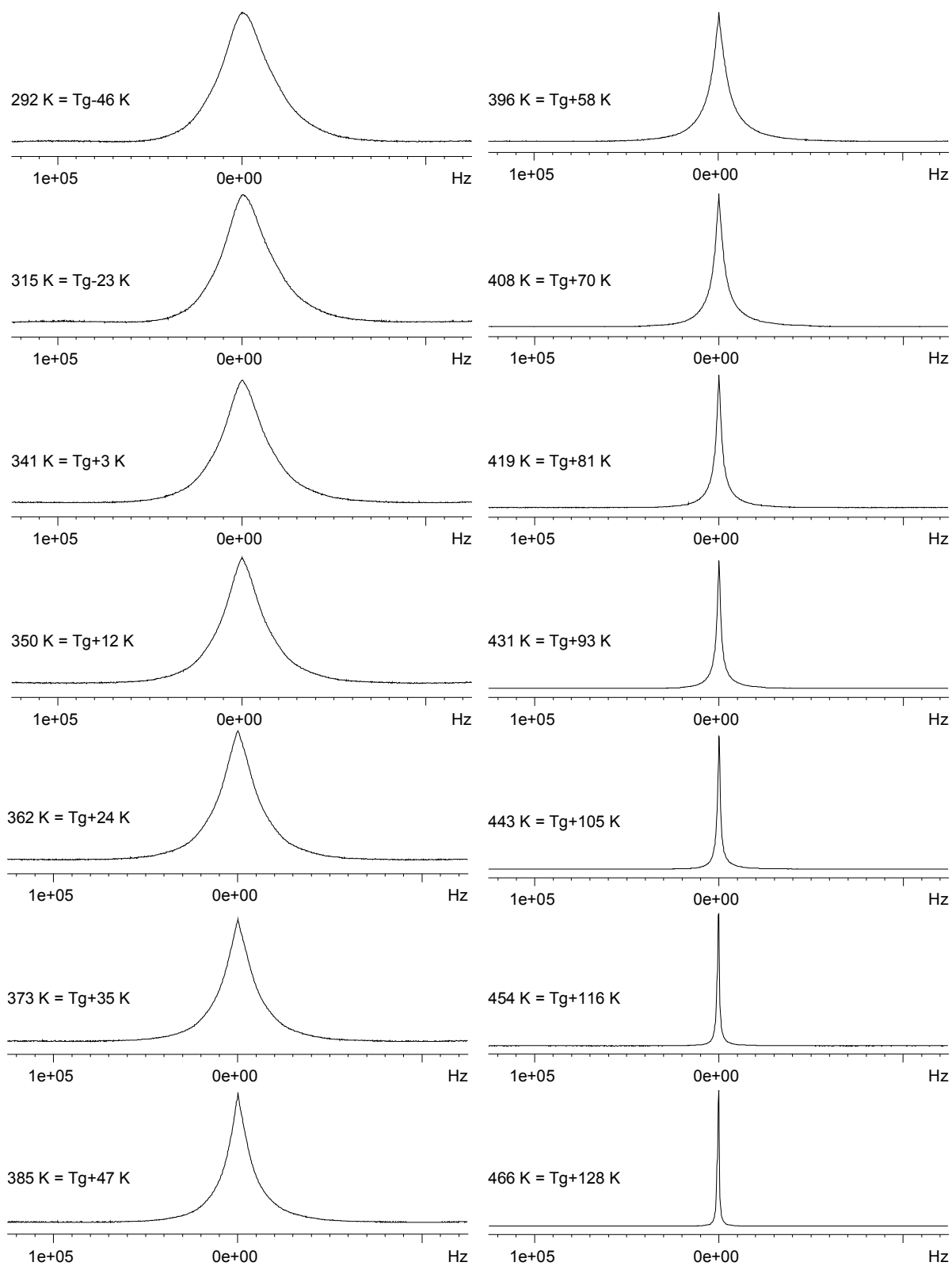


Figure 7- IV-2: Influence of the temperature on the shape of the ^1H spectrum of sample PEMA13C (spectra recorded at a ^1H Larmor frequency of 300.13 MHz, under static conditions).

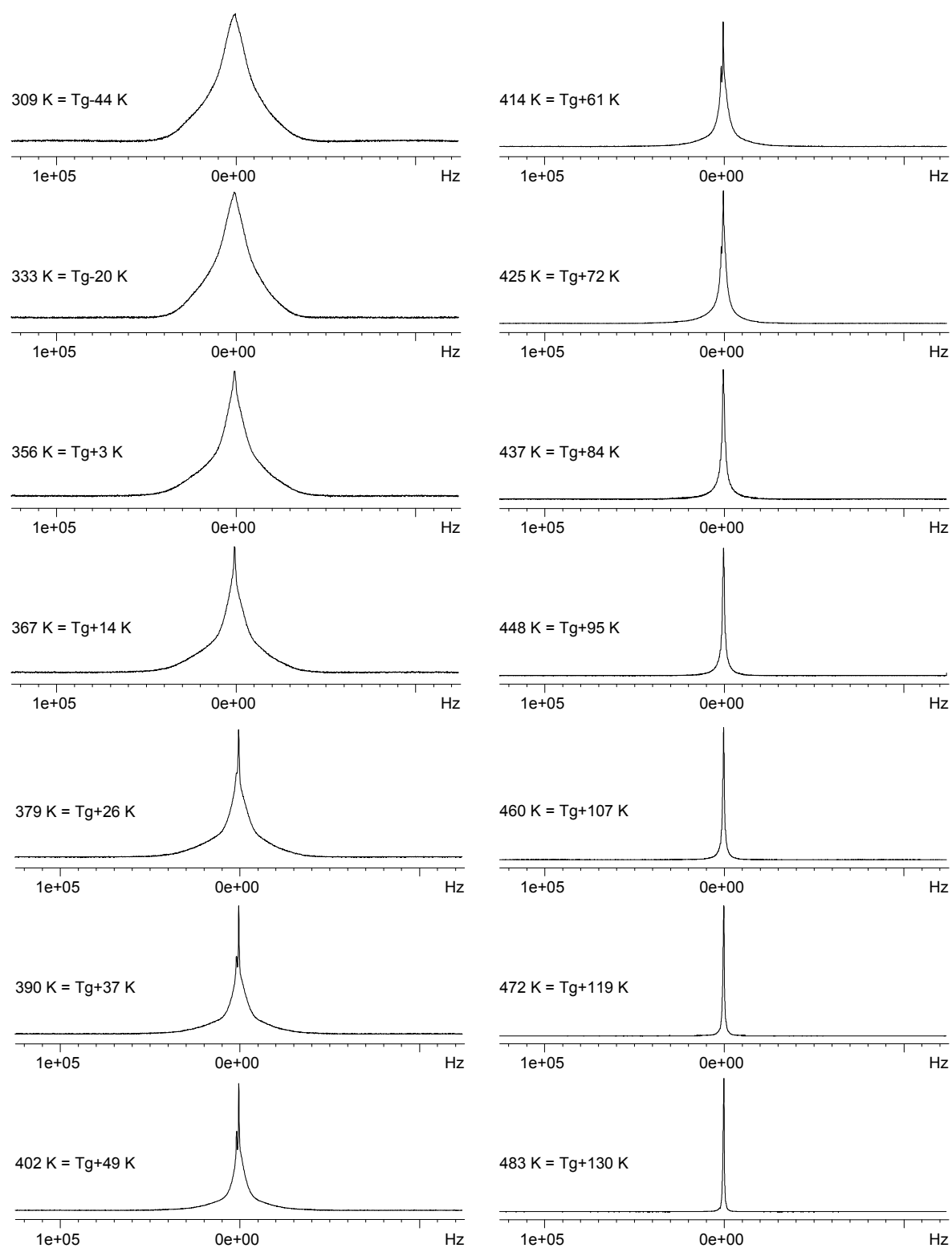


Figure 7- IV-3: Influence of the temperature on the shape of the ^1H spectrum of sample PEMADSC (spectra recorded at a ^1H Larmor frequency of 300.13 MHz, under static conditions).

Part 7, IV (Appendix) NMR spectra and SEC results

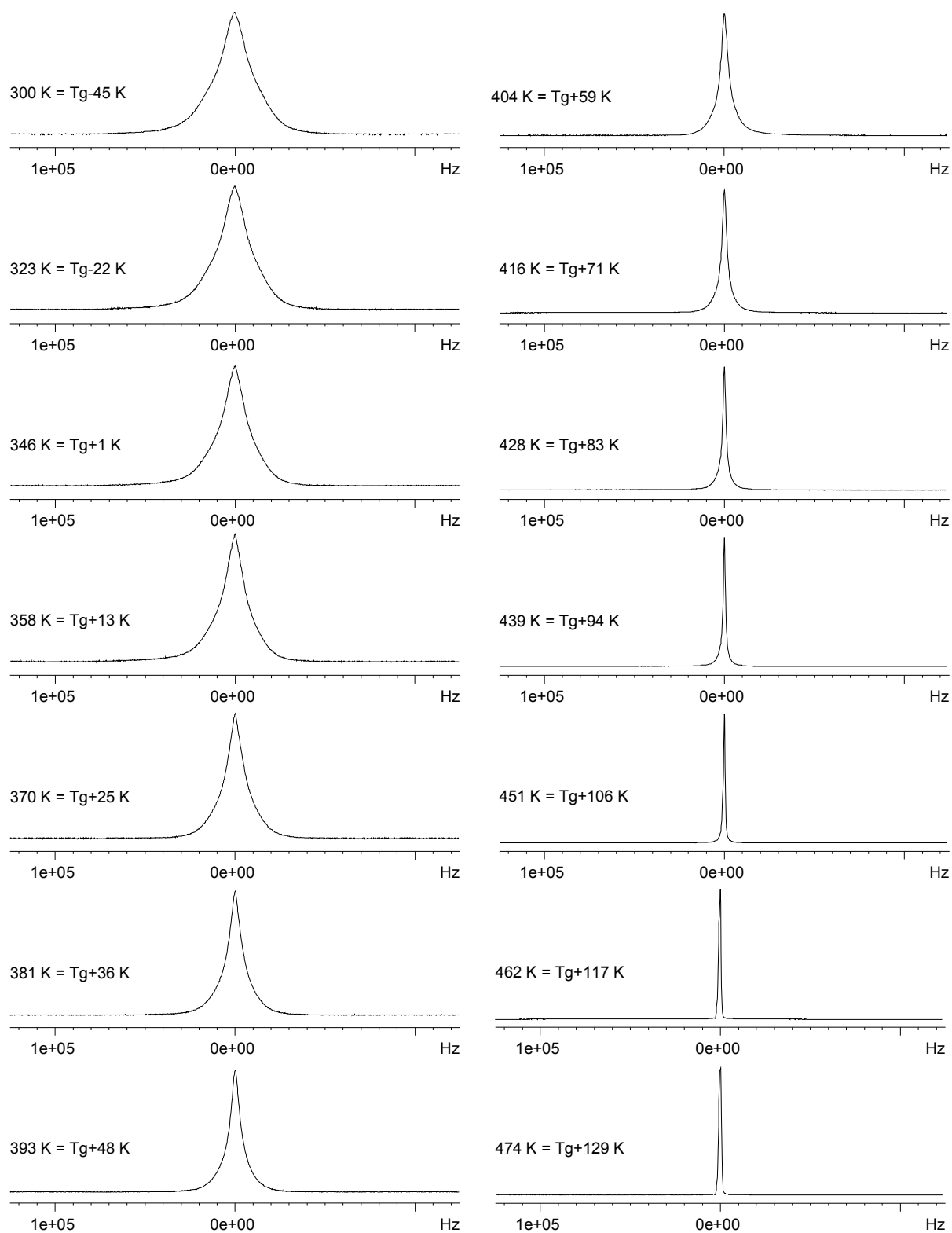


Figure 7- IV-4: Influence of the temperature on the shape of the ^1H spectrum of sample PEMADMC (spectra recorded at a ^1H Larmor frequency of 300.13 MHz, under static conditions).

Part 7, IV (Appendix) NMR spectra and SEC results

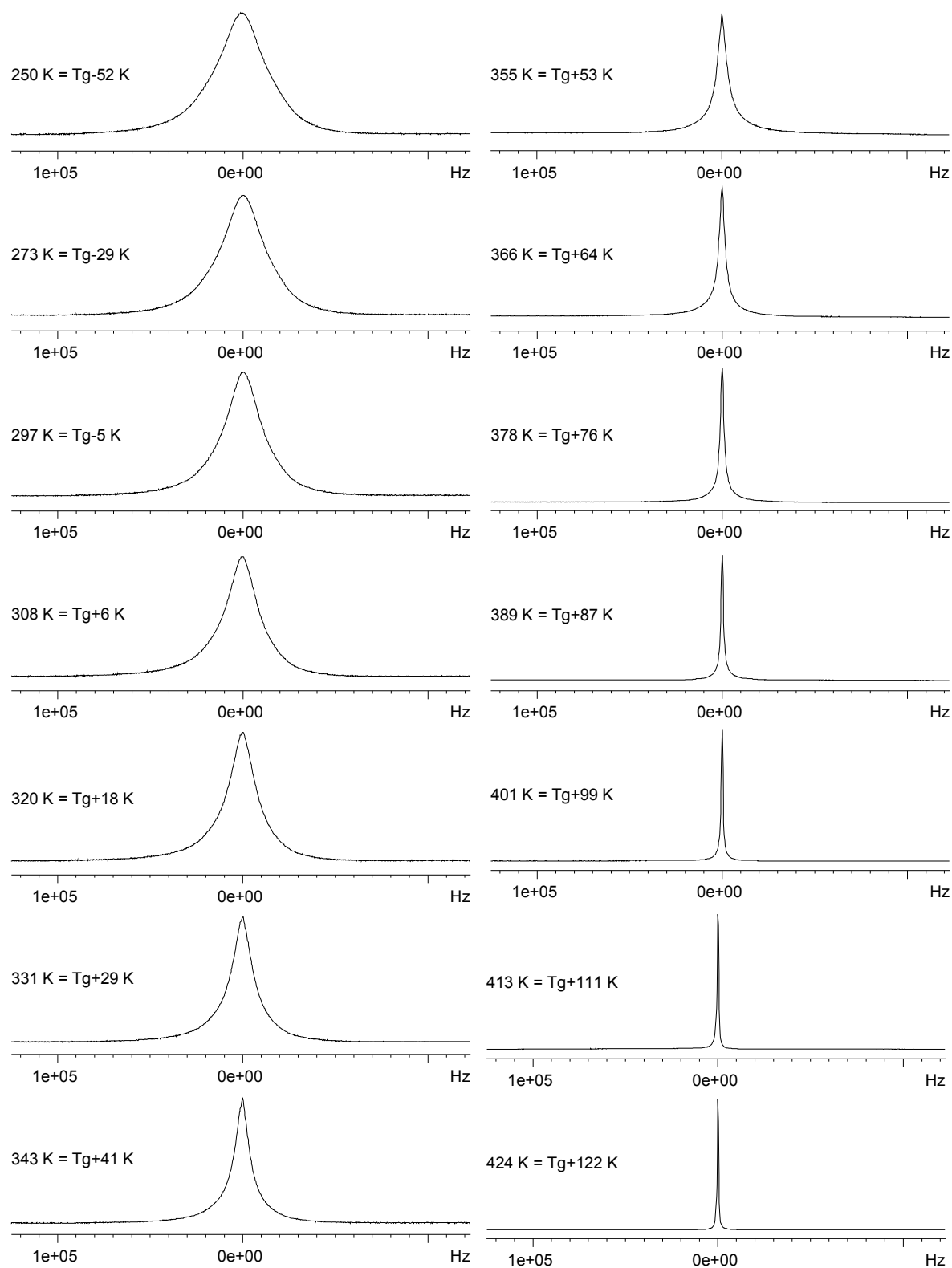


Figure 7- IV-5: Influence of the temperature on the shape of the ^1H spectrum of sample PBMA (spectra recorded at a ^1H Larmor frequency of 300.13 MHz, under static conditions).

Part 7, IV (Appendix) NMR spectra and SEC results

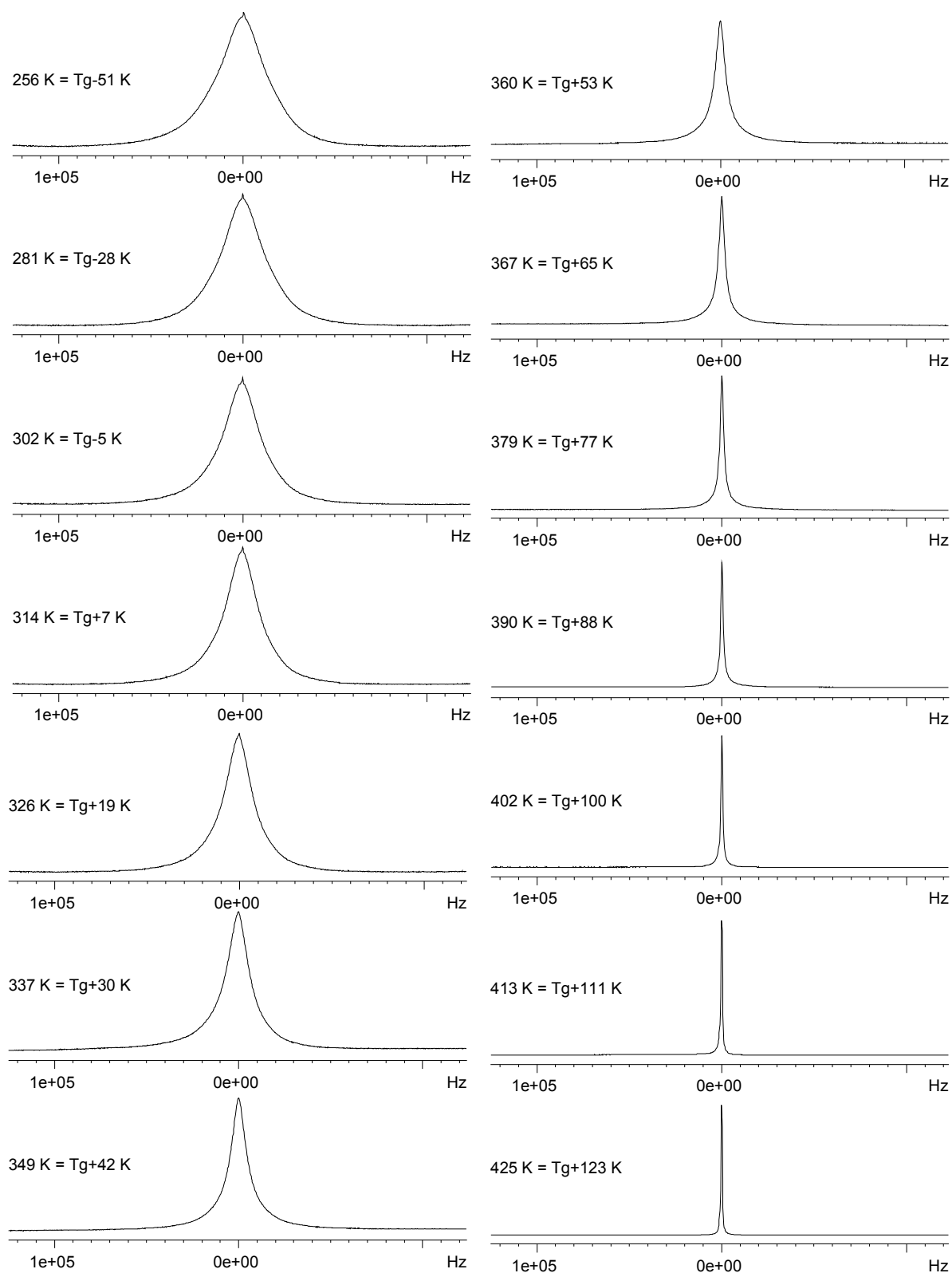


Figure 7- IV-6: Influence of the temperature on the shape of the ^1H spectrum of sample PBMA13C (spectra recorded at a ^1H Larmor frequency of 300.13 MHz, under static conditions).

Part 7, IV (Appendix) NMR spectra and SEC results

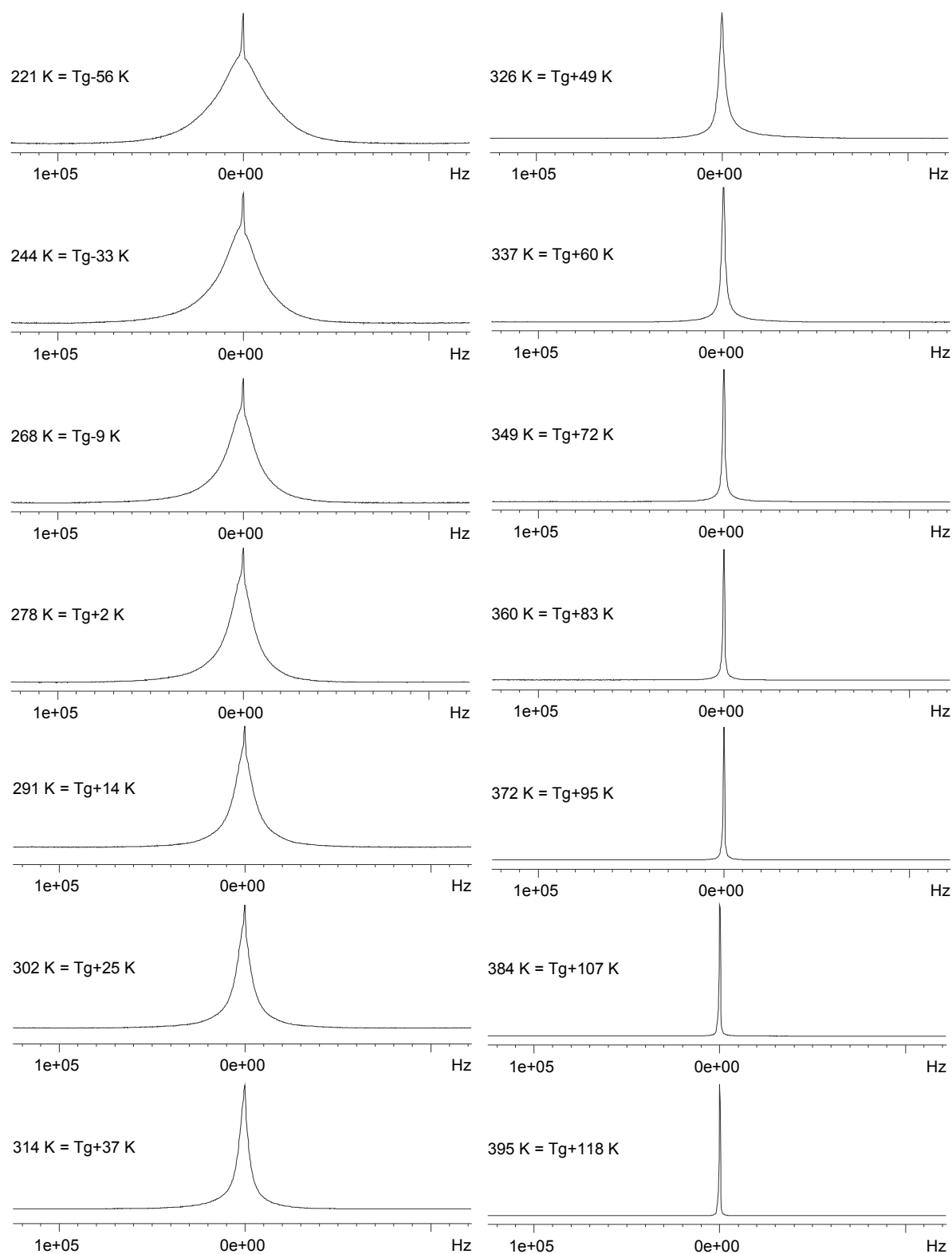


Figure 7- IV-7: Influence of the temperature on the shape of the ^1H spectrum of sample PHMA13C (spectra recorded at a ^1H Larmor frequency of 300.13 MHz, under static conditions).

2. 2D-WISE spectra

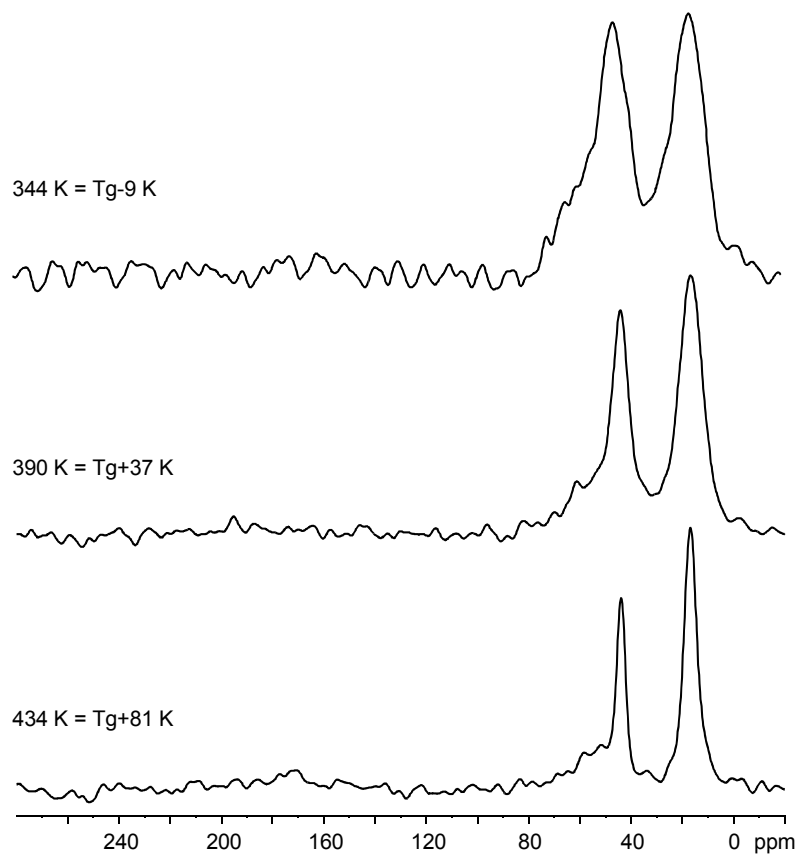


Figure 7-IV-8: 1D ^{13}C spectra extracted from the 2D-WISE spectra of sample PEMADSC (^1H Larmor frequency of 300.13 MHz, static, LG-CP and π -pulse during t_1).

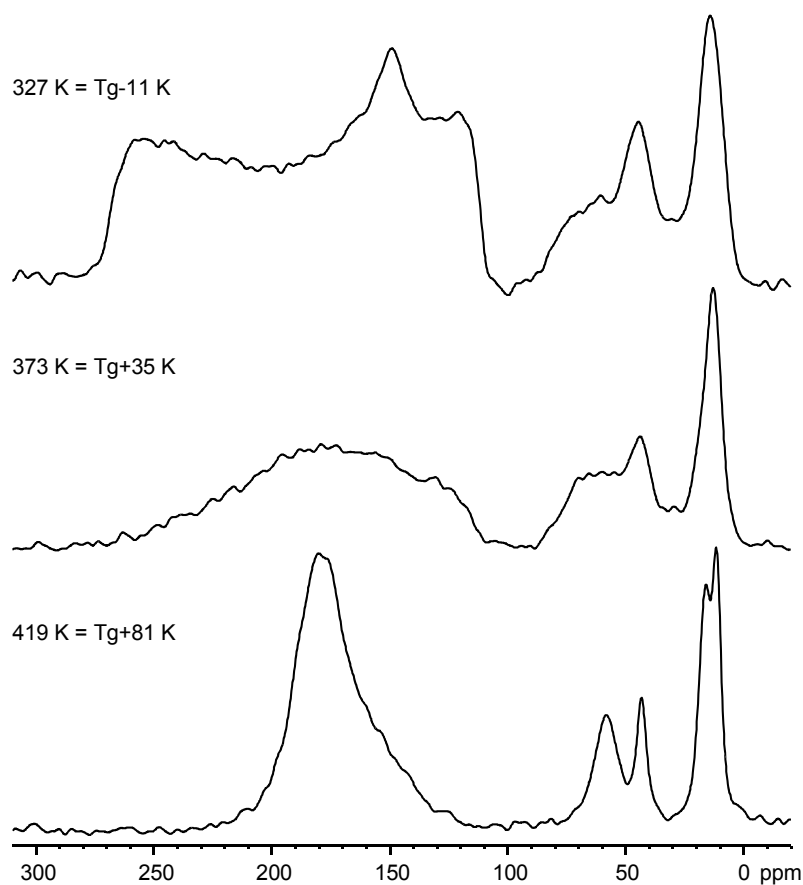


Figure 7-IV-9: 1D ^{13}C spectra extracted from the 2D-WISE spectra of sample PEMA13C (^1H Larmor frequency of 300.13 MHz, static, LG-CP and π -pulse during t_1).

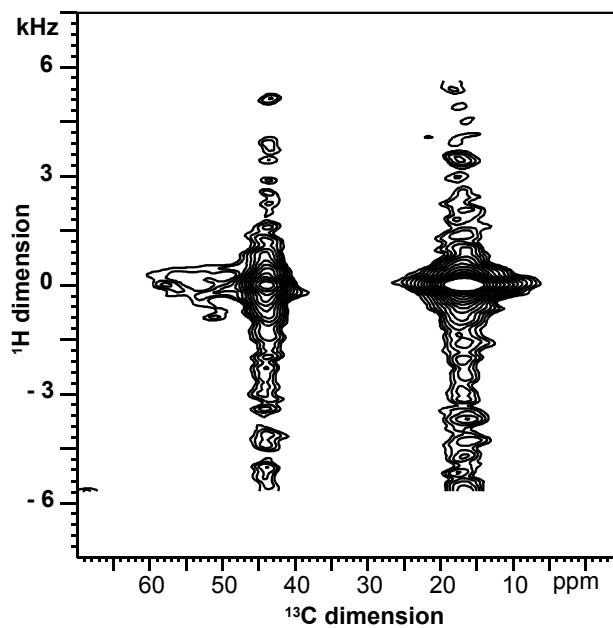
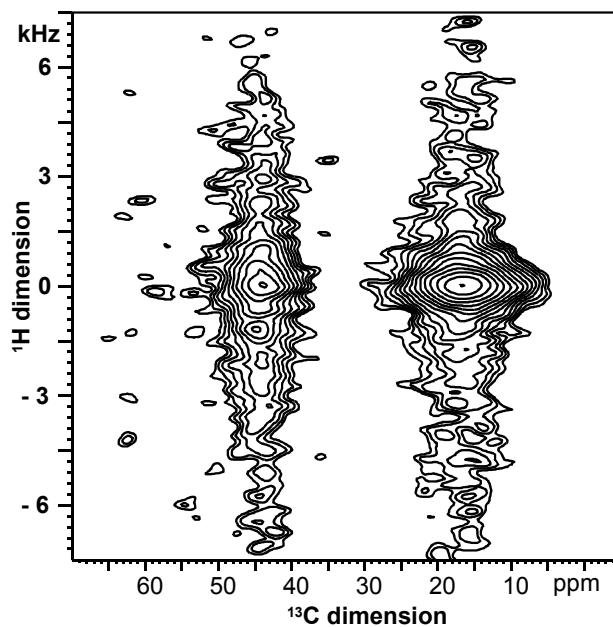
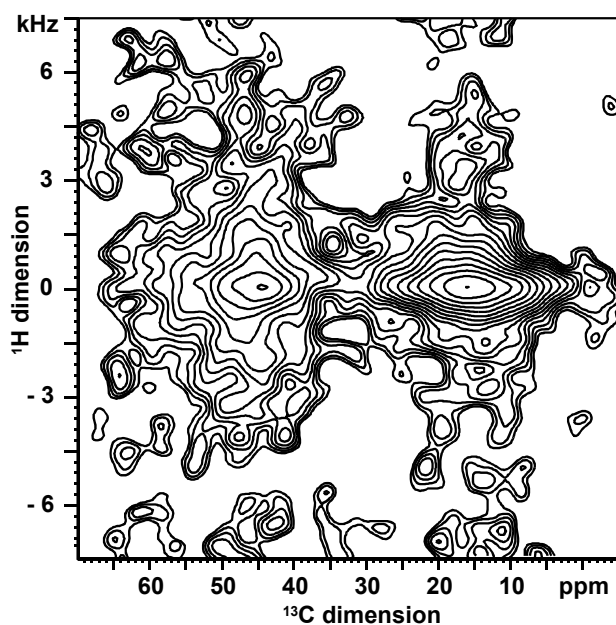


Figure 7- IV-10: Contour spectra extracted from the 2D-WISE spectra of sample PEMADSC (^1H Larmor frequency of 300.13 MHz, static, LG-CP and π -pulse during t_1); top: $T_g - 9$ k, middle: $T_g + 37$ K, bottom: $T_g + 81$ K.

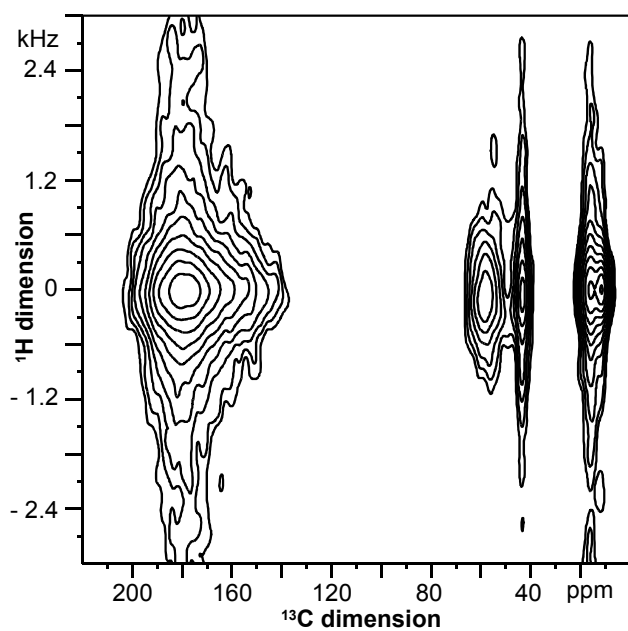
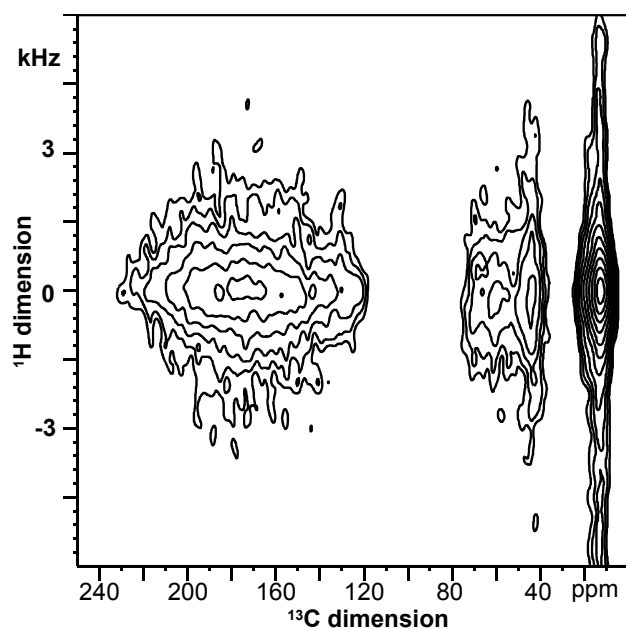
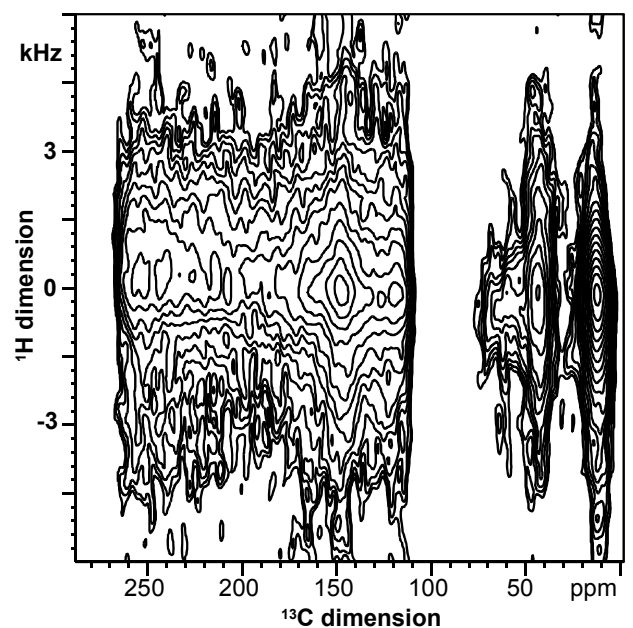


Figure 7-IV-11: Contour spectra extracted from the 2D-WISE spectra of sample PEMA13C (^1H Larmor frequency of 300.13 MHz, static, LG-CP and π -pulse during t_1); top: $T_g - 11$ K, middle: $T_g + 35$ K, bottom: $T_g + 81$ K.

3. NOE data

Sample (M_2)	T (K) / $T - T_g$ (K)	$q_{AB} \cdot \tau_C^{AB}$ (Hz)	τ_C^{AB} (s) from CH_3-CH_2	τ_C^{AB} (s) from M_2	Nb. of exp.
PEMA (342 kHz ²)	397 / 55	710±140 and 77±63	$1.8 \cdot 10^{-4} \pm 4 \cdot 10^{-5}$ and $1.9 \cdot 10^{-5} \pm 1.6 \cdot 10^{-5}$	$8.0 \cdot 10^{-5} \pm 1.6 \cdot 10^{-5}$ and $8.6 \cdot 10^{-6} \pm 7.1 \cdot 10^{-6}$	9
	409 / 67	275±8	$6.9 \cdot 10^{-5} \pm 2 \cdot 10^{-6}$	$3.08 \cdot 10^{-5} \pm 9 \cdot 10^{-7}$	8
	427 / 85	150±10	$3.8 \cdot 10^{-5} \pm 2 \cdot 10^{-6}$	$1.7 \cdot 10^{-5} \pm 1 \cdot 10^{-6}$	8
	442 / 100	93±9	$2.3 \cdot 10^{-5} \pm 2 \cdot 10^{-6}$	$1.0 \cdot 10^{-5} \pm 1 \cdot 10^{-6}$	17
	457 / 115	48±5	$1.2 \cdot 10^{-5} \pm 1 \cdot 10^{-6}$	$5.4 \cdot 10^{-6} \pm 5 \cdot 10^{-7}$	12
PEMADMC (240 kHz ²)	405 / 60	340±80 and 23±35	$6.4 \cdot 10^{-6} \pm 1.5 \cdot 10^{-6}$ and $4.3 \cdot 10^{-7} \pm 6.6 \cdot 10^{-7}$	$5.4 \cdot 10^{-5} \pm 1.3 \cdot 10^{-5}$ and $3.7 \cdot 10^{-6} \pm 5.6 \cdot 10^{-6}$	6
	425 / 80	136 and 3	$3.4 \cdot 10^{-5}$ and $8.5 \cdot 10^{-7}$	$2.2 \cdot 10^{-5}$ and $5.4 \cdot 10^{-7}$	1
	445 / 100	64±6	$1.6 \cdot 10^{-5} \pm 1 \cdot 10^{-6}$	$1.0 \cdot 10^{-5} \pm 1 \cdot 10^{-6}$	5
PBMA (447 kHz ²)	384 / 82	160±40 and 19±27	$4.0 \cdot 10^{-5} \pm 1.1 \cdot 10^{-5}$ and $4.8 \cdot 10^{-6} \pm 6.8 \cdot 10^{-6}$	$1.4 \cdot 10^{-5} \pm 4 \cdot 10^{-6}$ and $1.6 \cdot 10^{-6} \pm 2.3 \cdot 10^{-6}$	15
	387 / 85	100±30 and 12±13	$2.5 \cdot 10^{-5} \pm 8 \cdot 10^{-6}$ and $3.1 \cdot 10^{-5} \pm 3.6 \cdot 10^{-6}$	$8.5 \cdot 10^{-6} \pm 2.6 \cdot 10^{-6}$ and $1.1 \cdot 10^{-6} \pm 1.1 \cdot 10^{-6}$	10
	402 / 100	41±4	$1.02 \cdot 10^{-5} \pm 9 \cdot 10^{-7}$	$3.5 \cdot 10^{-6} \pm 3 \cdot 10^{-7}$	9
	417 / 115	24±1	$5.9 \cdot 10^{-6} \pm 2 \cdot 10^{-7}$	$2.02 \cdot 10^{-6} \pm 6 \cdot 10^{-8}$	8
	432 / 130	15±1	$3.8 \cdot 10^{-6} \pm 2 \cdot 10^{-7}$	$1.30 \cdot 10^{-6} \pm 8 \cdot 10^{-8}$	12
PBMA13C (319 kHz ²)	384 / 77	117±10	$2.9 \cdot 10^{-5} \pm 3 \cdot 10^{-6}$	$1.4 \cdot 10^{-5} \pm 1 \cdot 10^{-6}$	6
PHMA13C (447 kHz ²)	332 / 55	140±10	$3.5 \cdot 10^{-5} \pm 3 \cdot 10^{-6}$	$1.2 \cdot 10^{-5} \pm 1 \cdot 10^{-6}$	8
	349 / 72	78±6	$1.9 \cdot 10^{-5} \pm 1 \cdot 10^{-6}$	$6.6 \cdot 10^{-6} \pm 5 \cdot 10^{-7}$	8
	362 / 85	47±4	$1.3 \cdot 10^{-5} \pm 1 \cdot 10^{-6}$	$4.0 \cdot 10^{-6} \pm 4 \cdot 10^{-7}$	9
	377 / 100	28±2	$7.0 \cdot 10^{-6} \pm 7 \cdot 10^{-7}$	$2.4 \cdot 10^{-6} \pm 1 \cdot 10^{-7}$	8
	392 / 115	16±1	$4.0 \cdot 10^{-6} \pm 2 \cdot 10^{-7}$	$1.37 \cdot 10^{-6} \pm 8 \cdot 10^{-8}$	9

Table 7-IV-1: Correlation times of local molecular motion extracted from the NOE experiment with dipolar filter for model PnAMAs.

Sample	Process	$\log A$	A (s)	E_a/R	E_a (kJ.mol ⁻¹)	R^2	ref.
PEMA and PEMADMC	β -relaxation	-12.2	$6 \cdot 10^{-13}$	3.21	26.7	0.998	²²¹ , Θ O
		-13.7	$2 \cdot 10^{-14}$	3.77	31.3	0.9998	²²¹ , \oplus
	NOE from CH_3-CH_2	-12.2	$7 \cdot 10^{-13}$	3.30	27.4	0.973	p.w.
	NOE from M_2	-12.5	$3 \cdot 10^{-13}$	3.30	27.5	0.976	p.w.
PBMA and PBMA13C	β -relaxation	-20.6	$2.5 \cdot 10^{-21}$	5.83	48.5	0.995	¹⁵⁰
	NOE from CH_3-CH_2	-13.2	$6 \cdot 10^{-14}$	3.35	27.9	0.970	p.w.
	NOE from M_2	-14.2	$6 \cdot 10^{-15}$	3.56	29.6	0.970	p.w.
PHMA13C	β -relaxation	-21.2	$6 \cdot 10^{-22}$	5.65	47.0	0.990	¹⁵⁰
		-24.4	$5 \cdot 10^{-24}$	6.54	54.4	0.998	¹⁵⁰
	NOE from CH_3-CH_2	-10.6	$3 \cdot 10^{-11}$	2.05	17.0	0.997	p.w.
	NOE from M_2	-11.1	$9 \cdot 10^{-12}$	2.05	17.0	0.997	p.w.

Table 7-IV-2: Prefactor A and activation energy E_a for the relaxations processes detected in model PnAMAs and following an Arrhenius behavior; the abbreviations R^2 and p.w. designate respectively the coefficient of determination and the present work.

B. NMR spectra of model poly(n-alkyl acrylates)

1. ^1H static spectra

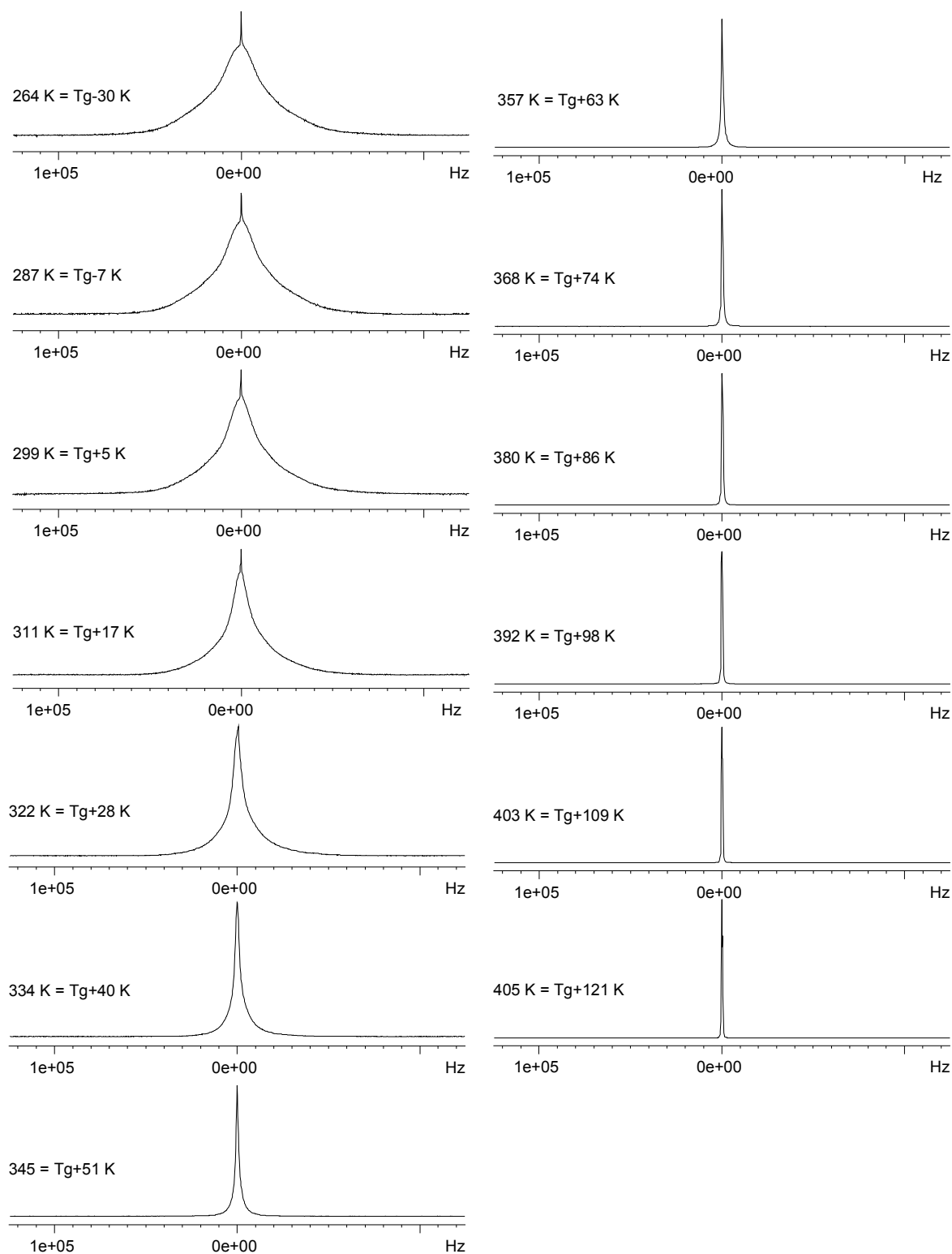


Figure 7- IV-12: Influence of the temperature on the shape of the ^1H spectrum of sample PMA (spectra recorded at a ^1H Larmor frequency of 300.13 MHz, under static conditions).

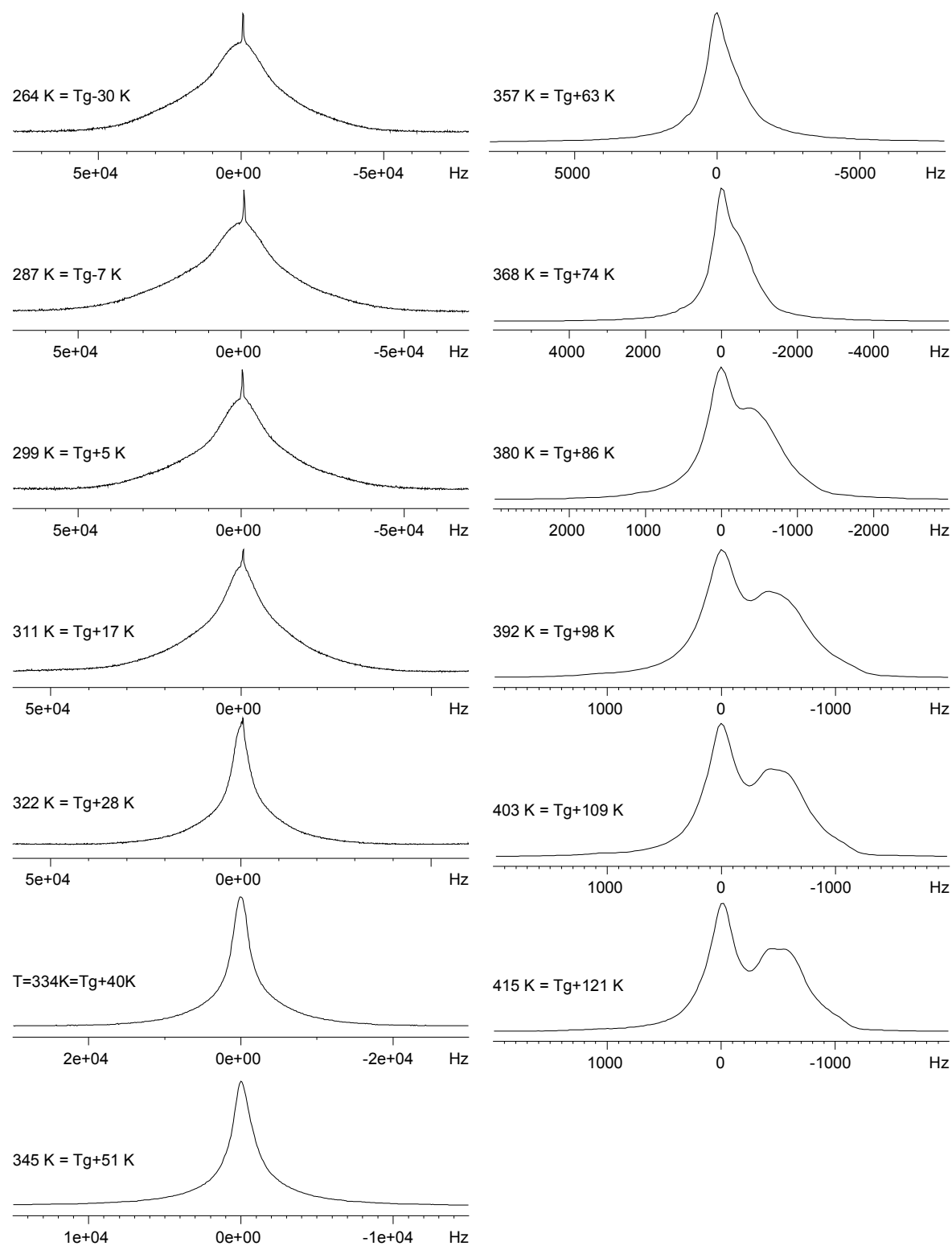


Figure 7- IV-13: Influence of the temperature on the shape of the ^1H spectrum of sample PMA (spectra recorded at a ^1H Larmor frequency of 300.13 MHz, under static conditions).

Part 7, IV (Appendix) NMR spectra and SEC results

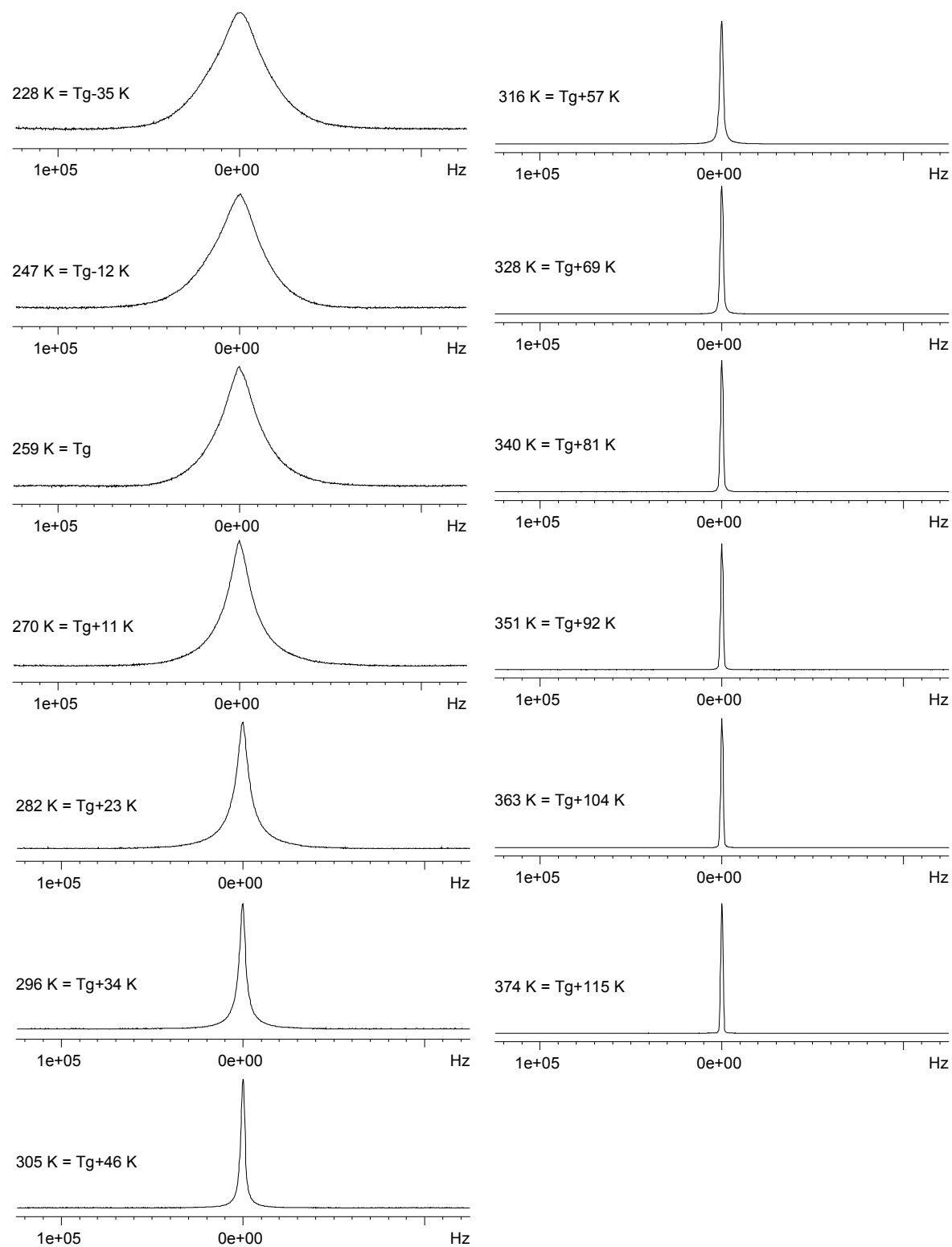


Figure 7- IV-14: Influence of the temperature on the shape of the ^1H spectrum of sample PEA (spectra recorded at a ^1H Larmor frequency of 300.13 MHz, under static conditions).

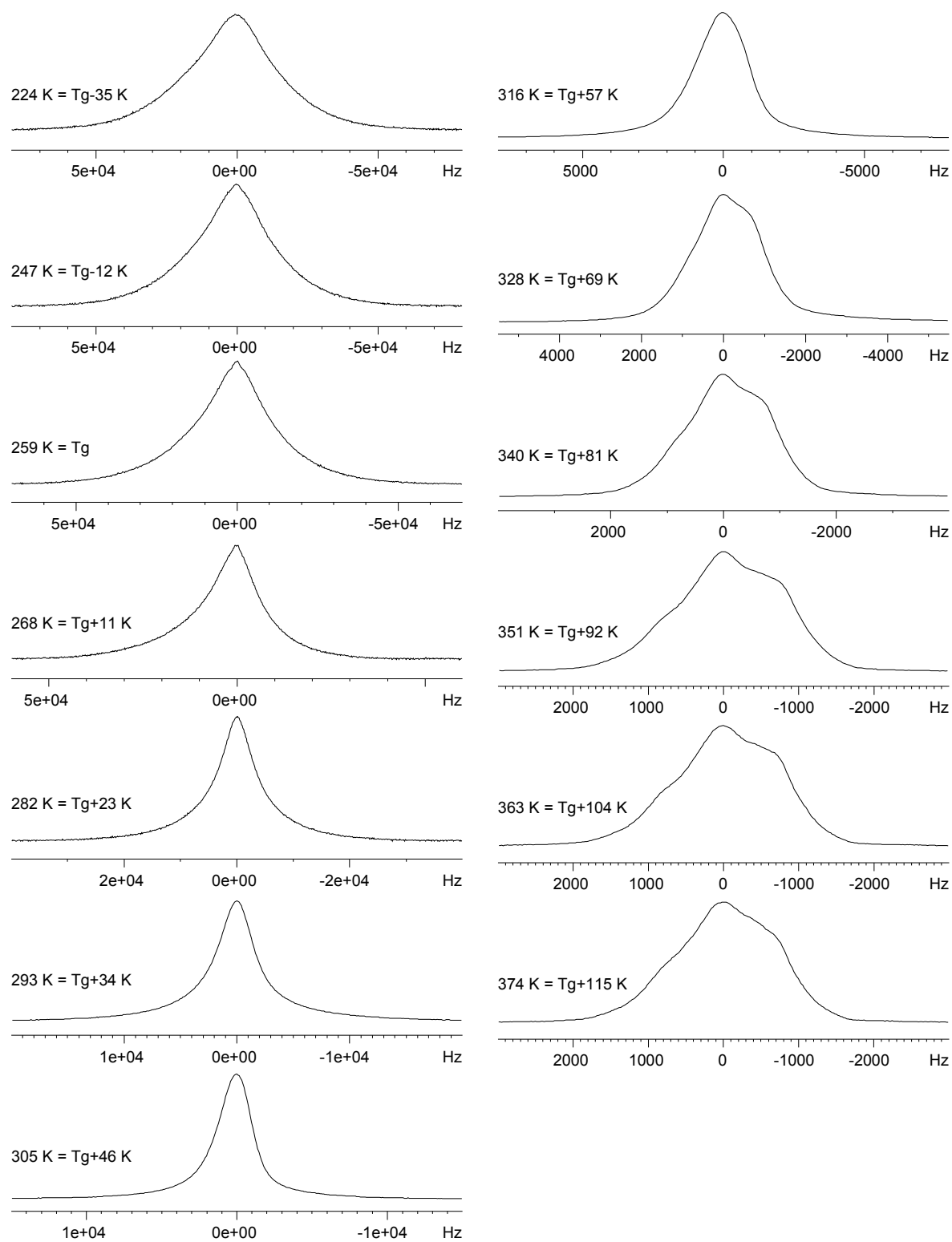


Figure 7- IV-15: Influence of the temperature on the shape of the ^1H spectrum of sample PEA (spectra recorded at a ^1H Larmor frequency of 300.13 MHz, under static conditions).

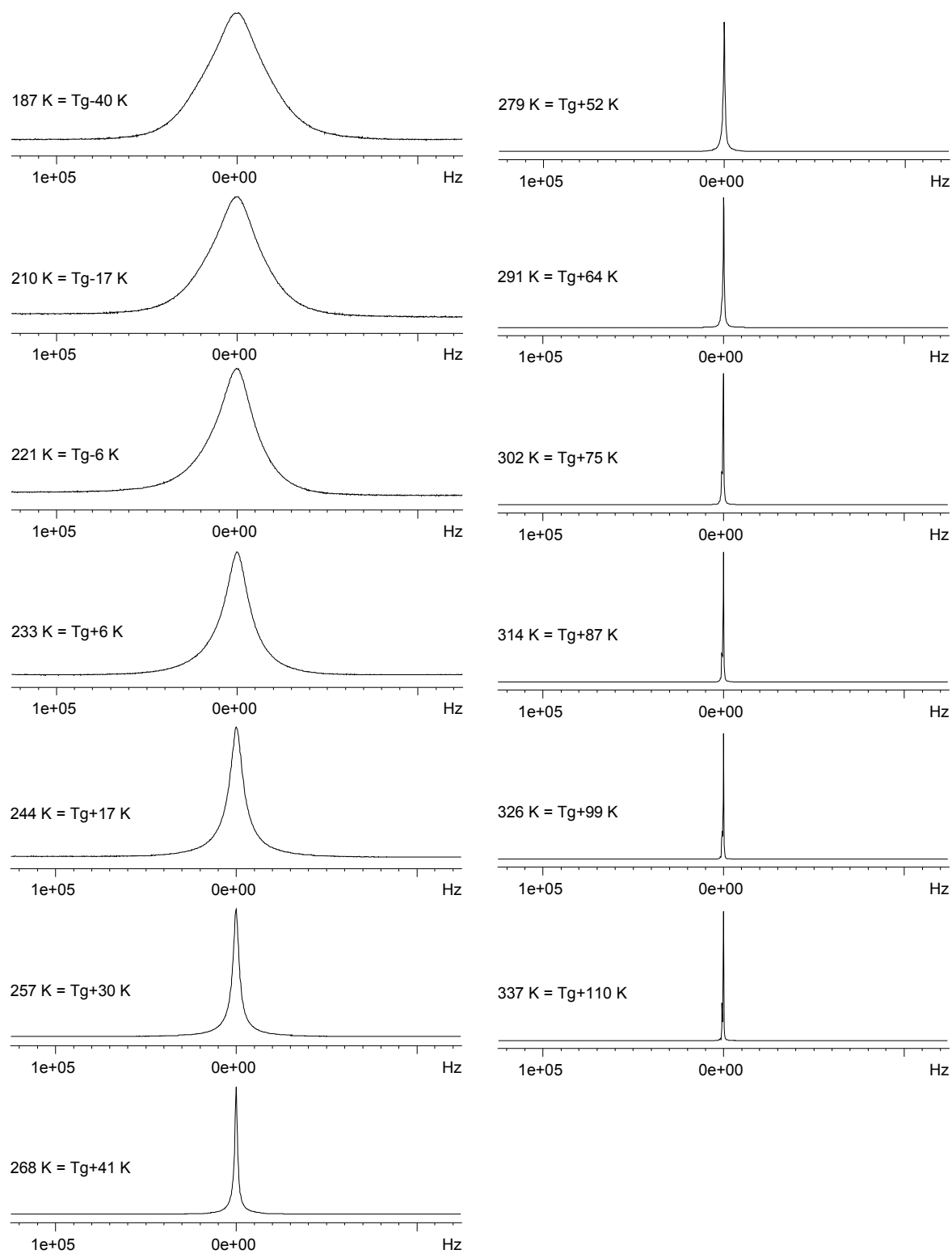


Figure 7- IV-16: Influence of the temperature on the shape of the ^1H spectrum of sample PBA (spectra recorded at a ^1H Larmor frequency of 300.13 MHz, under static conditions).

Part 7, IV (Appendix) NMR spectra and SEC results

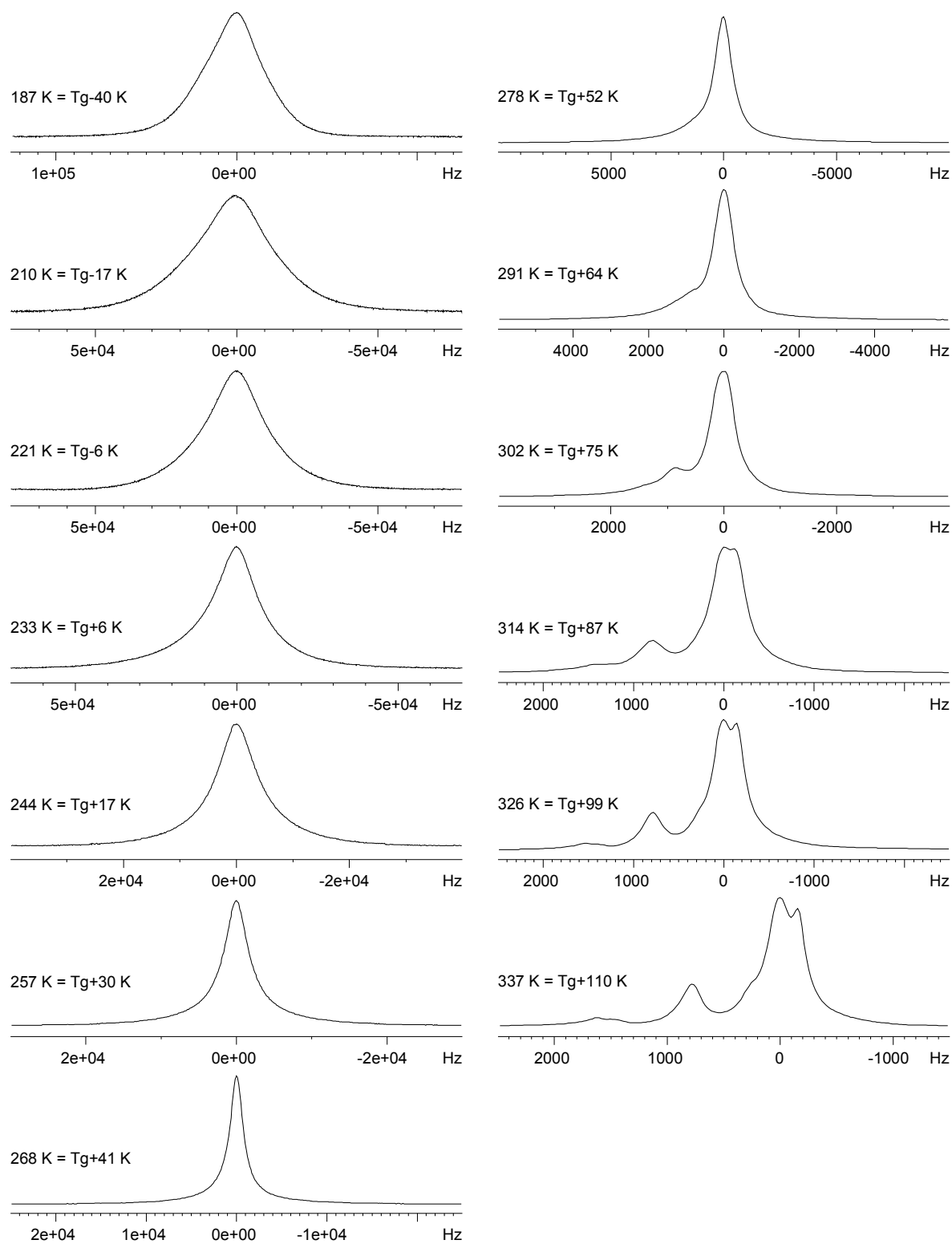


Figure 7-IV-17: Influence of the temperature on the shape of the ^1H spectrum of sample PBA (spectra recorded at a ^1H Larmor frequency of 300.13 MHz, under static conditions).

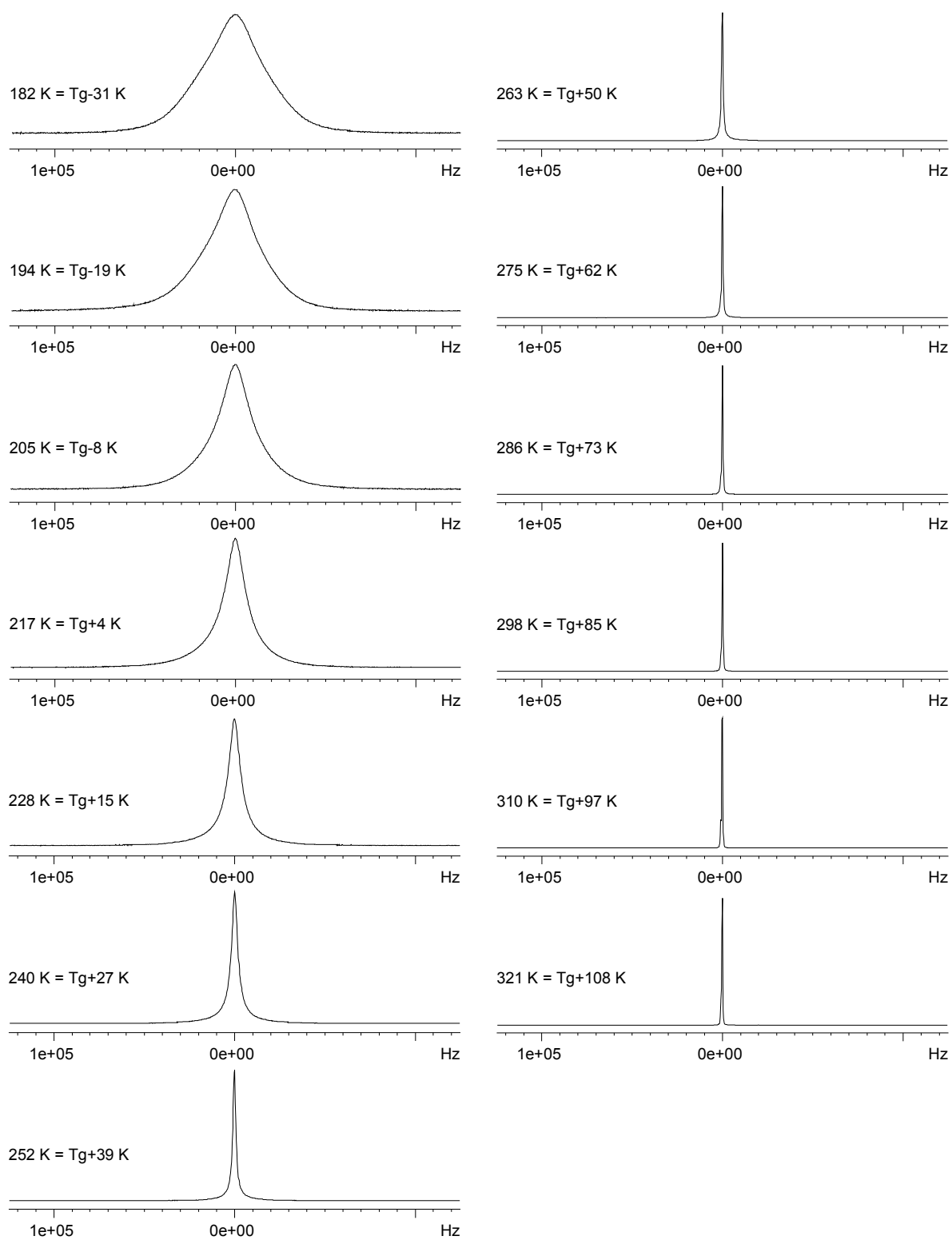


Figure 7- IV-18: Influence of the temperature on the shape of the ^1H spectrum of sample PHxA (spectra recorded at a ^1H Larmor frequency of 300.13 MHz, under static conditions).

Part 7, IV (Appendix) NMR spectra and SEC results

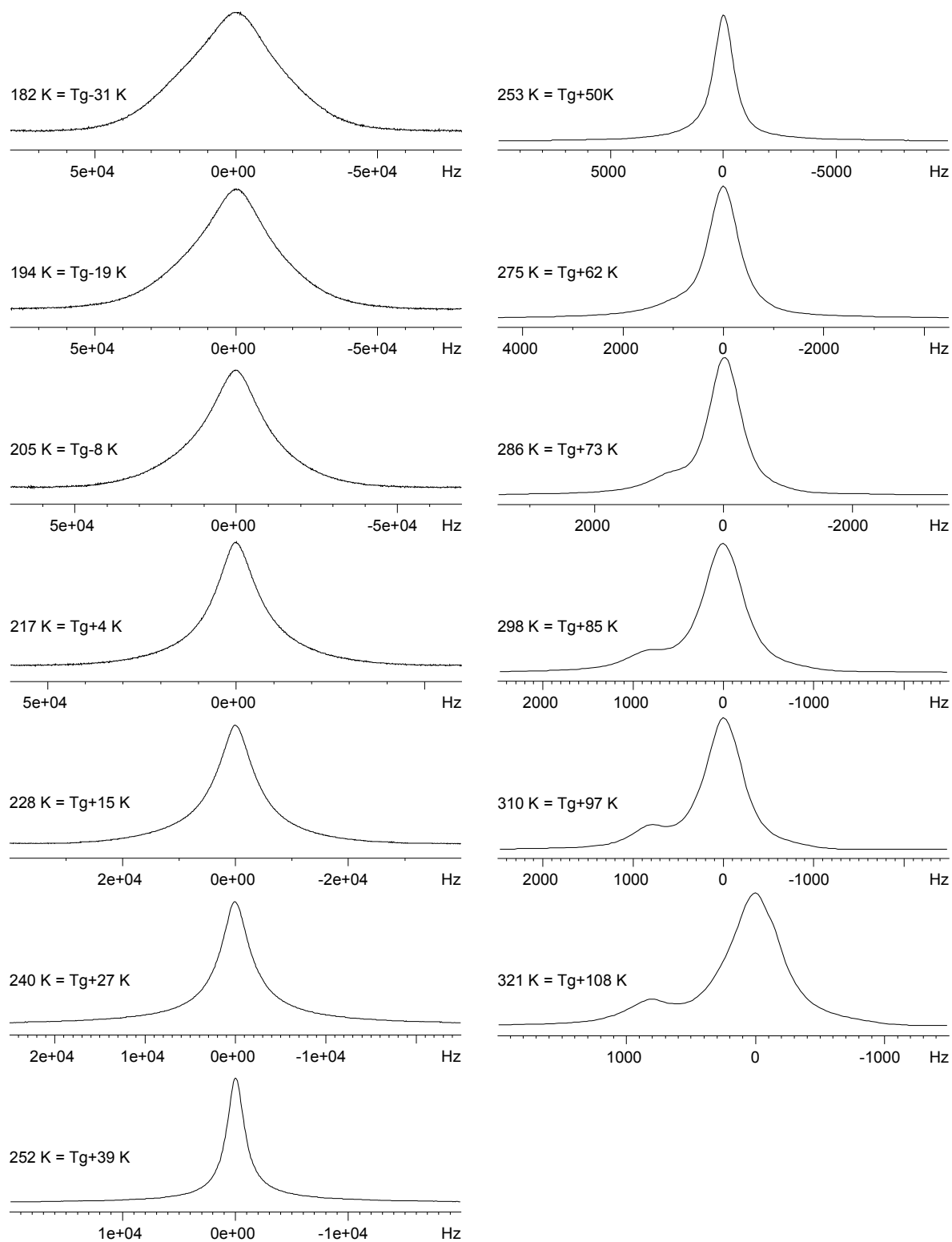


Figure 7- IV-19: Influence of the temperature on the shape of the ^1H spectrum of sample PHxA (spectra recorded at a ^1H Larmor frequency of 300.13 MHz, under static conditions)

2. 2D-WISE spectra

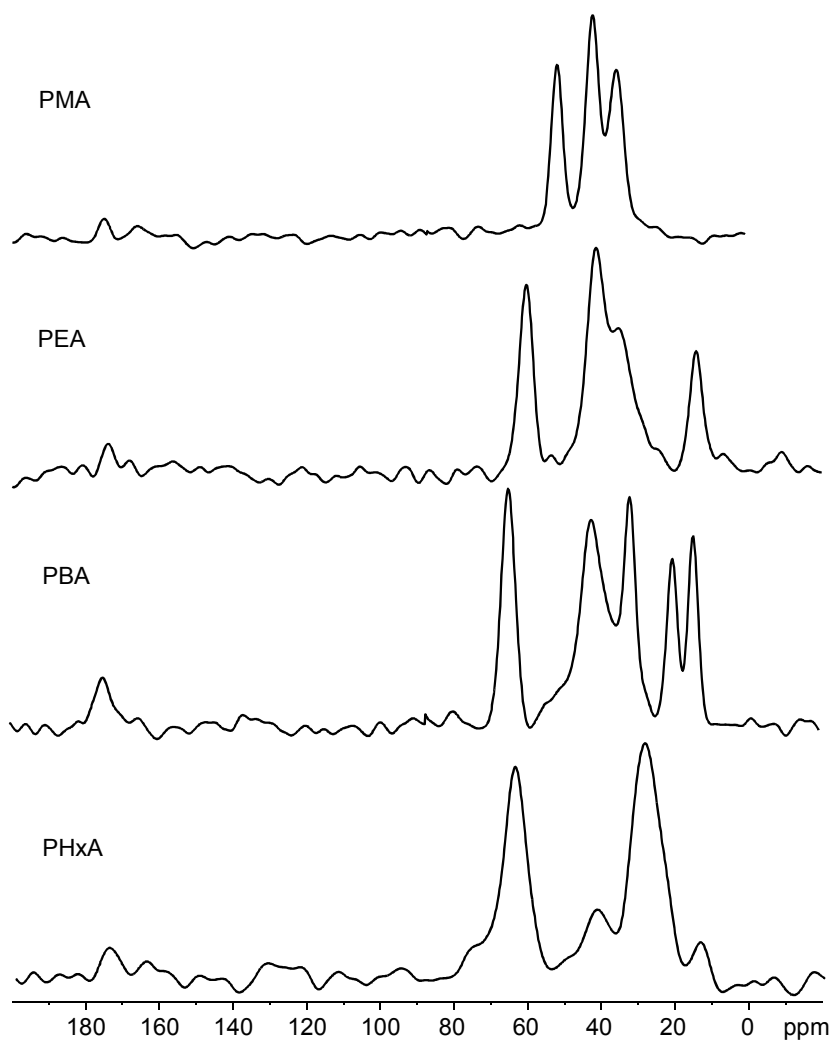


Figure 7- IV-20: 1D ^{13}C spectra extracted from the 2D-WISE spectra of model PnAAs at $T_g+70^\circ\text{C}$ (^1H Larmor frequency of 300.13 MHz, static, LG-CP and π -pulse during t_1).

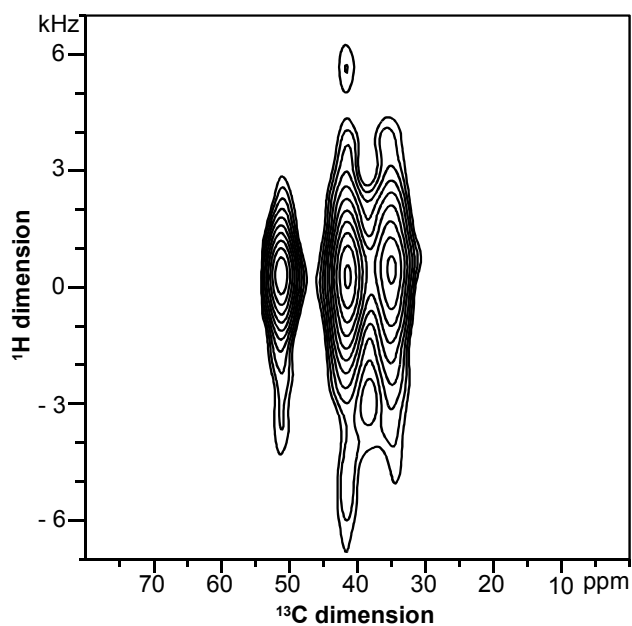


Figure 7- IV-21: Contour spectrum extracted from the 2D-WISE spectrum of sample PMA at $T_g+70^\circ\text{C}$ (^1H Larmor frequency of 300.13 MHz, static, LG-CP and π -pulse during t_1).

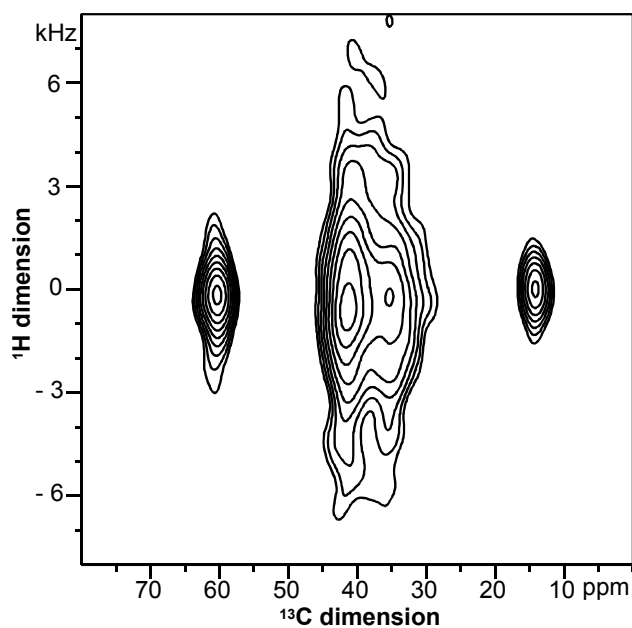


Figure 7-IV-22: Contour spectrum extracted from the 2D-WISE spectrum of sample PEA at T_g+70 °C (^1H Larmor frequency of 300.13 MHz, static, LG-CP and π -pulse during t_1).

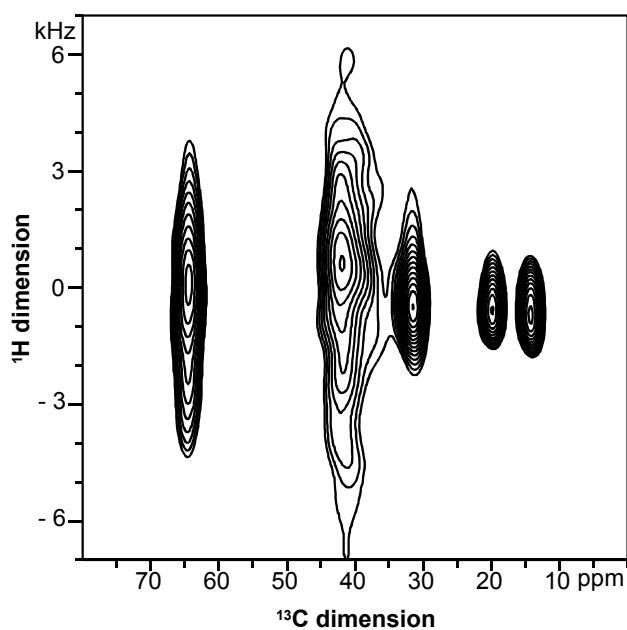


Figure 7-IV-23: Contour spectrum extracted from the 2D-WISE spectrum of sample PBA at T_g+70 °C (^1H Larmor frequency of 300.13 MHz, static, LG-CP and π -pulse during t_1).

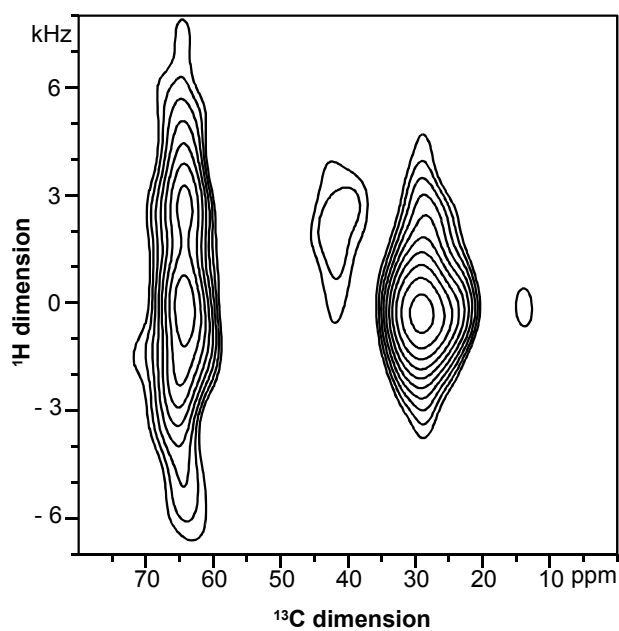


Figure 7-IV-24: Contour spectrum extracted from the 2D-WISE spectrum of sample PHxA at T_g+70 °C (^1H Larmor frequency of 300.13 MHz, static, LG-CP and π -pulse during t_1).

3. NOE data

Sample (M_2)	T (K) / $T - T_g$ (K)	$q_{AB} \cdot \tau_C^{AB}$ (Hz)	τ_C^{AB} (s) from CH_3-CH_2	τ_C^{AB} (s) from M_2	Nb. of exp.
PMA (322 kHz ²)	334 / 40	141.0±0.6	$3.54 \cdot 10^{-5} \pm 2 \cdot 10^{-7}$	$1.675 \cdot 10^{-5} \pm 7 \cdot 10^{-8}$	2
	368 / 74	26±1	$6.6 \cdot 10^{-6} \pm 3 \cdot 10^{-7}$	$3.1 \cdot 10^{-6} \pm 1 \cdot 10^{-7}$	9
	379 / 85	15±0.3	$3.76 \cdot 10^{-6} \pm 8 \cdot 10^{-8}$	$1.78 \cdot 10^{-6} \pm 4 \cdot 10^{-8}$	8
	394 / 100	9.0±0.3	$2.26 \cdot 10^{-6} \pm 7 \cdot 10^{-8}$	$1.07 \cdot 10^{-6} \pm 3 \cdot 10^{-8}$	7
PEA (442 kHz ²)	279 / 20	380±20	$9.6 \cdot 10^{-5} \pm 4 \cdot 10^{-6}$	$3.3 \cdot 10^{-5} \pm 1 \cdot 10^{-6}$	4
	299 / 40	145±8	$3.6 \cdot 10^{-5} \pm 2 \cdot 10^{-6}$	$1.25 \cdot 10^{-5} \pm 7 \cdot 10^{-6}$	7
	314 / 55	63±2	$1.58 \cdot 10^{-5} \pm 4 \cdot 10^{-7}$	$5.5 \cdot 10^{-6} \pm 1 \cdot 10^{-7}$	8
	328 / 69	25.8±0.5	$6.5 \cdot 10^{-6} \pm 1 \cdot 10^{-7}$	$2.23 \cdot 10^{-6} \pm 5 \cdot 10^{-8}$	9
	344 / 85	13±2	$3.3 \cdot 10^{-6} \pm 4 \cdot 10^{-7}$	$1.1 \cdot 10^{-6} \pm 1 \cdot 10^{-7}$	8
	359 / 100	8.2±0.6	$2.1 \cdot 10^{-6} \pm 2 \cdot 10^{-7}$	$7.1 \cdot 10^{-7} \pm 5 \cdot 10^{-8}$	9
PBA (375 kHz ²)	247 / 20	317±4	$8.0 \cdot 10^{-5} \pm 1 \cdot 10^{-6}$	$3.23 \cdot 10^{-5} \pm 5 \cdot 10^{-7}$	3
	267 / 40	110±20	$2.8 \cdot 10^{-5} \pm 4 \cdot 10^{-6}$	$1.1 \cdot 10^{-5} \pm 2 \cdot 10^{-6}$	20
	282 / 55	52±2	$1.31 \cdot 10^{-5} \pm 6 \cdot 10^{-7}$	$5.3 \cdot 10^{-6} \pm 2 \cdot 10^{-7}$	7
	291 / 64	31±1	$7.7 \cdot 10^{-6} \pm 3 \cdot 10^{-7}$	$3.1 \cdot 10^{-6} \pm 1 \cdot 10^{-8}$	9
	297 / 70	24±2	$6.1 \cdot 10^{-6} \pm 5 \cdot 10^{-7}$	$2.5 \cdot 10^{-6} \pm 2 \cdot 10^{-7}$	18
	312 / 85	15±2	$3.8 \cdot 10^{-6} \pm 5 \cdot 10^{-7}$	$1.5 \cdot 10^{-6} \pm 2 \cdot 10^{-7}$	9
	327 / 100	8.4±0.2	$2.11 \cdot 10^{-6} \pm 4 \cdot 10^{-8}$	$8.6 \cdot 10^{-7} \pm 2 \cdot 10^{-8}$	9
PHxA (335 kHz ²)	233 / 20	247±6	$6.2 \cdot 10^{-5} \pm 1 \cdot 10^{-6}$	$2.82 \cdot 10^{-5} \pm 7 \cdot 10^{-7}$	6
	253 / 40	100±20	$2.4 \cdot 10^{-5} \pm 4 \cdot 10^{-6}$	$1.1 \cdot 10^{-5} \pm 2 \cdot 10^{-6}$	9
	268 / 55	46±2	$1.15 \cdot 10^{-5} \pm 4 \cdot 10^{-7}$	$5.2 \cdot 10^{-6} \pm 2 \cdot 10^{-7}$	8
	275 / 62	34±2	$8.6 \cdot 10^{-6} \pm 6 \cdot 10^{-7}$	$3.9 \cdot 10^{-6} \pm 3 \cdot 10^{-7}$	9
	298 / 85	11.2±0.3	$2.81 \cdot 10^{-6} \pm 6 \cdot 10^{-8}$	$1.28 \cdot 10^{-6} \pm 3 \cdot 10^{-8}$	8
	313 / 100	6.0±0.1	$1.51 \cdot 10^{-6} \pm 3 \cdot 10^{-8}$	$6.8 \cdot 10^{-7} \pm 2 \cdot 10^{-8}$	8

Table 7- IV-3: Correlation times of local molecular motion extracted from the NOE experiment with dipolar filter for model PnAAs

Sample	Process	$\log A$	A (s)	E_a/R	E_a (kJ.mol ⁻¹)	R^2	ref.
PMA	local relaxation	-13.0	$9 \cdot 10^{-14}$	1.46	12.1	0.997	²⁴⁶
		-13.7	$2 \cdot 10^{-14}$	1.69	14.1	0.999	²⁵⁵
		-13.9	$1 \cdot 10^{-14}$	2.26	18.8	0.999	²⁵²
		-11.2	$6 \cdot 10^{-12}$	1.28	10.7	0.994	²⁵²
		-13.4	$4 \cdot 10^{-14}$	1.78	14.8	1	²⁴⁸
		-12.9	$1 \cdot 10^{-13}$	1.75	14.6	0.991	²⁵³
		-10.3	$5 \cdot 10^{-11}$	1.39	11.6	1	²⁵⁰
	NOE from CH_3-CH_2	-12.4	$4 \cdot 10^{-13}$	2.65	22.0	0.998	p.w.
	NOE from M_2	-12.7	$2 \cdot 10^{-13}$	2.65	22.0	0.998	p.w.
PEA	local relaxation	-11.6	$2 \cdot 10^{-12}$	0.97	8.1	0.982	²⁴⁶
		-14.4	$4 \cdot 10^{-15}$	1.52	12.6	0.998	²⁵⁵
		-9.1	$9 \cdot 10^{-10}$	0.98	8.1	0.995	²⁵⁰
		-12.8	$2 \cdot 10^{-13}$	2.00	13.5	0.999	²⁵³
	NOE from CH_3-CH_2	-11.8	$2 \cdot 10^{-12}$	2.17	18.0	0.994	p.w.
	NOE from M_2	-12.2	$6 \cdot 10^{-13}$	2.17	18.0	0.994	p.w.

PBA	β -relaxation	-13.8	$2 \cdot 10^{-14}$	2.17	18.0	0.982	²⁴⁶
		-13.0	$1 \cdot 10^{-13}$	2.11	17.5	0.993	²²⁹
	local relaxation	-13.3	$5 \cdot 10^{-14}$	1.21	10.1	0.987	²⁴⁶
		-12.8	$2 \cdot 10^{-13}$	1.20	10.0	0.996	²⁵⁵
	NOE from CH ₃ -CH ₂	-10.6	$3 \cdot 10^{-11}$	1.61	13.4	0.998	p.w.
NOE from M ₂	-10.2	$6 \cdot 10^{-11}$	1.61	13.4	0.997	p.w.	
PHxA	β -relaxation	no satisfying fit possible, E_a in the range from 15 to 25 kJ.mol ⁻¹					^{229,246}
	local relaxation	-13.1	$7 \cdot 10^{-14}$	1.22	10.2	0.997	²⁴⁶
	NOE from CH ₃ -CH ₂	-10.5	$3 \cdot 10^{-11}$	1.49	12.3	0.993	p.w.
	NOE from M ₂	-10.1	$9 \cdot 10^{-11}$	1.49	12.3	0.993	p.w.

Table 7- IV-4: Prefactor A and activation energy E_a for the relaxations processes detected in model PnAAs and following an Arrhenius behavior; the abbreviations R^2 and p.w. designate respectively the coefficient of determination and the present work.

C. NMR spectra of PSA samples

1. ¹H static spectra

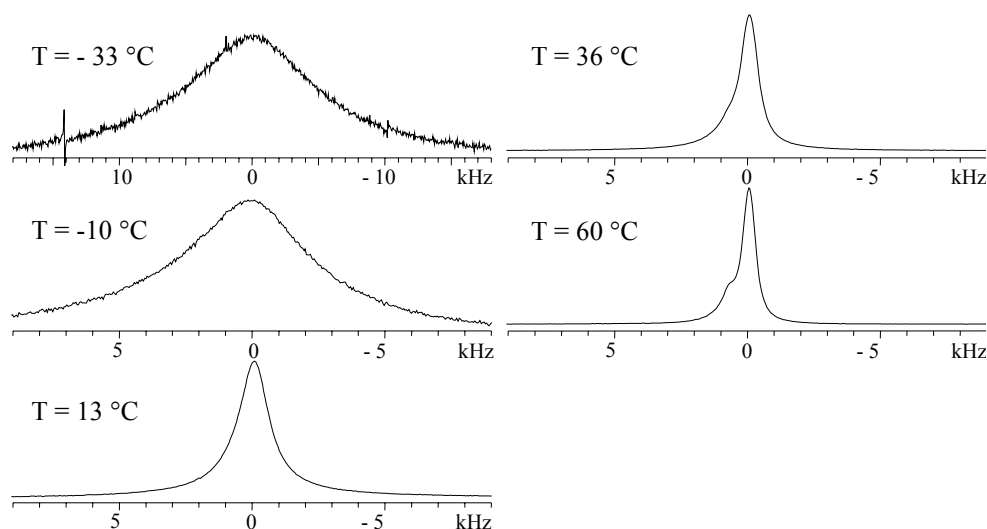


Figure 7- IV-25: Influence of the temperature on the shape of the ¹H spectrum of sample Homo2EHA (spectra recorded at a ¹H Larmor frequency of 300.13 MHz, under static conditions on a Bruker MSL300 spectrometer).

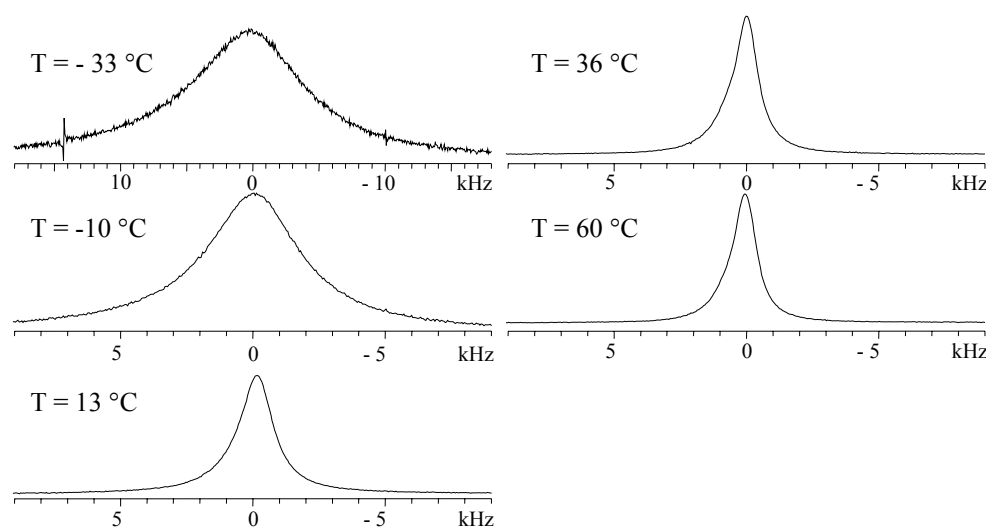


Figure 7- IV-26: Influence of the temperature on the shape of the ¹H spectrum of sample Copol1 (spectra recorded at a ¹H Larmor frequency of 300.13 MHz, under static conditions on a Bruker MSL300 spectrometer).

Part 7, IV (Appendix) NMR spectra and SEC results

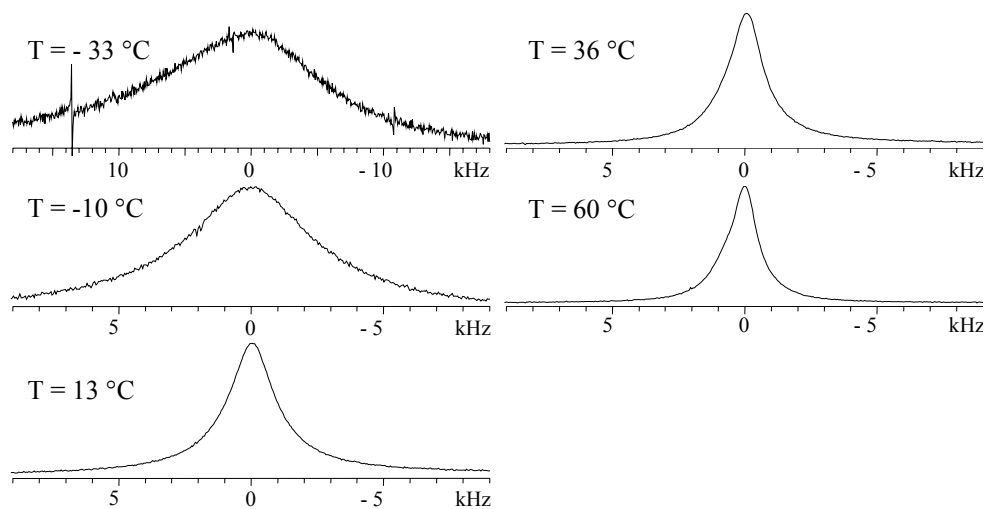


Figure 7-IV-27: Influence of the temperature on the shape of the ^1H spectrum of sample Copo2 (spectra recorded at a ^1H Larmor frequency of 300.13 MHz, under static conditions on a Bruker MSL300 spectrometer).

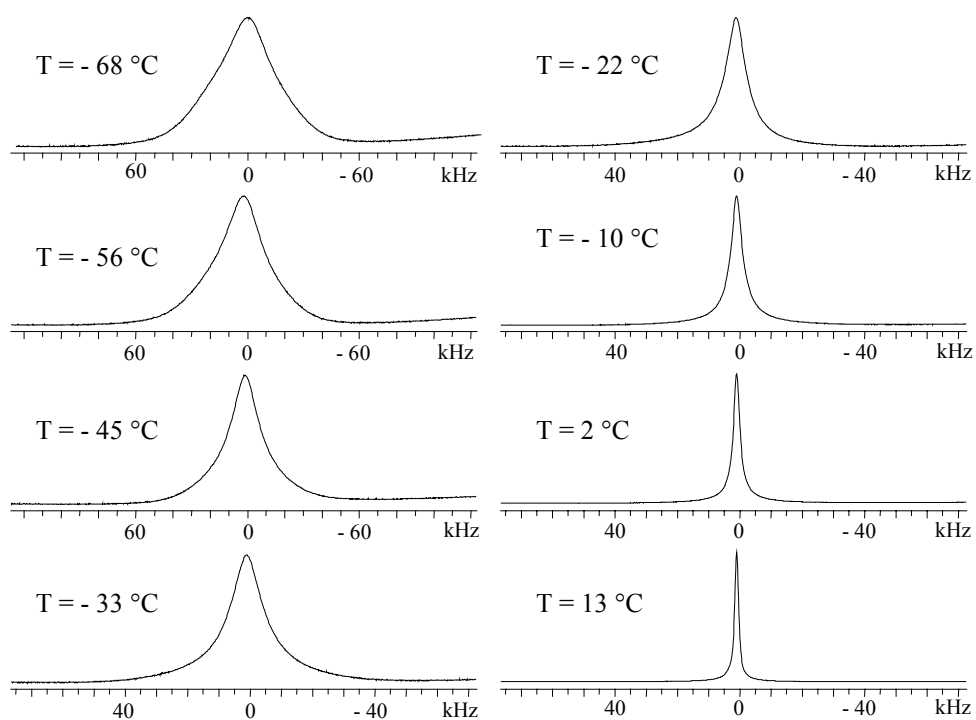


Figure 7-IV-28: Influence of the temperature on the shape of the ^1H spectrum of sample Copo2 (spectra recorded at a ^1H Larmor frequency of 300.13 MHz, under static conditions on a Bruker DSX300 spectrometer).

2. 2D-WISE spectra

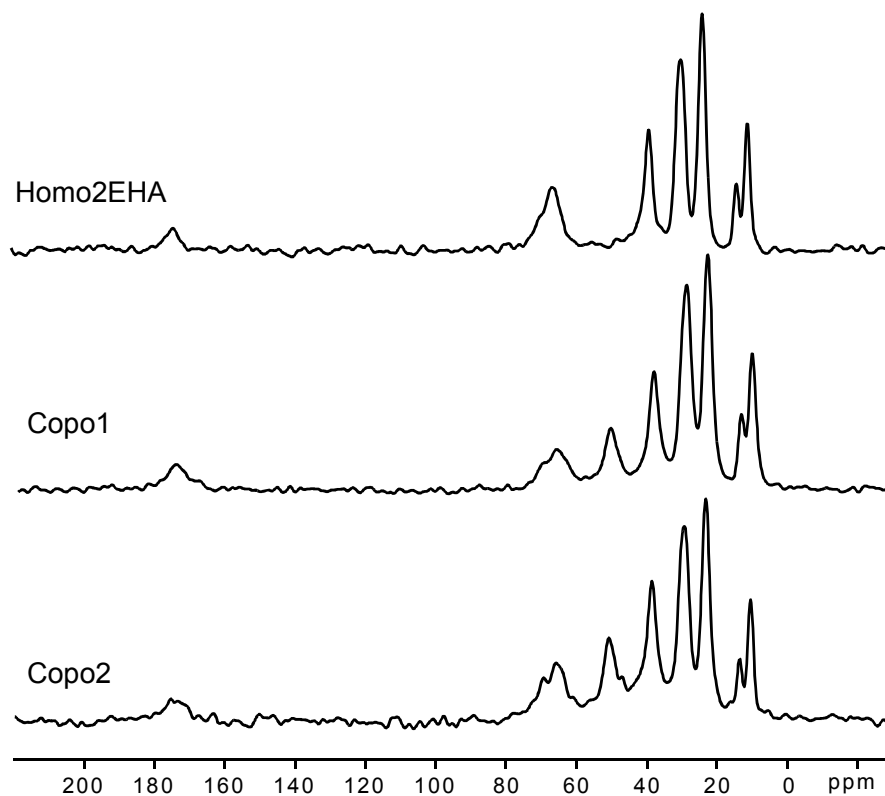


Figure 7- IV-29: 1D ^{13}C spectra extracted from the 2D-WISE spectra of model PSAs at room temperature (^1H Larmor frequency of 300.13 MHz, static, LG-CP and π -pulse during t_1).

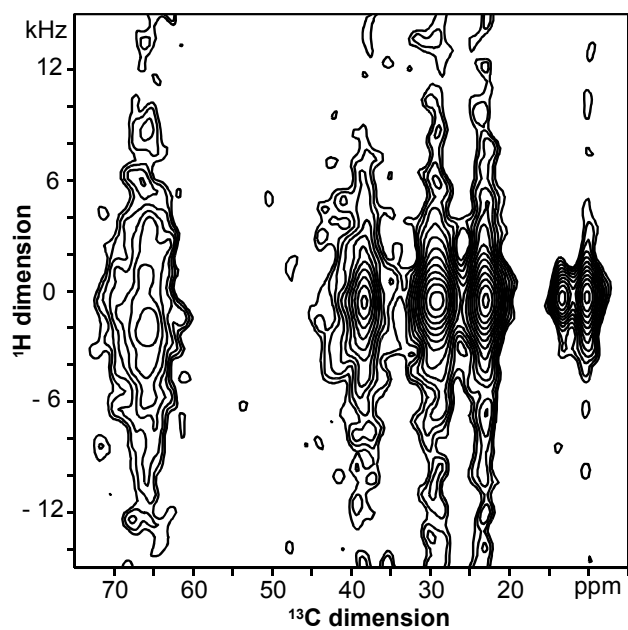
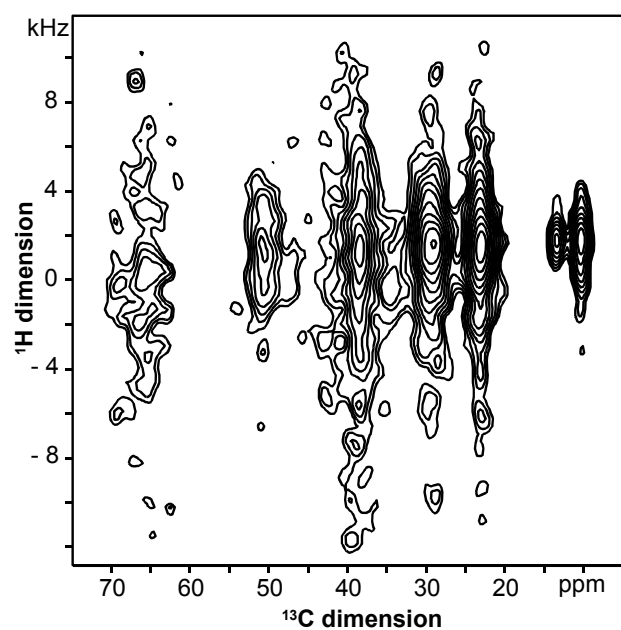
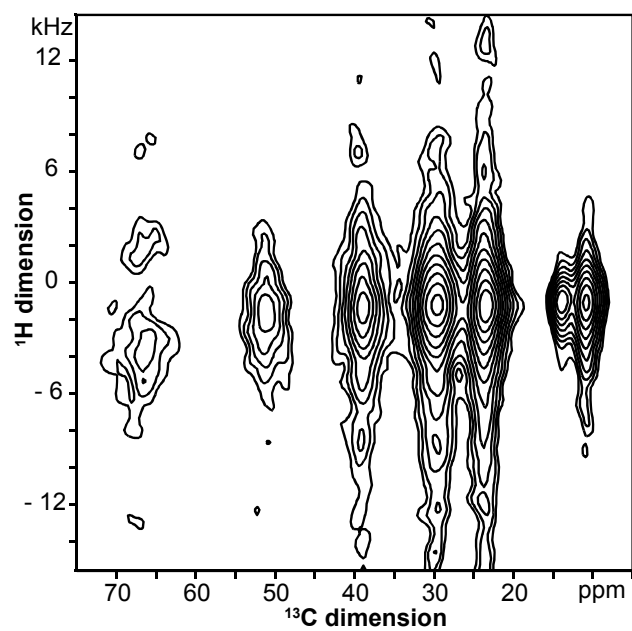


Figure 7- IV-30: Contour spectra extracted from the 2D-WISE spectra of PSA samples (^1H Larmor frequency of 300.13 MHz, static, LG-CP and π -pulse during t_1); top: sample Homo2EHA, middle: sample Copo1, bottom: Copo2.



3. NOE data

Sample	Temperature (K) / $T - T_g$ (K)	$q_{AB} \cdot \tau_C^{AB}$ (Hz)	τ_C^{AB} (s) from CH_3-CH_2	Number of experiments
Homo2EHA	298 / 85	35 ± 2	$8.8 \cdot 10^{-6} \pm 7 \cdot 10^{-7}$	9
Copo1	298 / 72	42 ± 5	$1.1 \cdot 10^{-5} \pm 2 \cdot 10^{-6}$	9
Copo2	298 / 73	42 ± 5	$1.0 \cdot 10^{-5} \pm 2 \cdot 10^{-7}$	9

Table 7- IV-5: Correlation times of local molecular motion extracted from the NOE experiment with dipolar filter for industrial PSAs

D. SEC results of poly(n-alkyl acrylates)

1. Plots of the intrinsic viscosity as a function of the molar mass

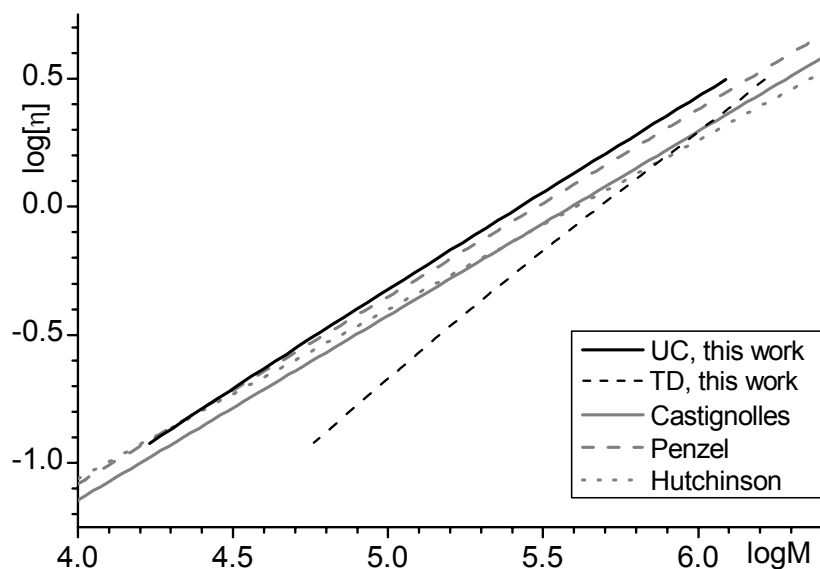


Figure 7- IV-31:
Intrinsic viscosity as
a function of the
molar mass on a log-
log scale for the
investigated PMA
sample, as well as
other PMA samples
(MHS parameters
from literature:
Castignolles,²⁰⁰
Penzel,²⁰⁹
Hutchinson^{210,211}).

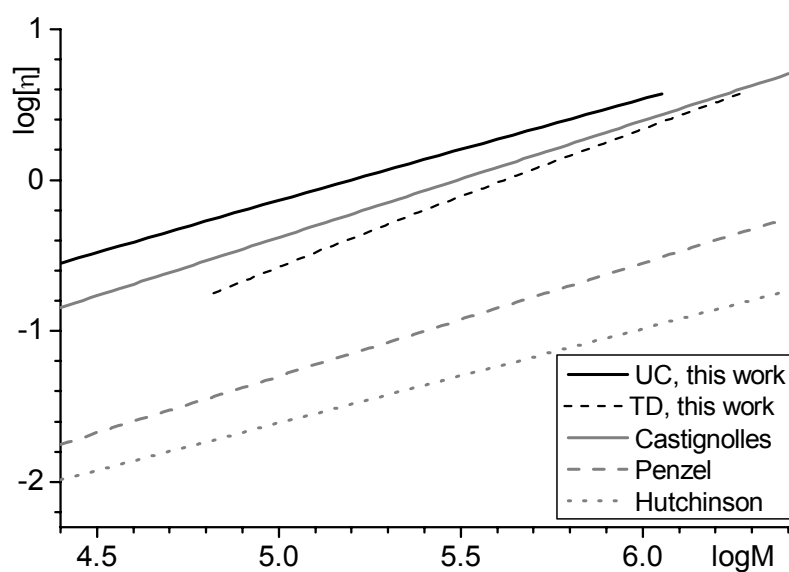


Figure 7- IV-32:
Intrinsic viscosity as a
function of the molar
mass on a log-log scale
for the investigated
PEA sample, as well as
other PEA samples
(MHS parameters from
literature:
Castignolles,^{200,286}
Penzel,²⁰⁹
Hutchinson²¹⁰).

Sample	K ($dL \cdot g^{-1}$)	α	Temperature	Ref.	Table 7- IV-6: Mark-Houwink- Sakurada (MHS) parameters for poly(n-alkyl methacrylates) in THF, used in the preceding figures.
PMA	$9.48 \cdot 10^5$	0.719	30 °C	200	
	$1.00 \cdot 10^6$	0.73	25 °C	209	
	$1.95 \cdot 10^6$	0.660		210,211	
PEA	$5.68 \cdot 10^5$	0.774	30 °C	200,286	
	$8.9 \cdot 10^5$	0.75	25 °C	209	
	$1.81 \cdot 10^6$	0.626		210	
PBA	$7.4 \cdot 10^5$	0.75	25 °C	209	
PHxA	$5.5 \cdot 10^5$	0.76	25 °C	209	

A critical comparison of the different sets of MHS parameters can be found in the Ph.D. thesis of Castignolles.²⁰⁰

2. Plots of the molar mass as a function of the elution volume

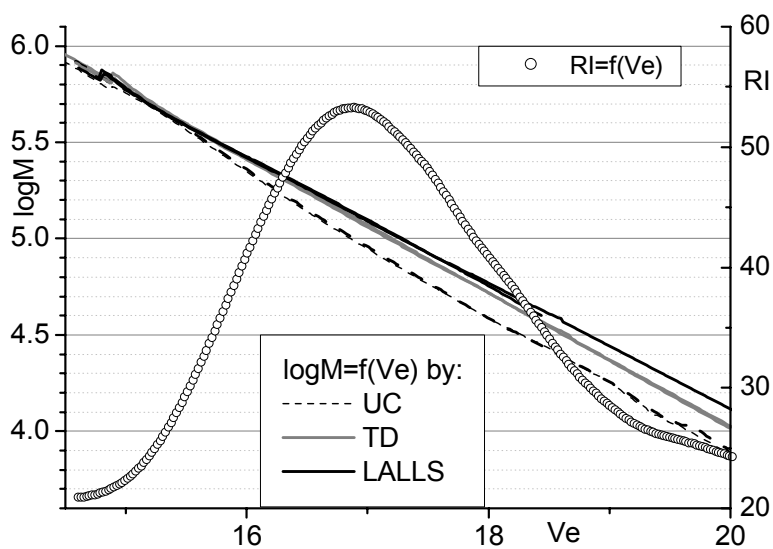


Figure 7- IV-33: Molar mass as a function of the elution volume for sample PMA, on a logarithmic scale; the different molar masses have been determined respectively by UC, TD and LALLS; the chromatogram is indicated for information (right scale).

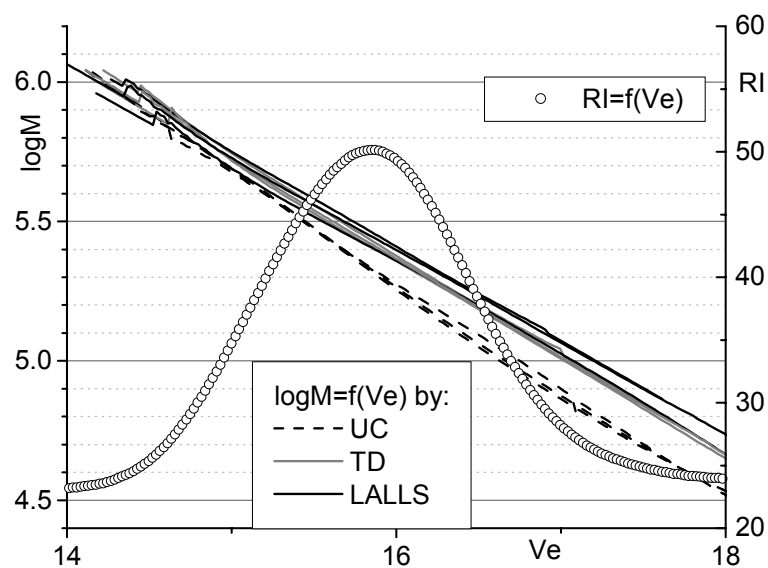


Figure 7- IV-34: Molar mass as a function of the elution volume for sample PEA, on a logarithmic scale; the different molar masses have been determined respectively by UC, TD and LALLS; the chromatogram is indicated for information (right scale).

V. Abbreviations and symbols

A. Investigated samples

PnAMA	poly(n-alkyl methacrylate)
PMMADMC	poly(methyl methacrylate), fully ^2H labeled on the main chain ($T_g = 398 \text{ K}$)
PEMA13C	poly(ethyl methacrylate), 20 % ^{13}C labeled at C=O ($T_g = 338 \text{ K}$)
PEMADSC	poly(ethyl methacrylate), fully ^2H labeled on the side chain ($T_g = 353 \text{ K}$)
PEMADMC	poly(ethyl methacrylate), fully ^2H labeled on the main chain ($T_g = 345 \text{ K}$)
PBMA	poly(n-butyl methacrylate), not isotopically labeled ($T_g = 302 \text{ K}$)
PBMA13C	poly(n-butyl methacrylate), 20 % ^{13}C labeled at C=O ($T_g = 309 \text{ K}$)
PHMA13C	poly(n-hexyl methacrylate), 20 % ^{13}C labeled at C=O ($T_g = 277 \text{ K}$)
PnAA	poly(n-alkyl acrylate)
PMA	poly(methyl acrylate) ($T_g = 294 \text{ K}$)
PEA	poly(ethyl acrylate) ($T_g = 259 \text{ K}$)
PBA	poly(n-butyl acrylate) ($T_g = 227 \text{ K}$)
PHxA	poly(n-hexyl acrylate) ($T_g = 213 \text{ K}$)
PSA	pressure sensitive adhesive
Homo2EHA	statistical copolymer of 99 % 2EHA and 1 % AA
Copo1	statistical copolymer of 80 % 2EHA, 19 % MA and 1 % AA
Copo2	statistical copolymer of 80 % 2EHA, 19 % MA, 1 % AA, and a crosslinker

B. Monomers, polymers and other chemicals

2EHA	2-EthylHexyl Acrylate
AA	Acrylic Acid
AIBN	Azo-bis-IsoButyroNitrile
a-PEMA	Atactic Poly(Ethyl MethAcrylate)
BA	n-Butyl Acrylate
DMF	DiMethylFormamide
EA	Ethyl Acrylate
MA	Methyl Acrylate
MMA	Methyl MethAcrylate
P2EHA	Poly(2-EthylHexyl Acrylate)
PBA	Poly(n-Butyl Acrylate)

PBMA	Poly(n-Butyl Methacrylate)
PE	PolyEthylene
PEMA	Poly(Ethyl MethAcrylate)
PHxMA	Poly(n-Hexyl MethAcrylate)
PMMA	Poly(Methyl MethAcrylate)
PIB	PolyIsoButylene
PS	PolyStyrene
PtBMA	Poly(t-Butyl MethAcrylate)
SIS	Styrene-Isoprene-Styrene triblock copolymer
THF	TetraHydroFurane
TMS	TetraMethylSilane

C. Nuclear magnetic resonance

1D	monodimensional
2D	two-dimensional
2D-WISE	two-dimensional WIdeline SEparation
δ	chemical shift
ε	number of orthogonal dimensions relevant for an effective spin diffusion process
τ	delay between two pulses in the dipolar filter of a spin diffusion experiment
B_0	static magnetic field
B_1	oscillating magnetic field
CP	Cross-Polarization
CPMG	Carr-Purcell-Meiboom-Gill
DD	Dipolar Decoupling
D_{eff}	effective diffusion coefficient of ^1H nuclear spin diffusion through flip-flops
DEPT	Distorsionless Enhancement Polarization Transfer
D_{Rouse}	diffusion coefficient of ^1H nuclear spin diffusion through chain translation
FID	Free Induction Decay
fwhm	Full Width at Half Maximum
LG-CP	Lee-Goldburg Cross-Polarization
MAS	Magic-Angle Spinning
NMR	Nuclear Magnetic Resonance
NOE	Nuclear Overhauser Effect
NOESY	Nuclear Overhauser Effect SpectroscopY

rf	RadioFrequency
S/N	Signal-to-Noise ratio
T ₁	time constant for spin-lattice relaxation (or transversal relaxation)
T _{1ρ}	time constant for relaxation under an applied B ₁ field
T ₂	time constant for spin-spin relaxation (or longitudinal relaxation)
t _m	mixing time

D. Others

ASTM	American Society for Testing and Materials
BASF AG	Badische Anilin- und SodaFabrik AktienGesellschaft
BL	Branching Level
CC	Conventional Calibration (in SEC)
CERDATO	Centre d'Etude de Recherche et Développement d'ATOfina
CRDE	Centre de Recherches de l'Est (Atofina)
DMA	Dynamic Mechanical Analysis
DSC	Differential Scanning Calorimetry
G', G''	storage, loss modulus
HPLC	High Performance Liquid Chromatography
IR	InfraRed
IUPAC	International Union of Pure and Applied Chemistry
LALLS	Low-Angle Laser Light Scattering (in SEC)
LCB	Long Chain Branch(ing)
MALDI-TOF-MS	Matrix-Assisted Laser Desorption Ionization – Time Of Flight Mass Spectrometry
M _e	average molar Mass between Entanglement
mm	syndiotactic triad
MM	Molar Mass
MPI-P	Max Planck Institute for Polymer Research
M _n	number-average molar mass
mr	atactic triad
M _w	mass-average molar mass
PSA	Pressure Sensitive Adhesive
rr	isotactic triad
SAFT	Shear Adhesion Failure Temperature
SAXS	Small-Angle X-ray Scattering

Part 7, V (Appendix) Abbreviations and symbols

SCB	Short Chain Branch(ing)
SEC	Size Exclusion Chromatography
$\tan\delta$	loss factor, or loss tangent
TD	Triple Detection (in SEC)
TDA	Triple Detection Array (for SEC)
T_g	glass transition temperature
TGA	ThermoGravimetric Analysis
UC	Universal Calibration (in SEC)
UV	UltraViolet
WAXS	Wide-Angle X-ray Scattering
WLF	Williams-Landel-Ferry

VI. Literature references

- (1) Penzel, E.; Polyacrylates, In *Ullmann's Encyclopedia of Industrial Chemistry*, 5th ed.; VCH Publishers, Inc.: New York, USA, 1992; vol. A21, pp 157-178.
- (2) Krenceski, M. A.; Johnson, J. F.; Temin, S. C. *J. Macromol. Sci.-Rev. Macromol. Chem. Phys.* **1986**, C26, 143-182.
- (3) History of Adhesives, <http://www.henkelca.com/student/history.asp>, Henkel Consumer Adhesives, Inc., 2004.
- (4) Schmidt-Rohr, K.; Spiess, H. W. *Multidimensional solid state NMR and polymers*, 1st ed.; Academic Press Ltd: San Diego, USA, 1994.
- (5) Wind, M., *Ph.D. thesis*, Johannes Gutenberg University, Mainz, Germany, 2001.
- (6) Egger, N.; Schmidt-Rohr, K.; Blumich, B.; Domke, W. D.; Stapp, B. *J. Appl. Polym. Sci.* **1992**, 44, 289-295.
- (7) Temin, S. C.; Pressure sensitive adhesives and products, In *Encyclopedia of Polymer Science and Engineering*, 2nd ed.; Wiley, 1988; vol. 13, pp 345-368.
- (8) Class, J. B.; Pressure sensitive adhesives, In *Encyclopedia of Material Science and Engineering*, 1st ed.; Bever, M. B., Ed.; Pergamon press, 1986; vol. 5, pp 3923-3928.
- (9) Fabris, H. J.; Knauss, W. G.; Synthetic polymer adhesives, In *Comprehensive Polymer Science*, 1st ed.; Allen, G.; Bevington, J. C., Eds.; Pergamon press, 1989; vol. 7, chap. 5, pp 139-141.
- (10) Jovanovic, R.; Dube, M. A. *J. Macromol. Sci.-Polym. Rev* **2004**, C44, 1-51.
- (11) Drew, R. G., 3M, USA, 1939, US2156380.
- (12) Bauer, W., Röhm & Haas AG, Germany, 1933, DE 575 327.
- (13) Bauer, W., Röhm & Haas AG, UK, 1929, GB 311,339.
- (14) Bauer, W., Röhm & Haas AG, USA, 1934, US 1,982,946.
- (15) Bauer, W., Röhm & Haas AG, France, 1930, FR 673.939.
- (16) Tobing, S. D.; Klein, A. *J. Appl. Polym. Sci.* **2000**, 76, 1965-1976.
- (17) Plessis, C., *Ph. D. thesis*, University of the Basque Country, Donasta - San Sebastian, Spain, 2000.
- (18) Grunlan, J. C.; Holguin, D. L.; Chuang, H. K.; Perez, I.; Chavira, A.; Quilatan, R.; Akhave, J.; Mehrabi, A. R. *Macromol. Rapid Commun.* **2004**, 25, 286-291.
- (19) Haller, W.; Henke, G.; Tauber, G.; Dierichs, W.; Gierenz, G.; Gruber, W.; Reckziegel, E.; Wegner, E.; Zoller, H.; Özelli, R.-N.; Herold, J.; Knop, B.; Brockmann, W.; Adhesives, In *Ullmann's Encyclopedia of Industrial Chemistry*, 5th ed.; VCH: New York, 1985; vol. A1, pp 221-247.
- (20) Glossary of terms, <http://www.pstc.org/publications/glossary.php>, PSTC, Glenview, Illinois, USA, 2004.
- (21) Creton, C.; Materials Science of Pressure-Sensitive Adhesives, In *Processing of Polymers*; Meijer, H. E. H., Ed.; VCH: Weinheim, 1997; vol. 18, chap. 15, pp 707-741.
- (22) Goulding, T. M.; Pressure-sensitive adhesives, In *Handbook of adhesive technology*, 1; Pizzi, A.; Mittal, K. L., Eds.; Marcel Dekker: New York, 1994; chap. 34, pp 549-564.
- (23) Bunker, S. P.; Wool, R. P. *J. Polym. Sci. Pol. Chem.* **2002**, 40, 451-458.
- (24) Auchter, G.; Aydin, O.; Zettl, A.; Acrylic adhesives, In *Handbook of pressure sensitive adhesive technology*, 3rd; Satas, D., Ed.; Satas and Associates: Warwick, RI, USA, 1982.
- (25) Tobing, S. D.; Klein, A. *J. Appl. Polym. Sci.* **2001**, 79, 2230-2244.
- (26) Tobing, S. D.; Klein, A. *J. Appl. Polym. Sci.* **2001**, 79, 2558-2564.
- (27) Hori, Y.; Sunakawa, M.; Takayama, K.; Matsuoka, N.; Moroishi, Y., Nitto Electric Industrial Co., Ltd., USA, 1985, US 4,500,683.

- (28) PSTC. *Test methods for pressure sensitive adhesives*, 13th ed.; PSTC: Glenview, Illinois, USA, 2000.
- (29) *ASTM standards (published one by one)*; ASTM: West Conshohocken, Pennsylvania, USA.
- (30) *FINAT Technical Handbook*, 6th ed.; FINAT: The Hague, Netherlands, 2001.
- (31) AFERA. 60 rue Auber, 94408 Vitry-sur-Seine, France.
- (32) Toyama, M.; Ito, T.; Moriguchi, H. *J. Appl. Polym. Sci.* **1970**, *14*, 2039-2048.
- (33) Lakrout, H.; Sergot, P.; Creton, C. *J. Adhes.* **1999**, *69*, 307-359.
- (34) Gent, A. N.; Hamed, G. R.; Bond strength: peel, In *Encyclopedia of Material Science and Engineering*, 1st ed.; Bever, M. B., Ed.; Pergamon press, 1986; vol. 1, pp 373-377.
- (35) Chan, H. K.; Howard, G. J. *J. Adhes.* **1978**, *9*, 279-304.
- (36) Yang, H. W.-H., Exxon Chemicals Patents, Inc., USA, 1993, WO 93/04097.
- (37) Zosel, A. *Int. J. Adhes. Adhes.* **1998**, *18*, 265-271.
- (38) Creton, C.; Hooker, J.; Shull, K. R. *Langmuir* **2001**, *17*, 4948-4954.
- (39) Roos, A.; Creton, C.; Novikov, M. B.; Feldstein, M. M. *J. Polym. Sci. Pt. B-Polym. Phys.* **2002**, *40*, 2395-2409.
- (40) Dhal, P. K.; Deshpande, A.; Babu, G. N. *Polymer* **1982**, *23*, 937-939.
- (41) Zosel, A. *J. Adhes.* **1991**, *34*, 201-209.
- (42) Plessis, C.; Arzamendi, G.; Leiza, J. R.; Alberdi, J. M.; Schoonbrood, H. A. S.; Charmot, D.; Asua, J. M. *J. Polym. Sci. Pol. Chem.* **2001**, *39*, 1106-1119.
- (43) Plessis, C.; Arzamendi, G.; Leiza, J. R.; Schoonbrood, H. A. S.; Charmot, D.; Asua, J. M. *Macromolecules* **2001**, *34*, 5147-5157.
- (44) Brown, K.; Hooker, J. C.; Creton, C. *Macromol. Mater. Eng.* **2002**, *287*, 163-179.
- (45) Chang, E. P. *J. Adhes.* **1997**, *60*, 233-248.
- (46) Kaelbe, D. H. *Trans. Soc. Rheol.* **1960**, *vol. IV*, 45-73.
- (47) Gent, A. N.; Kinloch, A. J. *Journal of Polymer Science Part A-2-Polymer Physics* **1971**, *9*, 659-668.
- (48) Gent, A. N.; Schultz, J. *J. Adhes.* **1972**, *3*, 281-294.
- (49) Andrews, E. H.; Kinloch, A. J. *Proc. R. Soc. London Ser. A-Math. Phys. Eng. Sci.* **1973**, *332*, 385-399.
- (50) Good, R. J.; Shoraka, F. *ACS Symposium Series* **1985**, *287*, 39-57.
- (51) Good, R. J.; Gupta, R. K. *J. Adhes.* **1988**, *26*, 13-36.
- (52) Zosel, A. *Colloid Polym. Sci.* **1985**, *263*, 541-553.
- (53) Zosel, A.; Fracture Energy and Tack of Pressure Sensitive Adhesives, In *Advances in Pressure Sensitive Adhesive Technology 1 (Handbook of PSA Technology)*; Satas, D., Ed.; Van Nostrand Reinhold: New York, 1992; pp 92-127.
- (54) Zosel, A. *J. Adhes.* **1989**, *30*, 135-149.
- (55) Lakrout, H.; Creton, C.; Ahn, D. C.; Shull, K. R. *Macromolecules* **2001**, *34*, 7448-7458.
- (56) Zosel, A. *J. Adhes. Sci. Technol.* **1997**, *11*, 1447-1457.
- (57) Creton, C.; Leibler, L. *J. Polym. Sci. Pt. B-Polym. Phys.* **1996**, *34*, 545-554.
- (58) Chiche, A.; Pareige, P.; Creton, C. *C. R. Acad. Sci. Ser. IV-Phys. Astrophys.* **2000**, *1*, 1197-1204.
- (59) Chikina, I.; Gay, C. *Phys. Rev. Lett.* **2000**, *85*, 4546-4549.
- (60) Gay, C.; Leibler, L. *Phys. Rev. Lett.* **1999**, *82*, 936-939.
- (61) Creton, C.; Lakrout, H. *J. Polym. Sci. Pt. B-Polym. Phys.* **2000**, *38*, 965-979.
- (62) Crosby, A. J.; Shull, K. R.; Lakrout, H.; Creton, C. *J. Appl. Phys.* **2000**, *88*, 2956-2966.
- (63) Claridge, T. D. W.; Introduction, In *High-Resolution NMR Techniques in Organic Chemistry*; Pergamon Press: Amsterdam, 1999; vol. 19, chap. 1, pp 1-12.

- (64) Claridge, T. D. W.; Introducing high-resolution NMR, In *High-Resolution NMR Techniques in Organic Chemistry*; Elsevier: Amsterdam, 1999; vol. 19, chap. 2, pp 13-44.
- (65) Abragam, A.; Introduction, In *The Principles of Nuclear Magnetism*, 1st ed.; Oxford University Press: Oxford, UK, 1961; chap. I, pp 1-18.
- (66) Mehring, M.; Homogenous, inhomogeneous and heterogeneous lineshapes, In *Principles of High Resolution NMR in Solids*, 2nd ed.; Springer-Verlag: Berlin, 1983; chap. 9-D, pp 303-304.
- (67) Abragam, A.; Dipolar line width in a rigid lattice, In *The Principles of Nuclear Magnetism*, 1st ed.; Oxford University Press: Oxford, UK, 1961; chap. IV, pp 97-132.
- (68) Abragam, A.; Theory of line width in the presence of motion of the spins, In *The Principles of Nuclear Magnetism*, 1st ed.; Oxford University Press: Oxford, 1961; chap. X, pp 424-479.
- (69) Andrew, E. R.; Magic angle spinning, In *Encyclopedia of Nuclear Magnetic Resonance*, 1st ed.; Grant, D. M.; Harris, R. K., Eds.; John Wiley and Sons Ltd.: Chichester, UK, 1996; vol. 5, pp 2891-2901.
- (70) Schaefer, J.; Stejskal, E. O.; Buchdahl, R. *Macromolecules* **1977**, *10*, 384-405.
- (71) Grimmer, A. R.; Bluemich, B.; Introduction to Solid-State NMR, In *NMR Basic Principles and Progress*, 1994; vol. 30, pp 1-62.
- (72) Hartmann, S. R.; Hahn, E. L. *Physical Review* **1962**, *128*, 2042-2053.
- (73) Schmidt-Rohr, K.; Clauss, J.; Spiess, H. W. *Macromolecules* **1992**, *25*, 3273-3277.
- (74) Lee, M.; Goldberg, W. I. *Physical Review* **1965**, *140*, A1261-A1271.
- (75) van Rossum, B. J.; de Groot, C. P.; Ladizhansky, V.; Vega, S.; de Groot, H. J. M. *J. Am. Chem. Soc.* **2000**, *122*, 3465-3472.
- (76) Schmidt-Rohr, K.; Spiess, H. W.; Multidimensional separation and correlation, In *Multidimensional solid-state NMR and polymers*, 1st ed.; Academic Press Ltd: San Diego, USA, 1994; chap. 6, pp 182-235.
- (77) Levitt, M. H.; Experiments on non-interacting spins, In *Spin dynamics*, 1st ed.; John Wiley and Sons Ltd: Chichester, UK, 2001; chap. 11, pp 315-336.
- (78) Hahn, E. L. *Physical Review* **1949**, *76*, 145-146.
- (79) Canet, D.; Dynamic phenomena in NMR, In *Nuclear magnetic resonance, concepts and methods*, 1st ed.; John Wiley and Sons Ltd: Chichester, England, 1996; chap. 4, pp 139-196.
- (80) Ernst, R. R.; Bodenhausen, G.; Wokaun, A.; Investigation of dynamic processes, relaxation, and chemical exchange, In *Principles of nuclear magnetic resonance in one and two dimensions*, 3; Oxford University Press: Oxford, UK, 1991; chap. 4.6, pp 201-220.
- (81) Mellinger, F.; Wilhelm, M.; Spiess, H. W. *Macromolecules* **1999**, *32*, 4686-4691.
- (82) Valtier, M.; Drujon, X.; Wilhelm, M.; Spiess, H. W. *Macromol. Chem. Phys.* **2001**, *202*, 1262-1272.
- (83) Suter, D.; Ernst, R. R. *Phys. Rev. B* **1985**, *32*, 5608-5627.
- (84) Schmidt-Rohr, K.; Spiess, H. W.; Domain sizes and internuclear distances from spin diffusion and dipolar couplings, In *Multidimensional solid-state NMR and polymers*, 1st ed.; Academic Press Ltd: San Diego, USA, 1994; chap. 13, pp 402-439.
- (85) Vanderhart, D. L. *Makromolekulare Chemie-Macromolecular Symposia* **1990**, *34*, 125-159.
- (86) Goldman, M.; Shen, L. *Physical Review* **1966**, *144*, 321-333.
- (87) Clauss, J.; Schmidt-Rohr, K.; Spiess, H. W. *Acta Polym.* **1993**, *44*, 1-17.
- (88) Reichert, D.; Hempel, G.; Poupko, R.; Luz, Z.; Olejniczak, Z.; Tekely, P. *Solid State Nucl. Magn. Reson.* **1998**, *13*, 137-148.

- (89) Tekely, P.; Potrzebowski, M. J.; Dusausoy, Y.; Luz, Z. *Chem. Phys. Lett.* **1998**, *291*, 471-479.
- (90) Landfester, K.; Spiess, H. W. *Acta Polym.* **1998**, *49*, 451-464.
- (91) Domjan, A.; Erdodi, G.; Wilhelm, M.; Neidhofer, M.; Landfester, K.; Ivan, B.; Spiess, H. W. *Macromolecules* **2003**, *36*, 9107-9114.
- (92) Kenwright, A. M.; Packer, K. J. *Chem. Phys. Lett.* **1990**, *173*, 471-475.
- (93) Mellinger, F.; Spindiffusionkoeffizienten, In *Entwicklung und Anwendung von Festkörper-NMR-Methoden zur Untersuchung industrieller Latices*, Ph.D. thesis, Mainz, Germany; Shaker Verlag: Aachen, Germany, 1998; chap. 5, pp 38-55.
- (94) Ernst, R. R.; Cross-relaxation and nuclear Overhauser effects, In *Principles of nuclear magnetic resonance in one and two dimensions*, 3; Oxford University Press: Oxford, UK, 1991; chap. 9.7, pp 516-527.
- (95) Overhauser, A. W. *Physical Review* **1953**, *92*, 411-415.
- (96) Overhauser, A. W. *Physical Review* **1953**, *89*, 689-700.
- (97) Bloch, F. *Physical Review* **1956**, *102*, 104-135.
- (98) Solomon, I. *Physical Review* **1955**, *99*, 559-565.
- (99) Mackor, E. L.; Maclean, C. J. *Chem. Phys.* **1965**, *42*, 4254-4261.
- (100) Noggle, J. H. *J. Chem. Phys.* **1965**, *43*, 3304-3316.
- (101) Hoffman, R. A.; Forsen, S. *J. Chem. Phys.* **1966**, *45*, 2049-2060.
- (102) Maclean, C.; Mackor, E. L.; Hilbers, C. W. *J. Chem. Phys.* **1967**, *46*, 3393-3398.
- (103) Anet, F. A. L.; Bourn, A. J. R. *J. Am. Chem. Soc.* **1965**, *87*, 5250-5251.
- (104) White, J. L.; Haw, J. F. *J. Am. Chem. Soc.* **1990**, *112*, 5896-5898.
- (105) Law, R. V.; Love, G. D.; Snape, C. E. *Energy Fuels* **1993**, *7*, 1148-1149.
- (106) Rajamohanam, P. R.; Ganapathy, S.; Ray, S. S.; Badiger, M. V.; Mashelkar, R. A. *Macromolecules* **1995**, *28*, 2533-2536.
- (107) Chai, M. H.; Niu, Y. H.; Youngs, W. J.; Rinaldi, P. L. *J. Am. Chem. Soc.* **2001**, *123*, 4670-4678.
- (108) Macchioni, A. *Eur. J. Inorg. Chem.* **2003**, 195-205.
- (109) Harvey, P. D. *Macromol. Symp.* **2004**, *209*, 67-79.
- (110) Palmas, P.; Tekely, P.; Mutzenhardt, P.; Canet, D. *J. Chem. Phys.* **1993**, *99*, 4775-4785.
- (111) Neuhaus, D.; Williamson, M.; The steady-state NOE for two spins, In *The nuclear Overhauser effect in structural and conformational analysis*, 1st ed.; VCH Publishers, Inc.: New York, USA, 1989; chap. 2, pp 23-61.
- (112) Macura, S.; Ernst, R. R. *Mol. Phys.* **1980**, *41*, 95-117.
- (113) Macura, S.; Ernst, R. R. *Mol. Phys.* **2002**, *100*, 135-147. Reprint from *Mol. Phys.*, **1980**, *41*, 95-117.
- (114) Levitt, M. H.; Relaxation, In *Spin dynamics*, 1st ed.; John Wiley and Sons Ltd: Chichester, UK, 2001; chap. 16, pp 513-570.
- (115) Neuhaus, D.; Williamson, M.; The kinetics of NOE, In *The nuclear Overhauser effect in structural and conformational analysis*, 1st ed.; VCH Publishers, Inc.: New York, USA, 1989; chap. 4, pp 103-140.
- (116) Kalk, A.; Berendsen, H. J. C. *J. Magn. Reson.* **1976**, *24*, 343-366.
- (117) Kaiser, R. *J. Chem. Phys.* **1965**, *42*, 1838-1839.
- (118) Wagler, T.; Rinaldi, P. L.; Han, C. D.; Chun, H. *Macromolecules* **2000**, *33*, 1778-1789.
- (119) Mirau, P. A.; Tanaka, H.; Bovey, F. A. *Macromolecules* **1988**, *21*, 2929-2933.
- (120) Heffner, S. A.; Mirau, P. A. *Macromolecules* **1994**, *27*, 7283-7286.
- (121) Hou, S. S.; Graf, R.; Spiess, H. W.; Kuo, P. L. *Macromol. Rapid Commun.* **2001**, *22*, 1386-1389.
- (122) Mirau, P. A.; White, J. L. *Magn. Reson. Chem.* **1994**, *32*, S23-S29.
- (123) Qiu, X. H.; Ediger, M. D. *Macromolecules* **2002**, *35*, 1691-1698.

- (124) Schmidt-Rohr, K.; Spiess, H. W. *Macromolecules* **1991**, *24*, 5288-5293.
- (125) Komoroski, R. A.; Maxfield, J.; Sakaguchi, F.; Mandelkern, L. *Macromolecules* **1977**, *10*, 550-556.
- (126) Qiu, X. H.; Moe, N. E.; Ediger, M. D.; Fetters, L. J. *J. Chem. Phys.* **2000**, *113*, 2918-2926.
- (127) Denault, J.; Prudhomme, J. *Macromolecules* **1989**, *22*, 1307-1316.
- (128) Smith, G. D.; Paul, W.; Monkenbusch, M.; Willner, L.; Richter, D.; Qiu, X. H.; Ediger, M. D. *Macromolecules* **1999**, *32*, 8857-8865.
- (129) Menger, E. M.; Veeman, W. S.; Deboer, E. *Macromolecules* **1982**, *15*, 1406-1411.
- (130) Gordon, S. L.; Wuthrich, K. *J. Am. Chem. Soc.* **1978**, *100*, 7094-7096.
- (131) White, J. L. *Solid State Nucl. Magn. Reson.* **1997**, *10*, 79-88.
- (132) Pollard, M.; Klimke, K.; Graf, R.; Spiess, H. W.; Wilhelm, M.; Sperber, O.; Piel, C.; Kaminsky, W. *Macromolecules* **2004**, *37*, 813-825.
- (133) Jeener, J., lecture, at *Ampere International Summer School II*, Basko Polje, Yugoslavia, 1971.
- (134) Aue, W. P.; Bartholdi, E.; Ernst, R. R. *J. Chem. Phys.* **1976**, *64*, 2229-2246.
- (135) Jeener, J.; Meier, B. H.; Bachmann, P.; Ernst, R. R. *J. Chem. Phys.* **1979**, *71*, 4546-4553.
- (136) Kumar, A.; Ernst, R. R.; Wuthrich, K. *Biochem. Biophys. Res. Commun.* **1980**, *95*, 1-6.
- (137) Kumar, A.; Wagner, G.; Ernst, R. R.; Wuthrich, K. *Biochem. Biophys. Res. Commun.* **1980**, *96*, 1156-1163.
- (138) Fritzhanns, T.; Hafner, S.; Demco, D. E.; Spiess, H. W.; Laukien, F. H. *J. Magn. Reson.* **1998**, *134*, 355-359.
- (139) Fritzhanns, T.; Demco, D. E.; Hafner, S.; Spiess, H. W. *Mol. Phys.* **1999**, *97*, 931-943.
- (140) Griesinger, C.; Sorensen, O. W.; Ernst, R. R. *J. Magn. Reson.* **1989**, *84*, 14-63.
- (141) Likic, V. A. *Concepts Magn. Resonance* **1996**, *8*, 423-436.
- (142) Madhu, P. K.; Kumar, A. *J. Magn. Reson.* **1997**, *127*, 168-172.
- (143) Landy, S. B.; Rao, B. D. N. *J. Magn. Reson. Ser. A* **1993**, *102*, 90-94.
- (144) Gao, J.; Penlidis, A. *J. Macromol. Sci.-Rev. Macromol. Chem. Phys.* **1996**, *C36*, 199-404.
- (145) Heatley, F.; Lovell, P. A.; Yamashita, T. *Macromolecules* **2001**, *34*, 7636-7642.
- (146) Lovell, P. A.; Shah, T. H.; Heatley, F.; Correlation of the extent of chain transfer to polymer with reaction conditions for emulsion polymerization of n-butyl acrylate, In *Polymer latexes, Preparation, Characterization, Applications*; Daniels, E. S.; Sudol, E. D.; El-Aasser, M. S., Eds., 1992; vol. 492, chap. 12, pp 188-202.
- (147) Plessis, C.; Arzamendi, G.; Leiza, J. R.; Schoonbrood, H. A. S.; Charmot, D.; Asua, J. M. *Macromolecules* **2000**, *33*, 4-7.
- (148) Plessis, C.; Arzamendi, G.; Alberdi, J. M.; Agnely, M.; Leiza, J. R.; Asua, J. M. *Macromolecules* **2001**, *34*, 6138-6143.
- (149) Ahmad, N. M.; Heatley, F.; Lovell, P. A. *Macromolecules* **1998**, *31*, 2822-2827.
- (150) Wind, M.; Graf, R.; Renker, S.; Spiess, H. W. *Macromolecular Chemistry and Physics* **2004**, in press.
- (151) Wind, M.; Brombacher, L.; Heuer, A.; Graf, R.; Spiess, H. W. *Solid State Nucl. Magn. Reson.* **2005**, *27*, 132-139.
- (152) Kuebler, S. C., *Ph.D. thesis*, Johannes Gutenberg University, Mainz, Germany, 1996.
- (153) Wind, M.; Graf, R.; Renker, S.; Spiess, H. W.; Steffen, W. *J. Chem. Phys.* **2005**, *122*, 0149061-01490610.

- (154) Lesko, P. M.; Sperry, P. R.; Acrylic and styrene-acrylic polymers, In *Emulsion Polymerization and Emulsion Polymers*, 1st ed.; Lovell, P. A.; El-Aasser, M. S., Eds.; John Wiley and Sons: Chichester, UK, 1997; chap. 18, pp 619-655.
- (155) Lovell, P. A.; Free-radical polymerization, In *Emulsion Polymerization and Emulsion Polymers*, 1; Lovell, P. A.; El-Aasser, M. S., Eds.; John Wiley and Sons: Chichester, UK, 1997; chap. 1, pp 3-35.
- (156) Alfrey, T.; Price, C. C. *Journal of Polymer Science* **1947**, *2*, 101-106.
- (157) Greenley, R. Z.; Q and e values for free radical copolymerization of vinyl monomers and telogens, In *Polymer Handbook*, 4th ed.; Brandrup, J.; Immergut, E. H.; Grulke, E. A., Eds.; Wiley interscience: New York, USA, 1999; section 2, p 309.
- (158) Davis, T., Propagation and transfer in free radical copolymerization, lecture, at *SML 01*, Il Ciocco, Italy, 2001.
- (159) Fukuda, T.; Ma, Y. D.; Inagaki, H. *Macromolecules* **1985**, *18*, 17-26.
- (160) Ma, Y. D.; Fukuda, T.; Inagaki, H. *Macromolecules* **1985**, *18*, 26-31.
- (161) Coote, M. L.; Davis, T. P. *Prog. Polym. Sci.* **1999**, *24*, 1217-1251.
- (162) Kine, B. B.; Novak, R. W.; Acrylic and methacrylic acid ester polymers, In *Encyclopedia of Polymer Science and Engineering*, 2nd ed.; Wiley, 1985; vol. 1, pp 234-299.
- (163) *Preparation, properties and use of acrylic polymers, CM 19*; Rohm and Haas Company, 1981.
- (164) Nemeč, J. W.; Bauer, W. J.; Acrylic and methacrylic acid polymers, In *Encyclopedia of Polymer Science and Engineering*, 2nd ed.; Wiley, 1985; vol. 1, pp 211-234.
- (165) Andrews, J. R.; Grulke, E. A.; Glass transition temperatures of polymers, In *Polymer Handbook*, 4th ed.; Brandrup, J.; Immergut, E. H.; Grulke, E. A., Eds.; John Wiley and Sons: New York, USA, 1999; section VI, pp 193-277.
- (166) Elias, H. G.; Glasübergänge, In *Makromoleküle*, 5th ed.; Elias, H. G., Ed.; Hüthig & Wepf: Basel, Switzerland, 1990; vol. 1, chap. 22.6, pp 845-860.
- (167) Fox, T. G. *Bull. Am. Phys. Soc.* **1956**, *1*, 123.
- (168) Loyen, K., Cerdato, Serquigny (France), *personal communication*, 2001.
- (169) Plazek, D. J.; Ngai, K. L.; The glass temperature, In *Physical Properties of Polymers Handbook*; Mark, E. J., Ed.; AIP press: New York, 1996; chap. 12, pp 139-159.
- (170) Grubisic, Z.; Rempp, P.; Benoit, H. *Journal of Polymer Science Part B-Polymer Letters* **1967**, *5*, 753-759.
- (171) Grubisic, Z.; Rempp, P.; Benoit, H. *J. Polym. Sci. Pt. B-Polym. Phys.* **1996**, *34*, 1707-1713. Reprint from *J. Polym. Sci. Pt. B-Polym. Lett.* **1967**, *5*, 753-759.
- (172) Netopilik, M.; Kratochvil, P. *Polymer* **2003**, *44*, 3431-3436.
- (173) Beuermann, S.; Buback, M.; Davis, T. P.; Gilbert, R. G.; Hutchinson, R. A.; Kajiwarra, A.; Klumperman, B.; Russell, G. T. *Macromol. Chem. Phys.* **2000**, *201*, 1355-1364.
- (174) Aqeel, S.; Lath, D.; Lathova, E.; Pavlinec, J.; Lacik, I. *Polym. Bull.* **2002**, *47*, 563-569.
- (175) Bruessau, R. J. *Macromol. Symp.* **1996**, *110*, 15-32.
- (176) Cho, D.; Park, I.; Chang, T.; Ute, K.; Fukuda, I.; Kitayama, T. *Macromolecules* **2002**, *35*, 6067-6069.
- (177) Reichl, S.; Beiner, M. **2004**, *to be published*.
- (178) Plessis, C.; Arzamendi, G.; Leiza, J. R.; Schoonbrood, H. A. S.; Charmot, D.; Asua, J. M. *Macromolecules* **2000**, *33*, 5041-5047.
- (179) Goni, I.; Gurruchaga, M.; Valero, M.; Guzman, G. M. *Polymer* **1993**, *34*, 1780-1785.

- (180) NMR spectra database of polymers, http://polymer.nims.go.jp/NMR/top_eng.html, National Institute for Materials Science, NIMS, Japan, 2004.
- (181) Brar, A. S.; Dutta, K. *Polym. J.* **1998**, *30*, 304-310.
- (182) Striegel, A. M.; Krejsa, M. R. *J. Polym. Sci. Pt. B-Polym. Phys.* **2000**, *38*, 3120-3135.
- (183) Heatley, F.; Lovell, P.; Yamashita, T. *Macromolecules* **2000**, *34*.
- (184) Jenkins, A. D.; Kratochvil, P.; Stepto, R. F. T.; Suter, U. W. *Pure Appl. Chem.* **1996**, *68*, 2287-2311.
- (185) Castignolles, P., *Ph.D. thesis*, Pierre et Marie Curie University, Paris VI, Paris, 2003.
- (186) Asua, J. M.; Beuermann, S.; Buback, M.; Castignolles, P.; Charleux, B.; Gilbert, R. G.; Hutchinson, R. A.; Leiza, J. R.; Nikitin, A. N.; Vairon, J. P.; van Herk, A. M. *Macromol. Chem. Phys.* **2004**, *205*, 2151-2160.
- (187) Voyutskii, S. S.; Ustinova, Z. M. *J. Adhes.* **1977**, *9*, 39-50.
- (188) Hahn, K.; Ley, G.; Schuller, H.; Oberthur, R. *Colloid Polym. Sci.* **1986**, *264*, 1092-1096.
- (189) Zosel, A.; Ley, G. *Macromolecules* **1993**, *26*, 2222-2227.
- (190) Atta-ur-Rahman. *Nuclear Magnetic Resonance - Basic Principles*; Springer: New York, 1986.
- (191) Farcet, C.; Bellenev, J.; Charleux, B.; Pirri, R. *Macromolecules* **2002**, *35*, 4912-4918.
- (192) Former, C.; Castro, J.; Fellows, C. M.; Tanner, R. I.; Gilbert, R. G. *J. Polym. Sci. Pol. Chem.* **2002**, *40*, 3335-3349.
- (193) Metz, G.; Wu, X. L.; Smith, S. O. *J. Magn. Reson. Ser. A* **1994**, *110*, 219-227.
- (194) McCord, E. F.; Shaw, W. H.; Hutchinson, R. A. *Macromolecules* **1997**, *30*, 246-256.
- (195) Chiefari, J.; Jeffery, J.; Mayadunne, R. T. A.; Moad, G.; Rizzardo, E.; Thang, S. H. *Macromolecules* **1999**, *32*, 7700-7702.
- (196) Plessis, C.; Arzamendi, G.; Leiza, J. R.; Schoonbrood, H. A. S.; Charmot, D.; Asua, J. M. *Ind. Eng. Chem. Res.* **2001**, *40*, 3883-3894.
- (197) Plessis, C.; Arzamendi, G.; Alberdi, J. M.; van Herk, A. M.; Leiza, J. R.; Asua, J. M. *Macromol. Rapid Commun.* **2003**, *24*, 173-177.
- (198) Ahmad, N. M.; Lovell, P. A.; Underwood, S. M. *Polym. Int.* **2001**, *50*, 625-634.
- (199) Castignolles, P.; Experimental Part, In *Cinétique de la polymérisation radicalaire des acrylates par polymérisation par LASER pulsé et chromatographie d'exclusion stérique multi-détection (PLP-SEC) - Analyse critique*, *Ph.D. thesis*; Pierre et Marie Curie University, Paris VI: Paris, 2003; Part 3, pp 84-104.
- (200) Castignolles, P.; Choix de la technique de détermination de la Distribution des Masses Molaires (MWD), In *Cinétique de la polymérisation radicalaire des acrylates par polymérisation par LASER pulsé et chromatographie d'exclusion stérique multi-détection (PLP-SEC) - Analyse critique*, *Ph.D. thesis*; Pierre et Marie Curie University, Paris VI: Paris, 2003; Part 4, pp 105-136.
- (201) Arzamendi, G.; Plessis, C.; Leiza, J. R.; Asua, J. M. *Macromol. Theory Simul.* **2003**, *12*, 315-324.
- (202) Nikitin, A. N.; Castignolles, P.; Charleux, B.; Vairon, J. P. *Macromol. Theory Simul.* **2003**, *12*, 440-448.
- (203) Barth, H. G.; Boyes, B. E.; Jackson, C. *Anal. Chem.* **1998**, *70*, 251R-278R.
- (204) Lehmann, U.; Kohler, W.; Albrecht, W. *Macromolecules* **1996**, *29*, 3212-3215.
- (205) Nielen, M. W. F. *Mass Spectrom. Rev.* **1999**, *18*, 309-344.
- (206) Castignolles, P.; Choix de la technique de détermination de la Distribution des Masses Molaires (MWD), In *Cinétique de la polymérisation radicalaire des acrylates par polymérisation par LASER pulsé et chromatographie d'exclusion*

- stérique multi-détection (PLP-SEC) - Analyse critique, Ph.D. thesis*; Pierre et Marie Curie University, Paris VI: Paris, 2003; Part 4, p 132.
- (207) Berek, D.; Bruessau, R.; Lilge, D.; Mingozzi, T.; Podzimek, S.; Robert, E., Repeatability and apparent reproductibility of molar masses values for homopolymers determined by size exclusion chromatography, <http://www.iupac.org/projects/posters01/berek01.pdf>, 2001.
- (208) Schaeffgen, J. R.; Flory, P. J. *J. Am. Chem. Soc.* **1948**, *70*, 2709-2718.
- (209) Penzel, E.; Goetz, N. *Angew. Makromol. Chem.* **1990**, *178*, 191-200.
- (210) Hutchinson, S. A.; Paquet, D. A.; Mc Minn, J. H.; Beuermann, S.; Fuller, R. E.; C., J. *Dechema Monographs* **1995**, *131*, 5th international workshop on polymer reaction engineering, 467-492.
- (211) Beuermann, S., *personal communication*, 2002.
- (212) Flory, P. J.; Determination of molecular weights and polymer dimensions by light scattering, In *Principles of Polymer Chemistry*, 1st ed.; Cornell University Press: Ithaca, NY, USA, 1953; chap. VII-2, pp 283-316.
- (213) Flory, P. J. *Principles of Polymer Chemistry*, 1st ed.; Cornell University Press: Ithaca, NY, USA, 1953.
- (214) Castignolles, P.; Annexes, In *Cinétique de la polymérisation radicalaire des acrylates par polymérisation par LASER pulsé et chromatographie d'exclusion stérique multi-détection (PLP-SEC) - Analyse critique, Ph.D. thesis*; Pierre and Marie Curie University, Paris VI: Paris, France, 2003; Part 8, pp 268-270.
- (215) Small, P. A. *Adv. Polym. Sci.* **1975**, *18*, 1-64.
- (216) Zimm, B. H.; Stockmayer, W. H. *J. Chem. Phys.* **1949**, *17*, 1301-1314.
- (217) *Model 302 TDA Detectors Instrument Manual*, ed. 0601, revision 1.21; Viscotek: Houston, Texas, USA.
- (218) Miller, R. L.; Boyer, R. F.; Heijboer, J. *J. Polym. Sci. Pt. B-Polym. Phys.* **1984**, *22*, 2021-2041.
- (219) Beiner, M.; Schroter, K.; Hempel, E.; Reissig, S.; Donth, E. *Macromolecules* **1999**, *32*, 6278-6282.
- (220) Beiner, M., *Habilitation thesis*, Martin Luther University, Halle-Wittenberg, Germany, 2003.
- (221) Wind, M.; Graf, R.; Heuer, A.; Spiess, H. W. *Phys. Rev. Lett.* **2003**, *91*, 1557021-1557024.
- (222) Kulik, A. S.; Beckham, H. W.; Schmidt-Rohr, K.; Radloff, D.; Pawelzik, U.; Boeffel, C.; Spiess, H. W. *Macromolecules* **1994**, *27*, 4746-4754.
- (223) Williams, M. L.; Landel, R. F.; Ferry, J. D. *J. Am. Chem. Soc.* **1955**, *77*, 3701-3707.
- (224) Adam, A.; Spiess, H. W. *Makromolekulare Chemie-Rapid Communications* **1990**, *11*, 249-259.
- (225) Beiner, M. *Macromol. Rapid Commun.* **2001**, *22*, 869-895.
- (226) Beiner, M.; Kabisch, O.; Reichl, S.; Huth, H. *J. Non-Cryst. Solids* **2002**, *307*, 658-666.
- (227) Hempel, E.; Huth, H.; Beiner, M. *Thermochim. Acta* **2003**, *403*, 105-114.
- (228) Pascui, O.; Beiner, M.; Reichert, D. *Macromolecules* **2003**, *36*, 3992-4003.
- (229) Beiner, M.; Huth, H. *Nat. Mater.* **2003**, *2*, 595-599.
- (230) Adam, G.; Gibbs, J. H. *J. Chem. Phys.* **1965**, *43*, 139.
- (231) Hiller, S.; Pascui, O.; Budde, H.; Kabisch, O.; Reichert, D.; Beiner, M. *New J. Phys.* **2004**, *6*, 10-25.
- (232) Arrighi, V.; Holmes, P. F.; McEwen, I. J.; Qian, H.; Terrill, N. J. *J. Polym. Sci. Pt. B-Polym. Phys.* **2004**, *42*, 4000-4016.
- (233) Reinsberg, S. A.; Heuer, A.; Doliwa, B.; Zimmermann, H.; Spiess, H. W. *J. Non-Cryst. Solids* **2002**, *307*, 208-214.

- (234) Tracht, U.; Wilhelm, M.; Heuer, A.; Feng, H.; Schmidt-Rohr, K.; Spiess, H. W. *Phys. Rev. Lett.* **1998**, *81*, 2727-2730.
- (235) Demco, D. E.; Hafner, S.; Fulber, C.; Graf, R.; Spiess, H. W. *J. Chem. Phys.* **1996**, *105*, 11285-11296.
- (236) Filip, C.; Hafner, S.; Schnell, I.; Demco, D. E.; Spiess, H. W. *J. Chem. Phys.* **1999**, *110*, 423-440.
- (237) Harris, R. K.; Becker, E. D.; De Menezes, S. M. C.; Goodfellow, R.; Granger, P. *Pure Appl. Chem.* **2001**, *73*, 1795-1818.
- (238) Homann, K. H., Abbreviated list of quantities, units and symbols in physical chemistry, <http://www.iupac.org/reports/1993/homann/index.html>, IUPAC, 1993.
- (239) Van Vleck, J. H. *Physical Review* **1948**, *74*, 1168-1183.
- (240) Slichter, C. P.; Magnetic dipolar broadening of rigid lattices, In *Principles of Magnetic Resonance*, 3rd; Springer Verlag: Berlin, Germany, 1990; chap. 3, pp 64-85.
- (241) Wang, Y. L.; Belton, P. S.; Tang, H. R. *Chem. Phys. Lett.* **1997**, *268*, 387-392.
- (242) Gee, B. *Solid State Nucl. Magn. Reson.* **2001**, *19*, 73-86.
- (243) Haase, J.; Oldfield, E. *J. Magn. Reson. Ser. A* **1993**, *101*, 30-40.
- (244) Knorgen, M.; Menge, H.; Hempel, G.; Schneider, H.; Ries, M. E. *Polymer* **2002**, *43*, 4091-4096.
- (245) Callaghan, P. T.; Samulski, E. T. *Macromolecules* **2000**, *33*, 3795-3802.
- (246) Pakula, T.; Kahle, S. *to be published*.
- (247) Schönhals, A.; Kremer, F.; Analysis of Dielectric Spectra, In *Broadband dielectric spectroscopy*; Kremer, F.; Schönhals, A., Eds.; Springer Verlag: Berlin, Germany, 2003; chap. 3, pp 59-98.
- (248) Buerger, D. E.; Boyd, R. H. *Macromolecules* **1989**, *22*, 2694-2699.
- (249) de Brouckere, L.; Offergeld, G. *Journal of Polymer Science* **1958**, *30*, 105-118.
- (250) Ribelles, J. L. G.; Duenas, J. M. M.; Pradas, M. M. *J. Appl. Polym. Sci.* **1989**, *38*, 1145-1157.
- (251) Ribelles, J. L. G.; Pradas, M. M.; Estelles, J. M.; Duenas, J. M. M.; Colomer, F. R. *Plast. Rubber Compos. Process. Appl.* **1992**, *18*, 169-179.
- (252) Kahle, S., Mainz, Germany, *personal communication*, 2004.
- (253) McCrum, N. G.; Read, B. E.; Williams, G.; Methacrylates and related polymers, In *Anelastic and dielectric effects in polymeric solids*; Dover Publications, Inc.: New York, USA, 1991; pp 238-299.
- (254) Mead, D. J.; Fuoss, R. M. *J. Am. Chem. Soc.* **1942**, *64*, 2389-2393.
- (255) Reissig, S., *Ph.D. thesis*, Martin Luther University, Halle, Germany, 1999.
- (256) Soen, T.; Yamashit.K; Kawai, H.; Ono, T. *Kolloid-Zeitschrift and Zeitschrift Fur Polymere* **1972**, *250*, 459-470.
- (257) Fioretto, D.; Livi, A.; Rolla, P. A.; Socino, G.; Verdini, L. *J. Phys.-Condes. Matter* **1994**, *6*, 5295-5302.
- (258) Fitzgerald, J. J.; Binga, T. D.; Sorriero, L. J.; Oreilly, J. M. *Macromolecules* **1995**, *28*, 7401-7406.
- (259) Hayakawa, T.; Adachi, K. *Polym. J.* **2000**, *32*, 845-848.
- (260) Jourdan, C.; Cavaille, J. Y.; Perez, J. *Polym. Eng. Sci.* **1988**, *28*, 1318-1325.
- (261) Williams, J.; Eisenberg, A. *Macromolecules* **1978**, *11*, 700-707.
- (262) Heijboer, J.; Baas, J. M. A.; Vandegraaf, B.; Hoefnagel, M. A. *Polymer* **1987**, *28*, 509-513.
- (263) Tanabe, Y.; Hirose, J.; Okano, K.; Wada, Y. *Polym. J.* **1970**, *1*, 107-115.
- (264) Gabrys, B.; Horii, F.; Kitamaru, R. *Macromolecules* **1987**, *20*, 175-177.
- (265) Kuebler, S. C.; Schaefer, D. J.; Boeffel, C.; Pawelzik, U.; Spiess, H. W. *Macromolecules* **1997**, *30*, 6597-6609.
- (266) Vorwerg, L.; Gilbert, R. G. *Macromolecules* **2000**, *33*, 6693-6703.

- (267) Mitsunobu, O. *Synthesis* **1981**, 1-28.
- (268) Powles, J. G.; Strange, J. H. *Proceedings of the Physical Society of London* **1963**, *82*, 6-15.
- (269) Bielecki, A.; Burum, D. P. *J. Magn. Reson. Ser. A* **1995**, *116*, 215-220.
- (270) Takahashi, T.; Kawashima, H.; Sugisawa, H.; Baba, T. *Solid State Nucl. Magn. Reson.* **1999**, *15*, 119-123.
- (271) Neue, G.; Dybowski, C.; Smith, M. L.; Hepp, M. A.; Perry, D. L. *Solid State Nucl. Magn. Reson.* **1996**, *6*, 241-250.
- (272) Beckmann, P. A.; Dybowski, C. *J. Magn. Reson.* **2000**, *146*, 379-380.
- (273) Langer, B.; Schnell, L.; Spiess, H. W.; Grimmer, A. R. *J. Magn. Reson.* **1999**, *138*, 182-186.
- (274) Grimmer, A. R.; Kretschmer, A.; Cajipe, V. B. *Magn. Reson. Chem.* **1997**, *35*, 86-90.
- (275) Kohler, F. H.; Xie, X. L. *Magn. Reson. Chem.* **1997**, *35*, 487-492.
- (276) Fischbach, I.; In *Supramolecular Order and Dynamics of Discotic Materials Studied by Solid-State NMR Recoupling Methods*, Ph.D. thesis; Johannes Gutenberg University: Mainz, Germany, 2003; p 82.
- (277) Kaye, A.; Stepto, R. F. T.; Work, W. J.; Aleman, J. V.; Malkin, A. Y. *Pure Appl. Chem.* **1998**, *70*, 701-754.
- (278) Schoff, C. K.; Rheological measurements, In *Encyclopedia of Polymer Science and Engineering*, 2nd ed.; Kroschwitz, J. I., Ed.; Wiley, 1988; vol. 1, pp 454-541.
- (279) Larson, R. G.; In *The structure and rheology of complex fluids*; Oxford University Press, New York, 1999; p 18.
- (280) Jenkins, A. D.; Loening, K. L.; Nomenclature, In *Comprehensive Polymer Science: the Synthesis, Characterization, Reaction and Applications of Polymers*, 1st ed.; Allen, G.; Bevington, J. C., Eds.; Pergamon Press: Oxford, 1989; vol. 1, chap. 2, pp 13-54.
- (281) Odian, G.; Stereochemistry of polymerization, In *Principles of polymerization*, 2nd ed.; John Wiley and Sons: New York, 1981; chap. 8, pp 566-651.
- (282) Jenkins, A. D. *Pure Appl. Chem.* **1981**, *53*, 733-752.
- (283) Litvinov, V. M.; Dias, A. A. *Macromolecules* **2001**, *34*, 4051-4060.
- (284) Vega, D. A.; Villar, M. A.; Valles, E. M.; Steren, C. A.; Monti, G. A. *Macromolecules* **2001**, *34*, 283-288.
- (285) Barth, P.; Hafner, S.; Denner, P. *Macromolecules* **1996**, *29*, 1655-1659.
- (286) Couvreur, L.; Piteau, G.; Castignolles, P.; Tonge, M.; Coutin, B.; Charleux, B.; Vairon, J. P. *Macromol. Symp.* **2001**, *174*, 197-207.

Summary

Industrial acrylic pressure sensitive adhesives (PSAs), poly(n-alkyl acrylate) and poly(n-alkyl methacrylate) model samples were investigated using predominantly solid-state NMR (nuclear magnetic resonance). The long term goal is to understand the influence of their microscopic properties on adhesion. Our contribution was to provide analytical tools to characterize branching, local dynamics and dynamic heterogeneity of poly(alkyl acrylates).

Several ^{13}C NMR techniques were compared for branching quantification in poly(alkyl acrylates) and single pulse excitation of the molten sample under magic angle spinning (MAS) was proved to be the most accurate. This provided the first reliable estimate of branching in poly(alkyl acrylates) and is directly applicable to crosslinked and multi-component industrial samples. This will help the understanding of the polymerization process for these samples.

In the context of a better understanding of the adhesion mechanism, an alternative method of multiple detection size exclusion chromatography (SEC) was presented to detect long branches (LCB) in soluble poly(alkyl acrylates). Extensive experimental and theoretical work will be necessary to obtain quantitative results. The use of solid-state NMR to quantify local motion of specific chemical sites in non isotopically labeled polymeric samples in the melt was investigated. The experimental scheme is the same as conventional ^1H spin diffusion with dipolar filter, previously widely used to quantify the size of dynamic heterogeneities in polymeric samples exhibiting a strong dynamic contrast. In poly(alkyl acrylates) and poly(alkyl methacrylates) with a weak dynamic contrast within the monomeric unit, the hindered dynamics of the side chains in alkyl nanodomains was quantified via cross-relaxation analysis.

Keywords: pressure sensitive adhesives (PSA), poly(alkyl acrylates), poly(alkyl methacrylates), long chain branching (LCB), solid-state nuclear magnetic resonance (NMR), dipolar filter, cross-relaxation (NOE), multiple detection size exclusion chromatography (SEC)

Résumé

Des adhésifs sensibles à la pression (PSAs) acryliques industriels, des polyacrylates et polyméthacrylates de n-alkyles modèles, ont été étudiés principalement par RMN (résonance magnétique nucléaire) du solide. Le but à long terme est de comprendre l'influence des propriétés microscopiques sur l'adhésion. Notre contribution est l'apport d'outils analytiques pour la caractérisation du branchement, de la dynamique locale et de l'hétérogénéité dynamique.

Après comparaison de plusieurs techniques de RMN ^{13}C , une méthode de quantification du branchement dans les poly(acrylates d'alkyles) par irradiation simple de l'échantillon fondu sous rotation à l'angle magique (MAS) a été proposée. Cela a permis la première estimation fiable du branchement dans les poly(acrylates d'alkyles) et est applicable directement aux échantillons industriels réticulés et multi-composants. Cela facilitera la compréhension du procédé de polymérisation.

Dans le cadre d'une meilleure compréhension du mécanisme d'adhésion, une méthode de chromatographie d'exclusion stérique (SEC) multi-détection a été proposée pour la détection des longues branches (LCB) dans les poly(acrylates d'alkyles) solubles. L'utilisation de la RMN du solide pour la quantification sélective de mouvements locaux dans des polymères fondus sans marquage isotopique a été étudiée. La technique expérimentale est la même que celle de la diffusion de spin ^1H conventionnelle avec filtre dipolaire, beaucoup utilisée antérieurement pour quantifier la taille d'hétérogénéités dynamiques dans des polymères ayant un fort contraste dynamique. Dans les poly(acrylates d'alkyles) et les poly(méthacrylates de n-alkyles), qui présentent un contraste dynamique faible au sein de l'unité monomère, la dynamique entravée des chaînes latérales dans les nanodomains alkyles a été quantifiée via une analyse de relaxation croisée.

Mots-clés : adhésif sensible à la pression (PSA), poly(acrylates d'alkyles), poly(méthacrylates d'alkyles), branchement long (LCB), résonance magnétique nucléaire (RMN) du solide, filtre dipolaire, relaxation croisée (NOE), chromatographie d'exclusion stérique (SEC) multi-détection